ACTA PHYSICA

ACADEMIAE SCIENTIARUM HUNGARICAE

REDIGIT
I. KOVÁCS

TOMUS XXXII FASCICULI 1–4

AKADÉMIAI KIADÓ, BUDAPEST
1972

ACTA PHYS. HUNG. APAHAQ 32 (1–4) 1–352 (1972)

ACTA PHYSICA

ACADEMIAE SCIENTIARUM HUNGARICAE

SZERKESZTI

KOVÁCS ISTVÁN

Az *Acta Physica* angol, német, francia vagy orosz nyelven közöl értekezéseket. Évente két kötetben, kötetenként 4–4 füzetben jelenik meg. Kéziratok a szerkesztőség címére (Budapest XI., Budafoki út 8.) küldendők.

Megrendelhető a belföld számára az Akadémiai Kiadónál (Budapest V., Alkotmány utca 21. Bankszámla 05-915-111-46), a külföld számára pedig a „Kultúra" Könyv- és Hírlap Külkereskedelmi Vállalatnál (Budapest I., Fő utca 32. Bankszámla 43-790-057-181 sz.), vagy annak külföldi képviseleteinél és bizományosainál.

The *Acta Physica* publish papers on physics in English, German, French or Russian, in issues making up two volumes per year. Subscription price: $16.00 per volume. Distributor: KULTURA Hungarian Trading Co. for Books and Newspapers (Budapest 62, P.O. Box 149) or its representatives abroad.

Die *Acta Physica* veröffentlichen Abhandlungen aus dem Bereich der Physik in deutscher, englischer, französischer oder russischer Sprache, in Heften die jährlich zwei Bände bilden.

Abonnementspreis pro Band: $16.00. Bestellbar bei: KULTURA Buch- und Zeitungs-Außenhandelsunternehmen (Budapest 62, Postfach 149) oder bei seinen Auslandsvertretungen.

Les *Acta Physica* publient des travaux du domaine de la physique, en français, anglais, allemand ou russe, en fascicules qui forment deux volumes par an.

Prix de l'abonnement: $16.00 par volume. On peut s'abonner à l'Entreprise du Commerce Extérieur de Livres et Journaux KULTURA (Budapest 62. P.O.B. 149) ou chez ses représentants à l'étranger.

«*Acta Physica*» публикуют трактаты из области физических наук на русском, немецком, английском и французском языках.

«*Acta Physica*» выходят отдельными выпусками, составляющими два тома в год.

Подписная цена — $16.00 за том. Заказы принимает предприятие по внешней торговле книг и газет KULTURA (Budapest 62, P.O.B. 149.) или его заграничные представительства и уполномоченные.

ACTA PHYSICA

ACADEMIAE SCIENTIARUM HUNGARICAE

REDIGIT
I. KOVÁCS

TOMUS XXXII

AKADÉMIAI KIADÓ, BUDAPEST
1972

ACTA PHYS. HUNG.

THIS VOLUME IS DEDICATED TO
Prof. L. JÁNOSSY
ON THE OCCASION OF HIS 60th BIRTHDAY

Acta Physica Academiae Scientiarum Hungaricae, Tomus 32 (1—4). pp. 5—16 (1972)

CENTRIFUGAL DISTORTIONS AND MULTIPLET STRUCTURE*

By

I. Kovács

DEPARTMENT OF ATOMIC PHYSICS, POLYTECHNICAL UNIVERSITY, BUDAPEST

(Received 24. VI. 1971)

Expressions are derived for the rotational energy levels of doublet states and the $^4\Sigma$ state of diatomic molecules that take into account the first and second correction terms of the centrifugal distortions of the spin-orbit, spin-spin and spin-rotation interactions in intermediate cases between Hund's cases a) and b). General formulas valid for Σ terms of any multiplicity are given in Hund's case b) taking into consideration the above-mentioned interactions. Applied to the $^2\Delta$ states of SnH and SnD molecules and to the $^4\Sigma$ states of GeH and SnH molecules the new expressions show better agreement with the experimental data than earlier formulas.

1. Introduction

Most of the observed molecular spectra exhibit a multiplet structure. The multiplying of a spectral line is due to the multiplying of the terms involved in the transition giving rise to the line in question. These multiplet terms are not accounted for by expressions obtained from the separable wave equation. To obtain multiplet term formulas in agreement with the experimental findings, several interactions have to be taken into consideration.

The multiplying of the terms can be due to two reasons: (i) the different orientations of the resultant spin momentum of the molecule involve different energies; or (ii) the different orientations of the resultant orbital angular momentum of the molecule entail different energy levels. The first case can be termed the case of S, or spin multiplets, and the second the L-multiplets. In this paper we shall deal with spin multiplets only. In this case, according as the spin momentum is coupled to the internuclear axis or to the axis of rotations, we speak of Hund's case a) or b). The energy values corresponding to Hund's case a) can be readily obtained from the separable wave equation including the diagonal terms of several interactions of the resultant spin momentum. The energy expressions obtained in this way will, however, seldom lead to values in agreement with experiment; this is understandable inasmuch as this limiting case practically means neglecting all but a few interactions, due to the neglection of the off-diagonal terms of several interactions. In the actual

* Dedicated to my friend, Prof. L. Jánossy, on his 60th birthday, with the heartiest congratulations and the best wishes for further successful work and a long and happy life.

molecule all interactions are operative to a greater or lesser extent. Results compatible with experimental findings can be obtained if these energy values are used initially, i.e. those of the unperturbed system, and the off-diagonal matrix elements of all interactions are taken into consideration by perturbation calculation. In this way we can obtain energies or term values intermediate between Hund's limiting cases which are capable of describing the gradual transition from one limiting case to another.

Although the so obtained term formulas show a good agreement with most observed multiplet terms, in some cases, especially in the case of hydrides, they cannot be applied successfully. The observed discrepancies usually consist of an apparent change of coupling constants with the rotational quantum number, J, and in addition the multiplet splitting deviates from the multiplet term formulas. In a few cases, especially in case of $^3\Pi$, $^3\Delta$ and $^4\Pi$ terms, the reason for these discrepancies was that the spin-spin and the spin-rotation interaction were left out of consideration. After taking these interactions into account these anomalies can be eliminated and the resultant spin coupling constant no longer changes with the rotational quantum number, but in case of doublet terms and of multiplet Σ terms the anomalies longer exist. Such cases are for instance, a $^2\Sigma$ term of YO, HgH and other hydrides and deuterides, a $^2\Pi$ term of SH, SiF and CCl, a $^2\Delta$ term of SnH and SnD, a $^3\Sigma$ term of O_2, N_2, a $^4\Sigma$ term of SnH, GeH, SiF, and a $^7\Sigma$ term of MnH molecules. Deviations from the usual multiplet term formulas of Σ terms for which the Hund's case b) gives a good approximation, however, could be partly interpreted by the second-order perturbation effect of the spin-orbit interaction. Such cases are the $^2\Sigma$ terms of HgH and YO molecules, the $^3\Sigma$ terms of the N_2 molecule and the $^7\Sigma$ term of the MnH molecule. These Σ terms of the remaining molecules belong to the intermediate case between the two Hund's cases due to the relative large spin-spin interaction. Taking into account the interaction between rotation and vibration it can be shown that the multiplet-splitting constant or, in other words, the spin-orbit coupling constant apparently varies with the rotational quantum number and so the anomalous behaviour of the $^2\Pi$ and $^2\Delta$ terms could be partly interpreted. All of the remaining anomalies can be explained very well by taking into account the centrifugal distortions of the spin-orbit, the spin-spin and the spin-rotation interactions. If the rotating molecule is not a rigid rotator then the centrifugal effect will influence the rotational energy and the energies of the spin interactions because the interaction constants obtained by the solution of the electronic part of the wave equation contain the internuclear distance as parameter and the latter increases with increasing rotation which may be very significant especially in case of hydride molecules. This effect for the rotational energy is already well known and for the spin-spin interaction was investigated by MIZUSHIMA and HILL [1] and by TINKHAM and STRANDBERG [2] in the case of $^3\Sigma$ terms. MIZUSHIMA and HILL

took into account the centrifugal distortion under the adiabatic expansion of the electronic and vibrational part of the wave function but assume a harmonic vibrational potential, while TINKHAM and STRANDBERG used a power-series expansion about the r_e equilibrium distance for the vibrational potential, for the rotational energy and for the spin-spin interaction. In the following we are going to investigate the centrifugal distortion not only for the rotational energy and for the spin-spin interaction but also for the spin-orbit and spin-rotation interactions and the theoretical results will be applied to the interpretation of the discrepancies appearing on the $^2\Delta$ terms of the SnH and SnD molecules and on the $^4\Sigma$ terms of the SnH and GeH molecules.

2. Theory

If certain members are omitted from the molecular wave equation

$$(\hat{H}-W)\psi = 0, \tag{1}$$

then it can be solved by the wave fuction as follows where ψ

$$\psi = \Phi R u, \tag{2}$$

where Φ depends on the electron and spin coordinates, R on the internuclear distance and u on the rotational coordinates. Multiplying Eq. (1) from left by Φ^* and integrating over all electron and spin coordinates we obtain

$$[\hat{H}_{\text{vibr}}+\hat{H}_{\text{rot}}+\hat{H}_{Sp}-(W-W_{el}(r))]Ru = 0. \tag{3}$$

Using a two-term power series expansion about the $W_{el}(r_e)$ minimum energy to express the dependence of the electronic energy on the inter-nuclear distance, we get for the vibrational Hamiltonian

$$\hat{H}_{\text{vibr}} = \bar{B}_e r_e^2 \hat{P}_r^2 + 1/2\, k r_e \xi^2 + \bar{b}\xi^3 \tag{4}$$

and in similar manner for the rotational Hamiltonian

$$\hat{H}_{\text{rot}} = \bar{B}_e(1 - 2\xi + 3\xi^2)\hat{R}^2, \tag{5}$$

where

$$\xi = \frac{r-r_e}{r_e}, \quad \bar{B}_e = \frac{h^2}{8\pi^2\mu r_e^2}, \quad k = 4\pi^2\bar{\omega}_e^2\mu. \tag{6}$$

μ is the reduced mass, $\bar{\omega}_e$ is the vibrational frequency measured in sec^{-1}, $\hat{P}_r$ is the vibrational operator, and $\hat{R}$ is the operator of the angular momentum of nuclear rotation.

The spin part of the Hamiltonian of a diatomic molecule can be written a

$$\hat{H}_{SP} = \hat{H}_{S0} + \hat{H}_{SS} + \hat{H}_{SR}. \tag{7}$$

$\hat{H}_{S0}, \hat{H}_{SS}$ and $\hat{H}_{SR}$ are the spin-orbit the spin-spin and the spin-rotation operators, respectively, and have the following forms

$$\begin{aligned} \hat{H}_{S0} &= \bar{A}(r)\,\hat{L}\hat{S}\,, \\ \hat{H}_{SS} &= \bar{\varepsilon}(r)\,[3\hat{S}_z^2 - \hat{S}^2]\,, \\ \hat{H}_{SR} &= \bar{\gamma}(r)\,\hat{R}\hat{S}\,, \end{aligned} \tag{8}$$

where $\hat{L}$ and $\hat{S}$ are the operators of the resultant orbital and spin momentum respectively. Owing to the dependence on the internuclear distance using a power series expansion about the minimum of potential energy we obtain for the coefficients of (8)

$$\begin{aligned} \bar{A}(r) &= \bar{A}_0 + \bar{\alpha}_1\,\xi + \bar{\alpha}_2\,\xi^2, \\ \bar{\varepsilon}(r) &= \bar{\varepsilon}_0 + \bar{\varepsilon}_1\,\xi + \bar{\varepsilon}_2\,\xi^2\,, \\ \bar{\gamma}(r) &= \bar{\gamma}_0 + \bar{\gamma}_1\,\xi + \xi + \bar{\gamma}_2\,\xi^2\,, \end{aligned} \tag{9}$$

where

$$\bar{A}_0 = (\bar{A})_{r=r_e},\ \bar{\alpha}_1 = r_e\left(\frac{\partial \bar{A}}{\partial r}\right)_{r=r_e},\ \bar{\alpha}_2 = \frac{1}{2}\,r_e^2\left(\frac{\partial^2 \bar{A}}{\partial r^2}\right)_{r=r_e}, \tag{10}$$

and similar expressions are valid for the other constants.

To explain the rotational structure it is not necessary to take into account the vibrational motion and consequently the vibrational dependence. The internuclear distance in the rotating molecule has to assume a value r such that the centrifugal force is cancelled by the restoring force generated by the slight deplacement $r - r_e$ from the equilibrium position r_e. Equating the centrifugal force to the restoring force, we obtain

$$\xi \cong \frac{\hbar^2}{\mu r_e^4\, k}\,\hat{R}^2\,. \tag{11}$$

Putting (11) in (5), (9) and (9) in (8) we obtain

$$\begin{aligned} \hat{H}_{\text{rot}} &= B\hat{R}^2 - D\hat{R}^4 + H\hat{R}^6\,, \\ \hat{H}_{S0} &= (A_0 + A_1\hat{R}^2 + A_2\hat{R}^4)\,\hat{L}\hat{S}\,, \\ \hat{H}_{SS} &= \left(\varepsilon_0 + \frac{2}{3}\,\tau\hat{R}^2 + \frac{2}{3}\,\varrho\hat{R}^4\right)(3\hat{S}_z^2 - \hat{S}^2)\,, \\ \hat{H}_{SR} &= (\gamma_0 + 2\sigma\hat{R}^2 + 2\varphi\hat{R}^4)\,\hat{R}\hat{S}. \end{aligned} \tag{12}$$

where all quantities are measured in cm^{-1} (dividing by hc in (5), (9) and neglecting all the flags above the symbols) and

$$B = \frac{h}{8\pi^2 \mu c r_e^2}\,;\; D = \alpha B, H = 3\alpha^2 B + \alpha^3 b\,,\; \alpha = \frac{4B^2}{\omega_e^2}\,,$$

$$A_1 = \alpha\alpha_1, A_2 = \alpha^2 \alpha_2\,,\; \tau = \frac{3}{2}\alpha\varepsilon_1,\; \varrho = \frac{3}{2}\alpha^2 \varepsilon_2\,, \tag{13}$$

$$\sigma = \frac{1}{2}\alpha\gamma_1, \varphi = \frac{1}{2}\alpha^2 \gamma_2.$$

Substituting (12) in (3) and solving the secular determinant

$$|<\Lambda,\Sigma|\, \hat{H}_{\text{rot}} + \hat{H}_{Sp}\, |\Lambda,\Sigma'> - F| = 0 \tag{14}$$

we obtain the new multiplet formulas.

3. Application for $^2\Delta$ terms

The spin-spin interaction does not give members for doublet terms and so — using the explicit form of the matrix elements of (12) given by Kovács and Vujisić [3] — after solving (14) we obtain the following expression for doublet terms for the intermediate case between Hund's case a) and b):

$$F_{\frac{1}{2}} = \nu_0' + B' J_A^2 - D[J_A^2(J_A^2+1) - \Lambda^2] + HJ_A^2\,[J_A^2(J_A^2+3) + 3\Lambda^2] - (1/2)\,\gamma_0 \mp \tag{15}$$
$$\mp \sqrt{\Lambda^2(A^* - 2B^* - \sigma)^2 + 4J_A^2[B^* + A_2\Lambda^2 - (1/2)(\gamma_0 + \sigma(J_A^2 - 1))]^2},$$

where

$$\begin{aligned} \nu_1' &= \nu_0 - (1/2)A_1\,\Lambda^2, \\ B' &= B - A_2\Lambda^2 - \sigma\,, \\ B^* &= B' - 2DJ_A^2 + H[J_A^2(3J_A^2+1) + \Lambda^2]\,, \\ A^* &= A_0 + A_1 J_A^2 + A_2\,[J_A^2(J_A^2+1) - \Lambda^2]\,, \\ J_A^2 &= (J+1/2) - \Lambda^2. \end{aligned} \tag{16}$$

In expression (15) we have taken into account the first and second centrifugal term of rotation energy and spin-orbit interaction and the first one for spin-rotation interaction in intermediate case between Hund's case a) and b). Putting $D = H = A_1 = A_2 = \gamma_0 = \sigma = 0$ in (15) we obtain the well known Hill—Van Vleck formula.

It is very interesting to note that the first centrifugal term of the spin-orbit interaction is similar to the correction term for the spin-orbit interaction

obtained by JAMES [4] treating vibration-rotation interaction, while the second term could not be derived from the latter interaction. The agreement of the first centrifugal term of the spin-orbit interaction with the JAMES correction is the reason that the JAMES formula was satisfactory where the first approximation proves to be sufficient.

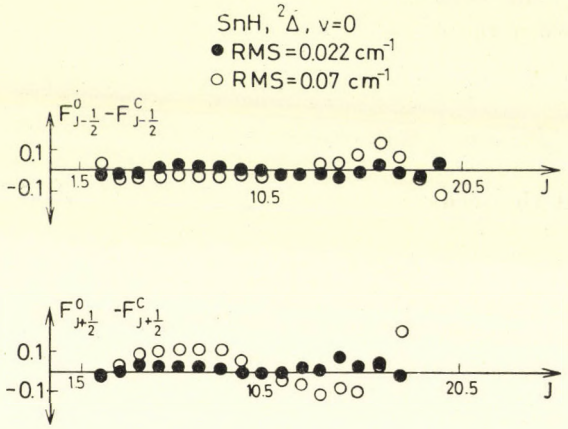

Fig. 1

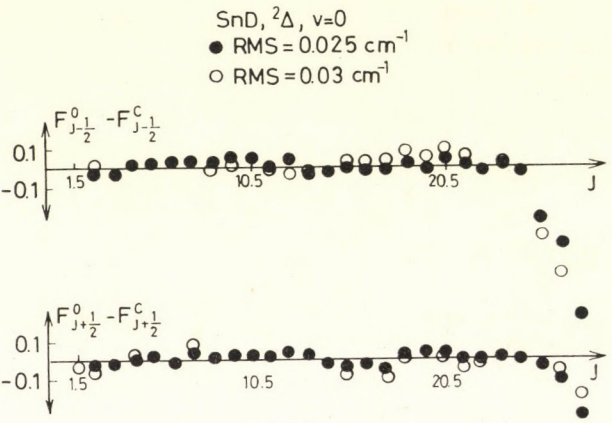

Fig. 2

While numerous examples of $^2\Pi$ and $^2\Delta$ states have been well analyzed, only two $^2\Delta$ states, namely those of SnH and SnD molecule, are selected for comparison with the results here obtained. KLYNNING, LINDGREN and ÅSLUND [5] have shown that the coupling constant of the spin-orbit interaction for $^2\Delta$ states depends on J. Applying the formula (15) to the term values of $^2\Delta$ state of both SnH and SnD molecules, it was found that, in case of SnH, it is not necessary to take into account the centrifugal correction term of the spin-

rotation interaction ($\sigma = 0$). The black circles show the differences between the observed and calculated term values according to (15), while the empty circles represent those according to JAMES' formula calculated by KLYNNING et al. [5]. The RMS error for SnH molecule decreases from the value of 0.07 cm^{-1} given by KLYNNING et al. to 0.022 cm^{-1}, and in case of SnD molecule from 0.04 cm^{-1} to 0.025 cm^{-1} (KOVÁCS and VUJISIČ [3]). As we can see the deviation between the observed and calculated term values shows no systematic trend except at the higher J values for the SnD molecule, which is probably caused by a perturbation. In his recently published paper VESETH [6] also found that the first centrifugal correction of the spin-orbit interaction is identical with the result obtained by JAMES (1964) using a different method of calculation but the second corrections are missing also in his paper.

4. Application for multiplet Σ states

The spin-orbit interaction in first order of magnitude does not give members for multiplet Σ terms and so is sufficient to take into account besides the rotational energy the energies of the spin-spin and spin-rotation interactions in (12). Taking into account that in most of the multiplet Σ terms, in general, the *Hund's case b)* form gives a good approximation and for Σ terms ($\Lambda = 0$) the rotational angular momentum $\hat{R}$ is identical to the angular momentum $\hat{N}$, (12) yields in general form for the energy of multiplet Σ states in Hund's case b)

$$F_N(N) = v_0 + T_N(N) + H_N^{SS}(N) + H_N^{SR}(N)\,, \tag{17}$$

where

$$T_N(N) = BN(N+1) - DN^2(N+1)^2 + HN^3(N+1)^3, \tag{18a}$$

$$H_N^{SS}(N) = \left[\varepsilon_0 + \frac{2}{3}\tau N(N+1) + \frac{2}{3}\varrho N^2(N+1)^2\right] \langle J, N\,|3\hat{S}_z^2 - \hat{S}^2|_b\, J, N\rangle, \tag{18b}$$

$$H_N^{SR}(N) = (\gamma_0 + 2\sigma N(N+1) + 2\varphi N^2(N+1)^2]\,\langle J, N\,|\hat{N}\hat{S}|_b\, J, N\rangle, \tag{18c}$$

$$\langle J, N\,|3\hat{S}_z^2 - \hat{S}^2|_b\, J, N\rangle = -\frac{(3/2)\,C(C+1) - 2N(N+1)\,S(S+1)}{(2N-1)\,(2N+3)}\,, \tag{18d}$$

$$\langle J, N\,|\hat{N}\hat{S}|_b\, J, N\rangle = \frac{1}{2}C, C = J(J+1) - N(N+1) - S(S+1)\,, \tag{18e}$$

and

$$N = J + S, J + S - 1, \ldots\ldots, |J - S|,$$

These formulas are valid for Σ terms of any multiplicity.

It is very interesting to note that the effect of perturbation by closer lying Π term of the same multiplicity in dependence on the rotational quantum number leads to correction terms of the same form as the first centrifugal correction members of the spin-spin interaction in (18b) and of the spin-rotation interaction in (18c). (The detailed form of these correction terms calculated for any multiplicity including septet terms can be found in the author's book (KOVÁCS, [7]). Therefore the experimentally determined constants τ and σ contain not only the effects of the centrifugal distortion but the perturbation effect by the neighbouring terms transferred by the spin-orbit interaction, too.

As a very simple example let us see the case of $^2\Sigma$ term. As can be easily seen in this case the spin-spin interaction does not give members and so substituted for $N = J - 1/2, J + 1/2$ and $S = 1/2$ and neglected the second correction the doublet splitting becomes

$$\Delta F_{12}(N) = \gamma_0(N+1/2) - 2\sigma N(N+1)(N+1/2), \tag{19}$$

The first member gives the usual doublet splitting and the second one is the deviation from the latter. Deviations of the above type were found, for instance, by HULTHÉN [8] at the levels $v = 0, 1, 2$ in the $X^2\Sigma^+$ ground state of the HgH molecule and also by UHLER and ÅKERLIND [9] at the $v = 0$ level of the $B^2\Sigma$ term of the YO molecule (see KOVÁCS, [7] p. 65). The fit between experiment and theory is seen to be fairly good, but as in his recently published paper VESETH [6] pointed out here and for the other hydrids and deuterides in the experimentally determined σ constant the centrifugal distortion gives much longer contribution than the perturbation effect by the neighbouring terms. Probably the situation is the same not only in the case of doublet Σ terms but also in the case of higher multiplicities among which two examples are mentioned here: deviation from the usual spin splitting at the $v = 0$ level of $A^3\Sigma^+$ term of the N_2 molecule (observed by CARROLL [10]) and at the $^7\Sigma^-$ term of the MnH molecule (observed by NEVIN [11]). In the last two cases, of course, besides the spin-rotation interaction (18c) also the spin-spin interaction (18b) is taken into account both inclusive till the first corrections (see KOVÁCS, [7] pp. 75, 101).

In case of Σ terms of triplet or higher multiplicity, however, especially when the coefficient of the spin-spin interaction ε_0 is larger than the others, the Hund's case b) approximation is no longer sufficient. This is the situation in the cases of the $^3\Sigma$ term of O_2 molecule and of $^4\Sigma$ terms of the GeH and SnH molecules. In such a case one can start from Hund's case a) for all interactions in (12) and taking into account the off-diagonal matrix elements of these interactions the secular determinant (14) is to be solved. The explicit form of the matrix elements for $^4\Sigma$ term are given by KOVÁCS and KORWAR [13]. The solutions of this secular equation provide the required multiplet energies

between Hund's case a) and b). These formulas are given by TINKHAM and STRANDBERG [2] for $^3\Sigma$ terms without taking into account the spin-rotation interaction and for $^4\Sigma$ term will be given as follows (see KOVÁCS and PACHER, [12]).

$$\begin{aligned} F_{J-3/2} &= U_+ - \sqrt{V_+^2 + Z_+^2}\,, \\ F_{J-1/2} &= U_- - \sqrt{V_-^2 + Z_-^2}\,, \\ F_{J+1/2} &= U_+ + \sqrt{V_+^2 + Z_+^2}\,, \\ F_{J+3/2} &= U_- + \sqrt{V_-^2 + Z_-^2}\,, \end{aligned} \tag{20}$$

where

$$\begin{aligned} U_\pm &= \nu_0 + B(j^2 \mp j + 1) - D(j^4 \mp 2j^3 + 7j^2 \mp 6j + 2) + H(j^6 \mp 3j^5 + \\ &+ 18j^4 \mp 31j^3 + 33j^2 \mp 18j + 4) - \frac{1}{2}\gamma_0(5 \mp j) - 2\tau(\mp j + 2) - \\ &- \sigma(\mp j^3 + 10j^2 \mp 10j + 6) - 2\varrho(\mp 2j^3 + 6j^2 \mp 6j + 4)\,, \end{aligned}$$

$$\begin{aligned} V_\pm &= 3\varepsilon_0 + B(\pm j - 2) - 2D(\pm j^3 - 3j^2 \pm 3j - 2) + \\ &+ H(\pm 3j^5 - 12j^4 \pm 25j^3 - 36j^2 \pm 24j - 8) + \frac{1}{2}\gamma_0(2 \mp j) + \\ &+ 2\tau(j^2 \mp j + 1) + \sigma(\mp j^3 + 4j^2 \mp 10j + 12) + 2\varrho(j^4 \mp 2j^3 + 7j^2 \mp 6j + 2), \end{aligned} \tag{21}$$

$$\begin{aligned} Z_\pm &= \sqrt{3(j^2 - 1)}\,[B - 2D(j^2 \mp j + 1) + H(3j^4 \mp 6j^3 + 13j^2 \mp 10j + 4) - \\ &- \frac{\gamma_0}{2} - \sigma(j^2 \mp 2j + 6)] \quad \text{and} \quad j = J + 1/2\,. \end{aligned}$$

The influence of the perturbation by other terms in intermediate case was investigated by HOUGEN [14]. HOUGEN in his first expressions added the perturbation matrix elements of the farther-lying terms transferred by the spin-orbit interaction to the matrix elements of the rotational perturbation and of the spin-spin interaction and solved the modified secular determinant so obtained. Meanwhile, however, the interaction between the spin and rotation, the second centrifugal correction of the rotational terms were neglected and even the first centrifugal correction was taken into account only in Hund's case b) form. In addition the above treated first and second centrifugal corrections of the spin-spin and of the spin-rotation interaction are missing.

Applying the HOUGEN's formula for the $^4\Sigma$ term of the GeH molecule KLYNNING [15] has found an RMS error of 0.137 cm^{-1} for the deviations between the observed and calculated term values (empty circles), while putting $\sigma = \varrho = 0$, (20) and (21) yield an RMS error of 0.118 cm^{-1} (black circles). For the detailed data see KOVÁCS and PACHER [12] (Fig. 3).

It is to note that after putting $\sigma = \varrho = 0$ formula (20) contains one constant less than the HOUGEN's formula. Because of the strong scattering of the experimental errors KLYNNING has neglected the points having larger deviations than 0.2 cm^{-1} and so obtained an RMS error of 0.106 cm^{-1}. In this case formula (20) gives an RMS error of 0.082 cm^{-1}. Owing to the strong scattering a better agreement with experiment cannot be expected here.

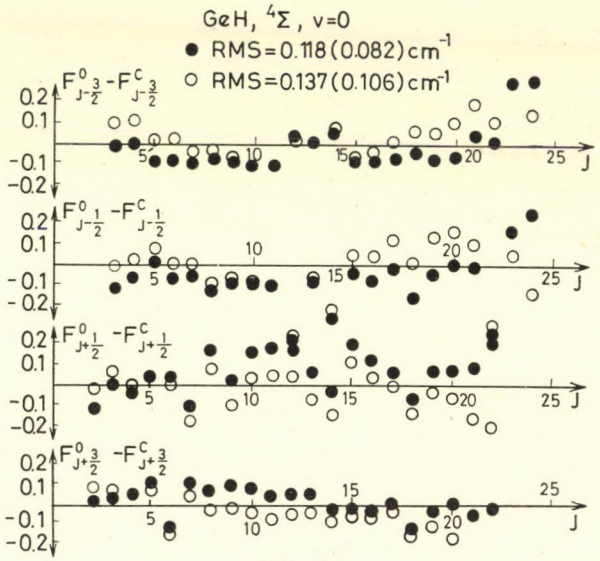

Fig. 3

Some further problem is shown in case of $^4\Sigma$ term of SnH molecule. Applying the above mentioned HOUGEN's formula deviations appear up to 10 cm^{-1} from the observed values. Therefore the preceding HOUGEN's formula was modified by KLYNNING, LINDGREN and ASLUND [5]. In the modified expressions the first and second centrifugal corrections of the rotational term were taken into account already in the intermediate form, although not in the entirely precise form, however, the spin-rotation interaction and the centrifugal corrections of the spin-spin and of the spin-rotation are still missing. Applying the modified HOUGEN's formula an RMS error of 0.15 cm^{-1} would be obtained with a little systematic trend.

The application of our formula in its form (20) and (21) does not give better results either. However, in both HOUGEN's formulas (in the first and the modified expressions) an effect missing in our expressions was partly taken into account. Namely due to the relative strong spin-spin interaction already in the electronic part of the Hamiltonian, i.e. in the non-rotating molecule the equilibrium internuclear distance will be slightly different for the states of

different orientation of the resultant spin momentum along the molecular axis. In case of SnH molecule, for instance, due to the large coupling constant the difference between the states with $\Omega = \pm 3/2$ and $\Omega = \pm 1/2$ is about 270 cm^{-1}. But, as can be seen from (8) and (10), since all of the coupling constants depend on the internuclear distance as parameter it follows that these constants have a little different values in the secular determinant (14) for the states with

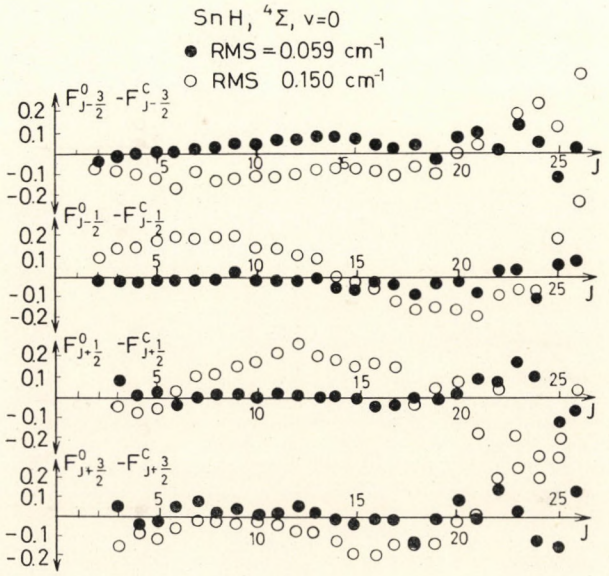

Fig. 4

$\Omega = \pm 3/2$ and $\Omega = \pm 1/2$ and it seems suitable to suppose that in the off-diagonal matrix elements the coupling constants are taking on the values of the arithmetical means of the above mentioned two different values The detailed calculation leads to the result that in (21) the B, D constants in $U_\pm$ and $V_\pm$ have different values than in $Z_\pm$ and in addition in $U_\pm$ τ^* stand instead of τ and in $V_\pm$ $2\tau(j^2 - 4) + 2\tau^*(5 \pm j)$ stand instead of $2\tau(j^2 \mp j + 1)$. So the modified form of (20) yields an RMS error of 0.059 cm^{-1} for $^4\Sigma$ term of the SnH molecule which is represented in Fig. 4, (see KOVÁCS and PACHER, [12]) by full circles. This value compared to the RMS error of 0.15 cm^{-1} obtained by KLYNNING, LINDGREN and ASLUND [5] seems to be a much better result.

Summarizing, it can be stated that most of the observed anomalies of the spin multiplets — in accordance with the experimental data — are correctly explained by the first and second correction terms of the centrifugal distortion.

REFERENCES

1. M. MIZUSHIMA and R. M. HILL, Phys. Rev.,**93**, 745., 1954.
2. M. TINKHAM and M. W. P. STRANDBERG, Phys. Rev., **97**, 937, 1955.
3. I. KOVÁCS and B. VUJISIČ, J. Phys. B., **4**, 1123, 1971.
4. T. C. JAMES, J. Chem. Phys., **41**, 631, 1964.
5. L. KLYNNING, B. LINDGREN, and N. ASLUND, Ark. Fys., **30**, 141, 1965.
6. L. VESETH, J. Phys. B., **3**, 1677, 1970.
7. I. KOVÁCS, Rotational Structure in the Spectra of Diatomic Molecules, Akadémiai Kiadó, Budapest, and Adam Hilger Ltd., London, 1969.
8. E. HULTHÉN, Z. Phys., **50**, 319. 1928.
9. U. UHLER and A. ÅKERLIND, Ark. Fys., **19**, 1, 1961.
10. P. K. CARROLL, Proc. Roy. Ir. Acad., **54A**, 369, 1952.
11. T. E. NEVIN, Proc. Roy. Ir. Acad., **50A**, 123, 1954.
12. I. KOVÁCS and P. PACHER, J. Phys. B., **4**, 1633, 1971.
13. I. KOVÁCS and V. M. KORWAR, J. Phys. B., **4**, 759, 1971.
14. J. T. HOUGEN, Can. J. Phys., **40**, 598, 1962.
15. L. KLYNNING, Ark. Fys., **32**, 563, 1966.

ЦЕНТРОБЕЖНЫЕ ИСКАЖЕНИЯ И МУЛЬТИПЛЕТНАЯ СТРУКТУРА

И. КОВАЧ

Резюме

Выведены выражения для вращательных уровней энергии дублетных и $^4\Sigma$ состояний двухатомных молекул с учетом первого и второго поправочных членов центробежных искажений спин-орбитального, спин-спинового и спин-варщательного в заимодействий в промежуточном случае, распологающемся между случаями а) и б) Хунда. Даны общие формулы для Σ термов любой мультиплетности в случае б) Хунда, в которых учитываются все вышеупомянутые виды взаимодействий. Полученные выражения применены к $^2\Delta$-состояниям молекул SnH и SnD, и к $^4\Sigma$-состояниям молекул GeH и SnH. При этом показано, что они дают результаты, более близкие к экспериментальным, чем дают известные ранее формулы.

Acta Physica Academiae Scientiarum Hungaricae, Tomus 32 (1—4), pp. 17—41 (1972)

RELATIVISTIC CORRECTIONS TO THE UNIVERSAL POTENTIAL*

By

R. GÁSPÁR and G. ERDŐS-GYARMATI

INSTITUTE OF THEORETICAL PHYSICS, KOSSUTH LAJOS UNIVERSITY, DEBRECEN

(Received 12. VII. 1971)

Atomic one-electron energies were calculated with the aid of a universal potential. For solution of the radial Schrödinger equation NOUMEROV's method was applied, while relativistic and spin-orbit coupling corrections were taken into account. The results are compared with experimental energy levels as well as with the results of other nonrelativistic and relativistic calculations.

Introduction

A very good description of atomic systems is given by the methods of HARTREE [1] and FOCK [2], but as solution of the HARTREE—FOCK (HF) equations is very laborious, simpler approximations, which can be applied to atomic calculations for all the elements, are very important. LATTER was the first to give numerical solutions of the Schrődinger equation for all the elements with an atomic one-electron potential [3]. To improve his results he considered relativistic effects. In 1963 HERMAN and SKILLMAN [4] solved the HF equations for all the elements with Slater's simplified exchange potential [5] (HFS method), relativistic and spin-orbit coupling effects were taken into account by perturbation method. A disadvantage of the HFS method is that the approximation introduced by SLATER for the exchange terms in the HF equations does not entirely compensate for the Coulomb self-interaction.

In this paper the atomic one-electron energies have been calculated with a universal potential [6], [7]. For the solution of the Schrődinger equation NOUMEROV's method has been applied according to [4]. The model makes it possible to determine the energies for all the atomic numbers as well as for all the states. Similar to [4] the relativistic and spin-orbit corrections have been taken into account by perturbation method. The results of the present calculation are compared with those of previous calculations and with experimental data .The promising results may stimulate further application of the above method, for instance to energy-band calculations.

* Dedicated to Prof. L. JÁNOSSY on his 60th birthday.

Universal potential

According to [6] the effective nuclear change, Z_p, of a neutral atom with atomic number Z is of the form

$$\frac{Z_p}{Z} = \frac{e^{-\lambda_0 x}}{1+A_0 x} . \tag{1}$$

By the aid of (1) the universal potential can be established for all the elements:

$$V = \frac{Z_p e}{r} , \tag{2}$$

where r is the distance of the electron from the nucleus, $-e$ is the charge of the electron,

$$\lambda_0 = 0.1837 , \qquad A_0 = 1.05 ,$$

$$x = \frac{r}{\mu} , \qquad \mu = \frac{0.88534137}{Z^{1/3}} a_0$$

and a_0 is the first Bohr radius.

In the statistical theory of atoms the potential of the exchange energy was given by DIRAC in the free electron approximation [8] as follows:

$$\gamma = -\frac{4}{3} \varkappa_a \varrho^{1/3} . \tag{3}$$

From (2) and (3) the potential field is

$$V = \frac{Z_p e}{r} + \frac{4}{3} \frac{\varkappa_a}{e} \varrho^{1/3} . \tag{4}$$

In (4) ϱ is the density of the electrons in the atom and

$$\varkappa_a = \frac{3}{4} \left(\frac{3}{\pi} \right)^{1/3} e^2 = 0.73855871 \, e^2$$

is a constant. Except in the immediate neighbourhood of the nucleus, the density distribution of the neutral atom can be well approximated [7] by

$$\left(\frac{\varrho}{Z^2} \right)^{1/3} = \frac{C e^{-\alpha x}}{1+Ax} \tag{5}$$

with

$$C = 3.1 a_0^{-1}, \; \alpha = 0.04, \; A = 9.$$

For the potential the above equations give the formula

$$V = \frac{Z_p e}{r} + \frac{4}{3}\varkappa_a \frac{1}{e}\varrho^{1/3} = \frac{Ze}{r}\,\frac{e^{-\lambda_0 x}}{1+A_0 x} + \frac{C'}{e}\,\frac{e^{-\alpha x}}{1+Ax}\,, \tag{6}$$

where

$$C' = \frac{4}{3}\varkappa_a Z^{2/3} C\,.$$

The potential (6) is spherically symmetrical. The total eigenfunction of the electron can be expressed as a product of a radial wave function $R(r)$, a spherical harmonics $Y(\vartheta\varphi)$ and a spin function μ. The wave function can be characterized with the principal n, azimuthal l, magnetic m and spin s quantum numbers

$$\Psi(n, l, m, s) = R_{l_n}(r)\,Y_{lm}(\vartheta\varphi)\mu_s. \tag{7}$$

The Schrődinger equation can be separated, its radial part being determined in Hartree units by

$$\frac{d^2 P_{nl}}{dr^2} + 2\left[(E^0_{nl} - V) - \frac{l(l+1)}{r^2}\right]P_{nl} = 0\,, \tag{8}$$

where

$$P_{nl}(r) = rR_{nl}(r)\,.$$

Relativistic and spin-orbit coupling corrections

The theoretical results are compared with the experimental energies in Table I, and it is found that serious deviations exist. Our results can be improved if relativistic corrections and spin-orbit coupling are taken into account. Our starting point is the relativistic Pauli equation for a one-electron system in Hartree units

$$-\frac{1}{2}\frac{d^2 P_{nl}}{dr^2} + \left[V(r) + \frac{l(l+1)}{r^2} - \frac{\alpha^2}{2}\left(E^0_{nl} - V(r)\right)^2 - \frac{\alpha^2}{4}\,\frac{dV(r)}{dr}\,\frac{d}{dr} - \right.$$
$$\left. - \frac{\alpha^2}{4}\begin{pmatrix} -l \\ l+1 \end{pmatrix}\frac{1}{r}\,\frac{dV(r)}{dr}\right]P_{nl} = E^1_{nl} P_{nl}\,, \tag{9}$$

where α is the fine structure constant.

Eq. (9) can be solved by the perturbation method. Let us introduce the following notations

$$H_0 = -\frac{1}{2}\,\frac{d^2}{dr^2} + V(r) + \frac{l(l+l)}{r^2}\,, \tag{10}$$

Table I

Absolute values of the unperturbed energy calculated with a one-electron universal potential for Cu and Hg (HARTREE units). The first, second and third lines show the values of the present work, the results of the HFS model and the experimental energy values, respectively

Z	1s	2s	2p	3s	3p	3d	4s
	328.466	39.0218	34.4837	5.02876	3.56012	0.961420	0.410164
29	325.22	39.438	34.873	4.677	3.214	0.729	—
	330.735	40.585	34.613	4.49	2.8183	0.12	—

Z	1s	2s	2p	3s	3p	3d	4s
	2795.87	437.493	452.909	108.315	100.292	83.9300	23.8111
80	2767.88	465.49	448.46	410.247	102.062	86.665	23.9669
	3060.85	546.8	476.126	131.25	110.416	86.07	29.65

4p	4d	4f	5s	5p	5d	6s
20.2702	13.4457	4.21619	3.76342	2.58767	0.678814	0.287561
20.3746	13.7152	4.6928	3.6857	2.5062	0.63516	0.28266
22.8	13.7	—	4.6	2.8666	0.5	—

$$H_m = -\frac{\alpha^2}{2}\,(E^0_{nl} - V(r))^2\,, \tag{11}$$

$$H_d = -\frac{\alpha^2}{4}\,\frac{dV(r)}{dr}\,\frac{d}{dr} \tag{12}$$

and

$$H_{s0} = -\frac{\alpha^2}{4}\begin{pmatrix} -l \\ l+1 \end{pmatrix}\frac{1}{r}\,\frac{dV(r)}{dr}\,, \qquad \begin{matrix} (j = l+1/2)\,, \\ (j = l-1/2)\,. \end{matrix} \tag{13}$$

Eq. (9) thus takes the form

$$(H_0 + H_m + H_d + H_{s0})\,P_{nl} = E^1_{nl}\,P_{nl}\,. \tag{14}$$

Here H_0 is the non-relativistic Hamiltonian. The relativistic mass-velocity correction, the Darwin correction and the spin-orbit coupling correction are produced by the operators H_m, H_d and H_{s0}, respectively. The zero-order non-relativistic wave equation

$$H_0\,R^0_{nl} = E^0_{nl}\,R^0_{nl} \tag{15}$$

Table II

The absolute values of the energy in various models for Cu^+ (HARTREE units). In the columns the corresponding results of the non-relativistic HARTREE (NR—H), non-relativistic HARTREE–FOCK (NR—HF), non-relativistic HARTREE–FOCK–SLATER without and with relativistic correction (NR—HFS), non-relativistic universal potential without and with relativistic correction (NR—U), relativistic DIRAC—SLATER (R—DS) models, and the experimental values of the X-ray-terms ($-E_{exp}$) are presented. The numbers in parentheses in the last column are SLATER values

Shell	j	NR–H Ref. [15]	NR–HF Ref. [13]	NR–HFS Ref. [4]	NR–HFS+ rel. corr. Ref. [4]	NR–U	NR–U+ rel. corr.	R–DS Ref. [15]	$-E_{exp}$ Ref. [11], [14]
1*s*	1/2	328.96	329.2	325.2	330.41	328.465	333.168	329.035	330.8 (331)
2*s*	1/2	39.2385	41.15	39.435	40.5135	39.0218	40.0367	40.279	40.5 (40.65)
2*p*	1/2	34.9325	35.915	34.87	35.8065	34.4837	35.4619	35.59	35.15 (35.4)
	3/2				35.049		34.6237	34.8125	34.45 (34.6)
3*s*	1/2	4.49545	5.3255	4.6775	4.8525	5.02876	5.19085	4.8205	4.5 (4.8)
3*p*	1/2	3.04045	3.6395	3.2145	3.3475	3.56012	3.69708	3.32235	2.88 (3.13)
	3/2				3.2515		3.58826	3.2235	2.8 (3.05)
3*d*	3/2	0.5997	0.8065	0.7295	0.746	0.961420	0.983846	0.7311	0.12 (0.4)
	5/2				0.7345		0.955790	0.71975	

Table III

Absolute values of the energy in various models for Hg (HARTREE units). In the columns the corresponding results of the non-relativistic HARTREE without and with relativistic correction (NR – H), non-relativistic HARTREE – FOCK – SLATER without and with relativistic correction (NR – HFS), non-relativistic universal potential without and with relativistic correction (NR – U), relativistic DIRAC – SLATER (R – DS) models and the experimental values of the X-ray-terms ($-E_{exp}$) are presented

Shell	j	NR – H Ref. [15]	NR – H + rel. corr. Ref. [15]	NR – HFS Ref. [4]	NR – HFS + rel. corr. Ref. [4]	NR – U	NR – U + rel. corr.	R – DS Ref. [15]	exp Ref. [11]
1*s*	1/2	2775.89	3044.47	2767.85	3077.35	2795.87	3055.88	3065.09	3060.85
2*s*	1/2	462.2	531.05	465.49	542.8	467.493	540.678	545.155	546.8
2*p*	1/2	446.055	514.905	448.46	519.45	452.909	526.255	523.875	523.45
	3/2		459.825		462.35		468.195	451.515	452.465
3*s*	1/2	108.495	125.84	110.245	130.3	108.315	127.057	130.07	131.25
3*p*	1/2	100.245	117.55	102.06	120.2	100.29252	118.532	120.34	120.95
	3/2		106.015		107.7		106.118	104.25	105.15
3*d*	3/2	85.235	88.43	86.665	91.65	83.9301	89·0297	88.005	88.2
	5/2		86.3		88.25		85.5060	84.535	84.65

4*s*	1/2	23.03	27.88	23.976	29.24	23.8111	28.6461	28.745	29.65
4*p*	1/2	19.44	24.29	20.3745	24.92	20.2702	24.7332	24.755	25.3
	3/2		21.305		21.93		21.8222	20.84	21.55
4*d*	3/2	12.89	13.84	13.715	14.935	13.4457	14.6404	13.9	14.15
	5/2		13.335		14.22		13.9051	13.16	13.4
4*f*	5/2	4.1825	4.2845	4.693	4.981	4.21619	4.48821	4.162	—
	7/2		4.226		4.807		4.27041	3.9995	—
5*s*	1/2	3.468	—	3.6857	4.768	3.76342	4.78702	4.6255	4.6
5*p*	1/2	2.2945	—	2.50615	3.3225	2.58766	3.42272	3.2105	3.4
	3/2		—		2.793		2.88820	2.5065	2.6
5*d*	3/2	0.4587	—	0.63515	0.772	0.678814	0.823891	0.5835	0.5
	5/2		—		0.6945		0.733251	0.508	—
6*s*	1/2	0.2341	—	0.28265	0.374	0.287561	0.380065	0.3487	0.3841

Table IV

The relativistic and spin-orbit coupling corrections in HARTREE units for alkaline elements. The notations are the following: E (NRL) is the non relativistic energy; E(VEL) is the relativistic mass-velocity correction; E(DAR) is the Darwin correction; E(S−O) is the spin-orbit parameter; E is the energy, correct to order α^2; $-E(K)$ is the experimental X-ray term

Z	Shell	$-E$(NRL)	$-E$(VEL)	$-E$(DAR)	$-E$(S−O)	$-E$	$-E(K)$
3	1s	2.12423480	0.00230352	−0.00532406	—	2.12122420	1.8
	2s	0.20058464	0.00007795	−0.00022165	—	0.20044090	—
11	1s	39.6758110	0.45434824	−0.39135161	—	39.7388080	39.465
	2s	2.75827790	0.03623653	−0.02661995	—	2.76789440	2.339
	2p	1.71468340	0.00397394	−0.00287359	−0.00570700	1.72719780 1.71007670	1.3125 1.124
	3s	0.21476370	0.00172387	−0.00136050	—	0.21512710	—
19	1s	131.85572	4.1146876	−3.29744620	—	132.67296	132.91
	2s	12.733210	0.422953	−0.27512523	—	12.884380	—
	2p	10.203932	0.0610991	−0.00851925	−0.0486276	10.353768 10.207885	10.985 10.875
	3s	1.1467713	0.0469457	−0.02986323	—	1.1638538	1.315
	3p	0.5823858	0.0056392	−0.00121147	−0.0042348	0.5952823 0.5825792	— —
	4s	0.1409854	0.0020316	−0.00135804	—	0.1416590	0.245

37	1s	552.43829	59.602946	−47.0982000	—	564.94303	559.825
	2s	72.567614	7.6121224	−4.69787630	—	75.481860	76.15
	2p	66.402153	1.2646360	−0.00316954	−0.7753110	69.220581 66.894648	68.715 66.52
	3s	11.155614	1.3179826	−0.77726521	—	11.696331	11.935
	3p	8.8079478	0.2443511	−0.00303987	−0.1184513	9.2861616 8.9308078	9.25 8.85
	3d	4.3286598	0.0464925	−0.00559471	−0.0191528	4.4270159 4.3312520	4.19 4.13
	4s	1.1938765	0.1864710	−0.10941173	—	1.2709358	1.135
	4p	0.62660570	0.02716929	−0.00091048	−0.01312732	0.69711915 0.63973717	0.65
	5s	0.13754984	0.00783304	−0.00467911	—	0.14070377	—
55	1s	1276.81730	290.430170	−230.430440	—	1336.81710	1325.15
	2s	192.397120	40.2318350	−24.6822350	—	207.946720	210.7
	2p	182.623880	6.99929950	0.12855195	−4.07656050	197.904850 185.675170	197.35 184.55
	3s	37.4554880	8.31591020	−4.82841390	—	40.9429850	44.8
	3p	32.8567710	1.72683070	0.01448100	−0.76102600	36.1201350 33.8370570	39.4 36.85

Table IV (continued)

Z	Shell	$-E$(NRL)	$-E$(VEL)	E(DAR)	$-E$(S−O)	$-E$	$-E(K)$
55	3*d*	23.6283560	0.44842651	−0.00493002	−0.12526020	24.4476330 23.8213320	27.2 26.55
	4*s*	6.12539980	1.67395570	−0.95867248	—	6.84068300	8.45
	4*p*	4.51434610	0.32809127	0.00059440	−0.13692116	5.11687410 4.70611060	6.6 6.2
	4*d*	1.68574760	0.06677810	−0.00237684	−0.01715694	1.80161970 1.71583500	2.9 2.75
	5*s*	0.55559829	0.21039820	−0.12050683	—	0.64548966	—
	5*p*	0.24306066	0.02490105	−0.00029706	−0.10105939	0.28885251 0.25707071	— —
	6*s*	0.10676555	0.01165528	−0.00673305	—	0.11168778	—
87	1*s*	3328.96680	1803.92730	−1443.48180	—	3689.41230	—
	2*s*	568.063760	266.906050	−163.741930	—	671.227880	—
	2*p*	552.174870	48.1306770	0.99267592	−27.3774710	656.053160 573.920750	— —
	3*s*	136.103270	63.8813490	−36.7988010	—	163.185810	—
	3*p*	127.093320	14.3638250	0.18978690	−6.00080200	153.648530 135.646130	— —

3*d*	108.687360	4.39089610	0.07253510	−1.03090520	116.243500 111.088980	— —
4*s*	31.5890250	16.7121400	−9.43286950	—	38.8682950	—
4*p*	27.4418050	3.83286880	0.03948497	−1.47216300	34.2584850 29.8419960	— —
4*d*	19.3659720	1.20930430	0.00878384	−0.22881278	21.2704980 20.1264340	— —
4*f*	8.13716720	0.28674932	−0.00494896	−0.05161981	8.62544680 8.26410810	— —
5*s*	5.52737700	3.80469770	−2.13499540	—	2.19707920	—
5*p*	4.04295370	0.80335877	0.00625175	−0.30238263	5.45732950 4.55018160	— —
5*d*	1.50286920	0.18812139	−0.00028487	−0.03508982	1.79597520 1.62052610	— —
6*s*	0.47429589	0.46660591	−0.26188790	—	0.67901389	—
6*p*	0.20368821	0.05333439	0.00007092	−0.02030946	0.29771245 0.23678406	— —
7*s*	0.10089316	0.02869522	−0.01616579	—	0.11342258	

Table V

The relativistic and spin-orbit coupling corrections in Hartree units for rare gases. The notations are the following: E(NRL) is the non-relativistic energy, E(VEL) is the relativistic mass-velocity correction, E(DAR) is the Darwin correction, E(S−O) is the spin-orbit parameter, E is the energy correct to order α^2, $E(K)$ is the experimental X-ray term

Z	Shell	$-E$(NRL)	$-E$(VEL)	$-E$(DAR)	$-E$(S−O)	$-E$	$-E(K)$
2	1s	0.90687656	0.00041395	−0.00180825	—	0.90548227	0.9
10	1s	32.0981430	0.30903203	−0.27275672	—	32.1344190	32.6
	2s	2.09621200	0.02332575	−0.01783124	—	2.10170650	1.78
	2p	1.21874120	0.00238062	−0.00226511	−0.00399293	1.22684260	0.795
						1.21486380	0.79
18	1s	117.213470	3.31040810	−2.66232300	—	117.861550	117.85
	2s	10.9890030	0.33553920	−0.21816490	—	11.1063780	—
	2p	8.65510400	0.04721050	−0.00785230	−0.03905580	8.77257380	9.05
						8.65540640	8.95
	3s	0.94338050	0.03518510	−0.02264410	—	0.95592140	—
	3p	0.45346960	0.00393420	−0.00101540	−0.00315200	0.46269260	—
						0.45323640	0.4
	1s	521.167870	53.4144190	−42.2044880	—	532.377800	527.525
	2s	67.7345030	6.77657210	−4.18537260	—	70.3257020	—

36	$2p$	61.7719910	1.12134420	0.00050992	−0.69115241	64.2761500 62.2026920	63.59 61.69
	$3s$	10.2207170	1.15655290	−0.68313490	—	10.6941350	—
	$3p$	7.98835750	0.21223712	−0.00320256	−0.10385719	8.40510650 8.09353490	7.81
	$3d$	3.75455290	0.03905798	−0.00529737	−0.01676798	3.83861750 3.75477760	— —
	$4s$	1.05850950	0.15863630	−0.09330153	—	1.12384420	—
	$4p$	0.53732028	0.02230820	−0.00085587	−0.01094256	0.58065773 0.54783004	0.355
54	$1s$	1228.50420	269.928750	−214.105360	—	1284.32760	1273.685
	$2s$	184.065220	37.2723720	−22.8692830	—	198.468310	200.51
	$2p$	174.486610	6.47311640	0.11674185	−3.775925600	188.631320 177.303540	187.87 176.09
	$3s$	35.4890460	7.65011070	−4.44402320	—	38.6951340	—
	$3p$	31.0219410	1.58207230	0.01251947	−0.69939884	34.0153310 31.9171340	— 34.605
	$3d$	22.0694390	0.40690835	−0.00543205	−0.11497237	22.8158330 22.2409710	— —
	$4s$	5.70578020	1.51974690	−0.87106216	—	6.35446490	—

Table V (continued)

Z	Shell	$-E$(NRL)	$-E$(VEL)	$-E$(DAR)	$-E$(S−O)	$-E$	$-E(K)$
54	$4p$	4.16203230	0.29520366	0.00030841	−0.12377812	4.70510060 4.33376630	5.065
	$4d$	1.47327830	0.05817147	−0.00230689	−0.01525855	1.57491850 1.49862570	— —
	$5s$	0.50382856	0.18368639	−0.10533181	—	0.58218313	—
	$5p$	0.21784468	0.02030443	−0.00028880	−0.00871323	0.25528677 0.22914708	0.4
86	$1s$	3249.91440	1722.88400	−1378.29460	—	3594.50380	—
	$2s$	553.054960	254.566860	−156.164130	—	651.457690	—
	$2p$	537.351380	45.8703900	0.94769222	−26.1005740	636.370610 558.068880	— —
	$3s$	131.910810	60.7406170	−34.9937280	—	157.657700	—
	$3p$	123.042270	13.6360830	0.17995580	−5.70199270	148.262290 131.156320	— —
	$3d$	104.928130	4.15690280	0.06764693	−0.97840289	112.087890 107.195880	— —
	$4s$	30.3945430	15.8066430	−8.92412410	—	37.2770120	—

86	4*p*	26.3353360	3.61490340	0.03402386	−1.39051090	32.7682850	—
						28.5967530	—
	4*d*	18.441012	1.13340350	0.00781439	−0.21541214	20.2284670	—
						19.1514060	—
	4*f*	7.50078470	0.26395338	−0.00511474	−0.04822699	7.95253130	—
						7.61494230	—
	5*s*	5.24725780	3.56206650	−1.99959400	—	6.80973020	—
	5*p*	3.80848570	0.74753483	0.00571320	−0.28193994	5.12561360	—
						4.27979380	—
	5*d*	1.36171490	0.17132361	−0.00039328	−0.03219610	1.62923350	—
						1.46825300	—
	6*s*	0.44103636	0.42175112	−0.23683400	—	0.62595348	—
	6*p*	0.18911604	0.04544038	0.00002843	−0.01736659	0.26931805	—
						0.21721825	—

Acta Physica Academiae Scientiarum Hungaricae 32, 1972

Table VI

The relativistic and spin-orbit coupling corrections in HARTREE units for elements of the fourth column of the periodical table. The notations are the following: E(NRL) is the non-relativistic energy; E(VEL) is the relativistic mass-velocity correction; E(DAR) is the Darwin correction; E(S—O) is the spin-orbit parameter; E is the energy, correct to order α^2; $E(K)$ is the experimental X-ray term

Z	Shell	$-E$(NRL)	$-E$(VEL)	$-E$(DAR)	$-E$(SO)	$-E$	$-E(K)$
6	1s	10.1925330	0.03893468	—0.04354071	—	10.1879270	10.52
	2s	0.49793248	0.00194962	—0.00214075	—	0.49774136	—
	2p	0.20996423	0.00008694	—0.00041073	—0.00048272	0.21060589 0.20915773	— —
14	1s	67.6068960	1.20292470	—0.99212571	—	67.8176950	67.85
	2s	5.47458870	0.10889100	—0.07426444	—	5.50921530	—
	2p	3.89942020	0.01377910	—0.00494549	—0.01438170	3.93701740 3.89387210	3.795 3.775
	3s	0.39228890	0.00836510	—0.00580620	—	0.39484790	—
	3p	0.17051100	0.00050390	—0.00032877	—0.00062180	0.17192990 0.17006430	— —
32	1s	405.453590	33.3338960	—26.3397630	—	412.447720	408.785
	2s	50.2436780	4.10284470	—2.54408040	—	51.8024420	—
	2p	45.0949930	0.666341520	—0.00702412	—0.42183136	46.5979730 45.3324790	45.855 44.71

32	3s	6.97401820	0.655844410	−0.39040070	—	7.23946190	6.51
	3p	5.18826230	0.114612700	−0.00336749	−0.05874349	5.41699460 5.24076410	4.51
	3d	1.90808410	0.01771869	−0.00397442	−0.00936209	1.94990460 1.90309420	0.98 0.96
	4s	0.62817824	0.07727281	−0.04598830	—	0.65946275	—
	4p	0.27902263	0.00869071	−0.00058270	−0.00461130	0.29635325 0.28251934	— —
50	1s	1044.7764	198.54839	−157.31351	—	1086.0073	1075.35
	2s	152.74014	27.034855	−16.598230	—	163.17676	164.415
	2p	143.95819	4.6593035	0.0760644	−2.7374845	154.16853 145.95607	153.035 144.67
	3s	28.244232	5.3812745	−3.1331209	—	30.492386	32.53
	3p	24.297366	1.0927761	0.0060681	−0.4899751	26.376161 24.906235	27.855 26.305
	3d	16.437633	0.2689369	−0.0067455	−0.0801690	16.940331 16.539486	18.155 17.85
	4s	4.2159560	1.0085628	−0.5801892	—	4.6443295	5.03
	4p	2.9316475	0.1880213	−0.0005241	−0.0805454	3.7802355 3.0385993	3.25
	4d	0.7828402	0.0314416	−0.0019220	−0.0091072	0.8396816 0.7941452	0.9 0.88

Table VI (continued)

Z	Shell	$-E$(NRL)	$-E$(VEL)	$-E$(DAR)	$-E$(S−O)	$-E$	$-E(K)$
50	5*s*	0.3394398	0.0998748	−0.0575892	—	0.3817254	—
	5*p*	0.1508040	0.0078585	−0.0002197	−0.0035278	0.1654985 0.1549149	0.05
82	1*s*	2943.36230	1425.5885	−1139.32720	—	3229.62360	3241.3
	2*s*	495.160270	209.42706	−128.449000	—	576.138320	584.25
	2*p*	480.201480	37.615524	0.78143897	−21.435484	561.469410 497.162960	559.95 480.2
	3*s*	115.885170	49.325255	−28.4320120	—	136.778410	141.9
	3*p*	107.581090	10.9994470	0.14403464	−4.61770340	127.959970 114.106860	131.1 113.1
	3*d*	90.6358990	3.31307270	0.05005999	−0.78843468	96.3643360 92.4221630	95.25 91.25
	4*s*	25.8958870	12.5515820	−7.09438230	—	31.3530870	33.05
	4*p*	22.1841810	2.83578680	0.02819969	−1.09779530	27.2432580 23.9503720	28.2 23.7
	4*d*	15.0067660	0.86508150	0.00447034	−0.16767200	16.3793340 15.5409740	16.2 15.4

82	$4f$	5.21106090	0.18543127	−0.00548849	−0.03623972	5.53596250 5.28228450	5.25 5.00
	$5s$	4.22153670	2.70728440	−1.52219780	—	5.40663330	5.6
	$5p$	2.96025890	0.55299674	0.00385694	−0.21038779	3.93788810 3.30622480	4.00 3.30
	$5d$	0.87630804	0.11441311	−0.00069677	−0.02223595	1.05623220 0.94555247	1.2 0.7
	$6s$	0.33041737	0.27118435	−0.15262655	—	0.44897516	—
	$6p$	0.14718676	0.02257056	−0.00007244	−0.00877763	0.18724014 0.16090726	— —

Table VII

The relativistic and spin-orbit coupling corrections in HARTREE units for Cu^{29}, Hg^{80} and U^{92}. The notations are the following: E(NRL) is the non-relativistic energy; E(VEL) is the relativistic mass-velocity correction; E(DAR) is the Darwin correction; E(S–O) is the spin-orbit parameter; E is the energy, correct to order α^2; $E(K)$ is the experimental X-ray term

Z	Shell	$-E$(NRL)	$-E$(VEL)	$-E$(DAR)	$-E$(S–O)	$-E$	$-E(K)$
29	1s	328.465870	22.4700730	—17.7673750	—	333.168570	330.735
	2s	39.0218660	2.69051710	—1.67562070	—	40.0367620	40.585
	2p	34.4837520	0.42926533	—0.00990639	—0.27938703	35.4618850 34.6237240	35.1 34.37
	3s	5.02875900	0.40524018	—0.24315432	—	5.19084490	4.49
	3p	3.56012470	0.06751074	—0.00310143	—0.03627346	3.69708090 3.58826050	2.875 2.79
	3d	0.96142044	0.00853149	—0.00293916	—0.00561110	0.98384609 0.95579056	0.12
	4s	0.41016398	0.04031745	—0.02429618	—	0.42618524	—
	4d	13.44570	0.7504364	0.0030964	—0.1470579	14.6404070 13.9051170	14.15 13.4
	4f	4.2161958	0.1530743	—0.00551603	—0.0311149	4.48821380 4.27040940	— —
	5s	3.7634216	2.3432873	—1.3189573	—	4.78702030	4.6

	5*p*	2.5876683	0.4714933	0.00309377	−0.1802334	3.42272220 2.88202190	3.4 2.6
	5*d*	0.67881406	0.0914712	−0.00077794	−0.0181279	0.82389120 0.73325130	0.5
	6*s*	0.28756135	0.2119391	−0.11943457	—	0.38006520	0.3841
80	1*s*	2795.87660	1292.21280	−1032.21080	—	3055.87860	3060.85
	2*s*	467.492990	189.248560	−116.063220	—	540.67830	546.8
	2*p*	452.90880	33.9333330	0.70618899	−19.353510	526.255340 468.194810	523.45 452.465
	3*s*	108.315240	44.2649360	−25.5226700	—	127.05750	131.25
	3*p*	100.292520	9.83556420	0.12802020	−4.1380715	118.53225 106.11803	120.95 105.15
	3*d*	83.9300760	2.94303780	0.04238770	−0.70473948	89.029720 85.506022	88.2 84.65
	4*s*	23.8111080	11.1293510	−6.29438150	—	28.646077	29.65
	4*p*	20.2702590	2.49790880	0.02436423	−0.97036166	24.733255 21.822170	25.3 21.55
92	1*s*	3738.72800	2252.61520	−1804.68250	—	4186.66060	4257.35
	2*s*	646.328540	335.444100	−205.844890	—	775.927750	801.3
	2*p*	629.522550	60.7097580	1.23931700	−34.4809900	760.433610 656.990640	771.1 632.1

Table VII (continued)

Z	Shell	$-E$(NRL)	$-E$(VEL)	$-E$(DAR)	$-E$(S−O)	$-E$	$-E(K)$
92	$3s$	158.197610	81.455510	−46.8976580	—	192.755460	204.25
	$3p$	148.477630	18.4517840	0.24439359	−7.67633490	182.526470 159.497470	190.7 158.3
	$3d$	128.606380	5.71297210	0.10015165	−1.32642660	138.398780 131.766650	136.95 130.75
	$4s$	37.9910260	21.8452330	−12.3151980	—	47.5210610	52.75
	$4p$	33.3973620	5.07663670	0.05344993	−1.93653030	42.4005090 36.5909180	46.15 38.30
	$4d$	25.4013950	1.64788320	0.01451147	0.30557988	26.9805290 25.4526300	28.65 27.05
	$4f$	11.7153000	0.42233239	−0.00363143	−0.07126401	12.4190570 11.9202090	14.2 13.95
	$5s$	7.07726360	5.21267590	−2.91997980	—	9.36995970	11.8
	$5p$	5.35712940	1.13138790	0.00944342	−0.42189675	7.34175420 6.07606390	9.3 7.25

	5*d*	2.33565700	0.28997519	0.00048162	−0.05233469	2.78311790 2.52144450	3.6
	5*f*	0.03125908	0.00000017	−0.00001895	−0.00001897	0.03131620 0.03118338	—
	6*s*	0.67759906	0.74058703	−0.41469507	—	1.00349100	—
	6*p*	0.30774643	0.10633405	0.00040822	−0.03988021	0.49424912 0.37460849	1.1
92	6*d*	0.05685283	0.00029369	−0.00006325	−0.00011631	0.05743221 0.05685065	—
	7*s*	0.11131291	0.03336578	−0.01876320	—	0.12591549	—

was solved for all orbitals of interest. In first order the corrected energy was obtained as

$$E^1_{nl} = E^0_{n'} + \int_0^\infty r^2 R^0_{nl} (H_m + H_d + H_{s0}) R^0_{nl} \, dr. \tag{16}$$

Numerical results and discussion

Eq. (15) was solved with the algorithm elaborated by HERMAN and SKILLMAN [4]. Determination of the energy correct to the order α^2 was done with the aid of formula (16). The differentiation occurring in (16) was carried out numerically with the Newton—Gregory polynomial; for the integration Simpson's rule was used [10].

In Table I the unperturbed energies E^0_{nl} are presented together with the results of the HFS model and the experimental results for all the states of Cu and Hg. It can be seen that for Cu the calculated values agree considerably better with the experimental values than in the case of Hg.

The results of various model calculations for Cu and Hg are compared in Tables II and III, respectively. In the columns are presented the corresponding results of the non-relativistic HARTREE (NR—H), non-relativistic HARTREE—FOCK (NR—HF), non-relativistic HARTREE—FOCK—SLATER without and with relativistic correction (NR—HFS), non-relativistic universal potential without and with relativistic correction (NR—U), relativistic DIRAC—SLATER (R—DS) models, and the experimental values of the X-ray terms ($-E_{\text{exp}}$). In the last column the numbers in parentheses are SLATER values. In the DIRAC—SLATER model (R—DS) the DIRAC equations are solved in SLATER approximation.

The uncorrected energy E^0_{nl}($-E$(NRL), the various corrections, the energy E^1_{nl} determined in the present work ($-E$) and the experimental energy ($-E(K)$) for the alkaline elements, the rare gases, the elements of the fourth column of the periodic table and some other elements (Cu^{29}, Hg^{80}, U^{92}) are presented in Tables IV, V, VI and VII, respectively. The Tables show that this technically very simple model gives good results for Cu even without relativistic corrections. These corrections increase the absolute value of the energies. It is interesting to note that for Cu this tendency improves the agreement with the experimental value only for the intermediate orbitals, whereas in the case of Hg the corrected values approximate the experimental ones at every state. The overall agreement is surprisingly good.

The numerical calculations were carried out on the ICT 1905 computer of the Central Research Institute in Fortran. Thanks are due to Prof. L. PÁL for granting machine time.

REFERENCES

1. D. R. Hartree, Proc. Cambridge Phil. Soc., **24,** 89, 1928.
2. V. Fock, Z. Physik, **61,** 126, 1930.
3. R. Latter, Phys. Rev., **99,** 510, 1955.
4. F. Herman and S. Skillman, Atomic Structure Calculations (Prentice-Hall, Inc., Englewood Cliffs, N. J., 1963).
5. J. C. Slater, Phys. Rev., **81,** 385, 1951.
6. R. Gáspár, Acta Phys. Hung., **2,** 151, 1952.
7. R. Gáspár, Acta Phys. Hung., **3,** 263, 1954.
8. P. A. M. Dirac, Proc. Camb. Phil. Soc., **26,** 376, 1930.
9. W. W. Piper, Phys. Rev., **123,** 1281, 1961.
10. Bálint Elemér, Közelítő Matematikai Módszerek, (Műszaki Kiadó, 1966).
11. A. E. Sandström, Encyclopedia of Phys. Edited by S. Flügge, (Springer-Verlag, Berlin 1957), Vol. **30,** p. 78.
12. E. Clementi, C. C. J. Roothaan and M. Yoshimine, Phys. Rev., **127,** 1618, 1962.
13. D. R. Hartree and W. Hartree, Proc. Roy. Soc. (London), A**157,** 490, 1936.
14. J. C. Slater, Phys. Rev., **98,** 1040, 1955.
15. D. Liberman, J. T. Waber and Don T. Cromer, Phys. Rev., **137,** A27, 1965.

РЕЛЯТИВИСТСКИЕ КОРРЕКЦИИ К УНИВЕРСАЛЬНОМУ ПОТЕНЦИАЛУ

Р. ГАШПАР и Г. ЭРДОШ-ДЯРМАТИ

Резюме

Мы вычисляем атомные одно-электронные энергии с помощью универсального потенциала. Радиальное уравнение Шредингера решаем методом Нумерова. Мы учитываем релятивистические коррекции, также коррекцию, происходящую из спин-орбитального взаимодействия. Полученные результаты сравниваем с данными, полученными из релятивистических ГФ вычислений, также с экспериментальными данными.

Acta Physica Academiae Scientiarum Hungaricae, Tomus 32 (1—4), pp. 43—48 (1972)

THE STABILITY OF LINEAR CHAINS*

By

T. SIKLÓS** and V. L. AKSIENOV

JOINT INSTITUTE FOR NUCLEAR RESEARCH, LABORATORY OF THEORETICAL PHYSICS, DUBNA, USSR

(Received 6. VII. 1971)

The dependence of the instability temperature of an anharmonic monoatomic linear chain on the external tension is investigated in the high temperature limit.

1. Introduction

The method formulated in [1] for deriving a self-consistent (S. C.) system of equations has already been applied to investigate the properties under low tension of anharmonic monoatomic linear chains displaying nearest-neighbour interaction [2] and of linear chains in pseudoharmonic approximation under small [3] and arbitrary external tension [4]. In the present paper the damping of the S. C. phonons is taken into account and the behaviour of linear chains with nearest-neighbour interaction under arbitrary external tension are considered in the high temperature limit.

2. S. C. system of equations for a linear chain

A linear chain of length L consisting of $N+1$ atoms of mass M is considered.

The one-phonon Green's function for the chain is [2]

$$G_k(\omega) = \ll A_k | A_k^+ \gg_\omega = \frac{2\omega_k}{\omega^2 - \omega_k^2 - 2\omega_k \Pi_k(\omega)}, \tag{1}$$

where ω_k is the phonon frequency defined in pseudoharmonic approximation by

$$\omega_k^2 = \frac{f(\Theta, l)}{f} \omega_{0k}^2. \tag{2}$$

Here ω_{0k} stands for the harmonic frequency corresponding to the strength constant f at external tension $P = 0$.

* Dedicated to Prof. L. JÁNOSSY on his 60th birthday.

** Present address: Central Research Institute for Physics of the Hungarian Academy of Sciences, Budapest, Hungary

The renormalized phonon frequencies ϵ_k and phonon widths Γ_k are determined approximately by

$$\epsilon_k \approx \omega_k + Re\, \Pi_k(\omega); \quad \Gamma_k = - Im\, \Pi_k(\omega + i\delta). \tag{3}$$

In the effective cubic approximation the self-energy operator takes the form

$$\Pi_k(\omega) = \frac{1}{8N} \frac{g^2(\Theta, l)}{f^3(\Theta, l)} \sum_{pp'} \left\{ \frac{(n_p + n_{p'} + 1)(\omega_p + \omega_{p'})}{\omega^2 - (\omega_p + \omega_{p'})^2} - \right.$$
$$\left. - \frac{(n_p - n_{p'})(\omega_p - \omega_{p'})}{\omega^2 - (\omega_p - \omega_{p'})^2} \right\} \omega_k \omega_p \omega_{p'} \Delta(p + p' - k), \tag{4}$$

where $n_p = [\exp(\omega_p/\Theta) - 1]^{-1}$.

The pseudoharmonic $f(\Theta, l)$ and the effective cubic $g(\Theta, l)$ strength constants in Eq. (2) and (4) are determined in the S. C. manner by

$$f(\Theta, l) = \frac{1}{2} \tilde{\varphi}''(l), \quad g(\Theta, l) = \frac{1}{2} \tilde{\varphi}'''(l), \tag{5}$$

where $\tilde{\varphi}(l)$ is the S. C. potential given by

$$\tilde{\varphi}(l) = \sum_{n=0}^{\infty} \frac{1}{n!} \left[\frac{1}{2} \overline{u^2(l)} \right]^n \varphi^{(2n)}(l). \tag{6}$$

Here $\varphi(l)$ stands for the interatomic pair potential. The mean square relative displacement of the neighbouring atoms $\overline{u^2(l)}$ can be expressed using the Green's function (1) as

$$\overline{u^2(l)} = \frac{1}{2Nf(\Theta, l)} \sum_k \frac{\omega_k}{\pi} \int_0^{\infty} d\omega \coth \frac{\omega}{2\Theta} [- Im\, G_k(\omega + i\delta)]. \tag{7}$$

In addition to depending on the temperature $\theta = kT$, the properties of the chain are determined also by the length of the chain $L = Nl$ or by the external tension P. According to [1], [2] these parameters satisfy the equation

$$P = - \frac{1}{2} \tilde{\varphi}'(l), \tag{8}$$

where l is the equilibrium separation of neighbouring atoms.

The thermal properties are determined by the internal energy E and the free energy F:

$$E = \langle H \rangle = \frac{N}{2}\{\tilde{\varphi}(l) + f(\Theta, l)\,\overline{u^2(l)}\} + 5\,\tilde{F}_3(\Theta). \tag{9}$$

$$F = \Theta \sum_k 2 \sinh(\omega_k/2\Theta) + \frac{N}{2}\{\tilde{\varphi}(l) - f(\Theta, l)\,\overline{u^2(l)}\} + \tilde{F}_3(\Theta), \tag{10}$$

where the effective cubic anharmonic contribution to the free energy is

$$\tilde{F}_3(\Theta) = \frac{1}{6}\sum_k \frac{1}{2\pi}\int_{-\infty}^{\infty} \frac{d\omega(\omega^2 - \omega_k^2)[-Im\,G_k(\omega + i\delta)]}{(e^{\omega/\Theta} - 1)\,\omega_k}. \tag{11}$$

We note here that in [1] in particular in Eq. (45) the approximation $Im\ G_k \cdot (\omega + i\delta) \approx \delta(\omega^2 - \xi_k^2)$ was employed in the integral over ω. But in this approximation the finite width of phonons is not taken into account. Here we do not employ this approximation and as in [5] we get more exact expressions for the internal and free energy.

Therefore both the dynamic (3) and thermodynamic (9), (10) properties of the anharmonic linear chain are determined by the S. C. system of equations (1), (2), (4)—(8). To solve these we introduce the interatomic pair potential $\varphi(l)$ into Eq. (7), which, as in [2]—[4], is taken as the model Morse potential.

Let us consider the case for which the external tension $P = \text{const.}$, but not necessarily small. It is convenient to introduce the reduced tension $P^* = P(r_0/D)$, where D is the depth of the potential and r_0 is the average distance between neighbouring atoms in the harmonic approximation. In the same way as in [4], taking $ar_0 = 6$, we get the following expressions for the pseudoharmonic renormalization of the frequency (dimensionless):

$$\alpha^2 = \frac{f(\Theta, l)}{f} = \frac{P^*}{3} + \frac{e^{-y}}{2}\left\{1 + \sqrt{1 + \frac{2P^*}{3}e^{y}}\right\};$$

the mean square relative displacement of neigbouring atoms (dimensionless):

$$y = 36\,[\overline{u^2(l)}/r_0^2] = \ln \frac{\alpha^2 - \dfrac{P^*}{6}}{\left(\alpha^2 - \dfrac{P^*}{3}\right)^2};$$

the S. C. potential:

$$\tilde{\varphi}(l) = -D\left\{\alpha^2 - \frac{P^*}{2}\right\}; \tag{12}$$

the equilibrium separation of neighbouring atoms:

$$l = r_0 \left\{ 1 + \frac{1}{12} \ln \frac{\alpha^2 - \dfrac{P^*}{6}}{\left(\alpha^2 - \dfrac{P^*}{3}\right)^4} \right\};$$

the effective cubic strength constant:

$$g(\Theta, l) = g\{\alpha^2 - P^*/9\},$$

where $f = Da^2$, $g = -3Da^3$.

Evaluation of the ω-integral in (7) is not so easy in the case of finite phonon widths as in the pseudoharmonic approximation [4] and should be done numerically. However, approximate expressions can be obtained for (7) if we investigate the high- and low-temperature limits separately.

3. High-temperature limit ($\Theta \gg \omega_D$)

With the assumption $F(p, p', \epsilon_k) = F(p, p', \omega_k)$ we can perform the summation required in [4] in the same way as it was done in [6], which gives the following results for (3) in the high-temperature limit:

$$\epsilon_k^2 \approx \omega_{0k}^2 \frac{f(\Theta, l)}{f} \left[1 - \Theta \frac{g^2(\Theta, l)}{2f^3(\Theta, l)} \right] = \omega_{0k}^2 \alpha_1^2(\Theta, l) , \tag{13}$$

$$\Gamma_k(\epsilon_k) \approx \Gamma_k(\omega_k) = \Theta \frac{g^2(\Theta, l)}{16 f^3(\Theta, l)} \omega_L [1 + \vartheta(\pi - kl)\, \vartheta(\pi + kl)], \tag{14}$$

where $\omega_L = (4f\ (\Theta, l)/M)^{1/2}$ is the maximum value of the pseudoharmonic vibrational frequency. In this approximation frequency renormalization leads only to a change of the strength constants and the renormalization factor does not depend on k.

Using (13) for the S. C. equation (7) we get:

$$\alpha_1^2 y(\alpha) = T^* \left\{ \left[1 - T^* D \frac{g^2(\Theta, l)}{f^3(\Theta, l)} \right]^{-1} + \frac{1}{24} \left(\frac{\alpha\pi}{\lambda T^*} \right)^2 \right\}, \tag{15}$$

where $T^* = \theta/D$ is the reduced temperature, and $\lambda = \pi D/\omega_{0L}$ is the dimensionless coupling constant of atoms.

Let us investigate the chain with strong coupling $\lambda \gg 1$. Using Eqs. (12) the S. C. equation (15) can be written in more convenient form

$$\left[1 - \left(\frac{P^*}{3T^*} - B \right) y \right]^2 e^y - \frac{y}{T^*} \left| 1 - \left(\frac{P^*}{6T^*} - B \right) y \right] = 0 , \tag{16}$$

where

$$B = 0.5\{2 + [1 + (2P^*/3)\, e^y]^{-1/2}\}^2 .$$

Eq. (16) has a substantially similar form and consequently a similar analytical behaviour, to the equations obtained in [7] for the f. c. c. lattice, so we shall give only the results here. The dependence of the instability temperature T_s^* on the reduced tension P^* is given in Fig. 1. For $P^* \leq P^*_1 \approx 1.5$ the chain has only one stable state, which exists if the temperature is sufficiently low ($T^* \leq T_s^*(P^*)$). For $T^* > T_s^*(P^*)$ the linear chain has another stable state only in the region $P^*_1 \leq P^* \leq P_c^*$ but here the mean square relative displacement of the atoms is much larger than in the first stable state. The

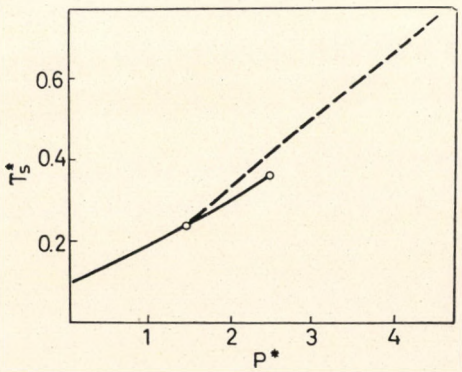

Fig. 1. The reduced instability temperature T_s^* as a function of the reduced tension P^*

critical tension is characterized by the disappearence of the vibrational instability of the first stable state S_1. In the high temperature limit we get the values $P_c^* \approx 2.5$ for the critical tension and $T_c^* \approx 0.37$ for the critical temperature.

When $P^* \geq P_1^*$ all stable states of the chain disappear at the temperature $T_d^*(P^*)$, which is given in Fig. 1 by the dotted line. Calculations show that Eq. (16) has only complex solutions in the region $T^* > T_d^*(P^*)$. We note here that in the case of a three-dimensional f. c. c. lattice [7] P^*_1 is small and the curve $T^*(P^*)$ is rather steep, while in the pseudoharmonic approximation [4] the curve $T_d^*(P^*)$ is described by the equation $P^* = 0$.

Thus, by taking into account the damping of the S. C. phonons we have found that at all positive tensions there exists a temperature above which a linear chain has no stable state, in contrast to the cases of the linear chain and f. c. c. lattice in the pseudoharmonic approximation.

Acknowledgement

It is a great pleasure to express our gratitude to Dr. N. M. PLAKIDA for valuable discussions and advice.

REFERENCES

1. N. M. PLAKIDA and T. SIKLÓS, phys.stat.sol., **33,** 103, 1969.
2. N. M. PLAKIDA and T. SIKLÓS, phys.stat.sol., **33,** 113, 1969.
3. N. M. PLAKIDA and T. SIKLÓS, Phys. Lett., **26A,** 342, 1968. Acta Phys. Hung., **26,** 387, 1969.
4. T. SIKLÓS, Acta Phys. Hung. **30,** 181, 301, 1971. Reports JINR 4E-5389, E4-5521, Dubna, 1970.
5. N. M. PLAKIDA and T. SIKLÓS, phys.stat.sol., **39,** 171, 1970.
6. K. N. PATHAK, Phys. Rev., **139,** Al569, 1965.
7. T. SIKLÓS and V. L. AKSIENOV, phys.stat.sol. (b) **50,** 171, 1972 Acta Phys. Hung. **31,** 335, 345, 1972, Reports JINR E4-5772, E4-5773 Dubna, 1971.

ОБ УСТОЙЧИВОСТИ ЛИНЕЙНОЙ ЦЕПОЧКИ

Т. ШИКЛОШ и В. Л. АКСЕНОВ

Резюме

Исследуется зависимость температуры неустойчивости ангармонической линейной цепочки от внешнего натяжения в пределе высоких температур.

Acta Physica Academiae Scientiarum Hungaricae, Tomus 32 (1—4), pp. 49—60 (1972)

DAS LEMMA VON WEYL ALS TRANSPORT- UND KOPPLUNGSVORSCHRIFT*

Von

HANS-JÜRGEN TREDER

INSTITUT FÜR RELATIVISTISCHE UND EXTRAGALAKTISCHE FORSCHUNG, STERNWARTE BABELSBERG POTSDAM-BABELSBERG, DDR

(Eingegangen: 10. VIII. 1971)

Das Lemma von WEYL verknüpft die koordinaten-kovarianten Ableitungen von raum-zeitlichen Tensoren mit den (lokal-) LORENTZ-kovarianten Ableitungen ihrer Messwerte und mit den (LORENTZ-kovarianten) Spinor-Ableitungen.

Auf Grund des Weylschen Lemmas sind die Lorentz-kovarianten Ableitungen auf die koordinaten-kovarianten zurückführbar. — Physikalisch bedeutet WEYLS Lemma für tensorielle Grössen eine Eichungsvorschrift für den freien Transport von Messeinrichtungen. Ferner sichert WEYLS Lemma, dass die durch die Fusion von Spinor-Feldern entstehenden Tensor-Felder derselben, aus dem EINSTEINschen Äquivalenzprinzip folgenden Vorschriften für den freien raum-zeitlichen Transport genügen, wie die originären Tensor-Felder.

WEYLS Lemma ist die allgemeine mathematische Begründung desjenigen, was mehr intuitiv als »Formalismus der kompensierenden Felder« verstanden wird.

I. Die mathematische Formulierung des Weylschen Lemmas

In der Raum—Zeit-Welt V_4 wird neben der Metrik g_{ik} ein orthonormiertes Vierbeinfeld $h^A{}_i$ (Tetradenfeld) eingeführt:

$$h^A{}_i\, h^B{}_k\, \eta_{AB} = g_{ik} \quad \begin{matrix}(i, k = 1, 2, 3, 4;\\ A, B = 1, 2, 3, 4),\end{matrix} \tag{1a}$$

$$h_A{}^i\, h_B{}^k\, g_{ik} = \eta_{AB} \quad (\eta_{AB} = \text{Minkowski-Tensor}). \tag{1b}$$

Mit einem Tetradenfeld $h^B{}_i(x^c)$ genügt auch die Linear-Kombination

$$\bar{h}^A{}_i = \omega^A{}_B\, h^B{}_i \tag{2a}$$

den Gleichungen (1), vorausgesetzt, dass auch die Koeffizienten $\omega^A{}_B$ den Orthonormalitätsbedingungen

$$\omega_B{}^A\, \omega^B{}_C = \omega^A{}_B\, \omega_C{}^B = \delta^A_C \tag{2b}$$

genügen. Die Matrix der homogenen Lorentz-Transformation wird durch die Bedingungen (2b) bestimmt; wir werden daher die Transformationen (2a, b) kurz als Lorentz-Rotationen der Tetraden bezeichnen. Die Matrix dieser

* Akademiker Prof. Dr. L. JÁNOSSY zum 60. Geburtstag zugeeignet.

Lorentz-Rotationen ist im allgemeinen eine Funktion der raum-zeitlichen Koordinaten $\omega^A{}_B = \omega^A{}_B(x^l)$. Die Transformationen (2) lassen sich somit auffassen als Lorentz-Rotationen in den Minkowskischen Tangentialräumen $M_4(P)$ zu den Punkten P: $\{x^l\}$ der Raum—Zeit-Mannigfaltigkeit V_4 [6].

Mit Hilfe der Tetraden $h^A{}_i$ werden einem Vektor T^i bzw. einem Tensor $T^i{}_k$ etc. natürliche Komponenten zugeordnet:

$$T^A = h^A{}_i\, T^i, \tag{3a}$$

$$T^A{}_B = h^A{}_i\, h_B{}^k\, T^i{}_k \tag{3b}$$

etc. Die Grössen (3a, b) sind Skalare in bezug auf Koordinatentransformationen der Raum—Zeit

$$x'^i = x'^i(x^l).$$

(Transformationen der EINSTEIN-Gruppe). Sie transformieren sich aber wie Vektoren bzw. Tensoren in bezug auf die Lorentz-Transformationen (2) in den Minkowskischen Tangentialräumen:

$$\bar{T}^A = \bar{h}^A{}_i\, T^i = \omega^A{}_B\, h^B{}_i = \omega^A{}_B\, T^B, \tag{4a}$$

bzw.

$$\bar{T}^A{}_B = \bar{h}^A{}_i\, \bar{h}_B{}^k\, T^i{}_k = \omega^A_C\, \omega^D_B\, T^C_D \tag{4b}$$

etc. Umgekehrt werden durch die reziproken Operationen

$$T^i = h_A{}^i\, T^A = h_A{}^i\, h^A{}_k\, T^k = \bar{h}_A{}^i\, \bar{T}^A, \tag{5a}$$

$$T^i{}_k = h_A{}^i\, h^B_k\, T^A{}_B = \bar{h}_A{}^i\, \bar{h}^B_k\, \bar{T}^A{}_B \tag{5b}$$

etc. den Lorentz-Tensoren T^A bzw. $T^A{}_B$ etc. raum-zeitliche Tensoren zugeordnet.

An die Stelle der Minkowskischen Tangentialräume $M_4(P)$ können auch die Spin-Räume $S_2(P), S^*{}_2(P)$ treten. Dem Vektor T_i wird dann ein hermitesymmetrischer Spinor zweiter Stufe zugeordnet:

$$T_{\alpha\dot\beta} = \sigma_{\alpha\dot\beta}{}^i T_i = \sigma_{\alpha\dot\beta}{}^A T_A = \sigma_{\alpha\dot\beta}{}^A h_A{}^i T_i \tag{6}$$

etc. Hierbei sind die

$$\sigma_{\alpha\dot\beta}{}^i(x^l) = \gamma_{\alpha\delta}\, \gamma_{\dot\beta\dot\gamma}\, g^{ik}\, \sigma^{\delta\dot\gamma}{}_k(x^l) \tag{7}$$

die koordinatenabhängigen metrischen Spinvektoren, die mit den konstanten Paulischen Spinmatrizen $\sigma_{\alpha\dot\beta}{}^A$, gemäss

$$\sigma_{\alpha\dot\beta}{}^k = \sigma_{\alpha\dot\beta}{}^A h_A{}^k(x^l) \tag{8}$$

zusammenhängen und dementsprechend den Orthonormalitätsbedingungen

$$\gamma_{\alpha\beta}\gamma_{\dot{\mu}\dot{\nu}} = \sigma_{\alpha\dot{\mu}}{}^{k}\sigma_{\beta\dot{\nu}}{}^{l}g_{kl} \tag{9a}$$

und

$$g_{kl} = \sigma^{\alpha\dot{\mu}}{}_{k}\sigma^{\beta\dot{\nu}}{}_{l}\gamma_{\alpha\beta}\gamma_{\dot{\mu}\dot{\nu}} \tag{9b}$$

genügen. Hierbei sind $\gamma_{\alpha\beta}$ und $\gamma_{\dot{\mu}\dot{\nu}}$ die metrischen Spinoren der Spin-Räume S_2 und S_2^*:

$$\gamma_{\alpha\beta} = -\gamma_{\beta\alpha}, \quad \gamma_{12} = \gamma_{\dot{1}\dot{2}} = 1 = -\gamma^{12} = -\gamma^{\dot{1}\dot{2}}. \tag{10}$$

— Umgekehrt ist jedem hermite-symmetrischen Spinor zweiter Stufe $T_{\mu\dot{\nu}} = T_{\dot{\nu}\mu}$ eindeutig ein Vektor T_i zugeordnet:

$$T_i = \sigma_i{}^{\mu\dot{\nu}}T_{\mu\dot{\nu}}. \tag{11}$$

Die Spinoren ψ_μ und $\psi_{\dot{\mu}}$ sind Skalare in bezug auf raum-zeitliche Transformationen; sie transformieren sich hingegen wie unimodulare Transformationen in den Spin-Räumen gemäss den Gesetzen

$$\overline{\psi}_\mu = \alpha_\mu{}^\nu\psi_\nu, \quad \overline{\psi}_{\dot{\mu}} = \alpha_{\dot{\mu}}{}^{\dot{\nu}}\psi_{\dot{\nu}} \tag{11a}$$

mit

$$|\alpha_\mu{}^\nu| = |\alpha_{\dot{\mu}}{}^{\dot{\nu}}| = 1. \tag{11b}$$

Bei einem Vektor T^i ist das gewöhnliche Differential

$$dT^i = T^i{}_{,l}\, dx^l \tag{12a}$$

kein Vektor, denn es gilt

$$(T'^i)_{,l}\, dx^l = \left(\frac{\partial x'^i}{\partial x^k}\, T^k\right)_{,l} dx^l = \left(\frac{\partial^2 x'^i}{\partial x^k \partial x^l}\, T^k + \frac{\partial x'^i}{\partial x^k}\, T^k{}_{,l}\right) dx^l. \tag{12b}$$

Daher wird das gewöhnliche Differential dT^i zum absoluten Differential

$$DT^i = dT^i + \Gamma^i{}_{kl}T^k dx^l = T^i{}_{;l}\, dx^l \tag{13a}$$

ergänzt, wobei die $\Gamma^i{}_{kl}$ die Koeffizienten des affinen Zusammenhanges sind, die dem Transformationsgesetz

$$\Gamma'^i{}_{kl} = \frac{\partial x'^i}{\partial x^r}\,\frac{\partial x^m}{\partial x'^k}\,\frac{\partial x^n}{\partial x'^l}\,\Gamma^r{}_{mn} + \frac{\partial x'^i}{\partial x^m}\,\frac{\partial^2 x^m}{\partial x'^k \partial x'^l} \tag{13b}$$

genügen müssen (und Lorentz-invariante Grössen sein sollen, d. h. nicht von der Wahl der Tetraden (2) abhängen). Ausser dem Transformationsgesetz

brauchen die Γ^i_{kl} keinen weiteren Bedingungen zu genügen. — Das absolute Differential für Tensoren ergibt sich dann einfach aus der Leibnizschen Regel, z. B.:

$$DT^i{}_k = dT^i{}_k + (\Gamma^i_{rl}\, T^r{}_k - \Gamma^r_{kl}\, T^i_r)\, dx^l. \tag{13c}$$

Analog dazu ist das gewöhnliche Differential eines Lorentz-Vektors T^A selbst kein Lorentz-Vektor, denn es gilt

$$d\bar{T}^A = (\omega^A{}_{B,l}\, T^B + \omega^A{}_B\, T^B{}_{,l})\, dx^l. \tag{14}$$

Indem zu (14) der Ausdruck

$$L^A{}_{Bl}\, T^B\, dx^l \tag{14a}$$

mit einer dem Transformationsgesetz

$$\bar{L}^A{}_{Bl} = \omega^A{}_C\, \omega_B{}^D\, L^C{}_{Dl} + \omega^A{}_D\, \omega_B{}^D{}_{;l} \tag{14b}$$

genügenden Lorentz-Affinität $L^A{}_{Bl}$ eingeführt wird, entsteht das Lorentz-kovariante Differential

$$DT^A = dT^A + L^A{}_{Bl}\, T^B\, dx^l = T^A{}_{|l}\, dx^l. \tag{14c}$$

Wiederum ist das Transformationsgesetz die einzige Forderung, die an die Lorentz-Affinität zu stellen ist. Ausserdem ist nur noch zu verlangen, dass sich die $L^A{}_{Bl}$ in bezug auf die Koordinatentransformationen in der V_4 wie ein Vektor transformiert:

$$L'^A{}_{Bl} = \frac{\partial x^k}{\partial x'^l}\, L^A{}_{Bk}. \tag{14d}$$

Die Bildung von Lorentz-kovarianten Differentialen für Lorentz-Tensoren folgt wieder aus der Leibnizschen Regel, z. B.:

$$DT^A{}_B = dT^A{}_B + (L^A{}_{Cl}\, T^C{}_B - L^C{}_{Bl}\, T^A{}_C)\, dx^l. \tag{14e}$$

Analog ist das gewöhnliche Differential $d\psi_\nu$ eines Spinors ψ_ν selbst kein Spinor, denn es gilt

$$d\bar{\psi}_\mu = (\alpha_\mu{}^\nu{}_{,l}\, \psi_\nu + \alpha_\mu{}^\nu\, \psi_{\nu,l})\, dx^l. \tag{15}$$

Durch Addition eines Terms

$$\Lambda^\alpha{}_{\mu l}\, \psi_\alpha \tag{16a}$$

mit der Spin-Affinität $\Lambda^\alpha{}_{\mu l}$, die den Transformationsgesetzen

$$\bar{\Lambda}^{\alpha}{}_{\beta l} = \alpha^{\alpha}{}_{\lambda}\,\alpha_{\beta}{}^{\mu}\,\Lambda^{\lambda}{}_{\mu l} + \alpha^{\alpha}{}_{\lambda}\,\alpha_{\beta}{}^{\lambda}{}_{,l} \tag{16b}$$

und

$$\Lambda'^{\alpha}{}_{\beta l} = \frac{\partial x^{k}}{\partial x'^{l}}\,\Lambda^{\alpha}{}_{\beta k} \tag{16c}$$

genügen soll, ist die kovariante Spinor-Ableitung

$$D\psi_{\nu} = d\psi_{\nu} - \Lambda^{\mu}{}_{\nu l}\,\psi_{\mu}\,dx^{l} = \psi_{\nu\,|\,l}\,dx^{l} \tag{16d}$$

definiert [2]. — Die Differentationsvorschrift für Spinoren höherer Stufe folgt wiederum aus der Leibnizschen Regel.

Da die raum-zeitlichen Affinitäten $\Gamma^{i}{}_{kl}$, die Lorentz-Affinitäten $L^{A}{}_{Bl}$ bzw. die Spinor-Affinitäten $\Lambda^{\alpha}{}_{\beta l}$ bzw. $\Lambda^{\dot{\alpha}}{}_{\dot{\beta} l}$ nur auf Grund der Transformationsgesetze definiert sind, sind sie zunächts völlig unabhängig voneinander. Die Beziehung zwischen der raumzeitlichen Affinität und der Lorentz-Affinität und die Beziehung zwischen der raum-zeitlichen Affinität und der Spinor-Affinität wird durch das Lemma von WEYL hergestellt[1].

Dieses Lemma besagt, dass, wenn eine der Gleichungen

$$T_{i,l} = 0\,, \tag{17a}$$

$$T_{A\,|\,l} = 0\,, \tag{17b}$$

oder

$$T_{\mu\dot{\nu}\,|\,l} = 0 \tag{17c}$$

gilt, auch die beiden anderen Gleichungen erfüllt sein sollten, d. h., dass die Operationen (3) oder (5) bzw. (6) oder (11), die die raum-zeitlichen Grössen mit den Lorentz-Grössen bzw. mit den Spinoren verknüpfen, mit den Operationen des kovarianten Differenzierens vertauschbar sein sollen.

Um dies zu erfassen, definiert man am einfachsten ein allgemein kovariantes Differential [7]: Für eine Grösse T^{Ai}, die in bezug auf den Index i ein raumzeitlicher Vektor und in bezug auf den Index A ein Lorentz-Vektor ist, definieren wir als allgemein-kovariantes Differential den Ausdruck

$$DT^{Ai} = (T^{Ai}{}_{,l} + L^{A}{}_{Bl}\,T^{Bi} + \Gamma^{i}{}_{rl}\,T^{Ar})\,dx^{l} = T^{Ai}{}_{|\,|\,l}\,dx^{l}. \tag{18}$$

(18) ist in der Tat wiederum in bezug auf $x'^{l} = x'^{l}\,(x^{k})$ ein raum-zeitlicher und in bezug auf (4) ein Lorentz-Vektor. — Genau so definieren wir für eine Grösse

[1] Die Postulate über den Zusammenhang der verschiedenen kovarianten Ableitungen, die wir hier als »Lemma von WEYL« bezeichnen, würden — in etwas speziellerer Form — von WEYL [9], [10] in die allgemein-relativistische Formulierung der Diracschen Wellengleichung eingeführt und dann auf etwas andere Weise in »Semi-Vektor-Kalkül« von EINSTEIN und MAYER [1] begründet.

$T^{\nu i}$, die einen raum-zeitlichen und einen Spin-Index trägt, als allgemein-kovariantes Differential den Ausdruck

$$DT^{\nu i} = (T^{\nu i}{}_{,l} + \Lambda^{\nu}{}_{\mu l}\, T^{\mu i} + \Gamma^{i}_{rl}\, T^{\nu r})\, dx^l = T^{\nu i}_{\;\;|||l}\, dx^l, \tag{19}$$

der in der Tat dieselben Transformationseigenschaften hat wie $T^{\nu i}$ selbst. Schliesslich ist:

$$DT^{A\nu} = dT^{A\nu} + (L^{A}_{\;Bl} T^{B\nu} + \Lambda^{\nu}{}_{\mu l}\, T^{A\mu})\, dx^l = T^{A\nu}{}_{|||l}\, dx^l. \tag{19a}$$

Insbesondere lautet also die allgemein-kovariante Ableitung der Tetraden $h^{A}{}_{i}$:

$$h^{A}{}_{i|||l} = h^{A}{}_{i,l} + L^{A}{}_{Bl}\, h^{B}{}_{i} - \Gamma^{r}{}_{il}\, h^{A}{}_{r}, \tag{20}$$

und die allgemein-kovariante Ableitung der metrischen Spin-Vektoren lautet

$$\sigma_{\mu\dot{\nu}}{}^{.k}{}_{|||l} = \sigma_{\mu\dot{\nu}}{}^{.k}{}_{.l} - \Lambda^{\alpha}{}_{\mu l}\, \sigma_{\alpha\dot{\nu}}{}^{.k} - \Lambda^{\dot{\alpha}}_{\dot{\nu} l}\, \sigma_{\mu\dot{\alpha}}{}^{.k} + \Gamma^{k}_{rl} \sigma_{\mu\dot{\nu}}{}^{.r}. \tag{21}$$

Durch allgemein-kovariantes Differenzieren der Gleichungen (3) und (6) sowie (5) und (11) finden wir nun

$$T^{A}{}_{||l} = T^{A}{}_{|||l} = h^{A}{}_{k|||l}\, T^{k} + h^{A}{}_{k}\, T^{k}{}_{;l}, \tag{22a}$$

$$T_{\mu\dot{\nu}|||l} = T_{\mu\dot{\nu}|||l} = \sigma_{\mu\dot{\nu}|||l}^{\;\;\;\;k} T_{k} + \sigma_{\mu\dot{\nu}}{}^{.k} T_{k;l} \tag{22b}$$

und

$$T^{i}{}_{|||l} = T^{i}{}_{;l} = h_{A}{}^{i}{}_{|||l}\, T^{A} + h_{A}{}^{i}\, T^{A}{}_{||l} = \sigma_{\mu\dot{\nu}|||l}^{\;\;\;\;i} T^{\mu\dot{\nu}} + \sigma_{\mu\dot{\nu}}{}^{.i}\, T^{\mu\dot{\nu}}{}_{|l}. \tag{22c}$$

Das Lemma von WEYL verlangt aber nun

$$T^{A}{}_{||l} = h^{A}{}_{k}\, T^{k}{}_{;l} \tag{23a}$$

und

$$T^{\mu\dot{\nu}}{}_{||l} = \sigma^{\mu\dot{\nu}}{}_{k}\, T^{k}{}_{;l}. \tag{23b}$$

Hieraus folgt, dass für die allgemein-kovarianten Ableitungen der $h^{A}{}_{i}$ und der $\sigma_{\mu\dot{\nu}}{}^{.k}$ gelten muss

$$h^{A}{}_{i|||l} = h_{A}{}^{i}{}_{|||l} = 0 \tag{24}$$

und

$$\sigma_{\mu\dot{\nu}|||l}^{\;\;\;\;k} = \sigma^{\mu\dot{\nu}}{}_{k|||l} = 0, \tag{25}$$

d. h. die Tetraden und die metrischen Spinvektoren müssen kovariant konstant sein (WEYL [10], EINSTEIN und MAYER [1]). Durch Auflösen von (24) erhalten wir die Beziehung zwischen den raum-zeitlichen Affinitäten und den Lorentz-Affinitäten

$$\begin{aligned} h_{A}{}^{i}\, h^{B}{}_{k}\, L^{A}{}_{Bl} &= \Gamma^{i}_{kl} - h_{A}{}^{i}\, h^{A}{}_{k,l} \\ &= \Gamma^{i}_{kl} + h_{A}{}^{i}{}_{,l}\, h^{A}{}_{k} \\ &= h_{A}{}^{i}{}_{;l}\, h^{A}{}_{k}. \end{aligned} \tag{26}$$

(26) ist daher lesbar als anholonome Transformation der $\Gamma^{i}{}_{kl}$ mit der Transformations-Matrix $h^{A}{}_{i}(x^{l})$ und dem Anholonomie-Objekt [5]:

$$h^{i}_{A,l}\, h^{A}{}_{k}\,. \tag{26a}$$

In der allgemeinen Relativitätstheorie sind die

$$L^{A}{}_{Bl} = -\gamma^{A}{}_{Bl} = -\,h^{k}{}_{B}\, h^{B}{}_{k\,;\,l} \tag{26b}$$

die Riccischen Rotations-Koeffizienten und die $\Gamma^{i}{}_{kl}$ die Christoffel-Affinität, so dass (26) hier identisch erfüllt ist (vgl. EISENHART [3]).

Durch Auflösen von (25) ergibt sich eine Beziehung zwischen den raumzeitlichen und den Spinor-Affinitäten:

$$\Lambda^{\alpha}_{\beta l} = \frac{1}{2}\,\sigma^{\alpha\dot{\mu}k}\,\sigma_{\beta\dot{\mu}k;\,l} + \frac{1}{2}\,\delta^{\alpha}_{\beta}\,\Lambda^{\mu}{}_{\mu l}\,. \tag{27}$$

Somit ist WEYLS Lemma diejenige Relation, die die Beziehungen zwischen dem raum-zeitlichen Tensor-Kalkül und dem Lorentz-kovarianten Kalkül sowie dem Spinor-Kalkül definiert. Die Eigenschaften der raum-zeitlichen Affinität werden über das Lemma von WEYL zu korrespondierenden Eigenschaften der Lorentz-Affinität und der Spinor-Affinität [8]. Genau dann sind die $h^{A}{}_{k}$ als anholonome Koordinaten interpretierbar; WEYLS Lemma beschreibt die anholonome Transformation der Affinitäten.

Insbesondere folgen aus der Metrizität und der Nichtmetrizität der raum-zeitlichen Übertragung $\Gamma^{i}{}_{kl}$ die Symmetrieeigenschaften der $L^{A}{}_{Bl}$ und der $\Lambda^{\alpha}{}_{\beta l}$. Allgemein gilt für die Vertauschung der beiden Lorentz-Indizes in der Lorentz-Affinität gemäss WEYLS Lemma (26):

$$L_{ABl} = h_{Ai}\, h^{i}_{B;l} = -\,h_{Ai;l}\, h^{i}{}_{B} = -\,L_{BAl} + h_{Bi}\, h_{Ak}\, g^{ik}{}_{;\,l}\,. \tag{28}$$

Für den Fall, dass die raum-zeitliche Affinität metrisch [3], [5] ist, d. h. dass das Lemma von Ricci

$$g^{ik}{}_{;\,l} = g_{ik;\,l} = 0 \tag{29}$$

erfüllt ist, ist die Lorentz-Affinität also antisymmetrisch in den vorderen Indizes [8]:

$$L_{ABl} = -\,L_{BAl}\,. \tag{30}$$

Damit wird gleichzeitig auch die Lorentz-Übertragung in dem Minkowski—Raum M_4 metrisch, d. h. es gilt:

$$\eta_{AB\|l} = 0\,. \tag{31}$$

Für die Vertauschung der Spin-Indizes in der Spinor-Affinität finden wir mit

$$\mathring{\Lambda}^{\alpha}{}_{\beta l} = \Lambda^{\alpha}{}_{\beta l} - \frac{1}{2}\delta^{\alpha}_{\beta}\Lambda^{\mu}{}_{\mu l}$$

aus (27) die Beziehung

$$\begin{aligned}\mathring{\Lambda}_{\alpha\beta l} &= \frac{1}{2}\sigma_{\alpha}{}^{\dot{\nu}r}\sigma_{\beta\dot{\nu}r\,;\,l} = \frac{1}{2}g^{rk}{}_{;\,l}\,\sigma_{\beta\dot{\nu}r}\sigma_{\alpha}{}^{\dot{\nu}}{}_{k} + \frac{1}{2}\sigma_{\alpha\dot{\nu}r\,;\,l}\,\sigma_{\beta}{}^{\dot{\nu}r} \\ &= \mathring{\Lambda}_{\beta\alpha l} + \frac{1}{2}g^{rk}{}_{;\,l}\,\sigma_{\beta\dot{\nu}r}\sigma_{\alpha}{}^{\dot{\nu}}{}_{k}.\end{aligned} \tag{32}$$

Gilt also das Lemma von Ricci, so wird die Affinität $\mathring{\Lambda}_{\alpha\beta l}$ symmetrisch in den vorderen Indizes:

$$\mathring{\Lambda}_{\alpha\beta l} = \mathring{\Lambda}_{\beta\alpha l},\ \mathring{\Lambda}_{\alpha\dot{\beta}l} = \mathring{\Lambda}_{\dot{\beta}\alpha l}. \tag{33}$$

Gilt dann noch $\Lambda^{\alpha}{}_{\alpha l} = 0$, so ist die Spinor-Übertragung metrisch, d. h. die kovariante Ableitung des metrischen Spinors verschwindet:

$$\gamma_{\alpha\beta\,|\,l} = -\Lambda_{\alpha\beta l} + \Lambda_{\beta\alpha l} = 0. \tag{34}$$

Gelten hingegen die Lemmata von Weyl (25) und Ricci (29) für:

$$\Lambda^{\alpha}{}_{\alpha l} - \Lambda^{\dot{\alpha}}{}_{\dot{\alpha} l} \neq 0$$

so ist die Spinor-Übertragung semi-symmetrisch.

II. Die physikalische Interpretation des Weylschen Lemmas

Die einfachen formalen Beziehungen von I haben nun einen bemerkenswerten physikalischen Inhalt. Wir betrachten zunächst den durch das Weylsche Lemma implizierten Zusammenhang zwischen der raum-zeitlichen und der Lorentz-Affinität; wir behandeln das Weylsche Lemma also in der Form (I. 24).

Der Transport einer vektoriellen Grösse längs einer raum-zeitlichen Kurve $\mathfrak{L} : x^l = x^l(s)$ ist gegeben durch

$$T^{i}{}_{;\,l}\frac{dx^l}{ds} = T^{i}{}_{;\,l}\ u^l = \frac{D}{Ds}T^{i} \quad \left(u^i = \frac{dx^l}{ds}\right). \tag{1}$$

Verschwindet (1), so erfolgt der Transport ausschliesslich unter dem Einfluss der geometrisierten universellen Kraft und ist dann ein freier Transport in der Raum—Zeit-Welt (Parallel-Transport im Sinne von Levi-Civita [4]).

Die Tetradenbeine $h^A{}_i$ repräsentieren ein System von vier normalen Massen (Etalons) — genauer ein System vom drei Normalmassstäben und einer Normaluhr [6]. Auf diese Etalons werden alle physikalischen Messgrössen bezogen und das Ergebnis dieser Operation sind die raum-zeitlichen Skalare [7]

$$T^A = h^A{}_i T^i, \tag{2}$$

die durch Projektion der raum-zeitlichen Grössen auf die Normalmasse entstehen.

Diese Normalmasse werden längs einer Kurve $\mathfrak{L}$ kräftefrei transportiert (d. h. ausschliesslich unter dem Einfluss der universellen geometrisierten Kraftfelder), wenn gilt

$$h^A{}_{i\,;l} \frac{dx^l}{ds} = h^A{}_{i\,;l}\, u^l = 0\,. \tag{3}$$

Aus WEYLs Lemma (24) folgt mit (3) das Verschwinden des Ausdrucks

$$L^A{}_{Bl}\, u^l \tag{4}$$

längs $\mathfrak{L}$, so dass bei Gültigkeit von (3) längs der Kurve $\mathfrak{L}$ für irgendeinen Messwert T^A der gewöhnliche Transport

$$\frac{dT^A}{ds} = T^A{}_{,l}\, u^l \tag{5a}$$

mit dem Lorentz-kovarianten Transport identisch wird:

$$T^A{}_{|l}\, u^l = (T^A{}_{,l} + L^A{}_{Bl}\, T^B)\, u^l = \frac{dT^A}{ds}\,. \tag{5}$$

Allgemein beschreibt in (5) der Term

$$L^A{}_{Bl}\, T^B\, u^l \tag{5b}$$

also den Einfluss, den die Änderung der Messgeräte während des Transports längs $\mathfrak{L}$ auf die Messwerte hat.

Auf Grund des Lemmas von WEYL ist dieser Einfluss der Änderung der Messgeräte einfach eine Folge der Wirkung von nichtgeometrischen Kräften auf die Messgeräte:

$$h_A{}^i\, L^A{}_{Bl}\, u^l = h_B{}^i{}_{;l}\, u^l \tag{6}$$

und verschwindet, wenn die Messgeräte längs $\mathfrak{L}$ frei bewegt werden. — Würde hingegen das Lemma von WEYL nicht eingeführt, so würden sich auch bei

einem kräftefreien Transport die Messwerte T^B längs der Kurve $\mathfrak{L}$ ändern, was so zu interpretieren ist, dass, wenn gemäss sich verändernden Messvorschriften gemessen wird, die Eichung der Messgeräte (im allgemeinen Sinne) beim Transport längs $\mathfrak{L}$ verändert wird. — Das WEYLsche Lemma schliesst hingegen eine solche (willkürliche) Umeichung der Messeinrichtungen aus.[1]

Somit hat für tensorielle physikalische Grössen das WEYLsche Lemma eine mehr gnosiologische Bedeutung. Die Bestimmung der Eichung der Bezugsgrössen durch das Weylsche Lemma geht hingegen unmittelbar in die Dynamik ein, wenn spinorielle physikalische Grössen zu behandeln sind.

Zur Darstellung der Dynamik von Spinorfeldern in einer allgemeinen Raum-Zeit V_4 reichen bekanntlich die metrischen Grössen der V_4, die g_{ik} (und die Konkomittanten ihrer Derivierten), nicht aus. Vielmehr gehen in die Feldgleichungen für spinorielle Felder die metrischen Spinvektoren $\sigma_{\mu\dot{\nu}}{}^{k}$ — und damit entsprechend I (8) die Tetraden $h^A{}_i$ — explicite ein, und die Feldgleichungen für die Spinorfelder enthalten über die kovarianten Spinor-Ableitungen die Spin-Affinitäten $\Lambda^{\alpha}{}_{\beta l}$ (während die raum-zeitlichen Affinitäten $\Gamma^{i}{}_{kl}$ nicht explicite auftreten).

Demnach ist die Dynamik von Spinorfeldern zunächts unabhängig von der Dynamik der Tensorfelder. In der Tat sind spinorielle Grössen ja auch nicht unmittelbar messbar und haben daher keine direkte physikalische Bedeutung. Jedoch entstehen durch hermitesymmetrische Verschmelzungen von Spinoren vektorielle (und allgemein tensorielle) Grössen. Es ist dann zu fordern, dass die Dynamik — insbesondere die Transportgesetze — für die durch Verschmelzung entstehenden Vektoren identisch sind mit denjenigen, die sich aus der raum-zeitlich-kovarianten Schreibweise der entsprechenden Transportvorschriften für die Vektoren ergeben.

Gilt also in Spinor-Schreibweise eine Transportvorschrift der Form

$$T_{\mu\dot{\nu}\,|\,l}\,u^l = 0 \qquad (\text{mit } T_{\mu\dot{\nu}} = T_{\dot{\nu}\mu}) \tag{7a}$$

(freier Transport längs $\mathfrak{L}$), so entsteht bei ihr durch Überschieben mit $\sigma^{\mu\dot{\nu}}{}_{k}$ die Transportvorschrift

$$\sigma^{\mu\dot{\nu}}{}_{k}\,T_{\mu\dot{\nu}\,|\,l}\,u^l = T_{k;\,l}\,u^l - \sigma^{\mu\dot{\nu}}{}_{k\,|\,|\,l}\,T_{\mu\dot{\nu}}\,u^l = 0\,. \tag{7b}$$

Andererseits gehört zu $T_{\mu\dot{\nu}}$ der Vektor $T_k = \sigma_k{}^{\mu\dot{\nu}}\,T_{\mu\dot{\nu}}$, und für dessen freien Transport längs derselben Kurve $\mathfrak{L}$ gilt die Transportvorschrift gemäss LEVI-CIVITA

$$T_{k;\,l}\,u^l = 0\,. \tag{8}$$

[1] Nach dem in I Gesagten werden in der allgemeinen Relativitätstheorie die »natürlichen Komponenten« $T^A = h^A{}_i T^i$ der Vektoren etc. und der Lorentz-kovariante Transport dieser Komponenten von vornherein so eingeführt, dass das Lemma von WEYL I (24) identisch erfüllt ist (siehe auch [7]).

Beide Transportvorschriften müssen nun identisch sein, da sie denselben physikalischen Tatbestand beschreiben: den freien Transport der Grösse T_k längs $\mathfrak{L}$. Dies verlangt aber, dass gilt

$$\sigma_{\mu\nu}{}^{k}{}_{|||l} u^l = 0 \tag{9}$$

und damit die Erfüllung des Lemmas von WEYL längs (der beliebigen Kurve) $\mathfrak{L}$.

Das Lemma von WEYL sorgt also dafür, dass die Transportvorschriften für Spinoren zu derselben Physik der Tensorfelder führen wie die raum-zeitlichen Transportvorschriften. Ein Verzicht auf das Lemma von WEYL in der Form (9) würde bedeuten, dass die durch die Fusion von Spinorfeldern entstehenden tensoriellen Felder einer anderen Dynamik genügen würden als Tensorfelder, die nicht als durch eine solche Fusion entstanden gedacht werden. (Wenn man einer solchen Annahme überhaupt einen physikalischen Sinn zurechnen kann, so wäre es der, dass die durch die Fusion von Fermi-Teilchen entstehenden Bose-Teilchen grundsätzlich auf andere Kraftfelder wirken als auf elementare Bose-Teilchen.)

Das WEYLsche Lemma für die Spinor-Übertragung impliziert natürlich die obigen Aussagen über den Transport von Messgrössen $T_A = h_A{}^i T_i$ im folgenden Sinne: Der freie Transport von metrischen Spinvektoren längs $\mathfrak{L}$ im Sinne von LEVI-CIVITA bedeutet

$$\sigma_{\mu\dot{\nu};}{}^{k}{}_{jl} u^l = 0. \tag{10}$$

Mit I(27) and I(27a) folgt damit

$$\Lambda^{\alpha}{}_{\beta l} = i\delta^{\alpha}_{\beta} \varphi_l . \tag{11}$$

Daher ist längs $\mathfrak{L}$ bei freiem Transport (10) des metrischen Spinvektors der gewöhnliche Transport eines hermitischen Spinors zweiter Stufe mit seinem Spinor-Transport identisch:

$$\psi_{\mu\dot{\nu}|||l} u^l = \psi_{\mu\dot{\nu},l} u^l . \tag{12}$$

Das auf Spinoren angewandte WEYLsche Lemma ist offenbar die elementarste und prinzipiellste Fassung desjenigen, was man neuerdings mehr intuitiv als Herleitung der Ankopplungsvorschrift für universelle (geometrisierte) Felder an die spinorielle Materie auf Grund der Forderung einer verallgemeinerten »Eich-Invarianz» erfassen will, wobei die universellen Felder als »kompensierende Felder» eingeführt werden. — Was in der allgemeinrelativistischen Theorie der Fermi-Felder tatsächlich geschieht, ist nach Einführung der kovarianten Spinor-Ableitung gemäss I(16) die »Eichung» dieser Ableitungen, d. h. die Bestimmung der zunächst frei verfügbaren Spinor-Affinität $\Lambda^{\alpha}{}_{\beta l}$ auf Grund des WEYLschen Lemmas.

Wir sehen auch, dass es kaum sinnvoll sein kann, in der allgemeinrelativistischen Spinor-Theorie auf das WEYLsche Lemma I(25) zu verzichten. Denn — im Gegensatz zu der rein messoperativen Bedeutung des WEYLschen Lemmas bei der Übertragungsvorschrift für Tensorfelder — ermöglicht das WEYLsche Lemma bei Spinorfeldern die Konsistenz der Fusions-Operationen mit den Übertragungsvorschriften für die Feldgrössen.

LITERATUR

1. A. EINSTEIN und W. MAYER, Semivektoren und Spinoren, Berliner Berichte, 1932, 522.
2. A. EINSTEIN und W. MAYER, Darstellung der Semi-Vektoren als gewöhnliche Vektoren von besonderem Differentations-Charakter. Ann. of Math, **35,** 104, 1934.
3. L. D. EISENHART, Non-Riemannian Geometry, New York, 1927.
4. T. LEVI-CIVITA, The Absolute Differential Calculus, London und Glasgow, 1926.
5. J. A. SCHOUTEN, Ricci-Calculus, Berlin, Göttingen, Heidelberg, 1954.
6. H.-J. TREDER, Lorentz-Gruppe, Einstein-Gruppe und Raumstruktur. In: H.-J. Treder (ed.) Entstehung, Entwicklung und Perspektiven der Einsteinschen Gravitationstheorie, Berlin, 1960.
7. H.-J. TREDER, General Relativity and General Lorentz-Covariance. Int. Journal of Theoret. Phys. **3,** 23, 1970.
8. H.-J. TREDER, On the Meaning of the General Covariant Derivations. GRG-Journal.
9. H. WEYL, Gravitation and the Electron, Proc. of National Academy of Sciences, USA, **15,** 323, 1929.
10. H. WEYL, Elektron und Gravitation. Zeitschr. f. Physik, **56,** 330, 1929.

ЛЕММА ВЕЙЛЯ КАК ПРАВИЛО ПЕРЕНОСА И СВЯЗИ

Х.-Й. ТРЕДЕР

Резюме

Сформулирована лемма Вейля, которой определяются общие соотношения между афинными связями $\Gamma^{i}{}_{Bl}$, наложенными на перенос пространственно-временных тензоров со связью вида $L^{A}{}_{Bl}$ для переноса тензоров Лоренца (то есть мер пространственно-временных тензоров) и спиноров. В частном случае метрических афинных связей, заданных уравнениями $g_{ik;\,l} = 0$, из леммы Вейля следуют свойства симметрии лоренцевых и спинорных связей. В общей теории относительности и в общем релятивистском спинорном исчислении лемма Вейла выполняется идентичным образом. В общем случае, по лемме Вейля можно прокалибровать процессы переноса локальных систем отсчета (нормальных эталонных систем), заданных тетрадами $h^{A}{}_{i}$. Для того, чтобы ковариантный спинорный анализ был совместим с операциями синтеза бозонов с ферми-частицами, необходимо, чтобы соотношения между спинорными и $\Gamma^{i}{}_{kl}$-связями удовлетворили лемме Вейля. Следовательно лемма Вейля определяет вид взаимодействия универсального геометрического поля с полем материи.

Acta Physica Academiae Scientiarum Hungaricae, Tomus 32 (1—4), pp. 61—74 (1972)

WEIGHT DIAGRAMS FOR THE GENERAL LINEAR GROUP IN FIVE DIMENSIONS*

By

J. McCONNELL

DUBLIN INSTITUTE FOR ADVANCED STUDIES, DUBLIN, IRELAND

(Received 27. IX. 1971)

Weight diagrams for irreducible representations of the Lie Algebra of the general linear group in five dimensions over the complex field are classified according to the shape of their boundaries. Weight multiplicities are examined and the reduction under the orthogonal group $O(5, C)$ of certain homogeneous integral irreducible representations of $GL(5, C)$ is deduced.

1. Weights and Young tableaux

The general linear group in five dimensions over the complex field $GL(5, C)$ is the set of all non-singular 5×5 matrices. If an infinitesimal transformation of the group is denoted by $I + \Sigma_A \varepsilon^A O_A$, the infinitesimal generators O_A are elements of a Lie algebra, which we shall denote by $gl(5, C)$. Since the O_A may be singular, they are not elements of a group.

The infinitesimal generators of any subgroup of $GL(5, C)$ are elements of a Lie algebra. Such a subgroup is the orthogonal group $O(5, C)$ and the corresponding algebra is denoted in Cartan's notation by B_2. It is a semi-simple Lie algebra of rank two and its root vector diagram is shown in Fig. 1. The different irreducible representations of B_2 may be characterized by two-dimensional weight diagrams, and the (m_1, m_2) coordinates of the highest weight of the representation denoted by $D(\lambda, \mu)$, where λ and μ are each a positive integer or zero, are

$$\frac{1}{2\sqrt{6}}(\lambda + 2\mu, \lambda) . \tag{1}$$

The weights in a B_2 diagram form a lattice, the difference between neighbouring points being a root vector. The diagrams are invariant for a rotation through an angle $\pi/2$ about the origin, for reflections in the $m_1 m_2$-axes and in lines through the origin that make an angle $\pi/4$ with the axes. The weight vectors corresponding to different weights are linearly independent, but linearly independent vectors do not necessarily correspond to different weights. The number of linearly independent vectors corresponding to a given weight is

* Dedicated to Prof. L. JÁNOSSY on his 60th birthday.

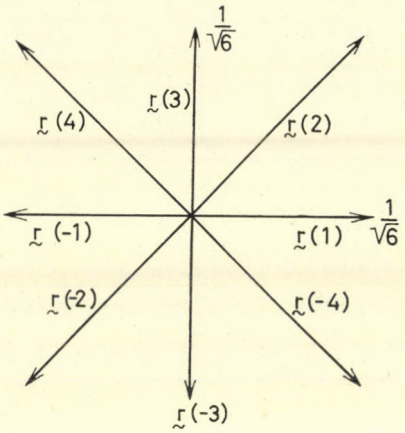

Fig. 1. The root vector diagram of B_2

called the multiplicity of the weight; if the multiplicity is unity, the weight is said to be simple. The boundary of the weight diagram for a $D(\lambda,O)$ is a square with sides parallel to the axes, which we denote by $\square$. The boundary for $D(O,\mu)$ is a square with sides inclined at an angle $\pi/4$ to the axes, and we denote this square by $\diamondsuit$. The boundary for a $D(\lambda,\mu)$ representation is octagonal, there being λ units each of length $1/\sqrt{6}$ in a vertical or horizontal side and μ units each of length $1/\sqrt{3}$ in a slant side. Further information on these and related matters may be found in McCONNELL [1] and in the literature quoted there.

The representation with $\lambda = 0$, $\mu = 1$ is the five-dimensional $D^{(5)}$ (0,1). All its weights are simple and its weight diagram is depicted in Fig. 2. The basis vectors x_1, x_2, x_3, x_4, x_5 are assigned to the weights in descending sequence. Now the Lie algebra B_2 has ten elements

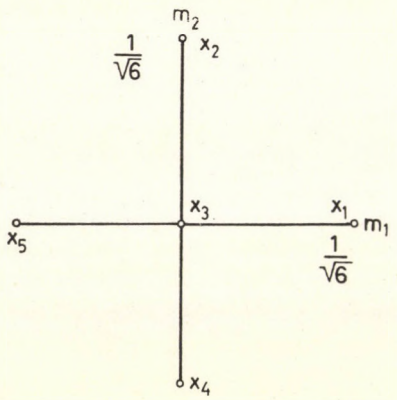

Fig. 2. The weight diagram for the $D^{(5)}$ (0,1) representation of B_2

$$H_1,\ H_2,\ E_1,\ E_2,\ E_3,\ E_4,\ E_{-1},\ E_{-2},\ E_{-3},\ E_{-4}$$

which satisfy well-known commutation relations. The matrices representing H_1, H_2 in any representation have eigenvalues m_1, m_2 which are the components of the weights of the representation. E_α displaces a vector with weight $\mathbf{m}$ to a vector with weight $\mathbf{m} + \mathbf{r}(\alpha)$, if this exists in the representation; otherwise it annihilates the vector. Thus for $D^{(5)}$ (0, 1)

$$H_1 x_5 = -\frac{1}{\sqrt{6}} x_5,\ H_2 x_5 = 0,$$

$$E_1 x_5 = \text{const. } x_3, \qquad E_2 x_5 = \text{const. } x_2, \qquad E_3 x_5 = 0.$$

Since x_1, x_2, x_3, x_4, x_5 are linearly independent, they are a basis of a five-dimensional linear vector space. We may take this as the space on which the elements of the group $GL(5, C)$ act or that on which the elements of the algebra $gl(5, C)$ act. Homogeneous integral irreducible representations of the group or of the algebra may be constructed by using Young diagrams (BOERNER [2]). To obtain an r^{th} rank tensor one makes a partition $[\lambda_1, \lambda_2, \lambda_3, \lambda_4, \lambda_5]$ of r such that

$$\lambda_1 \geq \lambda_2 \geq \lambda_3 \geq \lambda_4 \geq \lambda_5.$$

Having put down the corresponding diagram one constructs a Young tableau by filling numbers from 1 to 5 into the boxes in such a way that in any row the numbers are non-decreasing towards the right and that in any column they are increasing downwards. Let the tableau be (2)

a_1	a_2	.	.	.	.	a_{λ_1}
a_{λ_1+1}	.	.	.	.	$a_{\lambda_1+\lambda_2}$	
$a_{\lambda_1+\lambda_2+1}$	.	.	.	$a_{\lambda_1+\lambda_2+\lambda_3}$		
$a_{\lambda_1+\lambda_2+\lambda_3+1}$	.	.	$a_{\lambda_1+\lambda_2+\lambda_3+\lambda_4}$			
$a_{\lambda_1+\lambda_2+\lambda_3+\lambda_4+1}$	.	a_r				

(2)

and let us write down

$$x^{(1)}_{a_1} x^{a2}_{(2)} \ldots x^{(r)}_{a_r}, \tag{3}$$

where the x's are the basis vectors of the five-dimensional representation and the superscripts label the space to which each vector belongs. The tensor component for the tableau (2) is obtained by symmetrizing (3) with respect to the rows and antisymmetrizing with respect to the columns; we denote this tensor component by (4). The tensor components for all allowed entries in (2) are a basis for the irreducible representations of $GL(5, C)$ or of $gl(5, C)$ corre-

sponding to the partition $[\lambda_1, \lambda_2, \lambda_3, \lambda_4, \lambda_5]$, and the dimension of the representation is consequently the number of possible tableaux (2) that can be constructed for the partition.

$$\begin{bmatrix} a_1 & a_2 & \dots & a_{\lambda_1} \\ a_{\lambda_1+1} & \dots & a_{\lambda_1+\lambda_2} & \\ a_{\lambda_1+\lambda_2+1} & \dots & a_{\lambda_1+\lambda_2+\lambda_3} & \\ a_{\lambda_1+\lambda_2+\lambda_3+1} & \dots & a_{\lambda_1+\lambda_2+\lambda_3+\lambda_4} & \\ a_{\lambda_1+\lambda_2+\lambda_3+\lambda_4+1} & \dots & a_r & \end{bmatrix} \tag{4}$$

When an infinitesimal transformation $I+\Sigma_A \varepsilon^A O_A$ of $GL(5, C)$ is applied to $x^{(1)}_{a_1} x^{(2)}_{a_2}$, we obtain

$$(I+\Sigma_A \varepsilon^A O_A) x^{(1)}_{a_1} x^{(2)}_{a_2} = (x^{(1)}_{a_1}+\Sigma_A \varepsilon^A O_A x^{(1)}_{a_1})(x^{(2)}_{a_2}+\Sigma_B \varepsilon^B O_B x^{(2)}_{a_2}) =$$
$$= x^{(1)}_{a_1} x^{(2)}_{a_2}+\Sigma_A \varepsilon^A (O_A x^{(1)}_{a_1} \cdot x^{(2)}_{a_2}+x^{(1)}_{a_1} \cdot O_A x^{(2)}_{a_2}) + \dots$$

and therefore

$$O_A (x^{(1)}_{a_1} x^{(2)}_{a_2}) = O_A x^{(1)}_{a_1} \cdot x^{(2)}_{a_2}+x^{(1)}_{a_1} \cdot O_A x^{(2)}_{a_2}.$$

This is the rule for the application of an infinitesimal generator to a product. If x_{a_1}, x_{a_2} are weight vectors of weights $\mathbf{m}(a_1)$, $\mathbf{m}(a_2)$,

$$H_1(x^{(1)}_{a_1} x^{(2)}_{a_2}) = \big(m_1(a_1)+m_1(a_2)\big) x^{(1)}_{a_1} x^{(2)}_{a_2},$$

so that the weight of the product is the sum of the weights. It follows that the weight of (3) or of (4) is

$$\mathbf{m}(a_1)+\mathbf{m}(a_2)+\dots+\mathbf{m}(a_r). \tag{5}$$

The tensor component (4) which has the highest weight is that which has the greatest number of 1's, then the greatest number of 2's etc., viz.

$$\begin{bmatrix} 1 & 1 & \dots & 1 \\ 2 & 2 & \dots & 2 & \\ 3 & \dots & 3 & & \\ 4 & \dots & 4 & & \\ 5 & \dots & 5 & & \end{bmatrix}.$$

The weight of this is

$$\lambda_1 \mathbf{m}(1)+\lambda_2 \mathbf{m}(2)+\lambda_3 \mathbf{m}(3)+\lambda_4 \mathbf{m}(4)+\lambda_5 \mathbf{m}(5).$$

On referring to Fig. 2 we find that this is equal to

$$\frac{1}{\sqrt{6}}(\lambda_1-\lambda_5, \lambda_2-\lambda_4). \tag{6}$$

No other tensor component has this weight, so the highest weight of the representation of $gl(5, C)$ is simple.

We may associate this representation of $gl(5, C)$ with the irreducible representation of B_2, which has (6) as its highest weight. According to our earlier discussion and (1) the boundary of the weight diagram for this irreducible representation of B_2 will be $\diamond$ when $\lambda_2 - \lambda_4 = 0$ and this implies that

$$\lambda_2 = \lambda_3 = \lambda_4. \tag{7}$$

The boundary will be $\square$ when

$$\lambda_1 - \lambda_5 = \lambda_2 - \lambda_4$$

and therefore

$$\lambda_1 = \lambda_2, \lambda_4 = \lambda_5. \tag{8}$$

If neither (7) nor (8) is obeyed, the boundary will be octagonal.

In the following two sections we apply the notion of weight diagrams to the irreducible representations of $gl(5, C)$, study the question of multiplicities especially on the boundaries and point out how they may give a comparatively elementary method of finding the manner in which an irreducible representation of $GL(5, C)$ reduces under the orthogonal group $0(5, C)$.

2. Weight diagrams for irreducible representations of gl(5,C)

Corresponding to each tensor component (4) there is a weight and, if we put down the weight for every tensor component in accordance with (5), we shall have the weight diagram for the irreducible representation of $gl(5, C)$ corresponding to the partition $[\lambda_1, \lambda_2, \lambda_3, \lambda_4, \lambda_5]$. We distinguish between the irreducible representations with a highest weight related to a B_2 diagram with a boundary $\diamond$, a boundary $\square$ or an octagonal boundary.

We consider first the representations associated with $\diamond$. It will appear in the course of the calculations that we are about to perform that all the weights of the boundary of the B_2 diagram belong to the $gl(5, C)$ representation. Moreover it may easily be checked that no weight lies outside, and hence the boundary of the B_2 diagram is also the boundary of the $gl(5, C)$ diagram. The tensor component corresponding to the highest weight is:

$$\begin{bmatrix} 1 & 1 & \cdots & 1 & 1 \\ 2 & 2 & \cdots & 2 & \\ 3 & 3 & \cdots & 3 & \\ 4 & 4 & \cdots & 4 & \\ 5 & 5 & \cdots & 5 & \end{bmatrix}$$

and (6) shows that the highest weight is $(1/\sqrt{6})\ (\lambda_1 - \lambda_5, 0)$. We proceed from this along the boundary in the upper half-plane and examine the multiplicities of the weights. The tensor components at the next weight, obtained according to Fig. 2 by either replacement $1 \to 2$, $4 \to 5$, will be:

$$\begin{bmatrix} 1 & 1 & \cdots & 1 & 2 \\ 2 & 2 & \cdots & 2 & \\ 3 & 3 & \cdots & 3 & \\ 4 & 4 & \cdots & 4 & \\ 5 & 5 & \cdots & 5 & \end{bmatrix}, \qquad \begin{bmatrix} 1 & 1 & \cdots & 1 & 1 \\ 2 & 2 & \cdots & 2 & \\ 3 & 3 & \cdots & 3 & \\ 4 & 4 & \cdots & 5 & \\ 5 & 5 & \cdots & 5 & \end{bmatrix}.$$

The first is non-zero when $\lambda_1 > \lambda_2$, the second is non-zero when $\lambda_2 > \lambda_5$, so the multiplicity is 1 or 2 according as one or both the inequalities:

$$\lambda_1 - \lambda_2 \geq 1, \qquad \lambda_2 - \lambda_5 \geq 1$$

are satisfied. On going to the next weight we find similarly that its multiplicity is:

4 for $\lambda_1 - \lambda_2 \geq 2$, $\lambda_2 - \lambda_5 \geq 2$

2 for $\lambda_1 - \lambda_2 \geq 2$, $\lambda_2 - \lambda_5 = 1$ or $\lambda_1 - \lambda_2 = 1$, $\lambda_2 - \lambda_5 \geq 2$

1 for $\lambda_1 - \lambda_2 \geq 2$, $\lambda_2 = \lambda_5$ or $\lambda_1 = \lambda_2$, $\lambda_2 - \lambda_5 \geq 2$.

If s is the lesser of $\lambda_1 - \lambda_2$ and $\lambda_2 - \lambda_5$, then on proceeding along the boundary we obtain:

a weight at $\frac{1}{\sqrt{6}}\ (\lambda_1 - \lambda_5, 0)$ with multiplicity 1

a weight at $\frac{1}{\sqrt{6}}\ (\lambda_1 - \lambda_5 - 1, 1)$ with multiplicity 2

a weight at $\frac{1}{\sqrt{6}}\ (\lambda_1 - \lambda_5 - 2, 2)$ with multiplicity 2^2

. . . . . .

a weight at $\frac{1}{\sqrt{6}}\ (\lambda_1 - \lambda_5 - s, s)$ with multiplicity 2^s.

After this there is no increase in multiplicity. Indeed examining the tensor components we readily see that the multiplicities will decrease in a symmetrical way so as to be equal to unity at $(1/\sqrt{6})\ (0, \lambda_1 - \lambda_5)$. The same variation of multiplicity will be found on each side of the boundary.

It would clearly be difficult to derive expressions for multiplicities at internal points in the weight diagram for the general case, so we shall specialize to $\lambda_1 = r$, $\lambda_2 = \lambda_3 = \lambda_4 = \lambda_5 = 0$. This is the important case when the basis of the homogeneous integral irreducible representation of $gl(5, C)$ are totally symmetric functions. Then s is zero and all the weights on the boundary are simple. We examine the multiplicities in the first quadrant by constructing weight vectors.

We first construct totally symmetric basis vectors associated with weights on the positive m_1-axis, referring to Fig. 2 and (5). For bilinear expressions we can have at the centre the weights:

$$\mathbf{m}(3) + \mathbf{m}(3),\ \mathbf{m}(1) + \mathbf{m}(5),\ \mathbf{m}(2) + \mathbf{m}(4)$$

and these correspond, respectively, to the linearly independent basis vectors:

$$[33],\ [15],\ [24].$$

We note that, if at any stage we replace 33 by 15 or 24, we do not change the weight. To obtain the tensor components for the weight immediately to the right we make the replacement $5 \to 3$ or $3 \to 1$. We thus have for the origin and for the two weights to the right of it on the m_1-axis:

$$\begin{matrix} [33] & & & \\ [15], & [13], & [11], & \\ [24] & & & \end{matrix} \tag{9}$$

the multiplicities being 3, 1, 1, respectively.

For trilinear expressions we start with 333 at the centre, replace 33 by 15 or 24 displace:

$$\begin{matrix} [333] & [133] & & \\ [135] & , [115] & , [113] & , [111]. \\ [234] & [124] & & \end{matrix} \tag{10}$$

This is equivalent to 3 being added to the first set of terms of (9), and 1 being added to all terms. The latter produces a shift without change of multiplicity. For quadrilinear expressions we may start with [3333] and replacing 33 by 15 and 24 obtain $3 + 2 + 1$ components at the origin. On displacing (10) by addition of a 1 we get altogether:

$$\begin{matrix}[3333] & & & & \\ [1335] & [1333] & [1133] & & \\ [2334] \ , & [1135] \ , & [1115] \ , & [1113] \ , & [1111]. \\ [1245] & [1234] & [1124] & & \\ [1155] & & & & \\ [2244] & & & & \end{matrix}$$

The multiplicity structure is now evident. Coming left from the highest weight along the m_1-axis we see that the multiplicity of the first two weights is 1, the multiplicity of the second two is $1 + 2$, the multiplicity of the p^{th} two is $p(p+1)/2$. If $r=2t$ or $2t + 1$, the multiplicity of the origin is $(t+1)(t+2)/2$.

We next examine how the multiplicities of weights vary as we go from a point on the m_1-axis along a line in the first quadrant parallel to the boundary. Such a displacement is got from $1 \to 2$ or $4 \to 5$, and we find that we obtain for the boundary and for the next two layers of weights, respectively,

$$\begin{matrix}[11\ldots111], & [11\ldots112], & [11\ldots122], & \ldots & [12\ldots22], & [22\ldots22]; \\ [11\ldots113], & [11\ldots123], & [11\ldots223], & \ldots & [22\ldots23]; & \\ [11\ldots133], & [11\ldots233], & [11\ldots2233], & \ldots & & \\ [11\ldots115], & [11\ldots224], & [11\ldots2224], & \ldots & & \\ [11\ldots124], & [11\ldots125], & [11\ldots1225], & \ldots . & & \end{matrix}$$

We see that the first two give simple weights, that in the case of the third the replacement $4 \to 5$ adds nothing to $1 \to 2$ and that, as far as we have gone, the multiplicity here is 3. The reason for this constant multiplicity is that once 33 has appeared it can be replaced for the same weight only by 15 and 24. Now on commencing with [11...133] and making repeatedly the substitution $1 \to 2$ the 33 remains and gives multiplicity 3. The same reasoning will hold when we start with [11...1333], [11...13333], etc. and we conclude that the multiplicity remains constant along any line in the first quadrant parallel to the boundary. The same reasoning holds also for the other quadrants, so the multiplicities are constant along layers parallel to the boundaries, the multiplicities being those specified above for points on the m_1-axis.

Let us now consider weight diagrams for irreducible representations of $gl(5, C)$ that are associated with a B_2 boundary $\square$. Again it may be shown that this is also the boundary of the $gl(5, C)$ representation. According to (8) the tensor component corresponding to the highest weight is:

$$\begin{bmatrix} 11 & \ldots & 11 \\ 22 & \ldots & 22 \\ 3 & \ldots & 3 \\ 4 & \ldots & 4 \\ 5 & \ldots & 5 \end{bmatrix}.$$

To find the multiplicities on the boundary we could start at the highest weight and work down the vertical side. This is done by the replacements $2 \to 3$, $3 \to 4$. The $2 \to 3$ will occur for the first displacement only if $\lambda_2 - \lambda_3 \geq 1$, and the $3 \to 4$ will occur only if $\lambda_3 - \lambda_4 \geq 1$. However, even if $\lambda_3 = \lambda_4$, we can for later displacements have $3 \to 4$ from a 3 that had already been put into the second row by a $2 \to 3$ replacement. The specification of multiplicities will thus depend on inequalities involving $\lambda_2 - \lambda_3$, $\lambda_2 - \lambda_4$, $\lambda_3 - \lambda_4$. To avoid complications we restrict our investigations to the partition $[r^2]$, putting $\lambda_3 = \lambda_4 = \lambda_5 = 0$.

Starting with the highest weight $A\ (1/\sqrt{6})\ (r, r)$ we consider the points

$$B \frac{1}{\sqrt{6}}(r, r-1), \quad C \frac{1}{\sqrt{6}}(r, r-2), \ldots$$

vertically below A. The related tensor components are :

$$A \begin{bmatrix} 11 & \ldots & 11 \\ 22 & \ldots & 22 \end{bmatrix}$$

$$B \begin{bmatrix} 11 & \ldots & 11 \\ 22 & \ldots & 23 \end{bmatrix}$$

$$C \begin{bmatrix} 11 & \ldots & 111 \\ 22 & \ldots & 233 \end{bmatrix}, \quad \begin{bmatrix} 11 & \ldots & 11 \\ 22 & \ldots & 24 \end{bmatrix}$$

$$D \begin{bmatrix} 11 & \ldots & 1111 \\ 22 & \ldots & 2333 \end{bmatrix}, \quad \begin{bmatrix} 11 & \ldots & 111 \\ 22 & \ldots & 234 \end{bmatrix}, \quad \ldots .$$

Since 1 is not altered in a vertical displacement, the first row remains unchanged. As we go from A to B, we change 2 into 3 and this can be done in one way only. As we go from B to C, we change another 2 into 3. We then have 33 in the second row and we can remain with the same weight by replacing 33 with 24 but not with 15, since the first row is already filled with 1's. The multiplicity of C is therefore two. On going from C to D another 2 is changed into 3 and, as we can change 333 only into 234, there is no increase in multiplicity. E will contain in the second row 3333, which is replaceable by 2334 and 2244, so we have multiplicity three corresponding to zero, one or two 4's. The multiplicities of

$$A,\ B,\ C,\ D,\ E,\ F,\ G,\ \ldots \tag{11}$$

are, respectively,

$$1,\ 1,\ 2,\ 2,\ 3,\ 3,\ 4,\ \ldots . \tag{12}$$

We may by constructing tensor components find the multiplicities for all other weights in the diagram. Thus for

$$A',\ B',\ C',\ D',\ E',\ F',\ G',\ \ldots$$

situated at

$$\frac{1}{\sqrt{6}}(r-1, r),\ \frac{1}{\sqrt{6}}(r-1, r-1),\ \frac{1}{\sqrt{6}}(r-1, r-2),\ \text{etc.},$$

that is, along a layer parallel to (11), the multiplicities are, respectively,

$$1,\ 3,\ 4,\ 6,\ 7,\ 9,\ 10\ \ldots \tag{13}$$

and for

$$A''\frac{1}{\sqrt{6}}(r-2, r),\ B''\frac{1}{\sqrt{6}}(r-2, r-1),\ C''\frac{1}{\sqrt{6}}(r-2,\ r-2)$$

the multiplicities are, respectively,

$$2,\ 4,\ 9. \tag{14}$$

In calculating (12), (13), (14) we have tacitly assumed that the weights are not situated near the $m_1\ m_2$-axes. When they are, not all the above replacements are possible and the multiplicities will be consequently reduced.

3. Reduction under the orthogonal group O(5, C) of irreducible representations of GL(5, C)

In Section 1 we classified the homogeneous integral irreducible representations of $GL(5, C)$ by means of Young diagrams. If the 5×5 matrix for the transformation of the basic set x_1, x_2, x_3, x_4, x_5 belongs to the complex orthogonal group in five dimensions, the representation corresponding to a Young diagram may reduce into the direct sum of irreducible representations of $0(5, C)$. A closed formula for such a reduction is to be found in LITTLEWOOD [3] and in MURNAGHAN [4]. The derivation of this formula requires a deep study of group characters and also a knowledge of results from combinatorial mathematics that are not readily available. The application of the formula, moreover, requires theorems on the multiplication of Schur functions that are not easily established.

For these reasons it is worthwhile to see what use can be made of weight diagrams. We shall put down the weight diagram for an irreducible representation of the algebra $gl(5, C)$ corresponding to a Young diagram and subtract from it the weights of diagrams for irreducible representations of B_2 which are identifiable by their highest weights. This procedure will give the reduction under B_2 of the irreducible representations of $gl(5, C)$. By exponentiation we may deduce the reduction of the irreducible representations of $GL(5, C)$ under

$SO(5, C)$, which is the connected component of the exponential map of B_2 that contains the identity. However, since self-associate Young diagrams do not exist for an odd dimension (WEYL [5]), the irreducible representations of $O(5, C)$ are the same as those of $SO(5, C)$. We may therefore interpret the results of inspecting the weight diagrams in terms of the reduction of irreducible representations of $GL(5, C)$ under $O(5, C)$.

As a first example let us consider the irreducible representations of $GL(5, C)$ with totally symmetric bases. We saw in the previous section that the weight diagram corresponding to tensor components of rank r has a boundary $\diamond$ and consists of layers of successive multiplicities

$$1, 1, 1 + 2, 1 + 2, 1 + 2 + 3, 1 + 2 + 3, \ldots .$$

Now the B_2 weight diagram for a representation $D(0, \mu)$ has a boundary $\diamond$, the multiplicities are constant on layers parallel to the boundary and the multiplicities as we come in from the boundary are (MCCONNELL [6])

$$1, 1, 2, 2, 3, 3, \ldots .$$

We examine separately the cases of $r = 2t$ and $r = 2t + 1$. For the first we put down the multiplicities in layers for the representation $D[2t]$ of $gl(5, \mathfrak{a})$ and subtract the corresponding multiplicities for $D(0, 2t)$ proceeding from the origin to the boundary:

$D[2t]$ $1 + 2 + \ldots (t + 1), 1 + 2 + \ldots + t, 1 + 2 + \ldots + t, \ldots 1 + 2 + 3,$
$1 + 2 + 3, 1 + 2, 1 + 2, 1, 1$

$D(0,2t)$ $t + 1, \quad t, \quad t, \quad \ldots \quad 3, \quad 3, \quad 2, \quad 2, \quad 1, \quad 1$

difference $1 + 2 + \ldots t, 1 + 2 + \ldots (t - 1), 1 + 2 + \ldots + (t - 1), \ldots 1 + 2'$
$1 + 2, 1, 1, 0, 0$. The difference gives the multiplicities for $D[2t - 2]$, so for every weight of the diagram we have

$$\begin{aligned}
&\text{mult. } D[2t] = \text{mult. } D[2t - 2] + \text{mult. } D(0,2t)\\
&\text{mult. } D[2t - 2] = \text{mult. } D[2t - 4] + \text{mult. } D(0,2t - 2)\\
&\ldots\ldots\ldots\ldots\ldots\ldots\ldots\ldots\ldots\ldots\\
&\text{mult. } D[4] = \text{mult. } D[2] + \text{mult. } D(0, 4)\\
&\text{mult. } D[2] = \text{mult. } D[0] + \text{mult. } D(0, 2).
\end{aligned}$$

Since $D[0]$ is the one-dimensional $D(0, 0)$, we see that the multiplicity of any weight in the $D[2t]$ diagram is the sum of its multiplicities in the diagrams for

$$D(0, 2t), D(0, 2t - 2), \ldots D(0, 2), D(0, 0).$$

In the case of $r = 2t + 1$ we note that $D[1]$ is just $D(0, 1)$ and we deduce that the multiplicity of any weight in the $D[2t + 1]$ diagram is the sum of the multiplicities in the diagram for

$$D(0, 2t + 1),\ D(0, 2t - 1),\ \ldots\ D(0, 3),\ D(0, 1).$$

Thus by removing the weights of successive B_2 diagrams we may conclude that the $D[r]$ representation of gl(5, C) reduces under B_2 into the direct sum of representations as follows:

$$D[r] = D(0, r) \oplus D(0, r - 2) \oplus D(0, r - 4) \oplus \ldots \oplus \begin{cases} D(0, 1) \text{ for } r \text{ odd} \\ D(0, 0) \text{ for } r \text{ even.} \end{cases}$$

To relate the group algebras to the groups themselves we note first of all that on account of modification rules for the orthogonal group the irreducible representations of $O(5, C)$ are specified by a partition into two parts only. We denote such a representation by $\Delta(\lambda_1, \lambda_2)$, and we denote the irreducible representation of $GL(5, C)$ corresponding to the partition $[\lambda_1, \lambda_2, \lambda_3, \lambda_4, \lambda_5]$ by $\Delta[\lambda_1, \lambda_2, \lambda_3, \lambda_4, \lambda_5]$. We relate the representations of B_2 to those of $O(5, C)$ by pointing out that according to (1) and (6) the tensor component of the highest weight of the $D(\lambda, \mu)$ representation of B_2 belongs to $\Delta({}^1/_2\lambda + \mu, {}^1/_2\lambda)$. We therefore deduce from the last equation that the $\Delta[r]$ representation of $GL(5, C)$ reduces under $O(5, C)$ into the direct sum of irreducible representations as follows:

$$\Delta[r] = \Delta(r) \oplus \Delta(r - 2) \oplus \Delta(r - 4) \oplus \ldots \oplus \begin{cases} \Delta(1) \text{ for } r \text{ odd} \\ \Delta(0) \text{ for } r \text{ even.} \end{cases}$$

It is not difficult to see that there is no reduction of representations of $GL(5, C)$ that have totally antisymmetric bases. Indeed $D[1]$ is $D(0, 1)$, $D[1^2]$ is the ten-dimensional $D(2, 0)$, $D[1^3]$ is the same as $D[1^2]$ and $D[1^4]$ is the same as $D[1]$. Finally $D[1^5]$ has only one tensor component

$$\begin{bmatrix} 1 \\ 2 \\ 3 \\ 4 \\ 5 \end{bmatrix}$$

and is therefore the one-dimensional $D(0, 0)$.

Lastly we look at some representations whose bases are neither totally symmetric nor totally antisymmetric. As we have calculated the multiplicities for the partition $[r^2]$, we shall first of all study the representation $D[2^2]$. By

employing the method of the previous section we construct explicitly the tensor components for weights in the first quadrant. There will be related tensor components in the other quadrants, and altogether the multiplicities of weights diagram for the $D[2^2]$ representation of $gl(5, C)$ will be as shown in Fig. 3.

1	1	2	1	1
1	3	3	3	1
2	3	6	3	2
1	3	3	3	1
1	1	2	1	1

Fig. 3. The multiplicities of weights in the $D^{(50)}$ $[2^2]$ representation of $gl(5, C)$

The degree of representation being the sum of the multiplicities is 50. The highest weight $(1/\sqrt{6})$ (2, 2) is the highest weight of the $D(4, 0)$ representation of B_2, by (1). The multiplicities in this B_2 diagram are 1 on the boundary, 2 on the next layer, 3 at the origin (McConnell [6]), so the degree of the representation is 35. When the weights of $D^{(35)}$ (4, 0) are removed, the highest weight belongs to $D^{(14)}$ (0,2) and, when the weights of this representation are removed, there remains a single weight at the origin. The reduction of the $D[2^2]$ representation of gl(5, C) under B_2 is therefore

$$D^{(50)}[2^2] = D^{(35)}\ (4,0) \oplus D^{(14)}\ (0,2) \oplus D^{(1)}\ (0,0).$$

Consequently the reduction under $O(5, C)$ of the $\Delta[2^2]$ representation of $GL(5, C)$ is

$$\Delta[2^2] = \Delta(2^2) \oplus \Delta(2) \oplus \Delta(0).$$

By a somewhat longer calculation we find the reductions:

$$D^{(175)}\ [3^2] = D^{(84)}\ (6,0) \oplus D^{(81)}\ (2,2) \oplus D^{(10)}\ (2,0)$$

$$\Delta[3^2] = \Delta(3^2) \oplus \Delta(3,1) \oplus \Delta(1,1).$$

In the general case of $D[r^2]$ the use of weight diagrams will not easily give the complete reduction. It may, however, be seen that there occur in the reduction

$$D(2r,0) \oplus D(2r-4,2) \oplus D(2r-8,4) \oplus \ldots \oplus \begin{cases} D(2, r-1) \text{ for } r \text{ odd} \\ D(0, r) \text{ for } r \text{ even} \end{cases} \oplus D(2r-4,\ 0).$$

REFERENCES

1. J. McConnell, Weight Diagrams and their Application to the Reduction of Representations of the General Linear Group, Communications of the Dublin Institute for Advanced Studies, Series A, No. 20, 1971.
2. H. Boerner, Representation of Groups, North-Holland Publishing Company, 2nd ed., 1970, Chapter V.
3. D. E. Littlewood, The Theory of Group Characters, Oxford, Clarendon Press, 2nd ed, 1950, page 240, theorem II.
4. F. D. Murnaghan, The Orthogonal and Symplectic Groups, Communications of the Dublin Institute for Advanced Studies, Series A, No. 13, 1958, page 137.
5. H. Weyl, The Classical Groups, Princeton University Press, 1946, pages 155 and 164.
6. J. McConnell, Proc. Roy. Ir. Acad., A, **65**, 1, 1966.

ВЕСОВЫЕ ДИАГРАММЫ ДЛЯ ПЯТИМЕРНОЙ ПОЛНОЙ ЛИНЕЙНОЙ ГРУППЫ

ДЖЕМС МкҚОННЭЛЬ

Резюме

Проведена классификация весовых диаграмм для неприводимых представлений алгебры ли пятимерной полной линейной группы в комплексной области по форме их границы. Рассмотрены кратности веса и выведена формула приведения по ортогональным группам $O(5,C)$ для некоторых неприводимых однородных интегральных представлений $GL(5, C)$.

Acta Physica Academiae Scientiarum Hungaricae, Tomus 32 (1—4), pp. 75—81 (1972)

STOCHASTIC SPACES*

By

D. I. BLOKHINTSEV

JOINT INSTITUTE FOR NUCLEAR RESEARCH, DUBNA, USSR

(Received 11. X. 1971)

The phase fluctuations of the wave propagating in a stochastic homogeneous medium, particularly in a physical vacuum, are calculated. The notion of stochastic space is introduced. It is shown that to obtain convergent results in the relativistic case it is necessary to introduce a "cut-off" factor.

1. Introduction

This work is an extension of a method suggested earlier [1] for calculating wave propagation in a medium with random characteristics. A more perfect method of integrating the random phase equation is proposed, the averaging over the random phases is improved, and an application to quantum field theory is given.

In some cases it is found reasonable to introduce the notion of *stochastic space* [2].

2. Propagation of a plane wave

As the initial object we consider the plane wave:

$$\Psi_p(x) = u(p)\, e^{ipx}, \tag{1}$$

where

$$px = p^a x_a = Et - \vec{p}\vec{x},\ p(E, \vec{p}),\ E = \sqrt{p^2 + M^2}$$

is the wave momentum, the parameter M playing the role of the particle mass in quantum theory, and $u(p)$ is the wave amplitude.

If this wave is propagated in a medium with random characteristics, then as a first approximation we introduce a correction in the wave phase (1) which is assumed to be

$$\hat{S}(x) = px + \hat{\sigma}(x), \tag{2}$$

* Dedicated to Prof. L. JÁNOSSY on his 60th birthday.

where σ is a linear function of a certain random field $\hat{\Phi}(x)$. It is not difficult to show that this additional phase in the linear approximation satisfies the equation [1]*:

$$\frac{d\hat{\sigma}(x)}{d\tau} + \hat{F}(x) = 0 \tag{3}$$

where $\tau = nx$ and n is the vector with components $n^a = p^a/M$. It is obvious that $n^2 = 1$. Therefore τ is the proper time of the wave or, in quantum theory, the proper time of a particle with momentum p and mass M. $\hat{F}(x)$ is the linear function of the random field $\hat{\Phi}(x)$, which in the general case can be written

$$\hat{F}(x) = g n^\alpha n^\beta \ldots \hat{\Phi}_{\alpha\beta}(x)\,, \tag{4}$$

where g is a coupling constant and $\Phi_{\alpha\beta}(x)$ are the components of the field, $\hat{\Phi}(x)$, which may be a tensor of different rank.**

This field is expanded in the Fourier series

$$\hat{\Phi}_{\alpha\beta\ldots}(x) = \frac{1}{\sqrt{V}} \sum_k \frac{1}{\sqrt{2\omega_k}} e^\lambda_{\alpha\beta} \left\{ \hat{a}^+_{k\lambda}\, e^{ikx} + a_{k\lambda}\, e^{-ikx} \right\}. \tag{5}$$

Here $e^\lambda_{\alpha\beta}$ is the tensor defining the polarization of the wave (λ), and

$$\frac{\hat{a}^+_{k\lambda}}{\sqrt{2\omega_k}} \quad \text{and} \quad \frac{\hat{a}_{k\lambda}}{\sqrt{2\omega_k}}$$

are amplitudes of the random Fourier series. Vector k has components $k = (\omega_k \vec{k})$, $\omega_k = \omega(\vec{k})$. In particular, for the field obeying the Klein equation $\omega_k = \sqrt{k^2 + \mu^2}$, where μ is the particle mass for the field $\Phi(x) \cdot V = \mathrm{L}^3$ is the normalization volume. Below, this is assumed to be infinite. Expressing x as $x = x_{\parallel} + x_\perp$ | and $x_{\parallel} = n(nx) = n\tau$ by means of Eqs. (4) and (5), from Eq. (1) we obtain

$$\hat{\sigma}(x) = ig \frac{1}{\sqrt{V}} \sum_k \frac{1}{\sqrt{2\omega_k}} \frac{1}{\Omega_k(p)} (n^\alpha n^\beta \ldots e^\lambda_{\alpha\beta}) \left\{ \hat{a}^+_{k\lambda}\, e^{-ikx} - \hat{a}_{k\lambda}\, e^{-ikx} \right\} f(r_0, x_\perp), \tag{6}$$

where $f(\tau_0, x_\perp)$ is an arbitrary function of $x_\perp$ depending on the choice of initial conditions at $\tau = \tau_0$. In what follows it is assumed that $\tau_0 = -\infty$ and $f(-\infty, x_\perp) = 0$. The quantity $\Omega_k(p)$ is an invariant frequency:

$$\Omega_k(p) = \frac{1}{M}(kp). \tag{7}$$

* The notations used here are somewhat changed from those of [1] and a proper time τ is introduced instead of the time t.

** The spinor field is not considered when $\hat{F}(x)$ could not be a linear function of the spinor $\hat{\Phi}(x)$.

In all cases but that of a scalar field, the quantity $\hat{\sigma}(x)$ may be represented in the form

$$\hat{\sigma}(x) = p^{\alpha}\hat{\xi}_{\alpha}(x)\,, \tag{8}$$

where $\xi_{\alpha}(x)$ has the meaning of a random displacement of the coordinate x. This fact allows us to consider not only the initial space $R_4(x)$ (here called the reference space) but also the *stochastic* space $R_4(\hat{x})$. The coordinates of this latter space are connected with the coordinates of the points of the reference space by the transformation

$$\hat{X} = x + \hat{\xi}(x) \tag{9}$$

and are random quantities depending on the random field, so that labelling of events in the stochastic space is probabilistic.

The meaning of the concept of *stochastic space* or *stochastic geometry* in general goes beyond the scope of the present article (see [2], § 41, 44, 45).

3. Calculation of averages

We represent the Fourier amplitude $\hat{a}_{k\lambda}$ of the field in the form

$$\hat{a}^{+}_{k\lambda} = A_{k\lambda}\, e^{i\hat{\Theta}\,k\lambda},\ \hat{a}_{k\lambda} = \hat{A}_{k\lambda}\, e^{-i\hat{\Theta}k\lambda}\,; \tag{10}$$

where $Z\hat{A}_{k\lambda}$ and $\hat{\Theta}_{k\lambda}$ are real quantities. Eq. (6) can thus be rewritten in the form

$$\hat{\sigma}(x) = -\,2\sum_{k} N^{\lambda}_{k}\,\hat{A}_{k\lambda}\sin\,(kx+\hat{\Theta}_{k\lambda})\,, \tag{11}$$

where

$$N^{\lambda}_{k} = g\,\frac{1}{\sqrt{V}}\,\frac{1}{\sqrt{2\omega_k}}\,\frac{1}{\Omega_k(p)}\,(n^{\alpha}n^{\beta}\,\ldots\,e^{\lambda}_{\alpha\beta})\,. \tag{12}$$

In the theory of classic fields the random field distribution is specified by the functional $dw\{\hat{\Phi}(x)\} \geq 0$. This functional is here assumed to have the form

$$dw\{\Phi(x)\} = \prod_{k} e^{-\frac{A^2_k}{\Delta^2_k}}\,\frac{dA_k}{\sqrt{\pi}\,\Delta_k}\,\frac{d\Theta_k}{2\pi}\,. \tag{13}$$

i.e. there is normal distribution of amplitudes A_k with dispersion Δ_k, and uniform distribution of phases Θ_k. (For the sake of simplicity cep Λ and the polarization index for the amplitudes $\hat{A}_{kl}$ and phases $\hat{\Theta}_{k\lambda}$ have been omitted.)

From the definition of $dw\{\hat{\Phi}(x)\}$ we have for the average values of a) the wave $\Psi_p(x)$:

$$\langle \Psi_p(x) \rangle = U_p e^{ipk} \int e^{i\hat{\sigma}(x)} dw\{\hat{\Phi}(x)\} \tag{14}$$

and b) the interference correlation of two waves $\Psi_{p'}(y)$ and $\Psi_p(x)$:

$$\begin{aligned} \langle \overline{\Psi}_{p'}(y) \Gamma \Psi_p(x) \rangle = (U_p \cdot \Gamma u_p) \exp\{-i(p'y - px)\} \times \\ \times \int \exp\{-i\hat{\sigma}_{p'}(y)\} \exp\{-i\hat{\sigma}_p(x)\} dw\{\Phi(x)\}, \end{aligned} \tag{15}$$

where Γ is any spinor operator. Note that at $x = y$ and $\Gamma = \gamma^\mu$ (γ^μ is the Dirac matrix) correlation (15) coincides with the so-called "vertex" part known from quantum field theory.

Now inserting distribution (13) in Eq. (14) and integrating over A_k and Θ_k, we get

$$\int \exp\{i\hat{\sigma}(x)\} dw\{\Phi(x)\} = \exp\{-Q_p(x)\} = \prod_k R_k, \tag{16}$$

where

$$R_k = \exp\left\{-\frac{g^2}{2} \Delta_k^2 N_k^2 + \ln I_0\left(\frac{\Delta_k^2 N_k^2}{4}\right)\right\}. \tag{17}$$

Here $I(z)$ is the Bessel function. According to Eq. (12), $N_h = 1/\sqrt{V}$, so that as $V \to \infty^3$ the sum of InI_0 over k approaches the order of magnitude $0(1/V^2)$ and may be omitted. This justifies the native operation of replacing $\cos \Theta_k$ and $\sin \Theta_k$ in the exponential by their average values, which are equal to zero. Inserting (17) in Eq. (16) and making the transition to the limit $V \to \infty^3$ we obtain

$$R_p(x) = \frac{g^2}{2} \int \frac{d^3 k}{2\omega_k} \frac{\Delta_k^2}{\Omega_k^2(p)} (n^\alpha n^\beta \ldots e_{\alpha\beta}^\lambda)^2. \tag{18}$$

This equation is relativistically invariant if and if the dispersion Δ_k^2 is an invariant. Provided the field $\Phi(x)$ is not connected with a special direction in the Minkovsky space $R_4(x)$, then the only possibility is to assume that $\Delta_k^2 =$ const. is constant, i.e. that amplitudes A_k obey one and the same distribution law independently of the vector k. This supposition leads immediately to divergences in the integral (18): namely

$$Q_p(x) = \frac{g^2}{2} \ln \frac{p_{\max}}{M} \tag{19}$$

and $p_{\max} \to \infty$. At $\mu = 0$ there appears a divergency on the lower limit, too.

The correlation (15) is calculated in a similar manner. To make the calculation simpler we give the result for $x = y$:

$$\int \exp\{-i\hat{\sigma}_{p'}(x)\} \exp\{i\hat{\sigma}(x)\}\, dw\{\hat{\Phi}(x)\} = \exp[-Q_{pp'}(x)] \tag{20}$$

and in this case

$$Q_{p'p}(x) = \frac{g^2}{2}\int \frac{d^3k}{2\omega_k} \Delta_k^2 \sum_{\lambda} \left\{ e^{\lambda}_{\alpha\beta\ldots}\left[\frac{n_{\prime}{}^{\alpha} n'^{\beta}}{\Omega_k(p')} - \frac{n^{\alpha} n^{\beta}}{\Omega_k(p)}\right]\right\}^2. \tag{21}$$

This correlation, like the quantity (18), turns out to be divergent for $\Delta_k^2 =$ const. Note that Δ_k^2 may be considered as a form factor ensuring convergence of the inetgrals in (18) and (21). If it is considered as a function of the invariant $\Omega_k(p)$ (the remaining invariants from k and p are constant), then the quantities $\Theta_p(x)$ and $Q_{p'p}, (x)$ are invariant, too (which must be the case in relativistically invariant theory). The quantity $Q_p(x)$ is simply a number and $Q_{p'p}(x)$ a function of only $q^2, q = p' - p$ (if p' and p are on the mass shell, the invariant $qp = 0$ is zero).

4. The quantum field

In the case under consideration the random amplitudes $\hat{a}^{+}_{kl}$ and $\hat{a}_{k\lambda}$ are the operators obeying the commutation relations

$$[\hat{a}_{k\lambda}\, \hat{a}^{+}_{k'\lambda'}] = \delta_{kk'}\, \delta_{\lambda\lambda'}. \tag{22}$$

The average over the measure $dw\{\Phi(x)\}$ should now be replaced by the average over the wave functional $\Omega_0\{\Phi(x)\}\varrho$, which is an analogue of the quantity $\sqrt{dw_0\{\Phi(x)\}}\exp iS_0(\hat{\Phi})$ where $S(\hat{\Phi})$ is the functional phase and the mark 0 signifies the vacuum state of the field $\Phi(x)$. Using the usual notations we rewrite Eqs. (16) and (20) in the form

$$e^{-Q_p(x)} = \langle 0|e^{i\hat{\sigma}_p(x)}|0\rangle, \tag{16}$$

$$e^{-Q_{p'p}(x)} = \langle 0|^{-i\hat{\sigma}_{pi}(x)} \cdot e^{i\hat{\sigma}_p(x)}|0\rangle, \tag{20}$$

where $\langle 0|\hat{L}|0\rangle$ denotes the vacuum-expectation value of the field $\hat{\Phi}(x)$. Further calculations are based on the relations

$$\langle 0|\exp(\hat{A}^{+}_k + \hat{A})|0\rangle = \exp\frac{1}{2}[\hat{A}_{k'}\, \hat{A}^{+}_k] \tag{23}$$

$$\langle 0|\exp(\hat{A}^{+}_k + \hat{A}_k)\exp(\hat{A}^{+}_{k'} + \hat{A}_{k'})|0\rangle =$$

$$= \exp\left(\frac{1}{2}[\hat{A}_{k'}\, \hat{A}^{+}_k] + \frac{1}{2}[\hat{A}_{k'}\, \hat{A}^{+}_{k'}] + [\hat{A}_{k'}\, \hat{A}^{+}_{k'}]\right), \tag{23'}$$

where $[\hat{A}, \hat{B}]$ denotes the Poisson bracket, which is assumed to be the c-number. The calculation of the averages in Eqs. (16) and (20) with the help of Eqs. (23) and (23′) and the expression (12) for $N_{k\lambda}$ leads exactly to the classic formula (18) and (21), if $\Delta_k^2 = 1$.

Thus, the divergent result is a consequence of the assumption of *vacuum isotropy* ($\Delta_k^2 = \text{const.}$), which follows from the requirement of relativistic invariance.

Formula (21) is closely connected with the theory of so-called "coherent states" [5]. The model of the vertex in this latter differs from the considered fluctuations of the spinor particle coordinate $\xi(x)$ in that the zero harmonic is assumed to be predominant, so that the displacement $\xi(x)$ is independent of x.

It is useful to note that in the case of the vector field $\hat{\Phi}_a(x)$ the mean square displacement $\xi(x)$ defined by Eq. (8) is

$$\langle \xi_\alpha^2(x) \rangle = \frac{g^2}{M^2} \int \frac{d^3 k}{2\omega_k} \frac{1}{\Omega_p^2(p)} \sum_\lambda (e_\alpha^\lambda)^2 . \tag{24}$$

For $|\vec{p}| \ll M$, we obtain

$$\langle \xi_\alpha^2(x) \rangle = \frac{g^2}{M^2} \int \frac{d^3 k}{2\omega_k^2} \sum_\lambda (e_\alpha^\lambda)^2 . \tag{24'}$$

If $g = e$ is assumed to be equal to the electron charge and to denote its mass, Eq. (24′) coincides with the value of the square displacement of the electron coordinate $<\xi_\alpha^2(x)>$ which defines the Lamb shift of the level in the hydrogen atom (see [5,6]).

5. Gravitation

In [3] it was shown that if one considers the gravitational field fluctuations which arise from fluctuations of the energy-momentum tensor of the fields in the vacuum, one arrives at strongly divergent expressions for the fluctuations of the metric (length and time). The method developed here makes it possible to calculate the fluctuations of the wave phase which arise from zero-point fluctuations of the *free* gravitational field.

It is not difficult to show that in this case the function $\hat{F}(x)$ is

$$\hat{F}(x) = \frac{M}{2} \hat{h}^{\alpha\beta}(x) n_\alpha n_\beta , \tag{25}$$

where

$$\hat{h}^{\alpha\beta}(x) = \hat{g}^{\alpha\beta}(x) - g_z^\alpha \tag{26}$$

and $g^{\alpha\beta}$ is the metric tensor in the absence of gravitational waves. Among the quantities $\hat{h}^{\alpha\beta}(x)$ only four are independent. Bearing in mind these components, we represent $\hat{h}^{\alpha\beta}(x)$ as a series:

$$\hat{h}^{\alpha\beta}(x) = \frac{\gamma}{\sqrt{V}} \sum_k e_\lambda^{\alpha\beta}(a_{k\lambda}^{+} e^{ikx} + a_{k\lambda} e^{-ikx}). \tag{27}$$

In contrast to (5), a constant γ is introduced here which is defined in such a fashion that the energy of a gravitational wave should be equal to $\Sigma_k n_k h\omega_k$, where n_k are integers and $h\omega_k$ is the gravitational energy. On the other hand, this energy is expressed in terms of the integral of the energy-momentum pseudo-tensor (see e.g. [7]). This allows to determine the constant $\gamma^2 = \delta\pi k/c^2$, where k is the gravitational constant.

Performing the calculations analogues to those described in § 3 we are led to formulas (18) and (21) at $\Delta_k^{\varkappa} = 1$ and $g^2 = \gamma M^2$. If the usual dimensionality is restored, it is easy to satisfy oneself that in the case of the gravitational field the quantities $Q_p(x)$ and $Q_p{}'{}_p(x)$ are proportional to V^2gq, where q is the characteristic length defining the limits outside which the metric fluctuations may become essential.

It is seen from these calculations that, without artificially introducing a "cut-off" form factor, fluctuations of the phase $\hat{\sigma}(x)$ turn out to be indefinite. The same may be said about the fluctuations of the stochastic coordinate x in (9). This extreme dispersion of the averages $\langle \hat{\sigma}_p^2(x) \rangle$ and $\langle \xi_p^2(x) \rangle$ is due to the requirement of homogeneity of the vacuum ($\Delta_k^2 = \text{const}$). Physically it is clear that the above fluctuations can be restricted only by taking into account the effect of the particle itself on the vacuum; in other words, by taking into account a possible deformation of the vacuum in the vicinity of the particle. The introduction of the "cut-off" factor may be thought of as a formal procedure for doing this.

REFERENCES

1. Д. И. Блохинцев, ДАН СССР, **166,** 574, 1966.
2. Д. И. Блохинцев, «Пространство и время в микромире», Наука, 1970.
3. D. Blokhintsev, Nuovo Cimento, **16,** 382, 1960.
4. V. A. Matveev and A. N. Tavkhelidze, JINR, E2-5141, Dubna, 1970.
5. Я. А. Смородинский, УФН, **39,** 325, 1949.
6. Т. Вельтон. Сб. «Вопросы причинности в квант. механике», ИЛ (1955), см. также T. Welton, Phys. Rev., **74,** 457, 1948.
7. Л. Ландау, Е. Лифшиц, «Теория поля»: ГИФМЛ, § 100, 1960.

СТОХАСТИЧЕСКИЕ ПРОСТРАНСТВА

Д. И. БЛОХИНЦЕВ

Резюме

В работе вычисляются флюктуации фазы волны, распространяющейся в стохастически однородной среде, в частности, в физическом вакууме. Введено понятие стохастического пространства. Показано, что в релятивистском случае для получения сходящихся результатов необходимо вводить обрезающий форм-фактор.

Acta Physica Academiae Scientiarum Hungaricae, Tomus 32 (1—4), pp. 83—93 (1972)

CURRENT PROBLEMS OF HIGH ENERGY COSMIC RAY PRIMARIES*

By

J. G. WILSON

UNIVERSITY OF LEEDS, LEEDS, UK

(Received 13. X. 1971)

Problems of measurement of the total energy spectrum of primary cosmic ray particles beyond 10^{17} eV are discussed, with the most recent conclusion that no significant change in the slope of the spectrum at higher energies has yet been established.

The determination of the nature of particles of extreme energy presents much more difficult problems, and the relationship of studies of primary composition to details of shower development in the atmosphere as these are presented in model formulations is examined.

In 1946 I collaborated with LAJOS JÁNOSSY in a short study of the interpretation of the sea-level low-energy muon spectrum [1] and I feel it appropriate that my contribution to this collection should relate to a continuing interest in cosmic ray spectra.

We are here concerned with problems arising about the primary radiation of high energy, that is to say of energy greater than about 10^{17} eV. In terms of absolute quantity, whether of number of particles or of energy transfer, this high energy region is insignificant; its cosmological importance rests upon the very existence of processes of acceleration to this great energy, and upon problems of survival of such particles during their lifetime of transmission. For this purpose, knowledge of the nature of the particles, the mass-spectrum, is as relevant as is the spectrum of total-energy and accordingly the immediate problem is to describe high energy cosmic-ray primaries in terms of both mass composition and of energy distribution.

The total-energy spectrum is known with fair confidence at least to energy about 10^{19} eV: the most recent estimate of the integral spectrum, which refers strictly to $3.10^{17}\text{ eV} < E_p < 10^{19}\text{ eV}$ is [2]:

$$N(>E_p) = (4.5 \pm 0.2)\, 10^{-10} \left(\frac{E_p}{10^{17}}\right)^{-(2.24 \pm 0.04)} m^{-2}\, s^{-1}\, sr^{-1},$$

an expression which is unlikely to be seriously in error at values well below the lower limit, and from which there is no strongly positive evidence of deviation over the decade up to 10^{20} eV. This final statement is essentially

* Dedicated to Prof. L. JÁNOSSY on his 60th birthday.

tentative: it takes account of the fact that what slight evidence there is for some deviation between 10^{19} eV and 10^{20} eV is in the sense towards which all defects of treatment must be expected to move it. It is the residue of a very much larger deviation which is not sustained in the face of searching analysis, and there are no grounds for confidence that this residue is not of the same nature.

In comparison, our knowledge of the mass spectrum is rudimentary, typical work [3, 4, ;5, 6, 7] being directed towards the probably unrealistic distinction between a pure proton primary beam and a pure heavy-particle one. This situation bears strongly on the ideas which must be developed in shower studies in the next few years.

When a primary particle initiates a shower in the atmosphere, there are many parameters describing it which can be derived from current observational techniques: these may refer to a "number of (indistinguishable) particles", energy-loss in standard detector assemblies, the density of muons, radio signals at various frequencies, all of these either as point values or as lateral distributions from the shower axis. For the present article we ignore a major complication by considering only vertical showers.

Directly measured parameters are all fairly strongly related to total-energy but less strongly to mass-composition. However, derived parameters chosen to minimise sensitivity to total-energy can be obtained which are mass-sensitive. It is therefore a necessary procedure to obtain several directly measured parameters for each shower, for although in principle two alone are required, for reasons which will now be developed it is desirable that if possible more than one mass-sensitive parameter should be obtained, so that the degree to these are consistent is part of the information available.

The chain of development from an incident primary particle making its first interaction in the atmosphere to the derivation of a ground parameter descriptive of the particle in some way, involves a succession of stages at which there is a limitation of accuracy.

1. There are instrinsic fluctuations of shower development from identical primaries, while the actual form of this development is determined by incompletely understood features of high energy nuclear interactions. Our approach to the latter feature is to develop a range of "models" of the nuclear processes, and what follows after them [8], from which we discard those which are not consistent with what is directly observable of shower development. The influence on interpretation which arises from residual model uncertainties is approached by studies to determine to what extent a particular parameter is "model-sensitive". Those which are not form a still narrower range of acceptable models.

Similarly, chosen parameters may or may not be "fluctuation-sensitive", but the implications of this are more complex, for the degree of fluctuation

is likely to be a feature which is strongly mass-sensitive (since in a first approximation showers from primaries of mass N and total-energy E may be considered as superpositions of N separate showers from primaries of mass unity and of energy E/N). For a parameter chosen to be strongly related to total-energy but not to primary mass, a fluctuation-insensitive feature is required.

2. At these high energies all shower data come from sampling techniques: the actual sample at each detector is subject to statistical variations, and the derived signal from that detector to further instrumental uncertainties.

3. The various uncertainties noted above place a limit upon the accuracy of measured shower parameters in the broadest sense. For example, a parameter related closely to total energy and, as far as possible, mass-insensitive, is appropriate for the determination of a total energy spectrum. However, not only can the value of total energy derived from such measurements differ from the true one, but also the axis of the shower can be wrongly located. Since the spectrum is on the form "particles m^{-2} s^{-1} sr^{-1}", uncertainty of core (axis) location will be reflected in the reputed collecting area over which showers have been selected.

Against this background, certain general features of shower detecting systems arising at the determination both of total-energy and mass-composition of primary particles can be set out. But in doing so it remains to consider whether the aim is to ascribe to individually observed showers both a total-energy and a mass for the primary particle, or whether the more modest target to make very broad generalisations about the mass-composition of the primary beam is accepted. In terms of scientific value the latter must be considered insufficient, unless it is indeed all that can be obtained. It is unlikely that the primaries, when they reach the earth, can indeed be of simple mass-composition.

On all grounds the best total-energy estimate for each measured primary seems an essential first objective. This is so as strongly because of its relationship to the derivation of mass-sensitive parameters as in its own significance, for since most directly observable features are strongly sensitive to total-energy the precision of derived mass-sensitive features must depend upon the best possible information about total-energy.

This particular measurement has been the subject of detailed investigation, and general features have been established, if along rather predictable lines. For the immediate future it depends upon the traditional measurements either of all "particles" or of muons, rather than upon any prospective rapid development of the more recently identified shower features. The classical parameter, still widely used in the literature, is the "number of particles" (N) in the shower in the plane of observation. In parallel with this is the "number of muons" (N_μ) which refers to a much smaller number of individual par-

ticles, and which is therefore determined less well statistically in sampling detectors of similar area. Both suffer from the weakness that they peak at the shower axis, while, for the energy range that is the subject of this article, the sampling disposition of detectors ensures that for most showers no near-axial measurements are possible.

There is an unreality in quoting parameters towards which a significant and sometimes even a dominant part comes from a region totally unexplored! This is particularly so as regards the total "number of particles", for this quantity is known to show very large fluctuations near to the axis, and arising from the dominant influence of locally initiated cascades. What is quoted, in the event, in some publications, is based on information which does not include any knowledge of this region, and for which, therefore, some conventional value is introduced to cover the way in which particle density increases near the axis. It is not certain that the same convention for this purpose is used in all instances, and so that the various values of "N" in fact all refer to the same thing.

For muons this particular problem is less marked, since not only is the lateral structure for muons much flatter than that of all "particles", but also the muon component as a whole shows less marked fluctuations, and in particular is not dominated by the products of late nuclear interactions. In principle, however, this measurement also attaches weight to an important region in which no measurements are made.

It is now well-understood that relatively local fluctuations of shower development became less important with increasing distance from the shower axis, in fact in the region where direct observations are made for the more energetic showers, and some workers, particularly those associated with the collaborative studies from British Universities at Haverah Park, near Leeds, have for some time quoted their observational material in terms which exclude any claim to know what is taking place in the axial zone. It is likely, as indicated in previous paragraphs, that such a limitation does in fact apply to other measurements which do not explicitly refer to it, with the weakness that the precise terms of exclusion, or even its existance, are not set out.

We proceed therefore, from the starting point that total-energy measurements are to be derived from observations within the lateral spread of particles away from the axis and identified in relation to (i) the reduction of importance of intrinsic shower fluctuations with increasing axial distance, (ii) the disposition of detector elements, and (iii) the statistical weight of the observation, which gains from the use of large detectors, but which clearly falls off with axial distance. We further require that the manner of exclusion of near-axial data should be clearly defined.

Two approaches have been made to this problem. The earlier of these simply stated radial limits embracing the region containing suitable measure-

ments and was of the form $f(r_1, r_2)$ where 'f' might for example, have been "number of particles" or "number of muons", but was actually first applied at Haverah Park where it was related to another feature of importance.

The detectors use at Haverah Park are deep water-Čerenkov tanks, each unit is of area rather more than 2 m^2 and of depth 1.2 m. Čerenkov light is diffused upward, from the lining of the tank, and the disposition is designed to give uniform sensitivity for Čerenkov light emitted at any point in the detector, and in any direction. The measured signal is thus closely related to the energy loss of the shower complex in a depth of rather more than 0.1 atmosphere of water, and thus to a shower parameter identified by the mode of operation of a particular type of detector. With this detecting device, and at the relevant axial distances, the parameter sampled can be readily identified. Muons which remain relativistic through the full depth of detector contribute a signal proportional to their energy loss, that of any singly-charged relativistic particle. The electromagnetic cascade is almost completely absorbed, with a signal proportional to the total energy carried in it, while the residual contributions (slower muons, non-absorbed electromagnetic component) are both small and calculable. (While this article is deliberately confined, for brevity, to problems of vertically incident primaries, it is interesting to note that for strongly inclined showers, in which the component reaching sea-level consists entirely of energetic muons, these particular detectors remain essentially volume-sensitive, and, since the area presented in the direction of the shower does not vary greatly, of almost constant statistical accuracy).

This property, that detectors by their mode of operation define the precise feature of the shower complex detected, is brought out in a very clear way in deep water-Čerenkov tanks, but it has to be understood that it is something common to all detectors. An important property of water tanks 1.2 m deep is that the electro-magnetic component is almost completely absorbed. This is a clear-cut operation. However, the electromagnetic component in the shower regions under consideration carries by far the greater part of its energy as photons rather than as electrons, and the "number of particles" measurement, counting electrons as units and ignoring photons is a shower description which is definable only for very thin detectors in which electrons all contribute equally to the signal, and equally with muons, and no photons are converted to make any contribution. Such detectors have not been realised on the scale of many square metres required for the work on large showers. Geiger tubes, under thin covering, possibly offer the closest approximation, and it was the use of such counters, individually of small area and responding in a simple yes/no manner, which made the "number of particles" concept attractive. As normally used the shortcomings even of Geiger tubes in meeting this criterion are manifest. Scintillators offer yet a different example. They

are not 'thick', with near-total absorption properties, but certainly do not approximate to the ideal thin detector. The signal in them from an electron is not equivalent to that from a muon, nor are all photons ignored.

The detection and description of muons as a straightforward counting operation appears, and is in fact, more nearly achieved: muons are isolated by prior absorption of the electromagnetic component, and are thus counted above a well-determined energy threshold. Here again, however, except in a thin yes/no detecting decive, divided into detecting units for which this simple response is meaningful, the nature of a detector determines the instrumental spread of signal from relativistic muons, and in this way influences the statistical nature of the recorded information.

This discussion has been limited to modes of observation which lead to the limited range of parameters which in the immediate future seem certain to form a basis of the most reliable measurements of total-energy for individual primaries, and up to now relates specifically to the nature of the individual samples by whatever technique which form the basis of the determination of a parameter descriptive of an observable feature and intended to transcend details of sampling.

The choice of this parameter, however, must take account of the accuracy of samples, the disposition of detectors yielding the information, and background knowledge regarding, for example, the extent to which properties such as the lateral structure function (distance from the shower axis) may be assumed for a particular shower on the basis of measurements on others. Here two features are worth notice.

Firstly, for a particular detector and size of shower, there will be some range of axial distances from which the most reliable sample measurements are derived, this being determined by the reducing importance of intrinsic fluctuations in the shower at large distances from the core, set against the loss of statistical accuracy in a sampling detector of constant area as this distance increases. If the response of an array of detectors to a shower covers observations at a large range of axial distances, there will be a selection of these for which the observations will prove most reliable. The question must arise whether a local value based entirely within this most reliable region is not a better parameter than one expressed as an integrated effect over the full range of distances available for sampling. This distinction has been examined at Haverah Park and in the notation of work published for that station is that between '$E(r)$ and '$\varrho(r)$', the total enery loss integrated from 'r' metres from the axis outwards in the characteristic thickness and material of the detectors used, 1.2 m water, and the density of this loss measured at a single chosen distance 'r'. The significance of 'r' is not the same in these two notations. In the event the second has been chosen, both on account of its intrinsic internal precision, but also because it can take account of the fact that it can be related

to the actual disposition of detectors so as to be rather insensitive to the actual location of the shower axis. This feature is much more clearly apparent if actual examples are examined, but in the light of the following paragraphs it will not be pursued here.

The second point only modifies what has already been stated. Even if a very favourable parameter, itself of necessity related to distance from the shower axis, can be derived without the location of this axis, its use for the determination of the total-energy spectrum and also as basic data upon which measurements of other parameters can be founded, cannot take advantage of this property. The spectrum determination is essentially related to numbers of showers of which the axis falls within a defined area: the definition of this area is as necessary as the definition of the shower size parameter, and although one may attempt to define this area in such a way that uncertainties of core location move similar numbers of showers of a particular size into and out of it, this is an expedient which should surely be invoked as little as possible. Similarly other shower parameters may not inevitably have the same geometrical properties as those discussed above, and may require knowledge of the actual position of the axis of a more precise nature.

It thus appears that the observation of an optimum observable parameter (for the large showers which we are discussing in this article) (i) is best given as a unit area value at some most effective radial distance, and (ii) should preferably be related to the best possible location of the core position. The argument has been developed in relation to the Haverah Park system, and perhaps came first to attention there because the measurable feature was not one of those conventionally used in shower description and because the array had, from the outset, large distances between the detectors, but the broad argument seems to apply to the most effective use of whatever form of shower detection, which is currently sufficiently developed for the purpose, which is used.

The practical application of these principles presents complications, since all large detector systems are constrained by external factors, in respect of the total deployment of equipment. Accurate core location is certainly best accomplished with a rather closely spaced array of detectors in the region in which cores are to be located, on the other hand, the corresponding accurate determination of the characteristic parameter requires large area detectors at much larger spacings. This effect has not up to now been completely resolved, the most favourable conclusion will emerge if it proves that accurate direct core location is adequate if available only for a fraction of all showers used for spectrum measurements. This will depend upon the extent to which the lateral structure of showers, when it can be measured, is identical from one shower to another. If this is so within small limits, the location of core position for many showers with axes not falling in an area deliberately set out for most

accurate core location will be deduceable to a useful degree, if not to what is available for the most fully studied showers. This secondary level of core location may not be adequate for some workers now studying the more recently identified shower properties, and it may be that the most accurately determined core positions will alone provide them with suitable material.

The discussion of the preceding paragraphs refers to the problem of the use of the best understood, and at present the most reliably measurable shower features, and in particular that of their relationship with parameters directly chosen for total-energy studies. The connection of these measurements to total-energy has been refined to minimise the effects of intrinsic shower fluctuations, but it is still subject to the incompleteness of our knowledge of the basic features of shower development which we included in the phrase "model-sensitivity". The derived parameters, which must form a large part of the approach to primary mass composition are, however, even much more "model-sensitive" and the treatment of the whole problem of models is likely to prove the limiting factor in the full investigation of the primary radiation at energies above 10^{17} eV.

Critical comments on model problems must necessarily be of a detailed nature and these are outside the scope of this article: only some general factors will be considered.

The main object of study is the nucleonic cascade, its self-development and the way in which it feeds energy into the secondary components arising respectively from charged and neutral pions. The subsequent growth and transformations of these components is considered well understood. Interest centres on nuclear collisions, the survival of a leading particle, the development of an attendant nuclear component, and on pion production through the medium of double or single fireballs, isobars and other possible mechanisms. It is in this area, where even currently recognised phenomena allow wide scope for variations of treatment (since there are no alternative sources of information, or for that matter, within several orders on magnitude) that the quite striking differences in model predictions arise. Moreover, it cannot be excluded that hitherto unrecognised features are operative at these energies. In the comparison of showers from heavy primaries with those from protons, the nature of the first interaction of a heavy primary is a further area of uncertainty where the assumptions made are not always clearly presented.

To perform full Monte Carlo simulations in sufficient quantity for even the lower energy limit of the present discussion (10^{17} eV) is still very far from practicable and hence mixed treatments are invoked in which average value calculations are introduced whenever this seems permissable. It is fortunate for this essential simplification that attention should be focussed on the non-axial parts of showers where local deviations from the average are generally held to be minimal.

Broadly, two types of distinction may be expected to arise from model calculations. The treatment may bring out an average shower development, and particularly a region of maximum activity, roughly the region around shower maximum, which may be expected from a proton primary to move smoothly through the atmosphere with increasing energy. This feature is of importance for several reasons. It must be consistent with the predictions of its particular model for general observation, it is the region of special importance for certain of the parameters of value for composition studies (atmospheric Čerenkov light, radio emission), and, if it behaves as we imagine, is something which distinguishes the behaviour of protons from that of heavy primaries insofar as these may be thought of as leading to a superposition of protonlike sub-showers, each of correspondingly reduced energy. However, it is a characteristic of shower development which has some weaknesses for the purpose of distinguishing primary composition. While its sensitivity, in a simple way to primary composition may be confidently expected, it is something that is likely to be sensitive in a similar manner to any substantial variation of the details of interaction at energies near to that of the primary particle. Moreover, if measured features such as radio pulses from showers and Čerenkov light in the atmosphere are closely tied to it, they cease to be independent characteristics, and the significance of supporting agreement between their conclusions is limited.

It is for these reasons that some stress should be placed upon the second possible distinction: this is the extreme variations which may be expected to occur in shower development from proton primaries, arising from the very different configurations, as regards depth in the atmosphere, which are possible for the first two or three interactions of a proton primary which retains a significantly high proportion of its initial energy over these stages.

The significance of this shower property will be apparent. Probably the most important, if the simplest, question about primary composition is whether there are or are not any protons among the primaries, and if so, in what quantity? A property characteristic of protons in the most extreme fluctuations of behaviour would be expected to be totally smoothed out for heavier nuclei, even for alpha-particles, but would serve, subject to model capability, to estimate the amount of the whole proton fraction. It would have an incidence which would largely separate it from the considerations of average development which were the object of the last paragraph but one, and in this way would add in a quite important way to conclusions about mass. This diversity of derived parameters bearing upon the mass composition question should be regarded as undoubtedly valuable, not least because it is so unclear at present to what degree of detail this problem can be resolved in the relatively near future.

While the general purpose of this article is to comment upon ways of measuring the characteristics of the primary radiation, and in particular upon the background against which knowledge of the composition of primaries may be expected to be established, a rather discouraging feature of the total-energy spectrum, as it is expressed in paragraph three, should perhaps be noted in conclusion. The degradation of primary cosmic ray particles by interaction with the 3K radiation has, for some time, been regarded as an important test of the existence of this radiation, and is expected to come into operation rather abruptly somewhere in the region 10^{19}—10^{20} eV. Until recently it seemed established that the form of total-energy spectrum first put forward by LINSLEY [9] described at least the earlier part of this range, and this spectrum was much flatter than that at energies one or two decades lower with index perhaps as low as 1.6. Against so flat a spectrum any abrupt fall arising from 3K interaction would have been relatively easy to detect. Against the much steeper spectrum which is now proposed, and with the fuller understanding of the way in which weaknesses of treatment have an innate tendency to flatten the spectrum, one can only accept that the establishment of this most important cosmological feature will prove very much more difficult than has hitherto been supposed.

*

In this article I have drawn widely upon discussions with my colleagues in four universities who work at Haverah Park, and from their expert understanding of much of the detailed analysis upon which work in this field depends, for all of which I am most grateful.

REFERENCES

1. L. JÁNOSSY and J. G. WILSON, Nature **158**, 450, 1946.
2. D. ANDREWS, D. M. EDGE, A. C. EVANS, R. J. O. REID, R. M. TENNENT, A. A. WATSON, J. G. WILSON and A. M. WRAY, Paper EAS-17, 12th International Conference on Cosmic Rays, Hobart, Conference Papers (University of Tasmania), **3**, 995, 1971.
3. H. R. ALLAN, J. K. JONES, N. MANDOLESI, J. H. PRAH and P. SHUTIE, Paper EAS-50, 12th International Conference on Cosmic Rays, Hobart, Conference Papers (University of Tasmania), **3**, 1102, 1971.
4. J. C. EARNSHAW, A. C. MACHIN, K. J. ORFORD, D. R. PICKERSGILL and K. E. TURVER, Paper EAS-44, 12th International Conference on Cosmic Rays, Hobart, Conference Papers (University of Tasmania), **3**, 1081, 1971.
5. P. R. BLAKE, H. FERGUSON and W. F. NASH, Paper EAS-31, 12th International Conference on Cosmic Rays, Hobart, Conference Papers (University of Tasmania), **3**, 1043, 1971.
6. A. M. HILLAS, J. D. HOLLOWS, H. W. HUNTER and D. J. MARSDEN, Paper EAS-19, 12th International Conference on Cosmic Rays, Hobart, Conference Papers (University of Tasmania), **3**, 1007, 1971.
7. L. S. WILSON, J. ULRICHS, C. B. A. MCCUSKER, J. G. LOY and A. D. BRAY, Paper EAS-27, 12th International Conference on Cosmic Rays, Hobart, Conference Papers (University of Tasmania), **3**, 1025, 1971.
8. A. M. HILLAS, D. J. MARSDEN, J. D. HOLLOWS and H. W. HUNTER, Paper EAS-18, 12th International Conference on Cosmic Rays, Hobart, Conference Papers (University of Tasmania), **3**, 1001, 1971.
9. J. LINSLEY, Proc. 8th International Conference on Cosmic Rays (Jaipur), **4**, 77, 1963.

СОВРЕМЕННЫЕ ПРОБЛЕМЫ ИЗУЧЕНИЯ ПЕРВИЧНЫХ ЧАСТИЦ КОСМИЧЕСКОГО ИЗЛУЧЕНИЯ ВЫСОКОЙ ЭНЕРГИИ

Й. Г. ВИЛЬСОН

Резюме

Обсуждены проблемы измерения полного энергетического спектра первичных частиц космического излучения с энергией выше 10^{17} эв в свете новейших итогов, согласно которым до сих пор ещё не было установлено существенное изменение в наклоне спектральной кривой при высоких энергиях. Определение природы частиц с экстремально высокой энергией представляет собой более сложную задачу, и рассмотрена связь излучения первичного состава с деталями развития ливней в атмосфере в виде их модельных представлений.

Acta Physica Academiae Scientiarum Hungaricae, Tomus 32 (1—4), pp. 95—98 (1972)

REPRESENTATION OF BOSONS BY FERMIONS*

By

F. Bopp

SEKTION PHYSIK DER LUDWIG MAXIMILIANS-UNIVERSITÄT, MÜNCHEN, GFR

(Received 16. X. 1971)

Starting from the proposition that all quantum processes can be understood as a cooperation of a set of elementary processes (dichotomic processes), we prove how Bose processes can be represented by an enumerable set of Fermi operators.

1. Introduction

This paper is written on the occasion of the sixtieth birthday of Lajos Jánossy to whom that experiment [1] is due which clarifies so drasticly the fundamental difference between classical and quantum physics. We do not believe that it should be possible to return to classical physics. We rather believe that it should be possible to understand quantum physics independently from classical physics which only appears as an approximation. Both, classical and quantum physics, start as theories of their own right from fundamental basic ideas according to which either the one or the other system of mathematical principles is as evident [2] as the axioms of the Euclidean geometry in its own realm of ideas.

Classical physics may be derived from the idea that all events are to be understood as motions of matter points [3], quantum physics from the idea that all events are produced by creation and annihilation of fundamental particles, say, urfermions [4]. In the present paper we deal with the particular question, how to describe the creation and the annihilation of bosons by urfermion processes [5].

2. Representation of Bose by Fermi operators

To this end we introduce an infinite set of operators

$$\psi_n^+, \psi_n, \quad n = 1, 2, 3 \ldots, \tag{1}$$

which satisfy the commutation relation for fermions

$$\{\psi_m^+, \psi_n\} = \delta_{mn}, \{\psi_m^+, \psi_n^+\} = \{\psi_m, \psi_n\} = 0 \tag{2}$$

* Dedicated to Prof. L. Jánossy on his 60th birthday.

These operators may describe the creation and the annihilation of n bosons in one point and at once. Be $|n>$ the state vector for n bosons in a single point, we obtain for $n = 1, 2, 3 \ldots$

$$\psi_n^+ |0> = |n>, \psi_n |n> = |0>. \tag{3}$$

The latter equation follows from the first one if

$$\psi_n |0> = 0. \tag{4}$$

It is more convenient to consider the following combination of the ψ^+'s and ψ's:

$$\chi_n^+ = \psi_n^+ \prod_{l \neq n} \psi_l \psi_l^+, \chi_n = \psi_n \prod_{l \neq n} \psi_l \psi_l^+. \tag{5}$$

Hence

$$\chi_n^+ |0> = |n>, \chi_n |0> = 0, \tag{6}$$

and if $m, n \neq 0$:

$$\chi_m^+ |n> = 0, \chi_m |n> = \delta_{mn} |0>. \tag{7}$$

To prove these relations we must take into account that

$$\psi_l \psi_l^+ |0> = |0>. \tag{8}$$

The Eqs. (6) follow at once. If $m \neq n$, χ_m^+ and χ_m contain the factor $\psi_n \psi_n^+$ which annihilates $\psi_n^+ |0>$. If $m = n$, both Eqs. (6) are equivalent to

$$\psi_n^+ |n> = 0, \psi_n |n> = 0.$$

The Hilbert space is spanned by the vectors $|0>$, $|1>$, $|2> \ldots$ Any Hilbert vector may be written as

$$|\varphi> = \sum_{n=1}^{\infty} a_n |n>. \tag{9}$$

If we introduce the matrix with one column

$$a = \begin{pmatrix} (a_1) \\ (a_2) \\ (.) \\ (.) \\ (.) \end{pmatrix} \tag{10}$$

all transformations in the Hilbert space are given by matrices of the following kind:

$$A = \begin{matrix} (A_{00}, A_{01}, \ldots\ldots) \\ (A_{10}, A_{11}, \ldots\ldots) \\ (\ldots, \ldots, \ldots\ldots) \\ (\ldots, \ldots, \ldots\ldots) \\ (\ldots, \ldots, \ldots\ldots) \end{matrix} \tag{11}$$

Hence we obtain from (7):

$$(\chi_n)_{\alpha\beta} = \delta_{\alpha 0}\,\delta_{\beta n}\,, \quad (\chi_n^+)_{\alpha\beta} = \delta_{\alpha n}\,\delta_{\beta 0}\,. \tag{12}$$

It follows easily:

$$\begin{aligned} &\chi_m\,\chi_n = 0\,, \quad \chi_m^+\,\chi_n^+ = 0\,, \\ &(\chi_m^+\,\chi_n)_{\alpha\beta} = \delta_{m\alpha}\,\delta_{\alpha\beta}\,, \\ &(\chi_n\,\chi_m^+)_{\alpha\beta} = \delta_{mn}\,\delta_{\alpha 0}\,\delta_{\beta 0}\,. \end{aligned} \tag{13}$$

Therefore we may write any matrix (11) as

$$A = A_{00}\,\chi_1\,\chi_1^+ + \sum_{n=1}^{\infty} A_{0n}\,\chi_n + \sum_{m=1}^{\infty} A_{m0}\,\chi_{0n}^+ + \sum_{m,\,n=0}^{\infty} A_{mn}\,\chi_m^+\,\chi_n\,. \tag{14}$$

That is a function of all χ^+'s and χ's, and according to (5) one of all ψ^+'s and ψ's. Any matrix A may be written as a function of urfermion operators.

Finally we apply this simple theorem to the creation and annihilation operators for bosons:

$$a^+ = \begin{matrix} (0 & 0 & 0 & 0 & \ldots) \\ (\sqrt{1} & 0 & 0 & 0 & \ldots) \\ (0 & \sqrt{2} & 0 & 0 & \ldots) \\ (0 & 0 & \sqrt{3} & 0 & \ldots) \\ (\ldots & \ldots & \ldots & \ldots & \ldots) \end{matrix}, \quad a = \begin{matrix} (0 & \sqrt{1} & 0 & 0 & \ldots) \\ (0 & 0 & \sqrt{2} & 0 & \ldots) \\ (0 & 0 & 0 & \sqrt{3} & \ldots) \\ (0 & 0 & 0 & 0 & \ldots) \\ (\ldots & \ldots & \ldots & \ldots & \ldots) \end{matrix}. \tag{15}$$

It is well known that

$$a^+\,a = N\,, \quad a a^+ = N+1\,, \tag{16}$$

where N is the operator for the number of bosons, and

$$[a, a^+] = 1\,. \tag{17}$$

According to (14) we obtain from (15):

$$a = \chi_1 + \sum_{n=1}^{\infty} \sqrt{n+1}\;\chi_n^+\,\chi_{n+1}\,, \quad a^+ = \chi_1^+ + \sum_{n=1}^{\infty} \sqrt{n+1}\;\chi_{n+1}^+\,\chi_n\,. \tag{18}$$

That is the urfermion representation of bosons.

3. Conclusion

It is shown that we may go back to urfermions even in the case of bosons. In general, it will be very inconvenient to do it really. But we should bear it in mind if we are dealing with the basic ideas of quantum physics.

REFERENCES

1. L. JÁNOSSY and ZS. NÁRAY: On interference phenomena at low intensities of light; Hungarian Academy of Sciences, Central Research Institute of Physics; September 1957.
2. The notion "evidence" is often misunderstood and even rejected by mathematicians and physicists, and that for different reasons. Clearly, evidence has nothing to do in proofs, and it may not replace experience. But mathematical principles even of tentative theories must be developed from certain basic ideas by evidence. For that, evidence is necessary in the process of the mathematization of ideas.
3. F. BOPP: Grundlagen der klassischen Physik in gegenwärtiger Sicht; Sitzungsber. d. Bayer. Akad. d. Wiss.; Math.-naturw. Kl.; 1971, im Druck.
4. F. BOPP: Grundvorstellung der Quantenphysik; Beitrag zu Heisenberg-Festschrift, Vieweg, Braunschweig 1971, im Druck.
5. A. SOMMERFELD: Vorlesungen über Theoretische Physik, Bd. V, 1. Aufl., Dietrich'sche Verlagsbuchhandlung, Wiesbaden 1952, pp 331, 362. — W. HEISENBERG: Einführung in die einheitliche Feldtheorie der Elementarteilchen. Hirzel, Stuttgart, 1967, § 3.1.

ПРЕДСТАВЛЕНИЕ БОЗОНОВ С ПОМОЩЬЮ ФЕРМИОНОВ

Ф. БОПП

Резюме

Исходя из предположения, согласно которому каждый квантовый процесс может быть представлен как совокупность элементарных процессов (разветвляющихся процессов), рассмотрена возможность представления процессов, подчиняющихся статистике Бозе, с помощью счетного множества операторов Ферми.

Acta Physica Academiae Scientiarum Hungaricae, Tomus 32 (1—4), pp. 99—114 (1972)

COSMIC RAYS AT MANCHESTER AND DURHAM*

By

G. D. ROCHESTER and A. W. WOLFENDALE

DEPARTMENT OF PHYSICS, UNIVERSITY OF DURHAM, DURHAM, ENGLAND

(Received 20. X. 1971)

In this paper, offered as a tribute to L. JÁNOSSY on the occasion of his 60th birthday, the authors describe some of the experiments at Manchester with which he was associated and later work in the same field by the authors themselves at Durham.

The Manchester work covered a wide range of studies of showers, including electron-photon cascades and penetrating showers produced both by charged and neutral particles. Geiger counters were used as detectors and sophisticated arrangements were used to elucidate the shower characteristics and distinguish between the various types. Comparison with theory led to many important conclusions.

Technical innovations, in the form of neon flash-tubes and solid iron magnets. were used at Durham. An account is given of their use in studies of muons, extensive air showers, neutrinos and the search for quarks.

L. JÁNOSSY came to Manchester in 1938 as John Harling Fellow shortly after Professor BLACKETT was appointed to the Langworthy Chair of Physics and was one of a small, active group which included H. J. J. BRADDICK, A. C. B. LOVELL, G. D. ROCHESTER and J. G. WILSON. The group had close connections with other experimentalists and theorists in the U.K., for example, H. J. BHABHA, E. G. DYMOND, E. P. GEORGE, W. HEITLER, R. F. PEIERLS and E. J. WILLIAMS and often had distinguished scientists such as P. AUGER, W. HEISENBERG, G. P. S. OCCHIALINI and B. ROSSI as visitors. It was an exciting period with many new and strange things in the air, the positron, electron-photon showers and the meson. At Manchester the excitement was heightened by the genius and boundless energy of BLACKETT.

Before coming to Manchester JÁNOSSY had worked in HOLHÖRSTER's Laboratory at Potsdam, where he had made a detailed study of counters and counter systems and had produced some stimulating ideas on the origin of certain geomagnetic effects. In the nine years at Manchester he published some thirty letters and papers, his principal collaborators being D. BROADBENT, E. P. GEORGE, P. INGLEBY, P. LOCKETT, A. C. B. LOVELL, C. B. A. MCCUSKER, G. D. ROCHESTER, B. ROSSI and J. G. WILSON. He also had a long and intimate connection with HEITLER and was strongly influenced by his views on meson theory.

JÁNOSSY's main contributions at Manchester were concerned with all types of showers, indeed, the study of penetrating (or meson) showers, led

* Dedicated to Prof. L. JÁNOSSY on his 60th birthday.

directly to the discovery of heavy mesons and hyperons by ROCHESTER and BUTLER, and their colleagues.

JÁNOSSY's first work on electron-photon showers, the theory of which had been worked out in 1937 by BHABHA and HEITLER in the U.K. and by CARLSON and OPPENHEIMER in the U.S.A., was an attempt to check the theory as far as possible and to establish the origin and nature of the many types of 'soft' showers already observed. This work formed an important preliminary to the researches on meson showers for which the possible contribution of 'soft' showers had to be measured and allowed for. In 1938(a) electron showers produced in lead, in air and underground were studied and the conclusion was reached that most were secondary to the 'hard' component, and hence were due to knock-on electrons produced by the penetrating mesons. Again in 1938(b) it was shown that the absorption in lead and aluminium of the particles in electron-photon showers accorded closely with shower theory in that the spectral distribution followed a $1/E^2$ law and the tail of the absorption curve a Z^2 law, from which it followed that most of the particles in showers were electrons and photons and not a mixture of electrons and penetrating particles as was thought at the time. The puzzling features of the transition curve observed by SCHMEISSER and BOTHE, the so-called 'second maximum' could not be repeated. Later, however, GEORGE, JÁNOSSY and MCCAIG (1942) showed that a second maximum in the place found by SCHMEISSER and BOTHE could be produced spuriously by a suitable disposition of the shower producing layer.

An important piece of work on extensive air showers was carried out in this period with LOVELL (1938c). A counter array of spacing approximately 5m was set up and used to trigger a cloud chamber with a lead plate placed across a horizontal diameter. The photographs demonstrated that the shower particles were electrons. Some cloud chamber photographs also showed that quite high densities of particles occurred, much higher than assumed by AUGER and his collaborators who were the first to observe extensive air showers. Indeed the density found by JÁNOSSY and LOVELL was of the order of 700 particles per m^2 which meant that some of the showers contained at least 30,000 particles and therefore carried an energy of 10^{15} eV. This paper broke important new ground.

At about the same time JÁNOSSY began at first with ROSSI and then with one of the present authors a detailed study of the production of cosmic rays by non-ionizing agents. The questions posed were: Is the non-ionizing radiation all photons? Can the non-ionizing radiation produce penetrating particles?

The JÁNOSSY—ROSSI study of the photon component in 1940 was one of the first in this field and was excellent in conception and execution. It was shown that the cross section for pair production by photons was in

accord with the BHABHA—HEITLER theory for energies of about 10^8 eV. The dependence of the absorption coefficient on atomic number was also in fair agreement with theory. The differential photon spectrum was again as given by theory, namely, $\varrho(E) \propto 1/E$ for $E < E_c$ with $E_c = 1.5 \times 10^8$ eV for air.

A cloud chamber study with BOUND and ROCHESTER did not reveal any penetrating particles, but showed the importance of other effects like side showers. Much more elaborate apparatus involving anticoincidence shielding and considerable thicknesses of absorber was built later by JÁNOSSY

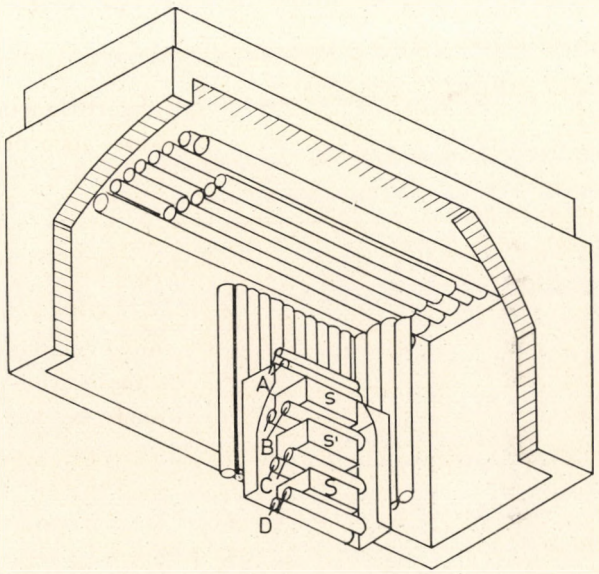

Fig. 1. Heavily shielded Geiger counter arrangement used by JÁNOSSY and ROCHESTER (1943) in a study of showers produced by neutral particles. ABC and D comprise a counter telescope to select penetrating particles

and ROCHESTER (1943). In these experiments excellent shielding from ionizing radiation either in the form of single charged particles or showers was devised. One of the more elaborate pieces of equipment is shown in Fig. 1. The leakage rate was less than 0.03% of the sea-level cosmic ray intensity. A careful study of the absorption of the primary non-ionizing radiation proved the existence of a penetrating non-ionizing radiation which could produce penetrating particles. Comparison of this with the results of ROSSI and REGENER, and SCHEIN and his co-workers at great altitudes, together with later work of JÁNOSSY and ROCHESTER on penetrating showers, identified the radiation as nucleonic. It was assumed that the penetrating particles so produced were mesons and the nucleons neutrons. A side product of this research was the development of a rapid process for making G.M. counters of high efficiency.

Parallel with the work on the non-ionising component went an experimental study of the puzzling problem of meson production. This work began in 1939 with P. INGLEBY and was a study of showers of penetrating particles since it was assumed, following extensive experiments on cosmic rays at sea level, that the penetrating shower particles were mesons. It was also assumed that the mesons were closely connected or were even identical with the Yukawa meson. JÁNOSSY and INGLEBY (1940) therefore dispersed a fourfold coincidence shower detector throughout a 50 ton block of lead such that no particle could penetrate less than 50 cm of lead. In the middle of the lead was a hodoscope which gave information on the numbers of ionising particles present. Penetrating showers were observed to be produced in the lead placed above the apparatus, the transition effect being completely different from that for the creation of 'soft' showers. With the then well-established cascade theory is was shown that the showers could not be due to very high energy electron cascades since electrons of energy 10^{19} eV would have been needed. Again with the help of the hodoscope records other non-genuine shower "events" e.g. double and triple knock-ons could be excluded. Further investigations were carried. out by JÁNOSSY and ROCHESTER, who in a long series of papers established the following facts:

(1) showers of penetrating particles like cosmic ray mesons exist, as were shown also by cloud chamber photographs (JÁNOSSY, MCCUSKER and ROCHESTER, 1941).

(2) these showers are produced by a nuclear active type primary which may be charged or uncharged, and they are not produced by the 'soft' component (JÁNOSSY and ROCHESTER 1943, 1944(a), 1944(b)).

(3) some extensive air showers contain penetrating particles (JÁNOSSY et al. 1945).

Following HAMILTON, HEITLER and PENG (1943) it was assumed that mesons are produced singly and that the observed groups of mesons arise from a plural process within the lead nucleus. Other good examples of photographs of groups of penetrating particles were observed over the period 1941—1945 by BOSTICK, HAZEN, WILSON POWELL in the U.S.A. and DAUDIN in France. However, perhaps the most comprehensive series was obtained by triggering a cloud chamber with a penetrating shower set (ROCHESTER, 1946) where in addition to groups of penetrating particles there were meson showers accompanied by an electronic component. It was shown that this component could not be secondary to the mesons, e.g. via knock-on processes and that if it came from the decay of mesons the lifetime of these particles must be very short, $\sim 10^{-10}$ sec. whence could not be one of the two mesons (the vector and pseudoscalar) assumed in the HAMILTON, HEITLER and PENG theory. Indeed, at about the same time OPPENHEIMER in the U.S.A. suggested that the most likely origin of the soft component of cosmic rays was the produc-

tion of electron showers via the decay of a very short lived meson into two photons high in the atmosphere. This meson was found at the Brookhaven accelerator in 1950. Not until 1947—48 was the mystery of the relation between the various mesons solved and the final answer is too well known to be repeated here.

The Manchester School of Cosmic Rays took on a new shape at the end of the War when BLACKETT, BRADDICK, LOVELL and WILSON returned, to be joined by BUTLER, ELLIOT and RUNCORN on the experimental side, and ROSENFELD, HAMILTON, PODOLANSKI, RAMSEY and TSU on the theoretical side. That the research got off to an excellent start was due mainly to BLACKETT's drive and initiative, but JÁNOSSY also helped enormously through his wide knowledge and his major book on Cosmic Rays, then in manuscript form. JÁNOSSY left Manchester to take up a Chair in Dublin in 1947.

This is not the place to record the contributions made by the Manchester School between the end of the War and 1955 by which date the principal members had dispersed to form daughter schools in many other universities. WILSON left in 1952 and founded a cosmic ray group in Leeds University which has specialised in extensive air showers and the continuous recording of cosmic ray neutrons; Professor BLACKETT took a large part of the School to Imperial College in 1953 and, although by that time his own research interests had moved to Paleomagnetism, a strong cosmic ray group was established under BUTLER, ELLIOT and NEWTH.

The Durham Cosmic Ray Group was started in 1955 when ROCHESTER moved there, and in a short time had an active group led by WOLFENDALE and MAJOR from Manchester. Since Durham is now one of the largest centres for cosmic ray research in the world, and has maintained close relations with Professor JÁNOSSY's School in Budapest it seems appropriate to give some account of research projects. The subjects chosen for review and comment are extensive air showers at Haverah Park, cosmic ray muons, neutrinos and the search for quarks. The first of these has been the special interest of ROCHESTER and the remainder of WOLFENDALE, who has taken the main responsibility for the Durham programme (MAJOR having moved over to accelerator physics).

The extensive air shower work stemmed from discussions between ex-Manchester workers at Durham, Imperial College, Leeds and a Harwell group of the need to set up a large array to study showers of above 10^{17} eV energy. An excellent site was obtained at Haverah Park within reasonable travelling distance of Leeds and not too far from Durham and Imperial College. The basic array consisted of very large volume water Čerenkov detectors spaced at 500 m. From the start a special feature was accurate timing which enabled the directions of the showers to be found. Durham, through ROCHESTER and TURVER, became active participants in 1963 and decided to extend

the facilities by the addition of a large "solid iron" magnet spectrograph with flash tube recording based on similar instruments developed by WOLFENDALE and a succession of research students starting in 1956. Durham also installed new arrays at 50m and 150m spacing thus extending the energy range down to 10^{15} eV and effectively making it possible to look at showers in the range 10^{15} eV—10^{18} eV. Leeds later added a 2 Km array bringing the upper limit to 10^{19}—10^{20} eV. A. SOMOGYI from Budapest joined the group in 1965 and helped in the final stages of the construction of the spectrograph. Accurate muon spectra and charge ratios were measured for the first time with this instrument in the range 5—100 GeV. These spectra are important because muons have the closest links of any shower particles with the first interaction in the atmosphere, and they carry most of the energy of the shower. The Mark I spectrograph ran successfully from 1964 until 1970 when it was replaced by the Mark II which had a much higher maximum detectable momentum. The Mark II instrument is now in operation. SOMOGYI's special contribution was to work out for the first time the effect of the earth's magnetic field on the muon distribution at sea level.

The main result of the spectrograph work has been to show that shower theory accounts well for the main muon distribution except at the highest energies where there is a marked excess of particles over theory (EARNSHAW et al. 1968). ORFORD and TURVER have attempted to interpret the excess as an indication that the primaries are heavy nuclei (e.g. $A \sim 20$) but, such are the difficulties of extensive air showers, an explanation in terms of primary protons and a change of particle interaction properties cannot be ruled out. Another entirely new feature was the demonstration, by KANNANGARA and TURVER, of the effects of large extensive air showers on the earth's electric field.

Apart from these new measurements other groups at Haverah Park have obtained the primary spectrum up to about 5×10^{19} eV, a tantalising limit already higher than might have been expected, and the observation that the primaries up to about 10^{19} eV seem to be isotropic. These observations raise many astrophysical questions of great interest. The problem of the expected degree of anisotropy for energetic primaries is being examined by OSBORNE from an analysis of galactic trajectories in a number of possible galactic magnetic field configurations; preliminary results indicate that unless the primaries above 10^{18} eV are heavy nuclei they cannot be contained in our galaxy.

WOLFENDALE's major work at Durham has been the development of neon flash tubes (first introduced by CONVERSI and GOZZINI in 1955) and solid iron magnets and their application to a number of Cosmic Ray problems, notably the measurement of muon spectra and charge ratios. The initial work was made possible by the loan of one of the BLACKETT-type electromagnets from the WILSON Double Magnet Spectrograph. WOLFENDALE and colleagues,

notably ASHTON, BROOKE and HAYMAN, used GM counters for the selection of single muons and trays of neon flash tubes to trace their trajectories through the spectrograph. They showed that a precision of measurement of about 1 mm at each level could be attained and that by employing a long arm the M.D.M. could be raised to 500 GeV/c. A "momentum selector" was added to help select particles of the highest momenta. The final spectrum due to HAYMAN and WOLFENDALE (1962) has largely been adopted as the 'standard' at sea level.

The pion spectrum was measured for the first time and the proton spectrum was determined. An interesting analysis using the proton and muon spectra and a simple interaction model yielded a primary spectrum which was steeper than had been previously thought. This observation, which has since been confirmed by more direct measurements, leads to quite a sharp change in slope of the primary spectrum at about 10^{15} eV which has interesting astrophysical significance.

In the course of this work it occurred to LLOYD and WOLFENDALE that because of the small interaction cross section of muons "solid" iron magnets could be used. Such magnets had been used formerly as magnetic lenses on a small scale in several experiments of great historical significance (e.g. the famous CONVERSI, PANCINI and PICCIONI experiment). The advantages of these magnets are low electrical power for a given magnetic field and the possibility of constructing magnets of great size and aperture quite cheaply.

Many experiments have been carried out with such magnets at Durham but perhaps the most interesting is one which has involved the construction of a 300-ton magnet. A diagram of this giant magnet, designed by WOLFENDALE and THOMPSON, and collaborators, AYRE et al. (1970), is shown in Fig. 2, and a photograph is given in Fig. 3. The magnet will form part of a spectrograph to extend the muon spectrum to 5000 GeV/c at various angles to the zenith. The spectrum will be measured not just because it is of basic importance to cosmic rays, but specifically to examine the implications of an important observation of KEUFFEL and his colleagues in the U.S.A. who find that muons of energies greater than 1000 GeV have a near isotropic distribution whereas conventional theory, which assumes that muons at sea level are produced largely by pions high in the atmosphere, predicts a $\sec\theta$ distribution for $\theta \lesssim 80°$ where θ is the angle with the zenith. A possible conclusion to be drawn from the KEUFFEL work is that the parents of very high energy muons are not pions (or kaons) but shorter lived particles, perhaps intermediate bosons. The 300 ton magnet will have scintillator selection and flash tube tray recording via a digital electrical method devised by AYRE and THOMPSON (1970). The digitised pulses from the tubes which have been set off by the muon will be fed "on-line" to a computer which will work out the momentum and sign. Preliminary measurements indicate that the equipment is working according

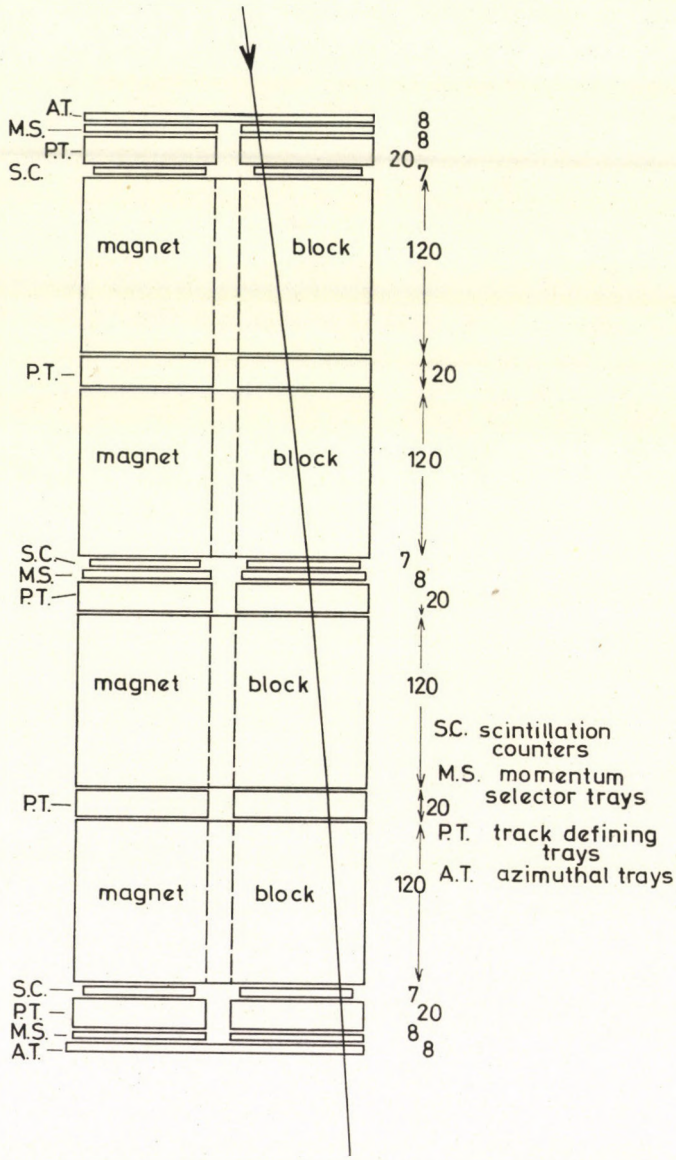

Fig. 2. M.A.R.S. — the Durham spectrograph (AYRE et al., 1970). The trajectory of a cosmic ray muon is indicated. The numbers are dimensions in cm.

to specification. The muon rate in the vertical direction above 7 GeV/c is 2200 hr^{-1} and above 500 GeV/c, 0.9 hr^{-1}. The spectrograph also provides a "beam" of high energy muons whose properties can be studied.

Groups in Durham have also studied neutrinos and looked for quarks. The neutrino work was part of a collaboration between scientists from the

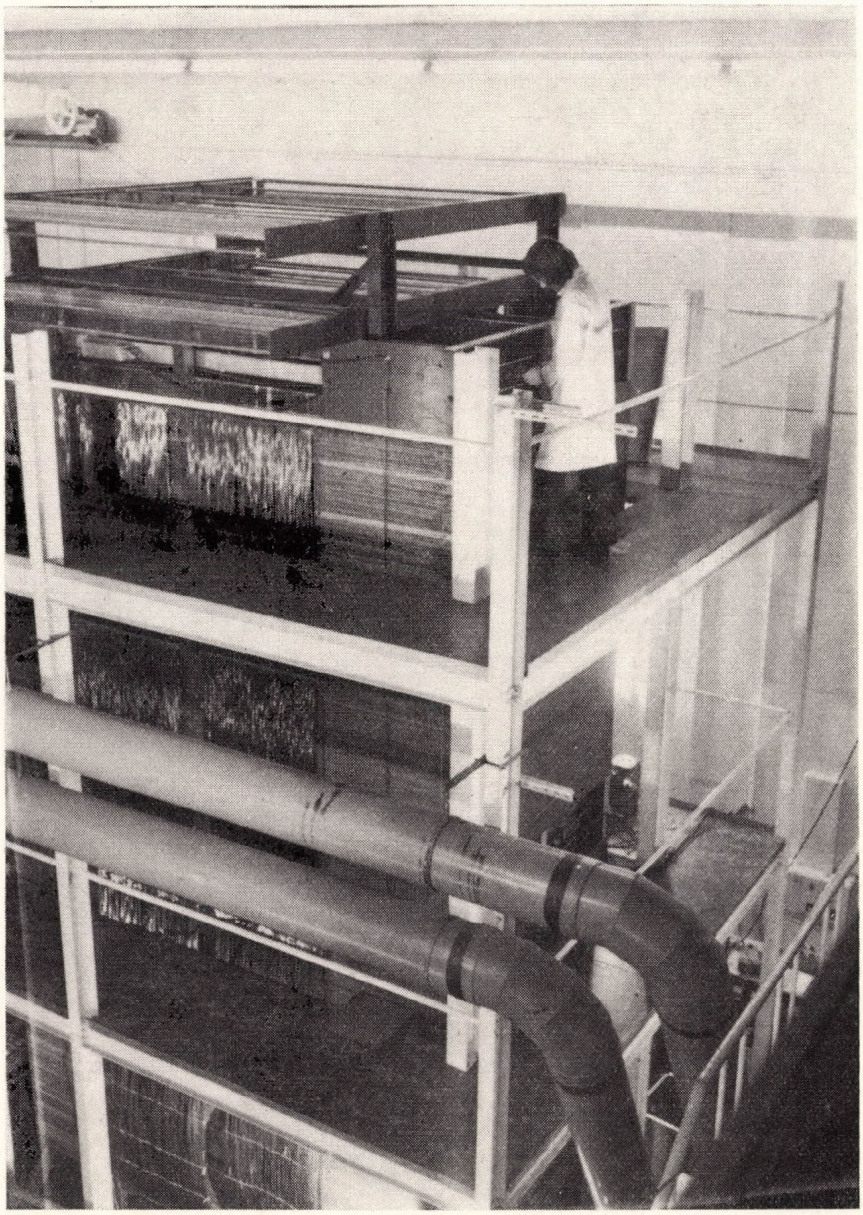

Fig. 3. Photograph of M.A.R.S. The windings for the electromagnet and the top tray of flash tubes can be seen

Tata Institute, Bombay, India, the Osaka City University in Japan, and Durham. WOLFENDALE was in charge of the Durham work, ably supported by OSBORNE and many research students.

Neutrino observations became a possibility when it was found at the large accelerators that the cross-section for muon neutrino nucleon interactions was very much higher than had been expected, the value up to 10 GeV being roughly 0.6 E_ν 10^{-38} cm^2 per nucleon (with E_ν in GeV); and that muons from the vertical beam were attenuated to such an extent deep underground that there was little danger of their being confused with the muons produced by neutrinos. In view of this the collaborating laboratories

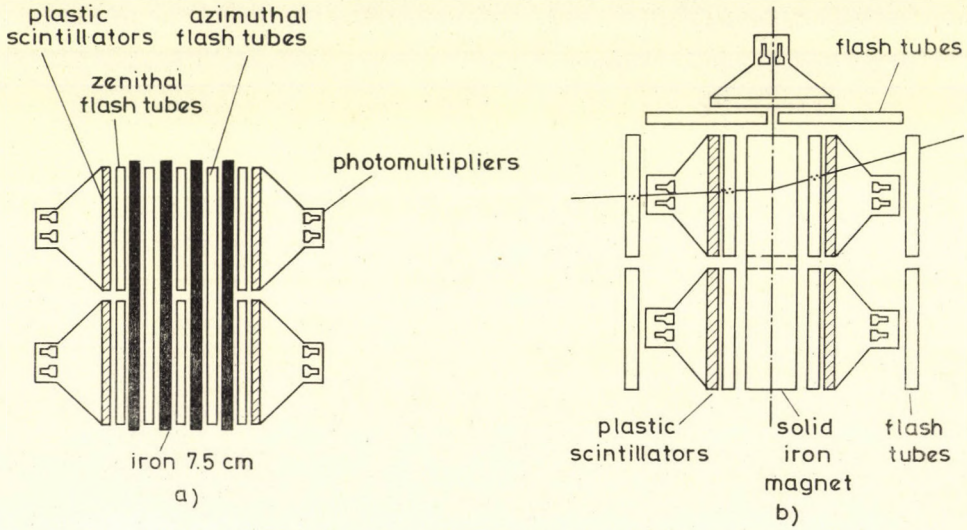

Fig. 4. Some of the detector arrangements used in the search for neutrino-induced muons deep underground (KRISHNASWAMY et al., 1971)

initiated in 1965 a search programme in the deep Kolar Gold Field Mines, a special feature being the introduction of neon flash tubes as visual detectors. Simultaneously with the Kolar experiment a joint American-South African project was initiated in the East Rand Proprietary Mine near Johannesburg. The basic trigger in the Kolar experiment was at first a fourfold coincidence between the pulses from a pair of photomultipliers viewing 1 m^2 of scintillation wall and a similar pair on the opposite wall and then later a two-fold from one wall only. Typical arrangements are shown in Fig. 4a and b. As seen in Fig. 4b some pieces of equipment were provided with blocks of magnetised iron in order to measure the energies of the muons. This disposition of the detectors was such as to favour muons moving in a horizontal direction. Seven blocks of detecting equipment were placed in a galley 7×10^5 g·cm^{-2} of rock, mean density 3.02 g·cm^{-3} below the earth's surface, at which depth the intensity of vertical muons was down by a factor of 10^8.

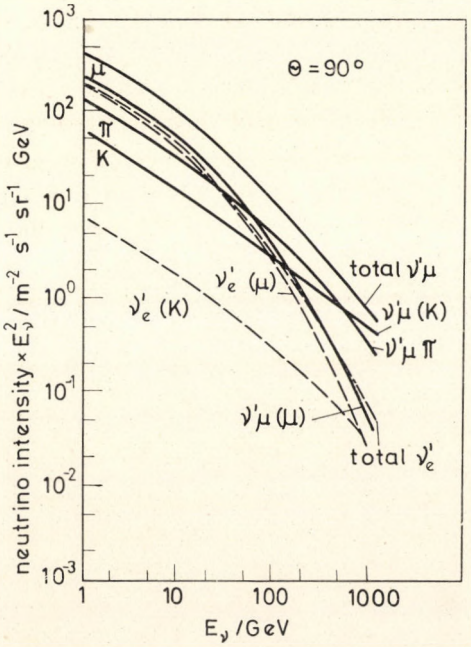

Fig. 5. Energy spectrum of cosmic ray neutrinos in the horizontal direction (OSBORNE et al., 1965). ν'_μ denotes $\nu_\mu + \bar{\nu}_\mu$ and ν'_e denotes $\nu_e + \bar{\nu}_e$

Many examples of muons and muon-type interactions were found. The expected flux of muon neutrinos from muon and kaon decay in the atmosphere was calculated by OSBORNE, SAID and WOLFENDALE in 1965 and by COWSIK, PAL and TANDON in 1966. The results of OSBORNE et al. are shown in Fig. 5 from which it will be noted that most of the neutrinos come from muon decay in the atmosphere. Neutrino interactions are expected to be mainly as follows:

$$\text{Elastic} \quad \nu_\mu^- + N \rightarrow N' + \mu$$
$$\text{Inelastic} \quad \nu_\mu + N \rightarrow N' + \mu + \pi' s$$

and with an intermediate boson, W,

$$\nu_\mu + N \rightarrow N + \mu + W \quad \text{(incoherent production)}$$
$$\nu_\mu + Z \rightarrow Z + \mu + W \quad \text{(coherent production)}$$

and $$\bar{\nu}_e + e \rightarrow W \quad \text{(Glashow Resonance)}$$

Muons will thus be generated in all these interactions and also by boson decay.

The predicted and observed 'events' are shown in Fig. 6 on various assumptions. The quantity E_0 signifies the energy at which the cross section

is assumed to saturate. It is seen that if the intermediate boson exists its mass, from this work, is likely to be greater than 3 GeV. There is some evidence that E_0 is finite, i.e. that the cross section saturates but the conclusion is not firm in view of a number of uncertainties about the neutrino flux and the magnitude of the coefficient in the energy-proportional total cross-section. The results from India and South Africa are in good accord. A full account of this work has recently been published by KRISHNASWAMY et al., 1971.

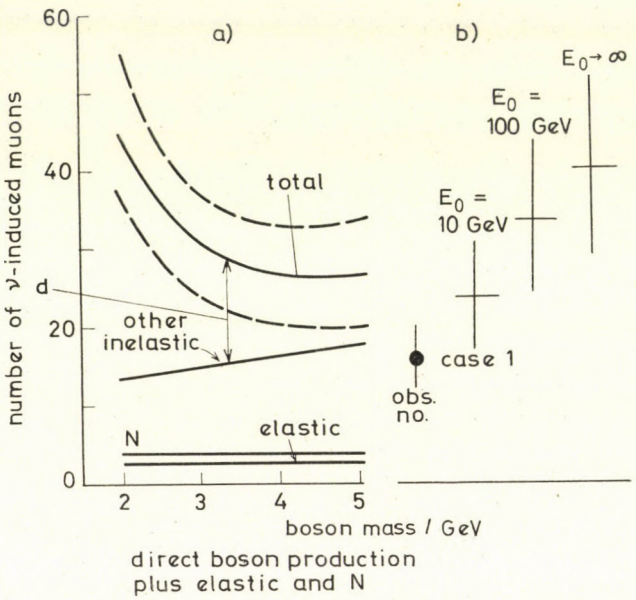

Fig. 6. Comparison of the observed number of events in the underground neutrino experiment (solid circle) with expectation for various assumptions about the mass of the intermediate boson and about the cut-off energy, E_0, of the linear increase of total inelastic cross section (KRISHNASWAMY et al., 1971)

In addition to this work Durham has in the past few years, mainly through ASHTON and his students, been actively engaged in the search for quarks, speculative particles which appear in theories of unitary symmetry. In the GELL-MANN and ZWEIG theories a triplet of charge states is predicted, that is, $-e/3$, $-e/3$ and $+2e/3$. The $2e/3$ state is expected to be stable while $-e/3$ state is expected to have a lifetime of the order of 10^{-10} sec against decay to the stable quark and a pion. Compound charge states of the type $4e/3$, $5e/3$ etc. are also expected. Alternative theories predict that quarks occur in quartets with charge e. Experiments at the great accelerators have failed to find these particles, suggesting that if they exist their masses are above 4 GeV. Since, however, particles of enormous energies occur in cosmic rays it seemed worthwile looking for them there.

A careful analysis of the production and interaction of quarks by cosmic ray primary particles led ASHTON to the conclusion that provided the mass is not too low quarks could occur at sea level. The easiest to detect should be the $e/3$ state since this particle would have characteristic signals most different from contaminating particles which will be mostly of charge e.

In the first experiment (ASHTON et al., 1968) an apparatus consisting of six plastic scintillators A, B, C, D, E, F, in coincidence and crossed neon flash tubes F_a, F_b, F_c, F_d, F_1, F_2, F_3, F_4 was set up as shown in Fig. 7. A G.M. telescope (G_a, G_b and G_c) allowed cosmic muons also to be recorded.

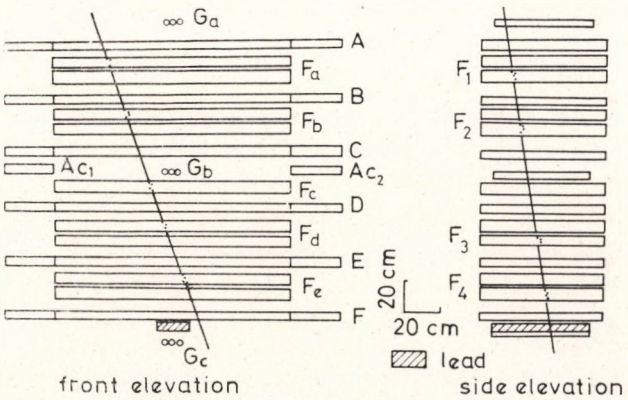

Fig. 7. Apparatus used in the search for fractionally charged quarks by ASHTON et al. (1968)

After a long run no events satisfied the rigid selection criteria, leading to the following upper limits for the quark flux at 90% confidence levels:

relativistic $e/3$ quarks 1.15×10^{-10} cm^{-2} s^{-1} sr^{-1}
relativistic $2e/3$ quarks 8.0×10^{-11} cm^{-2} s^{-1} sr^{-1}

In a second experiment ASHTON and KING (1971) looked for compound charge states by using a proportional counter scintillator telescope and a trigger requirement of an energy release of greater than 25 GeV in a thick iron plate. The scintillator was used to measure the energy and the proportional counters to estimate the charge of the initiating particle. Again, it was concluded that there were no certain quark candidates. The limit on the flux of particles of charges $4e/3$, $5e/3$ and $7e/3$ quarks is less than 8.2×10^{-10} cm^{-2} s^{-1} sr^{-1}.

In 1969, an important experiment was carried out in Sydney (CAIRNS et al., 1969) which claimed evidence for the existence of $2e/3$ quarks in air showers. A detailed statistical analysis of the problem of quark identification

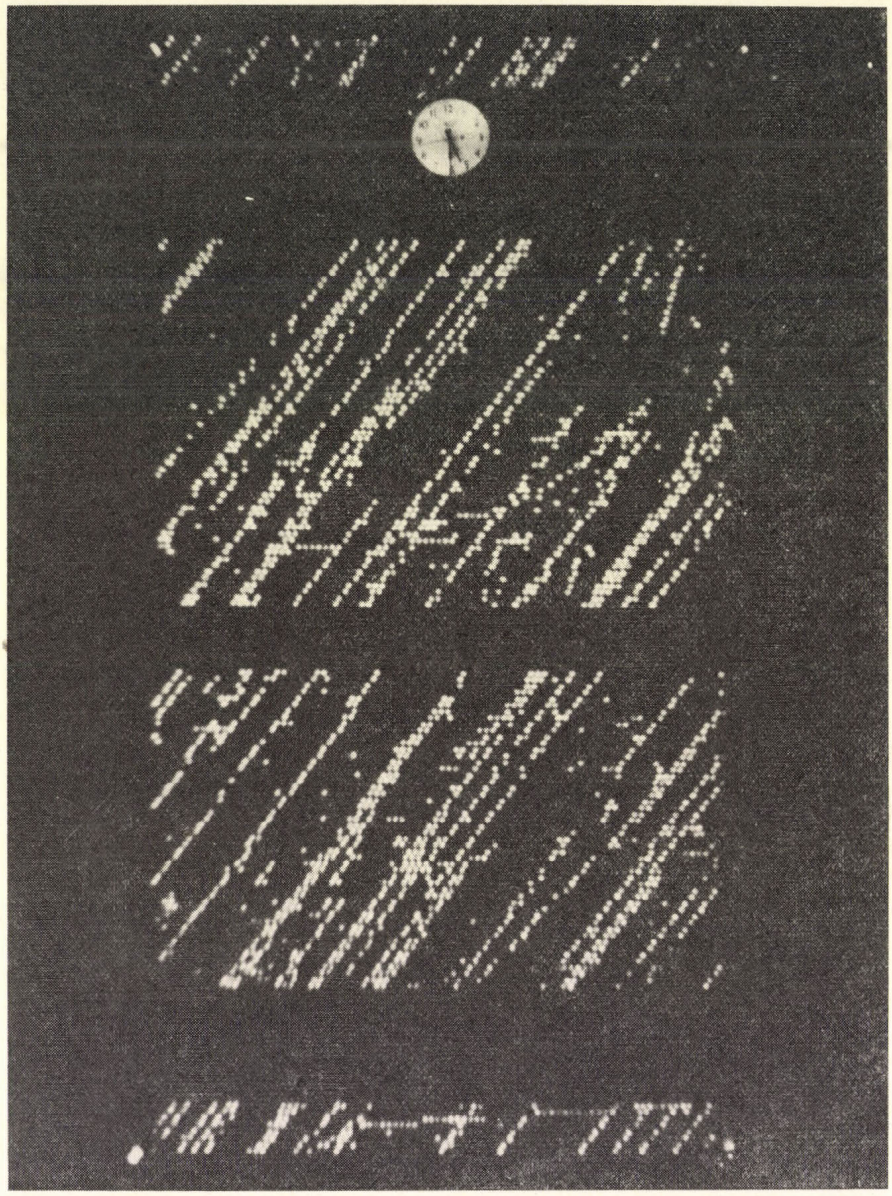

Fig. 8. Muon shower detected in the flash-tube chamber of ASHTON et al. (1971)

in cloud chamber observations was made by WOLFENDALE and P. KIRÁLY (a visitor from JÁNOSSY's laboratory) and it was shown that providing the technique was satisfactory (a proviso that had not, unfortunately, been demonstrated) the quarks were of the $e/3$ variety. An experiment was then

carried out by ASHTON, TSUJI and WOLFENDALE (1971) to search for $e/3$ quarks in extensive air showers. The method used the fact that the neon flash tube is sensitive to the ionisation loss of a particle in a quantitative fashion and hence it can in principle distinguish between different charges.

The apparatus takes the form of a flash tube chamber of volume 3 m $\times$ 1.5 m $\times$ 1 m, containing 11,670 flash tubes arranged so as to make possible three dimensional reconstruction of particle trajectories. The chamber is triggered by an extensive air shower array of liquid scintillation counters. A roof and walls of heavy absorber effectively eliminate low energy electrons. Particle densities of up to about 40 m^{-2} can easily be observed. A typical photograph of a fairly dense shower is shown in Fig. 8. So far the chamber has been run for 1771 hours and in this time no charge $e/3$ quark candidates have been seen, giving an upper limit of 2.6×10^{-10} $cm^{-2}s^{-1}sr^{-1}$ at the 90% confidence level; this is already below the Sydney rate for similar showers and particle densities.

Despite the absence of detected quarks in the experiments, the search is being continued and the upper limits will be depressed still further or, more hopefully, positive identifications made.

REFERENCES

F. ASHTON, R. B. COATS, G. N. KELLY, D. A. SIMPSON, N. I SMITH and T. TAKAHASHI, Proc. Phys. Soc. Al, 569, 1968.

F. ASHTON and J. KING, J. Phys., A4, L31, 1971.

F. ASHTON, K. TSUJI and A. W. WOLFENDALE, Proc. 12th Int. Conf. on Cosmic Rays, Hobart 3, 1162.

C. A. AYRE and M. G. THOMPSON, Acta Phys. Hung., 29, Suppl. 4, 541, 1970.

C. A. AYRE, J. M. B. BREARE, F. W. HOLROYD, M. G. THOMPSON, S. C. WELLS, and A. W. WOLFENDALE, Acta Phys. Hung., 29, Suppl. 4, 547, 1970.

I. CAIRNS, C. B. A. MCCUSKER, L. S. PEAK and R. L. S. WOOLCOTT, Phys. Rev., **186,** 1394, 1969.

M. CONVERSI and A. GOZZINI, Nuovo Cim., **2,** 189, 1955.

R. COWSIK, Y. PAL and S. N. TANDON, Proc. Ind. Acad. Sci., **53,** 217, 1966.

J. C. EARNSHAW, K. ORFORD, G. D. ROCHESTER, K. E. TURVER and A. E. WALTON, Cand. J. Phys., 46s, 122, 1968.

E. P. GEORGE, L. JÁNOSSY and M. MCCAIG, Proc. Roy. Soc., **180,** 219, 1942.

J. HAMILTON, H. HEITLER and H. W. PENG, Phys. Rev., **64,** 78, 1943.

P. J. HAYMAN and A. W. WOLFENDALE, Proc. Phys. Soc., **80,** 710, 1962.

L. JÁNOSSY, Proc. Roy. Soc., **167,** 499, 1938a.

L. JÁNOSSY, Proc. Cam. Phil. Soc., **34,** 614, 1938b.

L. JÁNOSSY and A. C. B. LOVELL, Nature, **142,** 716, 1938c.

L. JÁNOSSY and B. ROSSI, Proc. Roy. Soc., **175,** 88, 1940.

L. JÁNOSSY and P. INGLEBY, Nature, **145,** 511, 1940.

L. JÁNOSSY, C. B. A. MCCUSKER and G. D. ROCHESTER, Nature, **148,** 660, 1941.

L. JÁNOSSY and G. D. ROCHESTER, Proc. Roy. Soc., **181,** 399, 1943.

L. JÁNOSSY and G. D. ROCHESTER, Proc. Roy. Soc., **182,** 180, 1943.

L. JÁNOSSY and G. D. ROCHESTER, Proc. Roy. Soc., **183,** 181, 1944a.

L. JÁNOSSY and G. D. ROCHESTER, Proc. Roy. Soc., **183,** 186, 1944b.

L. JÁNOSSY, G. D. ROCHESTER and D. BORADBENT, Nature, **155,** 142, 1945.

M. R. KRISHNASWAMY, M. G. K. MENON, V. S. NARASIMHAM, K. HINOTANI, N. ITO, S. MIYAKE J. L. OSBORNE, A. J. PARSONS and A. W. WOLFENDALE, Proc. Roy. Soc., **323**, 489, 1971.
J. L. OSBORNE, S. S. SAID and A. W. WOLFENDALE, Proc. Phys. Soc., **86**, 93, 1965.
G. D. ROCHESTER, Proc. Roy. Soc., **187**, 464, 1946.

КОСМИЧЕСКИЕ ЛУЧИ В МАНЧЕСТЕРЕ И ДАРЕМЕ

Г. Д. РОЧЕСТЕР и А. В. ВОЛЬФЕНДАЛЕ

Резюме

В статье, посвященной Л. Яноши по случаю его шестидесятилетия со дня рождения описаны некоторые эксперименты, проведенные в Манчестере с его участием, и работы по той же области, которые были выполнены позднее самими авторами в Дареме.

Работы в Манчестере распространялись на довольно широкую область изучения ливней, включая слабопроникающие электронно-фотонные ливни, и проникающие ливни, образованные как заряженными так и нейтральными частицами. В качестве детекторов использовались счетчики Гейгера, и были применены сложные экспериментальные установки с целью различать ливни различных типов и наблюдать их характеристики. Сравнение результатов с теорией привело к целому ряду важных выводов.

В Дареме было проведено техническое усовершенствование экспериментальной аппаратуры, как применение неоновых вспыхивающих ламп и магнитов из железа. Подытожены результаты по их применению для изучения мюонов, широких атмосферных ливней, нейтрино, и для исследования кварков

Acta Physica Academiae Scientiarum Hungaricae, Tomus 32 (1—4), pp. 115—125 (1972)

RECHERCHES SUR UNE RÉINTERPRÉTATION CAUSALE DE LA MÉCANIQUE ONDULATOIRE RACCORDÉE AVEC LA POINTDYNAMIQUE

(DIFFUSIONS DES CORPUSCULES PAR UNE MARCHE POTENTIELLE)*

Par

T. MÁTRAI

CHAIRE DE PHYSIQUE A L'ÉCOLE SUPÉRIEURE PÉDAGOGIQUE »HO CHI MINH«, EGER

(Reçu 18. X. 1971)

Dans une note précédente [2], j'ai formulé l'équation eikonale des ondes BROGLIEnnes. Si nous attribuons un lieu de phase toujours précis à une particule, cette équation peut être considérée comme la généralisation quantique de l'équation Jacobienne. — Dans cette note je traite le mouvement linéaire d'une particule à quelle appartient un paquet d'onde Broglienne de profil Gauss, traversante une marche potentielle basse et s'y réfléchissant. J'ai réussi à demontrer qu'une telle particule — par rapport à sa situation de phase commençante — traverse vraiment la marche potentielle ou en rebondit, et cela précisément avec la probabilité donnée par la mécanique ondulatoire.

Enhardi par les travaux critiques de M. L. DE BROGLIE [1] dans une note précédente [2], j'ai formulé l'équation eikonale des ondes Brogliennes, qui — de la manière souhaitée — ne contient pas d'autres fonctions inconnues sauf la fonction eikonale réelle. Donc, si nous attribuons un lieu de phase et une orbite toujours précis à une particule libre, cette équation eikonale peut être considérée — même par sa forme — comme la généralisation de mécanique ondulatoire de l'équation Hamilton—Jacobienne, appartenant à une particule. L'incertitude du lieu de phase (q, p) de la particule selon HEISENBERG se montre par nécéssité dans cette conception pointdynamique causale de la mécanique ondulatoire aussi, mais seulement comme conséquence de la perturbation par la mesure de phase. Dans mon travail mentionné j'ai réussi à démontrer que, même dans cette interprétation, le carré de l'amplitude réelle dans la fonction complexe d'ondes Brogliennes mesure la densité rélative d'une multitude de particules affluent incohéremment. D'après ce modèle Zs. CSOMA [3] est récemment parvenu à des conclusions intéressantes et plausibles concernant le mouvement de l'électron dans l'état quantique d'un atome.

Pour vérifier la signification statistique éprouvée de la fonction d'ondes Brogliennes, j'étudie dans cette note le mouvement d'un point auquel appartient un paquet d'ondes Brogliennes à profil de Gauss, qui traverse une marche potentielle où s'y reflète. Je démontre qu'un tel point se rejette ou traverse alternativement la marche potentielle en dépendence de son »lieu initial«, c'est-à-dire, en conséquence du § 4 [2] précisément par une fréquence relative correspondant à la signification statistique de la mécanique ondulatoire.

* Dédié à M. le Professeur L. JÁNOSSY à l'occasion de son 60ième anniversaire.

§ 1. Introduction

Si dans un champ de forces, déterminées par le potentiel généralisé $V = V(\mathbf{r},t)$ l'on attribute un lieu $\mathbf{r}$ toujours précis et une impulsion précise

$$\mathbf{g} \equiv m\dot{\mathbf{r}} = \operatorname{grad} \varphi \tag{1,1}$$

à une particule libre de masse m, alors l'équation

$$\frac{1}{2m}\operatorname{grad}^2 S + \frac{\hbar^2}{4m^2}\left(\Delta \int_{t_0}^{t} \Delta S\, dt - \frac{1}{2m}\operatorname{grad}^2 \int_{t_0}^{t} \Delta S\, dt\right) + V + \frac{\partial S}{\partial t} = 0 \tag{1,2}$$

peut être considerée comme généralisation de l'équation pointdynamique Jacobienne, pour la mécanique ondulatoire. Dans cette équation t_0 est un temps initial quelconque, et la fonction d'action réelle S est l'intégrale totale de l'équation (1.2). Cette équation sera linéarisée par la transformation:

$$\psi = e^{-\frac{1}{2m}\int_{t_0}^{t} \Delta S\, dt + \frac{iS}{\hbar}}, \tag{1,3}$$

qui transpose la (1.2) dans l'équation Schrődingerienne, dépendant du temps pour la fonction complexe ψ des ondes Brogliennes.

§ 2. L'expression analitique du paquet d'ondes transitoire traversant la marche potentielle et s'y reflétant

Dans le [2] j'ai démontré que la forme d'ondes stationnaire (5,1) exclut le rejettement d'un point de masse sur la marche potentielle. Maintenant je démontre qu'une forme d'ondes transitoire plus générale — donnée par (3,2) dans [2] — permet le rejettement aussi et justement par la fréquence rélative, donnée par la mécanique ondulatoire. —

a) Pour construire, devant et derrière une marche potentielle, le champ d'ondes Brogliennes, qui se forme par un paquet d'ondes diffusant au profil Gaussienne, passant vers lui, écrivons tout d'abord un paquet d'ondes Brogliennes ψ, à la largeur

$$a' \equiv \sqrt{b/2m} \tag{2,1}$$

le paquet passe dans la direction de l'axe x, à une vitesse w appartenant à un point de masse m dans un champ au potential constant V_0, et doit atteindre à $x = 0$ justement au temps $t = 0$ [4]:

$$\psi(x,t) = \frac{1}{\sqrt{b+it\hbar}} \cdot e^{-\frac{i}{\hbar}(Et-mwx)-\frac{m(x-wt)^2}{2(b+it\hbar)}}, \tag{2,2}$$

où $E = (1/2)\, mw^2 + V_0$, b et A sont constants $(E > V_0 > 0)$*.
Il est assez facile de démontrer que le (2,2) est vraiment une solution de l'équation Schrődingerienne, qui dans notre cas peut être réduite à la forme suivante:

$$\frac{\hbar}{2m} \cdot \frac{\partial^2 \psi}{\partial x^2} + \hbar i \frac{\partial \psi}{\partial t} = V_0 \psi . \tag{2,4}$$

L'exponent négatif de (2,2) pourrait être écrit dans la forme convenable du quotient complexe:

$$\frac{i}{\hbar}(Et-mwx) + \frac{m(x-wt)^2}{2(b+it\hbar)} \equiv \frac{\frac{m}{2}x^2 - V_0 t^2 + ib\left(\frac{E}{\hbar}t - \frac{mw}{\hbar}x\right)}{b+it\hbar} . \tag{2,5}$$

b) Conformément au § 5 de [2], la marche potentielle doit se placer sur l'origo de l'axe x, notamment le potentiel doit être $V_0 = 0$ dans les lieux »d'au deça« $x < 0$, et $V_0 > 0$ dans les lieux »d'au delà« $x \geq 0$.

Nous choisissions la solution ψ de la (2,4) dans les lieux *d'au deça* sous forme de la somme

$$\psi(x < 0, V_0 = 0) \equiv \psi_1 = \varphi + \varrho , \tag{2,6}$$

où φ signifie un paquet d'ondes incident à la vitesse $w_1 > 0$, tandisque ϱ un pareil se *reflétant* à la vitesse $-w_1$ (cf. c).
Dans ce qui suit nous emploierons l'abréviation

$$mw_1 \equiv p \tag{2,7}$$

aussi.
Dans les lieux d'au delà nous voulons construire une unique solution ψ_2 de la (2,4) passant à la vitesse $w_2 > 0$ (cf. e) qui, en l'assemblant avec ψ_1 (cf. f) — nous fournira l'onde *refractée*. Celle-ci sera marquée par

$$\psi(x \geq 0, V_0 > 0) \equiv \psi_2 . \tag{2,8}$$

Pour ce domaine $(x \geq 0)$ nous emploierons l'abréviation:

$$mw_2 \equiv q . \tag{2,9}$$

* Entre la largeur a' et celle (a) de (3,2) dans [2], où $V_0 = 0$, il existe la relation suivante:

$$a'^2 - a^2 = \frac{7i\hbar t}{2m} . \tag{2,3}$$

Par conséquent on ne peut pas attendre, que la solution (3,2) de [2] puisse être transposée à (2,1) précedente, en choisissant le constant (a) d'une façon convenable.

c) Dans l'espace d'ondes d'au deça, l'onde φ incidente sera (pour la simplicité en posant $A = 1$ dans la (2,2), en usant de la (2,5) et (2,7), et en considérant que $V_0 = 0$ dans le domaine $x < 0$):

$$\varphi = \frac{1}{\sqrt{b+it\hbar}} \cdot e^{-\frac{\frac{i}{\hbar}(Et-px)+\frac{m}{2}x^2}{b+it\hbar}}. \tag{2,10}$$

Dans la ϱ se réfractante il est à écrire B ($\leqq A$) au lieu de A (=1), et $-p$ au lieu de p:

$$\varrho = \frac{B}{\sqrt{b+it\hbar}} \cdot e^{-\frac{\frac{i}{\hbar}(Et+px)+\frac{m}{2}x^2}{b+it\hbar}}. \tag{2,11}$$

Donc dans le sens de la (2,10) et (2,11)

$$\psi_1 = \frac{1}{\sqrt{b+it\hbar}} \cdot e^{-\frac{\frac{i}{\hbar}bEt+\frac{m}{2}x^2}{b+it\hbar}} \cdot \left(e^{\frac{\frac{i}{\hbar}bpx}{b+it\hbar}} + Be^{-\frac{\frac{i}{\hbar}bpx}{p+it\hbar}} \right). \tag{2,12}$$

d) Pour établir la B figurant dans la ψ_1, et pour construire la ψ_2 (cf. e), il faut écrire la ψ_1 donnée par (2,12) sous forme d'intégrale de *Fourier*. Dans ce but nous introduisons la notation suivante:

$$\psi_1^0 = \lim_{x \to -0} \psi_1(x,t). \tag{2,13}$$

Cette limite existe notamment dans le sens de la (2,12):

$$\psi_1^0 = (1+B) \cdot (b+it\hbar)^{-1/2} \cdot e^{-\frac{\frac{i}{\hbar}bEt}{b+it\hbar}}. \tag{2,14}$$

Nous cherchons une solution de (2,4), qui contient dans le domaine $x < 0$ un composant, se reflétant avec l'amplitude B et qui passe en (2,14) à l'endroit $x = 0$. Nous retrouvons une telle le plus simplement dans la forme de l'intégrale (ψ_1) d'une solution:

$$C(E) \cdot e^{-\frac{i}{\hbar}Et} \left(e^{+\frac{i}{\hbar}px} + B \cdot e^{-\frac{i}{\hbar}px} \right), \tag{2,15}$$

où $p \equiv \sqrt{2mE} > 0$. Ainsi

$$\psi_1(x,t) = \int_0^{+\infty} C(E) \cdot e^{-\frac{i}{\hbar}t} \cdot \left| e^{+\frac{i}{\hbar}px} + B \cdot e^{-\frac{i}{\hbar}px} \right| dE \tag{2,16}$$

est aussi sans doute une solution de (2,4). Par la, selon notre condition

$$\psi_1^0 \equiv \psi_1(0,t) = \int_0^{+\infty} C(E)\cdot e^{-\frac{i}{\hbar}Et}(1+B)\cdot dE\,, \tag{2,17}$$

d'où par le theorème de Fourier pour l'inversion:

$$C(E) = \frac{1}{2\pi\hbar}\cdot\int_{-\infty}^{+\infty}\frac{\psi_1^0(\tau)}{1+B}\cdot e^{+\frac{i}{\hbar}E\tau}\,d\tau\,. \tag{2,18}$$

En la substituant en (2,16), nous recevons:

$$\psi_1(x,t) = \frac{1}{2\pi\hbar}\int_0^{\infty}\int_{-\infty}^{+\infty}\frac{\psi_1^0(\tau)}{1+B}\cdot e^{+\frac{i}{\hbar}E\tau}\cdot e^{-\frac{i}{\hbar}Et}\cdot\left(e^{+\frac{i}{\hbar}px}+Be^{-\frac{i}{\hbar}px}\right)d\tau\,dE. \tag{2,19}$$

Si nous y substituons (2,14), la forme intégrale Fourierienne de ψ_1 sera:

$$\psi_1(x,t) = \frac{1}{2\pi\hbar}\int_0^{\infty}\int_{-\infty}^{+\infty}\frac{e^{-\frac{ibE\tau}{\hbar(b+i\tau\hbar)}}}{\sqrt{b+i\tau\hbar}}\cdot e^{\frac{i}{\hbar}E(\tau-t)}\cdot\left[e^{\frac{ipx}{\hbar}}+B\cdot e^{-\frac{ipx}{\hbar}}\right]d\tau\,dE. \tag{2,20}$$

e) Une simple calculation nous convincra du fait que, pour le domaine $x \geq 0$ il n'existe pas de solution de forme (2,2), qui puisse satisfaire toutes les exigences de raccordement:

$$\psi_2(0,t) = \psi_1^0\,, \tag{2,21}$$

$$\left(\frac{\partial\psi_2}{\partial x}\right)_{x=0} = \left(\frac{\partial\psi_1}{\partial x}\right)_{x=0}. \tag{2,22}$$

C'est pourquoi nous cherchons ψ_2 aussi dans la forme intégrale Fourierienne:

$$\psi_2(x,t) = \int_0^{\infty} C(E)\cdot e^{\frac{i}{\hbar}(qx-Et)}\,dE\,, \tag{2,23}$$

où $q \equiv \sqrt{2m(E-V_0)}$. A cause de (2,21):

$$\psi_1^0 = \psi_2(0,t) = \int_0^{\infty} C(E)\cdot e^{-\frac{i}{\hbar}Et}\,dE\,, \tag{2,24}$$

d'où d'après la formule d'inversion Fourierienne:

$$C(E) = \frac{1}{2\pi\hbar}\int_{-\infty}^{+\infty}\psi_1^0(\tau)\cdot e^{+\frac{i}{\hbar}E\tau}\,d\tau\,. \tag{2,25}$$

Substituons cela dans (2,23) et nous recevons:

$$\psi_2(x,t)=\frac{1}{2\pi\hbar}\int_0^{\infty}\int_{-\infty}^{+\infty}\psi_1^0(\tau)\cdot e^{\frac{i}{\hbar}E\tau}\cdot e^{\frac{i}{\hbar}[\sqrt{2m(E-V_0)}\,x-Et]}\,d\tau\,dE \tag{2,26}$$

et d'après (2,14) il en résulte:

$$\psi_2(x,t)=\int_0^{\infty}\int_{-\infty}^{+\infty}\frac{(1+B)\cdot e^{-\frac{ibE\tau}{\hbar(b+i\tau\hbar)}}}{\sqrt{b+i\tau\hbar}}\cdot e^{+\frac{i}{\hbar}E\tau}\cdot e^{+\frac{i}{\hbar}[\sqrt{2m(E-V_0)}\,x-Et]}\,d\tau\,dE\,. \tag{2,27}$$

Mais par la c'est seulement l'exigence de raccordement (2,21) qui est satisfaite. Pour accomplir (2,22), nous différentions les intégrales Fourieriennes (2,20) resp. (2,27) suivant x, en employant la règle connue de Leibniz par la dérivation de l'intégrande:

$$\frac{e^{-\frac{ibE\tau}{\hbar(b+i\tau\hbar)}}}{\sqrt{b+i\tau\hbar}}\cdot e^{+\frac{i}{\hbar}E(\tau-t)}\cdot\left(e^{+\frac{ipx}{\hbar}}\cdot\frac{ip}{\hbar}-B\cdot e^{-\frac{ipx}{\hbar}}\cdot\frac{ip}{\hbar}\right) \tag{2,27a}$$

et:

$$\frac{(1+B)\cdot e^{-\frac{ibE\tau}{\hbar(b+i\tau\hbar)}}}{\sqrt{b+i\tau\hbar}}\cdot e^{+\frac{i}{\hbar}E(\tau-t)}\cdot e^{\frac{i}{\hbar}\sqrt{2m(E-V_0)}\,x}\cdot\frac{i\sqrt{2m(E-V_0)}}{\hbar}\,. \tag{2,27b}$$

Les deux intégrales sont égales à l'endroit $x=0$, si

$$p(1-B)=q(1+B)\,,$$

d'où

$$B=\frac{p-q}{p+q}\,. \tag{2,28}$$

Nous voyons que, d'une façon réposante, cette forme B est identique au facteur d'amplitude à réflection de la solution stationnaire dans la [2] (5,1).
f) Nous calculons l'impulsion g dans le domaine $x<0$ d'après de (1,1) et [2] (2,12):

$$g=\frac{\hbar}{2i}\cdot\frac{\partial\psi_1/\partial x}{\psi_1}-\frac{\hbar}{2i}\cdot\frac{\partial\psi_1^*/\partial x}{\psi_1^*}\,. \tag{2,29}$$

En y introduisant le membre complexe:

$$g_1\equiv\frac{\hbar}{2i}\cdot\frac{\partial\psi_1/\partial x}{\psi_1}\,, \tag{2,30}$$

la g réelle donnée dans (2,29), se forme de la façon suivante:

$$g = g_1 + g_1^* \,. \tag{2,31}$$

Il suffit donc de calculer g_1 d'après (2,12) et (2,28). Le résultat de longues calculations élémentaires sera:

$$g = m\hbar^2\, dxt + b^2\, pd\, \frac{e^{2fd} - B^2\, e^{-2fd} + 2B \sin(kd)}{e^{2fd} + B^2\, e^{-2fd} + 2B \cos(kd)}\,, \tag{2,32}$$

où

$$d \equiv \frac{1}{b^2 + t^2\, \hbar^2}\,, \tag{2,32d}$$

$$f \equiv bp\, xt\,, \tag{2,32f}$$

$$k \equiv \frac{2\, b^2\, px}{\hbar}\,. \tag{2,32k}$$

Si $p = q$, la (2,32) passe dans la [2] (3,3) et indépendamment de cela, si $b \to \infty$: dans la [2] (5,4). D'après (1,1) l'équation orbitale cherchée: $x = x(t)$ serait fournie par l'équation différentielle ordinaire de premier ordre:

$$m\dot{x} = g\,. \tag{2,33}$$

Mais comme la forme de g donnée par (2,32) est transcendente, on peut à peine résoudre cette équation dans la forme fermée. Même d'une façon surprenante, la (2,33) a un point singulier à des valeurs

$$\left.\begin{aligned} t_n &= \frac{b \ln B}{(2n+1)\,\pi\hbar} \\ x_n &= \frac{(2n+1)\,\pi\hbar}{2\, b^2\, p} \end{aligned}\right\} n = 1, 2, 3, \ldots \tag{2,34}$$

des variables x, t, parce qu'ici la g, donnée par (2,32), prendra une forme indéfinie (0/0). Cette note ne croit pas de son devoir d'observer, si ce point singulier a un caractère de point nodal, un point de turbulence, ou de selle (cf. [5]). Même sans l'intégration de (2,33) nous pouvons faire des conclusions aux propriétés générales du mouvement du point. Nous pouvons accepter entre autres, que c'est l'apparition du point singulier qui rend possible pour le point, passant vers la marche potentielle, de retourner même plus avant.

§ 3. Conclusions pour la direction du mouvement orbital

I. *Si le point de masse atteint à la marche potentielle* $(x = 0)$, *il la traverse indispensablement et ne peut pas en retourner.*

À savoir l'expression (2,32), qui donne l'impulsion g du point à l'endroit de la marche $x = 0$, est toujours indispensablement positive, car dans le cas, où t est fini, l'équation se forme de la façon suivante:

$$g = \frac{b^2 p}{b^2 + t^2 \hbar^2} \cdot \frac{1 - \left(\frac{p-q}{p+q}\right)^2}{\left(1 + \frac{p-q}{p+q}\right)^2} = \frac{b^2 q}{b^2 + t^2 \hbar^2} > 0 \,. \tag{3,1}$$

II. *Après la réflexion du paquet d'ondes il y a des moments de temps* $t = \tau_n$ (>0), *quand le point, traversant certains endroits* $x = \xi_n (<0)$ *devant la marche potentielle, ne peut passer qu'en arrière* $\{g(\xi_n, \tau_n) < 0\}$.

A savoir une condition suffisante pour l'apparition de l'impulsion négative $(g < 0)$ est que le deuxième membre de la droite soit zéro dans la (2,32). Cela arrive indispensablement, si

$$\tau_n = \frac{b}{2\pi n \hbar} \ln \frac{p+q}{p-q}, \tag{3,2}$$

$$\xi_n = \frac{-\hbar}{4\pi n p} \cdot \left(4\pi^2 n^2 + \ln^2 \frac{p+q}{p-q}\right), \; n = 1, 2, \ldots \tag{3,3}$$

(Il est compréhensible, que le dénominateur du deuxième membre dans la droite de la (2,32) ne peut pas être zéro à côté de τ_n et ξ_n).

Cette conclusion diffère d'une façon intéressante du cas de l'onde Broglienne stationnaire traité par le § 5 [2], parce que celle-la atteste que, dans un cas transitoire, le point de masse peut passer sous certaines condititions non seulement vers la marche potentielle. Même dans le cas suivant seulement en arrière.

III. *Après la réflection du paquet d'ondes* $(t = 0)$ *nous trouvons pour le moment* $(t > 0)$ *de temps arbitraire des lieux* x_t *à une distance convenable, au deçà desquels chaque point de masse depuis le temp t ne peut que s'éloigner de la marche en arrière* $(g < 0)$.

En effet, en transformant le deuxième membre de la (2,32), en employant les abréviations (2,32, d, f, k), nous recevons:

$$g = \frac{mxt\hbar^2(e^{2fd}+B^2e^{-2fd}+2B\cos(kd))+b^2p(e^{2fd}-B^2e^{-2fd}+2B\sin(kd))}{d^{-1}(e^{2fd}+B^2e^{-2fd}+2B\cos(kd))}.$$

Ici le dénominateur est positif, parce que tous ses deux facteurs sont positifs. Mais le sous-multiple en parenthèse du premier membre du numérateur est aussi indispensablement positif, parce que le minimum de celui-ci forme un carré total.

Pour celà, en cas de $x < 0$, $t > 0$, la condition suffisante de sg $g = -1$ est que le sous-multiple en parenthèse du deuxième membre du numérateur:

$$e^{2fd}-B^2e^{-2fd}+2B\sin(kd)$$

soit negatif. Mais celà arrive indispensablement, si l'expression

$$e^{2fd}-B^2e^{-2fd}+2B$$

est négative, donc en employant la (2,28):

$$e^{2fd}+2\frac{p-q}{p+q} < \left(\frac{p-q}{p+q}\right)^2 \cdot e^{-2fd}. \tag{3,4}$$

Mais comme $x < 0$, un $x_t < 0$ appartient indispensablement à une $t > 0$ donnée afin que la (3,4) subsiste. A savoir la e^{-2fd} augmente sans limite, d'une façon monotone, ensemble avec $|x|$, alors qu'en même temps la e^{+2fd} converge en diminuant d'une façon monotone vers le zéro. C'est ce que nous avons voulu attester.

IV. *Même en cas d'ondes Brogliennes transitoires, ils passent par la marche potentielle justement tant de particules, qui peuvent être conclues d'après le rapport statistique légitime de la fonction d'ondes* $\psi(x, t)$.

Pour preuve, il faut remplir en pensée au temps de début $t \to -\infty$ le domaine $x < 0$ d'un tuyau de section droite $dy \cdot dz$ par une densité uniforme de particules. Il faut calculer, combien de particules n_2 passent par la surface de la marche dans le domaine $x > 0$ depuis le temps $t \to -\infty$ jusqu'au t fini.

D'après le § 4 [2], suivant cette condition de début, la $\psi\psi^* = A^2$ signifie la densité des particules à l'endroit du passage $x = 0$ à un t arbitraire. Alors le nombre n_2 des particules qui traversent la section droite $x = 0$ pendant le temps $-\infty$ et τ, est donné — selon une relation hydrodynamique bien connue — par l'intégrale de la

$$n_2 = \int_{-\infty}^{t} \psi(0,t) \cdot \psi^*(0,t)\, \dot{x}(0,t)\, dy\, dz\, dt \tag{3,5}$$

où l'expression $\dot{x}(0,t) = g(0,t)/m$, calculée d'après la (2,32), est positive dans la sens de (3,1). Donc en même temps $n_2 > 0$.

D'après la thèse Gaussienne, on peut transformer l'intégrale de surface en intégrale de volume, en l'adaptant pour le volume de forme de tuyau, s'étendant de $x = 0$ jusqu' à $x \to +\infty$.
En ce cas:

$$\int_{-\infty}^{t} \psi(0,t)\psi^*\cdot(0,t)\,\frac{g(0,t)}{m}\cdot dy\, dz\, dt = \int_{x=0}^{+\infty}\int_{-\infty}^{t} \operatorname{div}(\mathbf{x} g\psi\psi^*/m)\, dt\, dx\, dy\, dz. \tag{3,6}$$

Mais ici, en vertu de l'équation de continuité (1,4) et ensuite en conséquence des équations (1,8) et (2,12):

$$\operatorname{div}(\mathbf{x} g\psi\psi^*/m) = \partial(\psi\psi^*)/\partial t.$$

Pour cela le deuxième membre de la (3,6) sera simplifié en employant (2,21) et (2,22):

$$n_2 = \int_{x=0}^{+\infty} \psi_2\, \psi_2^*\, dx\, dy\, dz,$$

ce qui atteste justement notre thèse IV.

La concordance statistique, reçue pour le cas spécial précédent, nous donne l'espérance, que les résultats statistiques, calculés par la mécanique ondulatoire pour les phenomènes de diffusion plus compliqués, résultent aussi du modèle pointdynamique causal.

Remerciement

Même en ce lieu je remercie bien M. L. de BROGLIE, secrétaire perpétuel de l'Académie des Sciences Française, pour ses encouragements par lettre à continuer l'étude de ce thème.

BIBLIOGRAPHIE

1. L. DE BROGLIE, Étude critique des bases de l'interprétation actuelle de la mécanique ondulatoire, Gauthier V., Paris, 1963.
2. T. MÁTRAI, Acta Phys. Hung., **28**, 323, 1970.
3. Zs. CSOMA, Contributions à un modèle de dynamique ponctuelle pour la mécanique ondulatoire, Acta Phys. Hung., **31**, 389, 1972.
4. F. HUND, Einführung in die theor. Physik V., S. 201. Bibliogr. Inst., Leipzig 1950.
5. FRANK – MIESES, A mechanika és fizika differenciál- és integrál-egyenletei, I. 353. o. Műszaki KK, Bp. 1966.

ИССЛЕДОВАНИЯ ПО ПРИЧИННОЙ ТОЧЕЧНО-ДИНАМИЧЕСКОЙ РЕИНТЕРПРЕТАЦИИ ВОЛНОВОЙ МЕХАНИКИ

(Рассеяние на потенциальной ступени)

Т. МАТРАИ

Резюме

В предыдущей работе, исходя из критических работ Л. де Бройля, было выведено уравнение ейконала для волн де Бройля, в которое, согласно предварительным требованиям, кроме искомой реальной функции эйконала, другие неизвестные функции не входят. Значит, если же свободной микрочастице всегда приписываем точное значение фазы, то данное уравнение эйконала уже и по своему внешнему виду является одновременно и волновомеханическим обобщением уравнения Гамильтона-Якоби для микрочастицы.

В упомянутой работе удалось доказать и то, что вещественный квадрат амплитуды комплексной волновой функции де Бройля при такой интерпретации тоже является мерой относительной плотности потока микрочастиц, движущихся независимо друг от друга, то есть, плотности вероятности нахождения одной частицы.

В данной работе, с целью дальнейшей проверки принятой статистической интерпретации волновой функции, изучается движение такой материальной точки, к которой приписывается проходящий через потенциальную ступень, или же отражающийся от нее дебройлевский волновой пакет, имеющий вид распределения Гаусса. Доказано, что в зависимости от «начального значения фазы», она либо отражается от потенциальной ступени, либо проходит через нее, причем относительная частота этих событий точно совпадает с той, которая получается при статистическом истолковании волновой механики.

Acta Physica Academiae Scientiarum Hungaricae, Tomus 32 (1—4), pp. 127—133 (1972)

STATE VECTORS WITH VANISHING NORM AND THE PROBABILITY INTERPRETATION*

By

K. L. NAGY

INSTITUTE FOR THEORETICAL PHYSICS, ROLAND EÖTVÖS UNIVERSITY, BUDAPEST

(Received 18. X. 1971)

After an analysis of why theories with dipole states do not give a unitary physical S-matrix automatically, a reasonable unitarization procedure is proposed working even for these pathological cases.

1. In the last few years several definite questions have arisen concerning the physical unitarity of quantum theories with dipole (or multipole) ghost states [1—5]. These states were introduced into physical considerations by HEISENBERG in his unified theory of elementary particles [6] and in the LEE model [7]. He found that zero-norm energy eigenstates were associated with dipole states also possessing zero norm. Since these states prevent us from applying the immediate probabilistic interpretation accepted in an ordinary quantum theory, in the professional slang the states in question are called "ghosts". While an energy eigenstate satisfies the equation

$$(H - E) \mid E > = 0,$$

H being the Hamiltonian, the dipole ghost state $\mid D >$ satisfies

$$(H - E) \mid D > = \lambda E \mid E > \tag{1}$$

with some interesting consequences. For example, from the time-dependent Schrödinger equation

$$\mid E, t > = e^{-iEt} \mid E,\ 0>,$$

but

$$\mid D, t > = \{\mid D, 0 > - i\lambda E t \mid E,\ 0>\}\ e^{-iEt}. \tag{2}$$

In spite of the fact that these states were introduced in the framework of a state vector space with indefinite metric, where the possibility of a clear probabilistic interpretation is not guaranteed, it was thought that dipole theories automatically give a unitary physical S-matrix. A simplified reasoning went as follows [8, 9]:

* Dedicated to Prof. L. JÁNOSSY on his 60th birthday.

In an indefinite metric theory the eigenvectors of the Hamiltonian need not form a complete system. In dipole cases, therefore, a linearly independent dipole ghost state satisfying (1) must be attached to any eigenvector with zero norm $| 0; E >$

$$< 0; E | 0; E > = 0$$

in order to complete the whole state vector space. Then, because of the supposed completeness, the physical "in" state can be developed as follows:

$$\begin{aligned} | \text{phys; in} > = \Sigma a(n) \, | \text{ phys; out} > + \\ + \Sigma b(n) \, | \, 0; E; \text{ out} > + \Sigma c(n) \; D; \text{out} >. \end{aligned} \tag{3}$$

Since the left-hand side is an eigenstate, this equation was thought to hold only for $c(n) = 0$, in which case the physical S-matrix $<$ phys; out $|$ phys; in $>$ should be unitary.

However, it turned out in model theories [1, 4] that physical unitarity is violated; even in dipole cases the right-hand side of (3) can be developed in terms of energy eigenstates. This actually means, as was clearly demonstrated by NAKANISHI [5], that in the continuous spectrum (scattering states) the dipole state can be expressed as an appropriate superposition of energy eigenstates.

In Section 2 this problem will be discussed in general for the simplest case of one variable. Section 3 gives a proposal for extracting a new unitary physical S-matrix that is applicable even to theories of this type.

2. Let us suppose that we meet the following situation: In a certain theory, apart from apparent physical states, we have states satisfying

$$\begin{aligned} &(H - E) \, | \, E > = 0, \quad < E \, | \, E > = 0 \, , \\ &(H - E) \, | \, D > = \lambda E \, | \, E >, \quad < D \, | \, D > = 0, \\ &< D' \, | \, E > = < D \, | \, E' > = \delta(E' - E) \end{aligned} \tag{4}$$

i.e. a dipole ghost situation occurs. $| \, E >$ and $| \, D >$ are supposed to be linearly independent and form a complete system. E is real, but otherwise continuous. Now $| \, E >$ is already an eigenstate of H to E; but is there any other eigenstate? From the completeness a general state looks like

$$| \, E >_? = \int a(E') \, | \, E' > dE' + \int b(E') \, | \, D' > dE',$$

From $(H - E) \, | \, E >_? = 0$ one gets

$$\begin{aligned} (E' - E) b(E') = 0, \\ (E' - E) a(E') = - \lambda E' b(E') \end{aligned}$$

the solution of which is

$$b(E') = b\delta(E' - E),$$
$$a(E') = a\delta(E' - E) + \lambda bE\delta'(E' - E),$$

where δ' denotes differentiation with respect to the first argument. Therefore we have two linearly independent eigenstates

$$\begin{aligned} |\, E >_1 &= |\, E >, \\ |\, E >_2 &= |\, D > + \lambda E \int dE' \,|\, E' > \delta'(E' - E). \end{aligned} \tag{5}$$

and it is a matter of choice which of the sets $\{|\, E >, |\, D >\}$ or $\{|\, E >_1, |\, E_2 >\}$ we choose. For example

$$|\, D > = |\, E >_2 - \lambda E \int dE' \,|\, E >_1 \delta'(E' - E), \tag{6}$$

i.e. the dipole ghost is a superposition of eigenstates. A general state can be developed as

$$\begin{aligned} |\, A > = \int \alpha(E) \,|\, E > dE + \int \beta(E) \,|\, D > dE = \iint [\alpha(E')\delta(E' - E) - \\ - \lambda\beta(E')E'\delta'(E - E')] \,|\, E' >_1 dE dE' + \int \beta(E) \,|\, E >_2 dE. \end{aligned}$$

Thus we see that the argument given under (3) was rather hasty, indeed wrong. One realizes the following: in (3) the Σ-sign possesses only symbolic meaning, and if the state $|$ phys; in $>$ is developed in the form (3), $b(n)$ will contain $\delta'(E' - E)$ when

$$\begin{aligned} |\, \text{phys; in} > = \Sigma a(n) \,|\, \text{phys; out} > + \\ + \Sigma\beta(n) \,|\, E; \text{ out} >_1 + \Sigma c(n) \,|\, E; \text{ out} >_2, \end{aligned} \tag{7}$$

$\beta(n)$ and $c(n)$ may both have only $\delta(E' - E)$ — s. This is, in fact, what happens in the model treated in Section 3. The normalization properties of $|\, E >_1$, $|\, E >_2$ from (4) and (5) are

$$\begin{aligned} {}_1< E' \,|\, E >_1 &= 0, \; {}_1< E \,|\, E >_2 = \delta(E' - E), \\ {}_2< E' \,|\, E >_2 &= \lambda E'\delta'(E - E') + \lambda E\delta'(E' - E) = -\lambda\delta(E' - E). \end{aligned} \tag{8}$$

Thus

$$|\, E >_{II} = \frac{1}{\sqrt{\lambda}} \,|\, E >_2 ,$$

and

$$|\, E >_I = \sqrt{\lambda} \,|\, E >_1 + \frac{1}{\sqrt{\lambda}} \,|\, E >_2 \tag{9}$$

are linearly independent orthogonal ± 1 square norm eigenstates:

$${}_I< E' |\, E >_{II} = 0, \; {}_I< E' |\, E >_I = - \,{}_{II}< E' |\, E >_{II} = \delta(E' - E) . \tag{10}$$

This normalization shows that in spite of the "mysterious" δ' in (5) proper eigenstates can be found which are normalized in the usual sense. Therefore we may conclude by stating that the calculations accepted so far in the formal theory of scattering can be applied here also.

A procedure similar to (5) can also be carried out on the level of operators. In the reversed way, for example, starting from

$$H = \int E\,[A^*(E)A(E) - B^*(E)B(E)]\,dE,$$
$$[A(E), A^*(E')] = -\,[B(E), B^*(E')] = \delta(E - E'),$$

after introducing

$$\alpha(E) = \frac{1}{\sqrt{\lambda}}\,(A(E) - B(E)),$$

$$\beta(E) = \sqrt{\lambda}\,B(E) - \sqrt{\lambda}\,E \int dE'\delta'(E' - E)\,[A(E') - B(E')]$$

and allowing a partial integration, one gets

$$H = \int E[a^*(E)\beta(E) + \beta^*(E)\alpha(E) - \lambda\alpha^*(E)\alpha(E)]\;dE\,,$$
$$[\alpha(E), \beta^*(E')] = [\beta(E), \alpha^*(E')[= \delta(E - E'), \tag{11}$$

which corresponds to a dipole ghost Hamiltonian.

3. We have seen that in a theory with only dipole ghost states the unitarity of the physical S-matrix is not guaranteed automatically. Therefore in order to obtain a finite but unitary field theory it is rather fruitless to introduce auxiliary FROISSART fields [10]. What can be done then, with theories (e.g. LEE model or HEISENBERG's nonlinear spinor theory) where a dipole situation appears? If we wish to extract an unitary physical S-matrix, we must apply some sort of artifical unitarization procedure, as in any other theory with indefinite metric. A possibility is BOGOLJUBOV's prescription [11], which is always valid. In the LEE model HEISENBERG sorts out certain physically acceptable states [7]. Similar problems are treated also in [2].

Below a new proposal for a unitarization procedure — seemingly closely connected with HEISENBERG's and SUDARSHAN's [12] ideas — is worked out in detail for an earlier model [4] in which the Hamiltonian $H = H_0 + H_1$ with

$$H_0 = m_v\psi_v^*\psi_v + \int \omega(k)a^*(k)a(k)dk + \lambda A^*A,$$

$$H_1 = -\frac{1}{\sqrt{4\pi}}\int \frac{1}{\sqrt{2\omega}}\,(\psi_v^*\,a(k)\psi + \psi^*a^*(k)\,\psi_v)\,dk\,, \tag{12}$$

$$\psi = g\psi_N + g_1A + g_2B,\ \omega = \sqrt{k^2 + m^2}_\Theta,$$

where the prescription for the commutators is

$$\{\psi_V, \psi^*\} = \{\psi_N, \psi_N^*\} = \{A, B^*\} = \{B, A^*\} = 1, \qquad (13)$$
$$[a(k), \alpha^*(k')] = \delta(k - k');$$

all other commutators (anticommutators) vanish. In the $N - \Theta$ sector the general eigenstate of H looks like

$$|E> = (\alpha\psi_V^* + \psi_N^* \int \varphi(k)a^*(k)dk + A^* \int \varphi_1(k)\alpha^*(k)dk + \\ + B^* \int \varphi_2(k)a^*(k)dk)\,|0>, \qquad (14)$$

where $|0>$ the is real vacuum state, with ($\pm$ stands for in or out states)

$$\varphi = \frac{a}{\sqrt{4\pi k_0}}\delta(k-k_0) + \frac{\alpha g}{\sqrt{4\pi}\sqrt{2\omega}(\omega - E \mp i\varepsilon)},$$
$$\varphi_2 = \frac{c}{\sqrt{4\varphi k_0}}\delta(k-k_0) + \frac{\alpha g_2}{\sqrt{4\pi}\sqrt{2\omega}(\omega - E \mp i\varepsilon)}, \qquad (15)$$
$$\varphi_1 = \frac{b}{\sqrt{4\pi k_0}}\delta(k-k_0) + \frac{\lambda c E}{\sqrt{4\pi k_0^2}}\delta'(k-k_0) + \\ + \frac{\alpha}{\sqrt{4\pi}\sqrt{2\omega}(\omega - E \mp i\varepsilon)}\left(g_1 - \frac{\lambda g_2}{\omega - E \mp i\varepsilon}\right),$$
$$E = \sqrt{k_0^2 + m_\Theta^2},$$

a, b, c being arbitrary constants (depending, perhaps, on E). α can be determined from

$$h(E \pm i\varepsilon)\,\alpha \begin{matrix}\text{out}\\ \text{in}\end{matrix}(E) = \frac{k_0}{\sqrt{2E}}(ag + bg_2 + cg_1) + \frac{\lambda}{\sqrt{2E}}\left(\frac{k_0}{2E} - \frac{2E}{k_0}\right)cg_2, \qquad (16)$$

where

$$h(z) = m_v - z - (g^2 + 2g_1 g_2)\int \frac{k^2\,dk}{2\omega(\omega - z)} + \lambda g_2^2 \int \frac{k^2\,dk}{2\omega(\omega - z)^2}. \qquad (17)$$

Thus we have found there linearly independent eigenstates with (i; $a = 1$, $b = c = 0$), (ii; $a = c = 0$, $b = 1$), (iii; $a = b = 0$, $c = 1$). These are normalized to

$$<i;\ E' \mid i;\ E> \delta(k'_0 - k_0),\ <ii;\ E' \mid ii;\ E> = 0,$$
$$<iii;\ E' \mid iii;\ E> = -\lambda\left(\frac{3E}{k^2} - \frac{1}{E}\right)\delta(k'_0 - k_0), \qquad (18)$$
$$<i;\ E' \mid ii;\ E> = <i;\ E' \mid iii;\ E> = 0,$$
$$<ii;\ E' \mid iii;\ E> = \delta(k'_0 - k_0),$$

but a procedure similar to (9) gives orthonormalized eigenstates. We have shown that the physical $N-\Theta$ scattering state (i) gives a non-unitary S-matrix.

The proposal is: let us add to the physical scattering state (i) a zero-norm eigenstate (ii) with such a coefficient that for this new state the physical S-matrix should be unitary. It is easy to see that this state $|\, E;$ New phys.$>$ is (15) with ($a=1,\ c=0,\ b\neq 0$). First b must be determined from the unitarity requirement then one has to calculate

$$< a=1,\ b\neq 0,\ c=0,\ E';\ \text{in}\ |\ a=1,\ b\neq 0,\ c=0;\ E;\ \text{out}>.$$

From (14), (15) this matrix element turns out to be

$$\begin{aligned}
&< E';\ \text{New phys.;\ out}\ |\ E;\ \text{New phys.;\ in} > = \delta(k'_0-k_0)+\\
&+\alpha^*_{\text{out}}(E')\,\alpha_{\text{in}}(E)\left\{1+\frac{h(E-i\varepsilon)}{E-E'-i\varepsilon}+\frac{h(E'-i\varepsilon)}{E'-E-i\varepsilon}+\right.\\
&+\int\frac{k''^2\,dk''}{2\omega''(\omega''-E'-i\varepsilon)\,(\omega''-E-i\varepsilon)}\left[g^2+2g_1g_2-\right.\\
&\left.\left.-\lambda g_2^2\left(\frac{1}{\omega''-E'-i\varepsilon}+\frac{1}{\omega''-E-i\varepsilon}\right)\right]\right\}.
\end{aligned}$$

By using formal identities of the type

$$\frac{1}{(x'-x-i\varepsilon)^{n+1}}=P\,\frac{1}{(x'-x)^{n+1}}+i\pi\,\frac{(-1)^n}{n!}\,\delta^{(n)}(x'-x),$$

and the explicit form of h from (17), the S-matrix is found to be

$$S=e^{2i\pi\delta(E)}=1+\frac{i\pi k_0(g+b^*g_2)\,(g+bg_2)}{h(E+i\varepsilon)}\,. \tag{19}$$

For the trivial case $S=1$

$$b=-\frac{g}{g_2}\,. \tag{20}$$

From (16) the condition for the no-scattering case in general is

$$k_0(ag+bg_2+cg_1)+\lambda\left(\frac{k_0}{2E}-\frac{2E}{k_0}\right)cg_2=0\,,$$

which for $c=0$, $a=1$ gives (20). The sole non-trivial unitary S-matrix for the case ($a=1,\ b\neq 0,\ c=0$) is

$$S = \frac{h(E-i\varepsilon)}{h(E+i\varepsilon)},$$

which requires

$$h(E + i\varepsilon) + i\pi k_0(g + b^*g_2)(g + bg_2) = h(E - i\varepsilon).$$

Taking into account form (17) of h, this means

$$k_0(g+b^*g_2)(g+bg_2) = k_0(g+2g_1g_2) - \lambda g_2^2 \frac{E}{k_0},$$

from which b can be determined.

It is easy to see that this unitarization prescription is not unique — no other similar procedure is — and since it is proposed to re-define the physical states, the concrete example treated above can be considered as an application of SUDARSHAN's proposal [12] for dipole states.

REFERENCES

1. N. NAKANISHI, Progr. Theoret. Phys., **38,** 881, 1967.
2. H. P. DÜRR and E. RUDOLPH, Nuovo Cimento, **68A,** 411, 1969.
3. V. J. FAINBERG, private communication.
4. K. L. NAGY, Acta Phys. Hung., **28,** 245, 1969.
5. N. NAKANISHI, Phys. Rev. D., **3,** 1343, 1971.
6. W. HEISENBERG, Introduction to the Unified Field Theory of Elementary Particles, J. Wiley and Sons Ltd., London, 1967.
7. W. HEISENBERG, Nucl. Phys., **4,** 532, 1957.
8. R. ASCOLI and E. MINARDI, Nuovo Cimento, **8,** 951, 1958; Nucl. Phys., **9,** 242, 1958.
9. K. L. NAGY, State Vector Spaces with Indefinite Metric in Quantum Field Theory. Akadémiai Kiadó, Budapest, 1966.
10. M. FROISSART, Nuovo Cimento Suppl., **14,** 197, 1959.
11. N. BOGOLIUBOV, Proceedings of the 1958. International Conference on High Energy Physics, CERN. 1958.
12. E. C. G. SUDARSHAN, Phys. Rev., **123,** 2183, 1961; Phys.Rev., **133B,** 487, 1964; Indefinite Metric and Nonlocal Field Theories, Syracuse University preprint, No. SU-1206-137, 1967.

ВЕКТОРЫ СОСТОЯНИЯ С НОРМОЙ, ОБРАЩАЮЩЕЙСЯ В НУЛЬ, И ВЕРОЯТНОСТНАЯ ИНТЕРПРЕТАЦИЯ

К. Л. НАДЬ

Резюме

Проведен анализ причин, по которым теории с дипольными состояниями не обеспечивают автоматически унитарность физической S-матрицы. Предложен разумный приём для унитаризации, который применим и в таких необичных случаях.

Acta Physica Academiae Scientiarum Hungaricae, Tomus 32 (1—4), pp. 135—140 (1972)

THE MAGNETIC FIELD DEPENDENCE OF THE ANTIFERROMAGNETIC–FERROMAGNETIC TRANSITION TEMPERATURE IN FeRh*

By

L. PÁL, G. ZIMMER

CENTRAL RESEARCH INSTITUTE FOR PHYSICS, BUDAPEST

and

J. C. PICOCH, T. TARNÓCZI[1]

LABORATOIRE D'ELECTROSTATIQUE ET DE PHYSIQUE DU MÉTAL, C.N.R.S., GRENOBLE, FRANCE

(Received 19. X. 1971)

It was shown by measurements in static magnetic fields that, contrary to the results obtained by MCKINNON et al. in pulsed fields, the critical field for the antiferromagnetic—ferromagnetic (AFM—FM) transition in FeRh is a nearly linear function of temperature. The linear temperature dependence suggests that besides the electronic contribution there must be a considerable lattice contribution to the entropy change observed in the AFM—FM transition.

I. Introduction

The alloy FeRh furnishes a very interesting example of a first-order antiferromagnetic— ferromagnetic (AFM—FM) transition. Recent experimental data on this transition have been analyzed thermodynamically by J. M. LOMMEL [1], who concluded that the anomalous excess entropy of the ferromagnetic over the antiferromagnetic phase at the transition has a predominantly electronic origin. This is inferred principally from the experimental results of MCKINNON et al. [2], who showed that the critical field for inducing the transition varies with the square of temperature, from which it directly follows that the excess entropy has to be a linear function of the temperature.

In contrast with the quadratic temperature dependence observed by MCKINNON et al., ZAVADSKII et al. [3] found a linear temperature dependence in about the same temperature interval. The latter result implies that the electronic contribution to the entropy at the AFM—FM transition is neither exclusive nor preponderant.

In order to get more confident data on the temperature dependence of the critical field the measurements were repeated in static magnetic fields. In Section II the experimental method and the evaluation of data are described, while in Section III a detailed analysis of the possible discrepancies is given.

* Dedicated to Prof. L. JÁNOSSY on his 60th birthday.

[1] Visiting scientist. Present address: Central Research Institute for Physics, Budapest, Hungary.

II. Method of measurement

The magnetization versus temperature curves were measured by extraction technique on a spherical specimen of $Fe_{51,7}Rh_{48,3}$ of 3 mm diameter. The magnetic field, variable from zero to 82.3 kOe, was generated by a water-cooled Wood-type solenoid; the field strength was calculated from the precisely measured solenoid current. The sample temperature could be varied from 77 to 300 °K by the use of a special nitrogen cryostat supplied with a PID-type temperature controller. Although the temperature fluctuation of the specimen

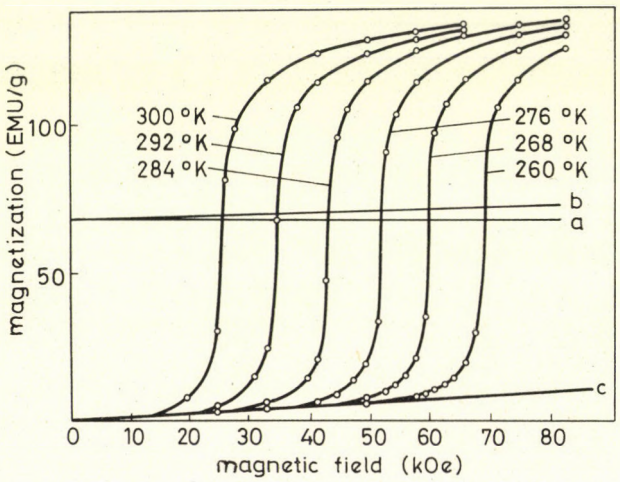

Fig. 1. FeRh magnetization curves at different temperatures. The temperature for each curve is given in °K. The critical field for AFM-FM transition is given by the intersection points of lines *a* or *b*. Line *c* is the magnetization curve for the pure AFM-phase

before extractions was smaller than ± 0.08 °K, during the measurements the temperature stability was not better than ± 0.4 °K. This resulted in a temperature inhomogeneity along the extraction path which could not be reduced significantly. However, this small uncertainty in the sample temperature did not seriously affect the form of the critical field versus temperature curve.

The flux change produced by sample extraction was measured with a ballistic galvanometer coupled to a Graphispot light follower. Before each magnetization measurement the sample was cooled to liquid nitrogen temperature, then heated in the absence of magnetic field to the temperature of the actual measurement and allowed to reach thermal equilibrium. The magnetization curves measured in increasing magnetic fields at different temperatures are shown in Fig. 1.

Although the AFM—FM transition is a first-order process, unfortunately the sharpness of the transition in real materials is not so pronounced that the

critical field can be defined unambigously, and thus one has to apply in some sense arbitrary definitions for the critical field. For instance, the critical field can be identified with the field value at which the field derivative of the magnetization is maximal (1), or the field at which the magnetization reaches half its maximum value (2). In the latter case it seems to be necessary to take into account also the high susceptibility of the AFM phase, while the relatively low intrinsic susceptibility of the FM phase can be neglected.

For the determination of the critical field we used the second definition. The straight lines *a* and *b* in Fig. 1 show the critical fields at different temperatures. Line *b* gives the corrected values and is so drawn that its intersection with the magnetization axis is equal to that of *a*, while its angle to *a* is half the angle between the magnetic field axis and the straight line *c* corresponding to the magnetization of the pure AFM phase. The correction for the intrinsic FM susceptibility, which somewhat increases the angle between *a* and *b*, has been omitted here, because its contribution to the magnetization is very small.

It should be noted that the definition of the critical field adopted here is consistent with the assumption that at the transition temperature half the sample consists of the AFM phase.

Fitting the measured values of the critical field by the least squares method to the polynominal

$$H_C = H_0 + H_1 T + H_2 T^2,$$

the following coefficients were obtained making use of the intersection points with *a*:

$$H_0 = 369.2 \quad \pm 40.0 \text{ kOe}$$
$$H_1 = 1.22 \quad \pm 0.29 \text{ kOe/°K}$$
$$H_2 = 0.00025 \pm 0.00051 \text{ kOe/°K}^2,$$

while with the intersection points with *b*:

$$H_0 = 442.6 \quad \pm 40.0 \text{ kOe}$$
$$H_1 = 1.73 \quad \pm 0.29 \text{ kOe/°K}$$
$$H_2 = 0.00114 \pm 0.00051 \text{ k°Oe/K}^2.$$

III. Discussion

First of all, it can be seen that the coefficients of the quadratic term are very small in both cases: the coefficient is practically zero, within the experimental error, in the first case and certainly positive — not negative, as found

by McKINNON et al. [2] — in the second case. This means that if $H_C = H_C(T)$ is a second-order polynomial of the temperature, its curvature must be opposite to that observed by McKINNON et al.

According to PÁL's [4] model, the relation of the transition temperature to the critical field is expressed by

$$T = T_0 - aH_C^{2/3},$$

which can be approximately inverted into the form

$$H_C = H_0 + H_1 T + H_2 T^2,$$

where H_1 is negative and H_2 positive. The positive sign of H_2 is consistent with our experiment, but one has to be careful in drawing any definite conclusion on the validity of PÁL's model in this case, since the coefficient of the quadratic term is only twice as large as its error.

The only certain conclusion is that the experimental data are in closer agreement with a linear than with a quadratic temperature dependence of the critical field. The curve of critical field versus temperature can be seen in Fig. 2. The straight line corresponds to the least squares fit of $H_C = H_0 + H_1 T$ to the experimental points. In Fig. 3 curve A shows the deviations of the experimental values from the expression $H_C = H_0 + H_1 T$ fitted by the least squares method, while curve B indicates the devitations from $H_C = H_0 + H_2 T^2$. There is no doubt that the deviations are larger in the latter than in the former case.

Let us look now at the possible causes of the difference between the pulsed field and the static field data. McKINNON et al. [2] defined the critical field as the value at which dM/dH is maximal. However, their experimental method did not determine precisely the value as so defined. Essentially the method consisted in placing the specimen in one of a matched pair of search coils belonging to a compensated inductive pick-up system that was located inside the pulse coils in the most uniform region of the magnetic field. In such an arrangement the voltage induced in the search coils originates exclusively from the specimen and is thus proportional to the time derivative of the magnetization. Since $\mathrm{d}M/\mathrm{d}t = \mathrm{d}M/\mathrm{d}H \cdot \mathrm{d}H/\mathrm{d}t$, the position of the maximum is dependent on the pulse shape. Since the value of $\mathrm{d}H/\mathrm{d}t$ remains initially practically constant but at higher fields shows an ever more rapid decrease as the field increases, the maximum position of $\mathrm{d}M/\mathrm{d}t$ is shifted towards increasingly lower fields as compared with the maximum of $\mathrm{d}M/\mathrm{d}H$. As the magnetic field grows (i.e. as the temperature decreases) the shift becomes ever larger. This causes a negative curvature in the measured $H_C = H(T)$ curve corresponding to a fictive quadratic term with negative coefficent.

Another problem arising in the measurements by pulsed field technique is the possible effect of the latent heat released or absorbed in the AFM—FM transition. The heat absorbed in the transition decreases the specimen tempera-

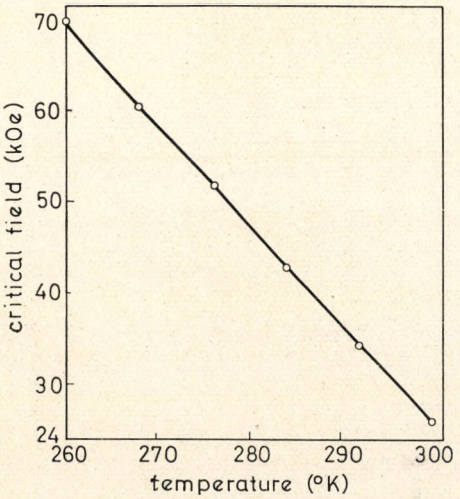

Fig. 2. Temperature dependence of the critical field for AFM-FM transition in FeRh. The straight line corresponds to the least squares fit of the equation $H_C = H_0 + H_1 T$ to the experimental points

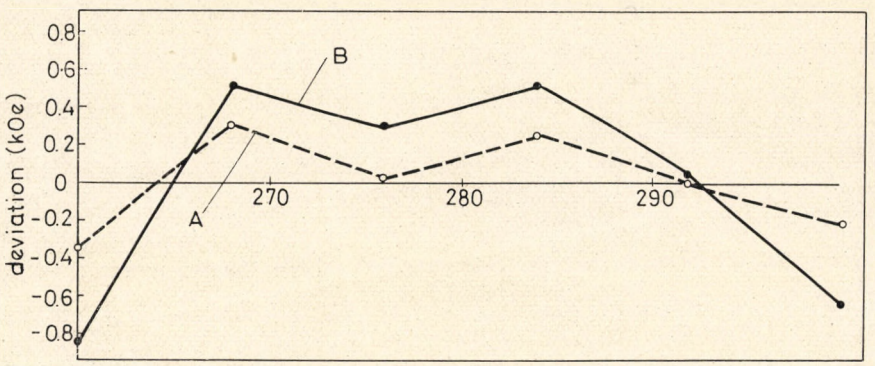

Fig. 3. Deviations of the experimental values from linear (*A*) and from quadratic (*B*) temperature dependence of the critical field H_C

ture, as in this case the system can be regarded as adiabatic. From the reported data the latent heat can be taken as 1 cal/g and the specific heat as 0.08 cal/gK°, and thus the temperature decrease can be estimated as 6—7°. If the specific heat and latent heat of the specimen are temperature-dependent, the temperature decrease will depend on the temperature which we associate with the criti-

cal field. These circumstances make questionable the preponderance of the electronic contribution to the excess entropy at the transition.

Assuming that the AF—F transition in FeRh can be described by an appropriate combination of the exchange-inversion and the electron entropy models, the two contributions with opposite signs could "straighten" the function $H_C = H_C(T)$. This would explain the nearly linear relationship shown by our measurements in static fields.

Acknowledgement

The authors are much indebted to Professor R. PAUTHENET for putting at their disposal the equipment of the High Magnetic Field Laboratory of the C.N.R.S., Grenoble, and for his helpful interest in their work.

REFERENCES

1. J. M. LOMMEL, J. Appl. Phys., **40**, 3880, 1969.
2. J. B. MCKINNON, D. MELVILLE and E. W. LEE, J. Phys. C: Metal Phys. Suppl., **1**, S46, 1970.
3. E. A. ZAVADSKII and J. G. FAKIDOV, Sov. Phys. Solid State, **9**, 103, 1967.
4. L. PÁL, Acta Phys. Hung., **27**, 47, 1969.

ЗАВИСИМОСТЬ ТЕМПЕРАТУРЫ АНТИФЕРРОМАГНИТНОГО-ФЕРРОМАГНИТНОГО ПЕРЕХОДА ОТ МАГНИТНОГО ПОЛЯ В FeRh

Л. ПАЛ, Д. ЦИММЕР, Й. Ц. ПИКОШ и Т. ТАРНОЦИ

Резюме

Путем измерений в статическом магнитном поле было показано, что в противоположность результатам, полученным Мак-Киннон и другими в импульсных полях, критическое поле для антиферромагнитного-ферромагнитного перехода в FeRh является почти линейной функцией температуры. Линейная температурная зависимость позволяет предполагать, что наряду с электронным компонентом должен иметь место значительный вклад решетки в изменение энтропии, наблюдаемой в антиферромагнитном-ферромагнитном переходе.

Acta Physica Academiae Scientiarum Hungaricae, Tomas 32 (1—4), pp. 141—147 (1972)

FURTHER MEASUREMENT ON THE $K_L - K_S$ REGENERATION AMPLITUDE ON HYDROGEN AT HIGH ENERGIES*

DUBNA—SERPUKHOV—BUDAPEST COLLABORATION

(Received 19. X. 1971)

The transmission regeneration amplitude of the long-lived K mesons was measured in the 14—42 GeV energy range. The phase of the difference of the forward scattering amplitudes, arg $(f-\bar{f})$, turned out to be $(-118 \pm 13)°$, whereas its module over the kaon momentum, $|f-\bar{f}|/p$, fell with increasing energy.

1. Introduction

In a former article [1] we have desribed the aim of the experiment, its theoretical basis, as well as the experimental lay-out together with some preliminary results. Here we should like to present results based on a much larger statistics and on a completed analysis in regard of avoiding possible systematic biases.

The measured quantity $f - \bar{f}$, the difference of the $K^\circ p$ and $\overline{K}^\circ p$ forward scattering amplitudes, can be compared with different theoretical predictions. First, if isotopic invariance holds for high-energy particle scattering, the following relation must be valid:

$$\begin{aligned} \Delta\sigma &\equiv \sigma_{\text{tot}}(K^+ n) - \sigma_{\text{tot}}(K^- n) = \\ &= \sigma_{\text{tot}}(K^\circ p) - \sigma_{\text{tot}}(\overline{K}^\circ p) = \\ &= \frac{4\pi}{p} Im\,(f-\bar{f}), \end{aligned} \tag{1}$$

where σ_{tot} is the total cross section of the process standing in the parentheses. The last relation was obtained from the optical theorem. Moreover, if the so-called POMERANCHUK theorem [2] is valid, $\Delta\sigma$ must vanish in the asymptotic energy region. Thus in observing a behaviour $\Delta\sigma \to 0$ as energy increases, the conditions for the validity of the POMERANCHUK theorem, e.g. the asymptotic character of the energy region, can be ascertained experimentally. The actual energy dependences of $|f-\bar{f}|$ and arg $|f-\bar{f}|$ are predicted theoretically from

* Dedicated to Prof. L. JÁNOSSY on his 60th birthday, to whom D. KISS, E. NAGY, L. URBÁN and G. VESZTERGOMBI would like to express their indebtedness and gratitude for the constant stimulation that his teaching has given them in their work.

the dispersion relations [3—5] and the Regge-pole models [6—8]. The regeneration experiment is thus a means of verifying these models as will be seen in the next Section.

2. Results and conclusions

The total numbers of events selected when the regenerator was present and without it were 2640 and 450, respectively. The backgrounds to be subtracted from these figures were 16% and 28%, respectively.

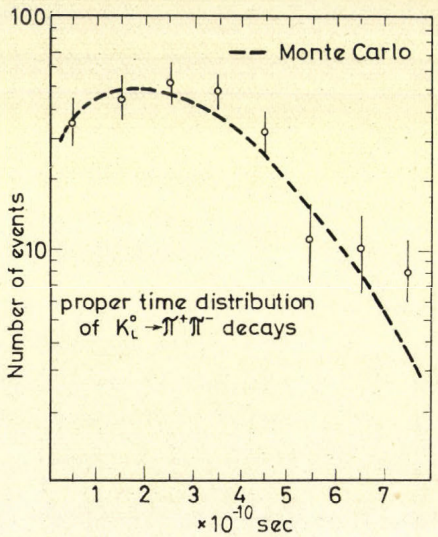

Fig. 1. The proper time distribution of $K_L \to \pi^+\pi^-$ events (circles). The dotted line shows the expected distribution calculated by Monte Carlo method

The detection efficiency $\varepsilon(p, t)$ was calculated as a function of kaon momentum, p, and proper time, t, using Monte Carlo method. The result was compared with the experimentally observed distributions, such as the proper time distribution of $K_L \to \pi^+\pi^-$ events when the regenerator was not employed. The similarity of the two distributions was satisfactory (Fig. 1).

In order to deduce ϱ from Eq. (1) of [1] one can proceed in different ways.

1a. Having determined experimentally the number of transmission-regenerated $K \to \pi^+\pi^-$ events (the circles e.g. in Fig. 4), one can fit to them the theoretical curve given by Eq. (1) of [1] using the Least Mean Squares (LMS) method. In doing so known quantities for γ_S, $\gamma(K_s \to \pi^+\pi^-)$, η_{+-} and Δm have been utilized [9]. It is also necessary to determine $M_H \cdot S_L(p)$, the total number of kaons decaying behind the regenerator. This was done using the $K_{\mu 3}$ and $K_{\pi 3}$ decay modes by applying Monte Carlo calculations [10].

in order to take into account the uncertainty in the K_L energy determination. With the assumption that the absorption of kaons does not vary in the 20—50 GeV energy region, the same spectrum can be obtained from the $K_L \to \pi^+\pi^-$ decays without regenerator. The observed spectrum can be seen in Fig. 2 together with a theoretical curve calculated after TRILLING [11]. The so-called monitor, M_H, turned out to be $M_H = (1.072 \pm 0.05)10^9$.

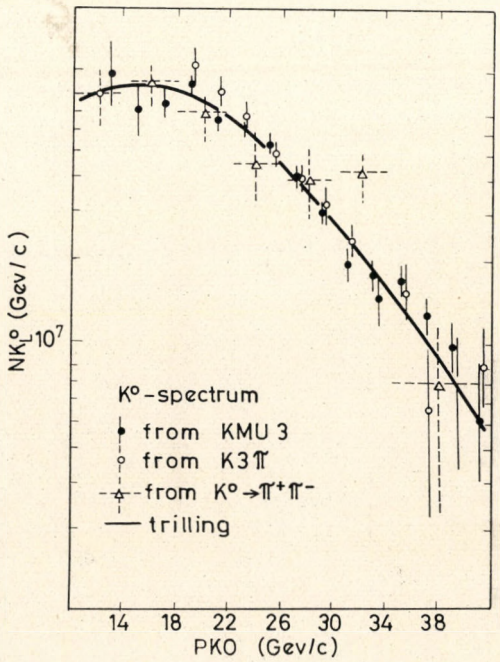

Fig. 2. The experimentally observed momentum spectrum of kaons behind the hydrogen regenerator. The full line shows theoretical expectation calculated in [11]

1b. To deduce ϱ by LMS fit it is not necessary to know $M_H S_L(p)$; on the contrary, if there is a sufficient number of proper-time bins the fit automatically produces the value of the parameter. In fact, the calculated values of $M_H S_L(p)$ coincide extremely well with the experimentally established ones, thus justifying the above procedure.

2. Again supposing that K_L absorption does not change with energy in hydrogen, we can rewrite Eq. (1) of [1] in the form:

$$\frac{N^H_{+-}}{N^V_{+-}} = \frac{M_H}{M_V}\left[\left|\frac{\varrho}{\eta_{+-}}\right|^2 e^{-\gamma_{st}} + 1 + 2\left|\frac{\varrho}{\eta_{+-}}\right| e^{-\frac{\gamma_{st}}{2}} \cos\left(\Delta m t + \Phi_s - \Phi_{+-}\right)\right], \qquad (2)$$

where N^V_{+-} and M_V are the same as the corresponding quantities N_{+-} and $M_H S_L(p)$ but refer to the case when regenerator is absent ($\varrho = 0$). The left-

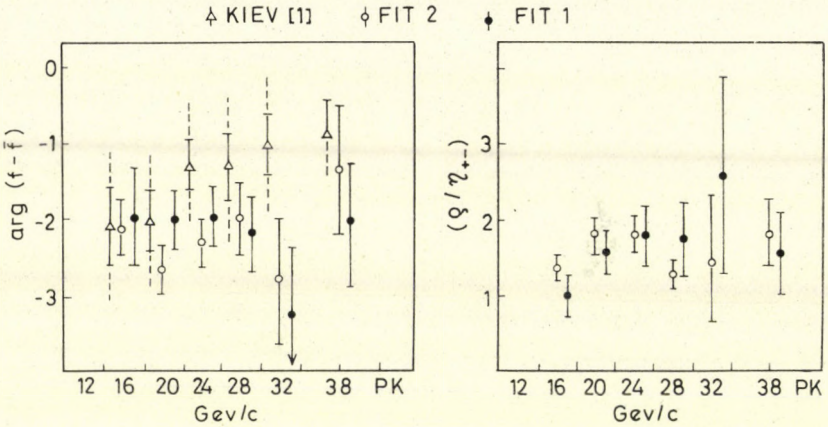

Fig. 3. The results of the two fitting procedures (full and empty circles). Preliminary results of the same experiments [1] (triangles) are also shown

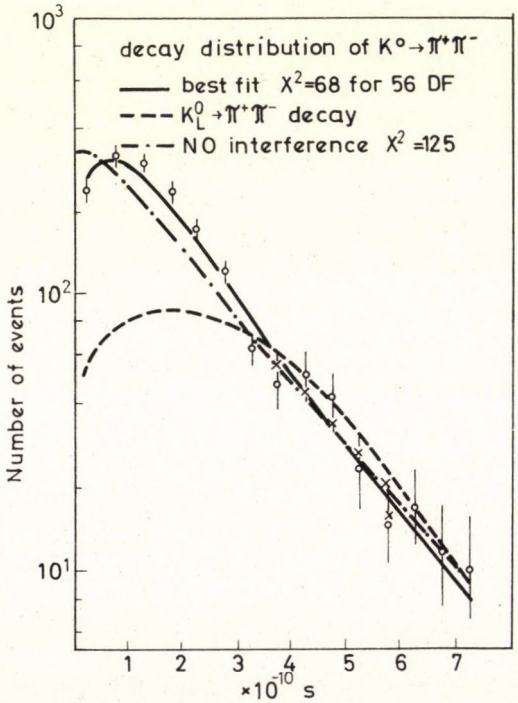

Fig. 4. Proper time distribution of all $K^0 \to \pi^+\pi^-$ events. The full line was obtained by an overall fit with constant phase hypothesis. Dotted lines correspond to no regeneration and no interference hypotheses

hand side is known experimentally, while M_H/M_V is the ratio of the total number of events with and without regenerator, which in the present case was 3.5 ± 0.06. The use of Eq. (2) in the LMS fitting procedure has the virtue that the efficiency and momentum spectrum functions do not intervene. On the other hand, one needs high statistics concerning the vacuum events.

The results of these two fitting procedures can be seen in Fig. 3. The two methods give essentially the same results. Since arg $(f - \bar{f})$ does not change appreciably with the energy, in agreement with the POMERANCHUK theorem and Regge pole models, we also carried out an overall fit over the six momentum intervals where arg $(f - \bar{f})$ was kept fixed. This yielded arg $(f - f) = -118^0 \pm 13^0$, with $\chi^2 = 68$ for 56 degrees of freedom. The curve corresponding to the best fit can be seen in Fig. 4, where for the sake of comparison curves with no interference and no regeneration are also shown.

For the modules of $(f - \bar{f})$ divided by p, the same overall fit yielded the values shown in Figs. 5 and 6. For comparison values of the same quantities measured in previous experiments but at lower energies are also shown. In Fig. 8 two kinds of theoretical curves can be seen: the full lines correspond to non-violation of the POMERANCHUK theorem ($\Delta\sigma = 0$), whilst the dotted lines

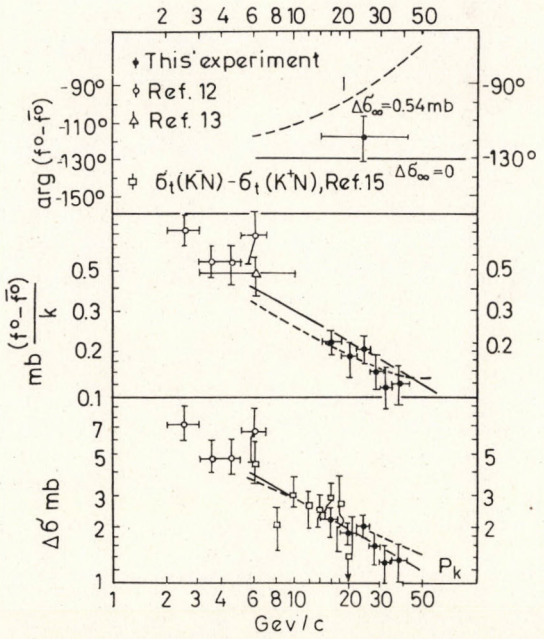

Fig. 5. The results of the overall fit. Theoretical curves were calculated using Regge-pole models. Full line — no violation, dotted line — small violation of the POMERANCHUK theorem. Results of previous measurements at lower energies are also shown

were obtained supposing small violation ($\Delta\sigma = 0.54$ mb) calculated using the Regge-pole models [5]. Our experimental points favour the former case, though a small violation cannot be excluded.

In Fig. 6 the theoretical curves were calculated using dispersion relations [4]. Here the full lines again correspond to the case of non-violation of the POMERANCHUK theorem, dotted lines signify weak violation ($\Delta\sigma = 2$ mb). Our experimental results seem to rule out this latter hypothesis in the given model with regard to both the phase and module of the difference of the forward scattering amplitudes.

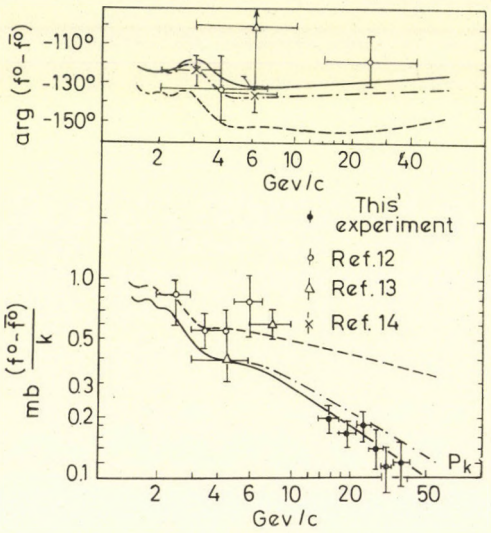

Fig. 6. Results of previous measurements together with those of the present experiment. The theoretical curves are predictions of dispersion relations. Full line — no violation, dotted lines — small violation of the POMERANCHUK theorem

REFERENCES

1. Dubna–Serpukhov–Budapest Collaboration, Acta Phys. Hung., **31,** 259, 1972 and С. Г. Басиладзе, Т. В. Беспалова, В. К. Бирулев, З. В. Борисовская, А. С. Вовенко, Д. Вестергомби, И. А. Голутвин, В. Я. Гвоздев, Н. Н. Говорун, Т. С. Григалашвили, Б. Н. Гуськов, Ю. А. Заневский, А. Запасник, И. М. Иванченко, И. Ф. Колпаков, Л. В. Комогорова, В. Д. Кондрашов, В. Г. Кривохижин, В. В. Кухтин, М. Ф. Лихачев, П. К. Маньяков, А. А. Митин, Н. А. Невская, В. П. Пугачевич, В. Д. Пешехонов, И. А. Савин, Е. А. Силаев, В. Е. Симонов, Д. А. Смолин, Г. Г. Тахтамышев, П. Т. Тодоров, А. С. Чвыров, М. Д. Шафранов, Сообщение ОИЯИ Р1-5361, 1970.
2. I. YA. POMERANCHUK, Zh. Eksp. i Teor. Fiz. **34,** 725, 1958.
3. M. LUSIGNOLI, M. RESTIGNOLI, G. VIOLINI, Nouvo Cim., **45A,** 792, 1966 and Phys. Letters, **24B,** 296, 1967.
4. И. Г. Азнаурян и Л. Д. Соловьев, ЯФ 12, 638, 1970.
5. М. Е. Вишневский, Н. Д. Галанина, Н. Н. Николаев и В. И. Чистилин Препринт ИТЭФ № 815 (1970 г.).

6. W. I. LYSIN, S. T. SUKHORUKOV and K. A. TER-MARTYROSIAN, Phys. Letters (to be published).
7. V. BARGER and R. PHILLIPS, Phys. Letters, **33B**, 425, 1970.
8. G. V. DASS, C. MICHAEL and R. PHILLIPS, Nucl. Phys., **B96**, 549, 1969.
9. Particle Properties, August 1970, Particle Data Group, Berkeley.
10. Г. Г. Тахтамышев. Препринт ОИЯИ № 2543 (1966 г.)
11. А. А. Борисов, С. Б. Нурушев, Л. Ф. Соловьев, В. Л. Соловьянов. Препринт ИФВЭ СЭФ 67—55 (1967 г.)
12. P. DARRIULAT, C. GROSSO, M. HOLDER, J. PILCHER, E. RADENMACHER, C. RUBBIA, M. SCIRE, A. SRANDE and K. TITTEL, Phys. Letters, **33B**, 433, 1970.
13. BUCHANAN, D. DRICKEY, F. RUDNICK, P. SHEPARD, D. STORK, H. TICHO, C. CHIEN, B. COX, L. ETTLINGER, L. RESVANIS, R. ZDANIS, E. DALLY, P. INNOCENTI and E. SEPPI, Contribution to the XVth International Conference on High Energy Physics, Kiev, 1970.
14. A. BRODY, W. JOHNSON, D. LEITH, J. LOOS, G. LUSTE, K. MORIYASU, B. SHEN, W. SMART, F. WINKELMANN, R. YAMARTINO and B. KEHOL, Contribution to the XVth International conference on High Energy Physics, Kiev, 1970.
15. K. J. FOLEY, R. S. JONES, S. J. LINDENBAUM, W. A. LOVE, S. OZAKI, E. D. PLATNER, C. A. QUARLES and E. H. WILLEN, Phys. Rev., **181, 5,** 1775, 1969.

ИЗМЕРЕНИЕ АМПЛИТУДЫ РЕГЕНЕРАЦИИ K_L-K_S НА ВОДОРОДЕ ПРИ ВЫСОКИХ ЭНЕРГИЯХ

СОВМЕСТНАЯ РАБОТА ДУБНА–СЕРПУХОВ–БУДАПЕШТ

Резюме

Амплитуда регенерации долгоживущих K мезонов была измерена при энергиях в 14—42 Гэв. Фаза различий амплитуд рассеяния вперед $\arg(f-f) = (-118 \pm 13)°$, а модуль над импульсом K-мезона $(f-f)/p$ падает вниз при возрастающей энергии.

Acta Physica Academiae Scientiarum Hungaricae, Tomus 32 (1—4), pp. 149—163 (1972)

ON THE EXCITATION MECHANISM AND OPERATION PARAMETERS OF THE 4416 Å He-Cd LASER*

By

M. JÁNOSSY, V. V. ITAGI** and L. CSILLAG

CENTRAL RESEARCH INSTITUTE FOR PHYSICS, BUDAPEST

(Received 19. X. 1971)

Measurements carried out on a 50 Hz a.c. excited He-Cd laser operating at 4416 Å indicated the possibility that two processes are involved in the excitation mechanism for this laser transition. It is suggested that the two processes are (1) Penning ionization of neutral Cd atoms by collisions with He metastables, and (2) electron — Cd ion collisions. The theory developed on the basis of the suggested excitation mechanism gives quantitative data on operation parameters of the laser.

1. Introduction

As a result of investigations performed on a d. c. operated He—Cd laser SILFVAST [1] has proposed that population inversion for the 4416 Å transition of Cd(II) is due to a Penning ionization process in which the upper laser state is excited by collisions of metastable He atoms with neutral Cd atoms, while depopulation of the lower laser state is achieved by the very fast 2144 Å ultraviolet transition. Measurements performed by SCHEARER and PADOVANI [2] show that the collision cross-section for the Penning reaction suggested by SILFVAST is high, being of the order of 10^{-15} cm^2, thus verifying that Penning ionization is indeed effective in populating the upper laser state in the He—Cd system.

Experiments on a 50 Hz a.c. excited He—Cd laser (CSILLAG et al. [3]) have indicated, however, that the excitation mechanism for the 4416 Å laser transition may be more complicated than that proposed by SILFVAST. The measurements showed it is possible that two processes take part in the excitation of the upper laser state, i.e. that Penning ionization alone is not sufficient to explain the phenomena observed on the 50 Hz a.c. excited laser.

In this article all experimental data obtained on the a.c. operated He—Cd laser are examined in detail and it is demonstrated that these can be interpreted by taking into account not only Penning ionization but also electron — Cd ion collisions. The theory developed on the basis of the suggested excitation mechanism gives quantitative data on operation parameters of the 4416 Å He—Cd laser.

* Dedicated to Prof. L. JÁNOSSY on his 60th birthday.

** Marathwada University, Aurangabad, India.

2. Experimental results

In the following the most important data obtained from experiments carried out on the 50 Hz a.c. operated He—Cd laser are summarized. Two different laser tubes, both of 4 mm inner diameter, were used in the measurements. One of the discharge tubes was 180 cm long, the necessary tube temperature being produced by a thermostatically controlled oil bath. The other was 130 cm long and was heated by means of an electrical furnace. The dependence of laser power on discharge current was measured using a dual beam

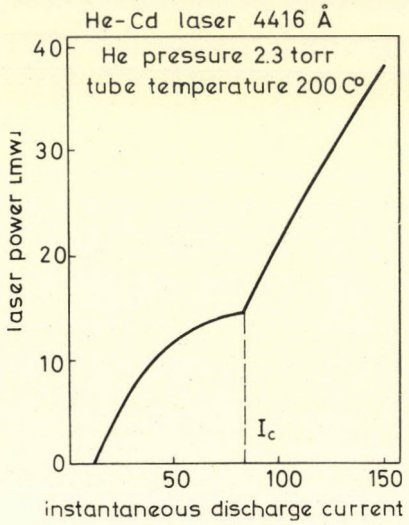

Fig. 1. Dependence of laser power on instantaneous discharge current for the 50 Hz a.c. excited He-Cd laser

oscilloscope, one beam recording the variation of laser power, the other the variation of discharge current, during a single excitation cycle.

a) The measurements showed an unusual dependence of a.c. laser power on discharge current in contrast to the linear relation found on d.c. lasers by SILFVAST [1], [4]. In the a.c. excited laser it was observed that laser power saturates in a current range of 50—100 mA but at higher current rises steeply again with increasing current (Fig. 1). The transition from the saturation range to the increasing one is always marked by a sharp break in the curve of laser power versus discharge current. Laser output becomes very noisy at currents above the critical current, at which the sharp increase in laser power occurs. The critical current I_c depends on He pressure, with increasing He pressure it shifts to lower currents in proportion to the reciprocal of the pressure p (Fig. 2). Above a certain He pressure, however, I_c does not depend anymore on p. The critical current also varies as the temperature (Cd concentration) in the

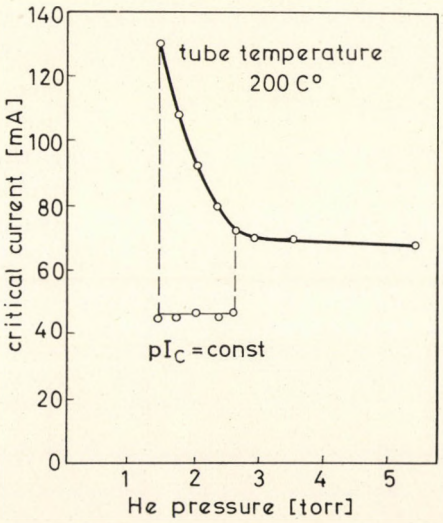

Fig. 2. Dependence of critical current on He pressure

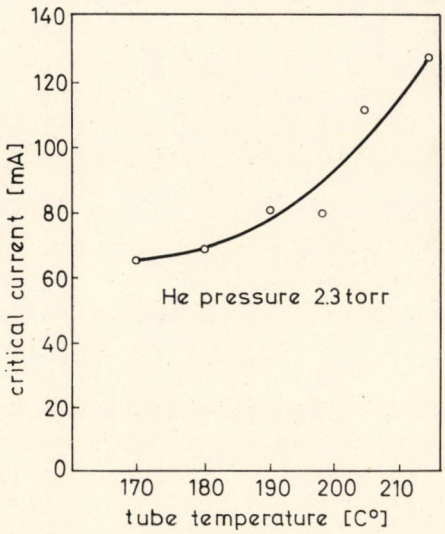

Fig. 3. Dependence of critical current on tube temperature

discharge tube is changed, becoming higher with increasing tube temperature (Fig. 3).

b) The same break in the intensity — current dependence was found for the spontaneous 4416 Å line viewed from the end of the laser tube; the effect was more or less pronounced for other spontaneous transitions of the ionic spectra of Cd (pronounced for 5378 Å, 5337 Å, 3250 Å, observable for 6360 Å,

6355 Å and others), but was not observed for spectral lines of neutral Cd. The intensity of neutral Cd lines showed a tendency to saturate in the current range in which the strong increase of intensity was found for the ionic spectral lines.

c) I_c was found to be equal to the lower current threshold for the occurrence of ionization waves (moving striations [5]) in the discharge tube. The presence of ionization waves was revealed by the sudden appearance of very strong, regular intensity fluctuations in the 4416 Å spontaneous side light as the discharge current exceeded I_c. The periodic intensity modulation due

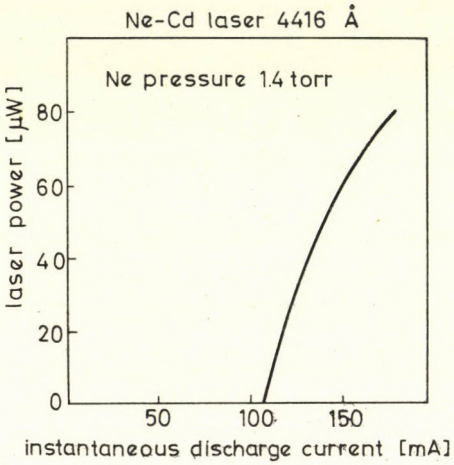

Fig. 4. Dependence of laser power on instantaneous discharge current for the 50 Hz a.c. excited Ne-Cd laser

to these fluctuations was nearly 100%, although noise amplitude in the laser output power was only 15% and modulation of discharge current was not more than a few %. According to data reported by PEPIN and DROUET [6] for d.c. discharges, the lower current threshold for the occurrence of ionization waves is related to saturation of the metastable atom population. The reported threshold current for a 1 cm diameter discharge tube containing pure He at a pressure of 2 torr is of the order of 100 mA, which roughly agrees with the value of I_c obtained in our 50 Hz a.c. operated He—Cd discharge.

d) CW laser oscillation at 4416 Å was also observed in a 50 Hz a.c. operated Ne—Cd discharge (CSILLAG et al. [7]). For this laser the dependence of laser power on discharge current is similar to that of the He—Cd laser in the current range above the critical current (Fig. 4). In the Ne—Cd laser the threshold current for laser action decreases with increasing Ne pressure and saturation occurs in laser output power.

3. Excitation mechanism

The break in the laser power — discharge current curve observed in the a.c. He—Cd laser is not due to any simple effect connected with a change of Cd vapour pressure caused by variation of the temperature of the discharge tube, since the same anomaly was not observed in a Ne—Cd discharge. The effect is thus certainly connected to atomic excitation processes in the He—Cd laser tube.

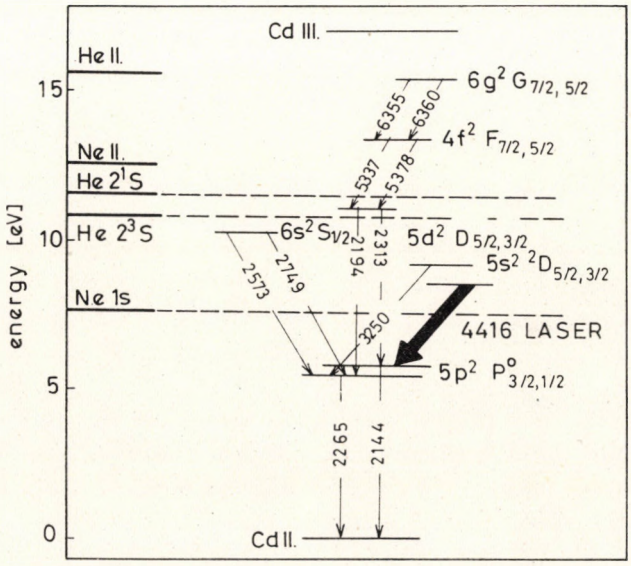

Fig. 5. Energy level diagram of the cadmium ion. Wavelengths are denoted in Å

Fig. 5 shows the energy level diagram of the Cd ion; the metastable and ion ground states of He and Ne which are important in respect of the excitation mechanism are also indicated. It can be seen that in contrast to the energy of the He metastables, the energy of Ne metastable atoms is not high enough to populate the upper $5s^{22}D_{5/2}$ level of the 4416 Å laser transition. Taking this together with the experimental fact that the low current ($I < I_c$) part of the laser power — discharge current curve does not appear in the Ne—Cd laser, it seems probable that in the low-current region the dominant excitation source of the $5s^{22}D_{5/2}$ state in the He—Cd laser is Penning ionization of neutral Cd atoms by collisions with He metastables, as suggested by SILFVAST.

On the other hand, the sharp increase of intensity at currents $I > I_c$ was found not only at 4416 Å, but also at other spontaneous transitions of the Cd ion. From Fig. 5 it can be seen that the energies of the 4*f* and 6*g* states from which these transitions originate are considerably higher than the energy of He

metastables. This shows that the sharp increase in intensity at currents above the critical current is not connected with any selective excitation by metastable states. This is also supported by the observation of laser oscillation at 4416 Å in the Ne—Cd discharge, where excitation by Ne metastables is ruled out on energetic grounds. It follows that the two effects are most likely due to electron excitation. Since the break observed in the He—Cd discharge occurs only in the ionic spectrum of Cd, excitation of the $5s^2$ and other ionic states in the high current region is probably due to collisions of electrons with ground-state Cd ions.

Inspection of the energy level diagram of the Cd ion shows that there is very strong cascading to the ion ground state from the $5s^2$ and other excited ionic states. Thus it is clear that Cd ions are to a great extent produced by cascades from higher energy ion states excited by Penning collisions.

We therefore suggest the following excitation mechanism for the 4416 Å He—Cd laser:

A) Penning ionization by collisions with He metastable atoms in the low current region $I < I_c$

$$\mathrm{He^M + Cd \rightarrow He + Cd^{+*} + e + \Delta E.}$$

The energy difference ΔE between He metastables and the upper laser state is taken away in the form of kinetic energy by the electron.

B) Two-step excitation in the high current region $I > I_c$ through:

I) Ionization of Cd by Penning collisions

$$\mathrm{He^M + Cd \rightarrow He + Cd^{+} + e + \Delta E.}$$

II) Electron excitation from Cd ion ground state

$$\mathrm{e + Cd^{+} \rightarrow e + Cd^{+*}.}$$

In process I cascades from higher energy ionic states make an important contribution to the population of the Cd ion ground state. Process II is strongly correlated with the appearance of ionization waves in the discharge tube. The exact role of ionization waves in the excitation mechanism is not clear, but it is possible that they cause local increases in the electron and Cd ion density and thereby raise the efficiency of process II in populating the upper laser state.

Excitation of the $5s^2\,^2D_{5/2}$ state by charge transfer collisions with He ions is not probable, since the energy of He ions is far off resonance with the upper laser state, and contributions by cascades from higher energy states are also negligible. It was shown by WEBB et al. [8], however, that charge transfer

collisions with He ions are efficient in populating the $4f$ and $6g$ states of the Cd ion, so it is likely that at low currents ($I < I_c$) charge transfer is the dominant process for excitation of these states.

Single-step electron excitation of the 4416 Å laser transition is not significant, since because of the high He pressure in the discharge tube relatively few high energy electrons capable of exciting the $5s^2{}^2D_{5/2}$ state from the neutral Cd ground state are present.

It is probable that excitation of the 4416 Å laser transition in a Ne—Cd discharge is analogous to the two-step process B, the role of He metastables being replaced by Ne metastable atoms. This suggestion is supported by the observation that the operation characteristics of the 4416 Å Ne—Cd laser are similar to those of the 4416 Å He—Cd laser in the current range above the critical current I_c.

4. Theory

In the following an expression aiming to describe the dependence of laser output power on various discharge parameters is derived on the basis of the suggested excitation mechanism.

We denote the populations of energy levels important in respect of the excitation mechanism by M (He metastables), N^+ (Cd ion ground state) and N (upper laser state). The population N' of the lower laser state will be neglected. If $N \gg N'$ holds, then the laser output power P can be taken as proportional to the population of the upper state. In the case of the 4416 Å transition of Cd(II) the spontaneous lifetime of the upper laser state is $\tau = 670$ nsec (KLEIN and MAYDAN [9]), while that of the lower one $\tau' = 3.4$ nsec (BAUMANN and SMITH [10]). The populations of excited states are only proportional to the lifetimes if the excitation rates to the two levels are equal. In our case, however, τ is so much longer than τ' that population inversion could take place even if the excitation rate to the lower level were two orders of magnitude faster than that to the upper. On this ground, taking into account also the high output power obtained from the He—Cd laser system, it is clear that $N \gg N'$ must be satisfied, at least to a first approximation.

We can now set up the rate equations for the three levels under discussion.

He metastables are produced by electron excitation and are lost by diffusion to the walls, by depopulating electron collisions, and by Penning deexcitation due to collisions with Cd atoms:

$$\frac{dM}{dt} = N_{He}\, n_e \langle \sigma_e v_e \rangle - \left(\frac{D}{\Lambda^2 p} + n_e \langle \sigma_D v_e \rangle + N_{cd} \langle \sigma_p v \rangle \right) M, \qquad (1)$$

where

N_{He}, $N_{c.}$, n_e = density of He atoms, Cd atoms and electrons;
v, v_e = velocity of He atoms and electrons;
σ_e, σ_D = cross-section for electron excitation and de-excitation of He metastables;
σ_p = cross-section for Penning collisions of He metastables with neutral Cd atoms;
D = diffusion coefficient for He metastables in He;
Λ = characteristic diffusion length (determined by the geometry of the discharge tube).

In the case of ground-state Cd ions we assume that a part of the population arises from cascades from the upper laser level, while contributions from other cascades and direct Penning excitation of Cd ions are taken into account by introducing a suitable factor $\alpha > 1$:

$$\frac{dN^+}{dt} = \alpha M N_{cd} \langle \sigma v \rangle - \frac{N^+}{\tau^+}, \tag{2}$$

where

σ = cross-section for Penning collisions which populate the upper laser state,
τ^+ = lifetime of Cd ions.

The upper laser level is populated by Penning collisions with He metastables and by collisions of electrons with Cd ions:

$$\frac{dN}{dt} = M N_{cd} \langle \sigma v \rangle + (n_e - n_c) \langle \sigma_e^+ v_e \rangle N^+ - \gamma N, \tag{3}$$

where σ_e^+ = cross-section for electron — Cd ion collisions,
γ = decay rate of upper laser level. (The rates of all processes leading to depopulation of this level are denoted together here.)

The ionization waves appear in the discharge tube above a sharp current threshold, this is taken into account by introducing a threshold electron density n_c in the electron — Cd ion collision term. Naturally, this term is zero if $n_e < n_c$.

Here we shall solve the equations for the stationary case. The solution obtained in this way is valid for the 50 Hz a.c. excited laser, since variations in time at 50 Hz excitation are much slower than the time factors of the elementary atomic collision processes.

Setting $dM/dt = 0$, $dN^+/dt = 0$, $dN/dt = 0$ and substituting M and N^+ from (1) and (2) into (3), we obtain

$$N = \frac{1}{\gamma} \frac{N_{He} n_e \langle \sigma_e v_e \rangle N_{cd} \langle \sigma v \rangle}{n_c \langle \sigma_D v_e \rangle + \dfrac{D}{\Lambda^2 p} + N_{cd} \langle \sigma_p v \rangle} [1 + \alpha (n_e - n_c) \langle \sigma_e^+ v_e \rangle \tau^+]. \quad (4)$$

The first term in (4) describes excitation of the upper laser state by Penning collisions, the second the two-step process of Penning ionization and electron — Cd ion collisions.

It follows from (4) that at a constant current ($n_e = \text{const}$) N is proportional to the product MN_{cd}. Our formula thus contains the results of SILFVAST [11], who verified the proportionality by direct measurements.

Considering the Penning collision term in (4), it can be seen that by increasing the discharge current (n_e is proportional to I) saturation occurs in N as a result of saturation of the He metastable density. The saturation electron density n_s is approximately

$$n_s \approx \frac{1}{\langle \sigma_D v_e \rangle} \left(\frac{D}{\Lambda^2 p} + N_{cd} \langle \sigma_p v \rangle \right). \quad (5)$$

Since the threshold current for the appearance of ionization waves is correlated with the saturation of the metastable density, we can take $n_c = n_s$. We obtain thus the observed laser power — discharge current dependence. By increasing the discharge current intermediate saturation occurs due to saturation of the He metastable density. At the critical current, however, electron excitation from the Cd ion ground state becomes effective and increases N significantly further. Although the increase in laser power is due to a two-step excitation process, laser output does not depend quadratically but only in a linear manner on discharge current. This can be seen clearly from (4), since when $n_e > n_c$ the He metastable density is already saturated, so that N becomes only a linear function of n_e.

The dependence of the critical current on He pressure and discharge tube temperature also follows from the first term of (4). Since n_c is proportional to I_c and $n_c = n_s$, this relation is given by (5). At low He pressures the diffusion term in (5) dominates over the Penning collision term, so

$$n_c \approx \frac{D}{\langle \sigma_D v_e \rangle \Lambda^2 p}. \quad (6)$$

Since $\langle \sigma_D v_e \rangle$ changes relatively slowly with variation of gas pressure it follows from (6), in accordance with experimental results, that at low He pressures n_c is inversely proportional to p. When p becomes high $N_{cd} \langle \sigma_p v \rangle \geqslant D/\Lambda^2 p$, and so n_c is determined by the Penning collision term and no longer depends on He pressure. The value of p where the p^{-1} dependence of n_c becomes constant is given by

$$\frac{D}{\Lambda^2 p} = N_{cd} \langle \sigma_p v \rangle . \tag{7}$$

To determine p in (7) we assume $\sigma_p \approx \sigma$ and approximate $\langle \sigma v \rangle$ by the product $\langle \sigma \rangle \langle v \rangle$. Inserting into (7) the values $D = 470$ cm^{2}torr sec^{-1}, given by PHELPS [12], $\sigma = 4 \times 10^{-15}$ cm^2, measured by SCHEARER and PADOVANI [2], $\Lambda^2 = 8 \times 10^{-3}$ cm^2, $N_{cd} = 3 \times 10^{13}$/cm^3 and $\langle v \rangle = 1.2 \times 10^5$ cm sec^{-1}, we obtain $p = 3.9$ torr, which agrees fairly well with the experimental value of 3 torr plotted in Fig. 2.

The temperature dependence of n_c at constant He pressure can be obtained in a similar way. It is found that at low temperatures $n_c \approx$ const., while at higher temperatures n_c increases in a nonlinear manner due to the non-linear relation between N_{cd} and the tube temperature T. The relation between n_c and T predicted by theory is clearly demonstrated in a qualitative manner by the experimental results shown in Fig. 4.

5. Optimum pressure

On the basis of the theory developed in the preceding section it is possible to calculate the optimum He pressure for laser operation at 4416 Å. This pressure is determined mainly by the pressure dependence of the electron — Cd ion collision term, since the first term in (4) — excitation of the upper laser state by Penning ionization — changes relatively slowly with variation of He pressure. The reason for this is discussed in the following.

If the geometry of the discharge tube is fixed, the energy of the electrons in a glow discharge is determined by the gas pressure only. Now at sufficiently high discharge currents $n_e \langle \sigma_L v_e \rangle \gg D/\Lambda^2 p + N_{cd} \langle \sigma_p v \rangle$, so the diffusion and Penning collision terms in the denominator of (4) can be neglected. Furthermore, the dependence of N on gas pressure arising from variation of the electron velocity distribution $f(v)$ in the electron excitation and de-excitation collision rates, $\langle \sigma_e v_e \rangle$ and $\langle \sigma_D v_e \rangle$, respectively, falls out, since these factors depend in a similar manner on gas pressure.

On the other hand, the electron — Cd ion collision rate $\langle \sigma_e^+ v_e \rangle$ is very sensitive to changes of gas pressure. In the case of electron-ion collisions the dependence of collision cross-section on electron energy differs from that of electron — atom collisions. Due to the Coulomb interaction between the negatively charged electron and positive ion, the electron is already distorted from a linear path at very large particle distances. Consequently the cross-section for electron — ion collisions has a sharp resonance maximum at the threshold excitation energy and falls off as E^{-1} at higher energies (see e.g. MOISEIWITSCH and SMITH [13]. Expressing the electron — Cd ion collision rate as a function of the energy of electrons

$$\langle \sigma_e^+ v_e \rangle = \sqrt{\frac{2}{m}} \int_0^\infty E^{1/2} f(E) \sigma_e^+(E) \, dE . \tag{8}$$

It is clear that the integral in (8) depends very strongly on the relative positions of the maxima of the collision cross-section σ_e^+ and the electron energy distribution $f(E)$. Since in our case $\sigma_e^+(E)$ is given and the energy at which $f(E)$ is maximum is determined by the gas pressure in the discharge tube, population of the upper laser state resulting from electron — Cd ion collisions is very sensitive to variation of He pressure.

On the basis of these considerations, at a discharge current $n_e \gg n_e$ and constant Cd concentration the upper laser state population N given by (4) can be approximated in a small He pressure range as

$$N \approx c_1 + c_2 p \langle \sigma_e^+ v_e \rangle \tag{9}$$

Here we have taken $N_{He} \sim p$, and in the first term a slow variation of N proportional to p has been neglected; c_1 and c_2 denote appropriate constants. Since p and $f(E)$ are both functions of the electron temperature kT in the discharge tube, we first determine the value of kT which gives maximum upper state population. If the optimum electron temperature is known, then it is possible to calculate the optimum He pressure for laser operation.

To evaluate $\langle \sigma_e^+ v_e \rangle$ according to (8) we take for the electron — Cd ion collision cross-section

$$\sigma_e^+ = \begin{cases} \dfrac{\sigma_0 E_0}{E} & \text{if } E \geq E_0 , \\ 0 & \text{if } E < E_0 , \end{cases} \tag{10}$$

where E_0 denotes the threshold excitation energy, (the energy difference between Cd ion ground state and the upper laser state) and σ_0 denotes the maximum collision cross-section.

The electron energy distribution in the discharge is assumed to be Maxwellian:

$$f(E) \, dE = \frac{2}{\sqrt{\pi}} (kT)^{-3/2} E^{1/2} e^{-E/(kT)} dE. \tag{11}$$

According to WADA and HEIL [14] there are departures from the Maxwellian distribution at energy values considerably higher than that corresponding to the maximum of $f(E)$. In this region, however, the contribution to the integral in (8) is small, so that no considerable error arises from the assumption.

On integration we obtain

$$\langle \sigma_e^+ v_e \rangle = \sqrt{\frac{8}{\pi m}} \sigma_0 E_0 (kT)^{-1/2} e^{-E_0/(kT)} . \tag{12}$$

The following relation exists between gas pressure and electron temperature:

$$\frac{\varepsilon}{p} = \text{const}\, kT\,, \tag{13}$$

where ε denotes the axial electric field in the positive column of the discharge. Since ε varies slowly with changing gas pressure, we can take p as inversely proportional to kT. The exact relation between p and kT is given later on by (17), however in the pressure range of interest (13) is a good approximation.

Inserting (12) and (13) into (9), we obtain

$$N \approx c_1 + c_2'(kT)^{-3/2}\, e^{-E_0/(kT)}, \tag{14}$$

where c_1 and c_2' are again appropriate constants.

Differentiating (14) with respect to kT yields the condition for maximum population

$$E_0 = \frac{3}{2} kT\,. \tag{15}$$

Since $3/2\, kT$ is the average energy of electrons in the discharge, (15) expresses the fact that optimum laser operation occurs when the average electron energy is equal to the energy necessary to excite ground state Cd ions to the upper laser state. Inserting the energy difference $E_0 = 8.57$ eV into (15) we obtain for the optimum electron temperature

$$kT = 5.71 \text{ eV}. \tag{16}$$

The electron temperature in the positive column is determined primarily by the high ionization potential He component; because of its very low concentration the effect of Cd is relatively small. Thus, the He pressure corresponding to a given electron temperature can be calculated from the following formula (see e.g. BROWN [15]):

$$\left(\frac{U_i}{kT}\right)^{-1/2} e^{U_i/(kT)} = 1{,}16 \times 10^7\, c^2\, p^2\, R^2\,, \tag{17}$$

where U_i = ionization potential,
R = discharge tube radius,
c = constant depending on type of gas used.

Inserting into (17) for He $U_i = 24.6\ eV$, $c = 3.9 \times 10^{-3}$, taking $kT = 5.71$ eV, and introducing for the tube diameter $d = 2R$, we obtain for optimum He pressure

$$p_{\text{opt}} \cdot d = 9 \text{ torr mm}. \tag{18}$$

Relation (18) is in good agreement with the experimental results of SILFVAST [1] and FENDLEY et al. [16], who give about 10 torr mm for the product of optimum He pressure and tube diameter in the case of d.c. He—Cd lasers. In the experiments performed on the 50 Hz a.c. excited laser $d = 4$ mm, so $p_{opt} = 2.25$ torr. This value is in excellent agreement with the measured optimum pressure of 2.3 torr.

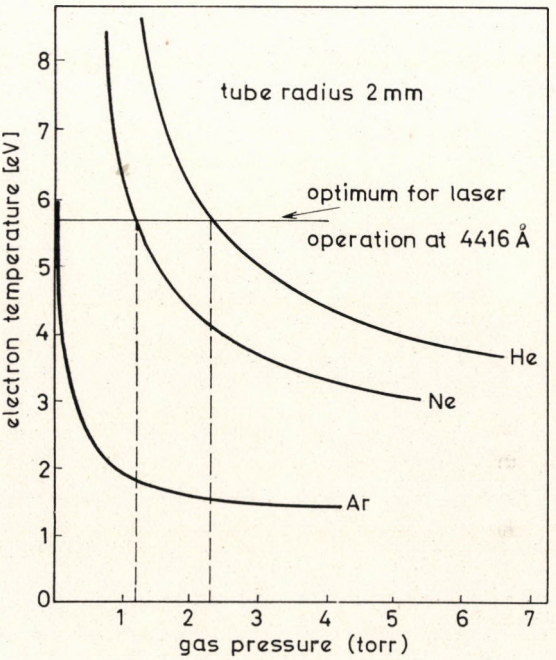

Fig. 6. Electron temperature as a function of gas pressure for He, Ne and Ar

If we assume an analogous two-step excitation mechanism consisting of Penning ionization and electron — Cd ion collisions for the Ne—Cd laser also, it is possible to determine the optimum pressure for 4416 Å laser operation in Ne. In the case of the Ne-Cd laser the term equivalent to the first one in (4) is missing, since direct excitation of the upper laser state by Penning ionization is not possible. The calculation is otherwise the same as that for He. Inserting now into (17) the data $U_i = 21.5$ eV and $c = 5.9 \times 10^{-3}$ for Ne and taking $kT = 5.71$ eV, we obtain for optimum Ne pressure

$$p_{opt} \cdot d = 4.8 \text{ torr mm}. \tag{19}$$

For a 50 Hz a.c. operated Ne—Cd laser with $d = 4$ mm, $p_{opt} = 1.2$ torr, which agrees well with the value $p_{opt} = 1.3$ torr measured by CSILLAG et al. [7].

Our results are illustrated in Fig. 6 where electron temperature is plotted on the basis of (17) as a function of gas pressure for He, Ne and also Ar. It can be seen that optimum He and Ne pressures for 4416 Å laser operation correspond to the same electron temperature in the discharge tube. In principle it should be possible to obtain laser action at 4416 Å using Ar also, provided the Ar pressure is chosen to give the proper electron temperature. This does not work in practice, however, as the optimum Ar pressure for $d = 4$ mm is of the order of 0.1 torr. At such low pressures there are relatively few Ar atoms present in the laser tube, thus Penning collisions of Ar metastables with neutral Cd atoms can not produce a sufficient density of Cd ions.

6. Conclusion

Our considerations on experimental results obtained with a 50 Hz a.c. operated He—Cd laser have indicated that two dominant processes take part in the excitation mechanism for the 4416 Å transition, the processes being interpreted as Penning ionization and electron — Cd ion collisions. The theory developed on the basis of the suggested excitation mechanism sucessfully explains experimental observations and gives quantitative data for the operation parameters of the 50 Hz a.c. excited He—Cd laser.

The question arises, however, of what is the situation in d.c. 4416 Å He—Cd lasers operated by cataphoretic techniques? The presence of two processes in the excitation mechanism is revealed very clearly in the 50 Hz a.c. laser by the observed laser power-discharge current dependence. The data on d.c. lasers (SILFVAST [1], [4]), in contrast, show that output power depends in a linear manner on discharge current. Two possibilities can be considered to explain this disagreement:

A) First of all it may be that the excitation mechanism for the 4416 Å transition of Cd(II) differs in 50 Hz a.c. and d.c. operated lasers. We feel, however, that this is not very probable, since variations in time at 50 Hz excitation are slow compared to the rates of atomic collision processes.

B) On the other hand, consideration of the laser power-discharge current dependence of the 50 Hz a.c. excited laser plotted in Fig. 1 shows that the departure from linearity due to the break in the curve is not more than 15%. It is possible, therefore, that since it is difficult to control discharge current and Cd concentration independently in d.c. operated cataphoretic He—Cd lasers the experimental circumstances of d.c. operation are not definite enough to reveal the small 15% difference from linearity. In the 50 Hz a.c. excited laser accurate measurements could be performed within stable circumstances by recording discharge current and laser power variation during a single excitation period using a double beam oscilloscope.

Acknowledgements

The authors wish to thank Mr. T. SALAMON, Mr. K. RÓZSA and Dr. P. VARGA for many valuable discussions and for their continuous interest in this work.

REFERENCES

1. W. T. SILFVAST, Applied Physics Letters, **13,** 169, 1968.
2. L. D. SCHEARER and F. A. PADOVANI, Journal of Chemical Physics, **52,** 1618, 1970.
3. L. CSILLAG, M. JÁNOSSY, K. KÁNTOR, K. RÓZSA and T. SALAMON, Journal of Physics D, 1970; Applied Physics **3,** 64.
4. W. T. SILFVAST, Applied Physics Letters, **15,** 23, 1969.
5. N. L. OLESON and A. V. COOPER, Advances in Electronics and Electron Physics, **24,** 155, Academic Press 1968.
6. H. PEPIN and M. G. DROUET, Physics Letters, **33A,** 31, 1970.
7. L. CSILLAG, V. V. ITAGI, M. JÁNOSSY and K. RÓZSA, Physics Letters, **34A,** 110, 1971.
8. C. E. WEBB, A. R. TURNER-SMITH and J. M. GREEN, Journal of Physics B 1970; Atomic and Molecular Physics, **3,** 134.
9. M. B. KLEIN and D. MAYDAN, Applied Physics Letters, **16,** 509, 1970.
10. S. R. BAUMANN and W. H. SMITH, Journal of the Optical Society of America, **60,** 345, 1970.
11. W. T. SILFVAST, Paper presented at Conference on Quantum Electronics, Kyoto, 1970.
12. A. V. PHELPS, Physical Review, **99,** 1307, 1955.
13. B. L. MOISEIWITSCH and S. J. SMITH, Review of Modern Physics, **40,** 238, 1968.
14. J. Y. WADA and H. HEIL, IEEE Journal of Quantum Electronics, QE-1, 327, 1965.
15. S.C. BROWN, Introduction to Electrical Discharges in Gases, Wiley and Sons Inc. 1966, 221.
16. J. R. FENDLEY JR., I. GOROG, K. G. HERNQVIST and C. SUN, R. C. A. Review, **30,** 422, 1969.

О МЕХАНИЗМЕ ВОЗБУЖДЕНИЯ И РАБОЧИХ ПАРАМЕТРАХ ЛАЗЕРА 4416 Å He—Cd

М. ЯНОШИ, В. В. ИТАГИ и Л. ЧИЛЛАГ

Резюме

Измерения, проведенные с He-Cd лазером возбужденным переменным током в 50 Гц в рабочем состоянии при 4416 A, показывают на возможность, что механизм возбуждения для этого лазерного перехода складывается из двух процессов. Согласно авторам этими двумя процессами являются пеннингова ионизация нейтральных атомов Cd путем столкновений с метастабильными атомами He и столкновения электрон-ион Cd. Теория, разработанная на основе изложенного механизма возбуждения дает количественные данные о рабочих параметрах лазера.

Acta Physica Academiae Scientiarum Hungaricae, Tomus 32 (1—4), pp. 165—176 (1972)

A SIMPLE EXTENSION OF THE ANALOGUE MODEL TO THE CASE OF SCALAR CURRENTS*

By

A. PATKÓS

DEPARTMENT OF ATOMIC PHYSICS, ROLAND EÖTVÖS UNIVERSITY, BUDAPEST

(Received 19. X. 1971)

An off-mass-shell continuation of the dual multiparticle amplitude is constructed in the analogue model for scalar particles. It is invariant under the $SL(2; R)$ group, factorizable in the direct channel and the hadronic form-factor has a reasonable asymptotic behaviour; analytic properties, however, are not satisfactory. In the scaling limit the two-current amplitude shows an automatic cut-off in the transversal momentum, which is proportional to the momentum transfer (not fixed), so that an anomalous dimension appears in the model.

Introduction

SUSSKIND quite recently proposed a simple model for meson—meson interactions [1], in which the mesons are considered to be bound scalar $q\bar{q}$ pairs. During the interaction momentum is transferred only to these "valence quarks" and not to the exchanged quanta. From this assumption he was able to get the Veneziano N-point function.

NIELSEN and SUSSKIND have emphasized that in the meson—current interaction the current can be coupled directly to the exchanged quanta [2]. This assumption seems to have experimental support in high-energy lepton-hadron processes. The parton picture offers a relatively good description of these processes and one can identify the exchanged quanta with partons.

Starting from this idea the above authors constructed hadronic form-factors with convenient properties in the $q^2 \sim 0$ region. (q^2 is the mass of the scalar current.) With further assumptions they succeeded in giving a reasonable model for deep inelastic electron—proton scattering as well.

The model contains certain arbitrariness concerning the cut-off to be applied in divergences appearing in the form-factor. The choice of the cut-off influences the behaviour of the form-factor considerably.

SUSSKIND has shown that the original harmonic oscillator model is equivalent to the analogue model of NIELSEN [3]. It would be of interest to know whether this equivalence can be maintained for the current amplitudes also and whether the problem of divergences appears in the analogue model.

* Dedicated to Prof. L. JÁNOSSY on his 60th birthday.

In Section 2 the extension of the analogue model to the current amplitude is rephrased. The scalar-current form-factor for mesons will be constructed without cut-off and a two-current amplitude derived. From the factorization of the amplitude in the s-channel we can deduce excitation form-factors.

The dual and asymptotic properties of the two-current amplitude are briefly discussed in Section 3 and finally in Section 4 the problem of the connection between the scaling and duality is investigated by means of a simple analogue model.

The extension of the analogue model

In the analogue model the equivalent picture of the world-sheet of SUSSKIND is a conducting plate of the same dimensions $-\infty \geq \lambda \leq +\infty$; $0 \leq \theta \leq \pi$ and uniform conductivity σ (see Fig. 1). If the meson is free, a

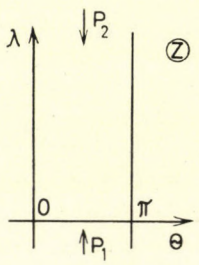

Fig. 1

four-momentum current flows in the sheet from a momentum source (p_1) at the point $\lambda = -\infty$ to source (p_2) at $\lambda = \infty$. Because of four-momentum conservation we have $p_1 = -p_2$. The current distribution ($p(\theta; \lambda)$) can be evaluated by solving the problem of the D. C. generated by the source distribution given above with the subsidiary condition $\int_0^\pi p(\Theta; \lambda) d\theta = p_1$. For uniform conductivity this gives a uniform current distribution independent of θ.

The amplitude for the interaction of an arbitrary number of particles and currents is given by NIELSEN's formula:

$$A = \frac{\int d(\text{conf.}) \exp\{-\sigma \int j^2 df\}}{\int d(\text{conf.})} . \tag{1}$$

Here $j(\theta; \lambda)$ describes the current distribution; $\sigma \int j^2 df$ is the total heat generation in the plate ($\delta^{(4)}(\Sigma p_i)$ is separated from A); and $\int d$ (conf.) denotes summation over all possible couplings of external momenta to the meson. We know [2] that the coupling of the on-mass-shell momenta is restricted to the boundary

of the plate ($\theta = 0; \pi$), whereas the currents can couple inside the sheet, too. Two further rules must be stated for constructing the amplitude:

a) Requiring the amplitude to be 1 in the case of a free hadron, one has to subtract the heat generation in the free hadron from $\sigma\int j^2 df$, so we have

$$A = \int d(\text{conf}) \exp\{-\sigma \int (j^2 - j_0^2)\, df\} / \int d(\text{conf}). \tag{1a}$$

One can see that this "0-point" heat is

$$H_0 = \lim_{|w_1|\to\infty} 2\sigma p^2 \ln |w_1| + \text{const.}, \tag{2}$$

where $w_1 = e^{iz_1}$; $z_1 = \theta_1 + i\lambda_1$ is the position of the source associated with the ingoing momenta p_1.

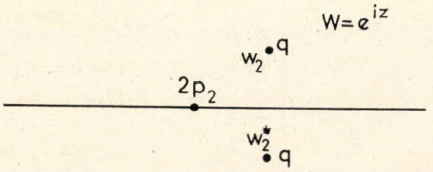

Fig. 2

b) The second remark concerns the requirement of λ-translation invariance, which is suggested by the proper-time interpretation of λ [1]. This is the partial consequence of the invariance of our amplitude under the transformation

$$w' = \frac{aw+b}{cw+d} \tag{3}$$

(a; b; c; d are real parameters with $|ab - cd| = 1$; $w = e^{iz}$, $z = \theta + i\lambda$). This property will be discussed in detail in Section 3. Because of the invariance one can fix the coupling of one of the currents at $\lambda = 0$.

With these two rules in mind let us construct the hadronic form factor (the meson—current—meson coupling).

We map the sheet into the upper half-plane by means of the function $w = e^{iz}$. In order to satisfy the boundary condition the half-plane will be reflected with respect to the real axis, without changing the signs of the sources (Fig. 2). The heat generated in the sheet can be evaluated from Ohm's law:

$$\begin{aligned}
H_{p_2 q} &= -\sigma p_2 q\ (\ln |w_q| + \ln |w_q^*|), \\
H_{qq} &= -\sigma q^2 \ln |w_q - w_q^*|, \\
H_{p_1 p_2} &= -\lim_{|w_1|\to\infty} 2\sigma p_1 p_2 \ln |w_1|, \\
H_{p_1 q} &= -\lim_{|w_1|\to\infty} \sigma p_1 q (\ln |w_1 - w_q| + \ln |w_1 - w_q^*|).
\end{aligned} \tag{4}$$

Expanding the sum $H_{p_1 p_2} + H_{p_1 q}$ in series at the point $w_1 = \infty$, one gets

$$H_{p_1 p_2} + H_{p_1 q} = -\lim_{|w_1| \to \infty} \sigma \left[2p_1(p_1+q) \ln |w_1| + \frac{1}{|w_1|}(\ldots) \right]. \tag{5}$$

Taking into account four-momentum conservation, it can be seen immediately that (5) tends to (2), so $H_{p_1 p_2} + H_{p_1 q}$ does not appear in (1a), as a consequence of our first rule. By the second rule:

$$| w_q | = 1, \text{ that is } H_{p_2 q} = 0.$$

We shall now use the so-called scale invariance property of the heat generation [3], which means that the expressions given by (4) are determined only up to an additive constant. In order to ensure agreement with the NIELSEN—SUSSKIND form-factor, this constant is required to be $-\ln \pi/\lambda_0$ in H_{qq} and 0 elsewhere (λ_0 is defined in [2]).

$$H_{qq} = -\sigma q^2 \ln \left(\frac{\lambda_0}{\pi} |w_q - w_q^*| \right), \tag{4a}$$

Substituting (4a) into (1a) one gets

$$F_\theta(q^2) = \left(\frac{2\lambda_0}{\sigma} \sin \Theta \right)^{\sigma q^2}. \tag{6}$$

One can now integrate over all possible values of θ, with a normalization factor in the integrand (omitting the denominator of (1a)):

$$F(q^2) = \int_0^\pi \frac{d\Theta}{N(\Theta)} \left(\frac{2\lambda_0}{\pi} \right)^{\sigma q^2} (\sin \Theta)^{\sigma q^2}. \tag{7}$$

If we choose $N(\Theta) = \sin^2 \Theta$ and $\sigma = 1$, we get the form-factor of [2] without using any cut-off. The choice of the form of $N(\theta)$ is determined by the interaction. In [2] $N(\theta) = \sin^2 \theta$ for charge-symmetric interactions, $N(\theta) = \sin^{1/2} \theta$ for electromagnetic interactions. In the following Section it will be shown that further restrictions appear if invariance of the volume element under real Moebius transformations is required. In order to investigate the excitation form-factors the two-current amplitude (Fig. 3) will be also discussed.

According to the first rule, the contribution of the p_1-source can be omitted. The other contributions are as follows (the procedure is the same as before):

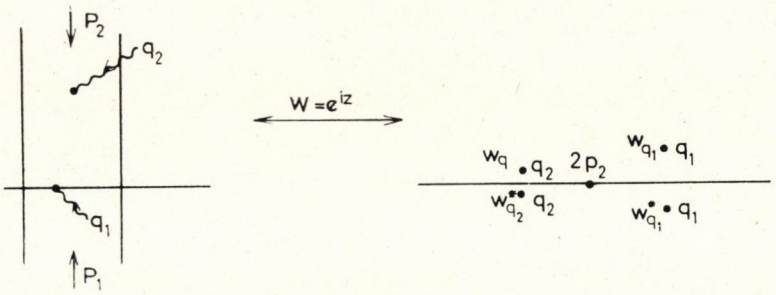

Fig. 3

$$H_{p_1 q_1} = 0\,;\; H_{q_1 q_1} = -\sigma q_1^2 \ln\left(\frac{\lambda_0}{\pi}\,|w_{q_1} - w_{q_1}^*|\right),$$

$$H_{p_2 q_2} = -\sigma p_2 q_1 \ln|w_{q_2}|^2;\; H_{q_2 q_2} = -\sigma q_2^2 \ln\left(\frac{\lambda_0}{\pi}\,|w_{q_2} - w_{q_2}^*|\right), \tag{8}$$

$$H_{q_1 q_2} = -\sigma q_1 q_2 [\ln|w_{q_1} - w_{q_2}| + \ln|w_{q_1} - w_{q_2}^*|],$$

The amplitude is

$$A = \int_0^\pi \frac{d\Theta_1}{N(\Theta_1)} \int_0^\pi \frac{d\Theta_2}{N(\Theta_2)} \int_0^1 \frac{du}{u}\, u^{\sigma(2p_2 q_2 + q_2^2)} |e^{i\Theta_1} - e^{i\Theta_2} u|^{\sigma q_1 q_2} |e^{i\Theta_1} - u e^{-i\Theta_2}|^{\sigma q_1 q_2} \cdot$$
$$\cdot (\sin\Theta_1)^{\sigma q_1^2} (\sin\Theta_2)^{\sigma q_2^2} \left(\frac{2\lambda_0}{\pi}\right)^{\sigma(q_1^2 + q_2^2)}, \tag{9}$$

(the new variable $u = e^{-\lambda q_2}$ has been introduced). The same amplitude can be derived (see Appendix) by the prescriptions of [1].

Now let us study the poles of (9) in the variable s. These poles occur from the region $u \sim 0$ and their residues are proportional to polynomials in $q_1 \cdot q_2$. The leading term describes the exchange of the pole on the leading trajectory and for the $s - c = J$ ($J = 0;\ 1;\ldots$) pole is:

$$\mathrm{Res}_J A = \int \frac{d\Theta_1}{N(\Theta_1)} \int \frac{d\Theta_2}{N(\Theta_2)} (\sin\Theta_1)^{\sigma q_1^2} (\sin\Theta_2)^{\sigma q_2^2} \left(\frac{2\lambda_0}{\pi}\right)^{\sigma(q_1^2 + q_2^2)} \cdot$$
$$\cdot (2q_1 q_2)^J (\cos\Theta_1 \cos\Theta_2)^J \frac{1}{J!}. \tag{10}$$

By factorization of (10) one gets the excitation form-factors shown in [2]:

$$F^J_{\mu_1 \ldots \mu_J}(q^2) = (\sqrt{2}\sigma)^J q_{\mu_1} \ldots q_{\mu_J} \int \frac{d\Theta}{N(\Theta)} (\sin\Theta)^{\sigma q^2} (\cos\Theta)^J \left(\frac{2\lambda_0}{\pi}\right)^{\sigma q_1} \frac{1}{\sqrt{J!}}. \tag{11}$$

Properties of the two-current amplitude

In this Section the properties of the amplitude (9) are briefly summarized.

Invariance of the intergrand under Sl(2; R) transformation [3].

Up to now a particular mapping of the $(\Theta; \lambda)$ sheet into the upper half-plane was used for the computation of the amplitude. In the case of an arbitrary mapping realizable by

$$w = \frac{ae^{iz}+b}{ce^{iz}+d}$$

the integrand in (1) becomes ($\sigma = 1$)

$$\begin{aligned} &|w_1-w_{q1}|^{2p_1q_1}|w_1-w_{q_2}|^{2p_1q_2}[|w_{q_1}-w_{q_2}|\,|w^*_{q1}-w_{q_2}|]^{q_1q_2}|w_{q_1}-w^*_{q\,1}|^{q_1^2}\cdot \\ &\cdot|w_{q_2}-w^*_q|^{q_2^2}|w_2-w_{q1}|^{2p_2q_1}|w_2-w_{q_2}|^{2p_2q_2}|w_2-w_1|^{2p_2q_1}. \end{aligned} \tag{12}$$

In order to ensure invariance of the amplitude under this change of the configuration of sources, that is under the $SL(2; R)$ transformations of the upper half-plane we have to multiply (12) by a factor $|w_2 - w_1|^{2p_1^2}$. But from (2) it can be seen that this is precisely the factor by which (1a) differs from (1). Therefore the meaning of the formal manipulation to assure $SL(2; R)$-invariance is similar to leaving the 0-point energy in the case of harmonic systems to ensure that the results are finite ($p_1^2 = p_2^2$ was assumed).

The invariance of the volume element

$$dV_N^M = \prod_{i=1}^{N} \frac{|dw_i|}{|w_{i+1}-w_i|}\, 2^M \prod_{k=1}^{M} \frac{d^2 w_k}{|w_k-w_k^*|^2} \tag{13}$$

can be demonstrated by direct evaluation (N is the number of particles on-mass-shell, M is the number of currents). The $SL(2; R)$ being a three-parameter group we can fix the positions of the two on-shell particles and partially that of one of the currents ($|w_3| = 1$), then one arrives at the same volume element as in (9) by putting $N = 2$, $M = 2$; $N(\Theta) = \sin^2\theta$.

Poles on the q_1^2 and q_2^2 planes

These poles arise from the region where θ_1 and θ_2 are approximately 0 or π and can be exhibited by integrating by parts at $\theta_i = 0;\pi$; they occur at $q_i^2 = 1; -1; \ldots$; if we use $N(\theta) = \sin^2\theta$. The residue of the two-fold pole at $q_1^2 = q_2^2 = 1$ coming from the region $\theta_1 = \theta_2 = 0$ or π is the dual amplitude

$$\int_0^1 du u^{-s-2}(1-u)^{-t-2}; \text{ for } N(\Theta) = \sin^2\Theta.$$

The contribution of the regions $\theta_1 = \theta_2 \pm \pi$ and $\theta_1 = 0;\pi$ can be identified with the parts of the amplitude which correspond to the $(s;u)$ and $(t;\ u)$ duality [1].

Poles on the s-plane

These poles arise from the $u \sim 0$ region at $s - c = J, J = 0;\ 1;\ldots,$ appearing independently of the actual value of θ.

Factorization in the s-channel

This problem has been investigated in Section 2. The residue contains the product of the two form-factors and a polynomial of $q_1 q_2$:

$$A = \sum_{J=1}^{\infty} \frac{F^J(q_1^2)\, F^J(q_2^2)}{J-(s-c)} (q_1 q_2)^J + \text{daughter poles}, \tag{14}$$

where

$$F^J(q^2) = (\sqrt{2})^J \int \frac{d\Theta}{N(\Theta)} (\sin\Theta)^{q_2} (\cos\Theta)^J \left(\frac{2\lambda_0}{\pi}\right)^{q^2} \frac{1}{\sqrt{\Gamma(J+1)}} .$$

Asymptotic behaviour in s

The main contribution comes from the region $u \sim 1$. The asymptotics depends strongly on the actual value of θ. If the currents couple on the edge of the interaction region, one obtains the dual part of the amplitude. But from the region $\theta_1 = \theta_2$, different rom 0; π, one would have a trajectory of a slope, which is half of that appearing in the dual part of the amplitude:

$$\lim_{s\to\infty} A_{\Theta_1=\Theta_2\neq 0;\ \pi} \sim \int du \int \frac{d\Theta}{N(\Theta)} (2p_2 q_2 + q_2^2)^{q_1 q_2} |1 - e^{-2i\Theta}|^{q_1 q_2} f(u). \tag{15}$$

Here $f(u)$ denotes the u-dependent part of the integrand. The part of the amplitude which comes from the region $0 < \theta_1 \neq \theta_2 < \pi$, has s-independent asymptotics.

The amplitude does not remain dual if we perform an analytic continuation from the mass-shell. It has inconvenient analytic properties in the t-channel due to the factor $|w_{q_1} - w_{q_2}|^{q_1 q_2}$. (The position of the t-channel poles depends on the actual value of q_i^2). This factor cannot be removed without fundamentally changing the physical content of the model.

It can be concluded that the amplitude has reasonable properties in the direct channel, but one is faced with having to exclude the $q_1 q_2$-poles in the crossed channel. Nevertheless the generality of the method presented here may be of interest for further investigations.

Scaling in the analogue model

NIELSEN and SUSSKIND imposed the scaling property on their model by considering the contributions of only those diagrams in which the two currents couple to the same exchanged quantum [2]. This assumption has an equivalent picture in the analogue model, which can be related directly to the parton model proposed by BJORKEN and PASCHOS [4]. If we identify $N^{-1}(\theta)$ with the density of partons [2] (this factor earlier played the role of the weighting factor in the summation of the contributions of different configurations), the longitudinal momentum carried by a parton at a given θ is $pN(\theta)/\pi$. The transversal part of the parton's momentum is neglected. Choosing

$$\sigma = \sigma_0 \delta(\Theta - \Theta q_1) \tag{16}$$

(for the q-current only), we restrict the coupling of both currents to the same parton.

The heat generation is given by

$$\begin{aligned} H_{qq} &= q^2 \int_0^{\lambda} d\Theta \, d\lambda' \sigma_0 \, \delta(\Theta - \Theta_1) = q^2 \, \lambda \sigma_0, \\ H_{pq} &= \frac{2p \cdot N(\Theta_1) q}{\pi} \int_0^{\lambda} d\Theta \, d\lambda' \, \sigma_0 \, \delta(\Theta - \Theta_1) = 2 \, pq \, \lambda \sigma_0 \, \frac{N(\Theta_1)}{\pi} \, . \end{aligned} \tag{17}$$

From Eq. (1a) the following amplitude can be evaluated:

$$\begin{aligned} A &= \int_0^{\infty} \frac{d\Theta}{N(\Theta)} \int_0^{\infty} d\lambda \, \exp \left\{ - \left[q^2 + \frac{2pq}{\pi} N(\Theta) \right] \sigma_0 \lambda \right\} = \\ &= \int_0^{\infty} \frac{d\Theta}{N(\Theta)} \, \frac{1}{\sigma_0 \left[q^2 + \frac{2pq}{\pi} N(\Theta) \right]} \, . \end{aligned} \tag{18}$$

The imaginary part of (18) is

$$\frac{1}{\pi} Im \, A = \int_0^{\pi} \frac{d\Theta}{N(\Theta) \sigma_0} \, \delta \left(q^2 + \frac{2p \cdot q}{\pi} N(\Theta) \right) = \frac{1}{2\nu} \int_0^{\pi} \frac{d\Theta}{N(\Theta) \, \sigma_0} \, \delta \left(x - \frac{N(\Theta)}{\pi} \right) \tag{19}$$

and gives the scaling law of ImA. In order to have a definite scaling function, we put $N(\theta) = \pi \sin^2 \theta$

$$\frac{1}{\pi} \nu \, Im \, A = \frac{1}{\sigma_0 \, \pi x^{3/2} \sqrt{1 - x^2}} \, , \tag{20}$$

where

$$x = \frac{q^2}{2\nu}\,;\quad \nu = -\,pq\,.$$

It is natural to try now to relate amplitude (9) in the BJORKEN limit [4] to the above picture. The aim will be to demonstrate that in the scaling limit the main contribution to the amplitude comes from the $\theta_1 = \theta_2$ region and that the amplitude shows the scaling property. We use (9) in the form given by Eq. (A3) with cut-off sums like (A4). (A3) has only technical advantages over (9); as we have seen, the results given by the two are identical. For the forward-scattering ($q_1 = -q_2$), we replace (A3) by

$$A = \int_0^\pi \frac{d\Theta_1}{N(\Theta_1)} \int_0^\pi \frac{d\Theta_2}{N(\Theta_2)} \int_0^1 dX\, X^{-s+c-1}\, e^{-q^2 \sum_k' \frac{\cos^2 k\Theta_1}{k} - q^2 \sum_k' \frac{\cos^2 k\Theta_2}{k}} \cdot e^{2q^2 \sum_k' \frac{\cos k\Theta_1 \cos k\Theta_2}{k} X^k} \tag{21}$$

Let us consider first the $s \to \infty$ limit only (Regge limit). The main contribution comes from the region $X \sim 1$. We introduce therefore the new variable $X = 1 - \frac{u}{s}$ and expand X^k in Newton binomial, which yields

$$A = \int \frac{d\Theta_1}{N(\Theta_1)} \int \frac{d\Theta_2}{N(\Theta_2)} \int \frac{du}{s}\, e^u\, e^{-q^2 \sum_k' \frac{1}{k} (\cos k\Theta_1 - \cos k\Theta_2)^2} \times \times e^{2q^2 \sum_k' \frac{\cos k\Theta_1 \cos k\Theta_2}{k}} \cdot \sum_{l=7}^{k}{}' \binom{k}{l} \left(-\frac{u}{s}\right)^l \tag{22}$$

Let us consider next the $q^2 \to \infty$ limit. The first exponent tends to 0 if $\theta_1 \neq \theta_2$, so expanding $\cos k\,\theta_2$ about $\theta_2 = \theta_1$, retaining only the first nonvanishing term, we acquire:

$$A = \int \frac{d\Theta_1}{N(\Theta_1)} \int \frac{d\Theta_2}{N(\Theta_2)} \int \frac{du}{s}\, e^{-q^2 \sum_k^{k_0}{}' k \sin^2 k\Theta_1 (\Theta_1 - \Theta_2)^2} \cdot \cdot e^u \cdot e^{\left[2q^2 \sum_k^{k_0}{}' \cos^2 k\Theta_1 - k \cos k\Theta_1 \sin k\Theta_1 (\Theta_2 - \Theta_1)/k \cdot \sum_{l=1}^{k}{}' \binom{k}{l} \left(-\frac{u}{s}\right)^l\right]}.$$

Using the definition

$$\lim_{q^2 \to \infty} e^{-q^2 \sum_k^{k_0}{}' k \sin^2 k\Theta_1 (\Theta_2 - \Theta_1)^2} \sqrt{q^2 \sum_k k \sin^2 k\Theta_1}\, \frac{1}{\sqrt{\pi}} = \delta(\Theta_2 - \Theta_1) \tag{23}$$

for the δ-function, we have

$$\lim_{\substack{q^2\to\infty\\ s\to\infty}} \int \frac{d\Theta_1}{N(\Theta_1)} \int \frac{d\Theta_2}{N(\Theta_2)} \int \frac{du}{s} \frac{\sqrt{\pi}}{\sqrt{q^2 \sum_k k \sin^2 k\Theta_1}} \delta(\Theta_2-\Theta_1)\, e^u \cdot \cdot \exp\left\{2q^2 \sum_k \frac{\cos^2 k\Theta_1}{k} \sum_{l=1}^{k} \binom{k}{l} \left(-\frac{u}{s}\right)^l\right\} \tag{24}$$

Finally, we keep $q^2/s = \bar{x}$ fixed. In this case only one term remains finite in the second exponent:

$$\lim_B A = \frac{1}{s\sqrt{q^2}} \int \frac{d\Theta_1}{N^2(\Theta_1)} \int du \times \times \sqrt{\frac{\pi}{\sum_k k \sin^2 k\Theta_1}} \cdot \exp\left\{\left(1-2\bar{x} \sum_k^{k_0} \cos^2 k\,\Theta_1\right) u\right\}. \tag{25}$$

Taking the u integration around $u \sim 0$:

$$\lim_B A = \frac{1}{s\sqrt{q^2}} \int \frac{d\Theta_1}{N^2(\Theta_1)} \sqrt{\frac{\pi}{\sum_k k \sin^2 k\Theta_1}} \frac{1}{1-2\bar{x} \sum_k \cos^2 k\Theta_1}. \tag{26}$$

After summing the divergent sums the θ_1-integration for the imaginary part can be made by means of the δ-functions

$$\lim_B s\sqrt{q^2}\, Im\, A \frac{1}{\pi} = \sqrt{\pi} \int \frac{d\Theta}{N(\Theta_1)} \frac{1}{\sqrt{\sum_k k \sin^2 k\Theta_1}} \delta\left(1-2\bar{x} \sum_k^{k_0} \cos^2 k\Theta_1\right). \tag{27}$$

The above demonstration confirms the assumption about the important region of θ-integration made in Eq. (16), but the power of ν multiplying ImA in the BJORKEN limit changes and its value is characteristic for the case of so-called anomalous dimensions, proposed in some field theoretical models of scaling. The physical basis for this change may be the different way of cutting-off the transversal momentum. In the naive analogue picture (Eq. (16)), there is no transversal part, but (as it can be seen from Eq. (23)) in the amplitude (9) the contributing region is proportional to $(\sqrt{q^2})^{-1}$.

*

I would like to thank DR. I. MONTVAY for his helpful discussions and encouragement.

Appendix

The two-current amplitude is derived by applying the prescription of [1].

The contribution from a given configuration $(\Theta_1; \Theta_2)$ is

$$T_{\Theta_1;\Theta_2} = \sum_{\{n_\mu^k\}} \langle 0|T(q_1;\Theta_1)|\{n_\mu^k\}\rangle \frac{1}{s - \sum' k n_\mu^k - c} \langle\{n_\mu^k\}|T(q_2;\Theta_2)|0\rangle, \tag{A1}$$

where $|\,0\,\rangle$ denotes the ground state of the meson, $|\{n_\mu^k\}\rangle$ denotes an excited state in the occupation number representation, and $T(q_1;\theta_1) = e^{iq_1 x(\Theta_1)}$ is the scalar vertex-operator with the second quantized four-position $X_\mu(\Theta;\lambda)$ given in [2]. If (A1) is rewritten in the coherent state basis and

$$T_{\Theta_1\Theta_2} = \sum_{\{n_\mu^k\}} e^{-q_1^2 \sum' \frac{\cos^2 k\Theta_1}{k} - \sqrt{2}\sum' \frac{\cos k\Theta_1}{\sqrt{k}}\alpha(k)\cdot q_1} \left(\prod_{\{k;\mu\}} \frac{\overleftarrow{\partial}}{\partial\alpha_\mu}\frac{\overrightarrow{\partial}}{\partial\beta_\mu}\right)^{n_\mu^k} \frac{1}{n_\mu^k!} \cdot \tag{A2}$$

$$\cdot\, e^{-q_1^2 \sum' \frac{\cos^2 k\Theta_2}{k} + \sqrt{2}\sum' \cos k\Theta_2 \beta(k)\cdot q_2} \frac{1}{s - \sum_{\mu;k} k n_\mu^k - c}\Bigg|_{\alpha_\mu=\beta_\mu=0}.$$

Using the identity

$$\int_0^1 dX X^{c-s-1+\sum' k n_\mu^k} = \frac{1}{s - c - \sum_k k n_\mu^k}$$

we get

$$T_{\Theta_1;\Theta_2} = \int_0^1 dX \sum_{n_\mu^k} \prod_{\mu k} \frac{1}{n_\mu^k!}\left(-\frac{2}{k} q_{1\mu} q_{2\mu} \cos k\Theta_1 \cos k\Theta_2\right)^{n_\mu^k} X^{c-s-1+k n_\mu^k}.$$

$$\cdot\, e^{-q_1^2 \sum_k^\alpha{}' \frac{\cos^2 k\Theta_1}{k}} e^{-q_2^2 \sum' \frac{\cos^2 k\Theta_2}{k}} = \tag{A3}$$

$$= \int_0^1 dX X^{c-s-1} \exp\left\{-q_1^2 \sum_k \frac{\cos^2 k\Theta_1}{k} - q_2^2 \sum_k \frac{\cos^2 k\Theta_2}{k} - \right.$$

$$\left. - 2q_1 q_2 \sum_k \cos k_1\Theta_1 \cos k\Theta_2 \frac{X^k}{k}\right\}.$$

As the exponent in the first exponential is divergent, it is necessary to introduce a cut-off. From [1] we have:

$$\sum_k^{k_0} \frac{\cos^2 k\Theta}{k} \approx -\frac{1}{2}\log\frac{2\lambda_0}{\pi} - \frac{1}{2}\log\sin\Theta. \tag{A4}$$

The third exponent can be evaluated without any cut-off:

$$\sum_k \cos k\Theta_1 \cos k\Theta_2 \frac{X^k}{k} = \frac{1}{2}[\ln|1 - Xe^{i(\Theta_1+\Theta_2)}| + h_1|1 - Xe^{i(\Theta_1-\Theta_2)}|]. \quad \text{(A5)}$$

Substituting (A4) and (A5) into (A3) $T_{\Theta_1\Theta_2}$ is obtained in its final form as:

$$T_{\Theta_2\Theta_1} = \int_0^1 dX X^{c-s-1} \left(\frac{2\lambda_0}{\pi}\right)^{q_1^2+q_2^2} (\sin\Theta_1)^{q_1^2} (\sin\Theta_2)^{q_2^2} \cdot \\ \cdot |1 - Xe^{i(\Theta_1+\Theta_2)}|^{q_1q_2} |1 - Xe^{i(\Theta_1-\Theta_2)}|^{q_1q_2}. \quad \text{(A6)}$$

The amplitude comes from (A6) by integrating over Θ_1 and and agrees with that given by (9) for $\sigma = 1$:

$$A = \int_0^\pi \frac{d\Theta_1}{N(\Theta_1)} \int_0^\pi \frac{d\Theta_2}{N(\Theta_2)} \int_0^1 dX X^{c-s-1} \left(\frac{2\lambda_0}{\pi}\right)^{q_1^2+q_2^2} (\sin\Theta_1)^{q_1^2} (\sin\Theta_2)^{q_2^2} \cdot \\ \cdot |1 - Xe^{i(\Theta_1-\Theta_2)}|^{q_1q_2} |1 - Xe^{i(\Theta_1+\Theta_2)}|^{q_1q_2}. \quad \text{(A7)}$$

The factorization in s is also clear from here, and the excitation form-factors are the same as in [1].

REFERENCES

1. L. Susskind, Nuovo Cim. **69A**, 457, 1970.
2. H. B. Nielsen and L. Susskind, Ref. TH-1230-CERN, 1970 Sept.
3. H. B. Nielsen and D. Fairlie, Nucl. Phys., **B20**, 637, 1970.
4. J. D. Bjorken and E. Paschos, Phys. Rev., **185**, 1975, 1969.

ПРОСТОЕ РАСПРОСТРАНЕНИЕ АНАЛОГОВОЙ МОДЕЛИ НА СЛУЧАЙ СКАЛЯРНЫХ ПОТОКОВ

А. ПАТКОШ

Резюме

Продолжение дуальной многочастичной амплитуды вне оболочки массы было построено в аналоговой модели скалярных частиц. Оно инвариантно при $SL(2; R)$ группе, факторизируется в прямом канале, а гадронический формирующий фактор показывает обоснованное асимптотическое поведение. Все же его аналитические свойства не являются удовлетворительными. Дуальная амплитуда в скалярном пределе показывает автоматический перерыв в поперечном моменте, который пропорционален переноса момента (не является константой). Поэтому в модели возникает аномальное измерение.

Acta Physica Academiae Scientiarum Hungaricae, Tomus 32 (1—4), pp. 177—180 (1972)

MEASUREMENT OF THE RELATIVE DEFLECTION OF TWO TORSION BALANCES IN THE 10^{-9} RAD SENSITIVITY RANGE*

By

K. KÁNTOR, L. OZSGYÁNI, M. PIPO and J. RÓNAKY

CENTRAL RESEARCH INSTITUTE FOR PHYSICS, BUDAPEST

(Received 19. X. 1971)

Using a simple method, a d.c. signal sensitivity of about $0{,}3 \times 10^{-9}$ A/10^{-9} rad was achieved in an apparatus designed for the measurement of the relative deflection of two torsion balances. This degree of sensitivity allows the EÖTVÖS experiment to be repeated with greater accuracy than has been attained hitherto. Signal sensitivity can be raised further by common electronic methods.

Higher accuracy repetitions [1, 2] of the famous Eötvös experiment concerning the equivalence of gravitational and inertial mass [3] and a number of recently published papers [4—7] have brought gravitational research into the foreground of modern physics. A newer repetition of the EÖTVÖS experiment in Hungary required the registration of changes in the angle difference between two torsion balances [8]. This was achieved by comparatively simple means, using a suitable optical arrangement and a laser source. This paper presents a brief description of the method.

Known methods for measuring the deflection of a mirror have until now employed photoelectric autocollimators, which can attain sensitivities of about 10^{-7}—10^{-8} rad, but only if mirror diameters of about 40 mm are used. R. HAKNER [9] proposed to use an optical path length of 15 m and a continuous 3 W laser source.

In our method two torsion balances (Fig. 1) consisting of the masses M_1 — M_4, respectively, were placed a distance 820 mm apart. The relative angle difference —φ — of the two mirrors T_1, T_2 attached to the two balances had to be measured with a sensitivity of 10^{-9} rad. A serious problem arose, however, because the variations of the gravitational field strength at the measuring place can make the balances deflect simultaneously as much as 10^{-5} rad.

The most suitable method of overcoming this strong "background noise" seems to be the familiar "optical-wedge" — mirror arrangement. In this arrangement the deflection angle of the incident light beam depends only on the value of φ. To determine the variation of φ (viz. the variation in the deflection $\delta = 2\varphi$ of the exit beam), a pair of silicon photodetectors D_1, D_2 was placed

* Dedicated to Prof. L. JÁNOSSY on his 60th birthday.

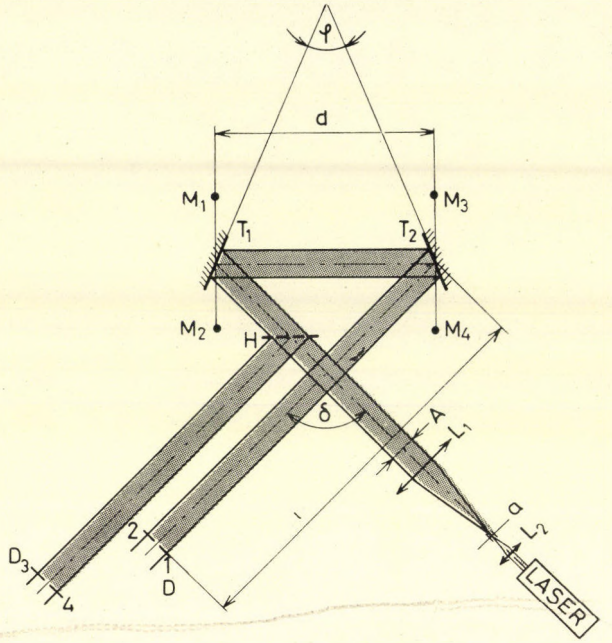

Fig. 1

at a given distance (l) into the exit beam, and the displacement of the spot on the detectors was measured by the difference signal produced.

Another problem was that the sensitivity of the balances had permitted the use of only a very thin fibre, which means that the diameter of the mirrors is limited and thus diffraction of the light beam is considerable. Taking into account all the different aspects, a mirror diameter of 20 mm and a free aperture beam of $A = 15$ mm were chosen. The measuring room permitted a light path of $l = 5000$ mm on the exit side, so that the displacement of the spot was 10^{-5} mm. The sensitivity of the silicon detector was 0.6—0.8 μA/μW, that of the recording galvanometer $0.3 \cdot 10^{-9}$ A. The required total intensity of the measuring spot was about 0.3 mW. The transmittance of the optical system, including losses by lenses, windows and a second reference beam (described below), was 0.2 and thus the intensity of the incident beam 1.5 mW.

For an objective lens (L_1) having a focal length of 840 mm, the optimal source diameter (a) is about 0.1 mm. The energy density in the pinhole aperture must therefore be 20 W/cm^2, which can be achieved only with a laser source. For this purpose a 2 mW He—Ne laser was used. The 632.8 nm wavelength light was focused into the pinhole aperture by a lens (L_2) with a focal length of 110 mm. This telescope system secured an ideal (Gaussian) light distribution for the measuring beam.

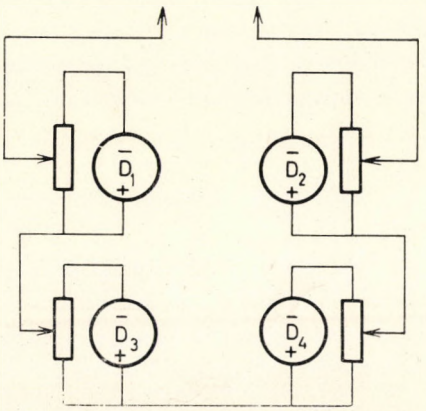

Fig. 2

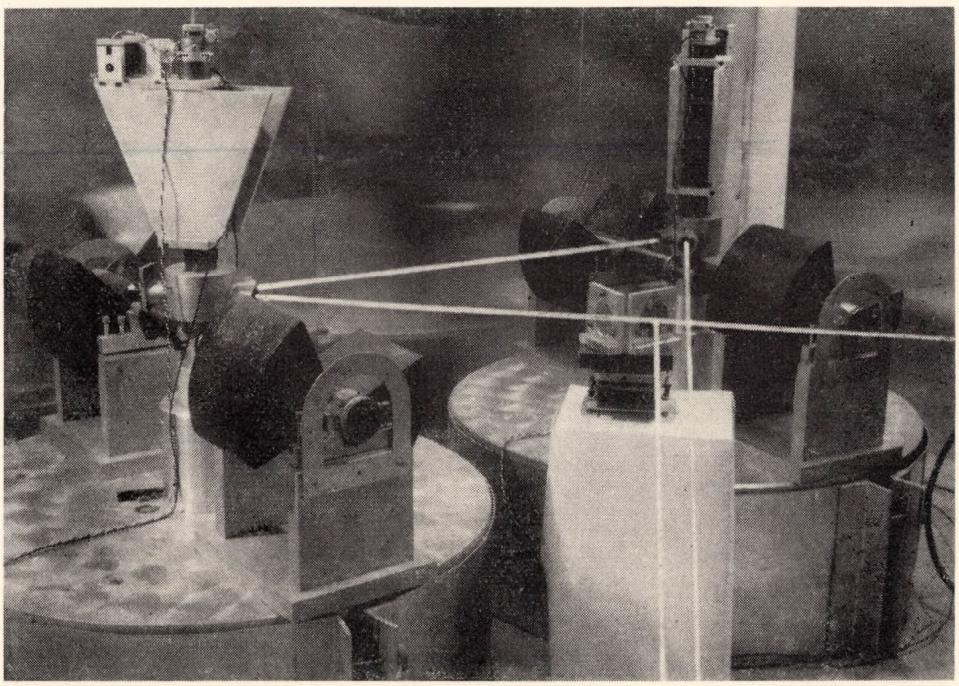

Fig. 3

The role of the reference beam coupled out of the semi-transparent mirror H was to eliminate errors arising from possible small displacements between the separate stone blocks supporting the optical elements and detectors. The reference spot fell on a second detector pair D_3, D_4 and the two detector pairs were connected in such a way (Fig. 2) that a simultaneous displacement of both the measuring and the reference spots did not affect the measuring signal.

Calibration of the total system up to 10^{-4} rad was performed with a Hilger autocollimator of 10^{-6} rad sensitivity. Deviations from linearity could be observed above 10^{-5} rad. For calibrating the high-sensitivity range a 60^0 hollow (air) prism was placed in the incident beam and the deviation inside the prism was varied by air pressure.

The whole system of optical ray paths, balances and detectors was placed under a separate shield to protect it against heat and air turbulence. Control and registration of air pressure change were carried out from another room.

The balance (without shield) and the ray path around them are shown in Fig. 3.

In the course of the calibration measurements of the apparatus a d.c. signal sensitivity of 0.3 10^{-9} A/10^{-9} rad was achieved, which agrees well with calculated values.

Acknowledgement

Thanks are due to the Physical Optical Laboratory of the Central Research Institute for Physics, Budapest, to the Hungarian Oil and Gas Trust, and to the Petroleum Machinery Factory, Budapest for designing, developing and producing the apparatus.

REFERENCES

1. J. Renner, MTA Mat. és TT. Ért., **53,** 542, 1955.
2. P. C. Roll, R. Krotkov and R. H. Dicke, Ann. of Phys., **26,** 442, 1964.
3. R. Eötvös, D. Pekár and E. Fekete, Ann. d. Phys., **4, 28,** 11, 1922.
4. L. B. Kreuzer, Phys. Rev., **169,** 1007, 1968.
5. J. Weber, Phys. Rev. Lett., **22,** 1320, 1969.
6. L. Ozsgyáni, Dissertation 1971. Hungarian Academy of Sciences.
7. J. W. Beams, Phys. Today, May, 1971.
8. M. Pipo, Investigation of the equivalence of the gravitational and inertial mass, in the accuracy range of 10^{-10},—10^{-10}, Dissertation 1971. Hungarian Academy of Sciences.
9. R. Hakner, Phys. Rev., **181,** 1723, 1969.

ИЗМЕРЕНИЕ ОТНОСИТЕЛЬНОГО ОТКЛОНЕНИЯ ДВУХ КРУТИЛЬНЫХ БАЛАНСОВ В ДИАПАЗОНЕ ЧУВСТВИТЕЛЬНОСТИ 10^{-9} РАД

К. КАНТОР, Л. ОЖДЯНИ, М. ПИПО и Й. РОНАКИ

Резюме

С помощью сравнительно несложного метода в аппарате, созданном для измерения относительного отклонения двух крутильных балансов, была получена чувствительность сигнала прямого тока в 0,3F 10^{-9} A/10^{-9}. Эта степень чувствительности позволяет повторить опыт Этвеша с большей точностью. Чувствительность к сигналу можно повышать далее с помощью обычных электронных методов.

Acta Physica Academiae Scientiarum Hungaricae, Tomus 32 (1—4), pp. 181—185 (1972)

SYMMETRIES OF WIGNER COEFFICIENTS AND THOMAE-WHIPPLE FUNCTIONS*

By

M. HUSZÁR

CENTRAL RESEARCH INSTITUTE FOR PHYSICS, BUDAPEST

(Received 19. X. 1971)

Wigner coefficients of the three-dimensional rotation group can be brought into the form of Thomae-Whipple functions. The symmetry group of order 72, discovered by Regge, is a straightforward consequence of 6 forms of the 120 Thomae-Whipple functions. The question whether the remaining 114 forms of these functions lead to new symmetries is investigated. It is shown that if the Regge group is enlarged by the transformations $j \to -j-1$, a group or order 1440 is obtained, which is exactly the group generated by the interrelations between the 120 Thomae-Whipple functions.

§1. Following the derivation of the Wigner coefficients for the rotation group it was recognized early that these coefficients possess a symmetry group of twelve elements, six of which are the permutations of three angular momenta and the remaining ones combinations of a space reflection and the above permutations. It was discovered by REGGE [1] that the Wigner coefficients are invariant under a larger symmetry group of 72 elements. These symmetries are exhibited by the following Table:

$$\begin{pmatrix} j_1 & j_2 & j_3 \\ m_1 & m_2 & m_3 \end{pmatrix} = \begin{bmatrix} -j_1+j_2+j_3 & j_1-j_2+j_3 & j_1+j_2-j_3 \\ j_1+m_1 & j_2+m_2 & j_3+m_3 \\ j_1-m_1 & j_2-m_2 & j_3-m_3 \end{bmatrix}. \qquad (1)$$

The full symmetry group of the Wigner coefficients consists of the permutations of three columns and three rows and of a reflection through the main diagonal. (To be strict, the Table has to be multiplied by $(-1)^{P(j_1+j_2+j)}$, where P is the parity of the permutation.) Thus we get a group of $3!\,3!\,2! = 72$ elements, which will be denoted by R_{72}.

An explicit form for the Wigner coefficients can be obtained by integration of the product of three D-functions, by solving recurrence formulas satisfied by the Wigner coefficients, by expanding certain spinor invariants in power series [1], etc. The final result obtained by any of these methods can be brought into the form of a generalized hypergeometric function ${}_3F_2$ of unit argument. The symmetry properties of these functions were derived a long time ago by

* Dedicated to Prof. L. JÁNOSSY on his 60th birthday.

THOMAE and WHIPPLE and, in fact, all 72 symmetries are straightforward consequences of these mathematical theorems.

§2. A simple analytic derivation for the Clebsch—Gordan coefficients utilizing a theorem of BURCHNALL and CHAUNDY, will be presented first. This derivation avoids rather cumbersome algebraic manipulations and gives the Clebsch—Gordan coefficients directly in a ${}_3F_2$ form, which is particularly suitable for the investigation of symmetry properties. To this end, consider representations of the rotation group in the form

$$D^j_{mn}(\varphi,\vartheta,\psi)=\eta e^{-i(m\varphi+n\psi)}n^j_{mn}\left(\sin\frac{\vartheta}{2}\right)^{m-n}\left(\cos\frac{\vartheta}{2}\right)^{m+n}\cdot \\ \cdot\,{}_2F_1\left(-j+m,j+m+1;m-n+1;\sin^2\frac{\vartheta}{2}\right), \tag{2}$$

where

$$n^j_{mn}=\frac{1}{\Gamma(m-n+1)}\sqrt{\frac{\Gamma(j+m+1)\,\Gamma(j-n+1)}{\Gamma(j-m+1)\,\Gamma(j+n+1)}}$$

and η is a phase factor $\eta=i^{|m-n|+m-n}$, which for $m\geq n$ reduces to $\eta=(-1)^{m+n}$. Eq. (2) is valid for $m\pm n\geq 0$. The remaining cases can be obtained by making use of the symmetry properties of D-functions.

Clebsch—Gordan coefficients can be defined by the following decomposition:

$$D^{j_1}_{m_1n_1}D^{j_2}_{m_2n_2}=\sum_{j_3=|j_1-j_2|}^{j_1+j_2}C^{j_3m_3}_{j_1m_1;\,j_2m_2}C^{j_3n_3}_{j_1n_1;\,j_2n_2}D^{j_3}_{m_3n_3}\,. \tag{3}$$

Let us recall a theorem by BURCHNALL and CHAUNDY [2] for the product of two ${}_2F_1$ hypergeometric functions:

$$\begin{aligned}&{}_2F_1(a,b;c;x)\,{}_2F_1(\alpha,\beta;\gamma;x)=\\&=\sum_{r=0}^{\infty}\frac{(a)_r\,(b)_r\,(\gamma)_r}{r!\,(c)_r\,(c+\gamma+r-1)_r}\,{}_3F_2\left[\begin{matrix}\alpha,1-c-r,-r\\ \gamma,1-a-r\end{matrix}\right]{}_3F_2\left[\begin{matrix}\beta,1-c-r,-r\\ \gamma,1-b-r\end{matrix}\right]\cdot\\&\cdot x^r\,{}_2F_1(a+\alpha+r,b+\beta+r;c+\gamma+2r;x)\qquad\left((a)_r\equiv\frac{\Gamma(a+r)}{\Gamma(a)}\right).\end{aligned} \tag{4}$$

Here ${}_3F_2$ is a generalized hypergeometric function of unit argument. In what follows it will be more convenient to work with the functions introduced by THOMAE and WHIPPLE [3], instead of ${}_3F_2$ functions. Using the identity* [3]

* The abbreviation $\Gamma\left[\begin{matrix}a,\,b,\,\ldots\,x\\ u,\,v,\,\ldots\,z\end{matrix}\right]=\dfrac{\Gamma(a)\,\Gamma(b)\,\ldots\,\Gamma(x)}{\Gamma(u)\,\Gamma(v)\,\ldots\,\Gamma(z)}$ is used. Further notations are those of [3].

$$F_p(0;45) = \Gamma\begin{bmatrix}\alpha_{023}, & \alpha_{024}, & \alpha_{025}\\ \alpha_{123}, & \alpha_{124}, & \alpha_{125}\end{bmatrix} F_p(1;24). \tag{5}$$

(α_{345} non-positive integer)

Eq. (4) can be rewritten as

$$\begin{aligned} {}_2F_1(a,b;c;x)\,{}_2F_1(\alpha,\beta;\gamma;x) = \sum_{r=0}^{\infty} \frac{(\alpha)_r(\beta)_r(c-a)_r(c-b)_r}{r!\,(c)_r(\gamma)_r(c+\gamma+r-1)_r} \cdot \\ \cdot {}_3F_2\left[\begin{matrix}a,\gamma-\alpha,-r\\ 1+a-c-r,1-\alpha-r\end{matrix}\right] {}_3F_2\left[\begin{matrix}b,\gamma-\beta,-r\\ 1+b-c-r,1-\beta-r\end{matrix}\right] \times \\ \times x^r\,{}_2F_1(a+\alpha+r,b+\beta+r;c+\gamma+2r;x). \end{aligned} \tag{6}$$

Before applying theorem (6), Eq. (2) is rewritten in the form

$$\begin{aligned} D^j_{mn}(\varphi,\vartheta,\psi) = \eta(-1)^{j-m} e^{-i(m\varphi+n\psi)} n^j_{mn}\,\Gamma\left[\begin{matrix}m-n+1, 2j+1\\ j+m+1, j-n+1\end{matrix}\right] \times \\ \times \left(\sin\frac{\vartheta}{2}\right)^{2j-m-n}\left(\cos\frac{\vartheta}{2}\right)^{m+n} {}_2F_1\left(-j+m,-j+n;-2j;\frac{1}{\sin^2\vartheta/2}\right). \end{aligned} \tag{7}$$

The series form of the ${}_2F_1$ function entering Eq. (2) terminates. Here, in Eq. (7), the terms of the series are merely written in the reverse order.

One gets the required decomposition (3). By applying the theorem of BURCHNALL and CHAUNDY in form (6) to the product of two D-functions given by Eq. (7) and changing the summation index to $j_3 = j_1 + j_2 - r$, the Clebsch-Gordan coefficients obtained are

$$\begin{aligned} C^{j_3 m_3}_{j_1 m_1; j_2 m_2} = \sqrt{2j_3+1}\,\Gamma\left[\begin{matrix}j_1+m_1+1, j_2-m_2+1, j_3-m_3+1,\\ j_1-m_1+1, j_2+m_2+1,\end{matrix}\right. \times \\ \left.\times \begin{matrix}j_3+m_3+1, j_1-j_2+j_3+1, -j_1+j_2+j_3+1\\ j_1+j_2-j_3+1, j_1+j_2+j_3+2\end{matrix}\right]^{1/2} \cdot \\ \cdot \frac{1}{\Gamma(j_3-j_2+m_1+1, j_3-j_1-m_2+1)} \times \\ \times {}_3F_2\left[\begin{matrix}-j_1+m_1, & -j_2-m_2, & -j_1-j_2+j_3\\ j_3-j_1-m_2+1, & j_3-j_2+m_1+1 & \end{matrix}\right]. \end{aligned} \tag{8}$$

It should be noted that identification of Clebsch—Gordan coefficients through Eq. (3) is not quite free of ambiguity, since C can contain an arbitrary real

factor $\alpha = \alpha(j_1, j_2, j_3)$ of unit modulus. In Eq. (8) the value of α has been chosen in such a way that no power of (-1) should appear on the right-hand side.

Wigner coefficients (1) are related to the Clebsch—Gordan coefficients by

$$\sqrt{2j_3+1}\, C^{j_3,-m_3}_{j_1 m_1 ; j_2 m_2} = (-1)^{j_1-j_2-m_3} \begin{pmatrix} j_1 & j_2 & j_3 \\ m_1 & m_2 & m_3 \end{pmatrix}. \tag{9}$$

§3. Out of the 72 symmetries of the Wigner coefficients, 12 are simple consequences of formula (8), as ${}_3F_2$ functions are invariant under permutations of the three numerator and two denominator parameters. This immediately gives $3!\ 2! = 12$ symmetries, so that in order to obtain 72 symmetries, six different forms of ${}_3F_2$ function have to be found.

It is easy to see which types of transformations are required to get the six ${}_3F_2$ functions. In REGGE Table (1) the sum of elements in any row or column is equal to $S = j_1 + j_2 + j_3$ and this sum remains unaltered by interchange of rows or columns, or by transposition through the main diagonal. Another characteristic of the ${}_3F_2$ function sum is closely related to S, as it can be seen from Eq. (8) that the sum of the denominator minus the sum of the numerator parameters is $s = j_1 + j_2 + j_3 + 2 = S + 2$. (This sum is responsible for the convergence of ${}_3F_2$ series when they contain an infinite number of terms. In the present case, however, no problem of convergence arises, since the ${}_3F_2$ series terminates.) Thus we have to search for such ${}_3F_2$ transformations which preserve the value of s. There are exactly six ${}_3F_2$ functions whose characteristic sum is equal to s. These are, $Fp(0; 45)$ (by definition this is proportional to the ${}_3F_2$ function entering eq. (8)), $Fp(4; 05)$, $Fp\ (5; 04)$, $Fn(1; 23)$, $Fn(2; 13)$ and $Fn(3; 21)$. It is important that these functions, and indeed all the Thomae—Whipple functions, are obtainable from $Fp(0; 45)$. It can be verified that in this way all the Regge symmetries are obtained.

§4. There exist 120 Thomae—Whipple functions and already six of them involve the R_{72} group. The question arises as to whether the remaining relations for these functions result in new symmetries for the Wigner coefficients. To see this, let us allow negative values of angular momenta. It can be seen from Eq. (2) that with the substitutions representations of the rotation group are merely multiplied by the phase $(-1)^{m-n}$. Hence, some of the angular momenta j_1, j_2, j_3 may be transformed into $j \to -j-1$. These transformations constitute a group of eight elements which fails to commute with REGGE transformations, and therefore the enlarged REGGE group G is not of order 8.72. To count the elements of G consider the subgroup which leaves the sum $S = j_1 + j_2 + j_3$ invariant. This is clearly the R_{72} group. The number of cosets in G with respect to the subgroup R_{22} is equal to the number of possible values of S. It can be seen by inspection that S can take the following values:

S	
$j_1 + j_2 + j_3$	1 of this type
$-j_1 + j_2 + j_3 - 1$	3 of this type*
$-j_1 - j_2 + j_3 - 2$	3 of this type
$-j_1 - j_2 - j_3 - 3$	1 of this type
$j_1 - m_1 - 1$	3 of this type
$j_1 + m_1 - 1$	3 of this type
$-j_1 - m_1 - 2$	3 of this type
$-j_1 + m_1 - 2$	3 of this type

* The values of S not indicated here explicitly can be obtained by permutation of the indices.

Altogether 20 cosets are obtained, so that if the R_{72} group is enlarged by transformations $j \to -j - 1$ a group of order $20.72 = 1440$ is obtained.

Let us investigate, finally, the question of how many different Thomae—Whipple functions are needed to cover this group of transformations, when two such functions are considered to be different if they cannot be transformed into each other by permutations of numerator or denominator parameters. It is evident that $144/12 = 120$ such functions are necessary, and these are the 120 Thomae—Whipple functions.

REFERENCES

1. T. Regge, Symmetry Properties of Clebsch-Gordan s Coefficients. Nuovo Cim., **10**, 544 1958.
2. J. L. Burchnall and T. W. Chaundy, The Hypergeometric Identities of Cayley, Orr and Bailey. Proc. London Math. Soc. (2) **50**, 56, 1948.
3. W. N. Bailey: Generalized Hypergeometric Series. Cambridge, 1935.

СИММЕТРИИ КОЭФФИЦИЕНТОВ ВИГНЕРА И ФУНКЦИИ ТОМЕ-ВИППЛА

М. ХУСАР

Резюме

Коэффициенты Вигнера можно привести к виду функций Томе—Виппла. Наличне группы симметрий порядка 72, обнаруженной Редже, является непосредственным следствием шести разных видов 120 функций Томе—Виппла. Рассмотрен вопвос о том, приводят ли остальные 114 видов этих функпий к новым свойствам симметрий коэффициентов Редже. Показано, что если группа порядка 1440, которая производится с помощью соотношений между 120 функциями Томе—Виппла.

Acta Physica Academiae Scientiarum Hungaricae, Tomus 32 (1—4), pp. 187—191 (1972)

ANGULAR CORRELATION IN ^{187}Re*

By

L. KESZTHELYI and I. DEMETER

CENTRAL RESEARCH INSTITUTE FOR PHYSICS, BUDAPEST

(Received 19. X. 1971)

The angular correlation coefficient of the 72—134 keV cascade of ^{187}Re was measured to be $A_2 = -0.006$ (2). This is an order of magnitude smaller than previous results.

1. Introduction

In the course of our program of measuring g-factors from the observed rotation of the angular correlation patterns caused by interaction of the magnetic moment of the excited state with the hyperfine field at the nucleus in Fe lattices, we wanted to determine the g-factor of the 134 keV 7/2-state of ^{187}Re. This state is populated in ^{187}W decay; the relevant data for the decay scheme [1] are presented in Fig. 1.

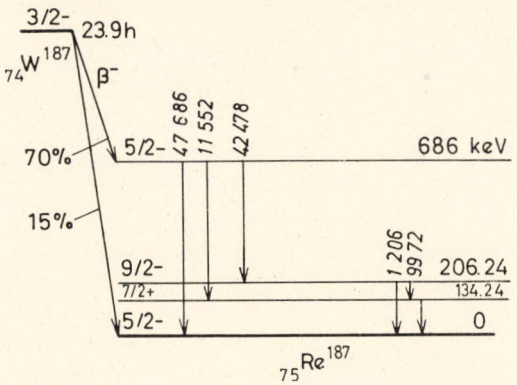

Fig. 1. Relevant features of the decay scheme of ^{187}W

According to the angular correlation measurement of MICHAELIS [2] the 72—134 keV cascade, which can be observed with good efficiency using a scintillation counter, has a small but measurable asymmetry $A_2 = -0.023$ (10), if no correction is made for the distributing 61 and 69 keV K X-ray back-

* Dedicated to Prof. L. JÁNOSSY on his 60th birthday.

ground produced by the internal conversion of 72 keV γ-radiation. A_2 increases a factor of two when corrected. We have remeasured this value using 2.56×2.56 cm and 2.56×0.6 cm NaI (Tl) crystals and obtained A_2 (uncorr) $= 0.031$ (2), which agrees within experimental error with the above value. NIGAM and BATTACHARYYA [3] recently reported that they got a value $A_2 = -0.017$ (11).

By using the known lifetime $\tau = 18$ ps and hyperfine field $H_{hf} = -760$ KGauss values and assuming $g = 1$, a value

$$\frac{R}{2} = \frac{W(135°, H\uparrow) - W(135°, H\downarrow)}{W(135°, H\uparrow) + W(135°, H\downarrow)} \approx 2\, b_2\, \omega\tau \approx 2 \cdot 10^{-3}$$

can be calculated as the expectation value for an alternating field magnetic experiment. Here, b_2 is the angular correlation coefficient if $\cos 2\vartheta$ is used instead of the expression $P_2(\cos\vartheta)$ and $W = g\mu_N H$ is the Larmor precession frequency (μ_N is the nuclear magneton). This $R/2$ value is rather small but it seemed to be measurable. A control experiment performed with a liquid Li_2WO_4 source and an external polarizing magnet gave $R/2 = +(0.3 \pm 2.6)\ 10^{-4}$. Two further measurements were performed on FeW alloys of 1 atom % W content irradiated in the reactor of this Institute. The first was measured without annealing, the second after annealing in argon at 900 °C for 9 hours. The results were $R/2 = (0.4 \pm 2.7) \cdot 10^{-4}$ and $(1.7 \pm 3.2) \cdot 10^{-4}$, respectively.

These results show that one of the parameters entering into the expression for $R/2$ is wrong. The value of b_2 could be checked easily by measuring the angular correlation, using a Ge (Li) counter to separate the 61 keV X-ray peak from the 72 keV γ-radiation.

2. Measurement of the angular correlation

The source was a Li_2WO_4 solution in a 8.5 mm diameter, 6.5 mm long teflon container. A 8 cm^3 coaxial Ge (Li) detector and a 2.5 cm $\times 2.5$ cm NaI (Tl) detector were placed 4 cm away from the source. Only the anisotropy $A = (I_{180°} - I_{90°})/I_{90°}$ was measured, the A_4 coefficient being neglected (it is very small according to MICHAELIS [2]). Fig. 2 shows the 61—72 keV peaks from the Ge (Li) detector in coincidence with the 134 keV peak in the scintillation counter. The efficiency of the Ge (Li) counter was about a factor of two smaller for 61 keV than for 72 keV radiation. The 72 keV peak contains about 15% 69 keV γ-radiation. The resolving time of the coincidence circuit was 10^{-7} sec, and in the control experiment, when the 480 keV—72 keV cascade was studied, 10^{-6} sec.

Firstly single-channel experiments were performed, with the single-channel analyser window set to 72 and then to 61 keV peaks. The sources were

carefully centered and the coincidence numbers were corrected for small centering errors (less than 0.5%), for radioactive decays, and for chance coincidences. The alloy source and liquid sources with W contents of 0.2, 2, and 20 mg were used to test whether a self-absoprtion effect exists or not. The data are collected in Table I. It can be seen that a very small asymmetry exists in the 72—134 keV cascade, which would explain the result of the magnetic experiment. A high asymmetry was obtained for the 480—72 keV radiation,

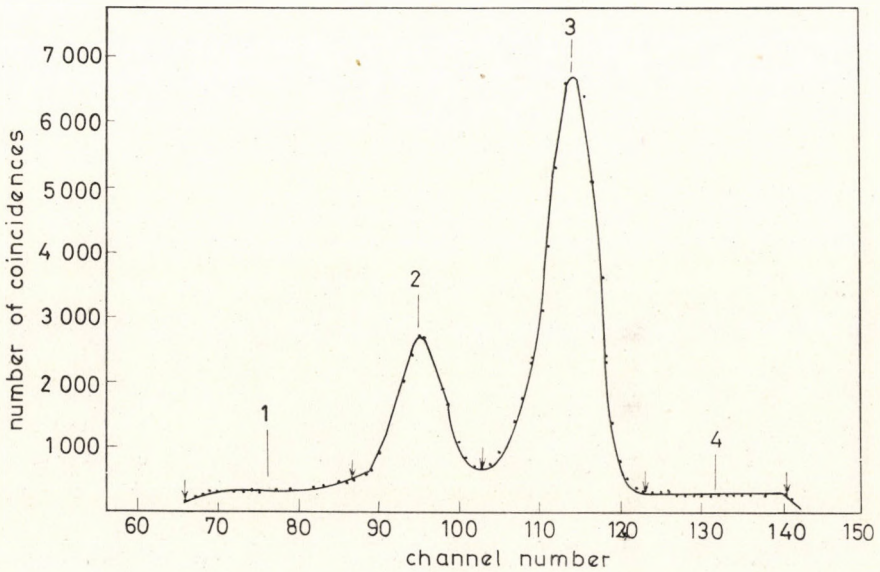

Fig. 2. Coincidence spectrum (61 + 72 keV) — 134 keV γ-radiations

in accordance with previous experiment [4]. There was, however, a —2.5% asymmetry on the 61 keV X-ray peak, too, showing that something is not in order in the experiment.

A broad-window experiment on Ge (Li) spectra containing the 61 + 72 keV peaks should yield the asymmetry of about —4% measured with the two scintillation counters. Therefore we have to get more asymmetry before and after the peaks in Ge (Li) spectra. These points were illuminated by a series of experiments in which the coincidence spectrum of the 61—72 keV region was measured with a multichannel analyser. As the data of Table I do not show any concentration dependence, within experimental error, the source containing 2 mg W was used. In the single-channel experiments the counters were not shielded, whereas in the series measured with the multichannel analyser both Pb and brass shields were placed on the Ge (Li) counter. Table II summarizes the results of this series. The asymmetry values were determined in four sections

Table I

Asymmetry values measured for different coincident radiations in ^{187}Re. Liquid sources are aqueous solutions of Li_2WO_4 of different W concentrations. All values are in %

Sample	72 keV–134 keV	61 keV–134 keV	480 keV–72 keV	480 keV–61 keV
Liquid sources:				
0.2 mg W	−0.7 (3)	−2.0 (6)		
2 mg W	−0.7 (4)	−2.4 (6)	−10.5 (5)	−2.6 (1.4)
20 mg W	−0.7 (5)	−3.2 (7)	−10 (1)	0 (3)
Alloy	−1.1 (3)	−2.9 (7)	− 3.5 (4)	−2.9 (7)

of the coincidence spectra: 1) below 61 keV; 2) at the 61 keV peak; 3) at the 72 keV peak; and 4) above 72 keV (see Fig. 2) for radiations in coincidence with 134 keV and with 480 keV γ-radiations.

The results clearly show that there is a backscattering effect of 72 keV and 134 keV radiation from the NaI (Tl) crystal. The energies of the γ-radiation Compton scattered at 180° are 56 keV and 87 keV, respectively. Without an absorber one gets a higher backscattering intensity at 90° than at 180°, which results in negative A values below the 61 keV peak, at the 61 keV peak, and above the 72 keV peak. The latter is due to concidences between the Compton continuum of higher energy γ-radiations in the scintillation counter and the backscattered "134" keV radiation. This is very high (−54%) in the case of coincidences with the 480 keV photopeak (Table II). The asymmetry changes sign if absorbers are used, because in this case the backscattering through 180° is effective but that through the hole of the shielding only partially so. The Pb shield is not very suitable, because the Pb X-rays are just in the 72—85 keV region and their contribution strongly depends on the geometry of the shieldings.

The asymmetry of the 72—134 keV cascade is very little affected by the different experimental circumstances. We believe it to be $A = 0.007$ (3), and

Table II

Asymmetry values measured for different coincident radiations in ^{187}Re in different sections of the spectra. All values are in %

Shield	134 keV				480 keV			
	1	2	3	4	1	2	3	4
None	−12 (2)	−3.0 (3)	−0.9 (5)	−20 (5)	−9 (2)	0 (2)	−9 (1)	−54 (6)
Pb	+ 7(4)	+3 (3)	−0.5 (10)	+17 (4)				
Brass	+ 5 (2)	0.3 (10)	−0.7 (6)	+ 5 (2)	−4.4 (12)	−0.6 (12)	−9 (1)	−18 (3)

corrected for the 69 keV K X-rays $A_{72\text{-}134} = -0.008$ (3). Hence the angular correlation coefficient $A_2 = -0.005$ (2), and corrected for finite angular resolution $A_2 = -0.006$ (2).

3. Discussion

The theoretical value of A_2 depends on the δ_1 and δ_2 mixing parameters of the first and second radiations of the cascade. The results of internal conversion measurements set upper limits for the quadrupole content of the two radiations [2] of $\delta_1^2/(1+\delta_1^2) \leq 0.01$ and $\delta_2^2/(1+\delta_2^2) \leq 0.25$. A value $\delta_2^2 = 0.038$ can be calculated from the known half-life of this state ($T_{1/2} = 1.3 \cdot 10^{-11}$ s) and the $B(E2)$ value [5] ($B(E2) = 1 \cdot 5 \cdot 10^{-48}$ cm$^4/e^2$ if the internal conversion coefficient $\alpha = 2.3$). Assuming $\delta_1 = 0$, and using $A_2 = -0.006$ (2), this gives $\delta_2 = +0.185$ (6), which is in very good agreement with the δ_2 obtained above.

The new A_2 value shows that the 72 keV radiation is nearly pure $E1$ radiation and that the 134 keV radiation is 96.5% $M1$ and 3.5% $E2$ in character.

REFERENCES

1. C. M. Lederer, J. Hollander and I. Perlman, Table of Isotopes, John Wiley, New York, London, Sidney, 1968.
2. W. Michaelis, Nucl. Phys., **45**, 573, 1963.
3. A. K. Nigam and R. B. Battacharyya, Nucl. Phys., **A164**, 1970.
4. D. A. Shirley in Hyperfine Structure and Nuclear Radiations ed. by D. A. Shirley and E. Matthias, North Holland, 1968, p. 979.
5. S. Koicki, A. Koicki and S. T. Wood, Nucl. Phys., **49**, 161, 1963.
6. P. K. McGowan and P. H. Stelson, Phys. Rev., **109**, 901, 1958.

УГЛОВАЯ КОРРЕЛЯЦИЯ В ^{187}Re

Л. КЕСТХЕЙИ и И. ДЕМЕТЕР

Резюме

Измерено, что коэффициент угловой корреляции каскада 72—134 кэв в ^{187}Re составляет $A_2 = -0{,}006$ (2). Это на порядок меньше, чем следует из предварительных результатов.

Acta Physica Academiae Scientiarum Hungaricae, Tomus 32 (1—4), pp. 193—198 (1972)

A SINGULARITY PROBLEM OF REGGE-POLE THEORY*

By

K. SZEGŐ and K. TÓTH

CENTRAL RESEARCH INSTITUTE FOR PHYSICS, BUDAPEST

(Received 19. X. 1971)

Reggeization of the unequal-mass scattering amplitude is examined. It is shown that there is a proper continuation to $s = 0$ of the Poincaré expansion of the scattering amplitude which does not lead to singularity and which is compatible with the dispersion relation and Regge behaviour.

1

In spite of the growing amount of experimental data, a complete, predictive theory is still lacking in high-energy elementary particle physics. Hence the importance of phenomenological and semi-phenomenological models. Perhaps the most successful of these is the Regge pole model, with its ability to connect the high-energy behaviour of the scattering amplitude with the elementary particle spectra, to fit the continually growing data with just a few parameters, and to systematize the particles.

To improve a model, or to understand its roots, it is necessary to concentrate on its defects. In what follows, we describe a famous singularity problem of the Regge pole theory and our solution to it.

2

Let us consider the $1 + 2 \to 3 + 4$ scattering process drawn in Fig. 1, for the sake of simplicity for spinless particles with $m_1 = m_3$, $m_2 = m_4$. We introduce, as usual, the invariants $s = (p_1 + p_2)^2$, $t = (p_1 - p_3)^2$, $u = (p_1 - p_4)^2$, satisfying $s + t + u = m_1^2 + m_2^2 + m_3^2 + m_4^2$. The physical domains of these variables are shown in Fig. 2.

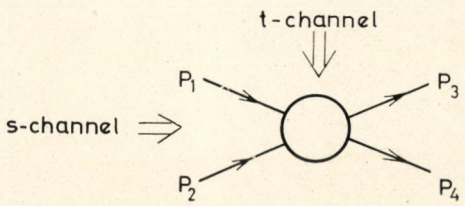

Fig. 1

* Dedicated to Prof. L. JÁNOSSY on his 60th birthday.

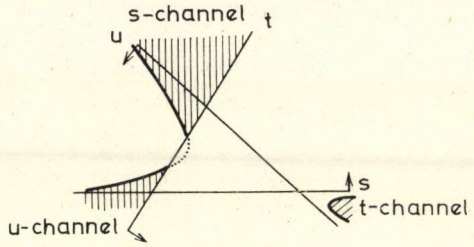

Fig. 2

Let ϑ be the scattering angle in the s-channel CM system, then the partial wave expansion of the $F(s, t)$ scattering amplitude in the s-channel will read

$$\langle p_3, p_4 | T | p_1, p_2 \rangle = (2\pi)^4 F(s,t)\, \delta^4(p_1+p_2-p_3-p_4) =$$
$$= (2\pi)^4 \delta^4(p_1+p_2-p_3-p_4) \frac{s}{(p_0+p)^2} \sum_j (2j+1) f(s,j) P_j(\cos\vartheta), \tag{1}$$

where

$$\cos\vartheta = \frac{s(t-u)+(m_1^2-m_2^2)^2}{[s-(m_1-m_2)^2][s-(m_1+m_2)^2]} \tag{1a}$$

and

$$f(s,j) = \frac{(p_0+p)^2}{s} \int_{-1}^{1} d(\cos\vartheta)\, F(s,t)\, P_j(\cos\vartheta)\,. \tag{1b}$$

Since the physical scattering amplitudes in the different channels are the real boundary values of the same complex, analytical function, we know that the analytical continuation of Eq. (1) will give the scattering amplitude in e.g. the u-channel.

This continuation is done by the so-called Watson—Sommerfeld trick. We recall its steps for the equal-mass case, when

$$\cos\vartheta = 1 + \frac{2t}{s-4m^2}\,. \tag{1c}$$

First, we write the sum in Eq. (1), using the theorem of residues, as a contour integral on the complex j-plane. To do this, we have to extend $f(s, j)$ to complex j values, and so we shall rewrite (1b) using the fixed s dispersion relation:

$$F(s,t) = \frac{1}{\pi} \int_{4m^2}^{\infty} \frac{A_t(s,t')}{t'-t}\, dt' + \frac{1}{\pi} \int_{-\infty}^{u_0} \frac{A_u(s,t')}{t'-t}\, dt'. \tag{2}$$

Inserting this into (1b) and performing the integration over ϑ, we get

$$f(s,j)=f_t(s,j)+f_u(s,j)=\frac{1}{\pi}\int_{4m^2}^{\infty}A_t(s,t')\,Q_j\left(1+\frac{2t'}{4m^2}\right)+$$
$$+(-1)^{j+1}\int_{4m^2}^{\infty}du'\,A_u(s,4m^2-s-u')\,Q_j\left(1+\frac{2u'}{s-4m^2}\right). \tag{3}$$

Denoting

$$f^{\pm}(s,j)=\frac{1}{\pi}\int_{4m^2}^{\infty}(A_t(s,t')\pm A_u(s,4m^2-s-t'))\,Q_j\left(1+\frac{2t'}{s-4m^2}\right) \tag{4}$$

we may cast (1) into the following form:

$$F(s,t)=\frac{1}{2}\sum_j(2j+1)\,P_j(\cos\vartheta)\left\{(1+e^{-i\pi j})f^-(s,j)+(1-e^{-i\pi j})f^+(s,j)\right\}=$$
$$=\frac{1}{2}\int_{C_1}\frac{dj(2j+1)}{\sin\pi j}\,P_j(-\cos\vartheta)\left\{(1+e^{-i\pi j})f^-(s,j)+(1-e^{-i\pi j})f^+(s,j)\right\}, \tag{5}$$

where C_1 is the contour drawn in Fig. 3.

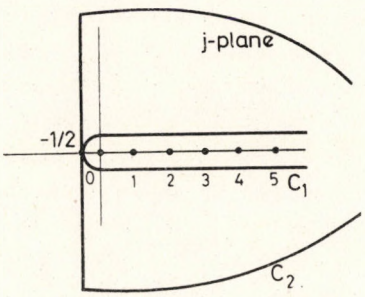

Fig. 3

Supposing that $f^{\pm}(s,j)$ are meromorphic functions on the complex Re $j\geq -1/2$ plane, we may deform C_1 to C_2:

$$F(s,t)=\frac{1}{2}\left(\int_{-1/2-i\infty}^{-1/2+i\infty}+\int_{\substack{\text{infinite}\\ \text{semicircle}}}\right)\frac{dj(2j+1)}{\sin\pi j}\,P_j(-\cos\vartheta)\{\ldots\}+$$
$$+\sum_{\text{poles}}\frac{(2\alpha+1)(1\pm e^{-i\pi\alpha})}{2\sin\pi\alpha}\,\beta_\alpha(s)\,P_\alpha(\cos\vartheta). \tag{6}$$

If $A_{t,u}$ are polynomially bounded, the contribution of the infinite semicircle is zero (which is why we introduced $f^{\pm}$; the same statement would not have been true for $f(s,j)$ [1]).

The above calculations were done in the s-channel. Now, if we continue s and t to such u-channel physical values that $|t| \gg 0$, $s \sim 0$, it is easy to show that the pole terms dominate over the background integral. Using the asymptotic form of the Legendre polynomials, we finally obtain

$$F(s,t) \sim \sum_{\text{poles}} \frac{(2\alpha+1)(1 \pm e^{-i\pi\alpha})}{2 \sin \pi\alpha} \beta_\alpha(s) |t|^\alpha. \tag{7}$$

This behaviour is in agreement with experiment.

3

If we were naive enough to play the same game for the unequal mass configuration, writing (1a) instead of (1c) everywhere, we should get into trouble at $s = 0$ in the u-channel (which is inside the physical domain), since there $\cos \vartheta = 1$, and $P_j(-\cos \vartheta)$ has a logarithmic singularity if $j \neq$ integer. Experiments, on the other hand, support the behaviour we got in Eq. (7).

This challenge of the Regge theory has inspired many physicists, and from different starting points (analytical approaches, group-theoretical considerations) they have always reached more or less the same result: if one supposes not one but an infinite number of Regge poles conspiring in a special way, the net result of such a family is the observed $|t|^\alpha$ behaviour. A survey of the literature can be found e.g. in [2].

As the singularity appears when we continue (6) to $s = 0$, in the group-theoretical considerations, people try to find expansions in terms of other groups, mostly in terms of SL(2, c) representations [3]. We suggest, however, that the singularity at $s = 0$ appears simply because the continuation was incorrect. We do not need expansions in terms of other groups just to find the correct continuation of formulae (1–6).

The partial wave expansion (1) is an expansion of the scattering amplitude in terms of the representations of the Poincaré group, which is the invariance group of the S-operator [4]. To continue the expansion, we have to continue (on the one hand) the representation matrix elements and (on the other hand) the expansion coefficients. We have already discussed the first question in [5] and we found that in the $s \to 0$ limit the representation matrix elements of the Poincaré group behave nicely if

$$sj(j+1) = \varepsilon^2/4 \tag{8}$$

is kept fixed. For instance, in a special case:

$$\lim_{\substack{s \to 0 \\ s(j+1)j \text{ fixed}}} P_j\left(1 + \frac{2st}{[s-(m_1-m_2)^2]\,[s-(m_1+m_2)^2]}\right) = J_0\left(\varepsilon \sqrt{\frac{|t|}{m_1 m_2}}\right), \tag{9}$$

This result was already known in another context. Although in Eq. (6) the representation matrix elements appear to be "sligthly deformed", one can prove that

$$\lim_{\substack{s\to 0 \\ sj(j+1)\to\varepsilon^2/4}} \frac{P_j(-\cos\vartheta)}{\sin \pi j} = \begin{cases} iH_0^{(1)}\left(\varepsilon\sqrt{\frac{|t|}{m\mu}}\right), & \text{for} \quad \operatorname{Im} j > 0. \\ iH_0^{(2)}\left(\varepsilon\sqrt{\frac{|t|}{m\mu}}\right), & \text{for} \quad \operatorname{Im} j < 0. \end{cases} \tag{10}$$

It is more difficult to discuss the continuation of the expansion coefficients. For a square-integrable function, the expansion coefficients are defined by (1b), and if we try to continue this expression, the integral diverges outside the s-channel. Hence we have to construct an expression which agrees with (1b) in the s-channel but will not diverge elsewhere. This can be done with the aid of the dispersion relations for the equal-mass case in Eqs. (3–4). Accordingly, in the u-channel, where $F(s, t)$ is not square integrable, we have an expansion reproducing the original function, but the expansion coefficients are not defined by the inverse transformation.

If the function to be expanded is given by a dispersion relation, it is useful to expand the Cauchy-kernel $1/t - t'$ [6]. This was done in [7], where we were able to show that

$$\frac{1}{t-t'\pm i0} = \begin{cases} \sum_j (2j+1) P_j\left(1+\frac{2st}{\Delta}\right) Q_j\left(1+\frac{2st'}{\Delta}\pm i0\right) & s\neq 0, \quad \text{(11a)} \\ \mp \frac{i\pi}{2m_1 m_2}\int_0^\infty \varepsilon d\varepsilon J_0\left(\varepsilon\sqrt{\frac{-t}{m_1 m_2}}\right) H_0^{(2)}\left(\varepsilon\sqrt{\frac{-t'}{m_1 m_2}}\right) & s=0 \quad \text{(11b)} \end{cases}$$

and

$$\lim_{\substack{s\to 0 \\ sj(j+1)=\varepsilon^2/4 \text{ fixed}}} (11a) = (11b).$$

These relations are true in a generalized function sense. Applying these results, one can check that

$$F(s=0,t) = \frac{1}{4\pi}\int_0^\infty \varepsilon d\varepsilon \left[f_t(0,\varepsilon)+f_u(0,\varepsilon)\right] \times \\ \times J_0\left(\varepsilon\sqrt{\frac{-t}{m_1 m_2}}\right) + \sum_{\text{poles}} \beta(\varepsilon_i) Y_0\left(\varepsilon_i\sqrt{\frac{-t}{m_1 m_2}}\right). \tag{12}$$

4

The last equation means that with the above-mentioned technique we have been able to continue Eq. (6) to $s = 0$ in such a way that

— no singularity appears;

— at every s value the expansion reproduces the scattering amplitude in the form of Eq. (2),

— at every s value we have an expansion in terms of the representations of the Poincaré group.

Let us now examine whether our expansion can reproduce the Regge behaviour of the scattering amplitude. On the j-plane, at $s = 0$, this behaviour is caused by the pole terms. However, on the ε-plane, at $s = 0$, the pole terms behave in another way, since

$$Y_0(z)_{|z|\to\infty} \sim \sqrt{\frac{2}{\pi z}} \sin(z - \pi/4). \tag{13}$$

Simple assumptions for $A_{t,u}$ (e.g. t^z) do not lead to poles at all on the ε-plane for Re $\varepsilon \geq 0$, but they do give a singularity at $\varepsilon = 0$ of $\varepsilon^{-(2\alpha+2)}$ type.

The "old" theory has predicted on the j-plane family of Regge poles with finite j values. These poles will, of course, appear on the ε-plane as well, since for $s \neq 0$ the j- and ε-planes are completely equivalent (c.f. Eq. (8)). Every pole at finite j value cumulates on the ε-plane at $\varepsilon = 0$, if $s \to 0$. Hence, it is obvious that the $\varepsilon = 0$ point will play an important role although it is far less easy to see how the cumulation of poles can give rise to an $\varepsilon^{-2\alpha-2}$ type singularity. But if this is assumed for $f_{t,u}(0, \varepsilon)$, we can reproduce the experimentally observed results, and such a simple assumption on the ε-plane is not unreasonable. If poles exist as well, they will give an oscillatory contribution, as one can see from Eq. (13). This is not supported by present experimental evidence.

We ought to mention that we did not find as simple an interpretation of the value of α on the ε-plane at $s = 0$, as there is in the "old" formalism: here α does not characterize Poincaré representations. In this respect further investigations are necessary.

REFERENCES

1. R. J. Eden et al., The Analytic S-Matrix, Cambridge U.P., 1966.
2. P. D. B. Collins and E. J. Squires, Regge Poles in Particle Physics, Springer, Berlin, 1968.
3. M. Toller, Nouvo Cim., **54**, 295, 1968; G. Domokos and G. L. Tindle, Phys. Rev., **160**, 1560, 1967. K. Szegő and K. Tóth, Nuovo Cim., **66A**, 371, 1970.
4. P. Moussa, CEA-R-3608, 1968.
5. K. Szegő and K. Tóth, KFKI-71-38; Annals of Phys., in print.
6. R. Hermann, preprint, Univ. of Cal. 8/67, 9/67, 10/67.
7. K. Szegő and K. Tóth, KFKI-71-60; Phys. Rev., in print.

О ПРОБЛЕМЕ ОСОБЕННОСТЕЙ В ТЕОРИИ РЕДЖЕ

К. СЕГЁ и К. ТОТ

Резюме

В настоящей статье исследуется разложение Редже для амплитуды рассеяния неравных масс. Авторы показывают, что имеется подходящее продолжение разложения Пуэнкаре амплитуды рассеяния, которое не приводит к особенности и совместимо с дисперсионными соотношениями и поведением типа Редже.

Acta Physica Academiae Scientiarum Hungaricae, Tomus 32 (1–4), pp. 199–205 (1972)

CONSTRUCTION OF THE EFFECTIVE LAGRANGIAN OF PIONIC PROCESSES FOR ARBITRARY SU(2) × SU(2) BREAKING*

By

P. HASENFRATZ

CENTRAL RESEARCH INSTITUTE FOR PHYSICS, BUDAPEST

(Received 19. X. 1971)

By assuming that SU(2) × SU(2) symmetry is broken by the isoscalar element of the representation (l, l), effective Lagrangians reproducing the results of current algebra and the PCAC assumption can be constructed by a direct method suggested by R. DASHEN and M. WEINSTEIN. The symmetry-breaking parts of these Lagrangians are the solutions (in closed form) of the differential equation for the breaking parts in Weinberg's formalism.

Effective Lagrangians, which give the amplitudes of pions in the lowest order of the momenta and the symmetry-breaking parameter, can be constructed for an arbitrary type of symmetry-breaking from one of DASHEN and WEINSTEIN's identities [1]. The results are WEINBERG's phenomenological Lagrangians in the case of the general pion field definition. Indeed, S. COLEMAN et al. [3] have pointed out that the phenomenological approximation with nonlinear Lagrangians is identical with the results obtained by current algebra. The mentioned identity is:

$$\langle \alpha + \pi_{\alpha_1}(p_1) + \pi_{\alpha_2}(p_2) + \ldots + \pi_{\alpha_n}(p_n) | S | \beta \rangle = f_\pi^n \langle \alpha | U^{(n)}(p_1, p_2, \ldots p_n) | \beta \rangle \quad (1)$$

with $U^{(n)}(p_1, p_2 \ldots p_n)$ defined to be the coefficient of f_π^n in the expansion of the exponential

$$T(\exp [i \int d^4 x \mathfrak{L}(x)]). \quad (2)$$

$\mathfrak{L}(x)$ is in general a sum of two parts, which can be obtained from

$$\begin{aligned} f_\pi \int_0^1 du \, \{ & \exp \left[-i f_\pi u \int d^3 x G(\varphi^2) \cdot \underline{\varphi} \cdot \underline{A}^\circ(x) \right] \\ & \cdot \left(\partial_\mu (G(\varphi^2) \underline{\varphi}) \, \underline{A}^\mu(y) \right) \exp \left[i f_\pi u \int d^3 z G(\varphi^2) \underline{\varphi} \cdot \underline{A}^\circ(z) \right] \} + \\ + f_\pi \int_0^1 du \, \{ & \exp \left[-i f_\pi u \int d^3 x G(\varphi^2) \underline{\varphi} \cdot \underline{A}^\circ(x) \right] \cdot \\ & \cdot \left(G(\varphi^2) \underline{\varphi} \cdot \partial_\mu \underline{A}^\mu(y) \right) \exp \left[i f_\pi u \int d^3 z G(\varphi^2) \underline{\varphi} \cdot \underline{A}^\circ(z) \right] \} \end{aligned} \quad (3)$$

if in the resulting expression we replace the terms $\partial_\mu \underline{\varphi} \underline{A}^\mu$ and $\underline{\varphi} \cdot \partial_\mu \underline{A}^\mu$ (linear in $\underline{\varphi}(x)$) with $\partial_\mu \underline{\varphi} \cdot \underline{\hat{A}}^\mu$ and $\underline{\varphi} \cdot \partial_\mu \underline{\hat{A}}^\mu$. Here $\underline{\varphi}(x)$ is a c-number isovector function:

* Dedicated to Prof. L. JÁNOSSY on his 60th birthday.

$$\underline{\varphi}(x) = \sum_{j=1} \underline{\varepsilon}_j \, e^{ip_j x} \tag{4}$$

ε_j being an isovector all of whose components except the α_j-th are equal to zero. Only those terms of the resulting expression should be kept for which all the p_j are distinct. $A_i^\mu(x)$ $(i = 1, 2, 3)$ are the axial vector currents encountered in the theory of weak interactions, and the barred quantities are defined as equal to the corresponding unbarred quantity with the pion pole removed. $G(\varphi^2)$ stands for an arbitrary function of φ^2.

Performing the operations in the first term of (3), we get

$$\frac{(\partial_\mu \underline{\varphi} \cdot \underline{\varphi})(\underline{\varphi} \cdot \underline{A}^\mu)}{\varphi} K(\varphi) + \frac{\sin f_\pi G\varphi}{\varphi} (\partial_\mu \underline{\varphi} \cdot \underline{A}^\mu) + (\partial_\mu \underline{\varphi} \, x \, \underline{\varphi}) \underline{V}^\mu \frac{\cos f_\pi G\varphi - 1}{\varphi^2}, \tag{5}$$

where

$$K(\varphi) = f_\pi \frac{\partial G}{\partial \varphi} + f_\pi \frac{G}{\varphi} - \frac{\sin f_\pi G\varphi}{\varphi^2}. \tag{6}$$

Let $|\alpha> = |\beta> = |0>$ in (1). In the lowest order we get contributions from direct and pole terms. Let us look for the contribution of the direct part. From the first term in (3) we obtain a part which is second order in pion momenta:

$$\left\{ <0 | \frac{1}{2!} (-i)^2 \int T(\mathfrak{L}(x) \mathfrak{L}(y)) \, d^4x \, d^4y \, | 0> \right\}_{| f_\pi^n}. \tag{7}$$

In the case of the direct diagram we can put a caret above the axial vector currents in (5), which gives

$$\left\{ \int d^4x \, d^4y \frac{-1}{2!} \left[\frac{(\partial_\mu \underline{\varphi} \cdot \underline{\varphi}) \varphi_\alpha(x)}{\varphi} K(\varphi) + \frac{\sin f_\pi G\varphi}{\varphi} \partial_\mu \varphi_\alpha(x) \right] \cdot \right.$$
$$\left. \cdot \left[\frac{(\partial_\nu \underline{\varphi} \cdot \underline{\varphi}) \varphi_\beta(y)}{\varphi} K(\varphi) + \frac{\sin f_\pi G\varphi}{\varphi} \partial_\nu \varphi_\beta(y) \right] <0 | \, T(\hat{A}_\alpha^\mu \hat{A}_\beta^\nu) \, | 0> \right\}_{| f_\pi^n}. \tag{8}$$

Here

$$<0 | \, (\hat{A}_\alpha^\mu \hat{A}_\beta^\nu) \, | 0> \to \delta_{\alpha\beta} g^{\mu\nu} \frac{-i}{4 f_\pi^2}.$$

Clearly we obtain the same result by putting $\underline{\varphi}(x) \to \underline{\pi}(x)$ in (8), sandwiching it between n pions, and calculating the direct diagram. Thus the kinetic part of the effective Lagrangian is

$$-\frac{1}{2} D_\mu \underline{\pi}(x) D^\mu \underline{\pi}(x), \tag{9}$$

where

$$D_\mu \underline{\pi} \equiv \frac{\sin f_\pi G\pi}{\pi} \partial_\mu \underline{\pi} + \frac{(\partial_\mu \underline{\pi} \cdot \underline{\pi})\underline{\pi}}{\pi} K(\pi), \qquad \pi \equiv \sqrt{\underline{\pi}^2}. \tag{10}$$

Let us compare this with the general form of the covariant derivative of WEINBERG [2]*:

$$D_\mu \underline{\pi} = \frac{1}{(f^2(\pi^2) + \pi^2)^{1/2}} \partial_\mu \underline{\pi} + \frac{1}{f^2(\pi^2)+\pi^2} \left(f'(\pi^2) + \frac{1}{2} v \right) \underline{\pi} \cdot \partial_\mu \pi^2, \tag{11}$$

where

$$v(\pi^2) = - \frac{f(\pi^2) - (f^2(\pi^2)+\pi^2)^{1/2}}{\pi^2}; \quad f'(\pi^2) \equiv \frac{df(\pi^2)}{d\pi^2}.$$

It can be seen immediately that the two expressions are the same, assuming

$$\sin f_\pi G\pi = \frac{\pi}{(f^2(\pi^2)+\pi^2)^{1/2}}. \tag{12}$$

To find the symmetry-breaking part of the Lagrangian let as assume that the strong interaction Hamiltonian can be decomposed at any time t into two parts

$$H = H_0(t) + \epsilon H_1(t) \quad \text{and} \quad H_1(t) = \int \mathcal{H}_1(x)\, d^3x,$$

where $H_0(t)$ possesses a chiral symmetry, and $\varepsilon H_1(t)$ transforms as some sum of irreducible tensors under the SU(2)×SU(2) group. The first-order term in ε comes from

$$< 0 | \frac{1}{1!} (-i) \int d^4x\, \mathfrak{L}(x) | 0 > \tag{13}$$

and its value can be obtained by evaluating the second part of (3). Here we must make a general chiral transformation on the $\partial_\mu \underline{A}^\mu(y)$ operator, assuming that the symmetry-breaking operator is the isoscalar element of the representation (l, l). Isoscalar and isovector . . . elements arise from the transformation, but because of (13) we must look only for the coefficient of the isoscalar part. Taking into account that

$$< 0 | \epsilon \mathcal{H}_1^{(l,l)}(0) | 0 > = - \frac{m_\pi^2}{4f_\pi^2} \frac{3}{2l(2l+2)} \tag{14}$$

one can see that the symmetry-breaking part of the effective Lagrangian is

$$\mathfrak{L}^{(l,l)}(x) = - i f_\pi G(\varphi^2) \frac{m_\pi^2}{4f_\pi^2} \frac{3}{l(2l+1)(2l+2)} \int_0^1 du\, Tr \{ \underline{\varphi} \underline{J}^{(l)} \cdot D^{(l)}(\underline{n}, 2\omega) \}_{|\varphi(x) \to \pi(x)}. \tag{15}$$

* There is a misprint in the expression of $D_\mu \underline{\pi}$ and $v(\pi^2)$ in [2].

In (15) $\underline{J}^{(l)}$ denotes the representation of the SU(2) generator and $D^{(l)}(\underline{n}, 2\omega)$ the matrix for the rotation $2\omega = 2(-\varphi f_\pi G u)$ about the axis $\underline{n} = \underline{\varphi}/\varphi$ of $(2l+1)$ dimensions (see Appendix). We find from the known form of $D^{(l)}$

$$\mathfrak{L}^{(l,l)}(x) = \frac{m_\pi^2}{4f_\pi^2} \frac{3}{l(2l+1)(2l+2)} \sum_{n=1}^{l} [\cos 2nf_\pi G\varphi - 1]_{|\underline{\varphi}(x) \to \underline{\pi}(x)} \tag{16}$$

($n = 1/2$ if l half-integer).

With the aid of (12) we get

$$\mathfrak{L}^{(l,l)}_{(x)} = \text{const} \cdot \text{Re}\left\{\frac{q^{l+1}}{q-1}\right\} + \text{const}. \tag{17}$$

where

$$q = \frac{f(\pi^2) + i\pi}{f(\pi^2) - i\pi}$$

and the constants may be obtained by demanding that the Taylor series of $\mathfrak{L}^{(l,l)}(\pi^2)$ start with $1/2\, m_\pi^2\, \pi^2$. The results can be summarized in the following theorem:

In the lowest order of the momenta and ε the pion's amplitudes are correctly calculated by using the effective Lagrangian (in the case of (l, l) -type symmetry-breaking)

$$\mathfrak{L}(x) = -\frac{1}{2} D_\mu \underline{\pi} D^\mu \underline{\pi} + \mathfrak{L}^{(l,l)}(x), \tag{18}$$

where $D_\mu \underline{\pi}(x)$ and $\mathfrak{L}^{(l,l)}(x)$ are defined by (10) (or (11)) and (16) (or (17)), respectively, calculating according to the usual Feynman rules but subject to the restriction that one keeps only tree diagrams. We can see, therefore, an explicit connection between the point of view of broken symmetry and WEINBERG's phenomenological Lagrangian formalism. Namely, $\mathfrak{L}^{(l,l)}(x)$ is the solution of the differential equation

$$\begin{aligned} &2\pi^2 \left(f(\pi^2) + \pi^2 g(\pi^2)\right)^2 \mathfrak{L}^{l,l''}(\pi^2) + \left(f(\pi^2) + \pi^2 g(\pi^2)\right) \cdot \\ &\quad \cdot \left[3f(\pi^2) + \pi^2 g(\pi^2) + 2\pi^2 \left(f(\pi^2) + \pi^2 g(\pi^2)\right)'\right] \mathfrak{L}^{(l,l)'}(\pi^2) + \\ &\quad + l(2l+2)\, \mathfrak{L}^{(l,l)}(\pi^2) = \text{const} \end{aligned}$$

$$g(\pi^2) = \frac{1 + 2f(\pi^2) f'(\pi^2)}{f(\pi^2) - 2\pi^2 f'(\pi^2)}, \tag{19}$$

which gives the symmetry-breaking Lagrangian in WEINBERG's method, as we can convince ourselves by direct substitution. The other solutions of (19) are $\sim Im\,(q^{l+1}/q-1)$, which are singular when $\pi^2 = 0$, and so are disregarded.

For the special case when $f(\pi^2) = -1/2 f_\pi (1 - f_\pi^2 \pi^2)$ we get [4]:

$$\mathfrak{L}^{(1/2,\,1/2)}(\pi^2) = \frac{m_\pi^2}{2}\,\pi^2\,\frac{1}{1+f_\pi^2\pi^2}\,, \tag{20a}$$

$$\mathfrak{L}^{(1,1)}(\pi^2) = \frac{m_\pi^2}{2}\,\frac{1}{(1+f_\pi^2\pi^2)^2}\,, \tag{20b}$$

$$\mathfrak{L}^{(2,2)}(\pi^2) = \frac{m_\pi^2}{2}\,\frac{1-6/5\,f_\pi^2\pi^2+f_\pi^4\pi^4}{(1+f_\pi^2\pi^2)^4}\,. \tag{20c}$$

20/a is the only closed solution which was given by WEINBERG [2]. The differential equation for this special pion field definition has been solved by W. SOLLFREY [4].

The author is very grateful for valuable discussions with A. FRENKEL and is indebted to Professor B. RENNER for a critical reading of the manuscript of the present paper [5].

Appendix

If x_i and y_i $(i = -l, \ldots 0, \ldots l)$ are the representations of the two independent SU(2) generators, then

$$\mathfrak{H}_1^{(l,l)} = x_k\, y^k. \tag{A.1}$$

Let us begin with the second term of (3). Because

$$\partial_\mu A^\mu(x) = -\,i\,[\underline{F}^5, \in \mathfrak{H}_1^{(l,l)}(x)] \tag{A.2}$$

we get

$$-i \in f_\pi G(\varphi^2) \int_0^1 du \left[\underline{\varphi}(y)\,\underline{F}^5,\, e^{-iuf_\pi G(\varphi^2)\underline{\varphi}(y)\underline{F}^5}\,\mathfrak{H}_1^{(l,l)}(y)\,e^{iuf_\pi G(\varphi^2)\underline{\varphi}(y)\underline{F}^5}\right], \tag{A.3}$$

where the $\delta^3(x - y)$ appearing in the equal time commutators has been used to exchange $\underline{A}^0 \to \underline{F}^5$. With the aid of A.1 we obtain

$$e^{-iuf_\pi G\underline{\varphi}\underline{F}^5}\,\mathfrak{H}_1^{(l,l)}\,e^{iuf_\pi G\underline{\varphi}\,\cdot\,\underline{F}^5} = (e^{-is\underline{\varphi}\underline{F}^{(+)}}\,x_j\,e^{is\underline{\varphi}\underline{F}^{(+)}})\,(e^{is\underline{\varphi}\underline{F}^{(-)}}\,y^j\,e^{-is\underline{\varphi}\underline{F}^{(-)}}) \tag{A.4}$$

$$= x_k \left(D^{(l)}(\underline{n}, \omega)\, D^{(l)}(\underline{n}, \omega)\right)_{kt} y^t = x_k\, D^{(l)}(\underline{n}, 2\omega)_{kt}\, y^t \tag{A.5}$$

$$(s = f_\pi G u)$$

where $D^{(l)}(\underline{n}, \omega)$ is the matrix of the rotation $\omega = -s\varphi$ about the axis $n = \dfrac{\varphi}{\varphi}$ in $(2l + 1)$ dimensions. Let us substitute A.5 in A.3

$$-i \in f_\pi G \int_0^1 du\, x_k \left\{\underline{\varphi}\underline{J}^{(l)} \cdot D^{(l)}(\underline{n}, 2\omega)\right\}_{kt} y^t \tag{A.6}$$

denoting by $\underline{J}^{(l)}$ the representation of the SU(2) generator. We must look for the isoscalar element from (A.6), because of (13), and this is the trace times $1/(2l+1)$. On the other hand

$$< 0 \mid \in \mathcal{H}_1^{(l,l)}(0) \mid 0 > = - \frac{m_\pi^2}{4f_\pi^2} \frac{3}{2l(2l+2)} \tag{A.7}$$

and so we obtain

$$\mathcal{L}^{(l,l)}(x) = - if_\pi G(\varphi^2) \frac{m_\pi^2}{4f_\pi^2} \frac{3}{l(2l+2)(2l+1)} \int_0^1 du Tr(\underline{\varphi}\underline{J}^{(l)} D^{(l)}(\underline{n}, 2\omega))|_{\underline{\varphi}\to\underline{\pi}(x)}. \tag{A.8}$$

The relation between $\underline{n}$, 2ω and the appropriate Euler angles is

$$\begin{bmatrix} \cos\frac{\Theta}{2} e^{i\frac{\Phi_1+\Phi_2}{2}} & i\sin\frac{\Theta}{2} e^{-i\frac{\Phi_2-\Phi_1}{2}} \\ i\sin\frac{\Theta}{2} e^{i\frac{\Phi_2-\Phi_1}{2}} & \cos\frac{\Theta}{2} e^{-i\frac{\Phi_1+\Phi_2}{2}} \end{bmatrix} \leftrightarrow$$

$$\leftrightarrow \begin{bmatrix} \cos\omega - i\frac{\varphi_3}{\varphi}\sin\omega & i(\varphi_1+i\varphi_2)\frac{1}{\varphi}\sin\omega \\ i(\varphi_1-i\varphi_2)\frac{1}{\varphi}\sin\omega & \cos\omega + i\frac{\varphi_3}{\varphi}\sin\omega \end{bmatrix}. \tag{A.9}$$

Expression A.8 is an isoscalar, so we can proceed in a special coordinate system: $\underline{\varphi} = (0, 0, \varphi) \to \Theta = 0$. It is easy to see that

$$Tr(\underline{\varphi}\underline{J}^{(l)} D^{(l)}(\Phi_1, \Theta, \Phi_2)) = \sum_{n=-l}^{l} n \cdot \varphi e^{-in(\Phi_1+\Phi_2)}. \tag{A.10}$$

By A.8 and A.9 we get (16). On the other hand

$$\mathcal{L}^{(l,l)} \sim \sum_{\substack{n=1 \\ (n=1/2)}}^{l} \cos(2nf_\pi G\varphi)|_{\underline{\varphi}\to\underline{\pi}} = \sum_{\substack{n=1 \\ (n=1/2)}} \mathrm{Re}\,(\cos f_\pi G\varphi + i\sin f_\pi G\varphi)\Big|_{\underline{\varphi}\to\underline{\pi}}^{2n}. \tag{A.11}$$

From (12) we get

$$(\cos f_\pi G\varphi + i\sin f_\pi G\varphi)^{2n} = \left(\frac{f+i\varphi}{f-i\varphi}\right)^n \equiv q^n. \tag{A.12}$$

Substituting (A.12) in (A.11) we obtain (17), because

$$Re\,\frac{q}{q-1} = \text{const.} \tag{A.13}$$

REFERENCES

1. R. Dashen and M. Weinstein, Phys. Rev., **183,** 1261, 1969,
2. S. Weinberg, Phys. Rev. **166,** 1568, 1968.
3. S. Coleman, J. Wess and B. Zumino, Phys. Rev., **177,** 2239, 1969.
4. W. Sollfrey, Phys. Rev., **173,** 1805, 1968.
5. P. Hasenfratz, KFKI-71-33 preprint.

ПОСТРОЕНИЕ ЭФФЕКТИВНОГО ЛАГРАНЖИАНА ПИ-МЕЗОННЫХ ПРОЦЕССОВ ДЛЯ ОЦЕНКИ SU(2) × SU(2) НАРУШЕНИЯ

П. ХАСЕНФРАТЦ

Резюме

Исходя из нарушения симметрии SU (2) × SU (2) изоскалярным элементом репрезентации (l, l) можно построить эффективный лагранжиан, воспроизводящий результаты алгебраических расчетов и предположения PCAC, с помощью прямого метода, который предложили Р. Дашен и М. Вейнштейн [1]. Нарушающие симметрию члены этих лагранжианов являются решениями (в замкнутой форме) дифференциального уравнения для нарушаюших членов в формализме Вейнберга [2].

Acta Physica Academiae Scientiarum Hungaricae, Tomus 32 (1–4), pp. 207–220 (1972)

SU(1,1) SPIN COEFFICIENTS*

By

Z. PERJÉS

CENTRAL RESEARCH INSTITUTE FOR PHYSICS, BUDAPEST

(Received 19. X. 1971)

A comparative discussion of SU(2) and SU(1,1) spinor algebras is presented. Spin coefficients are introduced in both formalisms. Although particular flat-space spin and coordinate frame is used, the fundamental relations are given in a covariant notation such that the method can easily be adapted to spinor fields in curved three-spaces also. The SU(1,1) spin coefficients are used to obtain the stationary axisymmetric gravitational equations in a form in which all the field quantities appear as spin coefficients of a flat hyperbolic three-space.

1. Introduction

The spin coefficient technique was brought into being by the physicists' struggle with the essentially nonlinear character of the gravitational equations of EINSTEIN. But since NEWMAN and PENROSE [1] developed the method, its uses have rapidly spread beyond the theory of general relativity, mostly due to the extreme flexibility lent to it by the alternative uses of spinor and vector pictures in visualizing the geometric meaning of spin coefficients. It is hard to give a comprehensive survey of all the papers involved in this field, but an attempt has been made to list some of the references containing the most important results [2].

Spin coefficients were introduced originally in the SL(2, C) spinor calculus, but their use had been extended to SU(2) and it will be shown in the present paper that the way of formulating the SU(2) calculus [3] is easily adapted to SU(1,1) spinors also. To facilitate comparison of the (already familiar) SU(2) with the SU(1,1) spin coefficient formalism, a parallel discussion will be given of spinor algebras (Section 2), connecting quantities (Section 3), the dyad notation (Section 4) and the field identities (Section 5). Although a particular flat-space coordinate and spin frame will be used throughout this paper, the covariant formulation of the basic relations opens the way for later applications to curved (Riemannian) spaces. For the same purpose, the field identities given in Section 5 contain curvature terms, although these are assumed to vanish in all other parts of the paper.

In Section 6, SU(1,1) spinor formalism is employed to bring the field equations of the stationary axisymmetric vacuum into a form in which all the

* Dedicated to Prof. L. JÁNOSSY on his 60th birthday.

field quantities are represented by spin coefficients. Research into the puzzling structure of the stationary axisymmetric gravitational equations has come into prominence since it was generally agreed [4] that the external gravitational field of black holes must be restricted by the requirements of time-independence and axial symmetry. We can use here a flat-space spinor calculus because, as is well known, the field equations of the problem can be formulated on a flat "background" three-space. It will be seen, however, that the invariance of the field equations against changing the signature of the metric (thus turning the Euclidean flat space into a Minkowski-type hyperbolic space) must be exploited in our construction. The final topic will be the solution of the static subclass of the fields by the method of SU(1,1) spin coefficients.

2. A simultaneous introduction to the algebras of SU(2) and SU(1,1) spinors

This Section presents a parallel discussion of the elements of both SU(2) and SU(1,1) spinor algebras. The notation adopted here was chosen as being the most convenient for the spin coefficient technique and follows closely the conventions of [3]. Where necessary, the parallel treatment of $SU(^{2}_{1,1})$ spinor algebras is achieved by a double-rowed notation. The upper row always refers to SU(2), the lower one to SU(1,1).

A one-index covariant spinor ξ_A is, by definition, a quantity of two complex components ($A = 0, 1$) which transforms according to the rule [5]

$$\hat{\xi}_A = U_A{}^B \xi_B . \tag{2.1}$$

Here the transformation matrix has the form [6]

$$[U_A{}^B] = \begin{bmatrix} \alpha & \beta \\ \mp\bar{\beta} & \bar{\alpha} \end{bmatrix}, \tag{2.2}$$

where the complex numbers α and β are restricted by the unimodularity condition

$$\alpha\bar{\alpha} \pm \beta\bar{\beta} = 1. \tag{2.3}$$

The 2×2 matrices $[U_A{}^B]$ given by (2.2) and (2.3), with respect to the matrix multiplication as a group operation, constitute the group $SU(^{2}_{1,1})$, with the upper and lower signs in the definition, respectively.

The transformation rule of one-index contravariant spinors is given by

$$\hat{\xi}^A = \xi^B (U^{-1})_B{}^A, \tag{2.4}$$

where U^{-1} is the inverse of U:

$$U_A{}^B(U^{-1})_B{}^C = \delta_A{}^C, \tag{2.5}$$

Thus the contraction $\xi^A\zeta_A$ is an invariant:

$$\hat{\xi}^A\,\hat{\zeta}_A = \xi^R\,(U^{-1})_R{}^A\,U_A{}^S\,\zeta_S = \xi^R\,\zeta_R. \tag{2.6}$$

In accordance with the unimodularity of **U**, the rules for raising and lowering spinor indices are:

$$\xi^A = \epsilon^{AB}\,\xi_B; \qquad \xi_A\,\xi^B = \epsilon_{BA}. \tag{2.7}$$

Here the "metric spinor"

$$[\epsilon_{AB}] = [\epsilon^{AB}] = \begin{bmatrix} 0 & 1 \\ -1 & 0 \end{bmatrix} \tag{2.8}$$

is left invariant by spin transformations. Definition (2.8) implies

$$\epsilon^{AC}\,\epsilon_{BC} = \delta_B^A. \tag{2.9}$$

There exists another invariant spinor. In order to show this, we take the complex conjugate of Eqs. (2.1) and (2.4):

$$\bar{\hat{\xi}}_{A'} = \bar{U}_A{}^{B'}\,\bar{\xi}_{B'}, \qquad \bar{\hat{\xi}}^{A'} = \bar{\xi}^{B'}(\bar{U}^{-1})_{B'}{}^{A'}. \tag{2.10}$$

The priming of spinor indices indicates that complex conjugates of spinors possess a different transformation property. We now introduce the Hermitian two-index spinor $a^{AB'}$, by

$$[a^{AB'}] = \begin{bmatrix} \pm 1 & 0 \\ 0 & 1 \end{bmatrix}. \tag{2.11}$$

Using the transformation rules (2.4) and (2.10) for spinor indices, it is easy to check that $a^{AB'}$ is invariant. By definition (2.11), $a^{AB'}$ has the property

$$a_{AB'}\,a^{CB'} = \pm\,\delta_A^C. \tag{2.12}$$

We define the ***adjoint*** of a spinor ξ_A by

$$\xi^{+A} = a^{AB'}\,\bar{\xi}_{B'}. \tag{2.13}$$

From (2.12) it follows that by adjoining the spinor ζ_A twice, we again get ζ_A, but in SU(2) with opposite sign:

$$\xi_A^{++} = \mp\,\xi_A. \tag{2.14}$$

We also have the relations for the complex conjugates of contracted spinors:

$$\bar{\xi}_{A'}\bar{\eta}^{A'}=\pm\,\xi^{+}_{A}\bar{\eta}^{+A};\qquad \bar{\xi}^{+}_{A'}\bar{\eta}^{A'}=\eta^{+}_{A}\xi^{A}. \tag{2.15}$$

3. The connecting quantities

The parallel discussion of SU(2) and SU(1,1) spinors will extend to this Section also. We now proceed to investigate the connection between SU $\binom{2}{1,1}$ spinors and geometric objects in a three-dimensional space. Throughout this Section we shall be contending with local relations in this space. Thus all the following relations hold in an arbitrary but fixed point P of the space; and so we shall not be concerned with whether or not this space is curved. It will be assumed that, at least locally, an appropriate coordinate system exists in which the metric takes the form

$$[g_{ij}]=\begin{bmatrix}\pm 1 & & \\ & \pm 1 & \\ & & 1\end{bmatrix};\quad \sqrt{g}\equiv(\det[g_{ij}])^{1/2}=1\,, \tag{3.1}$$

SU(1,1) spinors will therefore be related to objects in a Minkowski-type three-space (with indefinite metric).

In close analogy with the SL(2, C) spinor calculus [7], we introduce the connecting quantities σ^{i}_{AB} which are to be used later to relate spinors to tensors. The defining relation for the connecting quantities can be taken as

$$\sigma^{B}_{iA}\,\sigma^{C}_{B}+\sigma^{B}_{jA}\,\sigma^{C}_{iB}=g_{ij}\,\delta^{C}_{A}. \tag{3.2}$$

(Lower case Roman indices $i, j, k, \ldots$ denote tensor components with values 1,2 and 3.) In addition, symmetry of σ^{i}_{AB} in its spinor indices will be required:

$$\sigma^{i}_{AB}=\sigma^{i}_{BA}. \tag{3.3}$$

An appropriate solution of Eqs. (3.2) and (3.3) is

$$\begin{aligned}[\sigma^{1B}_{A}]&=\frac{1}{\sqrt{2}}\begin{bmatrix}0 & \pm 1\\ 1 & 0\end{bmatrix},\\ [\sigma^{2B}_{A}]&=\frac{1}{\sqrt{2}}\begin{bmatrix}0 & \pm i\\ -i & 0\end{bmatrix},\\ [\sigma^{3B}_{A}]&=\frac{1}{\sqrt{2}}\begin{bmatrix}1 & 0\\ 0 & -1\end{bmatrix}.\end{aligned} \tag{3,4}$$

For SU(2) the connecting quantities are simply the Pauli matrices divided by a common $\sqrt{2}$ factor. The explicit forms (3.4) of the SU(1,1) connecting quantities will be used in Section 6.

Using the expressions (3.4), we can easily prove the covariant identity

$$\sigma_{iA}^{B}\,\sigma_{jB}^{C}-\sigma_{jA}^{B}\,\sigma_{iB}^{C}=\mp\sqrt{2}\,i\,\epsilon_{ijk}\,\sigma_{A}^{kC}\,\sqrt{g}\,. \tag{3.5}$$

Another useful relation is obtained from (3.2) if we properly take into account the straightforward identity [8] $\epsilon_{A[B}\epsilon_{CD]}=0$:

$$\sigma_{iAB}\,\sigma_{CD}^{i}=-\frac{1}{2}(\epsilon_{AC}\,\epsilon_{BD}+\epsilon_{AD}\,\epsilon_{BC}). \tag{3.6}$$

There are two different ways of defining the adjoint of σ_{A}^{iB}, because we can take either $-a_{P'}^{B}$, $a_{A}^{Q'}\,\sigma_{ia'}^{P'}$, or $-a_{AP'}\,a^{Ba'}\,\bar{\sigma}_{ia'}^{P'}$ as the definition of the adjoint quantities. In order to retain the customary definition of matrix adjunction in the representation used here, we put

$$\sigma_{iA}^{+B}=-\,a_{AP'}\,a^{BQ'}\,\bar{\sigma}_{iQ'}{}^{P'}. \tag{3.7}$$

Thus, by (3.4), we are led to the adjunction properties of the connecting quantities:

$$\sigma_{iA}^{+B}=\mp\,\sigma_{iA}^{B}. \tag{3.8}$$

4. Spinor basis and spin coefficients

A normalized spinor basis and spin coefficients for SL(2, C) spinor fields were first introduced by NEWMAN and PENROSE [1]. The method was later on adjusted to SU(2) spinor fields by PERJÉS [3]. Since spin coefficients refer to differential (nonlocal) properties of the fields, it is relevant to ask whether or not we are considering spinors in a curved space. Although in the following we shall confine ourselves to flat space, it is not hard to prove that all the relations obtained remain valid in curved spaces, provided partial derivatives are properly replaced by covariant derivates. This assumes the introduction of covariant spinor derivatives, but this can be done along the lines of [7] and [3] without much difficulty [9]. As the comparative (double-rowed) treatment of SU(2) and SU(1,1) spinor calculi is of special use in this respect, it will be maintained throughout the present Section.

Let η_{A} be an arbitrary one-index spinor which is normalized by

$$\eta_{A}\,\eta^{+A}=1. \tag{4.1}$$

We choose a basic spinor dyad such that

$$\eta_{0A} \equiv \eta_A\,, \quad \eta_{1A} \equiv \eta_A^+\,, \tag{4.2}$$

where $\eta_{aA}(a = 0,1)$ are elements of the dyad. This basis in the spin space defines a complex vector basis in the three-space according to the relations

$$\begin{aligned} l^i &= \sqrt{2}\,\eta^A\,\eta_B^+\,\sigma_A^{iB}, \\ m^i &= -\,\eta^A\,\eta_B\,\sigma_A^{iB}, \\ \overline{m}^i &= \pm\,\eta^{+A}\,\eta_B^+\,\sigma_A^{iB}. \end{aligned} \tag{4.3}$$

An equivalent, but more compact, notation for the basic vector "triad" will also be used in the following;

$$z_{\mathrm{m}}^i = (l^i, m^i, \overline{m}^i)\,, \tag{4.4}$$

where m is a triad index ranging over the values 0, + and —. From the adjunction properties (3.8) of the connecting quantities, it can be ascertained that l^i is a real vector and that $\overline{m}^i$ is indeed the complex conjugate of m^i. The orthogonality properties of the basis follow from (3.6) and can be summarized as

$$z_{\mathrm{m}}^i\, z_{\mathrm{ni}} \equiv g_{\mathrm{mn}} = \begin{bmatrix} 1 & 0 & 0 \\ 0 & 0 & \pm 1 \\ 0 & \pm 1 & 0 \end{bmatrix}. \tag{4.5}$$

The physical components of an arbitrary tensor [10], say T_{ijk}, are given by $T_{\mathrm{mnp}} = T_{ijk}\, z_{\mathrm{m}}^i\, z_{\mathrm{n}}^j\, z_{\mathrm{p}}^k$; conversely, as is easily proven, the relations $T_{ijk} = T_{\mathrm{mnp}} z_i^{\mathrm{m}} z_j^{\mathrm{n}} z_k^{\mathrm{p}}$ also hold. Here we remark that triad indices are raised and lowered by means of the triad metric g^{mn} and its inverse g_{mn} (as given by (4.5)), respectively. In a similar fashion, spinors can be given in terms of their dyad components. For example,

$$\begin{aligned} \Phi_{ABC'} &= \Phi_{abc'}\,\eta_A^a\,\eta_B^b\,\overline{\eta}_{C'}^{c'}\,, \\ \Phi_{abc'} &= \Phi_{BCD'}\,\eta_a^A\,\eta_b^B\,\overline{\eta}_{c'}^{C'}, \end{aligned} \tag{4.6}$$

(dyad indices are chosen from the lower case Roman letters a, b, c, ... and take the values 0 and 1). The dyad components of a spinor, just like the physical components of tensors, are invariant scalar quantities. The algebraic properties of both spinors and tensors remain unaltered when transvecting with the basis. Care should be taken, however, over the order of dummy spinor indices (both ordinary and dyad), since converting the position of a dummy index pair results in a change of sign, due to the skew symmetry of the spinor "metric" (cf. Eq. (2.8)).

We now define the $SU(^2_{1,1})$ spin coefficients by the relations

$$\Gamma_{abcd} = (\partial_i \eta_{aA}) \eta_b^A \sigma^i_{CD} \eta_c^C \eta_d^D . \tag{4.7}$$

Here

$$\partial_i = \partial/\partial x^i . \tag{4.8}$$

As is easily inferred from the orthogonality (4.1) of the spinor base, the spin coefficients exhibit symmetry both in their first and the second pair of indexes:

$$\Gamma_{abcd} = \Gamma_{bacd} = \Gamma_{ab\dot{d}\dot{c}} . \tag{4.9}$$

Further relations among the spin coefficients can be deduced by considering their properties under adjunction. The rules for adjoining dyad components are needed at this point. Consider, for example, the dyad components of a one-index spinor, $\zeta_a = \zeta_A \eta_a^A$. From (2.15) we obtain

$$\begin{aligned} (\bar{\xi}_0) &= \pm \xi_A^+ \eta^{+A} = \pm \xi_1^+ , \\ (\bar{\xi}_1) &= - \xi_0^+ . \end{aligned} \tag{4.10}$$

The generalization of this rule for spinors with more than one index is a straightforward matter.

Taking into account all their symmetries, there are altogether five independent $SU(^2_{1,1})$ spin coefficients. We introduce an individual notation for these, according to the following Table.

$\Gamma_{abcd} =$

cd \ *ab*	00	0 1 / 1 0	11
00	$\frac{1}{\sqrt{2}} \sigma$	$\mp \frac{1}{2} \bar{\tau}$	$\pm \frac{1}{\sqrt{2}} \bar{\varrho}$
0 1 / 1 0	$-\frac{1}{2} \varkappa$	$\mp \frac{\epsilon}{2\sqrt{2}}$	$\mp \frac{1}{2} \bar{\varkappa}$
11	$\mp \frac{1}{\sqrt{2}} \varrho$	$-\frac{1}{2} \tau$	$-\frac{1}{\sqrt{2}} \bar{\sigma}$

(4.11)

The $2^{-1/2}$ factors are introduced here for practical reasons; the simplicity thus attained in the expressions containing spin coefficients will become clear shortly.

There exists a close relationship between spin coefficients and the well-known Ricci rotation coefficients given by

$$\gamma_{\mathbf{mnp}} = (\partial_j z^i_{\mathbf{m}})\, z^j_{\mathbf{p}} z_{\mathbf{n}i} \,. \tag{4.12}$$

This is most easily seen by using the equivalent form of (4.7),

$$\Gamma_{abcd} = \frac{1}{2}\, \epsilon^{pq}\, \sigma^i_{aq}\, \sigma^j_{cd}\, \partial_j \sigma_{ibp} \,. \tag{4.13}$$

We have

$\gamma_{\mathbf{mnp}} =$

p \ mn	-0	$+0$	$+-$
0	$\bar{\varkappa}$	$\varkappa$	ϵ
$+$	$\bar{\varrho}$	σ	$-\bar{\tau}$
$-$	$\bar{\sigma}$	ϱ	τ

(4.14)

Eq. (4.14) reveals the antisymmetry of the rotation coefficients in their first and second indices:

$$\gamma_{\mathbf{mnp}} = -\gamma_{\mathbf{nmp}} \,. \tag{4.15}$$

Hence we see that the quantity $\epsilon = \gamma_{+-0}$ is purely imaginary, $\epsilon = -\bar{\epsilon}$.

Like any tensor-type quantity, the vector operator of derivation can be transvected with the basis to yield the scalar operators

$$\partial_{\mathbf{m}} \equiv z^i_{\mathbf{m}}\, \partial_i \,, \tag{4.16}$$

An alternative individual notation for the scalar derivative operators will prove useful in the following; namely,

$$\begin{aligned} D &= z^i_0\, \partial_i = l^i\, \partial_i \,, \\ \delta &= z^i_+\, \partial_i = m^i\, \partial_i \,, \\ \bar{\delta} &= z^i_-\, \partial_i = \bar{m}^i\, \partial_i \,. \end{aligned} \tag{4.17}$$

Using the expressions (4.3) for the vector basis we have

$$\begin{aligned} D &= -\sqrt{2}\, \sigma^i_{01}\, \partial_i \,, \\ \delta &= \sigma^i_{00}\, \partial_i \,, \\ \bar{\delta} &= \mp \sigma^i_{11}\, \partial_i \,. \end{aligned} \tag{4.18}$$

5. The field identities

Though this paper is devoted to the flat-space spinor calculus, completeness requires that we formulate the field identities for the more general, curved-space case. In the present Section the three-space will therefore be considered to be a Riemannian space, with the metric signature $(\pm, \pm, +)$ as the geometric arena of the $SU(_1{}^2{}_1)$ spinor fields, respectively. The definition of the curvature tensor R_{ijkl} is given by the Ricci identities

$$v_{i\ [;j;k]} = \frac{1}{2} R^r_{ijk} v_r , \tag{5.1}$$

where v_i is an arbitrary vector field, and semicolon stands for the covariant derivation operation.

The equivalence of dyad and triad formalisms allows us to put down the field identities in the more simple triad notation. Applying the Ricci identities (5.1) to the basic vectors z^i_m and taking the triad projections [3], we get

$$\gamma_{mnp;q} - \gamma_{mnq;p} - \gamma^l{}_{mp}\gamma_{lnq} + \gamma_{mnl}(\gamma^l{}_{pq} - \gamma^l{}_{qp}) + \gamma^l{}_{mq}\gamma_{lnp} = R_{mnpq}. \tag{5.2}$$

The curvature tensor of a three-space can be decomposed into the Ricci tensor $R_{ik} = R^{\cdot j}_{ij\cdot k}$ and the curvature scalar $R = R^l_l$, since the conform tensor identically vanishes in this case [11]. In terms of triad components we have

$$R_{mnpq} = -g_{mp}R_{nq} + g_{mq}R_{np} - g_{nq}R_{mp} + g_{np}R_{mq} - \frac{1}{2}R(g_{mq}g_{np} - g_{mp}g_{nq}). \tag{5.3}$$

Another important relation is the commutation rule of the scalar derivatives given by [1.3]

$$\varphi_{;m;n} - \varphi_{;n;m} = (\gamma^{\cdot l}_{m\cdot n} - \gamma^{\cdot l}_{n\cdot m})\varphi_{;l}. \tag{5.4}$$

As a simple example of manipulating with triad labels in the above identities, we put down here the detailed form of the curvature scalar:

$$R = g^{mn}R_{mn} = R_{00} \pm 2R_{+-}. \tag{5.5}$$

Combining (5.2), (5.3) and (5.5) and using the detailed notation for rotation coefficients and scalar derivatives (Eqs. (4.14) and (4.17)), we obtain*

$$D\sigma - \delta\varkappa \mp \epsilon\sigma \mp \bar{\tau}\varkappa - \varkappa^2 \mp \sigma(\epsilon + \bar{\varrho}) \mp \varrho\sigma = -R_{++} \tag{5.6a}$$

$$D\varrho - \bar{\delta}\varkappa - \tau\varkappa - \varkappa\bar{\varkappa} \mp \sigma\bar{\sigma} \mp \varrho^2 = \mp 1/2\, R_{00} \tag{5.6b}$$

$$D\tau - \bar{\delta}\epsilon + \varkappa\bar{\sigma} - \varrho\bar{\varkappa} - \tau\epsilon - \epsilon\bar{\varkappa} \pm \bar{\tau}\bar{\sigma} \mp \tau\varrho = \mp R_{0-} \tag{5.6c}$$

$$\delta\tau + \bar{\delta}\bar{\tau} + \sigma\bar{\sigma} - \varrho\bar{\varrho} \mp 2\tau\bar{\tau} + \epsilon(-\bar{\varrho} + \varrho) = 1/2\, R_{00} \mp R_{+-} \tag{5.6d}$$

$$\bar{\delta}\sigma - \delta\varrho \mp \tau\sigma - \varkappa(\varrho - \bar{\varrho}) \mp \sigma\tau = \pm R_{0+}. \tag{5.6e}$$

* Am indebted to B. LUKÁCS for correcting these relations.

Similarly, the relations (5.5) can be written as

$$(D\delta - \delta D)\varphi = \pm \sigma\bar{\delta}\varphi \pm (\bar{\varrho} \pm \epsilon)\delta\varphi + \varkappa D\varphi, \tag{5.7a}$$

$$(\delta\bar{\delta} - \bar{\delta}\delta)\varphi = \pm \bar{\tau}\bar{\delta}\varphi \mp \tau\delta\varphi + (\bar{\varrho} - \varrho) D\varphi. \tag{5.7b}$$

An application of the SU(2) spin coefficient technique relying mainly on identities (5.6) and (5.7) has been discussed at length in [3]. Another example demonstrating the use of SU(1,1) spin coefficients will be given in the following Section. From here onwards we shall dispense with the double-rowed notation and confine our attention to the SU(1,1) spinor calculus in a flat hyperbolic space.

6. Application of SU(1,1) spin coefficients: The stationary axisymmetric vacuum

We consider here the vacuum as it is described in the framework of the general relativity theory. Under the assumption of stationarity and axial symmetry, the vacuum field equations of Einstein considerably simplify. As KRAMER and NEUGEBAUER [12] have pointed out, the corresponding Lagrangian can be written in the form

$$L = \nabla A \nabla A + \nabla B \nabla B - \nabla C \nabla C, \tag{6.1}$$

where the field quantitites A, B and C are invariant scalars in a fictitious Euclidean three-space, each of them being independent of the azimuthal angle. The usual notation for gradient and Laplacian operators (∇ and Δ, correspondingly) will be adopted.

By taking account of the constraint equation

$$A^2 + B^2 - C^2 = -1, \tag{6.2}$$

the field equations can be derived from the Lagrangian (6.1) and are of the form

$$\begin{aligned} \Delta A &= \lambda A, \\ \Delta B &= \lambda B, \\ \Delta C &= \lambda C, \end{aligned} \tag{6.3}$$

where $\lambda = L$ is the Lagrange multiplier.

From our point of view, it is essential to remark that the field equations (6.3) are unaffected if the signature of the metric is changed from $(+, +, +)$ to $(-, -, +)$. This can easily be seen if we introduce, for example, cylindrical coordinates ϱ, z, Φ, with

$$\begin{aligned} X &= \varrho \sin \Phi, \\ \mathrm{X} &= \varrho \cos \Phi, \\ Z &= z, \end{aligned} \tag{6.4}$$

X, Y and Z being the usual Cartesian coordinates. Due to the axial symmetry of the field variables, the g_{33} component of the metric

$$[g_{ij}] = \begin{bmatrix} 1 & & \\ & 1 & \\ & & \varrho^2 \end{bmatrix} \tag{6.5}$$

does not enter the field equations (6.3). Thus in place of (6.5) it is permissible to take the metric

$$[\hat{g}_{ij}] = \begin{bmatrix} -1 & & \\ & -1 & \\ & & \varrho^2 \end{bmatrix}. \tag{6.6}$$

Next, the coordinate transformation

$$\begin{aligned} x &= \varrho \, sh \, \Phi, \\ y &= \varrho \, ch \, \Phi, \\ z &= z \end{aligned} \tag{6.7}$$

leads to the metric form

$$[g_{ij}] = \begin{bmatrix} -1 & & \\ & -1 & \\ & & 1 \end{bmatrix}, \tag{6.8}$$

which was used in previous sections when developing the flat-space version of SU(1,1) spin coefficient technique.

In the coordinate system (6.7) we define a basic spinor η_A with the components

$$\eta_A = \begin{pmatrix} A+iB \\ C \end{pmatrix}. \tag{6.9}$$

The adjoint spinor η^{+A} is given by

$$\eta^{+A} = \bar{\eta}_{B'} a^{AB'} = (A - iB, C) \begin{pmatrix} -1 & 0 \\ 0 & 1 \end{pmatrix} = (-A + iB, C). \tag{6.10}$$

So $\eta_{0A} = (\eta_A, \eta_A^+)$ is a properly normalized SU(1,1) spinor base, with

$$\eta_A \eta^{+A} \equiv \eta_0 \eta^{+0} + \eta_1, \eta^{+1} = C^2 - A^2 - B^2 = 1. \tag{6.11}$$

In terms of the basic spinor η_A, the field equations take the spinor form

$$\Delta\eta_A = \lambda\eta_A \tag{6.12}$$

with

$$\lambda = -\nabla\eta_A \nabla\eta^{+A} = \partial_{BC}\eta_A \partial^{BC}\eta^{+A};\ \partial_{BC} \equiv \sigma^i_{BC}\partial_i . \tag{6.13}$$

A more convenient form of the field equations is acquired if we observe that

$$\begin{aligned}\epsilon_{BC}\epsilon_{DE}\Delta\eta_A &= (-\partial_{BD}\partial_{CE}+\partial_{CD}\partial_{BE}-\partial_{CE}\partial_{BD}+\partial_{BE}\partial_{CD})\eta_A = \\ &= 2(\partial_{CD}\partial_{BE}-\partial_{BD}\partial_{CE})\eta_A .\end{aligned} \tag{6.14}$$

Multiplying both sides of Eq. (6.12) by $\epsilon_{BC}\epsilon_{DE}$, we get

$$(\partial_{CD}\partial_{BE}-\partial_{BD}\partial_{CE})\eta_A = \frac{1}{2}\lambda\eta_A\epsilon_{BC}\epsilon_{DE} . \tag{6.15}$$

We now proceed to obtain the spin coefficient version of the field equations. Inserting Kronecker symbols

$$\delta^B_A = \eta_{rA}\eta^{rB} \tag{6.16}$$

into the expression (6.13) for λ gives

$$\lambda = \Gamma_{0abc}\Gamma^{abc}_1 . \tag{6.17}$$

Next, we contract the field equations (6.15) with $\eta^A_a\eta^B_b\eta^C_c\eta^D_d\eta^E_e$. After rearranging properly the derivative operators and making use of (6.17), we arrive at the set of spin coefficient equations

$$\begin{aligned}\partial_{cd}\Gamma_{0abe}-\partial_{bd}\Gamma_{0ace} &= \Gamma_{0abr}\Gamma^r_{e\cdot cd}-\Gamma_{0acr}\Gamma^r_{e\cdot bd}+\Gamma_{0aer}(\Gamma^r_{b\cdot cd}-\Gamma^r_{c\cdot bd})+ \\ &+\Gamma_{0rbe}\Gamma^r_{a\cdot cd}-\Gamma_{0rce}\Gamma^r_{a\cdot cd}+1/2\,\epsilon_{0a}\epsilon_{bc}\epsilon_{de}\Gamma_{0pqr}\Gamma_1^{pqr} .\end{aligned} \tag{6.18}$$

In the detailed notation we can write the above form of the field equations as

$$D\varkappa-2\delta\varrho = \sigma(\bar{\varkappa}-\tau)+\varrho(\varkappa+\bar{\tau})-2\varkappa\bar{\varrho} , \tag{6.19a}$$

$$D\varepsilon-2\delta\tau = -\varrho\bar{\varrho}+\sigma\bar{\sigma}+2\tau\bar{\tau}-\bar{\tau}\bar{\varkappa}+\tau\varkappa-2\varepsilon\bar{\varrho} . \tag{6.19b}$$

In addition, the spin coefficient equations which arise from the field identities (5.6) with the lower signs (corresponding to SU(1,1)) on imposing the flat-space condition $R_{mn} = 0$ are:

$$D\sigma-\delta\varkappa = -(\varrho+\bar{\varrho})\sigma-2\varepsilon\sigma-\varkappa\bar{\tau}+\varkappa^2 , \tag{6.20a}$$

$$D\varrho-\bar{\delta}\varkappa = -\varrho^2-\sigma\bar{\sigma}+\varkappa\tau+\varkappa\bar{\varkappa} , \tag{6.20b}$$

$$D\tau-\bar{\delta}\varepsilon = -\varrho\tau+\bar{\sigma}\bar{\tau}-\varkappa\bar{\sigma}+\varrho\bar{\varkappa}+(\bar{\varkappa}+\tau)\varepsilon , \tag{6.20c}$$

$$\delta\tau+\bar{\delta}\bar{\tau} = \varrho\bar{\varrho}-\sigma\bar{\sigma}-2\tau\bar{\tau}+\varepsilon(\bar{\varrho}-\varrho) , \tag{6.20d}$$

$$\delta\varrho-\bar{\delta}\sigma = 2\sigma\tau-\varkappa(\varrho-\bar{\varrho}) . \tag{6.20e}$$

The set consisting of Eqs. (6.19) and (6.20) is completely equivalent to the stationary axisymmetrie vacuum equations (6.3). The most interesting feature of the present formulation of the problem is that *the gravitational field quantities are represented here merely by spin coefficients* without any additional terms appearing in the field equations. This situation is to be compared with the SU(2) spinor form of the *stationary* gravitational equations [3], in which the excess of a complex vector field appears in the spin coefficient version of the field equations.

Although a more detailed study of the structure of field equations (6.19) and (6.20) lies beyond the scope of the present paper, it is perhaps useful to illustrate here with a very simple example the way of manipulating with SU(1,1) spin coefficient equations. Let us take the class of solutions for which

$$\varepsilon = \tau = 0, \ \varkappa = \bar{\varkappa}, \ \varrho = \bar{\sigma} \tag{6.21}$$

hold. Using the representation (3.4) for the connecting quantities and taking the spinor basis as in (6.9), we can prove that conditions (6.21) are characteristic of the static axisymmetric fields with [12] $B = 0$. Without relying on the detailed structure of the spin coefficients, however, we can find the solution of the field equations (6.19) and (6.20) by imposition of (6.21). We find that Eqs. (6.19b), 6.20c) and (6.20d) are identically satisfied. The remaining field equations are

$$D\varkappa - 2\delta\bar{\sigma} = -\sigma\varkappa + \bar{\sigma}\varkappa, \tag{6.22a}$$

$$D\sigma - \delta\varkappa = -(\sigma+\bar{\sigma})\sigma + \varkappa^2, \tag{6.22b}$$

$$\delta\bar{\sigma} - \bar{\delta}\sigma = \varkappa(\sigma - \bar{\sigma}). \tag{6.22c}$$

Comparison of Eqs. (6.22b) and (6.22c) with commutators (5.7) shows that the former are just the integrability conditions for a real scalar field Φ such that

$$\varkappa = D\Phi, \quad \sigma = \delta\Phi. \tag{6.23}$$

Further, taking the sum of Eqs. (6.22a) and (6.22c) and inserting (6.23), we obtain

$$(DD - \delta\bar{\delta} - \bar{\delta}\delta)\Phi = 0, \tag{6.24}$$

which is the Laplace equation written down in spin coefficient notation [13]. The solution of our problem is thus reduced to finding the solutions of the equation

$$\Delta\Phi = 0, \tag{6.25}$$

where, owing to the axial symmetry required for any solution Φ, no matter what signature is chosen for the metric.

In our representation, as is easily seen, the scalar Φ should be identified with $-2\ln(A+C)$, so it is not hard to prove that the procedure given in the above example is the spin coefficient version of obtaining Weyl's static axisymmetric solutions [14].

REFERENCES

1. E. T. NEWMAN and R. PENROSE, Journal of Math. Phys., **3,** 566, 1962.
2. Some important papers containing fundamental developments in the SL(2, C) formalism are listed here:
   E. T. NEWMAN and T. W. UNTI, Journal of Math. Phys., **3,** 891, 1962 (on the properties of asymptotically flat gravitational fields); E. T. NEWMAN and L. A. TAMBURINO, Journal of Math. Phys., **3,** 902, 1962 (exact solutions); A. JANIS and E. T. NEWMAN, Journal of Math. Phys., **6,** 902, 1965 (multipole moments in general relativity); E. T. NEWMAN and R. PENROSE, Journal of Math. Phys., **7,** 863, 1966 (Bondi-Metzner-Sachs group); E. T. NEWMAN and R. PENROSE, Proc. Roy. Soc. (London), **305A,** 175, 1968 (conserved quantities); E. T. NEWMAN and R. POSADAS, Phys. Rev., **187,** 1784, 1969 (equations of motion); W. BONNOR, Nature **225,** 932 (1970) (Maxwell equations).
3. Z. PERJÉS, Journal of Math. Phys., **11,** 3383, 1970.
4. W. ISRAEL, Phys. Rev. **164,** 1776 (1967); B. CARTER, Phys. Rev. Letts. **26,** 331, 1971.
5. Spinor indices are denoted by capital Roman letters A, B, C, . . ., to which the values 0 and 1 can be assigned and for which the Einstein summation convention holds.
6. According to the convention of BADE and JEHLE [7] whenever a matrix notation is used for a two-component quantity the first (second) index refers to the row (column), independently of the position of the indices. No confusion of matrix rows with our twofold notation for $SU(^{2}_{1,1})$ can occur, since the former are always enclosed in matrix brackets [ ].
7. W. L. BADE and H. JEHLE, Rev. Mod. Phys., **25,** 714, 1953.
8. F. A. E. PIRANI, Lectures on General Relativity, Brandeis Summer Institute in Theoretical Physics I. (Prentice-Hall, 1964).
9. Throughout this paper we assume that field quantities are differentiable as many times as we wish.
10. R. GEROCH, Ann. Phys. **48,** 526 (1968).
11. L. P. EISENHART, Riemannian Geometry (Princeton Univ. Press, 1950).
12. D. KRAMER and G. NEUGEBAUER, Commun. Math. Phys., **10,** 132, 1968, in German).
13. The complete spin coefficient form of Laplace's equation is given by
$$[DD-\bar{\delta}\bar{\delta}-\bar{\varepsilon}\delta+(\varrho+\bar{\varrho})D-(\varkappa+\bar{\tau})\bar{\delta}-(\bar{\varkappa}+\tau)\delta]\Phi=0.$$
   In obtaining (6.24), conditions (6.21) and (6.23) have been used.
14. For the conventional solution procedure, see, for example, J. L. ANDERSON: Principles of Relativity Physics (Academic Press, 1967), p. 393. Note, however, that the two sentences preceding Eq.(11 – 5.8) are erroneous and should be ignored, since this condition, being trivially satisfied by the field equations, yields no additional restriction on the field quantities.

СПИНОВЫЕ КОЭФФИЦИЕНТЫ SU (1,1)

З. ПЕРЬЕШ

Резюме

В статье излагается сравнительный анализ спинорной алгебры. Спиновые коэффициенты вводятся в формализм SU(2) и, соответственно, SU(1,1). Поскольку в настоящей статье используются спины в плоскости и координатная система, основные отношения ковариантной записи заданы таким образом, чтобы метод можно было легко применить также и относительно спинорных полей в кривом трехразмерном пространстве. Спиновые коэффициенты SU(1,1) используются для получения стационарных асимметричных уравнений притяжения в форме, где все количества полей принимают вид спиновых коэффициентов в плоском гиперболическом трехразмерном пространстве.

Acta Physica Academiae Scientiarum Hungaricae, Tomus 32 (1—4), pp. 221—239 (1972)

THE PHYSICS OF THE CORE OF THE POLYTECHNICAL UNIVERSITY'S TRAINING REACTOR*

By

F. SZABÓ, L. FRANKL, J. VALKÓ and L. TURI

CENTRAL RESEARCH INSTITUTE FOR PHYSICS, BUDAPEST

(Received 19. X. 1971)

A brief description is given of the measurements and calculations of the ZR-5 project which worked out the nuclear design of the Polytechnical University's Training Reactor. The system of programs — the reactor physical model — used in the calculations is described together with some of the experimental techniques, that have confirmed high precision and great potential value. It is emphasized that most nuclear aspects of reactor design and operation can be effectively studied with such a calculation model.

Introduction

Reactor physics studies in Hungary began with the installation of the WWRS reactor at the Central Research Institute for Physics, Budapest. The first problems were connected with approach to critical, reactor start-up, and reactor operation. Zero-power research — the basic tool for the investigation of fundamental reactor problems — separated quite soon, however. A large amount of experimental data accumulated from various clean, well-defined and precise measurements on a series of critical assemblies. Some theoretical investigations found their direct comparison with experiments during this time, but on the whole the study of reactor physics calculations had to be developed separately from contemporary experiments, because of the simple models used and the small computers available at that time. A new, theoretically sound and technically sophisticated calculational model was developed over the years 1966—69, the beginning of this period having been marked by the installation of a large computer in the Institute. This model was thoroughly checked with our previous experimental results and other experiments, and it proved satisfactory in a wide range of applications. As a result, when we undertook the investigation to be described below it became possible, for the first time, to perform measurements and theoretical calculations simultaneously on a given, real system. Comparison of the results has shown good agreement between measurements and calculations in all but a few explainable cases.

In the course of design, construction and putting into operation of the training reactor of the Polytechnical University in Budapest, the Central Research Institute for Physics completed the following tasks:

* Dedicated to Prof. L. JÁNOSSY on his 60th birthday.

1. Design of the reactor core; execution of critical experiments to determine the safe and optimal arrangement of the active zone; the necessary reactor physical measurements and calculation work.

2. Construction, production and installation of the active zone and its associated equipment.

3. Working out, design and building of the control, safety and measuring system.

4. Design, production and assembly of the rabbit system for activation analytical purposes.

5. Initial start-up and on-site adjustment of the reactor.

This paper deals only with the reactor physical measurements carried out on the ZR-5 critical assembly of the reactor and the accompanying calculations. A selection from the whole material [1], illustrating primarily the performance of the calculation methods, is presented.

Description of the active zone

The requirements and limitations laid down in preliminary studies were the following.:

1. Operational power of the reactor: max. 10 kW.

2. Fuel: bundles of type EK-10 rods [7]; max. number of bundles: 24.

3. Vertical irradiation channels to provide for simultaneous accommodation of 65 irradiation capsules of standard dimensions ($\varnothing 28 \times 100$ mm).

4. The reactor to be equipped with five horizontal irradiation channels, one of these tangential, the other four radial.

5. Three irradiation channels to be serviceable by the pneumatic rabbit system; of these one for irradiation with thermal neutrons.

6. The upper limit of excess reactivity: 0.7 $.

The final core of the ZR-5 critical assembly, selected after studies on three complete and some partial configurations, is presented in Fig. 1. The core consists of 22.75 fuel bundles. A sseen in the Figure, the reflector is partly graphite, partly water. Control of the system in ensured by two safety rods, one manual and one automatic control rod. The irradiation channels are situated in columns G and H and in the 8th and 9th rows. The thermal rabbits are in position G5, while the fast rabbit is in position D5.

The reactor physical model and the calculation methods

In the past 11 years a considerable amount of experimental results has accumulated from measurements on the ZR-1, ZR-2, ZR-3 and ZR-4 critical assemblies. This material provided an excellent basis for checking and improve-

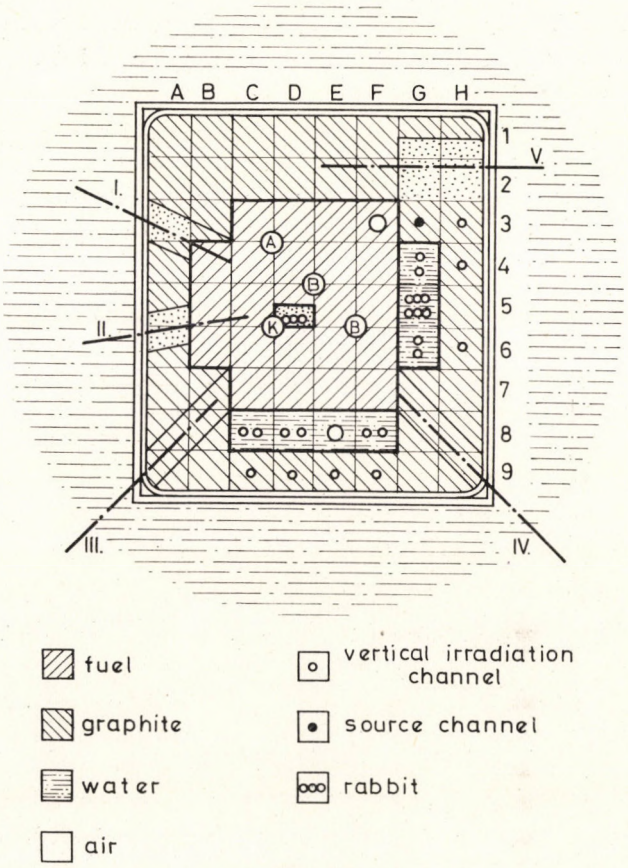

Fig. 1

ment of the reactor physical model program package used in the reactor physical calculations for the ZR-5 assembly. The general organization of the model is illustrated by Fig. 2; as detailed descriptions are presented elsewhere [3], [4], [5], [6], [7], only a short review is given here.

Cell calculations in the thermal region are made by the code THERMOS, those in the resonance region by RIFFRAFF, the two codes together providing group constants for the slowing-down calculation code GRACE. Group constants for homogeneous systems are calculated by code RAO4 in the resonance region. Few-group diffusion parameters for the criticality code SISYPHUS are given by GRACE. The logarithmic derivative of the thermal flux distribution on the surface of control rods is worked out by RAM. The first systematic testing of the THERMOS, RAO4, GRACE and SISYPHUS codes was carried out on the light-water-moderated ZR-2 system, which is constructed of EK-10 fuel elements, and on the beryllium-moderated homogeneous PF-4 intermediate system [8].

THERMOS. In the thermal range the integral transport code THERMOS can deal with a cylindrical elementary cell (21 mesh points, 15 energy groups in the region 0—1 eV). Besides being tested on the ZR-2 assembly, its results were checked with spectral index measurements on the 36% enriched, water-moderated and beryllium-reflected ZR-3 assembly and on the Argonaut reactor at Rossendorf. The comparisons showed a good agreement, so that group constants produced by THERMOS can be considered reliable.

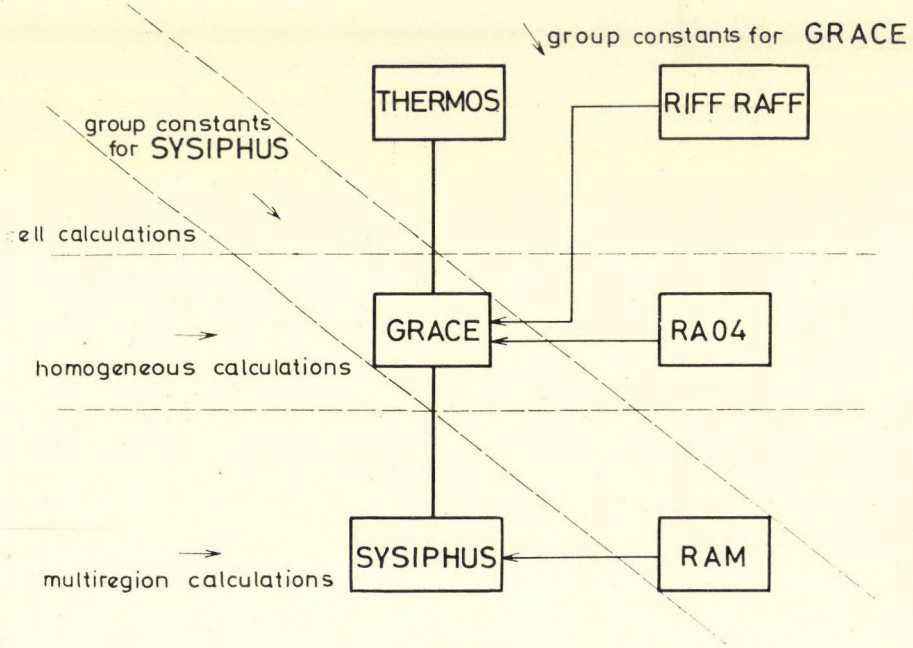

Fig. 2

RA04. This code is based on the integral formula of the homogeneous resonance; interactions between resonances are neglected. Inaccuracy of the resonance parameters influences the results in greater measure than the simplifications of the physical model. This code was applied with satisfactory results to the PF-4 and the 20% enriched, thermal, solid-homogeneous ZR-4 systems.

SISYPHUS. SISYPHUS solves the few-group diffusion equation in two dimensions (in XY or RZ coordinates). In two-group calculations it covers the system with a maximum of 3000 mesh points and, starting from geometrical data and group constants, determines the neutron fluxes in these mesh points and gives the k_{eff} of the system. With group constants given this is a purely mathematical problem, so verification was carried out on different published geometries. The main problems with this code are its convergence rate and running time.

GRACE. This code, which contains most of the difficult physics of the problem, is a 0-dimensional (asymptotic) 40-group program that provides the constants for the fast group. The use of the asymptotic approximation in the core region is justified, as a cosine spatial distribution is always formed there. The case is different in the reflector because here the spectrum is space-dependent; satisfactory results were achieved, however, by the introduction of a virtual, energy-dependent buckling.

The THERMOS and GRACE LIBRARY are organic parts of the model; they contain cross-sections and derived quantities for the elements used in practice.

Preparatory calculations (group constants)

For the calculation of thermal group constants a 17 mm square lattice was first considered. In the THERMOS calculations the cylindrical cell of equivalent area was described by 12 mesh points, and 10 energy groups were used in the 0—0.625eV range. Hydrogen scattering in the water was described by the Koppel—Young model. The program supplies the function $\Phi(r, E)$ for the cell (Fig. 3). Thermal group constants were produced from cross-sections by averaging with this $\Phi(r, E)$. As by-products the thermal utilization factor, f, and the average number of neutrons resulting from thermal absorption η, were obtained.

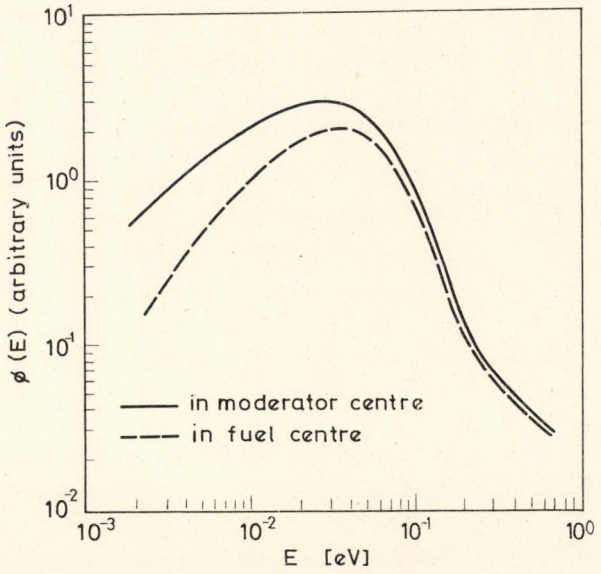

Fig. 3

Constants of the fast group were given by the code GRACE for several material compositions (core, reflector, etc.). By iteration to critical material buckling in the core material GRACE determined the spectrum that was to be used in the averaging of group constants. The resonance region was

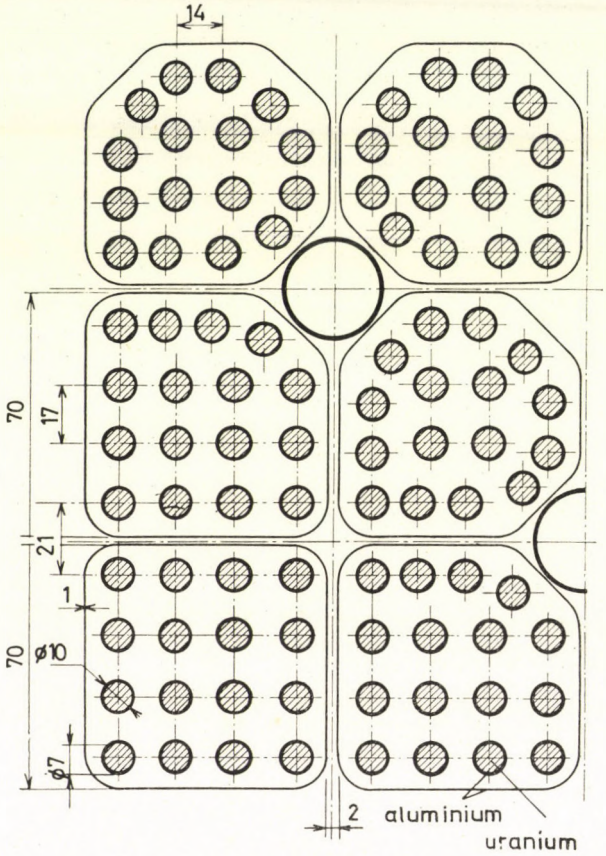

Fig. 4

taken into account by applying the so-called BIGG-type treatment. The energy-dependent buckling in the reflector was applied in the way already mentioned.

Group constants for the distorted lattice around the control and safety rods were determined with a THERMOS calculation in an equivalent cell of correspondingly distorted dimensions and with a fresh GRACE calculation.

Calculation of group constants took into account the bundle structure of the core (Fig. 4). As it did not seem satisfactory to mix the Al casettes and the water between the casettes with the material of the cells in a homogeneous

manner, the following procedure was adopted: With the above-mentioned group constants, applying a symmetry boundary condition on every side, a two-group SISYPHUS calculation was carried out for the elementary cell of the bundle lattice, which by definition consists of the 16 fuel rods in the bundle, the Al casette and 1 mm of surrounding water. As a results of the calculation the group constants for the different regions were averaged, weighting with the flux integrals over the material regions, and in this way the constants for the real core material, built up from the casettes, were obtained.

Calculation of flux distribution and k_{eff}

A cylindrical calculation was first executed for a graphite-reflected core with an equivalent — approximately critical — diameter. The axial flux shape obtained from this calculation was accepted in the course of all later computations, so that axial leakage was accounted for with an axial buckling fitted from it.

Correction curves that allowed lattice distortions and the presence of control-rod channels to be taken into account in a core originally treated as regular were likewise obtained from cylindrical calculations.

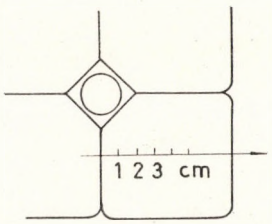

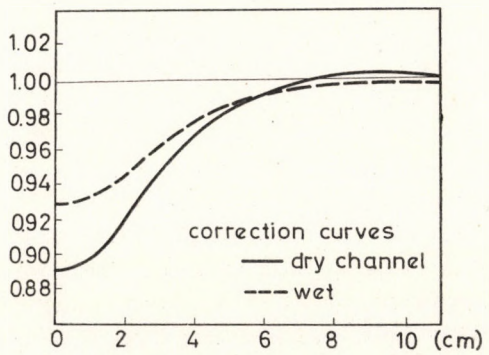

Fig. 5

The cylinder considered in these calculations was such that in its symmetry axis there is a control-rod channel around which the lattice is distorted in a region cylindrical in shape but in other respects approximating the real conditions; outside this region the lattice is regular. The flux distribution obtained was divided by the flux distribution present in an everywhere regular lattice, the quotient being the correction curve (Fig. 5). Calculations were made for the cases when there is water in the channel and when the rod channel is dry.

After the above preliminaries the exact calculation of the actual core in XY coordinates could be carried out. The section of the XY plane of the reactor was covered by a 54×54 mesh, making a total of 2916 points in each group. The mesh points were concentrated or spaced according to the expected curvature of the flux distribution. Allowance for the dry irradiation channel (position D5) was made difficult by the fact that the diffusion approximation is not suitable for dealing with air-filled cavities. It turned out, however, that the behaviour around such cavities could be described satisfactorily with the boundary condition of zero logarithmic derivative.

Calculation of reactivity worth

The criticality code SISYPHUS determines an eigenvalue λ at which the system is critical with a fictitious fuel having a group constant $\lambda \nu\Sigma_f$. If $\lambda = 1$ the system is truly critical; if $\lambda \neq 1$ the reactivity is $\varrho = 1 - \lambda$. Utilizing this, the reactivity worth of any change in the core can be calculated. The effect on reactivity of flooding the dry irradition channel and the safety channels with water was examined in this way. The changes in reactivity resulting from changing the fuel element bundles D4 and D7 for water were also calculated.

Methods of reactivity measurement

Of the methods suitable for measuring reactivity conditions in the reactor, one based on doubling-time measurement and another utilizing pulsed neutron source were adopted. The former is the simplest and quickest method, but its possibilities and accuracy are rather limited. As this measurement is made on a super-critical reactor, the reactivity range which can be directly covered is very narrow, and thus problems with fitting the ranges arise when determining higher values of reactivity in several steps. Several further difficulties are encountered because the doubling-time — reacticvity relation includes delayed neutron parameters for the given reactor core. In the course of our measurements the doubling-time — reactivity relation was calculated with Hughes delayed neutron parameters.

The far more complicated method based on measuring the reactivity by means of a pulsed neutron source can be applied in a broader range, but only in the region of negative reactivities; and it is not free of theoretical problems either [10].

The pulsed neutron reactivity measurements rely on determining the time dependence of the flux $\Phi(t)$ that appears after applying the pulse. A number of slightly different relations can be calculated between the line of the function $\Phi(t)$ and the reactivity, and the reactivity may accordingly be interpreted in a number of ways. For evaluation, determination of the function $\Phi(t)$ is necessary. This can be done from a measurement by fitting with the method of least squares. In the method of SIMMONS and KING [11] used in this work only the prompt fundamental mode decay constant (α) of the system and α_c belonging to the critical state are required, and the negative reactivity is approximately

$$\varrho \approx \left(\frac{\alpha}{\alpha_c} - 1\right)\beta_{\text{eff}}.$$

The approximation is worse at increasing subcritical reactivities.

For the measurements the NIG-200 neutron generator of the Central Research Institute for Physics was used [12]. The width of the neutron pulse is 150—500 μsec, the repetition time 15—75 msec. The signals were detected by BF_3 tubes and processed and directly tape-punched by an NTA-512 type analyser. The required α parameters were determined from the paper tape — completed by some control data — by our (RJO5) exponential function fitting program, utilizing the method of least squares.

Methods of neutron flux measurement

Detailed flux distribution measurements on the ZR-5 assembly served a double purpose: to find the optimal core configuration for the utilizable neutron flux, and to determine the flux values at 10 kW heat output in the irradiation and horizontal channels of this core configuration. Parallel to this — as a very important "by-product" — the detailed thermal neutron flux distributions were obtained in different planes of the active zone; these served at the same time for verification of our computing methods. The relative thermal neutron flux distributions in the active zone and in the vertical channels were measured by the activation method, with 0.8 mm diameter wires containing 10% dysprosium (axial distributions) and with wires cut into 0.8×20 mm pieces (radial distributions). The measurement of the activity distribution in the wires used for the axial measurements was carried out by an automatic device of our own design which made the decay correc-

tion itself. When carrying out measurements on a large scale, Dy is very advantageous as a detecting material, because its high cadmium ratio ($< R_{Cd} > 100$) means that the thermal neutron flux distribution is easily measurable without Cd shielding, which simplifies both the measuring technique and evaluation of the measurement results.

Measurements of the neutron flux and of integral quantities containing information about the neutron spectrum within an elementary cell have been performed for a long time and were used in the verification of cell calculation

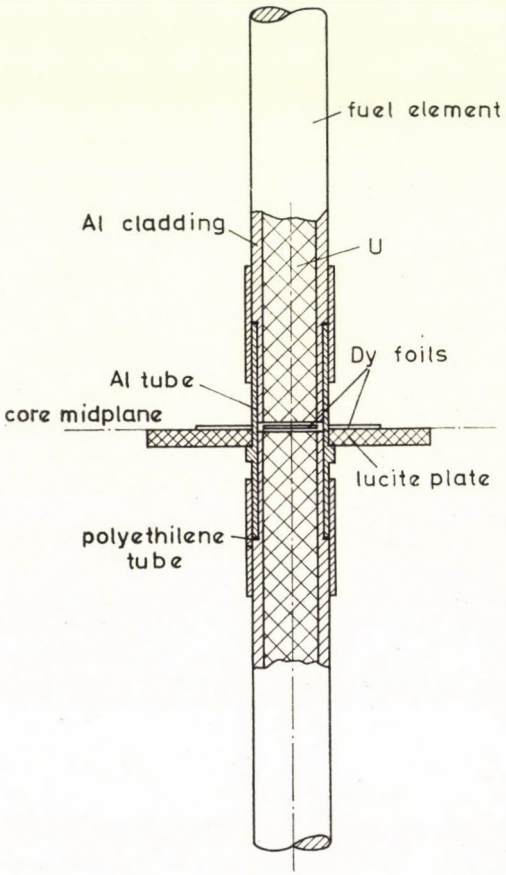

Fig. 6

methods. For this reason there was little emphasis on such measurements in the present experimental program. For the sake of greater completeness of our account, Fig. 6 shows the arrangement of a foil used for activation in the elementary cell. The thermal utilization factor, f, mentioned later was measured in this arrangement. In view of the low power of the ZR-5 assembly (8,5 Watt)

in the active zone and vertical channels, only thermal neutron flux measurements were carried out.

The optimal coupling of the horizontal channels to the active zone through reflector elements was studied with scintillation detectors in the thermal and epithermal energy regions.

Comparison of calculation and measurement results

With the methods discussed above, detailed measurements and calculations were carried out to study the parameteres of the reactor. This parallel use of calculations and measurements is of greatly increased significance compared to earlier practice. Some of the results are discussed below to illustrate how well a calculational model based on purely theoretical considerations can approximate the results of what are now highly accurate measurements. (Indeed, in a number of cases there is good reason to believe that where measurements are difficult to realize the results of calculation are more accurate than those obtained by measurements.)

The calculations directly gave the expected flux values at 10 kW operating power in each point of the core: the value calculated for the maximum flux in the middle of the core and in each irradiation channel was approximately 2.4×10^{11} neutron/cm^2 sec. Direct determination of this value required a very detailed flux measurement, but was nevertheless carried out in this case, with the same result.

In the course of the preliminary calculations a number of quantities were obtained — almost as by-products — which in earlier times were generally employed and which are still useful in cases where simple, quick, approximate results are of interest. These parameters can be measured routinely to a quite considerable accuracy. To illustrate this we mention two such parameters:

(a) The ratio of the average thermal flux in the moderator and in the fuel, Φ_M/Φ_U, had a measured value of 1.3193 ± 0.0079; the THERMOS calculation yielded 1.3355.

(b) One of the parameters of the four-factor formula, the thermal utilization factor, f, had a measured value of $0.8064 \pm 1\%$, while the THERMOS calculation gave 0.8021. In THERMOS this parameter can be calculated from the detailed function $\Phi(r, E)$, also determined by the code, but in real calculations (flux and k_{eff} calculations) only the function $\Phi(r, E)$ itself is used.

Reactivity measurements and calculations

One of the important aims of calculations was to ascertain the k_{eff} of the given assembly in different reactor conditions. The calculation of reactivity changes is always done using the k_{eff} of two conditions. The difference,

or reactivity worth, is:

$$\Delta\varrho = \varrho_1 - \varrho_2 = \lambda_2 - \lambda_1,$$

where λ is the eigenvalue already mentioned and $k_{\text{eff}} = 1/\lambda$. The ratio $\varrho/\beta_{\text{eff}}$ is the reactivity measured in dollars. Since $\beta_{\text{eff}} < 10^{-2}$, it is obvious that a reactivity difference of 1 \$ is smaller than a 1% effect in k_{eff}.

The core configuration shown in Fig. 1 (used as the starting point of measurements) possesses an excess reactivity of 0.91 \$ according to measurements, while the calculation yielded $k_{\text{eff}} = 1.001585$, which means that k_{eff} is accurate to about 0.5%. This accuracy satisfies the requirements expected from such calculations and represents more or less the limit of the possibilities of the model and method applied. Reactivity worths can be calculated more accurately because most of the errors in k_{eff} cancel out when the difference of two k_{eff} values is taken.

From the results of numerous measurements and calculations of reactivity worths we would like to mention the following:

(i) The measured and calculated worth values for a fuel bundle are 4.25 \$ and 4.8 \$ in position D4 and 2.3 \$ and 2.0 \$ in position D7, respectively.

(ii) The change in reactivity due to flooding of the dry channel of the

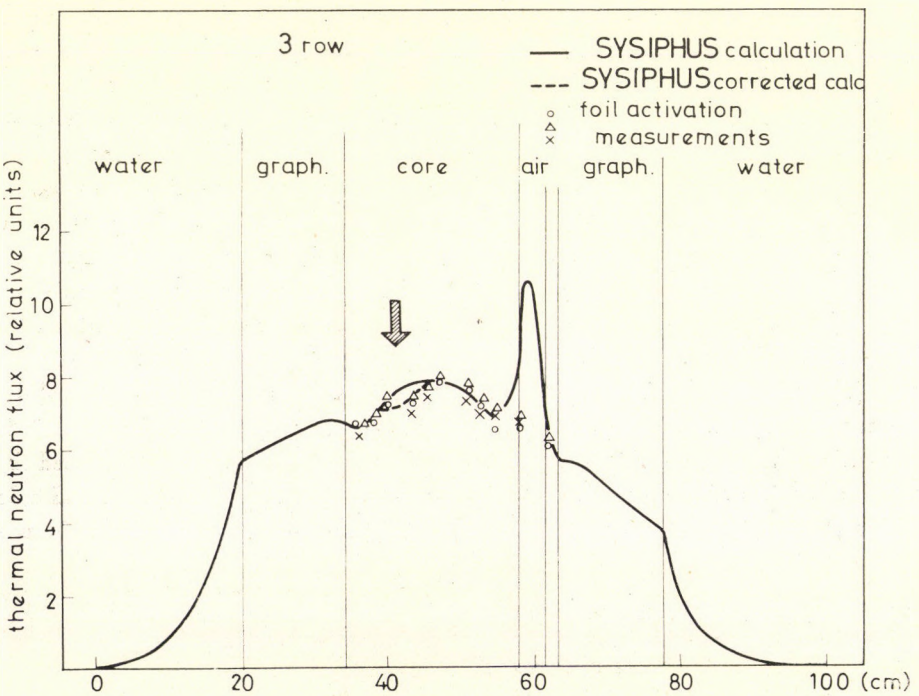

Fig. 7

safety rods — an important figure from the point of view of reactor safety — is 0.21 $ when measured, and 0.18 $ according to calculation.

(iii) The flooding of the large air cavity in the middle of the core was also studied; measurements indicated a reactivity change of —0.20 $, while the result of calculation was —0.71 $. The considerable difference between these results is due to the fact that the majority of errors entering into the calculation originate from the treatment of this cavity and appear here as the error in the k_{eff} difference.

Flux distributions

Figs. 7—16 show flux distributions measured and calculated along the axes passing through the centres of the fuel bundles along the rows and columns. These figures can be interpreted by comparing them with the map of the core (Fig. 1). Lattice distortions along the axes passing beside the wet and dry rod-channels are taken into account by the correction already mentioned: this is marked by a dotted line. The position of the rod channels is also marked in the figures: a blank arrow indicates the dry channel and a hatched one the

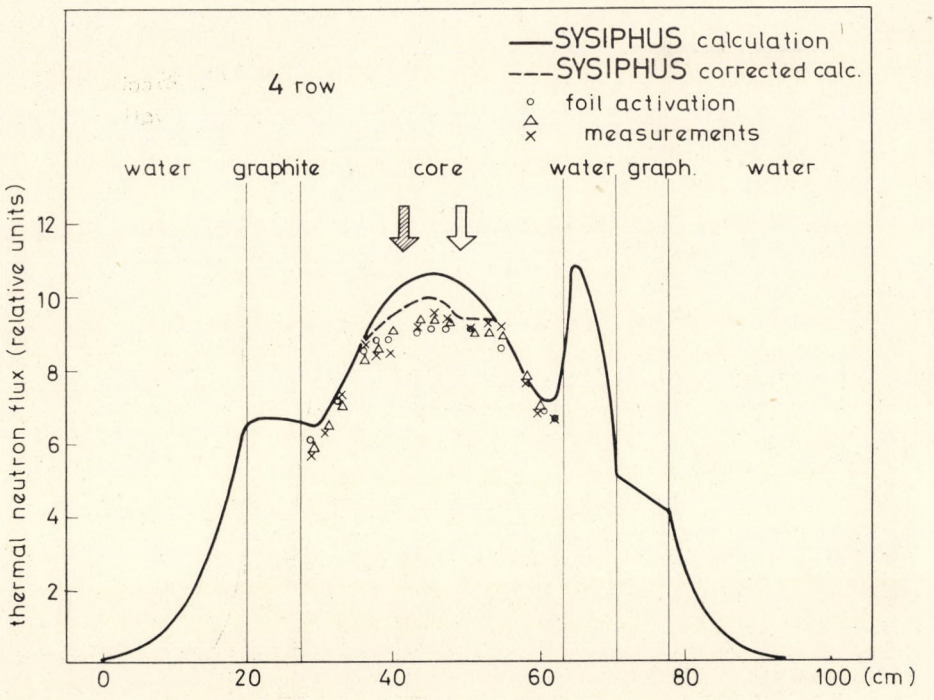

Fig. 8

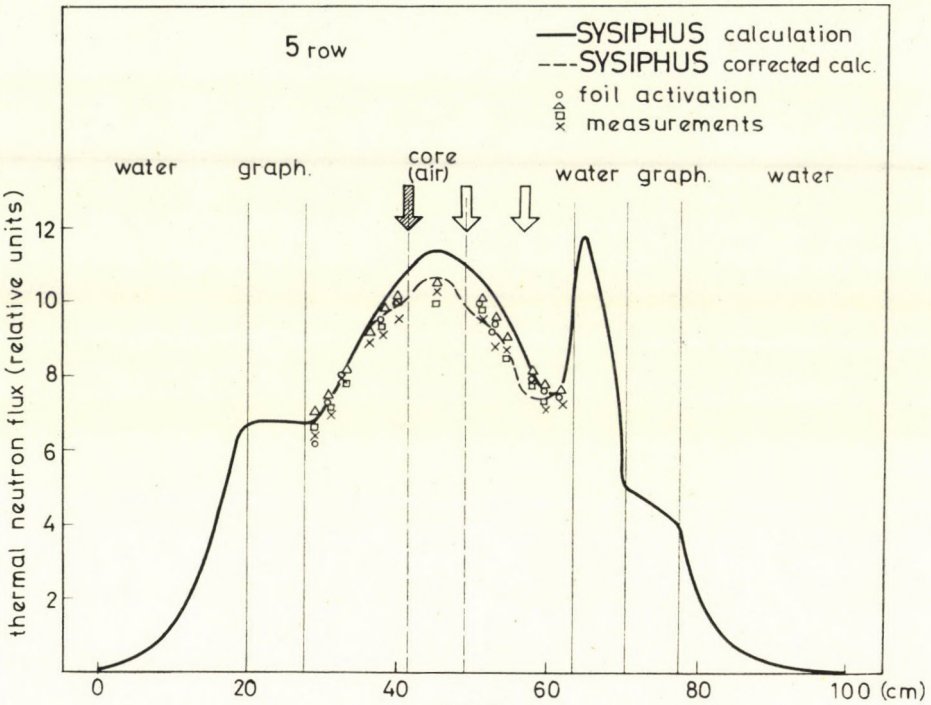
5 row
—SYSIPHUS calculation
---SYSIPHUS corrected calc.
foil activation measurements
water
graph.
core (air)
water
graph.
water
thermal neutron flux (relative units)
12
10
8
6
4
2
0
20
40
60
80
100 (cm)

Fig. 9

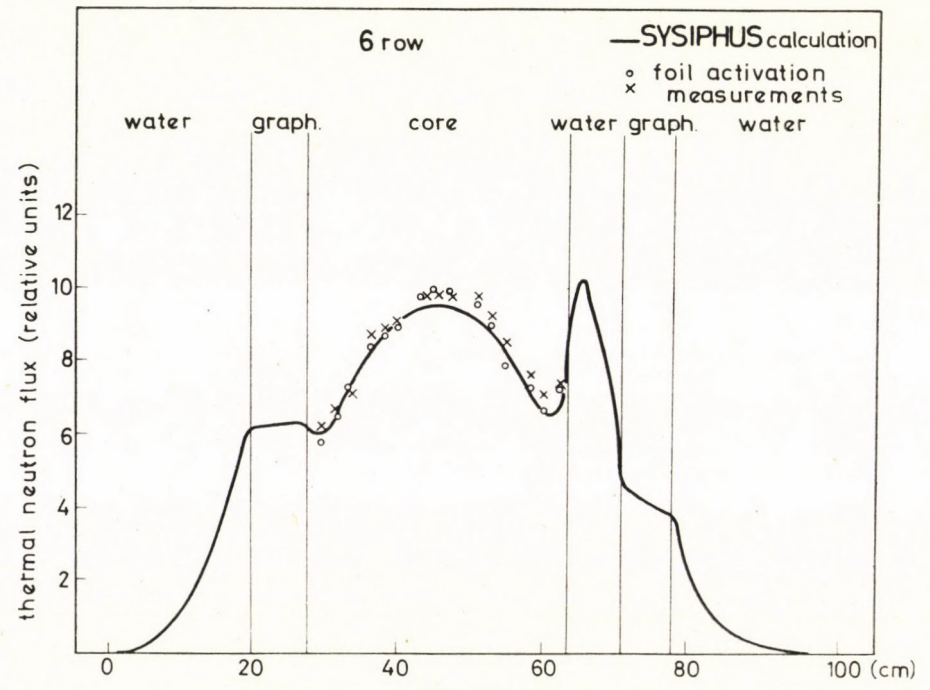
6 row
—SYSIPHUS calculation
foil activation measurements
water
graph.
core
water
graph.
water
thermal neutron flux (relative units)
12
10
8
6
4
2
0
20
40
60
80
100 (cm)

Fig. 10

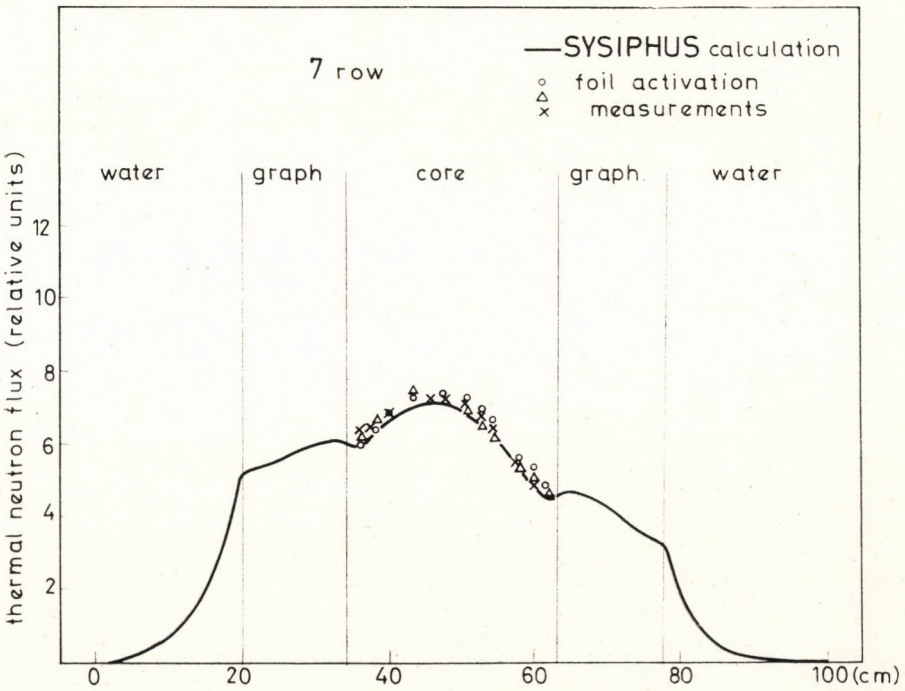
7 row
—SYSIPHUS calculation
foil activation measurements
water
graph
core
graph
water
thermal neutron flux (relative units)
12
10
8
6
4
2
0
20
40
60
80
100 (cm)

Fig. 11

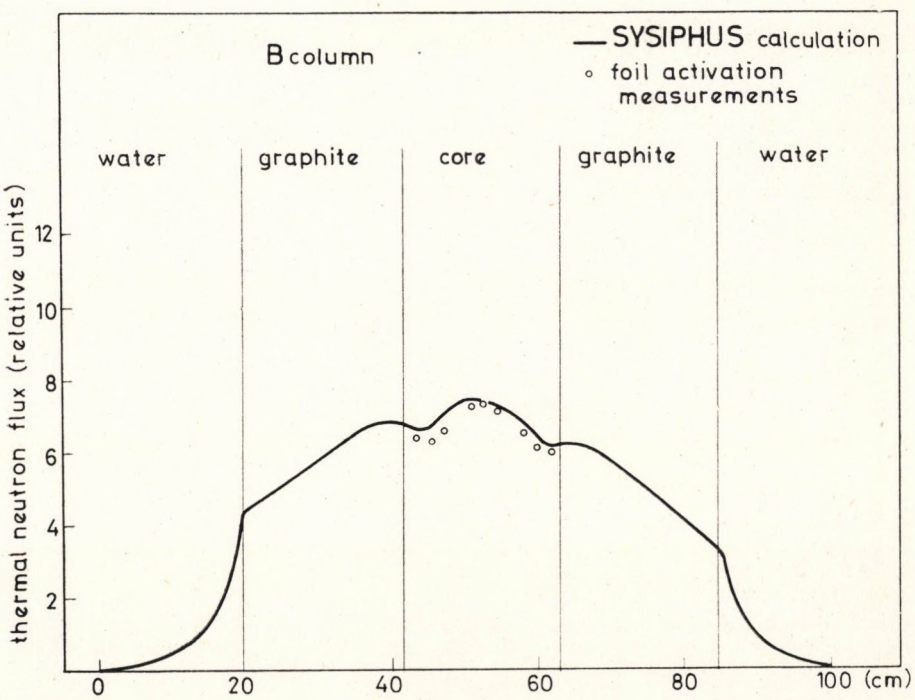
B column
—SYSIPHUS calculation
foil activation measurements
water
graphite
core
graphite
water
thermal neutron flux (relative units)
12
10
8
6
4
2
0
20
40
60
80
100 (cm)

Fig. 12

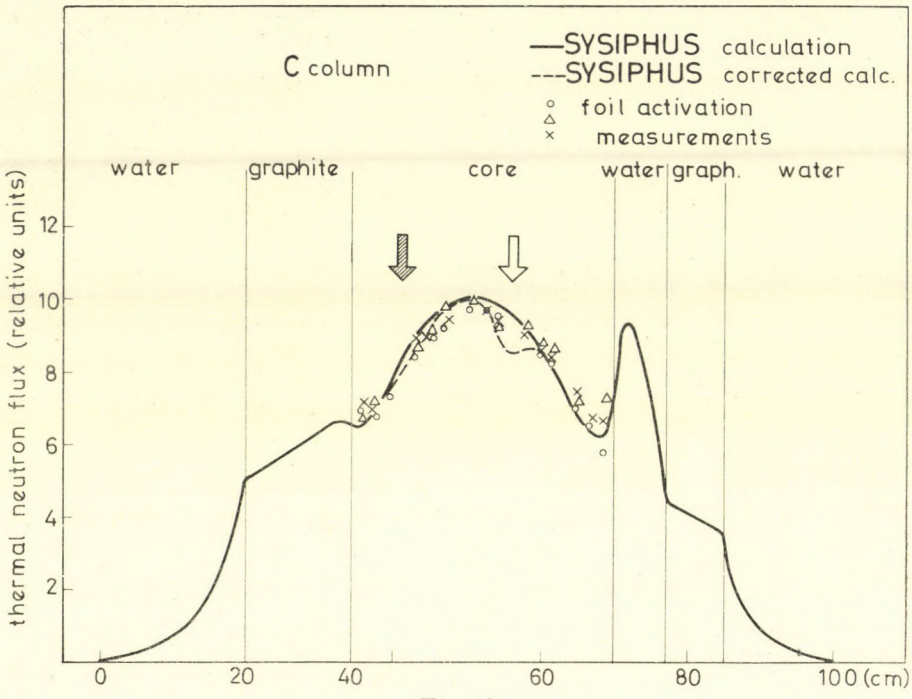
C column
—SYSIPHUS calculation
---SYSIPHUS corrected calc.
foil activation
measurements
water
graphite
core
water
graph.
water
thermal neutron flux (relative units)
12
10
8
6
4
2
0
20
40
60
80
100 (cm)

Fig. 13

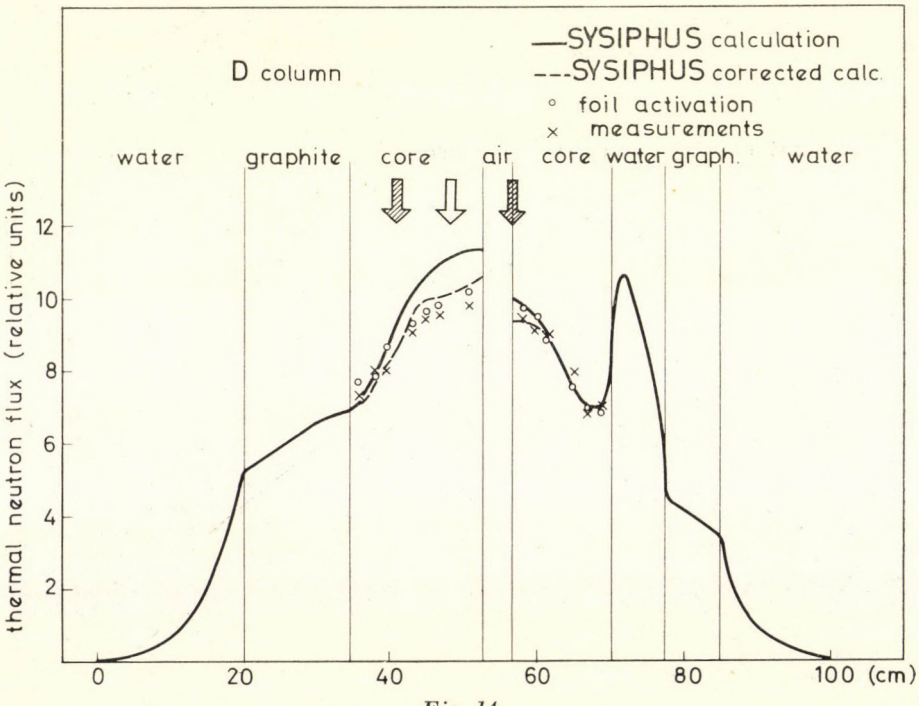
D column
—SYSIPHUS calculation
---SYSIPHUS corrected calc.
foil activation
measurements
water
graphite
core
air
core
water
graph.
water
thermal neutron flux (relative units)
12
10
8
6
4
2
0
20
40
60
80
100 (cm)

Fig. 14

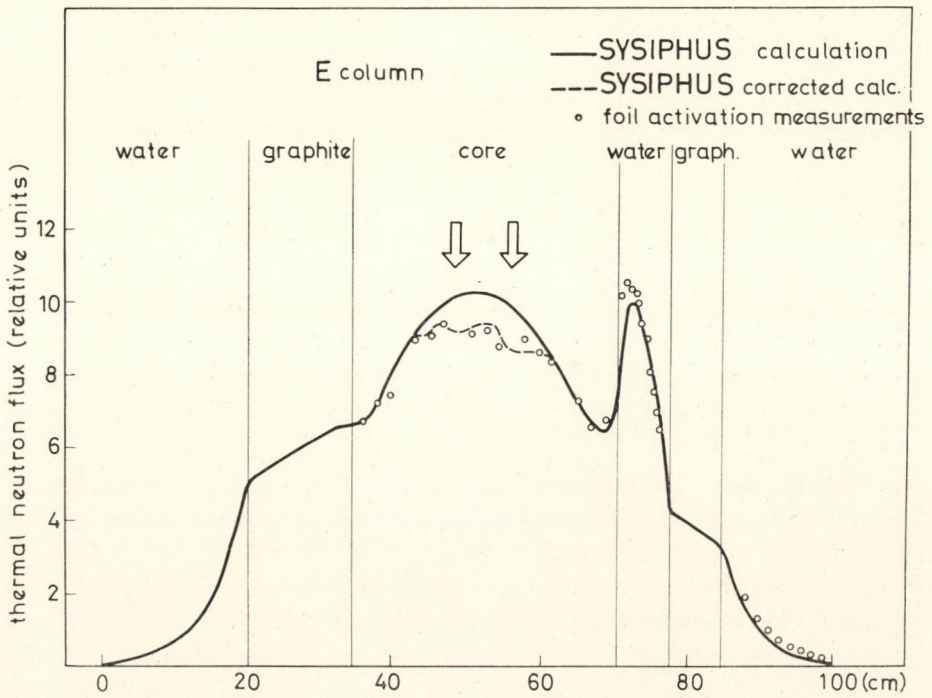
E column
—SYSIPHUS calculation
---SYSIPHUS corrected calc.
∘ foil activation measurements
water
graphite
core
water
graph.
water
thermal neutron flux (relative units)
2
4
6
8
10
12
0
20
40
60
80
100 (cm)

Fig. 15

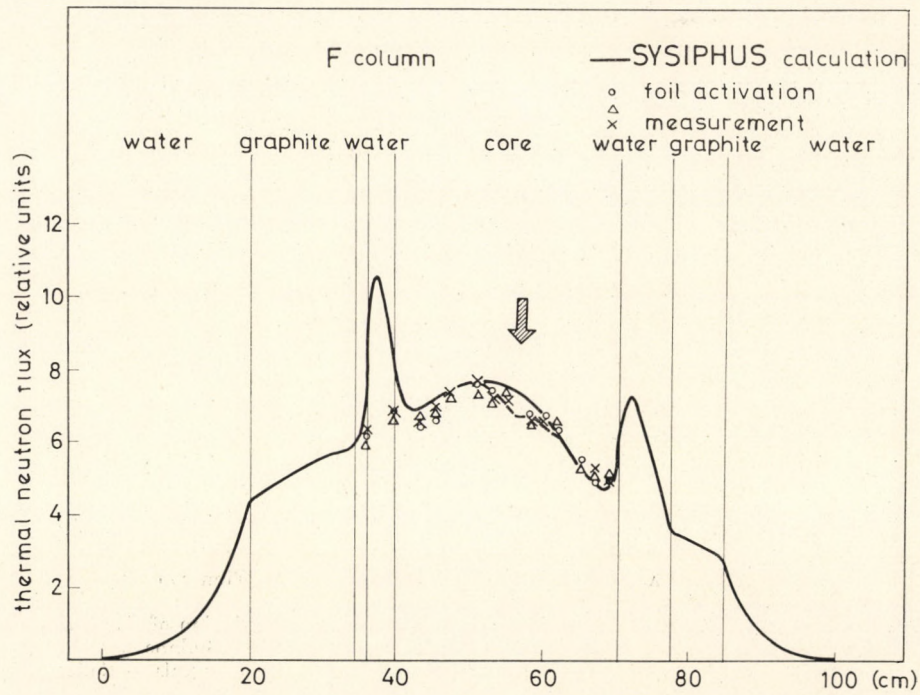
F column
—SYSIPHUS calculation
∘ foil activation
△ measurement
× measurement
water
graphite
water
core
water
graphite
water
thermal neutron flux (relative units)
2
4
6
8
10
12
0
20
40
60
80
100 (cm)

Fig. 16

wet channel. It can be observed that in the majority of cases this correction considerably improves the agreement of measurements and calculation.

It may be noted that all measurements have been normalized to the same reactor power by means of overlaps between the different sets of foils activated at different times. The calculated flux values are, of course, all consistent with another power. All measured values were normalized (with an integral requirement) to the calculations using a single normalization factor. The obtained agreement is thus much more remarkable than it would be if a separate normalization had been made in each figure.

The scattering of measurements repeated at different times (marked with different signs) indicates the reproducibility of measurements, but as there are probably systematic errors somewhat greater errors should be presumed in practice.

Conclusion

In the course of the calculations the values of thermal and fast neutron flux are obtained at approx. 3000 points of the system. The availability of such detailed flux data means that a range of problems connected with the design and operation of a reactor can be tackled which can only be treated by more roundabout methods, with ad hoc measurements or may indeed be absolutely inaccessible to direct measurement. Many different problems can be calculated for irradiated cores that cannot be handled or for working reactors that must not be disturbed, etc. It is for reasons such as these that the practice of utilizing a limited number of specially chosen and extremely precise measurements for checking the results of the calculations has come to be adopted world-wide, while in numerous practical problems the results of calculations are utilized instead of measurements. The measurements and calculations on the Polytechnical University's training reactor have proved that our calculation model is good enough to allow us, too, to follow this modern trend.

REFERENCES

1. A BME Oktató és Kutató reaktora. I. rész. Reaktorfizikai mérések és számítások, az aktív zóna kialakítása. KFKI report KFKI-71-69, Budapest.
2. F. Szabó, Light Water Enriched Uranium Lattice Experiments, III. Geneva Conf. A/Conf. 28/P/650 (1964).
3. J. Valkó, RJT1-THERMOS, to be published.
4. Z. Szatmáry and J. Valkó, GRACE — A Multigroup Fast Neutron Spectrum Code, KFKI report 14/1970, Budapest.
5. Z. Szatmáry and J. Vigassy, SISYPHUS — A Code for the Solution of Few-Group Diffusion Equations in Two-Dimension, KFKI-report 13/1970, Budapest.
6. Z. Szatmáry and Anna Bagyinszki, Calculation of Resonance Integrals — Codes RIFF-RAFF and RAO4, KFKI report 12/1970, Budapest.

7. Z. Szatmáry and Anna Bagyinszki, RAM — A Monte Carlo Code for the Determination of the Logarithmic Boundary Condition at the Surface of Control Rods, Seminar on Reactor Physics Calculation, 20—24 October 1969, Budapest.
8. V. A. Kuznetsov, et al., Experimental Study of Some Methods of Compensating Excess Reactivity in Intermediate Reactors, III. Geneva Conf. A/Conf. 28/P/375 (1964).
9. O. P. Tverbakk and J. M. Døderlein, KR-75 (1965).
10. G. Kosály and J. Valkó, Journal of Nuclear Energy, **25**, 297 1971.
11. B. E. Simmons and J. S. King, Nucl. Sci. Eng., **3**, 595, 1958.
12. Z. Szabó, Nuclear Instruments and Methods, **78**, 199, 1970.

ФИЗИКА АКТИВНОЙ ЗОНЫ УЧЕБНОГО РЕАКТОРА ПОЛИТЕХНИЧЕСКОГО УНИВЕРСИТЕТА

Ф. САБО, Л. ФРАНКЛ, Й. ВАЛКО и Л. ТУРИ

Резюме

Статья содержит краткое описание измерений и расчетов проекта ZR-5, на основании которых была создана ядерная конструкция учебного реактора Политехнического университета. Система использованных в расчетах программ, которая получила название физической модели реактора, описывается совместно с некоторыми элементами экспериментальной техники. Подтверждены высокая точность и большая потенциальная ценность таких расчетов. Авторы подчеркивают, что использование такой модели позволяет составить себе ясное представление о большинстве ядерных аспектов конструкции и функционирования реактора.

Acta Physica Academiae Scientiarum Hungaricae, Tomus 32 (1—4), pp. 241—259 (1972)

SYMMETRIES IN THE CLASSICAL THREE-BODY PROBLEM*

By

JULIA NYIRI

CENTRAL RESEARCH INSTITUTE FOR PHYSICS, BUDAPEST

(Received 19. X. 1971)

Classical Lagrangian and Euler equations of the three-body problem are given in different coordinate systems. This paper supplements quantum mechanical considerations, given before.

Introduction

Several authors (see e.g. [1—8]) have noticed that quantum mechanical three-body systems possess the symmetry of motion of a five-dimensional sphere with respect to both the free motion and elastic forces. As the quantum mechanical problem obviously has the same symmetry as the classical one, it seems to be worthwhile to consider the classical equations of motion from this point of view.

Arbitrary motions of three-body system can be described as rotations and deformations of a triangle formed by the three particles: the equations of motion of the triangle turn out to be very similar to the equations of two coupled tops, one of them reflecting the hidden (non-geometrical) symmetry of the deformational motion of the triangle.

The present paper collects different types of equations and formulae connected with the classical three-body problem.

I. Non-rotating triangles (examples)

In dealing with the three-particle system, let us first recall the system of coordinates introduced in [6]. The radius vectors $\vec{x}_i$ $(i = 1, 2, 3)$ of the three particles are fixed by the condition

$$\vec{x}_1+\vec{x}_2+\vec{x}_3=0. \tag{1}$$

The Jacobi coordinates $\vec{\xi}$ and $\vec{\eta}$ are given in the case of equal masses in the form

* Dedicated to Prof. L. JÁNOSSY on his 60th birthday.

$$\vec{\xi} = -\sqrt{\frac{3}{2}}(\vec{x}_1+\vec{x}_2),$$

$$\vec{\eta} = \frac{1}{\sqrt{2}}(\vec{x}_1-\vec{x}_2), \tag{2}$$

$$\xi^2+\eta^2 = x_1^2+x_2^2+x_3^2 = \varrho^2,$$

where ϱ is the radius of the five-dimensional sphere. Further, we introduce the complex vector

$$\begin{aligned} \vec{z} &= \vec{\xi}+i\vec{\eta}, \\ \vec{z}^* &= \vec{\xi}-i\vec{\eta}. \end{aligned} \tag{3}$$

Consider now a triangle with vertices x_1, x_2, x_3. The position of this triangle in space is characterized by the vectors $\vec{l}_1$ and $\vec{l}_2$, which together with the vector $\vec{l} = \vec{l}_1 \times \vec{l}_2$ form the moving coordinate system. They are connected with vectors z and z^* in the following way:

$$\begin{aligned} \vec{z} &= \frac{\varrho}{\sqrt{2}} e^{-i\frac{\lambda}{2}} \left(e^{i\frac{a}{2}}\vec{l}_1+ie^{-i\frac{a}{2}}\vec{l}_2\right), \\ \vec{z}^* &= \frac{\varrho}{\sqrt{2}} e^{i\frac{\lambda}{2}} \left(e^{-i\frac{a}{2}}\vec{l}_1-ie^{i\frac{a}{2}}\vec{l}_2\right), \end{aligned} \tag{4}$$

where $0 \leq a \leq \pi$, $0 \leq \lambda \leq 2\pi$. The variables λ and a determine the form of the triangle. Using expressions (4), we can write $\vec{\xi}$ and $\vec{\eta}$ in the form

$$\begin{aligned} \vec{\xi} &= \frac{\varrho}{\sqrt{2}} \left(\cos\frac{a-\lambda}{2}\vec{l}_1+\sin\frac{a+\lambda}{2}\vec{l}_2\right), \\ \vec{\eta} &= \frac{\varrho}{\sqrt{2}} \left(\sin\frac{a-\lambda}{2}\vec{l}_1+\cos\frac{a+\lambda}{2}\vec{l}_2\right). \end{aligned} \tag{5}$$

This means that we can consider $\vec{\xi}$ and $\vec{\eta}$ as a result of two transformations

$$\begin{pmatrix} \vec{\xi} \\ \vec{\eta} \end{pmatrix} = \frac{\varrho}{\sqrt{2}} \begin{pmatrix} \cos\frac{\lambda}{2} & \sin\frac{\lambda}{2} \\ -\sin\frac{\lambda}{2} & \cos\frac{\lambda}{2} \end{pmatrix} \begin{pmatrix} \cos\frac{a}{2} & \sin\frac{a}{2} \\ \sin\frac{a}{2} & \cos\frac{a}{2} \end{pmatrix} \begin{pmatrix} \vec{l}_1 \\ \vec{l}_2 \end{pmatrix}. \tag{6}$$

To make the picture clearer, let us consider the case of a non rotating triangle. We need for this purpose the expressions

$$\begin{aligned} \xi^2 &= \frac{\varrho^2}{2}(1+\sin a \sin\lambda), \\ \eta^2 &= \frac{\varrho^2}{2}(1-\sin a \sin\lambda), \end{aligned} \tag{7}$$

$$\vec{\xi}\vec{\eta} = \frac{\varrho^2}{2} \sin a \cos \lambda \,. \tag{8}$$

The angle Θ between vectors $\vec{\xi}$ and $\vec{\eta}$

$$\vec{\xi}\vec{\eta} = |\xi|\,|\eta| \cos \Theta \tag{9}$$

can be written in terms of our variables as

$$\cos \Theta = \frac{\cos \lambda \sin a}{\sqrt{1 - \sin^2 a \sin^2 \lambda}} \,. \tag{10}$$

Note that the components of the moment of inertia are

$$\varrho^2 \sin^2 \left(\frac{a}{2} - \frac{\pi}{4} \right), \quad \varrho^2 \cos^2 \left(\frac{a}{2} - \frac{\pi}{4} \right), \quad \varrho^2. \tag{11}$$

It is obvious that if $a = \text{const}$, the variations of λ lead to deformations of the triangle which do not affect the values of the momenta of inertia. We can write

$$\begin{aligned} |\xi| &= \frac{\varrho}{\sqrt{2}} \sqrt{1 + C \sin \lambda}\,, \\ |\eta| &= \frac{\varrho}{\sqrt{2}} \sqrt{1 - C \sin \lambda}, \\ \cos \Theta &= \frac{C \cos \lambda}{\sqrt{1 - C^2 \sin^2 \lambda}}\,, \end{aligned} \tag{12}$$

where $C = \sin a$.

For example, if $a = 0$ (i.e. $C = 0$), we have

$$|\xi| = \frac{\varrho}{\sqrt{2}}, \quad |\eta| = \frac{\varrho}{\sqrt{2}}, \quad \cos \Theta = 0\,. \tag{13}$$

In this case vectors $\vec{\xi}$ and $\vec{\eta}$ are orthogonal independently of the value of λ, and only similarity transformations of the triangle are possible. On the other hand, if $a = \pi/2$, then

$$\begin{aligned} |\xi| &= \frac{\varrho}{\sqrt{2}} \sqrt{1 + \sin \lambda}\,, \\ |\eta| &= \frac{\varrho}{\sqrt{2}} \sqrt{1 - \sin \lambda}\,, \\ \cos \Theta &= 1, \end{aligned} \tag{14}$$

i.e. the system is linear and the ends of the vectors $\vec{\xi}$ and $\vec{\eta}$ are oscillating about the point $\varrho/\sqrt{2}$. Expressing the positions of all three particles in the c.m. system in terms of $\vec{\xi}$ and $\vec{\eta}$:

$$\vec{x}_1 = -\frac{1}{\sqrt{6}}\vec{\xi} + \frac{1}{\sqrt{\eta}}\vec{\eta} = \sqrt{\frac{2}{3}}\left[\cos\frac{2\pi}{3}\vec{\xi} + \sin\frac{2\pi}{3}\vec{\eta}\right],$$

$$\vec{x}_2 = -\frac{1}{\sqrt{6}}\vec{\xi} - \frac{1}{\sqrt{2}}\vec{\eta} = \sqrt{\frac{2}{3}}\left[\cos\frac{4\pi}{3}\vec{\xi} + \sin\frac{4\pi}{3}\vec{\eta}\right], \tag{15}$$

$$\vec{x}_3 = \sqrt{\frac{2}{3}}\vec{\xi}$$

it will be easy to represent the position of the particles by their radius vectors. As an illustration, we consider the case $a = \pi/2$ for different values of λ:

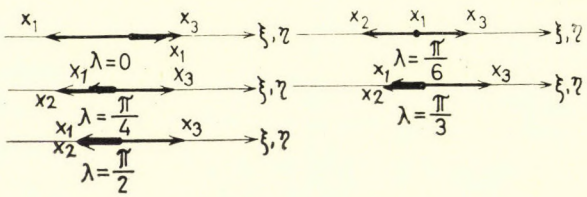

Consider now those deformations which are connected with the change of a i.e. those which do not leave the moment of inertia unaltered.
Let $\lambda = 0$, then

$$|\xi| = \frac{\varrho}{\sqrt{2}}, \quad |\eta| = \frac{\varrho}{\sqrt{2}}, \quad \sin a = \cos\Theta \tag{16}$$

The angle between $\vec{\xi}$ and $\vec{\eta}$ is

$$\Theta = \frac{\pi}{2} - a$$

and we have

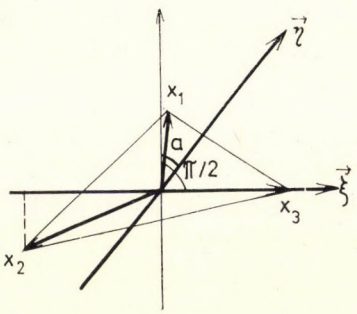

We list here a few particular cases:

$a = 0, \Theta = \frac{\pi}{2}$

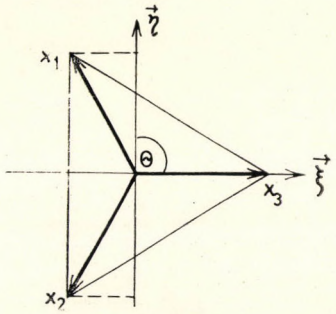

$a = \frac{\pi}{4}, \Theta = \frac{\pi}{4}$

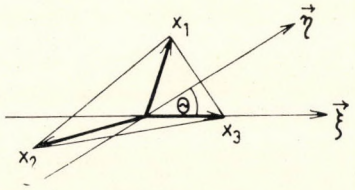

$a = \frac{\pi}{3}, \Theta = \frac{\pi}{6}$

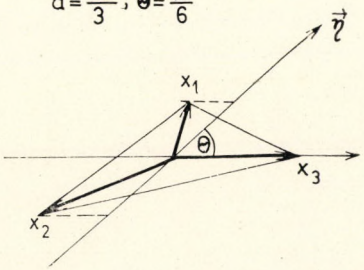

$a = \frac{\pi}{2}, \Theta = 0$

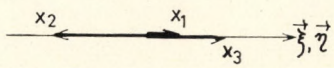

$a = \frac{3}{4}\pi, \Theta = -\frac{\pi}{4}$

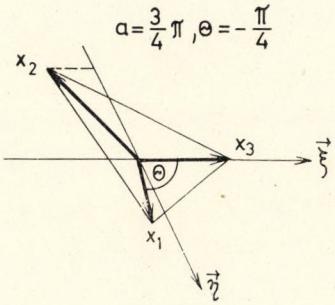

$a = \pi, \Theta = -\frac{\pi}{2}$

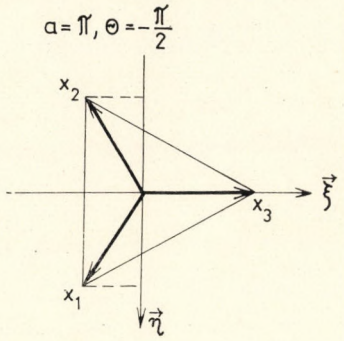

Considering the case $\lambda = \pi/2$, from the formulae

$$|\xi| = \frac{\varrho}{\sqrt{2}}\sqrt{1+\sin a}\,,$$

$$|\eta| = \frac{\varrho}{\sqrt{2}}\sqrt{1-\sin a}\,, \tag{17}$$

$$\cos\Theta = 0\,,$$

it can be easily seen that $\vec{\xi}$ and $\vec{\eta}$ are orthogonal and their lengths can oscillate between zero and ϱ.

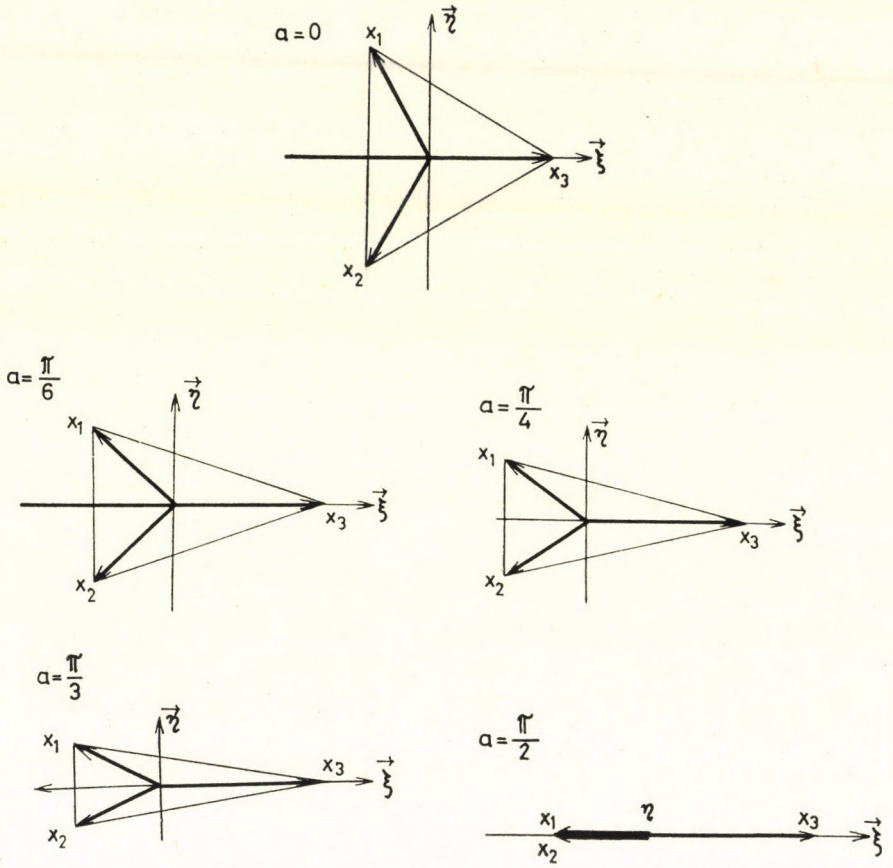

II. The free Lagrangian

In this Section we present the Euler equations. First of all, we have to construct the Lagrangian $L = T - U$. For free particles we have

$$L = T = \frac{1}{2}\left(\frac{ds}{dt}\right)^2, \tag{18}$$

Let us begin with the expression

$$d\vec{z} = \frac{1}{\varrho}\vec{z}\,d\varrho - \frac{i}{2}\vec{z}\,d\lambda + \frac{1}{2}e^{-i\lambda}(\vec{l}\times\vec{z})^*\,da - (d\vec{\omega}\times\vec{z}), \tag{19}$$

where $d\vec{\omega}$ is the infinitesimal rotation with projections $d\omega_i$ onto the fixed axes. The rotations about the moving axes are defined as

$$d\Omega_i = \vec{l}_i \, d\vec{\omega} \,. \tag{20}$$

They can be expressed in terms of the Euler angles in the form

$$\begin{aligned} d\Omega_1 &= -\cos\varphi_1 \sin\Theta d\varphi_2 + \sin\varphi_1 d\Theta, \\ d\Omega_2 &= \sin\varphi_1 \sin\Theta d\varphi_2 + \cos\varphi_1 d\Theta, \\ d\Omega_3 &= -d\varphi_1 - \cos\Theta d\varphi_2. \end{aligned} \tag{21}$$

From (19) we get

$$\begin{aligned} ds^2 = |dz|^2 = \varrho^2 \Big[\frac{1}{4} da^2 + \frac{1}{4} d\lambda^2 + \frac{1}{2} d\Omega_1^2 + \frac{1}{2} d\Omega_2^2 + d\Omega_3^2 - \\ - \sin a d\Omega_1 \, d\Omega_2 - \cos a d\Omega_3 \, d\lambda \Big] + d\varrho^2 . \end{aligned} \tag{22}$$

Obviously, the wanted expression will be

$$\begin{aligned} T = \frac{1}{2} \varrho^2 \Big[\frac{1}{4} \dot{a}^2 + \frac{1}{4} \dot{\lambda}^2 + \frac{1}{2} \dot{\Omega}_1^2 + \frac{1}{2} \dot{\Omega}_2^2 + \dot{\Omega}_3^2 - \\ - \sin a \dot{\Omega}_1 \dot{\Omega}_2 - \cos a \, \dot{\Omega}_3 \dot{\lambda} \Big] + \frac{1}{2} \dot{\varrho}^2 . \end{aligned} \tag{23}$$

Due to the formula

$$p_i = \frac{\partial T}{\partial \dot{q}_i} \tag{24}$$

we can write down the momenta

$$\begin{aligned} p_a &= \frac{1}{4} \varrho^2 \dot{a}, \\ p_\lambda &= \frac{1}{2} \varrho^2 \left(\frac{1}{2} \dot{\lambda} - \cos a \dot{\Omega}_3 \right), \\ p_{\Omega_1} &= \frac{1}{2} \varrho^2 (\dot{\Omega}_1 - \sin a \dot{\Omega}_2), \\ p_{\Omega_2} &= \frac{1}{2} \varrho^2 (\dot{\Omega}_2 - \sin a \dot{\Omega}_1), \\ p_{\Omega_3} &= \frac{1}{4} \varrho^2 (2\dot{\Omega}_3 - \cos a \dot{\lambda}), \\ p_\varrho &= \dot{\varrho} \end{aligned} \tag{25}$$

and the corresponding $\dot{p}_i$:

$$\begin{aligned}
\dot{p}_a &= \frac{1}{4}\varrho\dot{\varrho}\dot{a} + \frac{1}{2}\varrho^2\ddot{a}\,,\\
\dot{p}_\lambda &= \frac{1}{2}\varrho^2\left(\frac{1}{4}\ddot{\lambda} + \sin a\dot{a}\dot{\Omega}_3 - \cos a\ddot{\Omega}_3\right) + \varrho\left(\frac{1}{2}\dot{\lambda}\dot{\varrho} - \cos a\dot{\varrho}\dot{\Omega}_3\right),\\
\dot{p}_{\Omega_1} &= \frac{1}{2}\varrho^2(\ddot{\Omega}_1 - \cos a\dot{a}\dot{\Omega}_2 - \sin a\ddot{\Omega}_2) + \varrho(\dot{\varrho}\dot{\Omega}_1 - \sin a\dot{\varrho}\dot{\Omega}_2)\,,\\
\dot{p}_{\Omega_2} &= \frac{1}{2}\varrho^2(\ddot{\Omega}_2 - \cos a\dot{a}\dot{\Omega}_1 - \sin a\ddot{\Omega}_1) + \varrho(\dot{\varrho}\dot{\Omega}_2 - \sin a\dot{\varrho}\dot{\Omega}_1)\,,\\
\dot{p}_{\Omega_3} &= \frac{1}{2}\varrho^2(2\ddot{\Omega}_3 + \sin a\dot{a}\dot{\lambda} - \cos a\ddot{\lambda}) + \varrho(2\dot{\varrho}\dot{\Omega}_3 - \cos a\dot{\varrho}\dot{\lambda})\,,\\
\dot{p}_\varrho &= \ddot{\varrho}\,.
\end{aligned} \tag{26}$$

We can now construct the equations of motion

$$\frac{d}{dt}\frac{\partial T}{\partial \dot{q}_i} - \frac{\partial T}{\partial q_i} = 0\,. \tag{27}$$

To obtain the equations explicitly, we have to return to the Euler angles. Indeed, as $\dot{\Omega}_i$ are not derivatives of any angles Ω_i (that is why they are called quasi-coordinates), the Euler equation in terms of these quasi-coordinates must be written in another form.

Thus, instead of (23) we have to take the Lagrangian expressed in terms of the Euler angles:

$$\begin{aligned}
T = \frac{1}{2}\varrho^2\Big[&\frac{1}{4}\dot{a}^2 + \frac{1}{4}\dot{\lambda}^2 + \dot{\varphi}_1^2 + \frac{1}{2}\dot{\Theta}^2 + \frac{1}{2}\dot{\varphi}_2^2 + \frac{1}{2}\cos^2\Theta\dot{\varphi}_2^2 +\\
&+2\cos\Theta\dot{\varphi}_1\dot{\varphi}_2 + \sin a\left(\frac{1}{2}\sin 2\varphi_1\sin^2\Theta\dot{\varphi}_2^2 + \cos 2\varphi_1\sin\Theta\dot{\varphi}_2\dot{\Theta} -\right.\\
&\left.-\frac{1}{2}\sin 2\varphi_1\dot{\Theta}^2\right) + \cos a(\dot{\varphi}_1\dot{\lambda} + \cos\Theta\dot{\varphi}_2\dot{\lambda})\Big] + \frac{1}{2}\dot{\varrho}^2.
\end{aligned} \tag{28}$$

The equations of free motion are as follows:

$$\begin{aligned}
\frac{1}{2}\ddot{a} - \cos a&\left(\frac{1}{2}\sin 2\varphi_1\sin^2\Theta\dot{\varphi}_2^2 + \cos 2\varphi_1\sin\Theta\dot{\varphi}_2\dot{\Theta} - \frac{1}{2}\sin 2\varphi_1\dot{\Theta}^2\right) +\\
&+\sin a(\dot{\varphi}_1\dot{\lambda} + \cos\Theta\dot{\varphi}_2\dot{\lambda}) + \frac{1}{\varrho}\dot{\varrho}\dot{a} = 0\,,
\end{aligned} \tag{29}$$

$$\frac{1}{2}\ddot{\lambda}-\sin a(\ddot{a}\dot{\varphi}_1+\cos\Theta\dot{a}\dot{\varphi}_2)+\cos a(\ddot{\varphi}_1-\sin\Theta\dot{\Theta}\dot{\varphi}_2+\cos\Theta\ddot{\varphi}_2)+$$
$$+\frac{1}{\varrho}\dot{\varrho}\dot{\lambda}+\frac{2}{\varrho}\cos a(\dot{\varphi}_1\dot{\varrho}+\cos\Theta\dot{\varphi}_2\dot{\varrho})=0\,, \tag{30}$$

$$\ddot{\varphi}_1-\sin\Theta\dot{\Theta}\dot{\varphi}_2+\cos\Theta\ddot{\varphi}_2+\frac{1}{2}\cos a\ddot{\lambda}-$$
$$-\frac{1}{2}\sin a\left[\dot{a}\dot{\lambda}+\cos 2\varphi_1\sin^2\Theta\dot{\varphi}_2^2-2\sin 2\varphi_1\sin\Theta\dot{\varphi}_2\dot{\Theta}-\right. \tag{31}$$
$$\left.-\cos 2\varphi_1\dot{\Theta}^2\right]+\frac{1}{\varrho}(2\dot{\varphi}_1\dot{\varrho}+2\cos\Theta\dot{\varphi}_2\dot{\varrho}+\cos a\dot{\lambda}\dot{\varrho})=0\,,$$

$$\frac{1}{2}\sin a\cos 2\varphi_1\ddot{\Theta}+\frac{1}{2}\sin\Theta(1+\sin a\sin 2\varphi_1)\ddot{\varphi}_2-(1+\sin a\sin 2\varphi_1)\dot{\varphi}_1\dot{\Theta}+$$
$$+\sin a\left(\cos 2\varphi_1\sin\Theta\dot{\varphi}_1\dot{\varphi}_2+\frac{1}{2}\operatorname{cotan}\Theta\cos 2\varphi_1\dot{\Theta}^2+\right.$$
$$\left.+\sin 2\varphi_1\cos\Theta\dot{\varphi}_2\dot{\Theta}\right)+\cos a\left(\frac{1}{2}\sin 2\varphi_1\Theta\dot{a}\dot{\varphi}_2+\right. \tag{32}$$
$$\left.+\frac{1}{2}\cos 2\varphi_1\dot{\Theta}\dot{a}-\frac{1}{2}\dot{\lambda}\dot{\Theta}\right)+$$
$$+\frac{1}{\varrho}\left[\sin\Theta\dot{\varphi}_2\dot{\varrho}(1+\sin a\sin 2\varphi_1)+\sin a\cos 2\varphi_1\dot{\Theta}\dot{\varrho}\right]=0\,,$$

$$(1-\sin a\sin 2\varphi_1)\ddot{\Theta}+\frac{1}{2}\sin 2\Theta\dot{\varphi}_2^2+2\sin\Theta\dot{\varphi}_1\dot{\varphi}_2+$$
$$+\sin a\left(-2\cos 2\varphi_1\dot{\varphi}_1\dot{\Theta}+\cos 2\varphi_1\sin\Theta\ddot{\varphi}_2-2\sin 2\varphi_1\sin\Theta\dot{\varphi}_1\dot{\varphi}_2-\right.$$
$$\left.-\frac{1}{2}\sin 2\varphi_1\sin 2\Theta\dot{\varphi}_2^2\right)+\cos a(\cos 2\varphi_1\sin\Theta\dot{a}\dot{\varphi}_2^2- \tag{33}$$
$$-\sin 2\varphi_1\dot{a}\dot{\Theta}+\sin\Theta\dot{\varphi}_2\dot{\lambda})+\frac{2}{\varrho}(\dot{\Theta}\dot{\varrho}+\sin a\cos 2\varphi_1\sin\Theta\dot{\varrho}\dot{\varphi}_2-$$
$$-\sin a\sin 2\varphi_1\dot{\varrho}\dot{\Theta})=0$$

and finally,

$$\ddot{\varrho}-\varrho\left[\frac{1}{4}\dot{a}^2+\frac{1}{4}\dot{\lambda}^2+\dot{\varphi}_1^2+\frac{1}{2}\dot{\Theta}^2+\frac{1}{2}\dot{\varphi}_2^2+\frac{1}{2}\cos^2\Theta\dot{\varphi}_2^2+2\cos\Theta\dot{\varphi}_1\dot{\varphi}_2+\right.$$
$$+\sin a\left(\frac{1}{2}\sin 2\varphi_1\sin^2\Theta\dot{\varphi}_2^2+\cos 2\varphi_1\sin\Theta\dot{\varphi}_2\dot{\Theta}-\frac{1}{2}\sin 2\varphi_1\dot{\Theta}^2\right)+ \tag{34}$$
$$\left.+\cos a(\dot{\varphi}_1\dot{\lambda}+\cos\Theta\dot{\varphi}_2\dot{\lambda})\right]=0\,.$$

A few particular cases are considered in the following.

1) *Motion of the triangle in the plane:*

$$\dot{\Theta} = \dot{\varphi}_2 = 0 .$$

In this case the free Lagrangian can be written

$$T = \frac{1}{2}\varrho^2\left[\frac{1}{4}\dot{a}^2 + \frac{1}{4}\dot{\lambda}^2 + \cos a\,\dot{\varphi}_1\dot{\lambda} + \dot{\varphi}_1^2\right] + \frac{1}{2}\dot{\varrho}^2, \tag{35}$$

or, remembering that

$$\begin{aligned} p_{\varphi 1} &= \frac{1}{2}\varrho^2(2\dot{\varphi}_1 + 2\cos\Theta\dot{\varphi}_2 + \cos a\dot{\lambda}), \\ p_{\varphi 2} &= \frac{1}{2}\varrho^2(\dot{\varphi}_2 + \cos^2\Theta\dot{\varphi}_2 - \sin a \sin 2\varphi_1 \sin^2\Theta\dot{\varphi}_2 + \\ &\quad + 2\cos\Theta\dot{\varphi}_1 + \sin a\cos 2\varphi_1 \sin\Theta\dot{\Theta} + \cos a\cos\Theta\dot{\lambda}), \\ p_\Theta &= \frac{1}{2}\varrho^2(\dot{\Theta} + \sin a\cos 2\varphi_1 \sin\Theta\dot{\varphi}_2 - \sin a \sin 2\varphi_1\dot{\Theta}), \end{aligned} \tag{36}$$

in the form

$$T = \frac{1}{\varrho^2}\left[2p_a^2 + \frac{1}{\sin^2 a}\left(\frac{1}{2}p_{\varphi_1}^2 - 2p_{\varphi 1}p_\lambda\cos a + 2p_\lambda^2\right)\right] + \frac{1}{2}p_\varrho^2. \tag{37}$$

The equations of motion are in this case

$$\begin{aligned} &\frac{1}{2}\ddot{a} + \frac{1}{\varrho}\dot{\varrho}\dot{a} + \sin a\,\dot{\varphi}_1\dot{\lambda} = 0, \\ &\frac{1}{2}\ddot{\lambda} + \frac{1}{\varrho}\dot{\varrho}\dot{\lambda} - \sin a\,\dot{a}\dot{\varphi}_1 + \cos a\ddot{\varphi}_1 + \frac{2}{\varrho}\cos a\,\dot{\varphi}_1\dot{\varrho} = 0, \\ &\ddot{\varphi}_1 + \frac{1}{2}\cos a\ddot{\lambda} - \frac{1}{2}\sin a\dot{a}\dot{\lambda} + \frac{1}{\varrho}(2\dot{\varphi}_1\dot{\varrho} + \cos a\dot{\lambda}\dot{\varrho}) = 0, \\ &\ddot{\varrho} - \varrho\left(\frac{1}{4}\dot{a}^2 + \frac{1}{4}\dot{\lambda}^2 + \dot{\varphi}_1^2 + \cos a\dot{\varphi}_1\dot{\lambda}\right) = 0 . \end{aligned} \tag{38}$$

2) *Deforming triangle ;*

$$\dot{\Theta} = \dot{\varphi}_2 = 0 , \quad p_{\varphi 1} = 0 .$$

The free Lagrangian obtains the form

$$T = \frac{1}{2}\varrho^2\left(\frac{1}{4}\dot{a}^2 + \frac{1}{4}\dot{\lambda}^2\sin^2 a\right) + \frac{1}{2}\dot{\varrho}^2 = \frac{2}{\varrho^2}\left(p_a^2 + \frac{1}{\sin^2 a}p_\lambda^2\right) + \frac{1}{2}p_\varrho^2. \tag{39}$$

It should be noted that for $p_\varrho = 0$ this expression has the same form as the Lagrangian of the rotator. We see here an example of the hidden symmetry, which can be generalized to the case of a deforming rotator.

The equations of motion corresponding to the Lagrange function (39) are

$$\begin{aligned} &\frac{1}{2}\ddot{a} + \frac{1}{\varrho}\dot{\varrho}\dot{a} - \frac{1}{2}\sin a \cos a\dot{\lambda}^2 = 0, \\ &\sin a\left(\frac{1}{2}\ddot{\lambda} + \frac{1}{\varrho}\dot{\varrho}\dot{\lambda}\right) + \cos a\dot{a}\dot{\lambda} = 0, \\ &\ddot{\varrho} - \varrho\left(\frac{1}{4}\dot{a}^2 + \frac{1}{4}\sin^2 a\dot{\lambda}^2\right) = 0. \end{aligned} \tag{40}$$

If we add to the right-hand side forces depending only on ϱ, we get the equations of a non-rigid rotator.

III. Potentials for three-body systems

Two examples of interacting particles will be investigated.

1. *The harmonic oscillator potential:*

The equilibrium state of the three-particle system is an equilateral triangle of side ϱ_0, which can be described by the vectors $\vec{\xi}_0$ and $\vec{\eta}_0$:

$$\vec{\xi}_0 = \begin{pmatrix} 0 \\ \frac{\varrho_0}{\sqrt{2}} \end{pmatrix}, \quad \vec{\eta}_0 = \begin{pmatrix} \frac{\varrho_0}{\sqrt{2}} \\ 0 \end{pmatrix},$$

$$\vec{\xi}_0 \vec{\eta}_0 = 0, \quad \xi_0^2 - \eta_0^2 = 0. \tag{41}$$

The parameters a_0 and λ_0 corresponding to the equilibrium state will have the values

$$a_0 = \pi, \quad \lambda_0 = 0,$$

and consequently

$$\vec{z}_0 = \frac{\varrho_0}{\sqrt{2}}\left(e^{i\frac{\pi}{2}}\vec{l}_1 + ie^{-i\frac{\pi}{2}}\vec{l}_2\right). \tag{42}$$

Consider the motion of the three particles with the potential energy

$$U = \frac{1}{2}\left[(\xi-\xi_0)^2+(\eta-\eta_0)^2\right] = \frac{1}{2}\left(\varrho^2+\varrho_0^2-2\varrho\varrho_0 \sin\frac{a}{2}\cos\frac{\lambda}{2}\right). \tag{43}$$

From the formula

$$F_i = -\frac{\partial U}{\partial q_i} \tag{44}$$

we obtain

$$\begin{aligned} F_a &= \frac{1}{2}\varrho\varrho_0 \cos\frac{a}{2}\cos\frac{\lambda}{2}, \\ F_\lambda &= -\frac{1}{2}\varrho\varrho_0 \sin\frac{a}{2}\sin\frac{\lambda}{2}, \\ F_\varrho &= -\varrho+\varrho_0 \sin\frac{a}{2}\cos\frac{\lambda}{2}, \\ F_{\varphi_1} &= F_{\varphi_2} = F_\Theta = 0. \end{aligned} \tag{45}$$

Constructing $L = T - U$, it is now easy to get the equations of motion

$$\frac{d}{dt}\frac{\partial L}{\partial \dot{q}_i} - \frac{\partial L}{\partial q_i} = 0. \tag{46}$$

The equations

$$\frac{d}{dt}\frac{\partial L}{\partial \dot{\varphi}_i} - \frac{\partial L}{\partial \varphi_i} = 0$$

(where $\varphi_3 = \theta$) stay unchanged; instead of Eqs. (29), (30) and (34) we obtain

$$\begin{aligned} &\frac{1}{2}\ddot{a} - \cos a\left(\frac{1}{2}\sin 2\varphi_1 \sin^2\Theta\dot{\varphi}_2^2+\cos 2\varphi_1 \sin\Theta\dot{\varphi}_2\dot{\Theta} - \frac{1}{2}\sin 2\varphi_1\dot{\Theta}^2\right) + \\ &\quad + \sin a\,(\dot{\varphi}_1\dot{\lambda}+\cos\Theta\dot{\varphi}_2\dot{\lambda}) + \frac{1}{\varrho}\dot{\varrho}\dot{a} - \frac{\varrho_0}{\varrho}\cos\frac{a}{2}\cos\frac{\lambda}{2} = 0, \end{aligned} \tag{47}$$

$$\begin{aligned} &\frac{1}{2}\ddot{\lambda} - \sin a\,(\dot{a}\dot{\varphi}_1+\cos\Theta\dot{a}\dot{\varphi}_2)+\cos a\,(\ddot{\varphi}_1-\sin\Theta\dot{\Theta}\dot{\varphi}_2+\cos\Theta\ddot{\varphi}_2) + \\ &\quad + \frac{1}{\varrho}\dot{\varrho}\dot{\lambda} + \frac{2}{\varrho}\cos a\,(\dot{\varphi}_1\dot{\varrho}+\cos\Theta\dot{\varphi}_2\dot{\varrho}) + \frac{\varrho_0}{\varrho}\sin\frac{a}{2}\sin\frac{\lambda}{2} = 0 \end{aligned} \tag{48}$$

and

$$\ddot{\varrho}-\varrho\left[\frac{1}{4}\dot{a}^2+\frac{1}{4}\dot{\lambda}^2+\dot{\varphi}_1^2+\frac{1}{2}\dot{\Theta}^2+\frac{1}{2}\dot{\varphi}_2^2+\frac{1}{2}\cos^2\Theta\dot{\varphi}_2^2+2\cos\Theta\dot{\varphi}_1\dot{\varphi}_2+\right.$$

$$+\sin a\left(\frac{1}{2}\sin 2\varphi_1\sin^2\Theta\dot{\varphi}_2^2+\cos 2\varphi_1\sin\Theta\dot{\varphi}_2\dot{\Theta}-\frac{1}{2}\sin 2\varphi_1\dot{\Theta}^2\right)+ \quad (49)$$

$$\left.+\cos a(\dot{\varphi}_1\dot{\lambda}+\cos\Theta\dot{\varphi}_2\dot{\lambda})\right]+\varrho-\varrho_0\sin\frac{a}{2}\cos\frac{\lambda}{2}=0\,.$$

Let us consider again the case of a non-rotating triangle:

$$\dot{\Theta}=\dot{\varphi}_2=0 \quad \text{and} \quad p_{\varphi 1}=0\,, \quad \text{i.e.} \quad \dot{\varphi}_1=-\frac{1}{2}\cos a\dot{\lambda}\,.$$

The equations of motion assume the form

$$\frac{1}{2}\ddot{a}+\frac{1}{\varrho}\dot{\varrho}\dot{a}-\frac{1}{2}\sin a\cos a\dot{\lambda}^2-\frac{\varrho_0}{\varrho}\cos\frac{a}{2}\cos\frac{\lambda}{2}=0\,,$$

$$\sin^2 a\left(\frac{1}{2}\ddot{\lambda}+\frac{1}{\varrho}\dot{\varrho}\dot{\lambda}\right)+\sin a\cos a\dot{a}\dot{\lambda}+\frac{\varrho_0}{\varrho}\sin\frac{a}{2}\sin\frac{\lambda}{2}=0\,, \quad (50)$$

$$\ddot{\varrho}-\varrho\left(\frac{1}{4}\dot{a}^2+\frac{1}{4}\sin^2 a\dot{\lambda}^2\right)+\varrho-\varrho_0\sin\frac{a}{2}\cos\frac{\lambda}{2}=0\,.$$

If in this case we take $\varrho_0=0$, we will have

$$\frac{1}{2}\ddot{a}+\frac{1}{\varrho}\dot{\varrho}\dot{a}-\frac{1}{2}\sin a\cos a\dot{\lambda}^2=0\,,$$

$$\sin a\left(\frac{1}{2}\ddot{\lambda}+\frac{1}{\varrho}\dot{\varrho}\dot{\lambda}\right)+\cos a\dot{a}\dot{\lambda}=0\,, \quad (51)$$

$$\ddot{\varrho}-\varrho\left(\frac{1}{4}\dot{a}^2+\frac{1}{4}\sin^2 a\dot{\lambda}^2\right)+\varrho=0\,.$$

As an example, let us consider solutions for constant λ and a, illustrating a few cases of the deformed triangle in detail. The projections of the radius-

vectors $\vec{x}_i$; onto the axes $\vec{l}_1$ and $\vec{l}_2$ are as follows:

$$x_1^{(1)} = \frac{\varrho}{2}\left(\sin\frac{a-\lambda}{2} - \frac{1}{\sqrt{3}}\cos\frac{a-\lambda}{2}\right),$$

$$x_2^{(1)} = -\frac{\varrho}{2}\left(\sin\frac{a-\lambda}{2} + \frac{1}{\sqrt{3}}\cos\frac{a-\lambda}{2}\right),$$

$$x_3^{(1)} = \frac{\varrho}{\sqrt{3}}\cos\frac{a-\lambda}{2}$$

and (52)

$$x_1^{(2)} = \frac{\varrho}{2}\left(\cos\frac{a+\lambda}{2} - \frac{1}{\sqrt{3}}\sin\frac{a+\lambda}{2}\right),$$

$$x_2^{(2)} = \frac{\varrho}{2} - \left(\cos\frac{a+\lambda}{2} + \frac{1}{\sqrt{3}}\sin\frac{a+\lambda}{2}\right),$$

$$x_3^{(2)} = \frac{\varrho}{\sqrt{3}}\sin\frac{a+\lambda}{2}.$$

If $a = \text{const.}$, $\lambda = \text{const.}$ and $\varrho_0 \neq 0$, we obtain from (50)

$$\frac{\varrho_0}{\varrho}\cos\frac{a}{2}\cos\frac{\lambda}{2} = 0,$$

$$\frac{\varrho_0}{\varrho}\sin\frac{a}{2}\sin\frac{\lambda}{2} = 0, \tag{53}$$

$$\ddot{\varrho}+\varrho-\varrho_0\sin\frac{a}{2}\cos\frac{\lambda}{2} = 0.$$

It can be easily seen that in this case a and λ are multiples of π, and only similarity transformations are possible; for example:

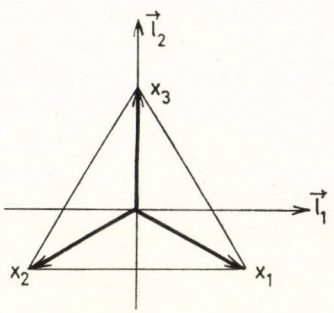

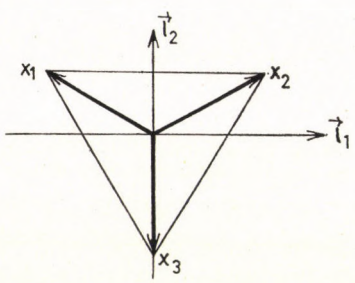

$$\lambda = 0, \quad a = \pi \qquad\qquad \lambda = 0, \quad a = 3\pi$$

$$x_1^{(1)} = \frac{\varrho}{2} \qquad\qquad x_1^{(1)} = -\frac{\varrho}{2}$$

$$x_2^{(1)} = \frac{\varrho}{2} \qquad\qquad x_2^{(1)} = -\frac{\varrho}{2}$$

$$x_3^{(1)} = 0 \qquad\qquad x_3^{(1)} = 0$$

$$x_1^{(2)} = -\frac{1}{2\sqrt{3}}\varrho \qquad\qquad x_1^{(2)} = \frac{\varrho}{2\sqrt{3}}$$

$$x_2^{(2)} = -\frac{1}{2\sqrt{3}}\varrho \qquad\qquad x_2^{(2)} = \frac{\varrho}{2\sqrt{3}}$$

$$x_8^{(2)} = \frac{\varrho}{\sqrt{3}}. \qquad\qquad x_3^{(2)} = -\frac{\varrho}{\sqrt{3}}.$$

If, on the contrary, $\varrho_0 = 0$, then the fixed value of a still does not determine the value of λ, so that arbitrary deformations are possible. We give in the following a few examples:

a) $\lambda = a$

$$x_1^{(1)} = -\frac{\varrho}{2\sqrt{3}} \qquad x_1^{(2)} = \frac{\varrho}{2}\left(\cos a - \frac{1}{\sqrt{3}}\sin a\right)$$

$$x_2^{(1)} = -\frac{\varrho}{2\sqrt{3}} \qquad x_2^{(2)} = -\frac{\varrho}{2}\left(\cos a + \frac{1}{\sqrt{3}}\sin a\right)$$

$$x_3^{(1)} = \frac{\varrho}{\sqrt{3}} \qquad x_3^{(2)} = \frac{\varrho}{\sqrt{3}}\sin a.$$

$$\lambda = a = 0 \qquad\qquad \lambda = a\,\frac{\pi}{2}$$

$$x_1^{(2)} = \frac{\varrho}{2}, \quad x_2^{(2)} = -\frac{\varrho}{2}, \quad x_3^{(2)} = 0 \qquad x_1^{(2)} = -\frac{\varrho}{2\sqrt{3}}, \quad x_2^{(2)} = -\frac{\varrho}{2\sqrt{3}}, \quad x_3^{(2)} = \frac{\varrho}{2}.$$

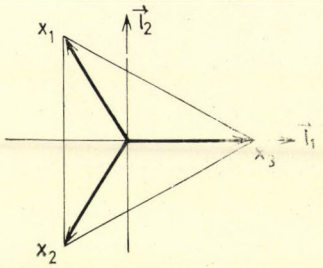

$$\lambda = a = \frac{\pi}{3}$$

$$x_1^{(2)} = 0, \quad x_2^{(2)} = -\frac{\varrho}{2}, \quad x_3^{(2)} = \frac{\varrho}{2}$$

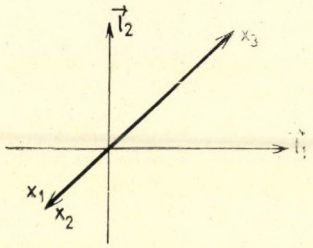

$$\lambda = a = \frac{\pi}{6}$$

$$x_1^{(2)} = \frac{\varrho}{2\sqrt{3}}, \quad x_2^{(2)} = -\frac{\varrho}{\sqrt{3}}, \quad x_3^{(2)} = \frac{\varrho}{2\sqrt{3}}.$$

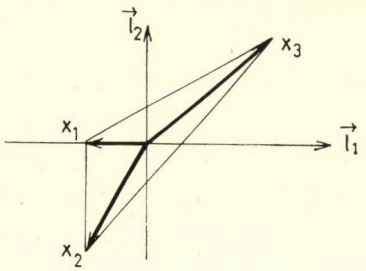

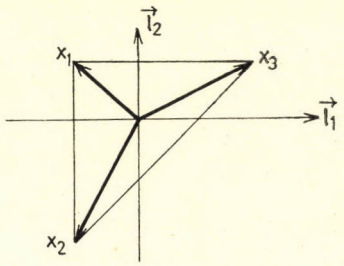

$$\lambda = a = \frac{\pi}{4}$$

$$x_1^{(2)} = \frac{\varrho}{2\sqrt{3}}\left(1 - \frac{1}{\sqrt{3}}\right), \quad x_2^{(2)} = -\frac{\varrho}{2\sqrt{2}}\left(1 + \frac{1}{\sqrt{3}}\right), \quad x_3^{(2)} = \frac{\varrho}{\sqrt{6}}$$

$$\lambda = a = \pi$$

$$x_1^{(2)} = -\frac{\varrho}{2}, \quad x_2^{(2)} = \frac{\varrho}{2}, \quad x_3^{(2)} = 0.$$

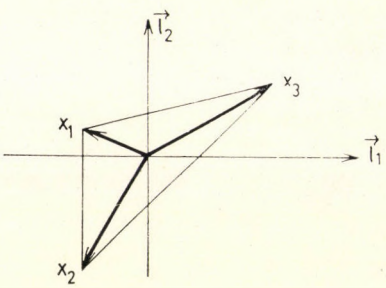

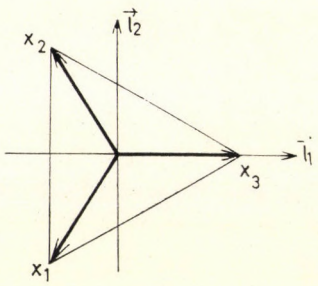

1) $a - \lambda = \dfrac{\pi}{3}$ $\quad x_1^{(1)} = 0$ $\quad x_1^{(2)} = \dfrac{\varrho}{2}\left(\cos\left(\lambda + \dfrac{\pi}{6}\right) - \dfrac{1}{\sqrt{3}}\sin\left(\lambda + \dfrac{\pi}{6}\right)\right)$

$$x_2^{(1)} = -\frac{\varrho}{2} \quad x_2^{(2)} = -\frac{\varrho}{2}\left(\cos\left(\lambda + \frac{\pi}{6}\right) + \frac{1}{\sqrt{3}}\sin\left(\lambda + \frac{\pi}{6}\right)\right)$$

$$x_3^{(1)} = \frac{\varrho}{2} \qquad x_3^{(2)} = \frac{\varrho}{\sqrt{3}}\sin\left(\lambda + \frac{\pi}{6}\right)$$

$$\lambda = 0, \quad a = \frac{\pi}{3}$$

$$x_1^{(2)} = \frac{\varrho}{2\sqrt{3}}, \quad x_2^{(2)} = -\frac{\varrho}{\sqrt{3}}, \quad x_3^{(2)} = \frac{\varrho}{2\sqrt{3}}$$

$$\lambda = \frac{\pi}{6}, \quad a = \frac{\pi}{2}$$

$$x_1^{(2)} = 0, \quad x_2^{(2)} = -\frac{\varrho}{2}, \quad x_3^{(2)} = \frac{\varrho}{2}$$

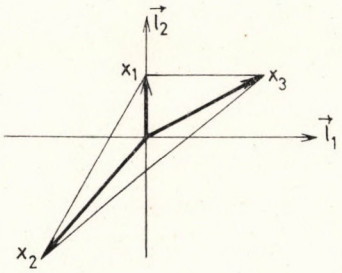

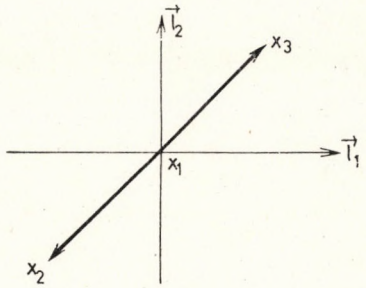

$$\lambda = \frac{\pi}{3}, \quad a = \frac{2\pi}{3}$$

$$x_1^{(2)} = -\frac{\varrho}{2\sqrt{3}}, \quad x_2^{(2)} = -\frac{\varrho}{2\sqrt{3}}, \quad x_3^{(2)} = \frac{\varrho}{\sqrt{3}}$$

$$\lambda = \frac{\pi}{2}, \quad a = \frac{5\pi}{6}$$

$$x_1^{(2)} = -\frac{\varrho}{2}, \quad x_2^{(2)} = 0, \quad x_3^{(2)} = \frac{\varrho}{2}$$

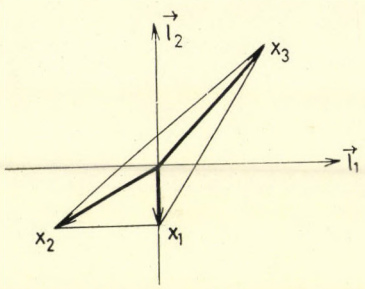

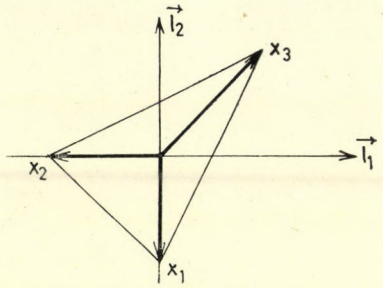

$$\lambda = \frac{2\pi}{3}, \quad a = \pi$$

$$x_1^{(2)} = -\frac{\varrho}{\sqrt{3}}, \quad x_2^{(2)} = \frac{\varrho}{2\sqrt{3}}, \quad x_3^{(2)} = \frac{\varrho}{2\sqrt{3}}$$

$$\lambda = \frac{5\pi}{6}, \quad a = \frac{7\pi}{6}$$

$$x_1^{(2)} = -\frac{\varrho}{2\sqrt{3}}, \quad x_2^{(2)} = -\frac{\varrho}{2\sqrt{3}} \; x_3^{(2)} = \frac{\varrho}{\sqrt{3}}.$$

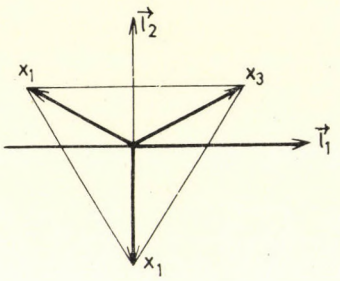

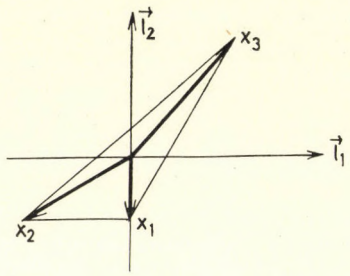

2. *The three-body problem in celestial mechanics (the Laplace case* [10]*). Self-consistent field in classical mechanics*

Suppose that an attractive Newtonian potential is acting between three particles. It can be shown that there exists a solution for which all three particles stay in the vertices of an equilateral triangle while each particle moves along an elliptic trajectory about the common center-of-mass as if there was a central body the mass of which is equal to the sum of masses of the three particles.

Suppose $\dot{a} = \dot{\Theta} = \dot{\varphi}_2$ is equal to zero. If the particles form an equilateral triangle, we have $a = 0$, and the distance between the particles is ϱ. The potential energy in this case is equal to $U = -3/\varrho$, so that the equations of motion take the form

$$\ddot{\varrho}-\varrho\left[\frac{1}{4}\dot{\lambda}^2+\dot{\varphi}_1^2+\dot{\varphi}_1\dot{\lambda}\right]+\frac{3}{\varrho^2}=0,$$
$$\frac{1}{2}\ddot{\lambda}+\ddot{\varphi}_1+\frac{\dot{\varrho}}{\varrho}\dot{\lambda}+\frac{2}{\varrho}\dot{\varphi}_1\dot{\varrho}=0. \tag{54}$$

Introducing a new variable

$$\dot{\psi}=\frac{1}{2}\dot{\lambda}+\dot{\varphi}_1. \tag{55}$$

we obtain the Kepler equations

$$\ddot{\varrho}-\varrho\,\dot{\psi}^2+\frac{3}{\varrho^2}=0,$$
$$\ddot{\psi}+\frac{2}{\varrho}\dot{\varrho}\dot{\psi}=0. \tag{56}$$

If we now express $\vec{x}_1$, $\vec{x}_2$ and $\vec{x}_3$ in terms of ϱ, we get the equations of three ellipses. It is easy to prove that in the case $a \neq 0$ the equations will not lead to the Kepler equations. It should be noted that the type of the solution is independent of the form of the potential; indeed, we use only the fact that the forces acting on any of the three particles are directed to the center-of-mass of the triangle.

REFERENCES

1. W. Zickendrath, Ann. of Phys., **35,** 18,1965; Phys. Rev., **159,** 1448, 1967.
2. J. M. Lévy-Leblond and M. Lévy-Nahas, J. Math. Phys., **6,** 1571, 1965.
3. А. М. Бадалян, Ю. А. Симонов, ЯФ, **3,** 6, 1966.
4. Ю. А. Симонов, ЯФ, **3,** 630, 1966.
5. R. C. Whitten and F. T. Smith, J. Math. Phys., **9,** 1103, 1968.
6. Ю. Нири, Я. А. Смородинский, ЯФ, **9,** 882, 1969.
7. J. Nyiri and Ya. Smorodinsky, JINR Preprint E2-4809, Dubna, 1969; ЯФ, 12, 202, 1970.
8. R. C. Whitten, J. Math. Phys., **10,** 1631, 1969.
9. J. Nyiri and Ya. Smorodinsky, JINR Preprint E2-5067, Dubna, 1970.

СИММЕТРИИ В КЛАССИЧЕСКОЙ ЗАДАЧЕ ТРЕХ ТЕЛ

Ю. НИРИ

Резюме

Классический лагранжиан и уравнения Эйлера задачи трех тел написаны в разных системах координат. Работа дополняет квантовомеханическое рассмотрение, данное раньше.

Acta Physica Academiae Scientiarum Hungaricae, Tomus 32 (1–4), pp. 261–274 (1972)

VARIATIONS OF COSMIC RAY INTENSITY IN CONSEQUENCE OF THE COROTATION EFFECT*

By

A. J. SOMOGYI

DEPARTMENT OF COSMIC RAYS, CENTRAL RESEARCH INSTITUTE OF PHYSICS, BUDAPEST

(Received: 19. X. 1971)

It is shown that corotation of cosmic ray particles with the drift velocity $v_d = \omega_s \times r$, where ω_s is the angular velocity of the rotation of the sun, must also take place outside the solar equatorial plane wherever the general conditions for corotation are fulfilled.

Predicted secondary effects of the corotation are: annual and semi-annual waves in the amplitude of the solar daily variation, a semi-annual wave in the phase of the solar daily variation, and an annual wave and north-south asymmetry in the total intensity of cosmic rays. The possibility of detecting these effects is discussed.

1. Introduction

1.1. The lack of diffusion of cosmic ray particles in directions perpendicular to the regular interplanetary magnetic field supposed to be arranged along Archimedes spirals gives rise to the so-called corotation effect [1, 2, 3] consisting in convection of cosmic ray particles with a drift velocity which, at the orbit of the earth, is known to be

$$\mathbf{v}_d = \boldsymbol{\omega}_s \times \mathbf{r}_e, \tag{1}$$

where $\omega_s = 2{,}7 \cdot 10^{-6}\,\mathrm{sec}^{-1}$ is the average angular velocity of the rotation of the sun and $\mathbf{r}_e$ is the sun–earth distance directed from the sun towards the earth.

The corotation effect has been invoked to account for the anisotropy of cosmic radiation manifested in the solar daily variation (= SDV) of the cosmic ray intensity [1, 2, 3]. There are, however, a few other, smaller effects which can be predicted on the basis of the corotation.

Some of these effects are at the present limit of detectability, others we cannot hope to detect at all yet. But what seems impossible today, may well be feasible tomorrow; at any rate, effects of the same order of magnitude and even of the same character as those to be dealt with in this paper are currently being investigated by many authors. It therefore seems appropriate to call attention to a simple mechanism which is contributing to building up

* Dedicated to Prof. L. JÁNOSSY on his 60th birthday, with best wishes.

phenomena that are currently absorbing much of the interest of cosmic ray investigators.

1.2. The phenomena to be dealt with in this paper are the following:

a) The drift velocity in three-dimensional space (i.e. is Eq. (1) valid at places far outside the solar equatorial plane?);

b) Yearly wave of the amplitude of the SDV;

c) Half-yearly wave of the amplitude of the SDV;

d) Half-yearly wave of the phase of the SDV;

e) Yearly wave of the isotropic part of cosmic ray intensity;

f) North-south asymmetry of cosmic ray intensity (i.e. the relation $I(\Phi,\Lambda) \neq I(-\Phi,\Lambda)$ where $I(\Phi,\Lambda)$ is the intensity of cosmic radiation outside of the magnetosphere in the direction characterized by the geographic coordinates (Φ,Λ)).

In view of the possibility spacecraft provide of making measurements far outside the ecliptic plane it is interesting to see what the corotation velocity sould be like at such places (Section 2). Results of Section 2 must be applied even when calculating corotation effects observed at the earth since the earth moves in a plane slightly different from that of the solar equator. In Sections 3—5 it will be shown that the corotation of cosmic ray particles contributes to the effects b — f observed at the earth. The contributions of corotation to effects c and e have already been discussed by McCracken and Rao [4]. The formula and conclusions they gave are refined in this paper.

1.3. Throughout this paper, the corotation effect will be considered in its simplest form, i.e. complete absence of diffusion in directions perpendicular to the field lines will be assumed, as well as absence of both energy loss and net radial flow of cosmic ray particles. Use will be made of the first approximation formula

$$S(\mathbf{e}) = S(\mathbf{e}_m)\cos\psi\,, \tag{2}$$

where $S(\mathbf{e})$ is the anisotropic part (extra current) of cosmic ray particles in the direction of the unit vector $\mathbf{e}$, and $\mathbf{e}_m$ is the direction in which $S(\mathbf{e})$ is maximum; $\cos\psi = \mathbf{e}\cdot\mathbf{e}_m$. Obviously, $\mathbf{e}_m$ shares the direction of $\mathbf{v}_d$, the corotation velocity.

At relativistic energies, $S(\mathbf{e}_m)$ can be expressed (see e.g. [5]) as

$$S(\mathbf{e}_m) = (2+\mu)(v_d/v)\cdot J\,, \tag{3}$$

where $v \approx c$ is the velocity of the particles, μ is the exponent of their energy spectrum, and J is the isotropic part of the intensity. Taking $\mu = 1{,}65$ and, in the vicinity of the earth, $v_d = 405$ km/sec, Eq. (3) yields $S(\mathbf{e}_m)/J = 0{,}63$ per cent, a value in general agreement with observations.

1.4. The discussion will be restricted to "free space" anisotropy. The actual magnitudes of the effects 1.2 b — f, as they may be observed under

the influence of the earth's magnetic field and atmosphere, can be derived from the "free space" values in the usual way.

2. The drift velocity in three dimensional space

We shall proceed by proving that Eq. (1), derived for conditions near the orbit of the earth, is valid also far away from the ecliptic plane, wherever the usual conditions of corotation, i.e. absence of diffusion across the field lines and zero net radial flux of particles, are fulfilled.

Let P be an arbitrary point within the modulation region where these conditions are met, and $\mathbf{r}$ be the radius vector pointing from the sun to P. It will be shown that the drift velocity of cosmic ray particles at the point P is

$$\mathbf{v}_d = \boldsymbol{\omega}_s \times \mathbf{r} .$$

To prove this, we must first determine the shape of the magnetic field line passing through P. The inclination of $\mathbf{r}$ to the equatorial plane of the sun should be denoted by $\varphi^{(h)}$. Because of the rotation of the sun, the field line passing through P will be twisted round a cone with an opening angle $\pi/2-\varphi^{(h)}$. It can easily be seen that the equation of a magnetic field line in a heliocentric system with x and y axes lying in the solar equatorial plane can be written in the form

$$x = \frac{w}{\omega_s}(\lambda_0^{(h)} - \lambda^{(h)}) \cos \varphi^{(h)} \cos \lambda^{(h)},$$

$$y = \frac{w}{\omega_s}(\lambda_0^{(h)} - \lambda^{(h)}) \cos \varphi^{(h)} \sin \lambda^{(h)},$$

$$z = \frac{w}{\omega_s}(\lambda_0^{(h)} - \lambda^{(h)}) \sin \varphi^{(h)},$$

$$\lambda^{(h)} < \lambda_0^{(h)},$$

where $\lambda^{(h)}$, the heliolongitude, is the parameter of the equation; $\varphi^{(h)}$, the heliolatitude, is constant; w is the velocity of the solar wind, and $\lambda_0^{(h)}$ is the heliolongitude at which $r = \sqrt{x^2+y^2+z^2} = 0$.

A simple calculation shows that the components of the unit vector $\mathbf{e}'$ pointing along the tangent of the field line in the sense corresponding to the movement towards the sun are

$$\begin{aligned} e'_x &= -(\beta x + y)/d, \\ e'_y &= (x - \beta y)/d, \\ e'_z &= -\beta z/d, \end{aligned} \tag{4}$$

where

$$\beta = \frac{w}{r\omega_s} = \frac{1}{\lambda_0^{(h)} - \lambda^{(h)}} > 0\,,$$

and

$$d = \sqrt{x^2 + y^2 + \beta^2 r^2} > 0\,.$$

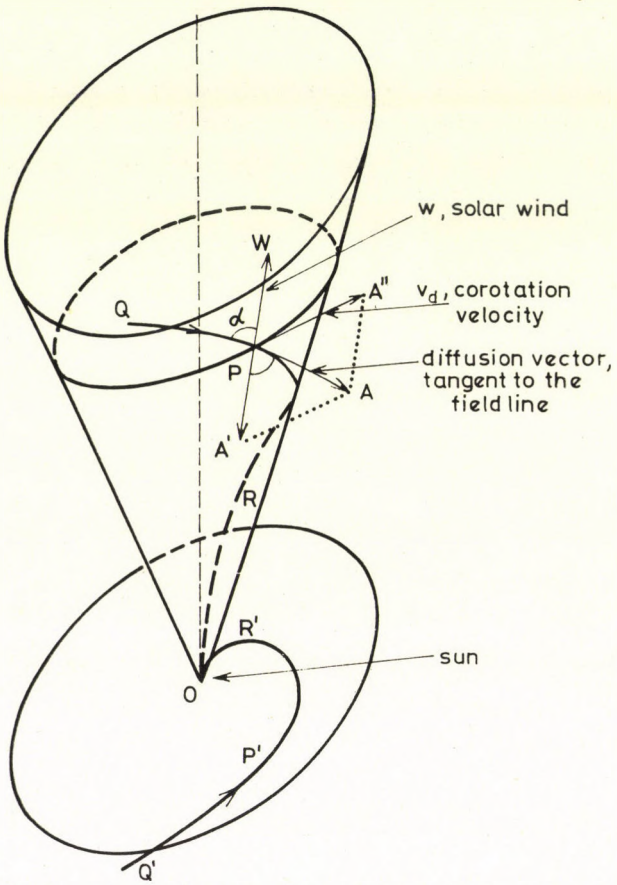

Fig. 1. Diagram showing the production of corotation in three dimensions. The curved ORPQ line is a magnetic field line, OR'P'Q' its projection onto the solar equatorial plane. PA'AA" defines a plane tangent to the cone. PA' is the orthogonal projection of PA, the diffusion vector, onto OP = r. PA' = PW if there is no net radial flow of particles

The value and direction of $\mathbf{v}_d$ can be determined on the basis of the assumptions that: a) diffusion of cosmic ray particles takes place along field lines only; and b) there is no net flux of cosmic ray particles along $\mathbf{r}$. These conditions imply (see Fig. 1) that $\mathbf{v}_d$ must be in the plane determined by $\mathbf{r}$ and $\mathbf{e}'$ i.e.

$$\begin{vmatrix} v_{d,x} & v_{d,y} & v_{d,z} \\ x & y & z \\ e'_x & e'_y & e'_z \end{vmatrix} = 0\,, \qquad (5)$$

and must be perpendicular to $\mathbf{r}$, i.e.

$$x\,v_{d,x}+yv_{d,y}+zv_{d,z}=0\,. \tag{6}$$

A simple calculation based on Eqs. (5) and (6) shows that $\mathbf{v}_d$ must be parallel to the solar equatorial plane (i.e. $v_{d,z}=0$) and tangential to the parallel circle with the radius

$$\sqrt{x^2+y^2}=r\cos\varphi^{(h)}\,.$$

It can be seen from Fig. 1 that

$$v_d=w\tan\alpha\,,$$

where

$$\cos\alpha=-\mathbf{e}'\mathbf{r}/r\,. \tag{7}$$

On the basis of Eqs. (4) and (7) we have

$$\tan\alpha=(\lambda_0^{(h)}-\lambda^{(h)})\cos\varphi^{(h)}\,,$$

and thus

$$v_d=r\omega_s\cos\varphi^{(h)}. \tag{8}$$

This, together with the direction of $\mathbf{v}_d$, proves that

$$\mathbf{v}_d=\boldsymbol{\omega}_s\times\mathbf{r}.$$

This is the velocity of a point fixed rigidly to the sun at the end of the radius vector $\mathbf{r}$. Thus $\mathbf{v}_d$ may be called "corotation velocity" in the three dimensional case also.

The direction of the anisotropy vector of cosmic rays is that of $\mathbf{v}_d$. It is thus everywhere parallel to the solar equator and tangential to the parallel circle. The amount of anisotropy is proportional to $\cos\varphi^{(h)}$, i.e. the cosine of the heliolatitude.

3. Derivation of the general formula for the corotation effect in free space

3.1. A detector viewing in the asymptotic direction $\mathbf{e}$ is sensitive to the extra current of cosmic ray particles

$$S(-\mathbf{e})=S(\mathbf{e}_m)\cos\psi\,,$$

with

$$\cos\psi=-\mathbf{e}\cdot\mathbf{e}_m$$

and (compare Eqs. [3] and [8])

$$S(\mathbf{e}_m) = (2+\mu)\frac{r\omega_s}{v} J \cos\varphi^{(h)},$$

where J is the isotropic part of the cosmic ray intensity, r and $\varphi^{(h)}$ are the heliodistance and heliolatitude, respectively, of the point of observation. The relative change of intensity as a consequence of corotation is thus

$$\frac{\Delta J}{J} = (2+\mu)\frac{r\omega_s}{v}\cos\varphi^{(h)}\cos\psi, \tag{9}$$

or in vectorial form

$$\frac{\Delta J}{J} = -\frac{2+\mu}{v}\mathbf{e}(\boldsymbol{\omega}_s \times \mathbf{r}). \tag{10}$$

In the case of observations made at the earth this reduces to

$$100\,\frac{\Delta J}{J} \approx 0{,}63\cos\varphi^{(h)}\cos\psi.$$

The problem consists of determining $\cos\varphi^{(h)}$ and $\cos\psi$.

3.2. Solar ecliptic coordinates will be used in what follows: hence φ will denote the ecliptic latitude ($\varphi = 0$ in the ecliptic plane) and λ the ecliptic longitude ($\lambda = 0$ for a vector pointing from the sun towards the place of the earth at the autumnal equinox; see Fig. 2). Let us restrict the discussion to observations made at the earth. It is easy to see that in this case

$$\cos\varphi^{(h)} = [1 - \sin^2\vartheta_s \sin^2(\lambda - \lambda_s)]^{1/2},$$

where ϑ_s is the inclination of the rotational axis of the sun to the direction normal to the ecliptic, and λ_s is the ecliptic longitude of the position of the earth when it crosses the equatorial plane of the sun in a direction inclined to the south of the solar equatorial plane. It is known that

$$\vartheta_s = 7{,}25°, \quad \text{and} \quad \lambda_s = 75{,}36°, \tag{11}$$

see e.g. [6].

The solar ecliptic latitude and longitude of the direction $\mathbf{e}_m$, which is the same as that of $\mathbf{v}_d$, should be denoted by (φ_m, λ_m). It can be shown that

$$\begin{aligned} \cos\lambda_m &= -\sin\lambda, & \sin\lambda_m &= \cos\lambda, \\ \cos\varphi_m &= \cos\vartheta_s/\cos\varphi^{(h)}, & \sin\varphi_m &= \sin\vartheta_s\cos(\lambda-\lambda_s)/\cos\varphi^{(h)}. \end{aligned} \tag{12}$$

3.3. **e**, the asymptotic direction of viewing of the detector, will be characterized by Φ, the (asymptotic) declination, and t, the angle by which the half-plane of the midnight meridian must be turned in the sense of the rotation of the earth to bring it into the position parallel to **e**. t has thus the character of a real solar time. It may be called the real solar time of the direction **e**, expressed in angular units (degrees). t is related to t', the solar mean time of the place of observation in the following way:

$$t = t' - \varepsilon - \eta, \tag{13}$$

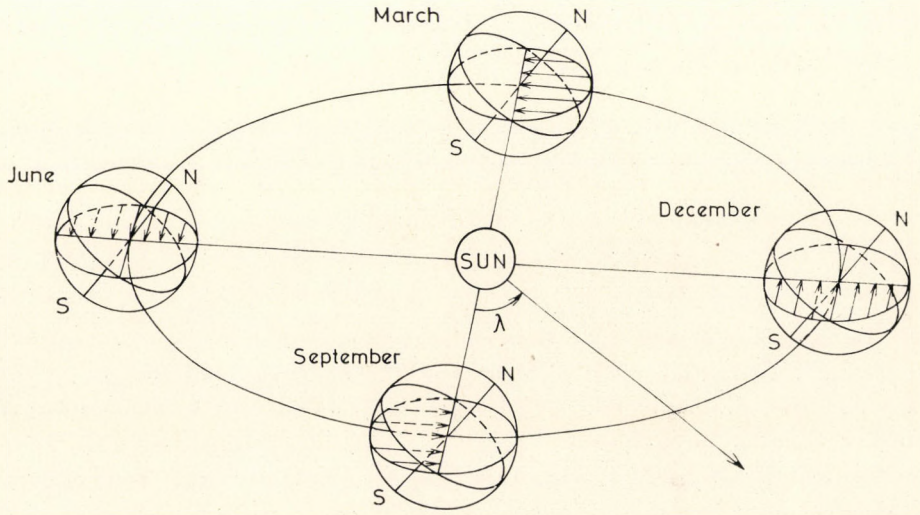

Fig. 2. Diagram showing the relative position of the equator to the direction of corotation throughout a year. The corotation direction is shown by arrows

where ε accounts for the magnetic deflection of the particles observed and η is the difference of the solar mean time and the real solar time.

Transforming the local equatorial coordinates (Φ, t) into ecliptic ones and calculating the angle of this direction formed with that of the corotation, one arrives at the conclusion that

$$\cos\varphi^{(h)} \cos\psi = B \cos\Phi \,[C \sin^2\chi \sin\lambda \cos\lambda \cos t - \\ - D \cos\chi \sin t] - C \sin\Phi \sin\chi \cos\lambda\,, \tag{14}$$

where

$$\chi = 23{,}45° \tag{15}$$

is the angle of the rotation axis of the earth to the normal direction of the ecliptic, while

$$B = (1-\sin^2\chi\sin^2\lambda)^{-1/2},$$
$$C = \cos\vartheta_s+\sin\vartheta_s\cos(\lambda-\lambda_s)/(\tan\chi\cos\lambda),$$
$$D = \cos\vartheta_s-\sin\vartheta_s\cos(\lambda-\lambda_s)\tan\chi\cos\lambda.$$

Note that by neglecting the inclination of the rotation axis of the sun to the normal direction of the ecliptic (i.e. by putting $\vartheta_s = 0$) we have $C = D = 1$. However, this inclination does have a small effect on corotation phenomena, as can be seen from Eq. (14).

On the basis of Eq. (14), the corotation effect (Eq. (10)) may be written as

$$\frac{\Delta J}{J} = S_m B\cos\Phi[C\sin^2\chi\sin\lambda\cos\lambda\cos t - D\cos\chi\sin t] - \\ - S_m C\sin\Phi\sin\chi\cos\lambda, \tag{16}$$

where the notation

$$S_m = (2+\mu)\frac{r\omega_s}{v} \approx 0{,}0063 \tag{16/a}$$

has been used for abbreviation.

An error of the order of $5.\ 10^{-3}$ in $\cos\varphi^{(h)}\cos\psi$ gives rise to an error of $\approx 3.10^{-5}$ in $\Delta J/J$ and may thus be neglected. Taking into account the numerical values of ϑ_s, λ_s, and χ (Eqs.[11]) and [15]), we may write, to an accuracy of better than $5.\ 10^{-3}$ that

$$B = 1{,}043-0{,}044\cos 2\lambda,$$

and thus

$$\frac{\Delta J}{J} = S_m\cos\Phi[(0{,}024+0{,}088\sin 2\lambda-0{,}024\cos 2\lambda)\cos t + \\ +(-0{,}943+0{,}025\sin 2\lambda+0{,}047\cos 2\lambda)\sin t] - \\ - S_m\sin\Phi[0{,}112\sin\lambda+0{,}423\cos\lambda]. \tag{17}$$

4. The solar daily variation

4.1. On the basis of Eq. (16), the amplitude of the SDV may be written as

$$a(\Phi,\lambda) = BS_m\cos\Phi[C^2\sin^4\chi\sin^2\lambda\cos^2\lambda+D^2\cos^2\chi]^{1/2},$$

or, on the basis of Eq. (17),

$$a(\Phi,\lambda) = 0{,}945\,S_m\cos\Phi[1+0{,}055\sin(2\lambda-116°)]. \tag{18}$$

It can be seen that the amplitude has a semiannual wave showing maximum changes of $\pm 5{,}5$ per cent of the amplitude itself. Times of maxima are 4th of January and 5th of July, approximately.

If the sun's axis were perpendicular to the ecliptic, the times of maxima would be 22nd of December and 23rd of June, as can be seen qualitatively from Fig. 2, which shows that the direction of corotation is parallel to the equator in December and June and has its maximum inclination to the equator in March and September. Hence the inclination of the sun's axis to the normal of the ecliptic causes the times of maxima of $a(\Phi, \lambda)$ to be delayed by about two weeks.

4.2. $a(\Phi, \lambda)$ the amplitude of the SDV has an annual wave as well, for the following reasons:

Eq. (9) shows that $\Delta J/J$ i.e. the relative change of intensity of cosmic ray particles, is proportional to r. This means simply that a rigid corotation with the sun must have larger velocities at larger distances from the sun. Now, the sun—earth distance displays a variation of $\pm 1{,}7$ per cent in a year because of the excentricity of the orbit of the earth, while r is maximum on the 2nd of July ($\lambda = 280°$) and minimum on the 1st of January ($\lambda = 100°$).

Thus

$$S_m = S_0[1 - 0{,}017 \sin(\lambda - 10°)].$$

Combining this with Eq. (18), we have, to the accuracy required:

$$a(\Phi, \lambda) = 0{,}945\, S_0 \cos\Phi[1 - 0{,}017 \sin(\lambda - 10°) + 0{,}055 \sin(2\lambda - 116°)]. \quad (19)$$

To illustrate the relative variation of $a(\Phi, \lambda)$ throughout a year as a consequence of variation of the value of the corotation velocity and its direction relative to that of the rotation axis of the earth the trigonometric function within the brackets of Eq. (19) is plotted in Fig. 3. It can be seen from this that the summer maximum of $a(\Phi, \lambda)$ is increased and amounts to about 7 per cent, whereas the winter maximum is decreased. There is a peak-to-peak change of about 12 per cent in $a(\Phi, \lambda)$ withinthe three month's period between about the 1st of April and the 1st of July.

4.3. The phase of the SDV may be expressed, on the basis of Eq. (14), as

$$\tan\tau = -C \sin^2\chi \sin\lambda \cos\lambda/(D \cos\chi),$$

or, on the basis of Eq. (17), as

$$\tan\tau = \frac{0{,}024 + 0{,}088 \sin 2\lambda - 0{,}024 \cos 2\lambda}{-0{,}943 + 0{,}025 \sin 2\lambda + 0{,}047 \cos 2\lambda} \approx \quad (20)$$

$$\approx -0{,}025 - 0{,}094 \sin 2\lambda + 0{,}024 \cos 2\lambda.$$

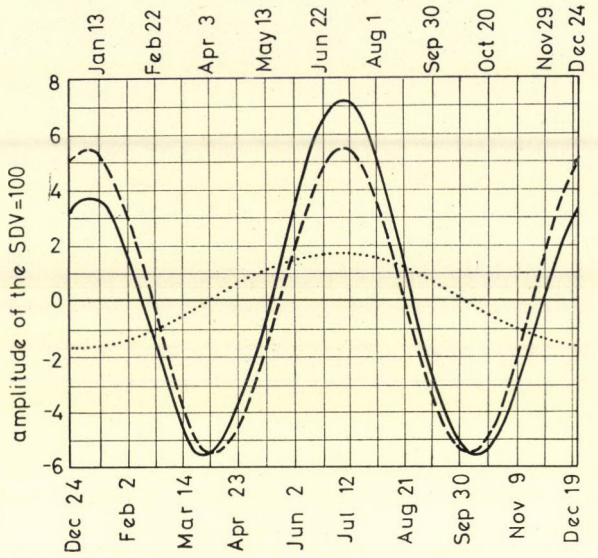

Fig. 3. Relative change of the amplitude of SDV in consequence of corotation: the trigonometric function within the brackets of Eq. (19).Curve I: annual wave with an amplitude of 1,7 per cent of the amplitude of the SDV. Curve II: semi-annual wave with an amplitude of 5,5 per cent of the amplitude of the SDV. Curve III: sum of I and II

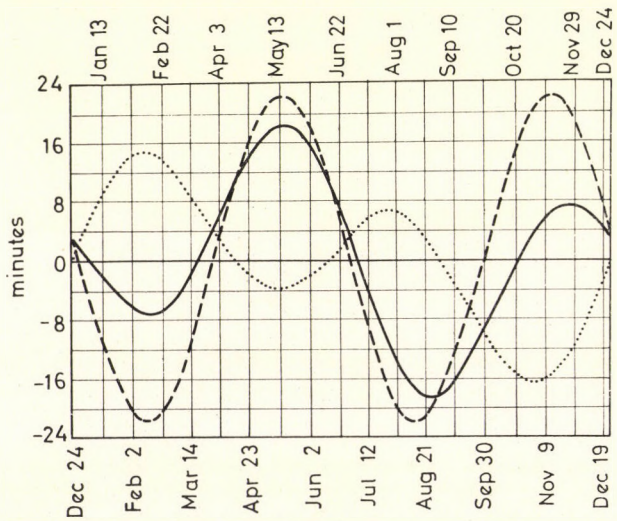

Fig. 4. Solid line: Annual change of the time of maximum (solar mean time) of the "free space" SDV. Dotted line: The same in real solar time, i.e. the trigonometric function on the RHS of Eq.(21). Dashed line: η, i.e. the difference of the solar mean time and the real solar time

Eq. (20) yields

$$t_m = 18^h\,06^{\min} + 22^{\min} \sin(2\lambda - 15°)$$

for the time of maximum of the SDV. t_m is expressed in "real solar time of the asymptotic direction of observation" (see Section 3.3). The time of maximum as expressed in local solar *mean* time of the point of observation will be (see Eq. (13) where the meanings of the symbols are also explained)

$$t'_m = \varepsilon + \eta + 18^h\,06^{\min} + 22^{\min} \sin(2\lambda - 15°). \tag{21}$$

The time-dependent part of the right-hand side of Eq. (21) is plotted in Fig. 4. It can be seen that there is a greater and a smaller maximum and similar minima in the yearly run of t'_m. The fastest change takes place between mid-May and mid-August: there is a successive retardation of about 36 minutes in the time of maximum of the SDV during these three months.

4.4. The effects reported on in this Section are of the order of 10^{-4} in the total intensity of radiation, and would thus be very difficult to detect. In addition, the variability of the direction and scattering efficiency as well as distortions of the spherical symmetry of the solar wind and the magnetic field frozen in to it may produce variations of the amplitude and phase of the SDV larger than those mentioned above.

Nevertheless, the effects described here certainly contribute to the variability of the amplitude and phase of the SDV. By the use of powerful detectors operating over very long undisturbed periods of several months, even the net effects might be revealed.

5. The annual wave and north-south asymmetry of cosmic ray intensity

5.1. The last term in the expression of $\Delta J/J$ (Eq (16)) should be denoted by $F(\Phi, \lambda)$:

$$F(\Phi, \lambda) = -S_m C \sin\Phi \sin\chi \cos\lambda. \tag{22}$$

This is independent of t and represents an annual change of the total intensity of cosmic radiation. Using numerical values (Eq. (17)), we have, to an accuracy of better than $1 \cdot 10^{-2}$,

$$F(\Phi, \lambda) = -0{,}44\, S_m \sin\Phi \cos(\lambda - 15°).$$

The relative amplitude of the annual wave represented by $F(\Phi, \lambda)$ is thus

$$\left(\frac{\Delta J}{J}\right)_{\text{annual amplitude}} \approx 0{,}28 \sin\Phi \text{ per cent},$$

with the time of maximum in the northern hemisphere falling on about the 5th of April, i.e. at about the *vernal* equinox (*not* the autumnal one; compare [4]).

Without the inclination of the sun's axis to the normal of the ecliptic, the maximum in the northern hemisphere would have been exactly at the vernal equinox. This can be seen, qualitatively, from Fig. 2 which shows that detectors in the northern hemisphere look at smaller angles to the anti-corotation direction in March than they do in September.

5.2. There are several other causes producing an annual wave of the cosmic ray intensity.

The seasonal variation of the atmospheric temperature should be mentioned in the first place. The mesonic component of cosmic radiation suffers an annual variation of the order of several per cent in consequence of atmospheric temperature changes. It seems to be hopeless to detect another sinusoidal wave simultaneously with an amplitude at least an order of magnitude smaller, even though there is a considerable phase lag between the two waves. The situation is much better with the nucleonic component, as the temperature effect of this is negligible. Yearly amplitudes of a few tenths of a per cent might be detected by neutron monitors with sufficient stability and statistical accuracy.

Other causes producing annual wave in the cosmic ray intensity are the following: a) the combined effect of the radial gradient of cosmic ray density in interplanetary space and the excentricity of the orbit of the earth, and b) the combined effect of the gradient of cosmic ray density perpendicular to the solar equatorial plane and the inclination of the ecliptic to the solar equatorial plane. These effects have been considered in a paper of SCHNEIDER and KORFF [7].

Eq. (22) (i.e. the underlying Eq. (16)) shows that the problem is still more complex: the variation of the angle between the earth's axis and the corotation direction constitutes a further, not negligible, source for the annual wave.

5.3. Eq. (16) also shows that the distribution of cosmic ray intensity is not symmetric with respect to the equator of the earth. Denoting by $(\Delta J)_{N-S}$ the difference

$$(\Delta J)_{N-S} = J(\Phi, \Lambda) - J(-\Phi, \Lambda)$$

of cosmic ray intensities measured in the asymptotic directions with geographic coordinates (Φ, Λ) and $(-\Phi, \Lambda)$, Eq. (16) shows that

$$(\Delta J)_{N-S}/J = -2S_m C \sin\Phi \sin\chi \cos\lambda,$$

or, on the basis of Eq. (17),

$$(\Delta J)_{N-S}/J = -0{,}55 \sin\Phi \cos(\lambda - 15^\circ) \text{ per cent.}$$

The north-south asymmetry depends on λ, i.e. on the season; it changes sign in January and July. Its maximum value amounts to about 0,55 sin Φ per cent and is reached in April. This asymmetry is a consequence of the fact that in the northern hemisphere the yearly wave described by Eq. (16) has a phase exactly opposite to that in the southern hemisphere. This suggests one way in which the asymmetry could be detected. Another way would be to intercalibrate two identical detectors, situated on different hemispheres, by means of a third, movable one.

North-south asymmetry can be produced by a gradient of cosmic ray density in a direction inclined to the equatorial plane of the earth, and especially by shock waves in the solar wind. Many investigations have been carried out along this line (see e.g. [8—12]). Eq. (16) points towards another mechanism which must not be neglected when analyzing north-south asymmetries.

6. Conclusion

A general formula has been derived for describing the effect of corotation of cosmic ray particles upon their intensity as observed on the rotating earth. The relative changes of intensity due to corotation are given in Eq. (10), (16), and — in numerical form — in Eq. (17).

Eq. (10) could be used to express cosmic ray intensity variations observed on a rotating spacecraft at any place within the solar system where corotation takes place.

So far as observations made at the earth are concerned, a number of interesting phenomena (viz. those listed in Section 1.2) can be predicted on the basis of Eq. (16). Although these effects have been studied experimentally by many authors, none of them is yet understood completely. It is the purpose of this paper to draw attention to another mechanism contributing to their development.

The north-south asymmetry dealt with in Section 5.3. deserves special interest. For it follows from the arguments presented that a certain amount of north-south asymmetry should prevail even in completely undisturbed periods. For polar looking stations and undisturbed periods, its maximum value amounts to about 0,5 per cent, which should not be difficult to detect by intercalibrating the two detectors.

Acknowledgement

The author wishes to express his high appreciation and great indebtedness to Professor L. JÁNOSSY for his expert guidance and friendly collaboration over many fruitful years.

REFERENCES

1. E. N. Parker, Planet. Space Sci., **12,** 735, 1964.
2. W. I. Axford, Planet. Space Sci., **13,** 115, 1965.
3. E. N. Parker, Proc. 9th Int. Conf. on Cosmic Rays London, The Inst. of Phys. and the Phys. Soc., **1,** 26, 1965.
4. K. G. McCracken and U. R. Rao, ibid., **1,** 213, 1965.
5. L. J. Gleeson and W. I. Axford, Astrophys. and Space Sci., **2,** 431, 1968.
6. C. W. Allen, Astrophysical Quantities, The Athlone Press, University of London, 1955.
7. S. M. Schneider and S. A. Korff, Proc. 11th Int. Conf. on Cosmic Rays, Budapest, Acta Phys. Hung., **29,** Suppl. **2,** 163, 1970.
8. N. Iucci and M. Storini, 12th Int. Conf. on Cosmic Rays, Hobart, Conference Papers, **2,** 588, 1971.
9. A. Hashim and M. Bercovitch, ibid., **2,** 596, 1971.
10. C. J. Hatton and M. C. Barker, ibid., **2,** 603, 1971.
11. S. P. Duggal and M. A. Pomerantz, ibid., **2,** 723, 1971.
12. S. P. Duggal and M. A. Pomerantz, Proc. 11th Int. Conf. on Cosmic Rays, Budapest, Acta Phys. Hung. **29,** Suppl., **2,** 351, 1970.

ВАРИАЦИИ ИНТЕНСИВНОСТИ КОСМИЧЕСКИХ ЛУЧЕЙ В РЕЗУЛЬТАТЕ ВРАЩАТЕЛЬНОГО ЭФФЕКТА

А. Й. ШОМОДИ

Резюме

В статье показано, что вращение частиц космического излучения с дрейфующей скоростью $v_d = \omega_s \times r$, где ω_s является угловой скоростью вращения солнца имеет место также и вне плоскости солнечного экватора, если выполнены общие условия вращения.

Вторичные эффекты вращения предсказаны: годовая и полугодовая волна в амплитуде суточной солнечной вариации, полугодовая волна в фазе суточной солнечной вариации, годовая волна и асимметрия север-юг в полной интенсивности космических лучей. Рассматривается также и возможность детектирования этих эффектов.

Acta Physica Academiae Scientiarum Hungaricae, Tomus 32 (1—4), pp. 275—287 (1972)

LOW LIGHT INTENSITY INVESTIGATIONS ON THE PHOTOELECTRIC EFFECT*

By

L. CSILLAG, M. JÁNOSSY and ZS. NÁRAY

CENTRAL RESEARCH INSTITUTE FOR PHYSICS, BUDAPEST

(Received 19. X. 1971)

Various features of the photoelectric effect were examined in a direct manner by irradiating very short light pulses of low intensity on to the photo-cathode of a photomultiplier. It was shown that the probability of the emission of a photo-electron during a time τ is proportional to the light energy absorbed by the photo-cathode, even when the absorbed energy is less than $h\nu$. The possibility of light energy accumulation occurring in the photoelectric effect process was also investigated. It was verified that during time intervals of the order of 10^{-9} sec such an energy accumulation phenomenon does not exist. Time statistical measurements of the emitted photo-electrons showed that these are released from the photo-cathode at random.

Introduction

The question of the nature of light has received great attention throughout the history of physical research but was taken up with renewed interest after the particle-wave duality problem was dealt with by quantum mechanics [1]. Although quantum-mechanics gave a satisfactory mathematical description of the phenomena, the consequences of the formal mathematical solution of the duality problem have been the subject of controversy ever since. Also experimental confirmation of the phenomena described by quantum theory was rather weak. Attention was drawn to the importance of these questions by L. JÁNOSSY, who for this reason started together with co-workers a series of experiments. The first of these experiments performed by A. ÁDÁM, L. JÁNOSSY and P. VARGA [2], based on a somewhat primitive photon concept, investigated the question of whether or not photons are split when a light beam is divided by a semi-transparent mirror into two coherent components. As only accidental coincidences were found between the pulses of two photomultipliers detecting the photons travelling in the two light beams, the experiment reinforced the particle interpretation, that photons are not split but take either one or the other path. In a second experiment, however, L. JÁNOSSY and ZS. NÁRAY [3] found that when they put mirrors in place of the two photomultipliers, so that the whole system formed a Michelson interferometer, interference took place even if only a single photon at a time was present in the interferometer.

* Dedicated to Prof. L. JÁNOSSY on his 60th birthday.

The conflicting results can be reconciled by assuming that light consists of classical electromagnetic waves and that the probability dp of a photo-electron being released by photoelectric effect from a photocathode during a time dt is proportional to the instantaneous light intensity $I(t)$:

$$dp = \alpha I(t)dt, \tag{1}$$

where the proportionality constant α denotes the efficiency of the photo-cathode.

Seen in the framework of this semi-classical picture the interference phenomenon is thus explained by the wave nature of light, while in the beam-splitting experiment the probabilities of the emission of photo-electrons from the two photomultipliers by two light beams of constant intensity in various intervals of time are independent, and so only accidental coincidences should occur, in agreement with the finding of ÁDÁM et al.

A more comprehensive theoretical analysis of the latter phenomenon by L. JÁNOSSY [4] took into account the fact that a real light beam shows fluctuations, which are caused mainly by the interference of wave bands emitted by individual atoms of the light source. If such a fluctuating light beam is divided by a semi-transparent mirror, the two components are coherent and show identical fluctuations and so should produce an enhancement of photo-electron pulse coincidences, unlike the case when two detecting photomultipliers are irradiated with incoherent light beams and only random coincidences occur. The rate of excess coincidences is closely connected with the coherence time of the light beam, which is of the same order of magnitude as the period of the fluctuations.

Measurements by GY. FARKAS, L. JÁNOSSY, ZS. NÁRAY and P. VARGA [5] verified the existence of excess coincidences and the experimental results showed a very good quantitative agreement with those predicted by the semi-classical theory.

The excess photo-electron coincidences are due to the fact that when two coherent light beams are incident on the two photo-cathodes, light fluctuations are in phase and simultaneous emission of photo-electrons occurs with a higher probability. The energy contained in the light beam during the average period of a fluctuation can be calculated with the following expression:

$$E = \frac{N\tau h\nu}{\alpha}, \tag{2}$$

where α denotes the efficiency of the photo-cathode used, N the number of photo-electron pulses registered in unit time, τ the average period of fluctuations and $h\nu$ the energy of the light quanta. With $N = 5 \cdot 10^4$ sec^{-1}, $\tau = 10^{-9}$ sec and $\alpha = 5 \cdot 10^{-2}$, we obtain

$$E = 10^{-3} h\nu,$$

which is much smaller than the energy corresponding to a single photon. This result supports the assumption that the release of a photo-electron by photo-electric effect is an instantaneous process the probability of whose occurrence is proportional to the instantaneous intensity of light, as expressed in (1). At low light intensities, however, the possibility of a different phenomenon arises, for it could be argued that under these conditions electrons gradually accumulate enough energy through excitation to escape from the photo-cathode. The early experiments of E. O. LAWRENCE and J. W. BEAMS [6] which showed that photo-electrons leave the photo-cathode immediately after the beginning of light irradiation in a time shorter than 3×10^{-9} sec did not shut out this possibility as the measurements were performed with light pulses of high intensity. The light-beating experiment of A. T. FORRESTER, R. A. GUDMUNSEN and P. O. JOHNSON [7] indicated that the photo-electron emission time is shorter than 10^{-10} sec, although their conclusion is somewhat questionable, since it was obtained in a rather indirect way.

In view of the importance of these considerations, it seemed to be necessary to carry out further experiments on the nature of light, namely to investigate the considered fundamental features of photoelectric effect in as direct a manner as possible. We therefore carried out a series of experiments using very short light pulses to verify the basic assumption of semi-classical theory on the emission of photo-electrons and to investigate the question of light energy accumulation within clear experimental conditions.

I. Experiment for verification of relation (1)

The experimental task is to show that by photoelectric effect the probability of the emission of a photo-electron is proportional to the instantaneous intensity of light. To connect (1) with quantities convenient for a direct experiment, consider a light pulse of duration τ falling on a photo-cathode. The probability P that a photo-electron will be released by the light pulse according to (1) is

$$P = \alpha E, \tag{3}$$

where $E = \int_0^\tau I(t)\,dt$ is the energy absorbed by the photocathode.

We have carried out the following experiment aiming to verify relation (3): the photo-cathode of a photomultiplier was irradiated with very short light pulses and the number of photo-electrons released in unit time was counted as a function of the energy of the incident light pulses.

This experiment was originally planned in the course of the earlier investigations of L. JÁNOSSY et al. but could not be carried out at that time, due to limitations following from the use of the conventional light sources then

available. The main problem from the experimental point of view was the generation of sufficiently short, uniform light pulses within carefully controllable circumstances. The method adopted [9] in the present experiment was to sweep the light beam of a He—Ne gas laser across a narrow slit using the system of a multisided rotating mirror surrounded by stationary mirrors depicted in Fig. 1.

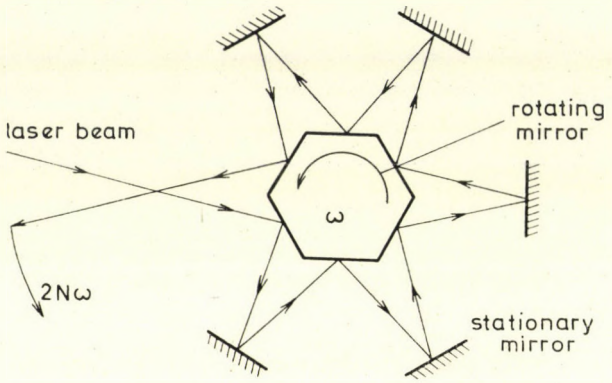

Fig. 1. Scheme of the rotating mirror system used for generation of light pulses

The energy of a single light pulse was determined by means of the expression

$$E = \gamma \frac{sW}{vhv}, \tag{4}$$

where the energy E is obtained in units of light quanta and the other symbols denote the following quantities:

v = velocity of light beam sweeping across the slit;
s = width of slit;
W = power carried in the non-rotating light beam;
hv = energy of light quanta;
γ = degree of attenuation.

Dark-current pulses in the detecting photomultiplier greatly disturb the measurements, since they resemble the pulses produced by the photo-electrons released by low intensity light pulses. The dark current was reduced by a factor of 10 by using magnetic defocusing [10] and the residual effects further diminished by application of a gating technique that activated the electronic counting system only at times when light pulses were actually incident on the photo-cathode. The gating was achieved by splitting the laser beam into two

parts at a semi-transparent mirror to produce simultaneously a gate light pulse for the coincidence circuit connected to the photomultiplier detecting the low-intensity light pulses.

Experimental arrangement

The apparatus is built up of two main parts: 1) an optical part for generation of light pulses, and 2) electronics for detection of photo-electrons released by low-intensity light pulses. (See Fig. 2)

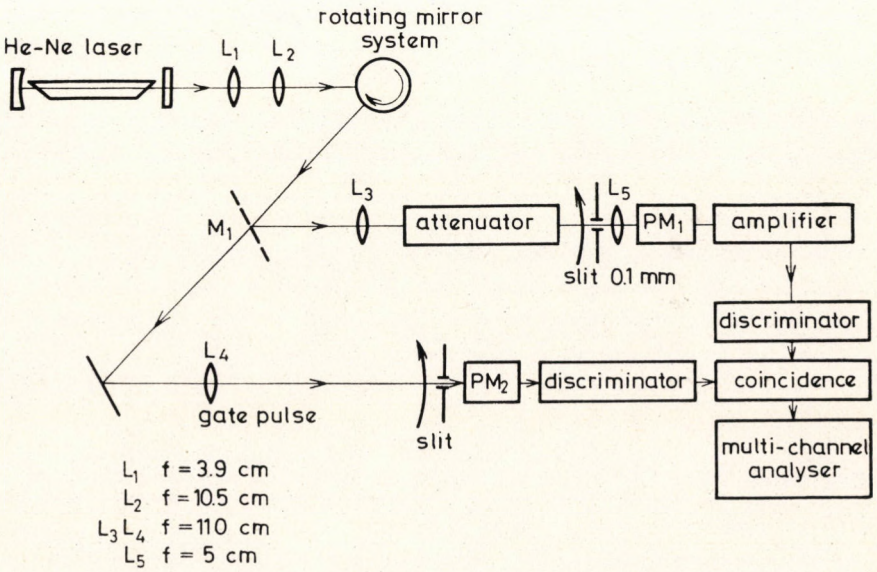

Fig. 2. Experimental arrangement for measurement of photo-electron emission probability

The light source was a d.c. excited He—Ne gas laser operating at $\lambda =$ $= 6328$ Å and 0.6 mW power. The inner diameter of the discharge tube was 2 mm, the laser resonator consisted of a large radius spherical mirror and flat mirror. This resonator configuration ensured TEM_{00} mode oscillation and a light beam of small divergence. The two mirrors were fixed to each other with four hollow invar rods through which water of constant temperature was run to stabilize the output power of the laser. Two lenses L_1 and L_2 helped to reduce beam divergence to the value of $\Theta = 2.5 \times 10^{-4}$ rad measured at half-intensity points of the beam. A semi-transparent mirror M_1 (reflectivity $= 30\%$) split the laser beam into two parts, the beam of higher intensity being used to produce the gate light pulse. Lenses L_3 and L_4 focused the light beams to obtain high intensity on the slits placed in front of the two photomultipliers PM_1 and

PM_2 detecting the low-intensity light pulses and gate light pulses, respectively. After passing through the slit the attenuated light beam was focused with lense L_5 directly on to the cathode of PM_1. The attenuator consisted of two parts: light was first attenuated by a filter (transmission $= 2 \cdot 10^{-3}$) and then passed through a system consisting of three polarizers [11]. By rotating the middle polarizer attenuation could be varied between 1 and 10^{-3} while keeping polarization state of light and geometry of the apparatus constant. A series of apertures was also placed in the path of the light beams to prevent as much as possible stray light from reaching the photomultipliers.

An electric motor spun the hexagonal rotating mirror at 7.700 rotations per minute. By reflecting the laser beam twice around the rotating mirror with the help of a semi-transparent mirror placed at the entrance of the system, light pulses of half duration $\tau = 1.5 \times 10^{-8}$ sec and a repetition rate of $n = 7.7 \times 10^2$ sec^{-1} could be generated. The energy of the light pulses was determined according to (4). The power carried by the non-attenuated laser beam was recorded with a Zeiss VTh8 type vacuum thermocouple. The sensitivity of the thermocouple was controlled by comparison with a directly calibrated black body calorimeter [12].

The reliability of the energy measurements was checked by comparing the measured efficiency of the detecting photomultiplier with the value given by cathalogue. The efficiency α was determined from

$$\alpha = \frac{n}{NE}, \tag{5}$$

where E = energy of incident light pulse;
N = number of light pulses incident in unit time;
n = number of photoelectrons counted in unit time.

The energy of the gate light pulses, according to measurements, was of the order of 10^5 $h\nu$, which was sufficient to produce electric pulses of constant amplitude at the output of PM_2. These uniform electric pulses were used directly to operate the coincidence circuit connected to PM_1. The photomultipliers PM_1 and PM_2 were of RCA 6810-A type, which have S-11 caesium antimonide cathodes. Since the amplitude of electric pulses arising at the output of PM_1 was only just sufficient to operate the coincidence circuit, these pulses were amplified by an 80 MHz wide-band amplifier to obtain stable electronic operation. The amplitude of the gating pulses coming from PM_2 was considerably higher than that of dark current pulses, so by the gating procedure dark current pulses could be excluded through suitable discrimination. By the detection of the low-intensity light pulses the discriminator placed after PM_1 was set to have a possible highest signal-to-noise ratio, this was achieved when the discrimination level was approximately equal to the amplitude of the largest

dark-current pulses. The time resolution of the coincidence circuit was 10^{-8} sec.

For the counting of pulses a multichannel analyser was used in multi-scaler operation. In this way it was possible to obtain not only the sum of photo-electrons arriving during the total measuring time, but also to count separately the number of pulses arriving in a given unit time. This made it possible to discover and eliminate many sources of stray light and to check on the stability of the whole apparatus during the course of the measurements.

Results of measurements

Results for the two series of measurements are plotted in Fig. 3. It can be seen that the results of the two series are consistent with each other and verify relation (3) down to an energy of 0.1 $h\nu$. Dark current pulses and the fraction of stray light pulses were counted together as background and corrected for. In the first run of measurements at the lowest energy 0.1 $h\nu$ the signal-to-noise ratio was 0.15; this was improved in the second run of measurements by a careful adjustment of discrimination level to 0.5. The lower part of Fig. 3 shows counts of pulses obtained with the multichannel analyser in the second run of measurements.The efficiency of the detecting photomultiplier determined from (5) was found to be $\alpha = 4 \times 10^{-3}$, which does not deviate significantly

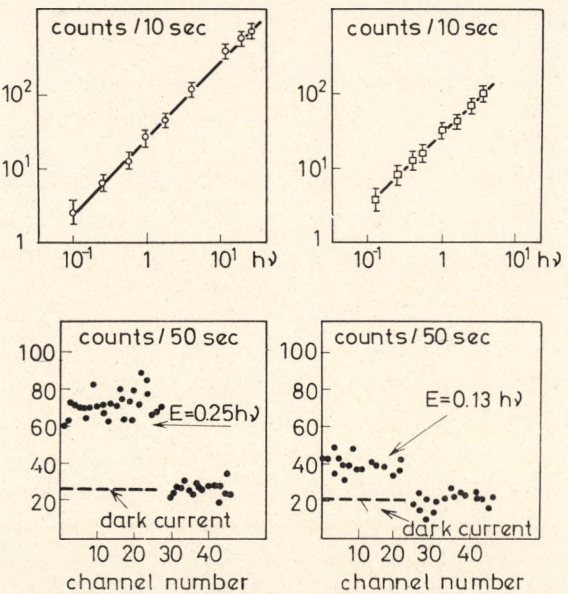

Fig. 3. Number of photo-electrons counted in unit time as a function of energy of light pulses. Circles and squares denote the results of the two series performed. The lower part of the figure shows counts obtained with the multichannel analyser

from the value 5×10^{-3} given by cathalogue. This agreement confirms the reliability of our energy measurements; the small deviation may be due to the fact that pulse discrimination introduces some loss in the electron pulses being counted.

It can be concluded that the probability of the release of a photo-electron by photoelectric effect is proportional to the light energy absorbed by the photo-cathode even when the energy absorbed is less than that of a single light quantum.

II. Experiment on the question of energy accumulation

The principle of the experiment is the following:

Consider two very short light pulses of low intensity falling on a photo-cathode with the shortest possible time delay. If there is an energy accumulation phenomenon within the photo-cathode, a photo-electron should be released with higher probability by the second pulse than by the first pulse.

Only slight modifications were required to the arrangement used in the preceding experiment. First of all it was necessary to generate light pulses of as short duration as possible. Secondly each light pulse was duplicated by splitting a part of the laser beam and delaying it on an optical path with the help of semi-transparent mirrors and the two light pulses were irradiated on to the photo-cathode of a single photomultiplier. The effect of energy accumulation was expected to show up through an increase in the number of photo-electrons released in unit time by the delayed light pulses.

The scheme of our modified experimental arrangement is shown in Fig. 4. A new rotating mirror system was constructed to generate light pulses of half-width $\tau = 5 \times 10^{-9}$ sec with a repetition rate of 4.6×10^3 sec^{-1}. As serious technical difficulties arose by the operation of the Fortuna-type electric motor, which rotated the hexagonal mirror at 46.000 rotations per minute, it was not possible to reduce further the duration of light pulses using this technique. A part of the laser beam was split and delayed 9×10^{-9} sec on a 270 cm path with the help of two semi-transparent mirrors M_2 and M_3. Dark current was reduced as before. The gate light pulse was adjusted, as shown in the inset of Fig. 4, so that the electronic system counted only photo-electrons released by the delayed light pulses. To reduce disturbing effects arising from the dead time of the coincidence circuit connected to the RCA 6810-A type detecting photomultiplier PM_1, the light pulses were attenuated to such low intensities that the probability of photo-electrons being released simultaneously by the two successive pulses was approximately two orders of magnitude smaller than the probability corresponding to the release of a photo-electron by a single pulse. This condition was fulfilled with light pulses of an energy of approximately 10 hv.

Stray light scattered mainly from the rotating mirror system and so falling time-dependently on photomultiplier PM_1 caused serious problems but could not be eliminated completely. The signal-to-noise ratio was about 4, the time resolution of the coincidence circuit 5×10^{-9} sec.

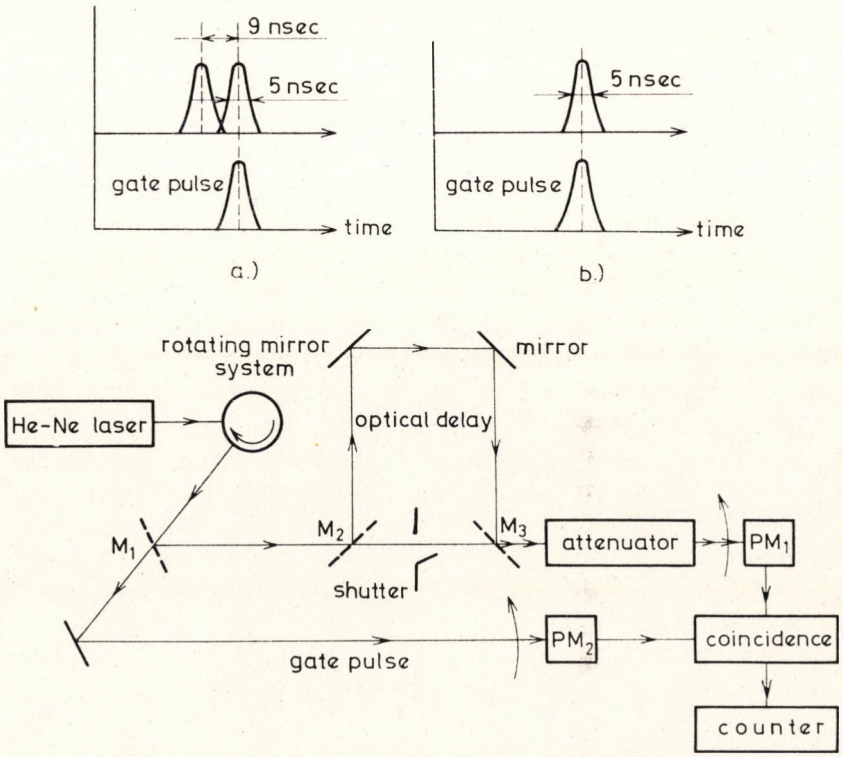

Fig. 4. Experimental arrangement for investigating light energy accumulation

Results of measurements

We measured the number of photo-electrons released in unit time by the delayed light pulses with the optical path between semi-transparent mirrors M_2 and M_3 unblocked (previous energy supply to electrons in photo-cathode by undelayed light pulse) and blocked (no previous energy supply), respectively. Background pulses were counted separately in both cases; these, dark-current pulses and the relatively small counting loss of about 2% due to dead-time effects of the electronics were corrected for in the evaluation of the measurements. Table I summarizes the results obtained from nine runs. It can be seen that the difference between the number of photo-electrons released in the two cases is in all cases within the limit of three times the standard error. The

Table I

Differences between the number of photo-electrons released with and without previous energy supply to electrons

No. of run	Difference %
1	-2.5 ± 2.5
2	$-5\ \pm2.1$
3	$+4\ \pm2.5$
4	$+10\ \pm5$
5	$-2\ \pm3$
6	$+4\ \pm2.5$
7	$+4.5\pm4$
8	$+0.7\pm4$
9	$-3\ \pm4$
Weighted mean square average	$(+0.1\pm1.1)$ %

weighted mean square average [13] of the results gives $(+0.1 \pm 1.1)\%$ for the difference, so it may be concluded that no energy accumulation phenomenon producing an effect larger than the order of a few percent is likely to exist at times in the 10^{-9} sec range.

III. Time statistical measurements

The time distribution of photo-electrons released by the low-intensity light pulses was investigated. The statistical measurements showed, as expected, that photo-electrons are released at random from the photo-cathode even when the energy of a single light pulse is less than the energy $h\nu$ of light quanta. This means that any of the extremely low-intensity light pulses is capable of releasing a photo-electron.

Assuming that photo-electrons are emitted independently from each other, the probability $P(N)$ that after a given start time $N-1$ incident light pulses will not, but the N-th pulse will, release a photo-electron is

$$P(N) = (1-\alpha E)^{N-1} \cdot \alpha E, \tag{6}$$

which if $\alpha E \ll 1$ can be written to a good approximation as

$$P(N) = \alpha E e^{-\alpha E(N-1)}. \tag{7}$$

The experimental task is to measure this distribution at various light pulse energy values. Our measurements were carried out using a multichannel analyser in the following way:

A pulse from a photo-electron starts the analyser. Every successive gate pulse shifts the analyser one channel further, so the l-th channel corresponds to the l-th light pulse incident on the photo-cathode. When the next photo-

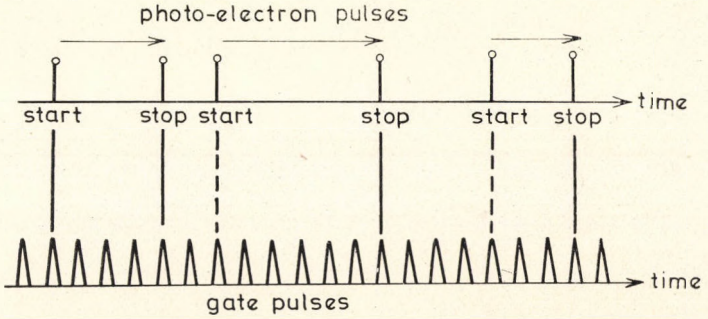

Fig. 5. Principle of the time distribution measurement of photo-electrons

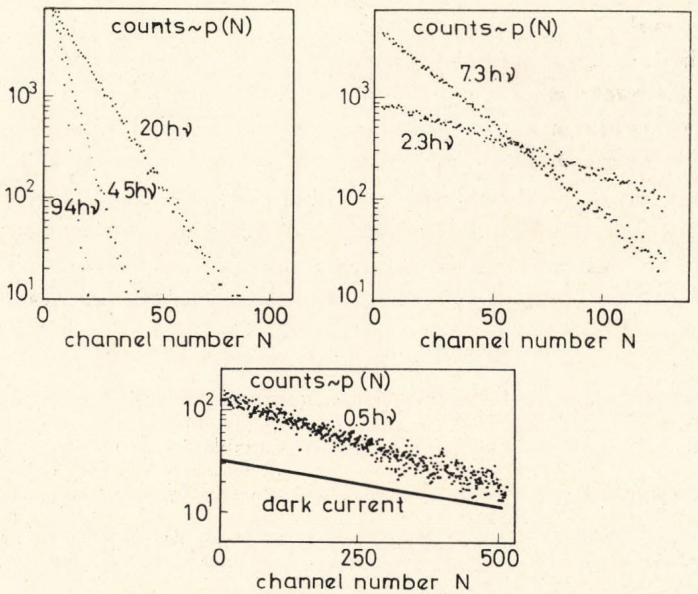

Fig. 6. Photo-electron time distributions obtained at various light-pulse energy values

electron is released, by the N-th light pulse, an event is stored in the N-th channel of the analyser, denoting that $N - 1$ light pulses have not, but exactly the N-th has, released a photo-electron. The next photo-electron pulse starts the process again, thus every second time interval between photo-electrons released from the low-intensity light pulses is analysed and stored in the appropriate channel (see Fig. 5). The duration of the time intervals is the number of non-emitting light pulses arriving in between.

The experimental arrangement was the same as that in Fig. 2. The measurements were carried out with light pulses of half-width $\tau = 5 \times 10^{-9}$ sec and a repetition rate of $n = 4.6 \times 10^3$ sec^{-1}. Due to instabilities arising from damage to the coating of the rotating mirror the measuring time of a statistical distribution had to be limited to the order of thirty minutes. This and the rate of dark-current pulses set a limit for the lowest intensity at which the photo-electron distribution could be measured.

The photo-electron time distributions obtained at various light pulse energy levels (Fig. 6) have the exponential form expected from theoretical considerations. In the case of the distribution corresponding to the lowest energy value the time distribution of dark-current pulses arriving in between is also indicated.

Conclusion

The results of our investigations carried out on the basis of the semi-classical theory of light using very short-duration, low-intensity light pulses verify in a direct manner various features of the photoelectric effect. Our measurements show that the probability of the emission of a photo-electron is proportional to the light energy absorbed by the photo-cathode down to an energy of 0.1 $h\nu$. It is verified that at times of the order of 10^{-9} sec light energy accumulation in the photo-cathode does not play any role in the photoelectric effect. The time distribution measurements of photo-electrons released by the low-intensity light pulses show that these are emitted at random from the photo-cathode.

Acknowledgement

We express our thanks to Mr. J. Tóth for valuable assistance in the performance of the experiments; to Mr. Cs. Hazay for help with the electronics; to Mr. T. Salamon for help in the preparatory part of the work; to Mr. P. Varga for his continuous interest and many helpful remarks; to Mr. J. Boros Gyevi for the evaporation of reflecting elements; to Mr. K. Kántor for measurements of various reflection and transmission data; and to Mr. F. Ádám for designing the frequency converter for the rotating mirror. Thanks for their help are due also to Miss J. Erdélyi and Mr. F. Kovács.

REFERENCES

1. M. Born, Optik 1933, Berlin, p. 456.
2. A. Ádám, L. Jánossy and P. Varga, Acta Phys. Hung., **4**, 301, 1955; Ann. der Physik, **16**, 408, 1955.
3. L. Jánossy and Zs. Náray, Acta Phys. Hung. **7**, 403, 1957; Nuovo Cimento Supplement, **9**, 588, 1958.
4. L. Jánossy, Nuovo Cimento, **6**, 111, 1957; **12**, 370, 1959.
5. Gy. Farkas, L. Jánossy, Zs. Náray and P. Varga Acta Phys. Hung., **18**, 199, 1965.
6. E. O. Lawrence and J. W. Beams, Phys. Rev., **32**, 478, 1928.
7. A. T. Forrester, R. A. Gudmunsen and P. O. Johnson, Phys. Rev., **99**, 1691, 1955.

8. L. Csillag, M. Jánossy, Zs. Náray and T. Salamon, Physics Letters, **27A**, 343, 1968. M. Jánossy and Zs. Náray, Physics Letters, **29A**, 479, 1969.
9. L. Csillag and M. Jánossy, Optics Technology, **1**, 97, 1969.
10. Gy. Farkas and P. Varga, Journ. Sci. Instr. **41**, 704, 1964.
11. H. E. Bennett, Applied Optics, **5**, 1265, 1966.
12. M. L. Császár, L. Csillag, I. Kertész and P. Varga, Reports of the Central Research Institute for Physics, **14**, 137, 1966.
13. L. Jánossy, Theory and practice of the evaluation of measurements. Clarendon Press, Oxford, 401, 1965.

ИССЛЕДОВАНИЕ ФОТОЭЛЕКТРИЧЕСКОГО ЭФФЕКТА ПРИ НИЗКОЙ ИНТЕНСИВНОСТИ СВЕТА

Л. ЧИЛЛАГ, М. ЯНОШИ и Ж. НАРАИ

Резюме

В статье излагаются эксперименты по исследованию фотоэлектрического эффекта, проведенные при очень низкой интенсивности света. Различные особенности фотоэлектрического эффекта можно исследовать прямым способом путем испускания очень коротких световых импульсов низкой интенсивности на фотокатод фотоэлектронного умножителя. Путем непосредственных измерений показано, что вероятность фотоэлектронной эмиссии в течение времени τ пропорциональна световой энергии, поглощенной фотокатодом даже и в том случае, если поглощенная энергия меньше, чем $h\nu$. Была исследована также и вероятность накопления световой энергии, которая встречается в процессе фотоэлектрического эффекта. Показано, что в отрезках времени порядка 10^{-9} сек такое явление накопления энергии не существует. Статистические измерения излученных фотоэлектронов показывают, что они беспорядочно испускаются фотокатодом.

Acta Physica Academiae Scientiarum Hungaricae, Tomus 32 (1—4), pp. 289—297 (1972)

ANISOTROPY AND HOT ELECTRON EFFECTS ON SEMICONDUCTING Si SAMPLES IN THE TEMPERATURE RANGE 1—300 °K*

By

I. KIRSCHNER, T. PORJESZ, J. BÁNKUTI and P. ZENTAI

LABORATORY FOR LOW TEMPERATURE PHYSICS, ROLAND EÖTVÖS UNIVERSITY, BUDAPEST

(Received 19. X. 1971)

The transport coefficients of Si single crystals were calculated assuming ellipsoid equienergetic surfaces. The results were checked by means of longitudinal Hall effect and anisotropy investigations. Hot electron measurements reflected the role of the interactions arising, determined the value of the critical field and produced a detectable size effect. The effects were measured in the [100], [110] and [111] planes and the dependence of the longitudinal Hall voltage on the angle between the directions of the electric and magnetic field was plotted.

Introduction

Low-temperature physics research in Hungary started at the Department for Atomic Physics of the Roland Eötvös University. In 1963 a research group was formed here setting the aim to cultivate this theme. In that time the leader of the Department was Professor L. JÁNOSSY, from whom we got a significant support to these researches.

In the past years we have been dealing with the galvanomagnetic, hot electron and anisotropy effects of semiconductors. These investigations have given enlightenment about charge carrier transport in semiconductors like InSb, Ge, Si and Si- (Ph—B) and furnished industrially important information concerning charge mobility, concentration, bound structure and impurity levels.

In the field of superconductivity we have investigated the effect of impurities on the critical parameters of superconductors. In the course of these researches we succeeded in taking into consideration — beside the change of the scattering mechanism — the change in the topology of the Fermi-surface as well.

Our experimental investigations have furnished the knowledge of the flux flow state of In—Bi alloys. The result of our measurements has given us impulse to elaborate a new model for the critical state of type II superconductors.

Our work carried out in the technics of low temperatures tended partly to build cryostates, partly to construct superconducting magnets, and to put into practice high pressure multiplicators.

* Dedicated to Prof. L. JÁNOSSY on his 60th birthday.

Moreover we have made studies in the field of thermodynamical stability, certain conclusions of which can be applied to physical phenomena of low temperatures as well.

During the course of these research works the Laboratory for Low Temperature Physics of the Roland Eötvös University came into being. Now, it is already working independently as a departmentlike unit with a definite research and teaching program.

The computation of transport coefficients

In the series expansion of the elements of the electric conductivity tensor with respect to the magnetic field H up to terms of the third order in H, there appear the following coefficients [1, 2]:

$$\begin{aligned}
\sigma_{ij}^0 &= \sigma_{ij}(H=0), \\
\sigma_{ijl}^0 &= \left(\frac{\partial\sigma_{ij}(H)}{\partial H_l}\right)_{H=0}, \\
\sigma_{ijlm}^0 &= \frac{1}{2!}\left(\frac{\partial^2\sigma_{ij}(H)}{\partial H_l \partial H_m}\right)_{H=0}, \\
\sigma_{ijlmn}^0 &= \frac{1}{3!}\left(\frac{\partial^3\sigma_{ij}(H)}{\partial H_l \partial H_m \partial H_n}\right)_{H=0},
\end{aligned} \tag{1}$$

where the index zero denotes independence from the magnetic field.

Supposing rotational ellipsoid equienergetic surfaces, the conductivity coefficients can be explicitly determined in case of Si samples. The charge carrier energy takes the form

$$\varepsilon(k) = -\frac{\hbar^2}{2}\left[\frac{k_1^2+k_2^2}{m_\perp} + \frac{k_3^2}{m_{||}}\right], \tag{2}$$

while the equation of motion is

$$v\Delta_r f - \frac{e}{\hbar}\left(E + \frac{1}{c}\, vxH\right)\Delta_k f = -\frac{f-f_0}{\tau}, \tag{3}$$

where k is the wave number vector, f_0 and f are the equilibrium and non-equilibrium distribution functions, E is the electric field intensity, e the electron charge, c the light velocity, $\hbar$ the Planck constant, τ the relaxation time, v the electron velocity, $m_1 = m_2 = m_\perp$ the transversal and $m_3 = m_{||}$ the longitudinal mass; further Δ_r and Δ_k denote the gradients with according to the coordinates and wave number vector, respectively.

If, moreover, the relaxation time approach is assumed to be valid, the collision term is

$$\left(\frac{\partial f}{\partial t}\right)_{\text{coll}} = -\frac{f - f_0}{\tau}. \tag{4}$$

In the case of longitudinal Hall effect it is necessary to compute σ_{ijlmn}. Therefore we must look for solutions of the form

$$f = f_0 + \sum_j f_j^{(1,0)} E_j + \sum_{j,l} f_{jl}^{(1,1)} E_j H_l + \sum_{j,l,m} f_{jlm}^{(1,2)} E_j H_l H_m + \sum_{j,l,m,n} f_{jlmn}^{(1,3)} E_j H_l H_m H_n, \tag{5}$$

where upper indices denote powers of the electric or magnetic field intensity. We shall suppose that $\nabla_r f = 0$ and we utilize the fact that for ellipsoids

$$f_{jlm}^{(1,2)} = \frac{e^3 \tau^3}{c^2} \sum_{r,p} \epsilon_{jlr} \epsilon_{rpm} \left(-\frac{\partial f_0}{\partial \varepsilon}\right) \frac{v_p}{m_r m_j}, \tag{6}$$

the contribution of the α-th ellipsoid to the i-th component of the current density is

$$j_i^{(\alpha)} = \frac{e^5}{c^3 m_i} n^{(\alpha)} \langle \tau^4 \rangle \sum_{j,l,m,n,p,r} \epsilon_{inp} \epsilon_{jlr} \epsilon_{rpm} \frac{1}{m_r m_j m_p} E_j H_l H_m H_n, \tag{7}$$

where ϵ_{xyz} and ϵ_{abc} are the elements of the permutation tensor, and $n^{(\alpha)}$ is the number of the conductivity electron states in the α-th ellipsoid. Introducing the notation

$$M_{ijlmn}^{(\alpha)} = \frac{1}{m_i m_j} \sum_{r,p} \frac{\epsilon_{jlr} \epsilon_{inp} \epsilon_{rpm}}{m_r m_p}, \tag{8}$$

we get

$$\sigma_{ijlmn}^{(\alpha)} = \frac{e^5}{6c^3} n^{(\alpha)} \langle \tau^4 \rangle M_{ijlmn}^{(\alpha)} \tag{9}$$

and summing for all the ellipsoids, the complete coefficient will be

$$\sigma_{ijlmn} = \sum_{\alpha} \sigma_{ijlmn}^{(\alpha)}. \tag{10}$$

The elements of the M_{ijlmn} tensor differing from zero are compiled in Table I [3].

Table I

i	j	l	m	n	r		$M^{(\alpha)}_{ijlmn}$	$\frac{1}{2}\,Mijlmn$
1	2	3	3	3	1	—	$1/m_1^2m_2^2$	$-b$
1	2	1	1	3	3	—	$1/m_1m_2^2m_3$	$-a$
1	3	1	1	2	2	+	$1/m_1m_2m_3^2$	a
1	3	2	2	2	1	+	$1/m_1^2m_3^2$	b
2	3	2	2	1	1	—	$1/m_1m_2m_3^2$	$-a$
2	3	1	1	1	2	—	$1/m_2^2m_3^2$	$-b$
2	1	2	2	3	3	+	$1/m_1^2m_2m_3$	a
2	1	3	3	3	2	+	$1/m_1^2m_2^2$	b
3	1	2	2	2	3	—	$1/m_1^2m_3^2$	$-b$
3	1	3	3	2	2	—	$1/m_1^2m_2m_3$	$-a$
3	2	3	3	1	1	+	$1/m_1m_1^2m_3$	a
3	2	1	1	1	3	+	$1/m_2^2m_3^2$	b
1	1	2	1	3	3	+	$1/m_1^2m_2m_3$	a
1	3	2	3	3	1	+	$1/m_1^2m_2m_3$	a
1	1	3	1	2	2	—	$1/m_1^2m_2m_3$	$-a$
1	2	3	2	2	1	—	$1/m^2m_2m_3$	$-a$
2	1	3	1	1	2	+	$1/m_1m_2^2m_3$	a
2	2	3	2	1	1	+	$1/m_1m_2^2m_3$	a
2	2	1	2	3	3	—	$1/m_1m_2^2m_3$	$-a$
2	3	1	3	3	2	—	$1/m_1m_2^2m_3$	$-a$
3	2	1	2	2	3	+	$1/m_1m_2m_3^2$	a
3	3	1	3	2	2	+	$1/m_1m_2m_3^2$	a
3	1	2	1	1	3	—	$1/m_1m_2m_3^2$	$-a$
3	3	2	3	1	1	—	$1/m_1m_2m_3^2$	$-a$

$$b = \frac{2}{m_\parallel^2 \cdot m_\perp^2} + \frac{1}{m_\perp^4}$$

$$a = \frac{1}{m_\parallel^2 \cdot m_\perp^2} + \frac{2}{m_\parallel^2 \cdot m_\perp^3}$$

Longitudinal Hall effect

The current density j flowing through the crystal, the magnetic field H_x and the longitudinal Hall field E_x are in the same plane. In our experiments the magnetic field was rotated in this plane. To investigate the longitudinal Hall effect only contributions of the third order in the magnetic field have to be considered. We calculated the component of the $j^{(1,3)}$ current density perpendicular to the electric field E in the three crystallographic planes. Let us examine the behaviour of $j_\perp^{(1,3)}$ in these cases. Making the computations in the chief axis system of the ellipsoids and retransforming, in the laboratory system we get the following results:

a. In the [100] plane no longitudinal Hall effect can be observed, because the conductivity matrix of the third order in H has no term containing only two number permutations in the indices *ilmn*;

b. In the [110] plane there is no longitudinal Hall effect either, because $H_1 = -H_2$ (see Fig. 1);

c. In the [111] plane, making use of the real value of the conductivity coefficients, we get

$$j_{\perp}^{(1,3)} = -\frac{e^5}{c^3}\langle\tau^4\rangle nEH^3\frac{b-a}{9\sqrt{2}}\sin 3\vartheta, \tag{11}$$

where ϑ denotes the angle between the electric and magnetic field intensity vectors (Fig. 2), while a and b are taken from Table I.

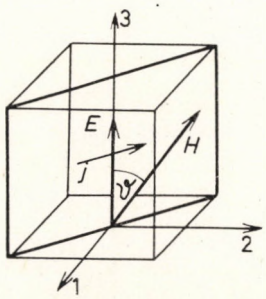

Fig. 1

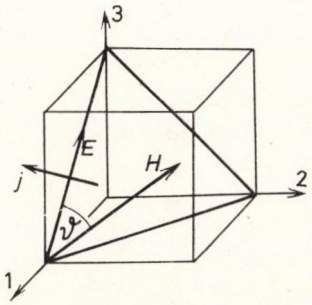

Fig. 2

Since here $j = j(j_1, 0, 0)$, the measurable quantity $E_{\varkappa}^{(1,3)}$ can be calculated

$$E_{\varkappa}^{(1,3)} = -\frac{e^5}{c^3}\frac{b-a}{9\sqrt{2}}\sigma^{-2}n\langle\tau^4\rangle j_1 H^3\sin 3\vartheta, \tag{12}$$

where some small terms have been neglected.

Anisotropy measurements

Our measuring equipment [4] was originally constructed for galvanomagnetic measurements [5] but was suitable for carrying out anisotropy investigations as well. The results of anisotropy effects measured on Si single crystals [6] are summed up in the following.

The voltage $U_{\varkappa}$ measured in the [100] and [110] planes is proportional to the sine of the angle ϑ. This is due to the transversal Hall voltage, which can arise because of the possibility of deviation of the directions of E and H.

It can be shown that the longitudinal Hall voltage must disappear in all cases when the magnetic field is parallel with one of the 2-, 3- or 4-fold symmetry axes. Thus, in the case of cubic symmetry the Hall voltage in the [100] and [110] planes must change with a periodicity of at least sin 4 ϑ.

Correspondingly, an angle dependence with a periodicity of sin 3 ϑ can be expected in the [111] plane.

The results of our measurements are shown in Figs. 3 and 4. It can be seen that the longitudinal Hall voltage varies as sin 3 ϑ. Its amplitude has been modulated by the transversal Hall voltage with sin ϑ. The longitudinal Hall voltage can be separated from the measured voltage by means of a third order polynomial fitted by the method of least squares.

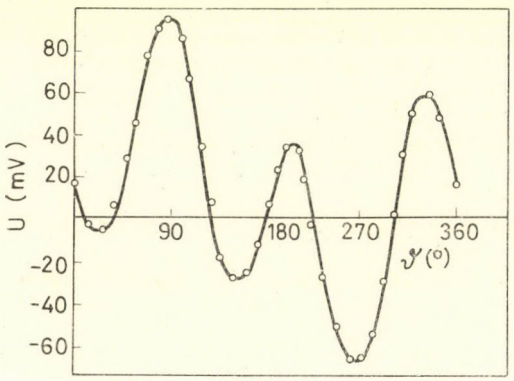

Fig. 3

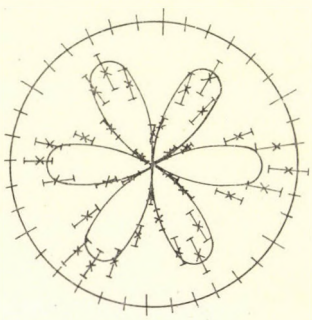

Fig. 4

The effect of non-equilibrium charge carriers on transport phenomena

In investigating the dependence of the transport coefficients on the magnetic field, it was assumed that they are independent of the electric field intensity. However, this supposition is valid up to a critical electric field intensity E_{crit} only. The hot electron effects [8] arising at field intensities above E_{crit} have led to the elaboration of two different sorts of computation methods for the dependence on electric field of the mobility of the charge carriers and of the different transport phenomena. (The exact solution of the Boltzmann equation cannot be given, because of the complicated electron—phonon interactions.) One solution — which neglects scattering on the optical phonons — has been found for a small interval over the critical field [9] but has only a small applicability. The model using the effective electron temperature [10, 11] is more generally applicable.

Our experiments have also verified this fact. In the measurements we examined the function

$$j = j(E) \tag{13}$$

from which the drift velocity v_d and, using the relation

$$v_d = \mu(E, T)E, \tag{14}$$

the dependence of the mobility on the field intensity can be computed. The measurements were made with the block arrangement of Fig. 5, where I is the high voltage impulse generator, M is the measuring equipment, consisting

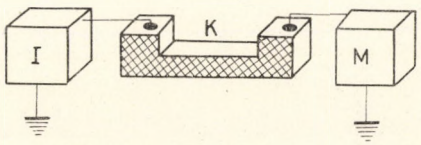

Fig. 5

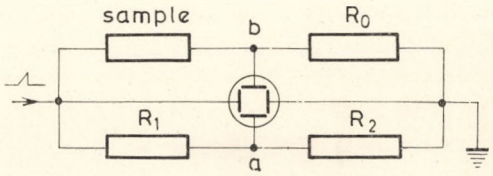

Fig. 6

of a small resistor and a parallel switched oscilloscope, while K is the semiconducting crystal to be measured. The horizontal deviation of the oscilloscope was proportional to the voltage given on the sample, the vertical one to the current through the sample, taken from the resistor.

The value of the critical electric field intensity was measured with the bridge switching system sketched in Fig. 6. The voltage applied to the bridge was small to ensure that linear Ohm's law was still valid, which in this case was achieved by choosing R_1 and R_2 to be such that in the linear interval at a given temperature there was no voltage difference between the points a and b. This meant that vertical deviation on the oscilloscope screen was observed only over the critical voltage.

Results of hot electron measurements

We measured the function $j(E)$ at 77 °K and 300 °K on a sample of 1 mm effective length with 2000 V pulses (i.e. a field intensity of 20 kV/cm). The results are represented in Fig. 7 by the broken lines.

The drift velocity of the charge carriers in a small electric field [12] is

$$v_d = \frac{4el}{3\sqrt{\pi\, m\, v_T}} E \tag{15}$$

while in a large one [13] it is

$$v_d = \left(\frac{\sqrt{2}\, c_f e l}{m v_T} E \right)^{1/2}, \tag{16}$$

where l is the average free path, v_T the thermal velocity, m the effective mass, c_f the phonon group velocity (or sound velocity) within the crystal.

In the transitional case between large and small spaces the value of v_d in (15) and (16) is equal, hence

$$E_{\text{crit}} = 1{,}51 \frac{c_f}{\mu_0}, \tag{17}$$

where we have introduced the notation $\mu_0 = el/mv_T$, which is equal to the value of the mobility in zero electric field.

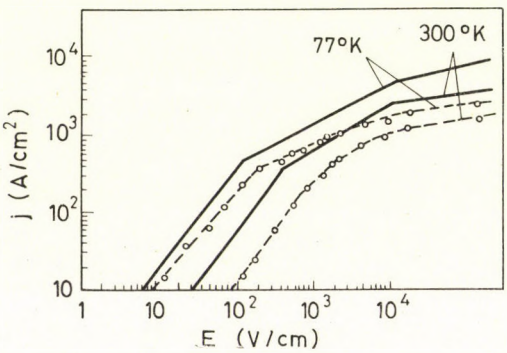

Fig. 7

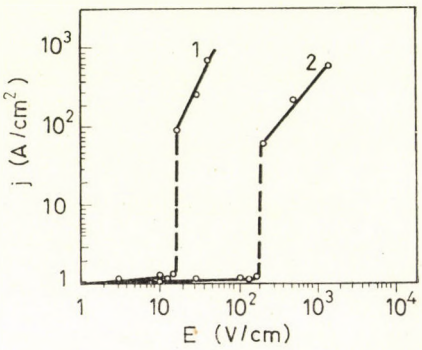

Fig. 8

If the value of the constant c_f is fitted to the measured values presented in Fig. 7, we get the drawn curves. If c_f is sound velocity within the crystal determined in any other way, then there is a significant deviation from the measured values. Our results show that acoustic phonons are not the only participants in interactions with the charge carriers.

The applicability of the model using the effective electron temperature is limited by the fact that the energy density of the electron gas originates first of all from the electron—electron interaction and not from the interaction between phonon and electron.

We measured the function $j(E)$ in the temperature interval of 1.6 °K—4.2 °K by taking the static characteristics (Fig. 8). In this interval temperature changes did not cause any detectable effect.

At the temperature of liquid helium a change in the number of charge carriers causes hot electron effects in the first line and not a change of the

mobility. If the energy of the carriers is sufficient to ionize the impurity, the number of charge carriers rises like an avalanche, and the value of the current increases suddenly.

The effect strongly depends on the size of the sample: in Fig. 8 we measured the curve 1, on a Si sample with dimensions of $5 \times 1 \times 1$ mm in the case of a longitudinally flowing current, while we obtained curve 2 on a sample of the same type with an effective length of 1 mm.

More detailed investigations showed that in samples smaller than the free path the collision and the energy transport decrease exponentially with size. In this temperature range, the critical field does not depend on the temperature.

REFERENCES

1. J. P. Jan, Solid State Phys., **5**, 1, 1957.
2. W. Mason, W. Hewith and R. Wick, J. Appl. Phys., **24**, 166, 1953.
3. И. Киршнер, Т. Порес, Й. Банкути, П. Зентаи: 10. Конф. физ. Техн. Низк. Темп. 26.9.—3.10. 1971. ,Варна. (Proc. Conf. p. 72., Sofia, 1971.)
4. I. Kirschner, T. Porjesz, E. Papp, Gy. Fricsovszky, I. Poór, I. Kovács és J. Bánkuti, Mérés és automatika, **17**, 101, 1969.
5. И. Киршнер, Т. Порес, Г. Фричовски, Й. Банкути, Е. Папп, П. Хорват: Acta Phys. Hung., **32**. No. 4. 1972. To be published.
6. J. Bánkuti, I. Kirschner, T. Porjesz und P. Zentai, 8. Intern. Konf. Phys. tiefen Temp. Dresden, 25—29, 11, 1969. (Proc. Conf. p. 77., Dresden, 1969.)
7. L. Grabner, Phys. Rev., **117**, 690, 1960.
8. G. J. Ryder and W. Shockley, Phys. Rev., **81**, 139, 1951.
9. R. S. Crandall, Phys., Rev., **169**, 585, 1968.
10. H. Fröhlich and B. V. Paranjape, Proc. Phys. Soc., **B69**, 21, 1956.
11. R. Stratton, Proc. Roy. Soc., **A 242**, 355, 1958, **A 246**, 406, 1958.
12. G. J. Ryder and W. Shockley, Phys. Rev., **82**, 330, 1951.
13. I. Kirschner és T. Porjesz, Magy. Fiz. Folyóirat, **16**, 112, 1968.

ВЛИЯНИЕ АНИЗОТРОПИИ И ГОРЯЧИХ ЭЛЕКТРОНОВ В ОБРАЗЦАХ ПОЛУПРОВОДНИКА Si ПРИ ТЕМПЕРАТУРНОЙ ОБЛАСТИ 1—300 °К

И. КИРШНЕР, Т. ПОРЕС, Й. БАНКУТИ и П. ЗЕНТАИ

Резюме

Предполагая эллипсоидальные изоэнергетические поверхности, вычислались транспортные постоянные монокристаллов Si. Мы проверяли результаты с помощью продольного эффекта Холла и исследования анизотропии. Наши измерения эффекта горячих электронов указали на роль возникающих взаимодействий, определили напряжение критического поля и было нами обнаружено и размерный эффект. Эффекты были измерены в плоскостях [100] [110] и [111] далее зависимость продольного напражения Холла в функции угла между направлениями электрического и магнитного поля была решена.

Acta Physica Academiae Scientiarum Hungaricae, Tomus 32 (1–4), pp. 299–304 (1972)

STUDY OF THE FIRST-ORDER ANTIFERROMAGNETIC-FERROMAGNETIC TRANSITION IN FeRh BY POSITRON ANNIHILATION METHOD*

By

A. ÁDÁM, L. CSER, ZS. KAJCSOS and G. ZIMMER

CENTRAL RESEARCH INSTITUTE FOR PHYSICS, BUDAPEST

(Received 4. XI. 1971)

In order to establish whether any change occurs in the electronic structure during the first-oder antiferromagnetic to ferromagnetic transition in FeRh taking place between the temperatures $T_1 = 300$ °K and $T_2 = 373$ °K, the angular correlation of γ-ray pairs arising from positron annihilation was measured in both phases. The angular correlation functions obtained at the two temperatures do not show any significant difference. This result is inconsistent with the theory explaining as due to excess electron entropy the difference between the entropy change measured during the transition and that calculated from the change in the lattice parameter.

Introduction

In ordered FeRh alloys of close to stoichiometric composition a first-order phase transition from a stable antiferromagnetic phase to a stable ferromagnetic phase on heating has been observed to take place by magnetic [1], [2] and neutron diffraction [3], [4], [5] methods. This transition does not cause any appreciable change in the symmetry of the CsCl-type crystal structure but involves an expansion of 1 per cent in the crystal volume [6].

To explain this transition, in his exchange inversion model KITTEL [7] postulated that a reversal of the sign of the exchange interaction between the sublattices occurs when the lattice parameter reaches a given value. This model was also adopted in the considerations of PÁL et al. [8]. The change of the specific entropy, S, during the phase transition was evaluated by KOUVEL [9], using the thermodynamical formula relating the transition temperature T_{crit} to the magnetic field H as

$$\frac{\partial T_{\text{crit}}}{\partial H} = -\frac{\Delta\sigma}{\Delta S},$$

where $\Delta\sigma$ is the change of magnetization during the transition. The measured value of $\Delta S = 14$ mJ/deg. g is, however, much larger than the contribution to entropy change $(\Delta S)_{\text{lat}} = 4.5$ mJ/deg. g estimated [9] from the change in the lattice parameter. This difference was initially attributed by KOUVEL to the

* Dedicated to Prof. L. JÁNOSSY on his 60th birthday.

behaviour of the induced magnetic moments of the Rh atoms [10]. The theory is that in the antiferromagnetic phase the distribution of the iron moments is such that the resultant exchange field is zero at the sites of the Rh atoms. If this were the case, the susceptibility would be expected to be strongly temperature dependent. Experimentally, however, the susceptibility in the antiferromagnetic phase is found to be constant [1] and consequently the Rh atoms can have no localized magnetic moments. Furthermore, though the Fe atoms produce an induced magnetic moment on the Rh atoms in the ferromagnetic phase, the contribution this makes to the entropy is probably of little importance.

More recently, KOUVEL [11] considered the possibility of a substantial contribution from the entropy of itinerant electrons. The entropy of conduction electrons is given by

$$S = \gamma T,$$

where γ is proportional to the density of states belonging to the Fermi surface. The electron entropy change involved in the phase transition can be expressed as

$$\Delta S = (\gamma_F - \gamma_{AF}) T_{\text{crit}}.$$

This means that if the electron entropy change contributes to a measurable extent to the entropy change of the phase transition, there should be a considerable alteration in the density of states close to the Fermi level. Any drastic alteration in the density of states would presumably affect the momentum space and should therefore be detectable by e.g. positron annihilation method

Principle of the method

In "free annihilation" of an electron—positron pair one or more γ-quanta are produced, although the emission probability of more than 3 quanta is negligibly small. The cross-section ratio of the two practically important annihilation types is $\sigma_2\gamma/\sigma_3\gamma = 372$ [12]. Annihilation of an electron-positron pair can be preceded by formation of an intermediate H-analog bound state: the parapositronium (p—Ps) if the resultant spin $S = 0$, and the orthopositronium (σ—Ps) if $S = 1$ (with lifetimes $\tau = 1.25 \cdot 10^{-10}$ sec and $1.4 \cdot 10^{-7}$ sec, respectively). By the law of conservation of momentum, parapositronium annihilation is accompanied by the emission of two, orthopositronium annihilation by emission of three γ quanta.

The lifetime of the long-lived orthopositronium is reduced if it interacts with its environment and exchanges or loses its electron. As this reduced lifetime is characteristic of the chemical properties and internal magnetic fields

of the environment, the measurement of positron lifetime thus provides a tool for the investigation of material structure.

Another positron annihilation method available for structural investigation is to measure the angular correlation of the annihilation γ-rays. This method was used in the present study.

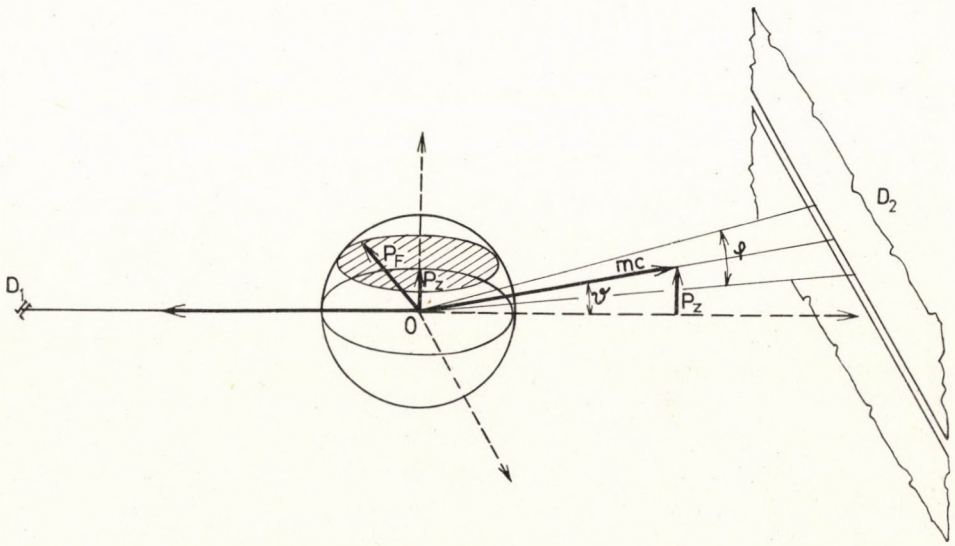

Fig. 1. D_1 is a point-detector, D_2 a line detector, and 0 is the point of annihilation

Let us briefly consider the information obtainable in this way from an ideal case (see Fig. 1). The positrons rapidly lose their energy to matter and are thermalized, so that the annihilation momentum of the electron – positron pair is practically equal to that of the electron. The two γ-quanta $E_1 = E_2 = mc^2 = 0.51$ MeV are emitted with high energies and small resultant momentum, hence the angle between the two γ-rays is close to 180° and the angle ϑ in Fig. 1 is correspondingly small. Assuming electrons are free and show a Fermi distribution having a maximum momentum p_F, with an ideal pair of detectors, one of which is infinitely long, the other point-like, we get a very simple angular correlation function of the form

$$N(\vartheta) = \pi \cdot (p_F^2 - p_z^2) = \pi m^2 c^2 (\Theta^2 - \vartheta^2),$$

that is, parabola for which $p_F = mc \cdot \Theta$. In a given angle ϑ those pulses are detected whose z-component has a constant value p_z and which are situated in the momentum field of the plane parallel to, at a distance p_z from, the median plane of the Fermi sphere, the area of which is given by the above expression.

Apart from having a parabolic form, distribution $N(\vartheta)$ also exhibits "tails" indicating annihilation on core electrons [13], [14].

Angular correlation measurements offer the possibility of studying not only the electron momentum distribution but also, if one chooses different relative z-axes in single crystals, its anisotropy, from which the shape of the Fermi surface can be inferred.

The positron annihilation method can be particularly useful for the study of changes in electron structure during phase transitions that cannot be followed precisely or (because a very low temperature is required) even detected at all by other methods.

Experimental apparatus

The angular correlation of the 0.5 MeV rays from 2γ annihilations was measured by two 50 mm$\times$50 mm NaI(Tl) scintillators mounted on 56 AVP photomultipliers. One of the detectors was rotated to different positions in the horizontal plane by a semi-automatically controlled driving motor. The angles were set by a modified arm used earlier for small-angle neutron scattering experiments. The angular correlation function was measured by a conventional fast-slow coincidence unit. The time resolution of the measuring equipment was chosen to be $\tau = 20$ nsec.

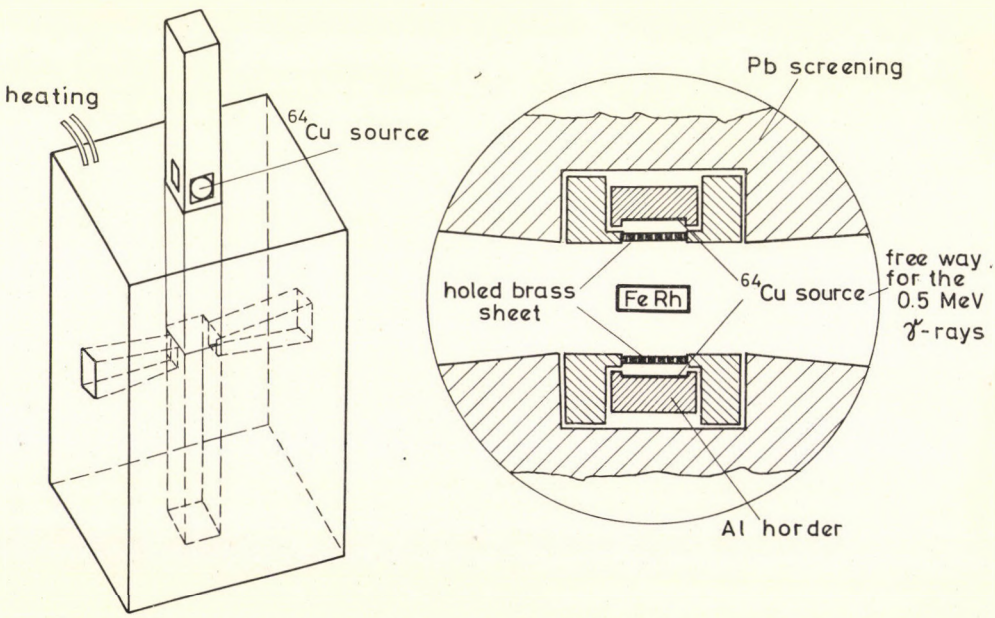

Fig. 2. ^{22}Na source and sample holder

Reactor-activated ^{64}Cu served as the positron source. The small dimensions of both the FeRh sample (5 mm diam., 1 mm thick) and the NaI(Tl) scintillators made it necessary to employ a source with the maximum activity permitted by health physical regulations. The source was prepared from two 99.99% copper discs (5 mm diam, 0.01 mm thick) activated separately to about 1 Ci. The thickness of the sample was limited, apart from by radiation safety considerations, also by the effective range of positrons. Because of its high activity, the source was handled in the manipulator cell of the reactor in source and sample holders prepared for this purpose (Fig. 2). The incidence into the detector of other than the pairs of rays originating in the sample was prevented by "collimation" of the positron sources with a perforated screen.

The temperature of the sample holder was controlled by an automatic thermostat. For temperature-dependence measurement of the sample a Thompson-bridge resistometer was used. The sample of $Fe_{49}Rh_{51}$ composition was prepared in the Solid State Physics Department of our Institute.

The measuring arrangement is shown in Fig. 3.

Experimental results and discussion

Since the sample was found to be still in the antiferromagnetic phase at $T_1 = 300$ °K and already in the ferromagnetic phase at $T_2 = 373$ °K (Fig. 4), the angular correlation function was measured at these two temperatures. The angular range covered was about 50 mrad in both cases. The angular correlation function was evaluated from the formula

$$N(\vartheta) = 2I_0 \cdot \omega_T \cdot \varepsilon_t \cdot \varepsilon_z \cdot \omega_1 \cdot p(\vartheta, \varphi) \cdot \Delta\vartheta,$$

where I_0 is the intensity of the source; ω_T the solid angle of the sample; ε_1, ε_2 the detector efficiencies; ω_1 the solid angle of one of the detectors; and $p(\vartheta, \varphi)$ is the probability that the solid angle Ω between the pair of gamma rays count-

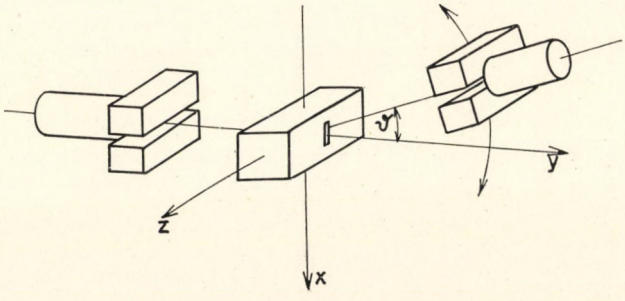

Fig. 3. The experimental set-up

ed by the detectors in the solid angle ω_1 and ω_2, respectively, is covered by the detector with slit width $\Delta\vartheta$ in the solid angle ω_2 (Fig. 5), which, assuming a Fermi distribution and detector of length l, is given by the function

$$p(\vartheta, \varphi) = \frac{l}{\Theta}\left(1 - \frac{\vartheta^2}{\Theta^2}\right).$$

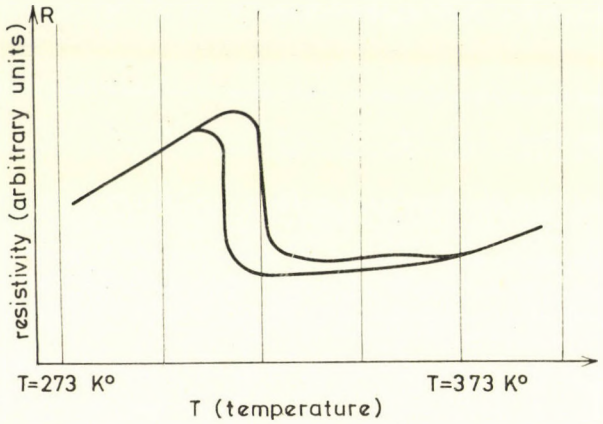

Fig. 4. Temperature dependence of the electronic resistivity of the FeRh-sample

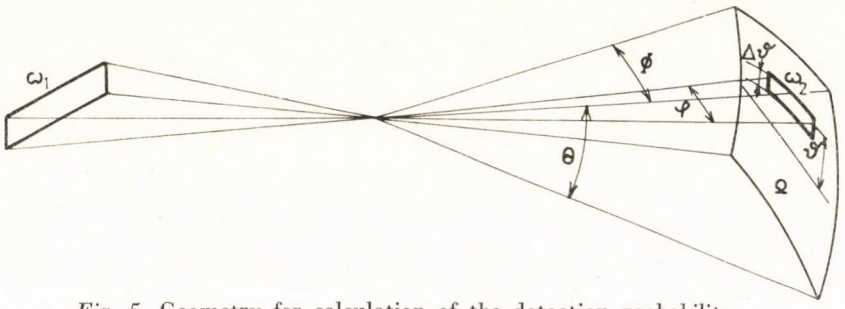

Fig. 5. Geometry for calculation of the detection probability

The number of random chance coincidences was taken to be negligible with the time resolution $\tau = 20$ nsec.

The function $N(\vartheta)$ measured in both phases was expected to yield two curves of different shapes which would permit a change in the electronic structure of the FeRh sample to be inferred. The measurements were repeated several times to average out minor electronic instabilities. The results are displayed in Fig. 6. The similarity of the two curves indicates that no significant change occurs in the electronic structure of FeRh as a result of the antiferro- to ferromagnetic transition.

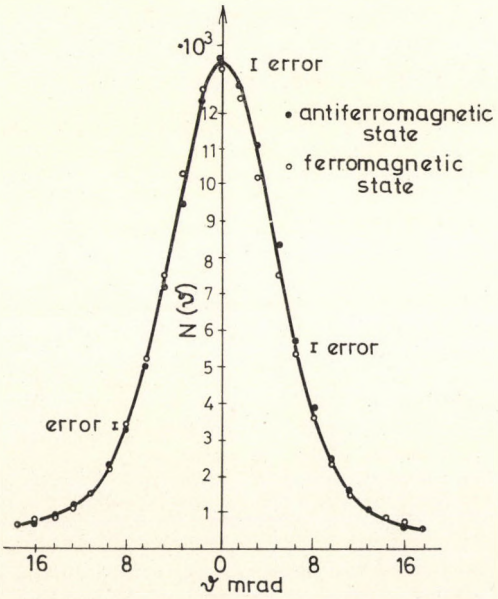

Fig. 6. The measured angular correlation for ferromagnetic and antiferromagnetic states

One cannot exclude here a possible dependence of the electron distribution on crystallographic direction, but the use of a polycrystalline sample averaged this out. Even if a sharp direction-dependent change does occur at the Fermi surface, its effect would be blurred by averaging. The difference between the averaged angular distributions at the two temperatures of the measurement cannot be more than 2%.

Acknowledgments

Authors are indebted to Prof. L. PÁL for suggesting the problem and to Dr. P. HRASKÓ for valuable discussions. Thanks are due to Mr. D. HORVÁTH and Miss MARIANNE LÁBADY for their help in the measurements as well as to Messrs I. VERESS and J. PAZONYI for designing and adjusting the mechanical parts of the measuring apparatus.

REFERENCES

1. J. S. KOUVEL and C. C. HARTELIUS, J. Appl. Phys. Suppl. **33,** 1343, 1962.
2. A. I. ZAKHAROV, A. M. KADOMTSEVA, R. J. LEVITIN i F. G. PONYATOVSKII, Zh. Eksp. Teor. Fiz., **56,** 2003, 1964.
3. L. MULDAWER and F. DE BERGEVIN J. Chem., Phys., **35,** 1905, 1961.
4. B. F. BERTAUT, F. DE BERGEVIN and G. ROULT, Compt. Rend., **256,** 1688, 1963.
5. G. SHIRANE, R. NATHANS and C. W. CHEN Phys., Rev., **134,** A1547, 1964.
6. F. DE BERGEVIN and L. MULDAWER, Compt. Rend., **252,** 1347, 1961.
7. C. KITTEL, Phys. Rev., **120,** 335, 1960.

8. L. PÁL, T. TARNÓCZI, P. SZABÓ, E. KRÉN and J. TÓTH Proc. Int. Conf. on Magnetism (1964) (London: The Institute of Physics and The Physical Society).
9. J. S. KOUVEL, C. C. HARTELIUS and P. E. LAWRENCE, Bull. Am. Phys. Soc., **8**, 54, 1963.
10. J. S. KOUVEL Journ. Appl. Phys., **37**, 1257, 1966.
11. P. TU, A. J. HEEGER, J. S. KOUVEL and J. B. COMLEY Journ. Appl. Phys., **40**, 1368, 1969.
12. A. ORE and J. L. POWELL Phys. Rev., **75**, 1969, 1949.
13. Positron Annihilation A. I. STEWART and L. O. ROELLIG, Academic Press, New York—London, 1967, p. 259.
14. A. T. STEWART, Can. J. Phys., **35**, 168, 1957.

ИССЛЕДОВАНИЕ АНТИФЕРРОМАГНИТНО–ФЕРРОМАГНИТНОГО ПЕРЕХОДА ПЕРВОГО РОДА В FeRh МЕТОДОМ АННИГИЛЯЦИИ ПОЗИТРОНОВ

А. АДАМ, Л. ЧЕР, Ж. КАЙЧОШ и Д. ЦИММЕР

Резюме

Для выяснения вопроса, изменяется ли электронная структура сплава FeRh при антиферро-ферромагнитном фазовом переходе, была измерена угловая корреляция двухфотонной аннигиляции позитронов в обоих фазах. ($T_1 = 300$°K и $T_2 = 373$°K.) Кривые угловой корреляции, померенные в обоих фазах, не отличаются друг от друга в пределах статистической точности измерения. Этот результат не подтверждает теоретическое предсказание о том, что электронная энтропия является движущей силой рассматриваемого фазового перехода.

Acta Physica Academiae Scientiarum Hungaricae, Tomus 32 (1—4), pp. 307—318 (1972)

НОВЫЕ РЕЗУЛЬТАТЫ ИССЛЕДОВАНИЙ РЕНТГЕНОВСКИХ ВСПЫШЕК НА СОЛНЦЕ*

С. Л. МАНДЕЛЬШТАМ

ФИЗИЧЕСКИЙ ИНСТИТУТ ИМ. П. Н. ЛЕБЕДЕВА АН СССР, МОСКВА, СССР

(Поступило 8. XI. 1971)

Измерения, выполненные на спутниках Земли «Интеркосмос-1» и «Интеркосмос-4», показали наличие значительной поляризации рентгеновского излучения вспышек на Солнце в области энергий около 10—20 кэв во время «импульсивной» стадии вспышек. Это показывает, что жесткое рентгеновское излучение солнечных вспышек обязано направленным пучкам ускоренных электронов. Исследование спектра рентгеновских вспышек, выполненное с помощью спектрометра с кристаллом с большим спектральным разрешением показало наличие в спектре линий ионов Fe XXV, Fe XXIV и Fe XXIII, причем получено доказательство существенной роли механизма диэлектронной рекомбинации. Электронная температура плазмы в области рентгеновской вспышки оказалась равной примерно $15—20 \cdot 10^6$ °К, температура ионов, измеренная по допплеровскому уширению линий Mg XII составляет $12—15 \cdot 10^6$ °К.

1. Введение

Одним из замечательных проявлений солнечной активности, являются т. н. вспышки на Солнце. Уже сравнительно давно было установлено, что иногда в активных областях, связанных с магнитными пятнами на Солнце, возникает внезапное сильное уярчение некоторого участка солнечной поверхности, особенно заметное в свете линии H_α. С развитием радиоастрономии, было установлено, что такие оптические вспышки, как правило сопровождаются всплесками радиоизлучения в сантиметровом, метровом и декаметровом диапазонах. Вспышки на Солнце вызывают ряд эффектов на Земле – нарушение состояния земной ионосферы, магнитные бури и т. д. С появлением спутников и ракет удалось непосредственно обнаружить агенты вызывающие эти явления — ими оказались вспышки рентгеновского излучения Солнца, сопровождающиеся появлением очень жесткого излучения — иногда вплоть до нескольких сотен кэв, и потоки ускоренных частиц — электронов, протонов и тяжелых ядер со скоростями от десятков кэв, до субрелятивистских, а также выбросы сгустков плазмы.

Масштаб времени солнечной вспышки составляет от нескольких минут до нескольких десятков минут. Во время сильной вспышки класса 3 выделяется полная энергия достигающая $\approx 10^{32}$ эрг (полная энергия излучения Солнца составляет $3{,}8 \cdot 10^{33}$ эрг/сек). Около половины энергии вспышки выделяется

* В честь 60-летия Профессора Л. Яноши.

ввиде электромагнитной энергии — от жесткого рентгена до метрового радиодиапазона и около половины — в виде ускоренных частиц [1].

Сильная вспышка захватывает площадь достигающую 10^{-3} видимой поверхности Солнца, толщина слоя — 10—100 км, т. е. объем области вспышки составляет 10^{29} см^3. Отсюда следует, что плотность энергии в области вспышки составляет $\approx 10^3$ эрг/см^3. Плотность тепловой энергии в хромосфере — около 3 эрг/см^3, т. е. вспышка происходит за счет дополнительного источника энергии. Этим источником является энергия магнитного поля в солнечной атмосфере. Во время вспышки, как показали исследования А. Б. Северного, происходит локальное высвобождение запаса магнитной энергии, соответствующее уменьшению величины магнитного поля на 100—200 гаусс (среднее поле в активной группе пятен — порядка 500 гаусс).

Здесь по существу кончаются твердо установленные факты. Каков механизм аннигиляции магнитного поля, каков механизм появления жесткого и оптического электромагнитного излучения и ускорения частиц — мы не знаем. Существует несколько гипотез, в частности, очень детально разработанная гипотеза предложена С. И. Сыроватским [2].

Существенное значение для понимания механизма солнечных вспышек имеет детальное исследование рентгеновского излучения вспышек. Рентгеновское излучение возникает в результате взаимодействия быстрых электронов с ионами в области вспышки ввиде тормозного и рекомбинационного непрерывного излучения и линейчатого излучения ионов. Таким образом это излучение характеризует электронную и ионную компоненту плазмы в области вспышки. Исследование рентгеновского излучения вспышек позволяет определить физические параметры плазмы — температуру и плотность частиц, а также локализацию, размеры и структуру области рентгеновских вспышек и их связь с областями оптических вспышек.

В настоящей статье приводятся результаты исследований рентгеновских вспышек, выполненных в последние годы в Физическом институте им. П. Н. Лебедева АН СССР группой в составе: И. Л. Бейгмана, Л. А. Вайнштейна, Б. Н. Васильева, И. А. Житника, В. Д. Иванова, В. В. Крутова, С. Л. Мандельштама, И. П. Тиндо, А. И. Шурыгина и др.

2. Исследование поляризации излучения рентгеновских вспышек

Исследование излучения рентгеновских вспышек, показывает, что оно большей частью состоит из двух компонент — жесткой «импульсивной» компоненты с временем нарастания в несколько секунд, длящейся несколько десятков секунд и жестким спектром и более медленной компоненты, длящейся до нескольких десятков минут и более мягким спектром; доминирующая роль импульсивной и медленной компонент обычно проявляется соответственно при $h\nu \gtrless$ 10—20 кэв [3].

Импульсивная компонента хорошо коррелирует по времени возникновения и длительности с микроволновыми радиовсплесками и ее максимум предшествует на 0,5—3 минуты максимуму оптической вспышки в H_α; медленная компонента хорошо коррелирует с основной фазой оптической вспышки. Можно полагать, что именно во время импульсивной фазы рентгеновских вспышек происходит ускорение частиц и выбросы плазмы, о которых говорилось выше. Поэтому представляется весьма существенным выяснить каков механизм возникновения жесткого рентгеновского излучения. Возникает ли оно благодаря нагреву плазмы до высокой температуры током или сжатием ее магнитным полем, как это, например, имеет место в лабораторных установках типа «тета-пинч», либо оно обязано направленным потокам ускоренных электронов, возникающих или вторгающихся в область вспышки.

Непосредственным способом выяснения этого вопроса является измерение поляризации этого излучения. Если имеется направленный пучек быстрых электронов, то ими вызывается тормозное излучение, которое, как показали А. А. Корчак и Г. Эльверт частично поляризовано [4, 5]. В случае направленных потоков электронов с энергиями в несколько десятков кэв, тормозное излучение значительно превосходит синхротронное излучение. Величина поляризации $P = \dfrac{I_\perp - I_{||}}{I_\perp + I_{||}}$, где $I_\perp$ и $I_{||}$ — соответсвенно интенсивность излучения в плоскости перпендикулярной и параллельной референтной плоскости, проходящей через направление движения электронов и направление движения фотонов, оказывается функцией отношения $h\nu/\varepsilon$, где $h\nu$ — энергия фотонов, а ε — энергия электронов. Для монохроматического направленного пучка электронов при наблюдении перпендикулярно движению электронов величина P изменяется от $+1$ до -1, проходя через ноль вблизи $h\nu/\varepsilon \approx 0{,}1$. Наличие распределения электронов по скоростям, а также непрямолинейное движение их в магнитном поле уменьшает предельные значения поляризации, не меняя качественной картины [4].

Поляризация излучения рентгеновских вспышек была нами впервые обнаружена на спутнике «Интеркосмос-I», запущенном 14 октября 1969 г. [6]. Эти измерения были повторены с большей точностью на спутнике «Интеркосмос-4», запущенном 14 октября 1970 г. Спутник «Интеркосмос-4» был идентичен спутнику «Интеркосмос-1»; продольная ось спутника была направлена на Солнце с точностью 1—2°, спутник медленно вращался вокруг этой оси. Поляризация излучения рентгеновских вспышек измерялась по угловой анизотропии томсоновского рассеяния. Схематическое изображение поляриметра приведено на рис. 1. Рентгеновское излучение вспышек рассеивается на бериллиевых пластинах и регистрируется тремя парами пропорциональных счетчиков фотонов, расположенными под углом в 120°. Область энергетической чувствительности счетчика, принимая что спектр импульсивной фазы имеет вид $(h\nu)^{-3,5}$ фот/см^2 сек. кэв [7] соответствовала примерно 15—

20 кэв. С целью уменьшения космического фона были использованы двухсекционные счетчики фотонов, включенные по схеме антисовпадений, амплитуда импульсов дискриминировалась по верхнему и нижнему уровню. Показания счетчиков суммировались за время 16 сек, и регистрировались на запоминающем устройстве спутника. Для контроля помех со стороны частиц

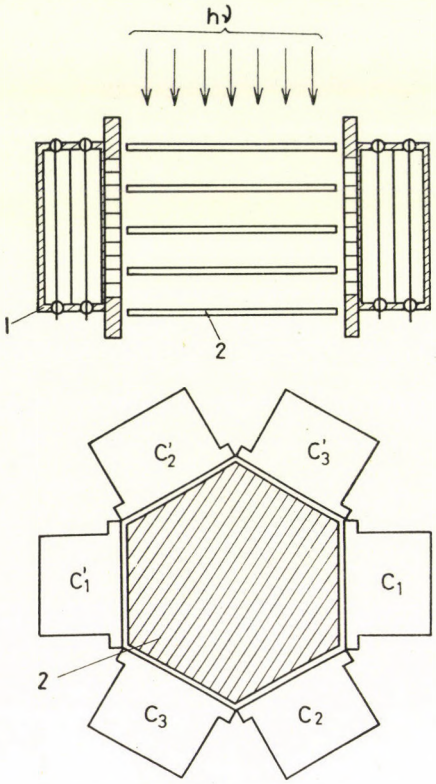

Рис. 1. Схематическое изображение рентгеновского поляриметра: 1(C'_{1-3}, C_{1-3})- двухсекционные счетчики фотонов, 2-бериллиевые пластины

радиационных поясов, служил контрольный счетчик, нечувствительный к рентгеновскому излучению.

На рис. 2, 3 и 4 приведены результаты измерений для вспышек 24/X кл. 2, 5/XI кл. 3B, 16/XI кл. 1N. Величина поляризации составляет $P \approx 0{,}2$. Угол поляризации остается примерно постоянным в течение 2—3 минут (небольшие монотонные изменения обусловлены медленным вращением спутника вокруг оси, направленной на Солнце, со скоростью лежащей в пределах 0—0,05°/сек). Затем начинаются сильные изменения угла поляризации — эти изменения соответствуют конечной стадии вспышки. Оценки показывают что они вероятно обусловлены «кажущейся поляризацией» из-за

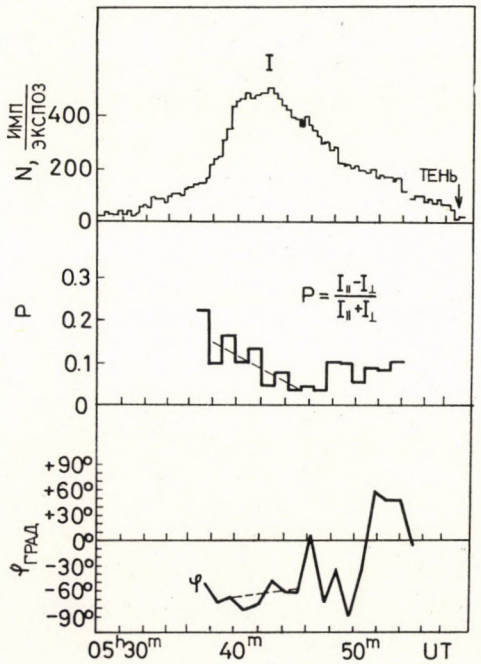

Рис. 2. Поток рентгеновского излучения, поляризация и угол поляризации во вспышке 24/X—70 г

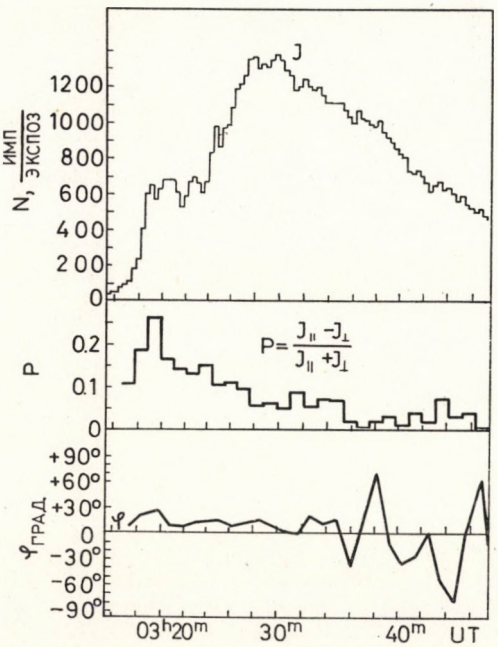

Рис. 3. Поток рентгеновского излучения, поляризация и угол поляризации во вспышке 5/XI—70 г

статистических флюктуаций показаний счетчиков в трех каналах, достигающих большой величины вследствие уменьшения абсолютного числа импульсов. Вспышки 5/XI и 16/XI показывают наличие второго максимума, что характерно для импульсивной фазы вспышек. Как видно из рисунков во время второго максимума, поляризация опять возрастает.

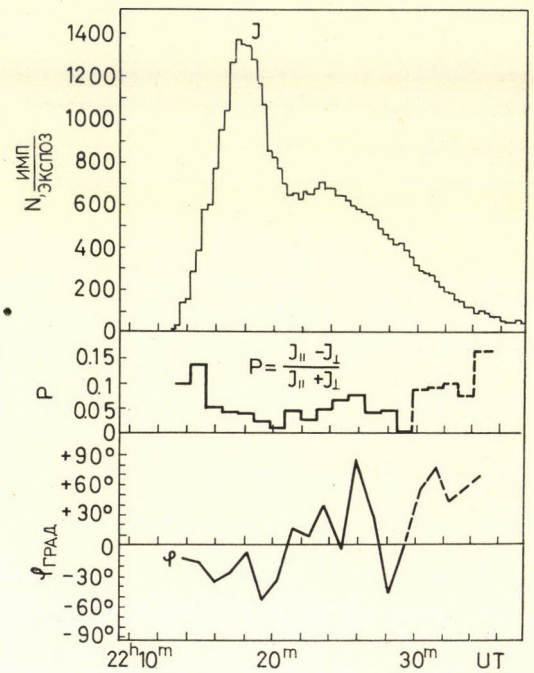

Рис. 4. Поток рентгеновского излучения, поляризация и угол поляризации во вспышке 16/XI—70 г

Приведенные результаты подтверждают результаты полученные на спутнике «Интеркосмос-1» и, как нам кажется, достаточно однозначно свидетельствуют о наличии в области вспышек в начальной стадии изученных нами вспышек, а также, по-видимгму, во время вторых максимумов, направленных потоков электронов с энергиями в несколько десятков кэв.

Время термализации электронов с начальной скоростью v равно

$$t_0 \approx \frac{\bar{l}}{\bar{v}} = \frac{m_e^2 v^3}{8\pi e^4 N_e \ln \Lambda} \approx \frac{6 \cdot 10^{-19} v^3}{N_e \ln \Lambda} .$$

При энергии электронов $\leqslant 10^5$ эв, $v \leqslant 1{,}8\ 10^{10}$ см/сек, и $N \geqslant 10^{-10}$ см$^{-3}$, $t_0 \leqslant 30$ сек.

Таким образом наличие поляризации излучения в течение нескольких

минут, по-видимому, свидетельствуют о том, что в области вспышек направленные потоки ускоренных электронов с энергией в несколько десятков кэв сохраняются в течение некоторого времени.

3. Исследования спектра рентгеновских вспышек

Информацию о параметрах плазмы в области рентгеновской вспышки — о температуре электронов и ионов и плотности электронов дает спектр рентгеновской вспышки. Спектр рентгеносвих вспышек изучался неоднократно с небольшим спектральным разрешением, главным образом с помощью про-

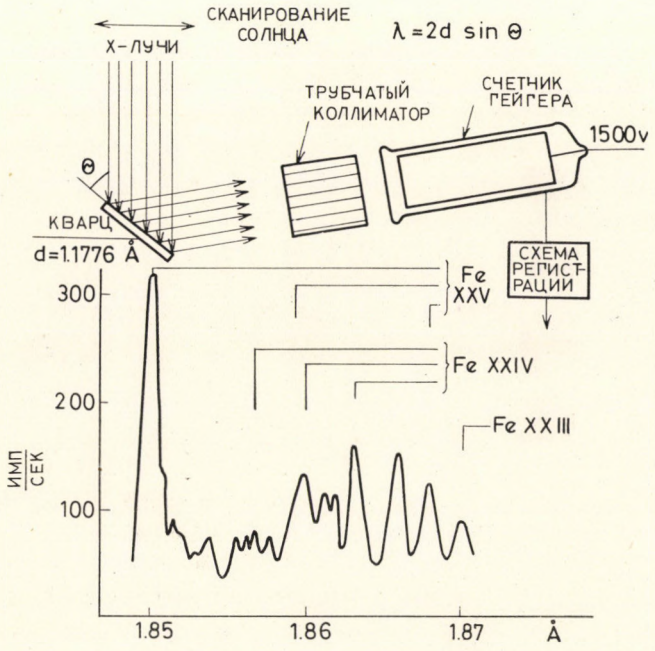

Рис. 5. Схема гелиоспектрометра

порциональных счетчиков фотонов. Однако более полную информацию можно получить, изучая линейчатый спектр вспышки. Мы исследовали спектр рентгеновской вспышки в области 1,8 Å — здесь расположены самые «горячие» линии, возбуждаемые в области вспышки — принадлежащие гелиеподобным ионам железа.

Исследования были также выполнены на спутнике «Интеркосмос-4». На рис. 5 изображена принципиальная схема гелиоспектрометра. Он состоит из кристалла кварца с постоянной $d = 1{,}1776$ Å и счетчика фотонов с берил-

Таблица I

Экспериментальные и вычисленные значения длин волн линий

Эксперимеит λ(Å)	Теоретический расчет	
	λ(Å)	переходы
1,850	1,850	FeXXV $1s^2\ {}^1S_0 - 1s2p\ {}^1P_1$
1,8525	1,852	FeXXIV $1s\ {}^2 2p^2 P_{1/2} - 1s2p^2\ {}^2S_{1/2}$
1,8555	1,855	FeXXV $1s^2\ {}^1S_0 - 1s2p\ {}^3P_2$
1,857	18565	FeXXIV $1s^2\ 2s\ {}^2S_{1/2} - 1s2s2p_1 P_{1/2}$
1,858	1,858	FeXXIV $1s^2\ 2p\ {}^2P_{1/2} - 1s2p^2\ {}^2P_{3/2}$
1,8585	1,859	FeXXV $1s^2\ {}^1S_0 - 1s2p\ {}^3P_1$
1,860	1,8605	FeXXIV $1s^2 2s\ {}^2S_{1/2} - 1s2s2p\ {}^2P_{3/2}$
1,8615		
1,863	1,8635	FeXXIV $1s^2 2s\ {}^2S_{1/2} - 1s2s2p\ {}^2P_{1/2}$ $1s^2 2p\ {}^2P_{1/2} - 1s2p^2\ {}^2D_{3/2}$
1,866	1,866	FeXXIV $1s^2 2p\ {}^2P_{3/2} - 1s2p^2\ {}^2D_{5/2}$
1,868	1,868	FeXXV $1s^2\ {}^1S^0 - 1s2s\ {}^3S_1$ EeXXIV $1s^2\ 2p\ {}^2P_{3/2} - 1s\ 2p^2\ {}^2D_{3/2}$
1,870	1,870	FeXXIII $1s^2 2s^2\ {}^1S^0 - 1s2s^2 2p\ {}^1P_1$

лиевым окном и выходом на телеметрию. Ось спутника направленная на Солнце, осуществляла три раза в течение каждого витка, а также по команде с Земли, сканирование диска Солнца. При этом изменялся угол Θ падения на кристалл параллельного пучка лучей от области вспышки и в соответствии с законом Брегга-Вульфа — длина волны, испытывающая отражение от кристалла. Этим осуществлялась регистрация спектра от 1,85 до 1,89 Å, что соответствовало $\Delta\Theta = 40'$. На рис. 6 изображен спектр вспышки кл. 3 16/XI—1970 г. в момент времени $1^h\ 51^m$UT. Ввиду отсутствия достаточно надежных лабораторных данных о длинах волн линий спектров FeXXIII, FeXXIV и FeXXV, мы произвели отождествление линий, опираясь на теоретические расчеты длин волн линий соответствующих переходов, выполненные методом возмущений [8]. Как показывает таблица, совпадение экспериментальных и вычисленных данных очень хорошее. Следует заметить, что впервые линейчатый спектр солнечной вспышки был получен в США Нейпертом с борта спутника OSO III; Нейпертом была сделана попытка отождествления линий, также опирающаяся на данные теоретических расчетов [9]. Однако разрешение в спектре Нейперта и точность расчетов значительно уступает данным, полученным на спутнике «Интеркосмос-4».

Таблица и рисунок показывают, что наряду с «оптическими» линиями иона FeXXV, наблюдаются внутриоболочечные переходы, соответствующие K_α — линиям ионов FeXXIV и FeXXIII. Наблюдаются также линии, которые можно рассматривать как результат заселения уровня $1s2p^2$ в ионе FeXXIV в процессе двухэлектронной рекомбинации иона FeXXV. Одна линия иона не отождествлена. Анализ условий возбуждения спектра, приведенного на рис. 6, приводит к выводу, что наблюдавшийся спектр в смысле соотношения интенсивности линий FeXXV $1s^2\,{}^1S_0$—$2s2p\,{}^1P_1$ $\lambda = 1{,}850$ Å и FeXXIV $1s^22p^2P_{3/2}$—$1s2p^2\,{}^2D_{5/2}$ $\lambda = 1{,}866$ Å соответствует электронной температуре плазмы в области вспышки $T_e \approx 20 \cdot 10^6$ °К, что хорошо согласуется с данными фильтровых измерений выполненных ранее [10].

Измерения ширины линии FeXXV $\lambda = 1{,}850$ Å, принимая форму линии Допплеровской, позволили впервые определить температуру ионов — она оказалась равной $T_e \approx 30 \cdot 10^6$ °К что, учитывая неточность измерений хорошо

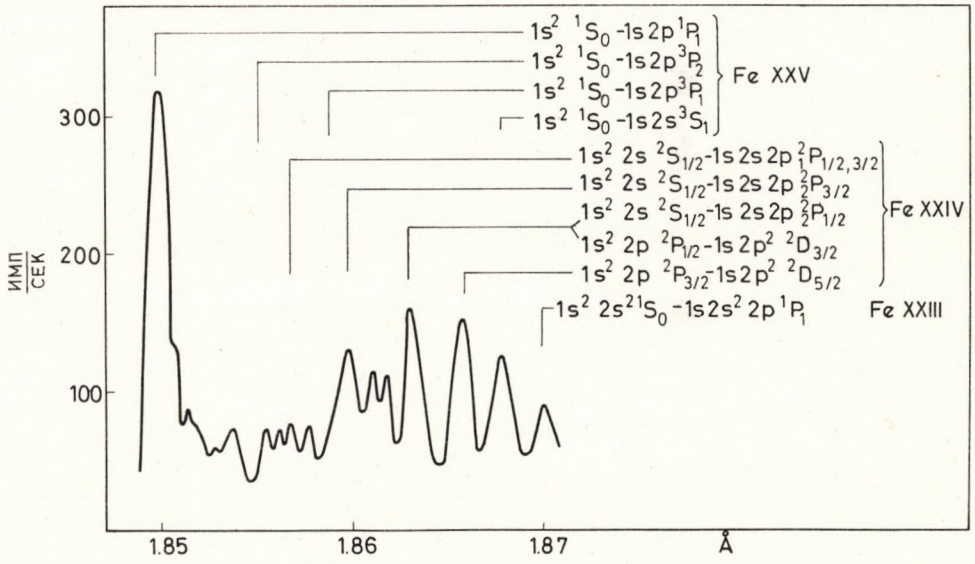

Рис. 6. Спектр в области 1,8—1,9 Å вспышки 16/XI—1970 г

согласуется со значением электронной температуры. Таким образом в области вспышки сравнительно быстро устанавливается равенство температур обеих компонент. Это подтверждается теоретической оценкой: время t_{eq} нагрева ионов электронной компонентой плазмы до $T_i \approx T_e$ составляет

$$t_{eq} \approx \frac{5{,}87}{Z_e^2 Z_i^2} \frac{A_i A_e}{N_e \ln \Lambda} \left(\frac{T_e}{A_e} + \frac{T_i}{A_i} \right)^{3/2} \approx 10^2 \text{ сек}.$$

На рис. 7 представлена форма линий дублета Mg XII $\lambda = 8{,}418$ Å и $\lambda = 8{,}423$ Å во время вспышки 24/X—1970 г., полученная на спутнике «Интеркосмос-4» для двух моментов времени. Эти линии Mg XII существуют в плазме в области температур $4 \cdot 10^6$—$4 \cdot 10^7$ °К и таким образом характеризуют горячие области вспышки. Измерения выполнены спектрогелиографом, ана-

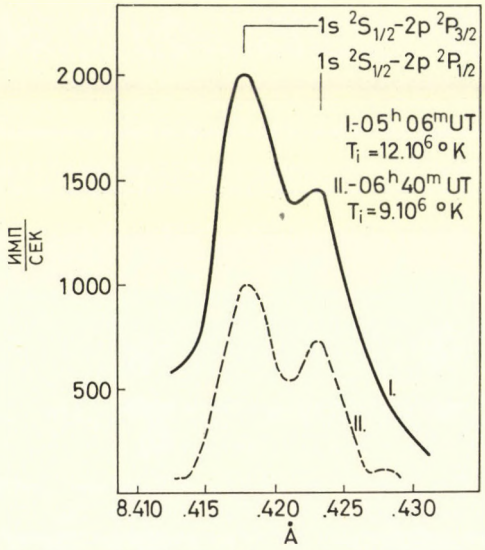

Рис. 7. Форма линий дублета Mg XII во время вспышки 24/X 1970

логичным, изображенному на рис. 5 с кристаллом кварца с постоянной $d = 4{,}246$ Å и счетчиком фотонов с алюминиевым окном. На рисунке видно уменьшение ширины линий и соответственно остывание плазмы во второй момент времени по сравнению с первым.

4. Заключение

Анализ изложенных выше результатов приводит к следующим выводам:

В начальной стадии вспышек в активную область вторгаются или в ней возникают направленные пучки быстрых электронов с энергией от нескольких десятков до нескольких сотен кэв. Эти электроны взаимодействуя с ионами плазмы вызывают поляризованное тормозное рентгеновское излучение, характерное для импульсивной фазы вспышки. Часть ускоренных электронов вызывает всплески микроволнового радиоизлучения. Этот процесс протекает, по-видимому, в течение 10—100 сек. Быстрые электроны термализуются и нагревают плазму в течение времени порядка 10 секунд. Следует, однако, иметь ввиду, что даже небольшая доля нетермализованных электронов может

давать существенный вклад в жесткое излучение $h\nu \geqslant 10$ кэв и поэтому жесткое излучение в импульсивной фазе вспышек следует характеризовать как нетепловое. Более мягкое излучение $h\nu \leqslant 10$ кэв, по-видимому, можно характеризовать как тепловое. Область рентгеновских вспышек аналогична области оптических вспышек — она имеет веретенообразную структуру с длиной волокна $\approx 100''$ и шириной $\approx 10—20''$, быстро изменяющуюся во времени, с яркими узлами [10].

Измерения спектрального состава излучения в широком диапазоне длин волн от 1 до 15 Å с помощью фильтров, однако, показывают что плазму нельзя описывать одной температурой, по-видимому, плазма в области рентгеновских вспышек состоит из двух компонент. Первая — более холодная компонента имеет температуру $T_1 \approx 7—9 \cdot 10^6$ °К и меру эмиссии $y_1 \approx 0{,}02—0{,}1$ (в единицах Баумбаха — 1В $\approx 3{,}2 \cdot 10^{49}$ см$^{-3}$); электронная плотность $N_e \approx 1—2 \cdot 10^{10}$ эл/см^3, возможно достигая иногда $10^{11}—10^{12}$ эл/см^3. Для мощных вспышек y_1, по-видимому, может быть в несколько раз больше, однако, сейчас трудно сказать связано ли это с большим объемом или большей электронной плотностью области вспышки. Вторая более горячая компонента плазмы имеет температуру $T_2 \approx 15—20 \cdot 10^6$ °К и меру эмиссии $y_2 \approx \approx (0{,}2—0{,}1) \cdot y_1$. По-видимому, эта более горячая область представляет собой не локализованное ядро, а совокупность горячих элементов, распределенных по всей области вспышки. Яркие узлы имеют, по-видимому, не большую температуру, а большую электронную плотность. Аналогичный вывод о дисперсном распределении горячих элементов был сделан также из сопоставления рентгеновского потока вспышки со вспышкой в H_α [11].

Следует далее заметить, что время заметного охлаждения нагретой плазмы составляет около 30 минут, тогда как наши данные указывают для некоторых вспышек на сравнительное малое изменение температуры вспышки за такое время. Это заставляет считать, что во всяком случае для длительных вспышек может иметь место длительное поступление энергии в область вспышки ввиде ускоренных электронов, однако, в значительно меньших масштабах чем при возникновении вспышки.

ЦИТИРОВАННАЯ ЛИТЕРАТУРА

1. C. de Jager, "Solar Flares and Space Research". North-Holland publ. Co. Amsterdam, 1969.
2. С. И. Сыроватский, Труды симпозиума по Солнечно-земной физике, Ленинград, 1970.
3. S. R. Kane and K. A. Anderson, Ap. J., **162,** 1003, 1970.
4. А. А. Корчак, а) Доклады АН СССР, **173,** 291, 1967. б) Геомагнетизм и Аэрономия V, 601, 1965.
5. G. Elvert a) "Structure and Development of solar active regions" IAU Symp. **35,** 444, 1968. b) Solar Physics, **15,** 234, 1970.
6. И. П. Тиндо, В. Д. Иванов, С. Л. Мандельштам, А. И. Шурыгин, В. А. Савельев, Космические исследования. IX, 116, 1971.
7. S. R. Kane and R. F. Donnely, Ap. J., **164,** 151, 1971.

8. Л. А. Вайнштейн, У. И. Сафронова, Астрономический журнал XLVIII, вып. 1, 1971.
9. G. Neupert, a) Ap. J., **149,** 79; 1967. b) Ap. J., **160,** 189, 1970.
10. И. Л. Бейгман, Л. А. Вайнштейн, Б. Н. Васильев, И. А. Житник, В. Д. Иванов, В. В. Корнеев, В. В. Крутов, С. Л. Мандельштам, И. П. Тиндо, А. И. Шурыгин, Космические исследования, IX, 123, 1971.
11. H. Zicsin, Solar Phys., **9,** 269, 1969.

NEW RESULTS OF X-RAY FLARE STUDIES

S. L. MANDELSTAM

Abstract

Measurements carried out with the satellites "Intercosmos-1" and "Intercosmos-4" showed a considerable polarization of the X-ray emission in the 10—20 keV range during the initial "impulsive" phase of solar flares. This shows that the hard X-rays of the solar flares are produced by directed beams of accelerated energetic electrons.

Investigations of the X-ray flare spectra, carried out with Bregg crystal spectrometers with high spectral resolving power, show lines of ions Fe XXV, Fe XXIV and Fe XXIII; the important role of dielectronic recombination process is confirmed. The electron temperature of the flare plasma is about 15—20· 10^6 °K and ion temperature 12—15 ·10^6 °K measured by the Doppler width of Mg XII lines was found.

Acta Physica Academiae Scientiarum Hungaricae, Tomus 32 (1—4), pp. 319—322 (1972)

THE PROBABILITY DISTRIBUTION OF OPTICAL FIELD EMISSION COUNTS*

By

J. BERGOU, GY. FARKAS and Z. GY. HORVÁTH

CENTRAL RESEARCH INSTITUTE FOR PHYSICS, BUDAPEST

(Received 19. XI. 1971)

The probability distribution of electron counts is derived for the case when electrons are released by the process of optical field emission, and measuring times are much shorter than the coherence time.

Of the several mechanisms for the detection of light that make use of the interaction of radiation with matter only photodetectors in which electrons are released by the incident light beam are dealt with. The emerging electrons carry information on the light so that a study of the photocount statistics allows the statistical properties of the light beam to be deduced.

The statistics of light emitted by thermal sources was first established by JÁNOSSY [1], [2] who showed that to a very good approximation it has a Gaussian character. This result was confirmed experimentally by JÁNOSSY et al. [3].

The situation is strictly modified when a laser is employed as the light source, as by using suitable optical instruments the statistical properties of a laser beam can be altered in a continuous manner from those of the phase and amplitude-stabilized case to those of the thermal beams. The intensity distribution for the first case can be described to a good approximation by the δ function. Detailed theoretical and experimental investigations have been carried out by many authors [see e.g. ARECCHI [4] and the references quoted therein] using a laser beam and first-order photoelectric effect as photodetecting process.

It appears, however, that when high-intensity light beams are utilized — which can be obtained today with solid state lasers — besides the usual linear photoelectric phenomena, electrons released by higher-order photoelectric effect and in a direct manner by optical field emission may play a role in the detection process. The photocount statistics also has been investigated in detail for higher-order photoelectric effect [5—11]. The possibility of optical field emission at high intensities was supported experimentally by KRASYUK PASHININ and PROKHOROV [12].

The aim of this work is to give an approximate formula for the probability distribution of optical field emission counts. According to our calculations

* Dedicated to Prof. L. JÁNOSSY on his 60th birthday.

the field emission counting statistics differs from that of the photoelectric effect, so it could be possible to distinguish experimentally between the two processes on this basis.

The electron current obtained in the process of field emission at optical frequencies was first expressed as the function of the incident light intensity $I(t)$ by KELDYSH [13] and BUNKIN and FEDOROV [14]. For the following calculations we need the differential probability $P(t)\Delta t$ of counting one electron in the time interval t, $t + \Delta t$ expressed in terms of the electron current:

$$P(t)\,\Delta t = \alpha\, I(t) \exp\left\{-\frac{\beta}{\sqrt{I(t)}}\right\}\Delta t\,, \tag{1}$$

where α and β are constants, and high-order corrections in the intensity are neglected. The probability $p(n, T, t)$ of counting n electrons in the time interval $(t, t + T)$ is given [9] by the Poisson distribution

$$p(n, T, t) = \frac{1}{n!}[U(T, t)]^n\, e^{-U(T,t)}, \tag{2}$$

where $U(T, t)$ denotes the integral of the differential electron counting probability over the time interval $(t, t + T)$

$$U(T,t) = \alpha \int_t^{t+T} I(t') \exp\left\{-\frac{\beta}{\sqrt{I(t')}}\right\} dt'\,. \tag{3}$$

If, as is usually the case, the radiation field is stationary and ergodic, $p(u, T, t)$ will be independent of t and may be written as $p(n, T)$. Generally, the intensity contains the fluctuations of the radiation field. In that case $p(u, T)$ follows from (2) by averaging over the time t. In the ergodic case this procedure can be replaced by ensemble averaging, where the average is to be taken over the ensemble of $U(T, t)$:

$$p(n, T) = \int p(n, T, U)p(U)dU\,. \tag{4}$$

We evaluate $p(n, T)$ under the following two assumptions:

1. T is much shorter than the coherence time of light: $T \ll 1/\Delta\nu$, so that after the integration denoted in (3) is carried out $U(T, t)$ reduces to

$$U(T,t) = \alpha I(t)\, T \exp\left\{-\frac{\beta}{\sqrt{I(t)}}\right\}.$$

2. Fluctuations of the radiation field are ignored: $p(U)dU = \delta(U - \langle u \rangle)\, dU$, viz. we are dealing with a laser operating in a single mode. In this case the ensemble averaging denoted in (4) yields the following expression:

$$p(n, T) = \frac{1}{n!} \int U^n e^{-U} \delta(U - \langle U \rangle)\, dU = \frac{1}{n!} \left[\alpha \bar{I} T e^{-\frac{\beta}{\sqrt{\bar{I}}}} \right]^n \exp \left\{ -\alpha \bar{I} T e^{-\frac{\beta}{\sqrt{\bar{I}}}} \right\}, \tag{5}$$

where $\bar{I}$ denotes the average intensity, It can be seen that (5) is the usual Poisson distribution with parameter

$$U = \alpha \bar{I} T e^{-\frac{\beta}{\sqrt{\bar{I}}}}.$$

On these assumptions the Poisson distribution also results for the counting statistics of linear and higher-order photoelectric effects [5—11], but with a different parameter $\alpha \bar{I}^k$, where k is the order of the effect. Thus by measuring the intensity dependence of the parameter it becomes possible to distinguish between photoelectric effect and optical field emission.

We hope to return to the problem of what modifications to the above result are to be expected if the statistics of real laser fields are considered and the measuring time is comparable to the coherence time of light.

The intensity range in which the pure field emission process occurs (i.e. where the formula (1) is valid) high enough to be perfectly realized. However, investigations carried out for the nonlinear photoelectric effects [12, 15, 16] have recently shown that in lower intensity ranges the influence of the field emission appeared. Therefore the role of the statistics is immediately comparable to the experimental results.

REFERENCES

1. L. JÁNOSSY, Il Nuovo Cimento, **6,** 111, 1957.
2. L. JÁNOSSY, Il Nuovo Cimento, **12,** 369, 1959.
3. GY. FARKAS, L. JÁNOSSY and ZS. NÁRAY, Acta Phys. Hung., **18,** 199, 1965.
4. F. T. ARECCHI, Proc. of Int. School of Phys. "Enrico Fermi" ed. R. J. Glauber "Quantum Optics", Academic Press, 1969.
5. J. MEADORS, **QE—2** 638, 1966.
6. Y. R. SHEN, Phys. Rev., **155,** 921, 1967.
7. M. C. TEICH and P. DIAMENT, J. Appl. Phys., **40,** 625, 1969.
8. S. CARUSOTTO, G. FORNACCA and E. POLACCO, Phys. Rev., **165,** 1391.
9. П. П. Барашев и А. Д. Гладун, Усп. Физ. Наук, **98,** 493, 1969.
10. F. SHIGA and S. IMAMURA, Phys. Lett., **25A,** 706, 1967.
11. GY. FARKAS, Acta Phys. Hung., **29,** 415, 1970.
12. И. К. Красюк, П. П. Пашинин, А. М. Прохоров, ЖЭТФ, 1606, 1970.
13. L. В. Келдыш, ЖЭТФ, 47, 1945, 1964.
14. Ф. В. Бункин, М. В. Федоров, ЖЭТФ, **48,** 1341, 1965.
15. А. П. Силин, Физ. Твер. Тела, **12,** 3553, 1970.
16. GY. FARKAS, Z. GY. HORVÁTH and I. KERTÉSZ, Preprint, KFKI, 1972.

РАСПРЕДЕЛЕНИЕ ФОТОЭЛЕКТРОННЫХ ОТСЧЕТОВ, ЭМИССИОННЫХ ОПТИЧЕСКИМ ПОЛЕМ

Я. БЕРГОУ, Д. ФАРКАШ и З. Д. ХОРВАТ

Резюме

Распределение вероятности электронных отсчетов определяется для того случая, когда электроны испускаются в процессе эмиссии под действием оптического поля и времена измерения гораздо короче времени когерентности. Из многих механизмов детектирования света, в которых используется взаймодействие света с веществом рассматриваются только фотодетекторы, где электроны испускаются под действием падающих пучков света. Испускаемые электроны несут информацию о свете, и поэтому изучение отсчета фотоэмиссионных электронов позволяет делать выводы о статистических свойствах светого пучка.

Acta Physica Academiae Scientiarum Hungaricae, Tomus 32 (1—4), pp. 323—340 (1972)

CHECKING MICROSCOPIC CAUSALITY AND REVERSIBILITY IN K-MESON DECAY*

By

G. MARX

DEPARTMENT OF ATOMIC PHYSICS, ROLAND EÖTVÖS UNIVERSITY, BUDAPEST

(Received 19. XI. 1971)

The available experiments have indicated that neutral K decays violate CP and T symmetries, but conserve CPT symmetry, which is strictly related to local causality. The accuracy of this indication is discussed. The possibility that a stronger CP and T asymmetry existed at the time of the Big Bang is suggested and its implications for leptonic charge values are investigated.

Symmetries and asymmetries in the K°—$\overline{K}^\circ$ system

The celebrated CPT theorem states that in a relativistic field theory, subject to the principle of causality, CPT must be a strict symmetry [1]. As usual, C stands for charge conjugation, P for space reflection, T for time reversal and CPT is the product of the three transformations. CPT symmetry is supported by the observed equality of the masses and lifetimes of particles and antiparticles, but in the light of the observed faint CP asymmetry of neutral K-meson decays it has become necessary to check both T and CPT to the same accuracy. The possibility of accurate investigation is offered by the $K^\circ - \overline{K}^\circ$ system. Let us summarize briefly the formulas in which such investigations rest [2].

State vectors describing the unstable neutral K mesons have the following structure:

$$K(t) > = a_+(t) \mid K^\circ > + a_-(t) \mid \overline{K}^\circ > + \text{orthogonal decay products.} \quad (1)$$

Here $\mid K^\circ >$ and $\mid \overline{K}^\circ >$ are simultaneous eigenvectors of the strong Hamiltonian H_0 and of the hypercharge Y:

$$[H_0,\ Y] = 0, \quad [H_0, CP] = 0, \quad \{Y, CP\} = 0, \quad (2)$$

$$H_0 \mid K^\circ > = m_0 \mid K^\circ >, \qquad H_0 \mid \overline{K}^\circ > = m_0 \mid \overline{K}^\circ >, \quad (3)$$

$$Y \mid K^\circ > = + \mid K^\circ >, \qquad Y \mid \overline{K}^\circ > = - \mid \overline{K}^\circ >. \quad (4)$$

If we turn on the weak perturbation H with the properties

* Dedicated to Prof. L. JÁNOSSY on his 60th birthday.

$$H_{\text{total}} = H_0 + H, \qquad [H, Y] \neq 0, \tag{5}$$

K° and $\overline{K}^\circ$ will not be steady-state solutions any longer. The time dependence of $| K(t) >$ in Eq. (1) is given by the Weisskopf—Wigner theory [2]:

$$i \frac{\partial}{\partial t} \begin{bmatrix} a_+ \\ a_- \end{bmatrix} = \mathcal{H} \begin{bmatrix} a_+ \\ a_- \end{bmatrix}, \tag{6}$$

where $\mathcal{H}$ is the effective Hamiltonian in the subspace of neutral K mesons. This non-Hermitian two-by-two matrix is parametrized as follows:

$$\mathcal{H} = \frac{M_S + M_L}{2} + \frac{M_S - M_L}{2} \begin{bmatrix} \sin 2\delta & e^{2\varepsilon} \cos 2\delta \\ e^{-2\varepsilon} \cos 2\delta & -\sin 2\delta \end{bmatrix}. \tag{7}$$

M_S, M_L, ε and δ are complex numbers. The components of $\mathcal{H}$ are given by perturbation theory, e.g.

$$\mathcal{H}_{++} = m_0 + \langle K^\circ | H | K^\circ \rangle + \sum_r \langle K^\circ | H | r \rangle \cdot \left[\frac{\mathcal{P}}{m_0 - E_r} - i\pi\delta(m_0 - E_r) \right] \langle r | H | K^\circ \rangle + \ldots$$

$$\mathcal{H}_{+-} = \langle K^\circ | H | \overline{K}^\circ \rangle + \sum_r \langle K^\circ | H | r \rangle \cdot \left[\frac{\mathcal{P}}{m_0 - E_r} - i\pi\delta(m_0 - E_r) \right] \langle r | H | \overline{K}^\circ \rangle + \ldots$$

The eigensolutions of Eq. (6) are:

$$| K_S > e^{-iM_S t} = \frac{N_S}{\sqrt{2}} [e^{\varepsilon}(\cos\delta + \sin\delta) | K^\circ > + e^{-\varepsilon}(\cos\delta - \sin\delta) | \overline{K}^\circ >] e^{-iM_S t},$$

$$| K_L > e^{-iM_L t} = \frac{N_L}{\sqrt{2}} [e^{\varepsilon}(\cos\delta - \sin\delta) | K^\circ > - e^{-\varepsilon}(\cos\delta - \sin\delta) | \overline{K}^\circ >] e^{-iM_L t}. \tag{8}$$

K_S may be identified with the observed short-lived neutral K meson, K_L with the observed long-lived neutral K meson. The real and imaginary parts of the eigenvalues M_S and M_L give the experimental mass and lifetime of the corresponding particles:

$$M_S = m_S - \frac{i}{2\tau_S}, \qquad M_L = m_L - \frac{i}{2\tau_L}. \tag{9}$$

It will be shown that the two other complex numbers, ε and δ, describe the CP, T and CPT asymmetries of the neutral K subspace. If Nature were described exactly by the Hamiltonian H_0 possessing the properties (2), $e^{-icY} \cdot H_0 \cdot e^{icY}$ would evidently be identical with H_0. If we turn on the small perturbation H with the property (5), this will no longer be true:

$$H_{\text{new}}(c) = e^{-icY} H_{\text{tot}} e^{icY} = H_0 + H(c) \quad \text{with} \quad H(c) = e^{-icY} H e^{icY}. \tag{10}$$

It is still true, however, that the matrix elements of $H(c)$ are identical with those of H up to some phase factor, if they are taken between two eigenstates of Y:

$$\langle y_1 | H(c) | y_2 \rangle = e^{-ic(y_1 - y_2)} \langle y_1 | H | y_2 \rangle .$$

The hypercharge Y is almost always accompanied by electric or baryonic charges. The latter generate superselection, and consequently the physical states are in most cases Y eigenstates. This means that for such states H_{tot} and $H_{\text{new}}(c)$ are physically equivalent. The only important exceptions are the K_S and K_L states, these being superpositions of the two Y eigenstates K^0 and $\bar{K}^0$:

$$< K^0 | H(c) | K^0 > = < K^0 | H | K^0 >, \; < K^0 | H(c) | \bar{K}^0 > = e^{-2ic} < K^0 | H | \bar{K}^0 >,$$
$$< \bar{K}^0 | H(c) | \bar{K}^0 > = < \bar{K}^0 | H | \bar{K}^0 >,$$
$$< \bar{K}^0 | H(c) | K^0 > = e^{2ic} \; < \bar{K}^0 | H | K^0 >,$$

consequently, replacing H_{tot} by $H_{\text{new}}(c)$ entails the replacement

$$\varepsilon \to \varepsilon - ic, \; c = \text{arbitrary real value.}$$

By exploiting this freedom the imaginary part of ε can always be modified arbitrarily, for instance, with the appropriate c value a replacement $H_{\text{tot}} \to H_{\text{new}}(c)$ can make $\text{Im}\varepsilon$ even zero.

CP and CPT transformations produce $\bar{K}^0$ from K. The time reversal T does not affect a K^0 or $\bar{K}^0$ at rest, as both are spinless particles:

$$CP \mid K^0 > = e^{ia} \mid \bar{K}^0 >, \qquad CP \mid \bar{K}^0 > = e^{i\bar{a}} \mid K^0 >,$$
$$CPT \mid K^0 > = e^{ib} \mid \bar{K}^0 >, \qquad CPT \mid \bar{K}^0 > = e^{i\bar{b}} \mid K^0 >,$$
$$T \mid K^0 > = e^{i(b-\bar{a})} \mid K^0 >, \qquad T \mid \bar{K}^0 > = e^{i(\bar{b}-\bar{a})} \mid \bar{K}^0 >.$$

Here CP is unitary, while CPT and T are antiunitary operators. From the conditions

$$(CP)^2 = (CPT)^2 = 1 \tag{11}$$

one has $\bar{a} = -a$, $\bar{b} = b$. Using the combinations

$$e^{iaY}CP \quad \text{and} \quad e^{-ib}CPT$$

as new CP and CPT operators, which also obey Eqs. (2) and (11), one has simply

$$CP \mid K^0 > = \mid \bar{K}^0 >, \quad CPT \mid K^0 > = \mid \bar{K}^0 >, \quad T \mid K^0 > = \mid K^0 >. \tag{12}$$

Now, by making use of Eqs. (8) and (12) it is easy to verify that

$$\begin{aligned} &\text{i) if } [H, CP] = 0, && \text{then } \mathcal{H}_{++} = \mathcal{H}_{--}, \mathcal{H}_{+-} = \mathcal{H}_{-+}, \text{ i.e. } \varepsilon = \delta = 0; \\ &\text{ii) if } [H, CPT] = 0, && \text{then } \mathcal{H}_{++} = \mathcal{H}_{--}, \text{ i.e. } \delta = 0; \\ &\text{iii) if } [H, T] = 0, && \text{then } \mathcal{H}_{+-} = \mathcal{H}_{-+}, \text{ i.e. } \varepsilon = 0. \end{aligned} \tag{13}$$

Parameter ε is the measure of CPT asymmetry, while δ the measure of T asymmetry in the neutral K subspace. In an exactly CP-, T- and CPT-symmetric world we would have

$$\begin{aligned} \mid K_1 > &= \frac{1}{\sqrt{2}}[\mid K^0 > + \mid \bar{K}^0 >], \qquad CP \mid K_1 > = + \mid K_1 >. \\ \mid K_2 > &= \frac{1}{\sqrt{2}}[\mid K^0 > - \mid \bar{K}^0 >], \qquad CP \mid K_2 > = - \mid K_2 >. \end{aligned} \tag{14}$$

K_L decays indicate a faint violation of the CP symmetry, so the parameters ε and δ cannot be large. For small values of ε and δ the effective Hamiltonian may be written as

$$\mathcal{H} = \frac{M_S + M_L}{2} + \frac{M_S - M_L}{2}(\sigma_1 + 2i\varepsilon\sigma_2 + 2\delta\sigma_3), \tag{15}$$

and the eigenvectors are

$$K_S > = \mid K_1 > + (\varepsilon - \delta) \mid K_2 >, \qquad \mid K_L > = \mid K_2 > + (\varepsilon - \delta) \mid K_1 >. \tag{16}$$

Experimental facts

If CP were an exact symmetry, K_1 and K_2 would be observable particles. By conserving the CP quantum number the K_1 meson would decay into $\pi\pi$, the K_2 meson into three particles. The fact that both $K_S \to \pi\pi$ and $K_L \to \pi\pi$

decays have been observed means a breakdown of CP symmetry. This breakdown is characterized by the complex numbers

$$\eta_{+-} = \frac{\langle \pi^+ \pi^- \mid H+\ldots \mid K_L \rangle}{\langle \pi^+ \pi^- \mid H+\ldots \mid K_S \rangle}, \quad \eta_{00} = \frac{\langle \pi^0 \pi^0 \mid H+\ldots \mid K_L \rangle}{\langle \pi^0 \pi^0 \mid H+\ldots \mid K_S \rangle}. \tag{17}$$

The experimental decay rates and the phases of the interference terms in the time dependence of $K \to \pi\pi$ events enable us to compute the empirical values of these asymmetry parameters [3]:

$$\begin{aligned} &| \eta_{+-} | = (1.95 \pm 0.03) \cdot 10^{-3}, \quad | \eta_{00} | = (1.95 \pm 0.12) \cdot 10^{-3}, \\ &\arg \eta_{+-} = 43.6^0 \pm 3.3^0, \qquad \arg \eta_{00} = 43^0 \pm 19^0. \end{aligned} \tag{18}$$

Similar parameters of the $K \to \pi\pi\pi$ decays are:

$$\eta_{+-0} = \frac{\langle \pi^+ \pi^- \pi^0 \mid H+\ldots \mid K_S \rangle}{\langle \pi^+ \pi^- \pi^0 \mid H+\ldots \mid K_L \rangle}, \qquad \eta_{000} = \frac{\langle \pi^0 \pi^0 \pi^0 \mid H+\ldots \mid K_S \rangle}{\langle \pi^0 \pi^0 \pi^0 \mid H+\ldots \mid K_L \rangle}. \tag{19}$$

The observed time dependence of the neutral $K \to \pi^+\pi^-\pi^0$ decay gives [3]

$$\eta_{+-0} = (0.15 \pm 0.15) + i(-0.05 \pm 0.24). \tag{20}$$

No attempt to measure η_{000} has been reported, but if the dominating $\pi\pi\pi$ final state is characterized with isospin $I = 1$, one may expect

$$\eta_{000} = \eta_{+-0}. \tag{21}$$

For leptonic decays let

$$\eta_{\pi-e+\nu} = \frac{\langle \pi^- e^+ \nu \mid H+\ldots \mid K_S \rangle}{\langle \pi^- e^+ \nu \mid H+\ldots \mid K_L \rangle}, \quad \eta_{\pi+e-\nu} = \frac{\langle \pi^+ e^- \nu \mid H+\ldots \mid K_S \rangle}{\langle \pi^+ e^- \nu \mid H+\ldots \mid K_L \rangle}. \tag{22}$$

The nonvanishing value of these parameters does not necessarily indicate a CP breakdown, because the final states are not CP eigenstates. The parameters can be expressed in terms of other parameters which have more direct physical meanings.

$$x = \frac{\langle \pi^- e^+ \nu \mid H+\ldots \mid K^0 \rangle}{\langle \pi^+ e^- \nu \mid H+\ldots \mid K^0 \rangle}, \quad \bar{x} = \frac{\langle \pi^+ e^- \nu \mid H+\ldots \mid \bar{K}^0 \rangle}{\langle \pi^+ e^- \nu \mid H+\ldots \mid \bar{K}^0 \rangle} \tag{23}$$

characterize the violation of the $\Delta Y = \Delta Q_{\text{hadron}}$ selection rule. It is easy to show that

$$\eta_{\pi^- e^+ \nu} = \frac{1+x'}{1-x'}, \quad \eta_{\pi^+ e^- \nu} = -\frac{1+\bar{x}'}{1-\bar{x}'} \tag{24}$$

with

$$x' = xe^{-2\varepsilon}(1+\delta)+\delta, \quad \bar{x}' = \bar{x}e^{2\varepsilon}(1-\delta)-\delta. \tag{25}$$

The consequences of symmetry assumptions are the following:

$$\bar{x} = x^*, \text{ if } [H, CPT] = 0,$$

$$x = x^* \text{ and } \bar{x} = \bar{x}^*, \text{ if } [H, T] = 0.$$

Numerical analysis of $K \to \pi e \nu$ experiments [3] makes use of an assumed CPT symmetry:

$$\eta_{\pi^- e^+ \nu} = \frac{1+x}{1-x} = -\eta^*_{\pi^+ e^- \nu} \qquad \text{for } [H, CPT] = 0. \tag{26}$$

The observed value is [3]

$$x = (+24 \pm 30) \cdot 10^{-3} + i(-8 \pm 28) \cdot 10^{-3}. \tag{27}$$

Evidently $\xi = \mathrm{Im}x$ is a measure of CP and T breakdown in the $\Delta Y = \Delta Q_{\text{hadron}}$ violating leptonic decay.

The charge asymmetry of $K_L \to \pi^{\mp} e^{\pm} \nu$ decays is an easily observable quantity:

$$\alpha = \frac{\Gamma(K_L \to \pi^- e^+ \nu) - \Gamma(K_L \to \pi^+ e^- \nu)}{\Gamma(K_L \to \pi^- e^+ \nu) + \Gamma(K_L \to \pi^+ e^- \nu)} =$$

$$= \frac{|\langle \pi^- e^+ \nu | H \ldots | K_L \rangle : \langle \pi^+ e^- \nu | H + \ldots | K_L \rangle|^2 - 1}{|\langle \pi^- e^+ \nu | H \ldots | K_L \rangle : \langle \pi^+ e^- \nu | H + \ldots | K_L \rangle|^2 + 1},$$

which can be written in the simple form

$$\alpha = 2 \,\mathrm{Re}\, \varepsilon \frac{1-|x|^2}{|1-x|^2} + \beta, \tag{28}$$

where $\beta = 0$ in the case of CPT symmetry. The experimental value is [3]

$$\alpha = (3 \cdot 27 \pm 0.42) \cdot 10^{-3}. \tag{29}$$

Numerical analysis of the K asymmetries

In order to learn as much from these data as possible we shall first exploit the unitarity. From Eq. (6) one can deduce

$$-\frac{d}{dt}\langle K(t)|K(t)\rangle=\langle K(t)|\Gamma|K(t)\rangle\,. \tag{30}$$

Here $-1/2\,\Gamma$ is the anti-Hermitian part of $\mathfrak{H}$, while according to the rules of perturbation theory it is given by the formula

$$\langle K\,|\Gamma|\,K'\rangle = 2\pi \sum_r \langle K\,|H+\ldots|\,r\rangle\,\delta(m_0-E_r)\,\langle r\,|H+\ldots|\,K'\rangle\,.$$

Let us substitute the expression

$$|\,K(t)\rangle = u\,|\,K_s\rangle\, e^{-iM_S t}+v\,|\,K_L\rangle\, e^{-iM_L t}$$

into Eq. (30). Since u and v are arbitrary constants,

$$\langle K_S\,|\Gamma|\,K_L\rangle=\frac{1}{2}\langle K_S|K_L\rangle\left[\frac{1}{\tau_S}+\frac{1}{\tau_L}+2i\Delta m\right], \tag{31}$$

or, because $\tau_S \ll \tau_L$,

$$\langle K_S|\Gamma|K_L\rangle \simeq \frac{1}{2\tau_S}\langle K_L|K_S\rangle\,(1+i\tan z)\,,$$

where according to the experimental data [3]

$$z=\tan^{-1}(2\tau_S\Delta m)=42.94^0\pm 0.26^0. \tag{32}$$

Only the final states with branching ratios above 1% will be taken into account:

$$\begin{aligned}\langle K_S\,|\Gamma|\,K_L\rangle = {}& \frac{1}{\tau_S}\left\{\eta_{+-}\,B\,(K_S\to\pi^+\pi^-)+\eta_{00}\,B\,(K_L\to\pi^0\pi^0)\right\}+\\ &+\frac{1}{\tau_L}\left\{\eta^*_{+-0}\,B\,(K_L\to\pi^+\pi^-\pi^0)+\eta^*_{000}\,B\,(K_L\to\pi^0\pi^0\pi^0)+\right.\\ &+\eta^*_{\pi^-e^+\nu}\,B\,(K_L\to\pi^-\,e^+\,\nu)+\eta^*_{\pi^+e^-\nu}\,B\,(K_L\to\pi^+\,e^-\nu)+\\ &\left.+\eta^*_{\pi^-\mu^+\nu}\,B\,(K_L\to\pi^-\mu^+\nu)+\eta^*_{\pi^+\mu^-\nu}\,B\,(K_L\to\pi^+\,\mu^-\,\nu)\right\}.\end{aligned}$$

As a consequence of the smallness of τ_S/τ_L our formula is too insensitive for the data to be substituted into the second parenthesis, so we shall make use of assumption (21) and write

$$\begin{aligned}&B(K_S\to\pi^+\pi^-)=1-B(K_S\to\pi^0\pi^0),\\ &B(K_L\to\pi^+\pi^-\pi^0)+B(K_L\to\pi^0\pi^0\pi^0)=B(K_L\to 3\pi),\end{aligned}$$

$$B(K_L \to \pi^- e^+ \nu) + B(K_L \to \pi^+ e^- \nu) + B(K_L \to \pi^- \mu^+ \nu) + \\ + B(K_L \to \pi^+ \mu^- \nu) = 1 - B(K_L \to 3\pi),$$

$$B(K_L \to \pi^- e^+ \nu) - B(K_L \to \pi^+ e^- \nu) = B(K_L \to \pi^- \mu^+ \nu) - \\ - B(K_L \to \pi^+ \mu^- \nu).$$

We arrive at the result

$$-\frac{1}{2}\langle K_S|K_L\rangle (1+i\tan z) = \eta_{+-} + (\eta_{+-} - \eta_{00})\, B(K_S \to \pi^\circ\pi^\circ) +$$

$$+\frac{\tau_S}{\tau_L}\eta^*_{+-0}\, B(K_L \to 3\pi) +$$

$$+\frac{\tau_S}{\tau_L}\left(\frac{\eta_{\pi^- e^+\nu} + \eta_{\pi^+ e^-\nu}}{2} + \alpha\frac{\eta_{\pi^- e^+\nu} - \eta_{\pi^+ e^-\nu}}{2}\right)[1 - B(K_L \to 3\pi)]\,.$$

The experimental branching ratios are [3]

$$B(K_S \to \pi^\circ\pi^\circ) = 0.313 \pm 0.005, \quad B(K_L \to 3\pi) = 0.340 \pm 0.008. \tag{33}$$

If the smallness of x' is taken into account

$$\frac{1}{2}(\eta_{\pi^- e^+\nu} - \eta_{\pi^+ e^-\nu}) \simeq 1\,,$$

$$\frac{1}{2}(\eta_{\pi^- e^+\nu} + \eta_{\pi^+ e^-\nu}) \simeq (x - \bar{x}) + 2\delta\,,$$

but if CPT symmetry is assumed on the right-hand side of the last equation we can put simply $2i\xi$. Finally,

$$\frac{1}{2}\langle K_S|K_L\rangle = \mathrm{Re}\,\varepsilon - i\,\mathrm{Im}\,\delta = \\ = \frac{1}{1+i\tan z}\left\{\eta_{+-} - (\eta_{+-} - \eta_{00})\, B(K_S \to \pi^\circ\pi^\circ) + \right. \tag{34}$$

$$\left. + \frac{\tau_S}{\tau_L}(\alpha + 2i\xi) - \frac{\tau_S}{\tau_L}(\alpha + 2i\,\xi - \eta^*_{+-0})\, B(K_L \to 3\pi)\right\}.$$

All numbers on the right-hand side of the unitarity equation (34) have been measured and are quoted above, so we can compute $\mathrm{Re}\,\varepsilon$ and $\mathrm{Im}\,\delta$:

$$\mathrm{Re}\;\varepsilon = (1.49 \pm 0.09)\cdot 10^{-3}, \quad \mathrm{Im}\;\delta = (-0.04 \pm 0.18)\cdot 10^{-3}. \tag{35}$$

Knowing Re ε, the value of β can be obtained from Eq. (28):

$$B = (0.15 \pm 0.50) \cdot 10^{-3}. \tag{36}$$

A more detailed knowledge of the asymmetry parameters is offered by detailed analysis of $K \to \pi\pi$ decays, for which the most complete set of experimental data is available.

As the spin of K is zero, the orbital angular momentum of the $\pi\pi$ final state is also zero. Bose statistics allows $I = 0$ and $I = 2$ in this final state. The K_S branching ratio gives

$$\left| \frac{\langle \pi^\circ \pi^\circ | H + \ldots | K_S \rangle}{\langle \pi^+ \pi^- | H + \ldots | K_S \rangle} \right|^2 = \frac{1}{2} \left| \frac{1 - \sqrt{2}\, p}{1 + p/\sqrt{2}} \right|^2,$$

where

$$p = \frac{\langle \pi\pi, I = 2 | H + \ldots | K_S \rangle}{\langle \pi\pi, I = 0 | H + \ldots | K_S \rangle} \tag{37}$$

is the ratio of the $\Delta I > 1/2$ amplitude to the $\Delta I = 1/2$ amplitude in the CP-allowed $K_S \to \pi\pi$ decay. From the experimental value (33) one gets

$$\text{Re } p = 0.026 \pm 0.006. \tag{38}$$

The CP-forbidden $K_L \to \pi\pi$ transitions may have two different sources: either the CP impurity of the K_L eigenstate (the presence of K_1 being characterized by ε—δ) or a direct jump of CP in the $K_2 \to \pi\pi$ transition (to be characterized by new parameters γ_0 and γ_2; see Fig. 1). We define

$$\varepsilon_0 = \frac{\langle \pi\pi, I = 0 | H + \ldots | K_L \rangle}{\langle \pi\pi, I = 0 | H + \ldots | K_S \rangle}, \quad \varepsilon_2 = \frac{\langle \pi\pi, I = 2 | H + \ldots | K_L \rangle}{\langle \pi\pi, I = 0 | H + \ldots | H_S \rangle}. \tag{39}$$

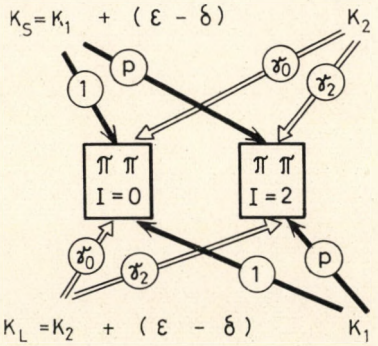

Fig. 1. $K \to \pi\pi$ amplitudes

In accordance with the isospin decomposition of the $\pi^+\pi^-$ and $\pi^0\pi^0$ states one can write

$$\eta_{+-} = \frac{\varepsilon_0 + \frac{\varepsilon_2}{\sqrt{2}}}{1 + \frac{p}{\sqrt{2}}}, \quad \eta_{00} = \frac{\varepsilon_0 - \varepsilon_2\sqrt{2}}{1 - p\sqrt{2}}. \tag{40}$$

If the only source of $K_L \to \pi\pi$ transitions were the K_1 impurity, one would have

$$\frac{\varepsilon_2}{\varepsilon_0} = \frac{\langle \pi\pi, I=2 \,|H+\ldots|\, K_L\rangle}{\langle \pi\pi, I=2 \,|H+\ldots|\, K_L\rangle} = \frac{\langle \pi\pi, I=2 \,|H+\ldots|\, K_S\rangle}{\langle \pi\pi, I=0 \,|H+\ldots|\, K_S\rangle} = p.$$

The other source might be the CP-breaking $K_2 \to \pi\pi$ transition. Let us write

$$\langle \pi\pi, I \,|H+\ldots|\, K^0\rangle = A_I e^{i\delta_I}, \; \langle \pi\pi, I \,|H+\ldots|\, \bar{K}^0\rangle = \bar{A}_0 e^{i\delta_I}. \tag{41}$$

Here δ_I is the scattering phase shift of the strong $\pi\pi$ final state interaction at $E = m_0c^2$ with isospin I. With a certain amount of hesitation π-meson physics says, that [3]

$$\delta_2 - \delta_0 = -39^0 \pm 18^0. \tag{42}$$

In the case of CP symmetry one would have $A_I = \bar{A}_I$, so direct CP breakdown in the $K_2 \to \pi\pi$ transition is characterized by the two complex parameters

$$\gamma_0 = \frac{A_0 - \bar{A}_0}{A_0 + \bar{A}_0}, \quad \gamma_2 = \frac{A_2 - \bar{A}_2}{A_2 + \bar{A}_2}. \tag{43}$$

(Up to the first order of perturbation theory Re $\gamma_I \neq 0$ indicates CP and CPT breakdown, Im $\gamma_I \neq 0$ indicates CP and T breakdown.) By making use of Eqs. (14), (16), (39), (40), (41) and (43) one arrives at the following relations:

$$\varepsilon_0 = \gamma_0 + \varepsilon - \delta = \frac{2\eta_{+-} + \eta_{00}}{3} + \frac{2}{3} p\,(\eta_{+-} - \eta_{00}), \tag{44}$$

$$\gamma_2 - \gamma_0 = \frac{\varepsilon_2}{p} - \varepsilon_0 = \frac{\sqrt{2}}{3} \frac{\eta_{+-} - \eta_{00}}{p} \left(1 - \frac{p}{\sqrt{2}} + p^2\right). \tag{45}$$

(Here all the CP asymmetry parameters have been taken into account in the first order; no other parameters have been neglected.) Re p is known experimentally, and it is easy to show that

$$p = \frac{A_2 + \bar{A}_2}{A_0 + \bar{A}_0} e^{i(\delta_2 - \delta_0)} \frac{1 + \gamma_2(\varepsilon + \delta)}{1 + \gamma_0(\varepsilon + \delta)}.$$

Now if $K \to \pi\pi$ is dominated by the CP-symmetric weak interaction for both $I = 0$ and $I = 2$ final states, one can write

$$p = \pm \left|\frac{A_2}{A_0}\right| e^{i(\delta_2 - \delta_0)} + CP \text{ asymmetric terms} = \\ = \pm (0.44 \pm 0.013)\, e^{i(-39^\circ \pm 18^\circ} + CP \text{ asymmetric terms.} \tag{46}$$

Substituting the experimental values (18) and (46) into formulas (43) and (44) one obtains

$$|\varepsilon_0| = (1.95 \pm 0.06) \cdot 10^{-3}, \qquad \arg \varepsilon_0 = 44.7^0 \pm 6.7^0,$$
$$|\gamma_2 - \gamma_0| = (2.12 \pm 7.5) \cdot 10^{-3}, \quad \arg (\gamma_2 - \gamma_0) = \text{unknown}. \tag{47}$$

The information available on CP-breaking parameters of the neutral K meson system are summarized in the following Table:

Table I

Source of information	Irreversibility (T asymmetry)	Acausality (CPT asymmetry)
Unitarity	Re $\varepsilon = 1.49 \pm 0.09$	Im $\delta = -0{,}04 \pm 0.18$
$K \to \pi\pi$, $I = 0$	Im $(\varepsilon + \gamma_0) = 1.32 \pm 0.24$	Re $(\delta - \gamma_0) = 0.11 \pm 0.19$
$K \to \pi\pi$, $I = 2$	$\lvert$ Im $(\gamma_2 - \gamma_0)\rvert < 9.6$	$\lvert$ Re $(\gamma_2 - \gamma_0)\rvert < 9.6$
$K \to \pi e \nu$	$\xi = -8 \pm 28$	$\beta = 0.15 \pm 0.50$
		(all values in 10^{-3} units).

The Table shows that CP and T symmetries are definitely broken in neutral K meson decays, but there is no indication of any CPT breaking of comparable strength. Nature thus reveals herself to be irreversible microscopically, although even here she behaves causally (Fig. 2).

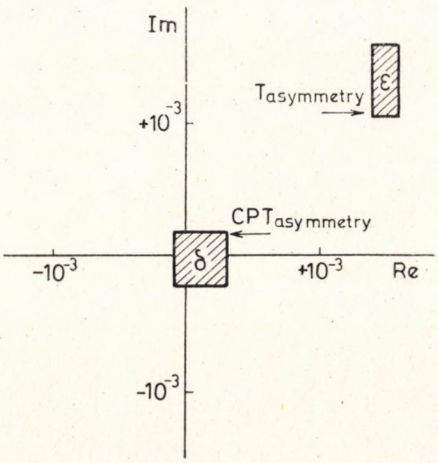

Fig. 2. Strength of T and CPT violation (Empirical values of ε and δ)

The minimum model

The only asymmetry parameter significantly differing from zero is ε. It is therefore very tempting to assume that all the observed asymmetries are explained by this single parameter, which characterizes the time-odd part of the effective Hamiltonian $\mathcal{H}$ [5]:

$$\mathcal{H} = \frac{M_S+M_L}{2} + \sigma_1 \frac{M_S-M_L}{2} + i\varepsilon\,\sigma_2 (M_S-M_L)\,. \tag{48}$$

Let us check the confidency of this "minimum model".

By exploiting the possibility of the $H_{\text{tot}} \to H_{\text{new}}(c)$ replacement (10) we can make $\text{Im}\,\gamma_0 = 0$ (WU–YANG convention [6]), which gives

$$\varepsilon = (1.49 \pm 0.09) \cdot 10^{-3} + i(1.32 \pm 0.24) \cdot 10^{-3}. \tag{49}$$

By assuming that $\beta = \text{Re}\,\gamma_I = \delta = 0$ (exact CPT symmetry) and $\text{Im}\,\gamma_2 = \xi = 0$ (the microscopic irreversibility is concentrated into the neutral K eigenstates produced by the effective Hamiltonian (48) and no further irreversibility is to be found in the decay matrix elements), we obtain the unique relations

$$\eta_{+-} = \eta_{00} = \varepsilon = \varepsilon_0 = p^{-1}\varepsilon_2 \text{ for the minimum model.} \tag{50}$$

The unitarity relation tells us that the phase of this complex number is equal to the z quoted in Eq. (32). Its real part can be obtained also from the charge asymmetry of the leptonic decays. So by writing

$$\lambda = (1+i\tan z)\,\frac{1-\text{Re}\,x}{1+\text{Re}\,x}\,\frac{\alpha}{2} \text{ for the minimum model,} \tag{51}$$

we can collect three independent pieces of experimental information about the strength of the time-reversal asymmetry:

$$\varepsilon = \begin{cases} \eta_{+-}, & |\,\eta_{+-}\,| = (1.95 \pm 0.03) \cdot 10^{-3}, \quad \arg\,\eta_{+-} = 43.6^0 \pm 3.3^0, \\ \eta_{00}, & |\,\eta_{00}\,| = (1.95 \pm 0.12) \cdot 10^{-3}, \quad \arg\,\eta_{00} = 43.2^0 \pm 19^0, \\ \lambda, & |\,\lambda\,| = (2.13 \pm 0.27) \cdot 10^{-3}, \quad \arg\,\lambda = 42.9^0 \pm 0.3^0. \end{cases} \tag{52}$$

The coincidence of these three values makes it understandable that this "minimum model" is very popular among theoreticians (Fig. 3).

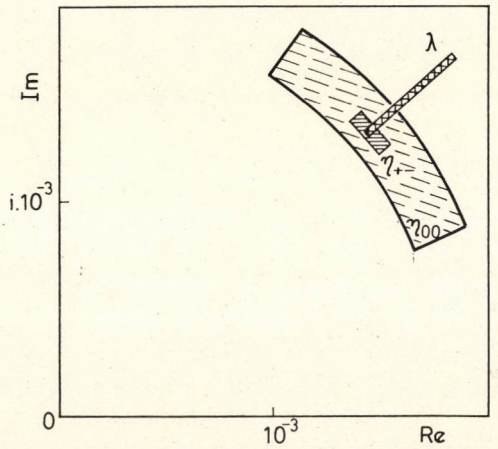

Fig. 3. Consistency of the minimum model

Conclusion and outlook

Let us try to formulate the moral of our numerical results. What can we say about the *CP*-odd Hamiltonian

$$H' = \frac{1}{2}\left[H_{\text{tot}} - (CP)^{-1} H_{\text{tot}} (CP)\right], \tag{53}$$

which explains the experimental ε value (49), but gives zero for γ_I?

$$\varepsilon = \frac{2\tau_S}{1 - i \tan z} \operatorname{Im} \langle \bar{K}^0 | H' + \ldots | K^0 \rangle \,. \tag{54}$$

The predictions for the measurable quantity

$$\omega = \left| \frac{\eta_{+-} - \eta_{00}}{\eta_{+-} + \eta_{00}} \right|$$

for the case when H' is built up purely from hadronic operators, and is characterized with a definite SU(3) property ($< I_1, Y_1 \mid H' \mid I_2, Y_2 > \neq 0$ only for definite values of $\Delta I = |I_1 - I_2|$ and $\Delta Y = |Y_1 - Y_2|$) are summarized in Table II [7]. (g' is the dimensionless coupling constant characterizing the strength of H').

Table II

ΔY	ΔI	g'	ω	
0	0	10^{-3}	137^{-1}	← millistrong
	1	10^{-3}	1	
	2	10^{-3}	1	
	3	10^{-1}	137	
1	1/2	10^{-8}	137^{-1}	← milliweak
	3/2	10^{-8}	1	
	5/2	10^{-6}	1	
2	0	10^{-11}	10^{-10}	superweak
	1	10^{-13}	10^{-10}	
	2	10^{-11}	10^{-8}	
$n > 2$		10^{-23+5n}	10^{-10}	

The experimental finding $\omega \ll 1$ can be explained in three different ways: with superweak, milliweak, or millistrong realizations of the millistrong model. A choice among these possibilities would be possible only with asymmetry experiments performed outside neutral K-meson physics.

What about the coupling constant of a hypothetical CPT-violating interaction? We know that

$$|\delta| = \left| \frac{i\tau_S}{1 - i \tan z} \langle K^0 | H - (CPT)^{-1} H (CPT) + \right.$$

$$\left. + \text{higher order terms} \, |K^0\rangle \right| < 3 . 10^{-4} ,$$

If the CPT-odd part of the Hamiltonian were characterized by the selection rule $\Delta Y = 0$ or 1 or 2, the corresponding upper limits on its coupling constant would be $10^{-14}, 10^{-9}, 10^{-4}$. We can state that a CPT asymmetry with a strength comparable to the T asymmetry can be excluded experimentally only for $\Delta Y = 0$ transitions.

Coming back to the definitely observed T asymmetry, we still have to answer the puzzling question: If Nature is irreversible even microscopically, why does she hide this property so well? Is it a primary fact that the coupling constant g' in the odd coupling (53) is small, or may we ask for an explanation of the faintness of the T asymmetry?

Well, it is known that no exotic particles can be found in the recent Table of Particle Properties. For this reason we are allowed to think in terms

of quarks: only such particles and such vertices are of importance for Nature, which can be built up simply by quarks. On the other hand, it is exceedingly difficult to write down a coupling which is invariant against all transformations but C and T. One is forced to use the scalar product of γ_μ and ∂_μ (with the current odd and the momentum even with respect to C). Examples:

$$\bar{\psi}\gamma_\mu\psi \cdot \partial_\mu\bar{\psi}\psi \qquad \text{corresponding to } \omega_\mu \cdot \partial_\mu\varepsilon,$$

$$\bar{\psi}\gamma_5\partial_\mu\psi \cdot \bar{\psi}\gamma_5\gamma_\mu\psi \qquad \text{corresponding to } \mathbf{A}_{1\mu} \cdot \mathbf{B}_\mu,$$

$$\bar{\psi}\gamma_\mu\psi \cdot \bar{\psi}\gamma_5\psi \cdot \partial_\mu\bar{\psi}\gamma_5\psi \qquad \text{corresponding to } (\boldsymbol{\pi}\boldsymbol{\rho}_\mu)\partial_\mu\eta\,.$$

(Here ω, ε, A_1, B, π, ϱ and η stand for the field operators of the corresponding mesons.) These structures are realized by rare particles (excited, bound quark pairs) or by sophisticated centrifugal barriers. This offers an explanation of why it is so hard to observe the T asymmetry in Nature, but we have still not succeeded in clarifying the CP puzzle. We have shown only that it may be related to another unsolved problem of Nature: to the quark puzzle.

A further possibility is that C and T asymmetries are faint only in the present state of the world. If we want to write a T-odd expression in place of g', the simplest possibility is to put a time derivative there. If the world is in a more or less steady state now, this time derivative will give a small number. It may be that this can provide the explanation for the effective faintness of C and T breakdowns. We shall follow this line of thought in the Appendix.

The present analysis — following similar ones published in earlier years by other authors — was prepared to fulfil a request to give a review on CP breakdown at the Conference on Nuclear Weak Interactions at Zagreb, in July 1971. The author is highly indebted to Dr. D. TADIČ and to the staff of the Institute Ruder Boskovič for their kind hospitality in Zagreb, and also to Dr. A. FRENKEL for his stimulating discussions and criticism, especially concerning the phase conventions, and to Mr. A. S. SZALAY for his help in computer programming.

Appendix

Charge asymmetry in particle physics and in the universe

PONTECORVO has pointed out [8], that the lifetime of the double beta decay observed for Te-130 by T. KIRSTEN et al. is in accordance with the prediction of the lepton-conserving weak interaction theory, but the ratio of the decay rates Te-128 to Te-130 favours a double beta decay without neutrinos. Both he and H. PRIMAKOFF [9] speculated that the CP non-conservation observed in K decays with the strength $|\varepsilon|\, g^2_{\text{weak}} \simeq 10^{-3}\, g^2_{\text{weak}}$ (g_{weak} is the weak coupling constant) may be related to a lepton non-conserving interaction of the same strength observable in double beta decay. Keeping this coincidence of the two

coupling constants in mind, I would like to call attention to another possible relation.

The isotropy of black body radiation at 2.7 °K is a strong hint of the Big Bang origin of the Universe. The only astronomical observation contradicting this theory is the low helium content of certain Population II stars. It has been pointed out by FOWLER and HOYLE that the existence of a non-vanishing leptonic charge in the Universe could solve this discrepancy. (The formation of helium from hydrogen might be prevented by surplus neutrinos.) As charge asymmetry and time-reversal asymmetry are connected by the CPT theorem, one can speculate about the possibility, that matter will behave in a very charge-symmetric manner during periods when the Universe is rather symmetric against time reversal (i.e. the present) but that the same matter would behave in a very charge-asymmetric manner, when the Universe is changing very fast in time (i.e. in the seconds following the Big Bang). Perhaps the superweak charge asymmetry of the leptonic K decays and the asymmetrically positive leptonic (and baryonic) charge of our present Universe are consequences of the same interaction. Several ways are open to us when we try to build up a model which is able to realize such a speculation. One example will be sketched here. A fundamental interaction Hamiltonian which is invariant against C, P and T may have the following structure:

$$H = g' \cdot H',$$

where g' is a nowadays slowly varying expression playing the role of an effective coupling constant, and H' is an effective local vertex which is odd against CP and T. The effective coupling constant g' may be something like

$$g' = a \frac{d}{dt} \ln b,$$

where a is odd against CP and b is a quantity characterizing the cosmologica state of the Universe, e.g. its density. (g' must be symmetric under local Lorentz transformations.) The CP- and T-asymmetric local interaction will be strong for small values of t but very faint for large values. Matter behaved very charge asymmetrically at the moments of the Big Bang, but it behaves in a practically charge-symmetric way today.

The electric charge Q is related to the long-range Coulomb force, but the baryonic charge B and the leptonic charge L are related to short range interactions. It has been stressed by J. A. WHEELER that a black hole (a mass concentration producing a geometrical singularity) may absorb and practically destroy B and L (their short range shrinks to zero range), but not so Q (i.e. electric lines of forces remain of infinite length). It is interesting in this connec-

tion that our Universe at present shows itself to be charged from the baryonic and leptonic point of view (more protons, electrons and neutrinos than antiparticles), but neutral from the electric point of view. One may dare to advance the following hypothesis:

The completely symmetric Hamiltonian of our world contains a term in which the effective coupling constant g' is big for small t values and small for large t values. This part of the Hamiltonian behaves as C and T asymmetric in small space-time regions, as have been detected in the faint charge asymmetry of neutral K meson decays. At the time of the Big Bang, however, the same interaction worked much harder, producing a much stronger attraction between antibaryons ($B < 0$) and antileptons ($L < 0$) than between baryons ($B > 0$) and leptons ($L > 0$). The black holes formed by gravitational collapse during the infancy of the Universe thus absorbed more antibaryons and more antileptons and so left the originally neutral Universe in a state which for practical purposes can be described with positive B and L charges. This effective leptonic charge prevented the formation of a high helium concentration.

In the present underdeveloped state of empirical cosmology it is probably too early to build up a quantitative theory from this hypothesis. We must wait for a better understanding of the helium puzzle from astronomy and for a better understanding of charge-asymmetric decays from particle physics. Nevertheless, it remains empirical fact that the process of the leptonic K decay is charge asymmetric and that the state of the Universe is charge asymmetric. The dynamics of K mesons shows a tiny microscopic irreversibility in Hilbert space, and the history of the Universe shows a shocking cosmological irreversibility in Minkowski space. It is very tempting to contemplate on what the connection between these facts might be.

REFERENCES

1. G. Lüders, K. Danske Vidensk. Selks. Mat. Fys. M. **28,** 165, 1954. W. Pauli, Niels Bohr and the Dev. of Physics, Pergamon, London, 1955.
2. See e.g. T. D. Lee and L. Wolfenstein, Phys. Rev., **160B,** 1490, 1965. G. Marx, Fortschritte der Physik, **14,** 695, 1966.
3. All the quoted experimental data are taken from the Review of Particle Properties, Rev. Mod. Phys. April, 1971 and from the world averages presented at the Amsterdam Conference on High Energy Physics, July, 1971.
4. J. S. Bell and A. Steinberger, Proc. Oxford Conference on High Energy Physics, 1967. K. R. Schubert et al., Physics Letters, **31B,** 662, 1970.
5. L. Wolfenstein, Nuovo Cimento, **42A,** 17, 1966.
6. C. S. Wu and C. N. Yang, Phys. Rev. Letters, **13,** 380, 1964.
7. A. Frenkel and G. Marx, Acta Phys. Hung., **27,** 87, 1969.
8. B. Pontecorvo, Phys. Letters, **26B,** 630, 1968.
   V. Gribov and B. Pontecorvo, Phys. Letters, **28B,** 493, 1969.
9. H. Primakoff and D. H. Sharp, Phys. Rev. Letters, **23,** 501, 1969.
   H. Primakoff and S. P. Rosen, Phys. Rev., **184,** 1925, 1969.

ПРОВЕРКА СОХРАНЕНИЯ МИКРОСКОПИЧЕСКОЙ ПРИЧИННОСТИ И ОБРАТИМОСТИ В СЛУЧАЕ РАСПАДА К-МЕЗОНОВ

Г. МАРКС

Резюме

Обсуждается строгость выводов, согласно которым, имеющиеся экспериментальные результаты свидетельствуют о том, что при нейтральном К-распаде нарушаются *CP*-, и *T*-симметрии, но сохраняется *CPT*-симметрия, которая строго связана с локальной причинностью. Выдвинута гипотеза о возможности существования ещё более сильной *CP*- и *T*-асимметрии во время «Биг Бенг»-а (большого взрыва). Рассмотрены вытекающиеся отсюда возможные следствия относительно значений лептонных и барионных зарядов.

Acta Physica Academiae Scientiarum Hungaricae, Tomus 32 (1—4), pp. 341—352 (1972)

A NEW ATTEMPT AT A UNIFIED FIELD THEORY*

By

D. IVANENKO

MOSCOW STATE UNIVERSITY, MOSCOW, USSR

(Received 14. XII. 1971)

It is attempted to construct an improved version of the non-linear spinor field theory originally proposed by the author and HEISENBERG. A new perturbation theory dissimilar to the Tamm—Dancoff one is used for the case of degenerate vacuum. Furthermore, a new propagator is introduced and the existence of unitary symmetry is supposed to hold from the very beginning, i.e. essentially a non-linear theory of quarks is proposed.

Many beautiful papers by L. JÁNOSSY have stimulated efforts to build up a more unified picture of physical reality without the need to dispense with the older attempts in this direction. The present article is intended as a review of the situation of the non-linear spinor field theory that is advocated by the author and in well-known papers of the HEISENBERG—DÜRR group and which seems to offer a promising basis for such a unified theory, if a due account is taken of gravitation and cosmology.

§ 1. Non-linear spinor theory

The starting point of the theory is the Dirac (Weyl) equation supplemented by some non-linear terms of the ψ^3 type proposed earlier [1, 3]: $\gamma_\mu \partial_\mu \psi + l^2(\psi^3) = 0$. This is a genuine, primordial non-linearity, like Einsteinian General Relativity or the Born—Infeld model of electrodynamics, as contrasted with induced non-linearities including those of ψ^3 type arising by means of quantum vacuum effects (virtual mutual transmutations of all interacting fields). It is instructive to compare our treatment with that of HEISENBERG. Briefly, HEISENBERG and DÜRR choose as their fundamental field operator a spinor-isospinor and pseudovector type of all five possible forms of (IVANENKO—BRODSKY) non-linearities; they use the new (and rather cumbersome) Tamm—Dancoff approximation method for calculations and introduce an indefinite metric in Hilbert space and ground state (vacuum) degeneracy with respect to the isospin; a specific form of propagator is constructed and a (rather artificial) spurion model is invented to explain strangeness. The propagator (removing infinities) is

* Dedicated to Prof. L. JÁNOSSY on his 60th birthday.

$$G=(\sigma p)\left[-\frac{1}{p^2+m^2-i\varepsilon}+\frac{1}{p^2-i\varepsilon}+\frac{m^2}{(p^2-i\varepsilon)^2}\right]. \tag{1}$$

With this approach one gets the following chief results:

1. the (average) baryonic mass, as expressed by the self-interaction constant, is

$$ml=5{,}8; \tag{1}$$

2. the masses of the baryonic octet are semi-qualitatively good, but the masses of 0^- mesons poor (up to factor 1/2):

Λ: 1,09 (1,19)
π: 0,27 (0,15) (empirical values in parentheses)

3. Sommerfeld's fine structure constant is obtained (but by means of some empirical values) in semi-quantitative agreement [2].

Work at Moscow University has aimed, chiefly through investigations by NAUMOV and younger colleagues [4], at the construction of a more convincing version of the theory. This approach retains the non-linear ψ^3 term as well as HEISENBERG's important suggestions of an indefinite metric and vacuum degeneracy, but

1) it permits the application of a modified perturbation theory in the degenerate vacuum case, 2) it has a more satisfactory propagator and 3) it admits unitary symmetry from the beginning. Roughly speaking, then, the group is trying to build a theory of non-linear quarks. Let us examine each of these points in turn.

1) The Lagrangian is reconstructed in a form permitting the inclusion of all symmetry-breaking effects in zeroth approximation:

$$\mathfrak{L}=\mathfrak{L}_0+\mathfrak{L}_{\text{int}}=(\mathfrak{L}_0+\mathfrak{L}_{\text{brok}})+(\mathfrak{L}_{\text{int}}-\mathfrak{L}_{\text{brok}})=\mathfrak{L}_0'+\mathfrak{L}_{\text{int}}'. \tag{2}$$

For the γ_5-invariant model, with $\mathfrak{L}_{\text{brok}}=m\bar{\psi}\psi$, this yields the mass value from the equation

$$m^2\ln(1+p_0^2/n^2)=p_0^2+\frac{16\pi^2}{3\,l^2} \tag{2a}$$

(p_0 is the cut-off impulse).

Convincing support for this perturbation method is obtained by checking it with the old HEISENBERG propagator, which yields even better hadronic masses; for example,

$$\pi\text{: } 0{,}13(0{,}15), \quad \eta\text{: } 0{,}58(0{,}58) \text{ etc.}$$

2) The new proposed propagator, which corresponds to a field operator taking into account not only physical states, but also ghost states of vanishing norm and dipole states

$$\psi = f(x) + a_1 Z(x) + a_2 d(x), \tag{3}$$

is

$$G = -\frac{\hat{p}+im}{p^2+m^2-i\varepsilon} + \frac{\hat{p}+im}{p^2+\mu^2-i\varepsilon} + \frac{\lambda\mu(\mu-m)(\hat{p}+i\mu)}{(p^2+\mu^2-i\varepsilon)^2}. \tag{4}$$

If we analyse the amplitude of nucleon – nucleon scattering, applying the self-consistency condition of equality of the mass of the physical particle and the m value in the propagator, we get

$$ml = 7{,}4, \qquad \mu = 1{,}1\, m.$$

Moreover, from the requirement of a pole at the vanishing square of a transferred impulse (existence of photons!), we obtain for the fine structure constant [4]

$$\alpha = 1/115. \tag{5}$$

This last result can be considered as satisfactory, since it is obtained by a clear-cut method, without use of any empirical values, and permits further refinements.

3) Let us account $SU(3)$ symmetry from the beginning and choose vector non-linearity for our massless quarkian pre-matter, which is in line with the suggestion of some group theoretical arguments (MARSHAK–MUKUNDA) and leads also to better empirical values of masses. Considering the vacuum state to be degenerate with respect to chirality and isospin, we get for the Λ-quark a mass which is some 17% heavier than other quark masses, in nice agreement with phenomenological evaluations.

Let us consider now the scattering of quark by antiquark $q + \bar{q} \to q + \bar{q}$ and the scattering of three quarks, recalling that mesons and baryons are built from quark and antiquark or, correspondingly, from three quarks. Then, analysing carefully the scattering and crossing symmetric amplitudes, one gets the desired hadronic masses, viz.

	π	η	K^*	N	Λ	Σ	Δ	Ω
Theory	1	4,2	7,1	8	10	11	9	12
Exp.	1	4	6,5	7	8	9	9	12

These results can be considered as satisfactory for the present in view of the preliminary, exploratory state of non-linear theory. It may be remarked

that in HEISENBERG formalism vector mesons do not seem to be obtained with any degree of reliability; the decuplet baryonic masses are calculated by us in non-linear spinor theory for the first time [4].

Without entering into details we draw attention to the possibility of constructing non-linear spinor equations by applying the formalism of non-linear representations of some internal symmetries. Writing the transformations of the internal group as

$$\psi_{a\lambda} \to \tilde{\psi}_{a\lambda} = \psi_{a\lambda} + \delta t_\mu T^\mu_{ab}(f)\, \psi_{b\lambda}(x), \tag{6}$$

where f are invariants of transformations (for example, $f = \bar{\psi}\tau\psi$) and $T(f)$ are generators of the internal group satisfying the commutation relations generalizing the linear case. In the simple case of the $SU(2)$ group one gets some essentially non-linear solutions for T:

$$T^{\pm} = \pm \frac{id}{4\xi\sqrt{4\xi+\alpha}}\, e^{\pm i\varkappa}(f_2\tau^1 - f_1\tau^2) - \frac{\sqrt{\xi}}{\sqrt{4\xi+\alpha}}(\tau^1 + i\tau^2), \tag{7}$$

$$\xi = f_1^2 + f_2^2, \quad \varkappa = \arcsin\frac{f_2}{\sqrt{f_1^2+f_2^2}}.$$

Defining the corresponding covariant (self-compensating or non-linear) derivative, which transforms as

$$\mathfrak{D}_\nu \psi \to \tilde{\mathfrak{D}}_\nu \psi = \mathfrak{D}_\nu \psi + \delta t_\mu T^{(\mu)} \mathfrak{D}_\nu \psi \tag{8}$$

we get a strongly non-linear, a bit complicated construction for this derivative:

$$\mathfrak{D}_\nu \psi = \partial_\nu \psi + \frac{i}{2(f_1^2+f_2^2)}[(f_1\partial_\nu f_2 - f_2\partial_\nu f_1)\tau^3 - \ldots]\psi \tag{9}$$

for which, the corresponding non-linear equation [8]

$$i\gamma\mathfrak{D}\psi + \Phi\psi = 0 \tag{10}$$

(Φ is an arbitrary function of invariants) is invariant under Lorentz $\times SU(2)$ transformations.

Fusion of non-linear quark equations

Let us now proceed with an approximative, but unexpectedly quick method of dealing with non-linear quarks by admitting a basic equation with quark mass already included (but not massless quarkian pre-matter):

$$(\gamma p)\psi + m\psi - l^2(\bar{\psi}\psi)\psi = 0 \tag{11}$$

(Nambu's 3 triplets scheme understood). Applying a generalized fusion condition

$$\frac{\partial}{\partial x}(\varphi\psi) = 2\frac{\partial\varphi}{\partial x}\psi \tag{12}$$

with meson and baryon operators

$$\begin{aligned} \mathfrak{M} &= \frac{\lambda_0^2}{2}\langle T\psi_A\,\psi^B\rangle\,, \\ \psi_{ABC} &= \frac{\lambda_0^3}{3!}\langle T\psi_A\,\psi_B\,\psi_C\rangle\,, \end{aligned} \tag{13}$$

(T is a symmetrizing operator), one gets with KURDGELAIDZE [5] equations for hadrons, generalizing the Bargman—Wigner and Yang—Mills equations; e.g. for baryons

$$\begin{aligned} (\gamma p)_A^{A'}\psi_{A'BC} + m\,\psi_{ABC} = \frac{1}{10}(l/\lambda_0)^2(\mathfrak{M}_A^D\,\psi_{DBC} + \\ + \mathfrak{M}_B^D\psi_{ADC} + \mathfrak{M}_C^D\psi_{ABD} - 3\,\mathfrak{M}_D^D\,\psi_{ABC})\,. \end{aligned} \tag{14}$$

Moreover, in the same manner one obtains the description of the interactions of quarks with mesons. We are, therefore, now in a position to calculate all hadronic magnetic moments and coupling constants. In some cases the previous results are obtained by our easier calculations, but many new ones are also predicted, up to properties of the Ω particle. For instance

$$\begin{aligned} &g^{\text{scalar}}_{\bar{q}_1\pi^0 q_1} = -\,g^{\text{sc}}_{\bar{q}_2\pi^0 q_2}\,; \quad \mu_{q_1} = \frac{2}{3} + \varkappa_q\left(\frac{1}{m_\varrho} + \frac{1}{3m_\omega}\right); \\ &\mu_p = 1 + \frac{\varkappa_p}{3}\left(\frac{5}{m_\varrho} + \frac{1}{m_\omega}\right); \quad \mu_n = -\left\{\frac{2}{3} + \frac{\varkappa_n}{3}\left(\frac{5}{m_\varrho} - \frac{1}{m_\omega}\right)\right\}; \\ &\mu_{\Xi^0} = -\left\{\frac{2}{3} + \frac{m_{\Xi^0}}{9}\left(\frac{3}{m_\varrho} + \frac{1}{m_\omega} + \frac{8}{m_\Phi}\right)\right\}; \quad \mu_\Lambda = -\left(\frac{1}{3} + \frac{2}{3}\frac{\varkappa_\Lambda}{m_\Phi}\right). \end{aligned} \tag{15}$$

(Here the magnetic moments are constructed either from quarks or are obtained from baryonic equations.) We believe that this rather bold method also deserves attention for essentially permitting rapid reconstruction of the consequences of group theoretical method and for promising further non-linear corrections — all this with a single self-interaction constant.

§ 2. Gravitation

Tetrads

The tetradic treatment of General Relativity is now very popular in connection with the analysis of reference systems. One hopes that the energy problems may be clarified in this way. (MILLER, RODICHEV, TREDER, SCHWINGER, IVANITSKAYA and others). It should be stressed once more that tetradic "revision" of General Relativity is necessary, as the interaction of fermions with gravitation requires introduction of tetrads (FOCK—IVANENKO coefficients, analysed in subsequent works of SCHRÖDINGER, DIRAC, WHEELER, BERGMANN, HAYASHI, cf. reviews of BADE-JEHLE, FIERZ, PETRIAEVA). One consequence of this is that we are led to propose tetrads $h_\alpha(a)$ — and not the metric $g_{\alpha\beta}$ — as the basic potentials, or field components, of the gravitational field. Even considered independently from fermionic matter (r.h. side of equations), tetradic formalism seems to lead to a generalization, and not just a useful reformulation, of General Relativity, as some supplementary conditions are needed (MØLLER, RODICHEV, or SCHWINGER types).

As to the energy problem, we point to an interesting investigation by RODICHEV and FROLOV, who obtained an energy expression starting from the tetradic Lagrangian

$$\mathfrak{L}_G = \frac{1}{2G} h(\Delta_{abc}\Delta^{bac} - \Delta_{ab}{}^{a}\Delta_{c}{}^{bc}) \tag{16}$$

(here Δ_{abc} are Ricci coefficients) and using invariance under

$$\delta x^\sigma = h^\sigma(a)\,\omega^a. \tag{17}$$

(Of course, one could just as well begin with the full scalar Lagrangian analogous to R rather than G.) Imposing RODICHEV's quasi-harmonic conditions [6]

$$\frac{\partial}{\partial x^\sigma}\left(hh^\sigma(a)\right) = 0$$

one gets the following reasonable expression for the energy of the gravitational field:

$$t^\mu(a) = -2a'\left\{2\Delta(b, lt)\,c(la, b) - \frac{1}{2}\delta(at)\,R\right\} h^\mu(t), \qquad a' = \frac{c^4}{8\pi\varkappa}. \tag{18}$$

Here c is a nonholonom expression. (This is covariant under coordinate transformations but not covariant under orthogonal tetradic localized transforma-

tions i.e. those with variable parameters.) A fine condition (very anschaulich when compared with the analogous electromagnetic case) for a pure gravitational radiation field, requiring isotropic character of $t^{\mu}(4)$, was proposed on these lines by DOZMOROV [8]:

$$t^{\mu}(a)\ t_{\mu}(b) = 0. \tag{19}$$

He verified directly that this condition is satisfied by existing wave solutions.

One may ask about the connection of this condition with algebraic classification: In a very satisfactory way one can show that this condition leads indeed to solutions of the N type (or $\mathrm{II}^{\mathrm{nd}}$ degenerate type), as required by other criteria of LICHNEROWICZ, BEL, also of MALDYBAYEVA's proposal, refined by NIKOLAENKO [9]

$$\bar{\Box}\Omega_{\alpha\beta} = 0. \tag{20}$$

Here $\bar{\Box}$ is the generalised d'Alembertian constructed by means of external differentiation and codifferentiation operators, $\bar{\Box} = d\delta = \delta d$, and is topologically and metrically self adjoint; $\Omega_{\alpha\beta}$ is the curvature tensor form built from the Riemannian tensor.

Compensating fields

A powerful formalism of "compensating" fields has been developed, especially by SAKURAI. Consideration of internal space transformation with non-constant but localized parameters depending on space-time coordinates necessitates the substitution of the ordinary derivative by a compensating one and the introduction of corresponding fields (vector mesons). Not only photons are recognized as "compensons", but it is found that gravitation also can be considered as a kind of compensating field after one has localized previously globally constant coefficients of the Lorentz transformations (UTIYAMA, BRODSKY—IVANENKO—SOKOLIK; KIBBLE, FROLOV [10]).

Introducing the compensating derivative (in this case an essentially conventional covariant derivative)

$$Q^{A}_{|a} = h^{\sigma}_{a} Q^{A}_{,\sigma} - \Delta_{a}{}^{m} I_{m}{}^{A}{}_{B} Q^{B} \tag{21}$$

by means of generators $I_{m}{}^{A}{}_{B}$ and compensating fields h^{σ}_{a}, Δ^{m}_{a} (which for the Poincaré group coincide with tetrads and Ricci coefficients), and building the simplest Lagrangian, one gets Einstein's equation alongside the supplementary equation (after variation over Ricci's)

$$K_{\alpha\beta}{}^{\mu} = \varkappa(S_{\alpha\beta}{}^{\mu} + \delta^{\mu}_{[\alpha} S_{\beta]\nu}{}^{\nu}), \tag{22}$$

where the spin moment tensor (r.h. side) generates torsion (tensor on l.h. side). The Lagrangian itself is a function of the field tensor, which in our case coincides with the Riemannian curvature tensor:

$$F^{m}_{ab} = 2h^{\nu}_{[a} \Delta_{b],\nu} + 2\Delta_{c}{}^{m} h_{[\tau,\sigma]} h^{\sigma}_{a} h^{\tau}{}_{b} - C_{n}{}^{m}{}_{q} \Delta^{n}_{a} \Delta^{q}_{b} . \tag{23}$$

It has been pointed out (RODICHEV, KIBBLE, PERES) that parallel displacement, by the FOCK—IVANENKO method of spinors in the space endowed with torsion leads to a non-linear ψ^3-type term in the Dirac equation of precisely the type discussed above. The quantization of the torsions has been investigated by VLADIMIROV. One sees that torsionic generalisation is suggested strongly, but not required, by tetradic and compensational treatment of gravitation. Recently TRAUTMAN and PONOMARIOV considered empirical implications of a simple concrete model of torsion (Copenhagen GR6 report, 1971).

Variable constant of gravitation

There have been plenty of theories of non-geometrized gravitation as the spin 2-field. A recent interesting version by SALAM and STRATHDEE [17] proposed to use real f-mesons as carriers of a gravitation strong enough to play even the role of cutting-off factor.

In recent years the discussion of scalar-tensor theory (STT) has became fashionable in the hands of JORDAN [11], while BRANS—DICKE have revived Dirac's interesting suggestion of a variable gravitation constant. STT has attacked even the collapse problem. Some people indicate that nothing essentially new is gained here (KIP THORNE, DUKLA); whereas others believe that no collapse arises in STT and that arbitrarily large star masses are permitted (e.g. MUATSAKANIAN, who insisted on the point-like behaviour of $r = 0$).

Without claiming to settle definitely the difficult collapse problem, we may draw attention to the work of GORELIK [12] on several important points. First of all, it is easy to prove the complete equivalence of two central symmetric solutions in STT: on the one hand, Heckmann's form, using Schwarzschild-type coordinates (in which nothing like a gravitational radius appears) and, on the other hand, the Brans—Dicke—Salmona form, written in isotropic coordinates, which explicitly exhibits gravitational radius. Now, if Gerock's notion of the singular region is applied and its topological dimensionality investigated, writing with the GORELIK equations of geodetics and looking for their behaviour at small r, one sees that two incomplete radial geodetics, corresponding to different angles, are not equivalent in the Gerock sense, so that, paradoxically, the metrical "point" $r = 0$ represents rather a $(2 + 1)$-dimensional

surface (2-space + time). (This analysis can, of course, be performed both in Heckmann or Brans—Dicke—Salmona coordinates.) We see, then, that one must be at any rate cautious in trying to connect the presumed absence of collapse in STT with the apparent — but in reality non-existent — difference of two types of solutions.

Another important conclusion can be drawn from the geodetics equations; namely, that the time needed by a falling particle to reach singularity, as judged by infinitely distant observer's clock, is finite $\triangle r \sim (\triangle r)^{2/3}$, in contrast to the Schwarzschild General Relativity case. Thus, observation of the last stages of a star contraction should, in principle, permit a distinction to be made between STT and General Relativity. This interesting consequence is obtained for positive values $\omega > 0$ of the dimensionless interaction constant connecting scalar and metrical fields in STT; for $\omega < 0$ and $|\omega| \gg 1$ one obtains the same $(2 + 1)$ -dimensionality of a singular surface, but the test particle will take infinite time to reach the singularity. In this connection it is necessary to remark also that to pass from STT to General Relativity requires not only constancy of the scalar field but also that $|\omega| \to \infty$, so that KIP THORNE's suggestion that the Black Holes of STT are similar to conventional GR Black Holes may be too great a simplification.

Quantum gravidynamics

We shall not enter here into discussion of the various difficult basic and technical problems of quantization of gravity (which is almost equivalent to quantization of space-time itself), but draw attention to two questions only. The first is connected with the polarization of spinor vacuum by the gravitational field, which was already considered by us some time ago (BRODSKY—IVANENKO). Using techniques like the powerful Schwinger method, one can get the supplement to the Lagrangian, expansion of which yields the first correction identifiable with a cosmological term:

$$\mathfrak{L}' = \frac{1}{32\,\pi^2\,\tau_0^2} = \Lambda$$

(τ_0 is the cut-off parameter).

We see here, therefore, the necessary appearance of a cosmological term, also of a quantum character. Further terms lead to R^2 corrections, moreover the quantum gravidynamics seems to fall in the series of renormalizable theories (B. DE WITT). The appearance of quadratic quantum scalar terms is in harmony with classical suggestions about such generalization.

The most important quantum gravitational processes seem to be anticipated principally as metrics fluctuations (WHEELER), which even seem to

lead to drastic topological changes (TREDER, DAUTCOURT) that realize in a complicated fashion the hypothesis of discrete space-time (AMBARZUMIAN—IVANENKO, SHILD, SNYDER, KOISH, FINKELSTEIN and others).

Secondly, there is a multitude of mutual transmutation of gravitations and quanta of ordinary matter (IVANENKO, developed by SOKOLOV, VLADIMIROV, WHEELER—BRILL, PIIR, KORKINA and others) and production of gravitons by electromagnetic scattering etc. (DE SABBATA, HALPERN et al.). All this is extremely important for the analysis of the Big Bang and the first weeks of expansion (ZELDOVICH—NOVIKOV), as well as for evaluation of the present day concentration of relicts and newly produced gravitons (VLADIMIROV, DE SABBATA [13, 14] et al., CARMELI), not to speak of fundamental epistemological features of the transmutation of ordinary matter into an apparently geometrized form of physical reality. Anyhow such gravitational transmutations help to unify all sides of physical reality.

§ 3. Cosmology and elementary particles

On our hypothesis, all cosmological asymmetries induce (or are reflected in) analogous asymmetries of vacuum ground states, these latter leading via the Goldstone theorem to real particles. The chief cosmological asymmetries are:

1) Preponderance of baryons (protons over antiprotons, etc). If conservation of baryonic number (B) is absolute, this does not lead to goldstons. (But here one must be cautious, in view of WHEELER's arguments in favour of a changing B at collapse and pointing in this respect to the BRODSKY—IVANENKO formalism of anomalous spinors).

2) The Universe seems to possess a large value of hypercharge and non-vanishing strangeness. If our hypothesis is admitted, one is led to accept violation of the unitary SU(3) symmetry, with probably vector mesons playing the role of goldstons; strictly speaking, the violators — goldstons-compensons are here ω and φ mesons, being mixture of octet and singlet, like the part played by photons as mixture of singlet and isotriplet, leading to their role as goldstons-violators of SU(2), and corresponding compensons at the same time being.

3) A fundamental asymmetry is given to the Universe by the Friedman—Hubble expansion. Is it possible that in a contracting Universe one would have a preponderance of antibaryons? (The same point was stressed by SAKHAROV). KURDGELAIDZE tried to evaluate the order of magnitude of the influence of the effective cosmological force due to expansion by introducing the factors $(1 \pm F)$ $(F = \varrho/\varrho_{\text{crit}})$ in the field operators. They aimed in this way to explain the anomalous K° decays, which point to non-conservation of T-parity.

4) The average non-vanishing curvature induces a departure from flatness in vacuum metrics, which leads to gravitons as corresponding goldstons (HEISENBERG [2], IVANENKO, PHILIPPS, THIRRING, TREDER [16]).

5) The difference of the proton *vs* neutron concentration — which yields a non-vanishing cosmological isospin (I or I_3) — induces degeneracy of the vacuum and leads to photons as corresponding goldstons (and at the same time compensons). This last example was thoroughly discussed by HEISENBERG. To be quite clear, we may emphasize once more that is seems unreasonable to limit oneself by connecting photons — as goldstons — with a definite cosmological asymmetry in isospin: on the contrary, it is attractive to assume that this specific connection is not an accidental one but that all cosmological asymmetries have their counterpart in vacuum degeneracies and corresponding particles as goldstons.

6) Conformal invariance seems to be of a fundamental nature, but is apparently broken in the microworld by the rest masses of particles, which in our view may be due to the existence of the cosmological term. May be electron is the corresponding goldston, possessing the smallest rest mass? Certainly the conventional Goldstone theorem leads to massless bosons, but it must be generalized to cover the indefinite metrics of Hilbert space. It may then be that massless fermions (neutrinos) are also goldstons (HEISENBERG); the evident connection between goldstons and compensons also points to the possibility of non-vanishing mass at generalized goldstons.

7) We shall not discuss here the possibility of goldstons reflecting further plausible cosmological asymmetries due to leptons (non-vanishing leptonic number, non-vanishing spirality, muonic number). A curious possibility arises that the diminishment of an eventual anisotropy in the course of expansion may entail the disappearance of certain conservation laws as well as corresponding goldstons (Dirac's magnetic monopoles?).

Concluding this short review of some promising points of this new unified theory, there seems to be reason to be moderately optimistic that a suitable basis can be provided by a non-linear unitary invariant spinor field taking account of quantized gravitation, preferably in tetradic form, and of cosmological characteristics.

REFERENCES

1. D. IVANENKO, Actual problems of gravitation (Tbilissi, 1968), G R5-Theses (Tbilissi, 1968).
2. W. HEISENBERG, Introduction to the Unified Field Theory of Elementary Particles, (N. Y. 1966).
3. D. IVANENKO, Sov. Phys., **13**, 141, 1938; Convegno sulla Relativita Generale (Firenze, 1964).
D. IVANENKO and A. M. BRODSKY, JETP, **24**, 384, 1953.

4. A. I. Naumov, JETP, **47**, 914, 1964; Nucl. Phys., **7**, 664, 1968; Transact. High Schools (Tomsk), N5, 1965; Transact. Moscow Univ., N2, 1967;
N. S. Demidova and A. I. Naumov, Transact. (Vestnik) Moscow Univ. (Phys.), N2, 1970.
A. I. Naumov and Nguen Ngoc Giao, Transact. (Vestnik) Moscow Univ. (Phys.) 1971.
A. D. Smirnov, Transact. (Vestnik) Moscow Univ., 1971.
5. D. F. Kurdgelaidze and A. Bassiuni, Nucl. Phys., **9**, 432, 1969; (Vestnik) Transact. Moscow Univ. (Phys.), N3, 115, 1969; N4, 107, 1969.
6. V. I. Rodichev, Transact. High Schools (Phys.) Tomsk., N1, 132, 1965; Actual problems of gravitation (Tbilissi, 1968).
V. A. Fock and D. Ivanenko, C. R. Paris, **188**, 1470, 1929.
H. J. Treder, Mitteil. Institut Kosm. Phys., Potsdam, 1968–70.
7. B. N. Frolov, Transact. (Vestnik) Moscow Univ. (Phys.), N2, 1964.
8. I. Dozmorov, Transact. High. Schools (Tomsk), N7, 156, 1968, N10, 17, 1968, ibid. 1971.
9. V. M. Nikolaenko, Transact. High. Schools (Tomsk) N1, 1971.
10. A. M. Brodsky, D. Ivanenko and H. Sokolik, JETP, **41**, 1037, 1961;
B. N. Frolov, Transact. (Vestnik) Moscow Univ. (Phys.), N6, 48, 1968., in "Actual problems of Grav". (Tbilissi, 1968).
11. P. Jordan, Die Expansion d. Erde. Braunschweig, 1966;
D. Ivanenko and M. Sagitov, Transact. (Vestnik) Moscow Univ. (Astron.), N6, 83, 1961;
E. Aman, Transact. High School (Tomsk), 1971.
12. T. E. Gorelik, Transact. (Vestnik) Moscow Univ., 1971.
13. Yu. S. Vladimirov, JETP, **45**, 251, 1963;
S. N. Gupta, Proc. Ph. Soc. A **65**, 608, 1952.
14. V. de Sabbata et al., Nuovo Cim., B, **54**, 134, 1968.
15. D. Ivanenko, Nuovo Cim., A, **51**, 244, 1967;
D. Ivanenko, GR5-Theses, Tbilissi, 1968.
16. H. J. Treder, in "Physics, Logic, History", Ed. W. Yourgrau, A. D. Breck, Plenum Press., NY, 1970.
17. A. Salam and I. Strathdee, Preprint Trieste IC 70/38.

НОВЫЕ ВАРИАНТЫ ЕДИНОЙ ТЕОРИИ

Д. ИВАНЕНКО

Резюме

Мы продолжаем построение наиболее объединенной картины физической реальности, связывая локальную теорию с гравитацией. Базой является единая теория элементарных частиц, исходящая из нелинейного обобщения дираковского уравнения (Иваненко—Бродский—Гейзенберг), причем с унитарно симметричной волновой функцией («нелинейные кварки»).

Тогда улучшенный пропагатор Наумова позволяет вычислить массы адронов, в том числе барионных резононов декуплета в удовлетворительном согласии с опытом. Быстрый, хотя и более грубый метод «слияния» Курдгелаидзе позволил получить магнитные моменты барионов. Теория гравитации существенно использует тетрадный формализм, ставший необходимым для описания фермионов (коэффициенты Фока—Иваненко). Взаимные трансмутации гравитонов и частиц со своей стороны объединяют разные категории физической реальности. Мы попрежнему считаем правдоподобной нашу гиотезу о связи космологических и вакуумных асимметрий (расширение Вселенной, преимущественная концентрация барионов и т. д.).

INDEX

A kiadásért felel az Akadémiai Kiadó igazgatója Műszaki szerkesztő: Zacsik Annamária

A kézirat nyomdába érkezett: 1972. II. 15. — Terjedelem: 31 (A/5) ív, 109 ábra

72.73128 Akadémiai Nyomda, Budapest — Felelős vezető: Bernát György

NOTES TO CONTRIBUTORS

I. PAPERS will be considered for publication in Acta Physica Hungarica only if they have not previously been published or submitted for publication elsewhere. They may be written in English, French, German or Russian.

Papers should be submitted to

Prof. I. Kovács. Editor
Department of Atomic Physics, Polytechnical University
Budapest 112. Budafoki út 8, Hungary

Papers may be either articles with abstracts or short communications. Both should be as concise as possible, articles in general not exceeding 25 typed pages, short communications 8 typed pages.

II. MANUSCRIPTS

1. Papers should be submitted in two copies. Articles should be accompanied by abstracts in the language of the paper together with a copy of the title, name of author(s) and abstract in Russian if the paper is in English, French or German, and in one of the latter three languages if the paper is in Russian. If a translation of the abstract cannot be provided, this will be arranged by the Editor.

2. The text of papers must be of high stylistic standard, requiring minor corrections only.

3. Manuscripts should be typed in double spacing on good quality paper, with generous margins.

4. The name of the author(s) and of the institutes where the work was carried out should appear on the first page of the manuscript.

5. Particular care should be taken with mathematical expressions. The following should be clearly distinguished. e.g. by underlining in different colours: special founts (italics, script, bold type, Greek, Gothic, etc.); capital and small letters; subscripts and superscripts, e.g. x^3, x_3; small l and 1; zero and capital O; in expressions written by hand: e and l, n and u, ν and v, etc.

6. References should be numbered serially and listed at the end of the paper in the following form: J. Ise and W. D. Fretter, Phys. Rev., *76*, 933, 1949.

For books, please give the initials and family name of the author(s), title, name of publisher, place and year of publication, e.g.: J. C. Slater, Quantum Theory of Atomic Structures, I, McGraw-Hill Book Company Inc., New York, 1960.

References should be given in the text in the following forms: Heisenberg [5] or [5].

7. Captions to illustrations should be listed on a separate sheet, not inserted in the text.

III. ILLUSTRATIONS AND TABLES

1. Each paper should be accompanied by two sets of illustrations, one of which must be ready for the blockmaker. The other set attached to the copy of the manuscript may be rough drawings in pencil or photocopies.

2. Illustrations must not be inserted in the text.

3. All illustrations should be identified in blue pencil by the author's name, abbreviated title of the paper and figure number.

4. Tables should be typed on separate pages and have captions describing their content. Clear wording of column heads is advisable. Tables should be numbered in Roman numerals (I, II, III, etc.).

IV. MANUSCRIPTS not in conformity with the above Notes will immediately be returned to authors for revision. The date of receipt to be shown on the paper will in such cases be that of the receipt of the revised manuscript.

Reviews of the Hungarian Academy of Sciences are obtainable at the following addresses:

ALBANIA
Drejtorija Qëndrone e Përhapjes dhe Propagandimit të Librit
Kruga Konferenca e Pazes
Tirana

AUSTRALIA
A. Keesing
Box 4886, GPO
Sydney

AUSTRIA
Globus
Höchstädtplatz 3
A-1200 Wien XX

BELGIUM
Office International de Librairie
30, Avenue Marnix
Bruxelles 5
Du Monde Entier
5, Place St. Jean
Bruxelles

BULGARIA
Hemus
11 pl Slaveikov
Sofia

CANADA
Pannonia Books
2, Spadina Road
Toronto 4, Ont.

CHINA
Waiwen Shudian
Peking
P. O. B. 88

CZECHOSLOVAKIA
Artia
Ve Smečkách 30
Praha 2
Poštovní Novinová Služba
Dovoz tisku
Vinohradská 46
Praha 2
Mad'arska Kultura
Václavské nám. 2
Praha 1
Slovart A. G.
Gorkého
Bratislava

DENMARK
Ejnar Munksgaard
Nörregade 6
Copenhagen

FINLAND
Akateeminen Kirjakauppa
Keskuskatu 2
Helsinki

FRANCE
Office International de Documentation et Librairie
48, rue Gay Lussac
Paris 5

GERMAN DEMOCRATIC REPUBLIC
Deutscher Buch-Export und Import
Leninstraße 16
Leipzig 701
Zeitungsvertriebsamt
Fruchtstraße 3–4
1004 Berlin

GERMAN FEDERAL REPUBLIC
Kunst und Wissen
Erich Bieber
Postfach 46
7 Stuttgart S.

GREAT BRITAIN
Blackwell's Periodicals
Oxenford House
Magdalen Street
Oxford
Collet's Subscription Import Department
Dennington Estate
Wellingsborough. Northants.
Robert Maxwell and Co. Ltd.
4–5 Fitzroy Square
London W. 1

HOLLAND
Swetz and Zeitlinger
Keizersgracht 471–487
Amsterdam C.
Martinus Nijhof
Lange Voorhout 9
The Hague

INDIA
Hind Book House
66 Babar Road
New Delhi 1

ITALY
Santo Vanasia
Via M. Macchi 71
Milano
Libreria Commissionaria Sansoni
Via La Marmora 45
Firenze

JAPAN
Kinokuniya Book-Store Co. Ltd
826 Tsunohazu 1-chome
Shinjuku-ku
Tokyo
Maruzen and Co. Ltd
P. O. Box 605
Tokyo-Central

KOREA
Chulpanmul
Phenjan

NORWAY
Tanum-Cammermeyer
Karls Johansgt 41–43
Oslo 1

POLAND
RUCH
ul. Wronia 23
Warszawa

ROUMANIA
Cartimex
Str. Aristide Briand 14–18
Bucureşti

SOVIET UNION
Mezhdunarodnaya Kniga
Moscow G–200

SWEDEN
Almqvist and Wiksell
Gamla Brogatan 26
S–101 20 Stockholm

USA
F. W. Faxon Co. Inc.
15 Southwest Park
Westwood Mass. 02090
Stechert Hafner Inc.
31. East 10th Street
New York, N. Y. 10003

VIETNAM
Xunhasaba
19, Tran Quoc Toan
Hanoi

YUGOSLAVIA
Forum
Vojvode Mišića broj 1
Novi Sad
Jugoslovenska Knjiga
Terazije 27
Beograd

Acta Phys. Hung. Tom. 32. No. 1—4 Budapest, 10. XI. 1972. Index: 26.022